BIOMARKERS IN GENITOURINARY CANCERS, VOLUME I

EDITED BY: Eric A. Singer, Paula Alexandra Quintela Videira and Marco Borghesi

PUBLISHED IN: Frontiers in Oncology

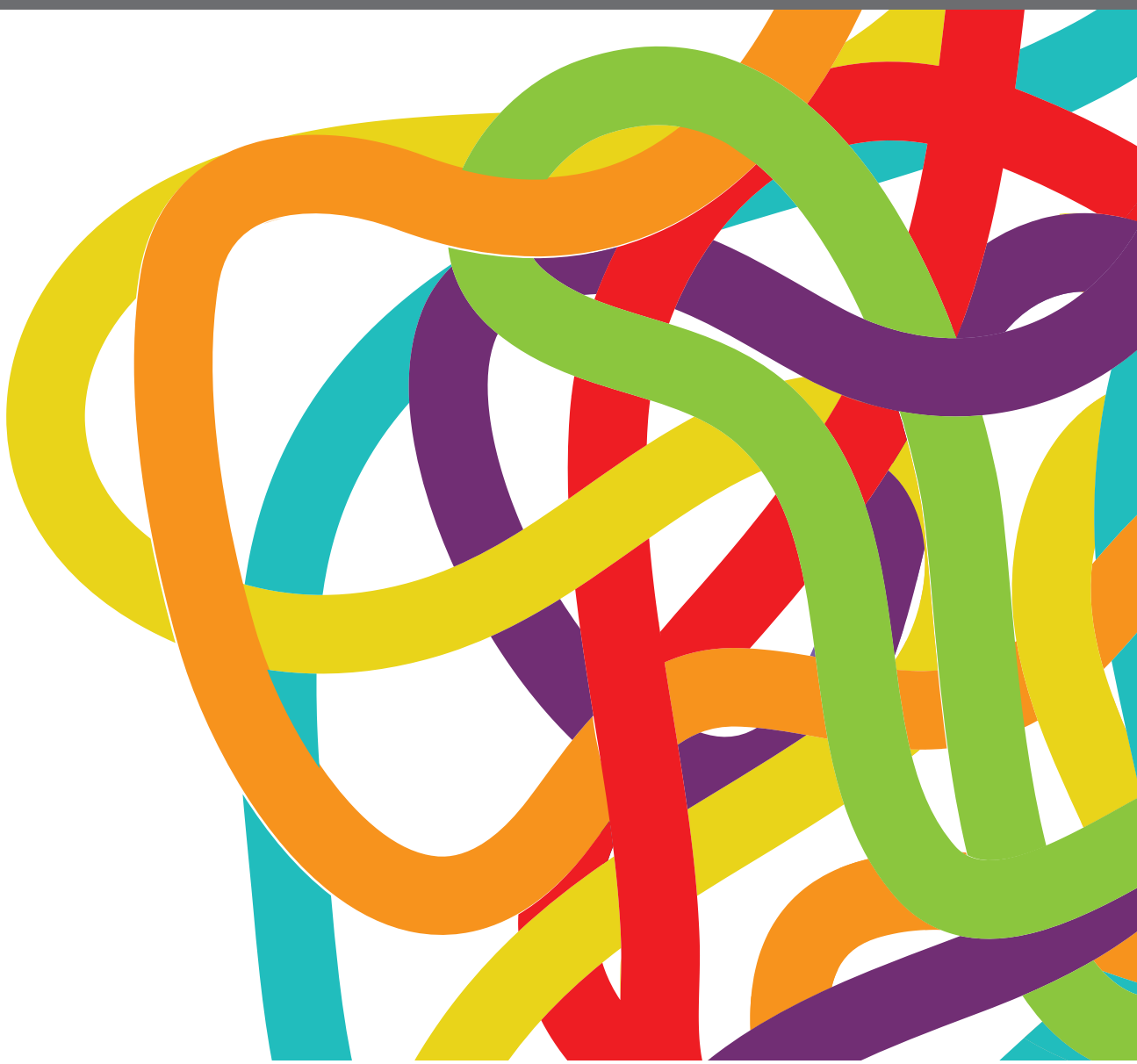

frontiers Research Topics

Frontiers eBook Copyright Statement

The copyright in the text of individual articles in this eBook is the property of their respective authors or their respective institutions or funders. The copyright in graphics and images within each article may be subject to copyright of other parties. In both cases this is subject to a license granted to Frontiers.

The compilation of articles constituting this eBook is the property of Frontiers.

Each article within this eBook, and the eBook itself, are published under the most recent version of the Creative Commons CC-BY licence. The version current at the date of publication of this eBook is CC-BY 4.0. If the CC-BY licence is updated, the licence granted by Frontiers is automatically updated to the new version.

When exercising any right under the CC-BY licence, Frontiers must be attributed as the original publisher of the article or eBook, as applicable.

Authors have the responsibility of ensuring that any graphics or other materials which are the property of others may be included in the CC-BY licence, but this should be checked before relying on the CC-BY licence to reproduce those materials. Any copyright notices relating to those materials must be complied with.

Copyright and source acknowledgement notices may not be removed and must be displayed in any copy, derivative work or partial copy which includes the elements in question.

All copyright, and all rights therein, are protected by national and international copyright laws. The above represents a summary only. For further information please read Frontiers' Conditions for Website Use and Copyright Statement, and the applicable CC-BY licence.

ISSN 1664-8714
ISBN 978-2-88976-215-6
DOI 10.3389/978-2-88976-215-6

About Frontiers

Frontiers is more than just an open-access publisher of scholarly articles: it is a pioneering approach to the world of academia, radically improving the way scholarly research is managed. The grand vision of Frontiers is a world where all people have an equal opportunity to seek, share and generate knowledge. Frontiers provides immediate and permanent online open access to all its publications, but this alone is not enough to realize our grand goals.

Frontiers Journal Series

The Frontiers Journal Series is a multi-tier and interdisciplinary set of open-access, online journals, promising a paradigm shift from the current review, selection and dissemination processes in academic publishing. All Frontiers journals are driven by researchers for researchers; therefore, they constitute a service to the scholarly community. At the same time, the Frontiers Journal Series operates on a revolutionary invention, the tiered publishing system, initially addressing specific communities of scholars, and gradually climbing up to broader public understanding, thus serving the interests of the lay society, too.

Dedication to Quality

Each Frontiers article is a landmark of the highest quality, thanks to genuinely collaborative interactions between authors and review editors, who include some of the world's best academicians. Research must be certified by peers before entering a stream of knowledge that may eventually reach the public - and shape society; therefore, Frontiers only applies the most rigorous and unbiased reviews.
Frontiers revolutionizes research publishing by freely delivering the most outstanding research, evaluated with no bias from both the academic and social point of view. By applying the most advanced information technologies, Frontiers is catapulting scholarly publishing into a new generation.

What are Frontiers Research Topics?

Frontiers Research Topics are very popular trademarks of the Frontiers Journals Series: they are collections of at least ten articles, all centered on a particular subject. With their unique mix of varied contributions from Original Research to Review Articles, Frontiers Research Topics unify the most influential researchers, the latest key findings and historical advances in a hot research area! Find out more on how to host your own Frontiers Research Topic or contribute to one as an author by contacting the Frontiers Editorial Office: frontiersin.org/about/contact

BIOMARKERS IN GENITOURINARY CANCERS, VOLUME I

Topic Editors:
Eric A. Singer, The State University of New Jersey, United States
Paula Alexandra Quintela Videira, New University of Lisbon, Portugal
Marco Borghesi, University of Genoa, Italy

Citation: Singer, E. A., Videira, P. A. Q., Borghesi, M., eds. (2022). Biomarkers in Genitourinary Cancers, Volume I. Lausanne: Frontiers Media SA.
doi: 10.3389/978-2-88976-215-6

Table of Contents

frontiers | Frontiers in Oncology

EDITORIAL
published: 08 July 2022
doi: 10.3389/fonc.2022.965294

Editorial: Biomarkers in Genitourinary Cancers, Volume I

Paula Alexandra Videira[1,2]*, *Marco Borghesi*[3] and *Eric A. Singer*[4]

[1] Research Unit on Applied Molecular Biosciences (UCIBIO) – Applied Molecular Biosciences Unit, Department of Life Sciences, NOVA School of Science and Technology, Universidade NOVA de Lisboa, Caparica, Portugal, [2] Associate Laboratory i4HB - Institute for Health and Bioeconomy, School of Science and Technology, NOVA University Lisbon, Caparica, Portugal, [3] Dipartimento di Scienze Chirurgiche e Diagnostiche Integrate, University of Genoa, Genoa, Italy, [4] Kidney Cancer Program, Rutgers Cancer Institute of New Jersey and Rutgers Robert Wood Johnson Medical School, New Brunswick, QC, United States

Keywords: biomarkers, genitourinary cancer, bladder cacner, prostate cancer, renal cancer

Editorial on the Research Topic

Biomarkers in Genitourinary Cancers, Volume I

Genitourinary cancers are known as significant causes of mortality worldwide. This heterogeneous group includes, among others, the most common cancer in men, prostate cancer, the most common form of kidney cancer, renal cell carcinoma (RCC), and the 10th most common cancer, bladder cancer. These entities present biological diversity with various histological subtypes and a poor prognosis when metastatic.

There has been considerable progress in treating patients with genitourinary cancers due to the improved understanding of their pathological mechanisms and the identification of meaningful biomarkers. The treatment progress has led to a fundamental paradigm shift in treatments. For example, our current understanding of the immunogenicity of these tumours has improved tremendously. Thanks to that, today, immunotherapy is a reliable strategy to improve the outcomes of patients with metastatic urothelial carcinoma, renal cell carcinoma, and prostate cancer. However, there is still a critical need to enrich our understanding of additional molecular mechanisms.

Along with the mechanisms, there is an urgent requirement to identify novel biomarkers to progress the diagnosis and prognosis of genitourinary cancers and their treatment. Biomarkers have become a significant focus of research, primarily on how they can help predict response to systemic therapy, identify treatment resistance, and avoid toxicities. Biomarkers that reveal the mutated tumour suppressor genes, the altered signalling pathways and the aberrantly expressed molecules help select potentially responsive patients to a given therapy. In this way, biomarkers improve outcomes and reduce costs related to ineffective treatments, and, most importantly, they significantly upsurge patients' quality of life.

This Research Topic named Biomarkers in Genitourinary Cancers includes an interesting and up to date palette of publications from prominent research and clinical groups focused on identifying significant and emerging prognostic and predictive biomarkers. These biomarkers encompass non-

OPEN ACCESS

Edited and reviewed by:
Ronald M. Bukowski, Cleveland Clinic, United States

***Correspondence:**
Paula Alexandra Videira
p.videira@fct.unl.pt

Specialty section:
This article was submitted to Genitourinary Oncology, a section of the journal Frontiers in Oncology

Received: *09 June 2022*
Accepted: *14 June 2022*
Published: *08 July 2022*

Citation:
Videira PA, Borghesi M and Singer EA (2022) Editorial: Biomarkers in Genitourinary Cancers, Volume I. Front. Oncol. 12:965294. doi: 10.3389/fonc.2022.965294

coding RNA, serum proteins, gene expression, and glycans, among other entities identified in patients' cohorts, samples and in the increasing number of public databases.

BLADDER CANCER

The review by Zhang et al. discussed biomarkers which predict bladder cancer lymphatic metastasis. The authors particularly emphasised the influence of non-coding RNA, its specific roles and prediction imaging models. In addition, they highlight non-coding RNA's contribution to providing accurate diagnostic methods for future clinical applications.

Wang et al. showed that among the non-coding RNA, the miR-20a-5p correlates with the recurrence of bladder cancer. Furthermore, the author reinforced that serum miR-17-92 cluster is overexpressed in bladder cancer. They also proposed a model composed of the three miR cluster members as a promising noninvasive biomarker for bladder cancer diagnosis.

Li et al. constructed a prognostic signature to improve the prognosis prediction of advanced Bladder Urothelial Carcinoma based on ferroptosis-related genes. They used TCGA and another patient cohort, identified differentially expressed genes associated with overall survival, and generated a prognostic risk signature through LASSO regression analysis.

Xie et al. reported a novel model based on the ten inflammatory response-associated genes that can predict survival time for transitional bladder cancer. In addition, the authors provide clues for treatment strategies according to the drug sensitivity.

Beyond genes, Carvalho et al. underscored the sialyl Tn as a cancer-associated glycan to detect urothelial bladder cancer cells in urinary samples that can serve as follow-up and long-term retrospective screening. In addition, the authors demonstrated that the microfluidic devices, which the authors called UriChip, can successfully be used to detect cancer cells in urine, paving the way for the development of a sialyl Tn -based medical devices.

PROSTATE CANCER

Basourakos et al. highlight recent advances in using tissue-based genomic tests to select the best treatments for prostate cancer and the existing evidence supporting their clinical use. Chiu et al. showed that the Prostate Health Index density (PHID), a diagnostic indicator calculated based on serum biomarkers and prostate volume is an efficient predictor of clinically significant prostate cancer (csPCa). Therefore, they suggested, the PHID risk table to be used in standard clinical practice to screen men at the highest risk of having csPCa.

Shi et al. explored The Cancer Genome Atlas (TCGA) and other public databases the Oncomine and found that in prostate cancer, lysophosphatidic acid receptor 1 (LPAR1) is positively correlated with chemokine/chemokine receptors, probably regulating the migration of immune cells. LPAR1 is a potential prognostic biomarker and plays an essential part in immune infiltrates in prostate cancer.

RENAL CELL CARCINOMA

Kidney renal clear cell carcinoma (KIRC) and renal papillary cell carcinoma (KIRP) are the most common RCC types. Zhou et al. showed that the extracellular matrix protein collagen triple helix repeat containing 1 (CTHRC1) can predict tumour stage, metastasis and immune infiltration in KIRP and KIRC. This is due to the CTHRC1 role in modulating the tumour microenvironment and the authors also showed that its overexpression in KIRP and KIRC may be due to copy number variations (CNV) and DNA methylation.

Li et al.'s performed a systematic review to investigate the prognostic value of aspartate transaminase (AST) to alanine transaminase (ALT) ratio, also known as De Ritis ratio. The authors concluded that De Ritis ratio significantly correlates with worse survival in patients with RCC. An elevated De Ritis ratio before treatments may serve as a prognostic biomarker in patients with RCC, although further studies are still necessary to validate this biomarker .

Cui et al. study suggested that Apolipoprotein C1 (APOC1) is a diagnostic and prognostic biomarker for clear cell Renal Cell Carcinoma (ccRCC). The author identified elevated APOC1 gene expression in databases and then, using tissue microarray, confirmed a significant correlation between APOC1, the tumour size and histological grade. Understanding the underneath tumorigenic mechanism may convert APOC1 into a new therapeutic target for the treatment of ccRCC.

On the other hand, Huang et al. analysed transcriptome data of ccRCC. They demonstrated that the ALDOB, EFHD1, and ESRRG genes are potential targets for medical therapy and could serve as diagnostic biomarkers for ccRCC.

Zhu et al. investigated why ccRCC carrying wild-type Von Hippel–Lindau (VHL) tumour suppressor gene are more invasive and show higher morbidity. Applying applied bioinformatics approaches, these authors elected six survival-related differentially expressed RNAs upregulated in patients carrying wild type VHL, which helped to calculate risk scores predicting malignancy and prognosis.

Studies conducted by Lv et al. highlighted the clinical significance of CD146 in ccRCC and provided novel insights into the immune function of CD146 in the tumour microenvironment . In another research article, the Lv et al. team showed that Fibrinogen-like Protein 1 (FGL1) facilitates the epithelial-to-mesenchymal transition (EMT) process and modulates the tumour microenvironment, which promotes ccRCC progression and metastasis. The authors suggest that targeting FGL1 can potentially improve the clinical outcomes of ccRCC patients.

Zhang et al. put into evidence, in ccRCC, the role of pyroptosis, a programmed cell death with a highly inflammatory profile. The authors used gene expression data to show that pyroptosis regulators and pyroptosis index associated with the development and prognoses of ccRCC. Moreover, the

authors validated the gene AIM2 the most significant immune-related pyroptosis regulator. AIM2 was therefore proposed as a predictor of the response to immunotherapy.

In non-metastatic RCC, Shang et al. demonstrated that neutrophil-associated NETosis and systemic lymphocyte perturbations occurred in patients with tumour thrombus and worse prognosis. This was replicated by a neutrophil-to-lymphocyte ratio ≥4 and considered an independent risk factor for patients . These two studies prove that assessing the cell death patterns may indicate the tumour status and guide therapeutic decisions. On the other hand, in metastatic RCC, Maruzzo et al. showed that thyroid hormones, when they reach a low fT3/fT4 ratio at baseline, are a decisive prognostic factor in patients under systemic treatment and independent of other biomarkers currently used in clinical practice.

In two patients with metastatic ccRCC, and different sensitivity to axitinib–pembrolizumab combination Seront et al. found that in the case with decreased 68Ga metabolism it accompanies a decrease in size and number of lesions and, therefore a better response to treatment. The authors suggested that in ccRCC, 68Ga-Prostate-Specific Membrane Antigen (PSMA)-Positron Emitted Tomography (PET) predicts early response to systemic therapy. These studies confirm the relevance of PSMA as a predictive biomarker due to its significant expression in neovasculature.

OTHER GENITOURINARY CANCERS

Nonaka et al. reported a rare case of Solitary fibrous tumours (SFT), which rapidly progressed to death after admission, which contrasted with SFT typical favourable prognosis. The authors screened for known mutation and gene expression. They reported the first evidence that mutations in the tumour suppressor gene TP53 mutations and downregulation of NAB2-STAT6 fusion gene expression associates with dedifferentiation of tumours and subsequent malignancy.

In summary, this Research Topic summarised recent findings in the quest for reliable and meaningful biomarkers in genitourinary cancers. Such biomarkers are often identified based on large cohorts of patients and using computer-aided tools to guarantee new prognostic biomarkers, and promising therapeutic targets.

AUTHOR CONTRIBUTIONS

PV drafted the manuscript. ES revised the manuscripts. All authors made a substantial, direct, and indirect contribution to the work and approved it for publication.

FUNDING

This work was also financed by national funds from FCT - Portugal, in the scope of the project UIDP/04378/2020 and UIDB/04378/2020 of the Research Unit on Applied Molecular Biosciences - UCIBIO and the project LA/P/0140/2020 of the Associate Laboratory Institute for Health and Bioeconomy - i4HB.

ACKNOWLEDGEMENTS

We sincerely appreciate all submissions and contributing authors and reviewers for this Research Topic.

Conflict of Interest: The authors declare the absence of any commercial or financial relationships that could be construed as a potential conflict of interest.

Publisher's Note: All claims expressed in this article are solely those of the authors and do not necessarily represent those of their affiliated organizations, or those of the publisher, the editors and the reviewers. Any product that may be evaluated in this article, or claim that may be made by its manufacturer, is not guaranteed or endorsed by the publisher.

Copyright © 2022 Videira, Borghesi and Singer. This is an open-access article distributed under the terms of the Creative Commons Attribution License (CC BY). The use, distribution or reproduction in other forums is permitted, provided the original author(s) and the copyright owner(s) are credited and that the original publication in this journal is cited, in accordance with accepted academic practice. No use, distribution or reproduction is permitted which does not comply with these terms.

frontiers in Oncology

ORIGINAL RESEARCH
published: 10 June 2020
doi: 10.3389/fonc.2020.00846

LPAR1, Correlated With Immune Infiltrates, Is a Potential Prognostic Biomarker in Prostate Cancer

Jingqi Shi[1†], Dongbo Jiang[1†], Shuya Yang[1†], Xiyang Zhang[1], Jing Wang[1], Yang Liu[1], Yuanjie Sun[1], Yuchen Lu[2] and Kun Yang[1]*

[1] Department of Immunology, The Fourth Military Medical University, Xi'an, China, [2] School of Basic Medicine, The Fourth Military Medical University, Xi'an, China

Prostate cancer is a common malignancy in men worldwide. Lysophosphatidic acid receptor 1 (LPAR1) is a critical gene and it mediates diverse biologic functions in tumor. However, the correlation between LPAR1 and prognosis in prostate cancer, as well as the potential mechanism, remains unclear. In the present study, LPAR1 expression analysis was based on The Cancer Genome Atlas (TCGA) and the Oncomine database. The correlation of LPAR1 on prognosis was also analyzed based on R studio. The association between LPAR1 and tumor-infiltrating immune cells were evaluated in the Tumor Immune Estimation Resource site, ssGSEA, and MCPcounter packages in R studio. Gene Set Enrichment Analysis and Gene Ontology analysis were used to analyze the function of LPAR1. TCGA datasets and the Oncomine database revealed that LPAR1 was significantly downregulated in prostate cancer. High LPAR1 expression was correlated with favorable overall survival. LPAR1 was involved in the activation, proliferation, differentiation, and migration of immune cells, and its expression was positively correlated with immune infiltrates, including CD4+ T cells, B cells, CD8+ T cells, neutrophils, macrophages, dendritic cells, and natural killer cells. Moreover, LPAR1 expression was positively correlated with those chemokine/chemokine receptors, indicating that LPAR1 may regulate the migration of immune cells. In summary, LPAR1 is a potential prognostic biomarker and plays an important part in immune infiltrates in prostate cancer.

Keywords: lysophosphatidic acid receptor 1, tumor-infiltrating immune cells, chemokines, migration, prostate cancer

OPEN ACCESS

Edited by:
George Kulik,
Wake Forest University, United States

Reviewed by:
Sanja Štifter,
University of Rijeka, Croatia
Mohammed Imran Khan,
University of Western Ontario, Canada

****Correspondence:***
Kun Yang
yangkunkun@fmmu.edu.cn

† These authors have contributed equally to this work

Specialty section:
This article was submitted to Genitourinary Oncology, a section of the journal Frontiers in Oncology

Received: *06 December 2019*
Accepted: *29 April 2020*
Published: *10 June 2020*

Citation:
Shi J, Jiang D, Yang S, Zhang X, Wang J, Liu Y, Sun Y, Lu Y and Yang K (2020) LPAR1, Correlated With Immune Infiltrates, Is a Potential Prognostic Biomarker in Prostate Cancer. Front. Oncol. 10:846. doi: 10.3389/fonc.2020.00846

INTRODUCTION

Prostate cancer is a common malignancy in men worldwide (1). It is also the second leading cause of death related to cancer around the western countries. Although several drugs for patients who were suffering from castration-resistant prostate cancer have been approved (2, 3), such as enzalutamide and abiraterone, there is still an urgent need for treating patients who have no response to androgen depravation therapy. The tumor microenvironment (TME) has been reported to be associated with prostate cancer progression (4–6). Immunotherapy, a promising strategy, showed antitumor effects in prostate cancer (7, 8). Recent studies have found that the tumor-infiltrating immune cells affect the prognosis of a patient and the antitumor efficacy of immunotherapy (9–12). However, the molecular immune-related mechanisms in prostate cancer remain ambiguous. Therefore, the

identification of novel therapeutic biomarkers associated with immune infiltrates in prostate cancer is urgently needed.

Lysophosphatidic acid receptor 1 (LPAR1) is one of the G protein-coupled receptors and binds with lysophosphatidic acid (LPA) (13). It is involved in diverse biological functions, including chemotaxis (14), proliferation (15), cell differentiation (16), platelet aggregation (17), and tumor progression (13). A set of papers indicated that LPAR1 is a prognostic biomarker in various cancers and takes an important part in the development of prostate cancer (18–20). However, the LPAR1-correlated functions and mechanisms in tumor immunology and tumor progression remain to be explored.

The rapid development of high-throughput sequencing makes it possible to explore the mechanisms in diseases (21). The Cancer Genome Atlas (TCGA) is a landmark project that contains 32 human cancers through genome sequencing, making an effort to understand the molecular basis of cancer. It has been made available in order to figure out the function of LPAR1 in prostate cancer at a large scale.

Integrative analysis and several visualization methods were used in this present study to explore the mechanism of LPAR1 in prostate cancer. We investigated the LPAR1 expression levels and analyzed the correlation of LPAR1 and the prognosis of patients. Gene Ontology (GO) analysis, Gene Set Enrichment Analysis (GSEA), and several methods were also utilized to explore the potential function of LPAR1 in tumor progression and immune microenvironment. The findings suggested the potential mechanisms of LPAR1, giving us new insights into the important role of LPAR1 in prostate cancer.

MATERIALS AND METHODS

Data Source and Processing

The prostate adenocarcinoma (PRAD) clinical and molecular data (including mRNA expression and mutations) was extracted from the TCGA Data Portal (https://tcga-data.nci.nih.gov/tcga/) through the TCGAbiolinks (22) R package. In terms of the gene expression profile, we downloaded two types of data including raw counts data and transcripts per kilobase of per million mapped (TPM) data, one of the normalized gene expression estimations. We got the mRNA expression information of 52 normal patients and 499 tumor patients and the clinical information of 499 patients. In addition, the GSE6956 dataset was extracted from GEO database, including 69 tumor patients and 18 normal patients with prostate cancer.

Oncomine Database Analysis

The Oncomine microarray database was used for analysis (https://www.oncomine.org/). We screened the mRNA levels of LPAR1 in various types of cancers. *P*-value <0.05 and fold change >2 were restricted as the thresholds.

GO Analysis and GSEA

We separated all patients into two groups based on the median value of LPAR1 mRNA expression data. The log2 fold change and *p*-value calculated by DEseq2 (23) package were used as ranking metric. The GO terms (C5 collection in GSEA) were divided into three sub-collections: biological process (BP), molecular function, and cellular component. It is one of the most frequently used databases for pathway annotation. The two enrichment analyses were based on the BP sub-collection, which contains 7,350 genes. For the GO analysis, we used the Cytoscape (24) software and the ClueGO (25) app to analyze the function of differentially expressed genes (DEGs) with p-value < 0.01 and GO term network connectivity score equal to 0.6. As for GSEA, there is no need for the screening of differentially expressed genes. Hence, those genes that have a limit change in the transcriptional level but are functionally important can be retained. Compared to conventional GO and Kyoto Encyclopedia of Genes and Genomes enrichment analyses, GSEA retains more information. For GSEA, we made use of the clusterprofiler (26) R package in R studio, and the C5 collection was the gene set used in the present analysis.

TIMER Database Analysis

The Tumor Immune Estimation Resource (TIMER) (27) is an integrative web server for evaluating tumor-infiltrating immune cells across diverse cancer types (https://cistrome.shinyapps.io/timer/). The TIMER includes more than 10,000 samples across multiple cancer types of the TCGA. It applies a partial deconvolution linear least square regression method to calculate the abundance of immune infiltrates. We evaluated the correlation between LPAR1 expression and immune infiltrates in tumors, including CD8+ T cells, CD4+ T cells, dendritic cells, neutrophils, B cells, and macrophages.

Immune Infiltrates in Tumor Tissues

The Microenvironment Cell Populations counter (MCPcounter) method (28) and single-sample GSEA (ssGSEA) method (29) were used to calculate the level of tumor-infiltrating immune cells based on PRAD mRNA TPM data. The ssGSEA marker genes were extracted from the paper of Bindea et al. (30) and it included 24 types of immune cells. Figures were generated with a pheatmap R package.

Protein–Protein Interaction Analysis

The LPAR1 and chemokines/chemokine receptors were searched in a protein–protein interaction (PPI) network *via* the STRING database (https://string-db.org/). The minimum required interaction cutoff is 0.4. The edges between nodes represent protein–protein associations. The edge with blue color means that the two nodes have known interactions from curated databases. The yellow color means textmining. The black color means that the two nodes have a co-expression. The purple color means that the interactions of the two nodes were experimentally determined.

Statistical Analysis

The statistical analysis and the graphical work in this study were mainly conducted by R programming language with several packages, such as DEseq2 package, survival package, and TCGAbiolinks package. The survival curve based on log-rank test was depicted with Kaplan–Meier method. Univariate survival analysis was based on Cox proportional hazards model. Hazard

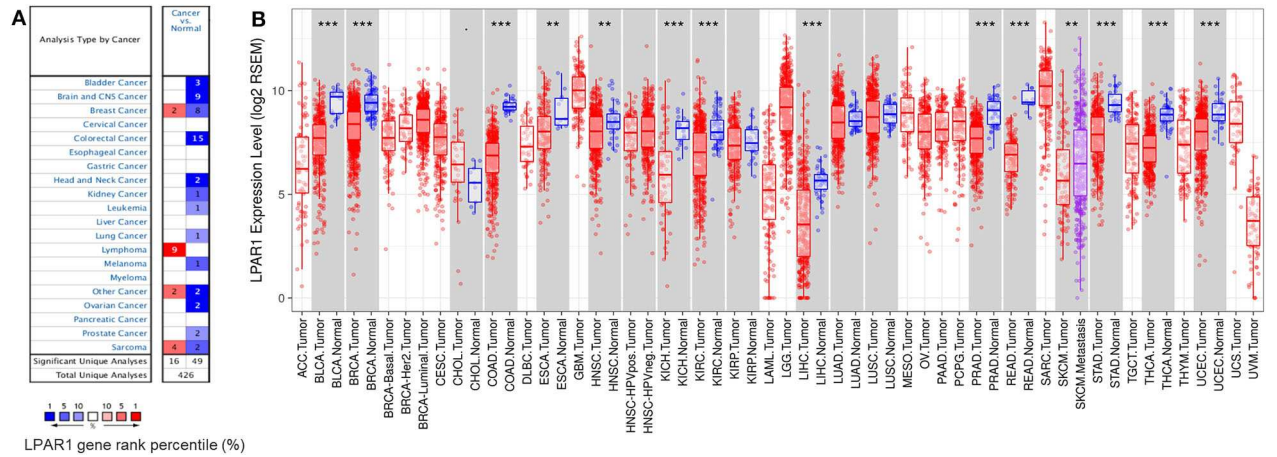

FIGURE 1 | Lysophosphatidic acid receptor 1 (LPAR1) expression levels in different kinds of human cancers. **(A)** LPAR1 profile in different types of human cancers compared with normal tissues based on the Oncomine database. **(B)** The LPAR1 expression levels between tumor and normal tissue among all The Cancer Genome Atlas datasets were analyzed by the Tumor Immune Estimation Resource (**$P < 0.01$, ***$P < 0.001$).

ratio (HR) and log-rank test were used for comparing the overall survival between patients in different groups. Throughout the study, the threshold of statistical significance was $P < 0.05$.

RESULTS

LPAR1 mRNA Expression Was Downregulated in Diverse Cancers

To compare the mRNA expression levels of LPAR1 in normal and tumor tissues, we used the Oncomine database to determine the LPAR1 expression among multiple cancer types. This analysis indicated that LPAR1 was highly expressed in lymphoma and lowly expressed in prostate cancer, bladder cancer, brain and central nervous system cancer, head and neck cancer, colorectal cancer, kidney cancer, lung cancer, leukemia, melanoma, and ovarian cancer (**Figure 1A**). To further validate the LPAR1 expression in different cancers, we explored the differential gene expression between tumor and normal tissue among all TCGA datasets *via* TIMER database and show it in **Figure 1B**. LPAR1 was significantly lowly expressed in PRAD, breast invasive carcinoma (BRCA), bladder urothelial carcinoma (BLCA), colon adenocarcinoma (COAD), rectum adenocarcinoma (READ), head and neck cancer (HNSC), esophageal carcinoma (ESCA), kidney renal clear cell carcinoma (KIRC), kidney chromophobe (KICH), liver hepatocellular carcinoma (LIHC), thyroid carcinoma (THCA), stomach adenocarcinoma (STAD), and uterine corpus endometrial carcinoma (UCEC). In brief, LPAR1 was downregulated in colorectal cancer, breast cancer, kidney cancer, head and neck cancer, and prostate cancer based on the Oncomine database and TCGA.

Association of LPAR1 Expression and Immune Cell Populations

The association between LPAR1 and tumor-infiltrating immune cells in multiple cancer types was based on the TIMER database, including breast cancer, head and neck cancer, colorectal cancer, kidney cancer, and prostate cancer (**Figure S1**). We found that LPAR1 impacted tumor-infiltrating immune cells in prostate cancer (**Figure 2A**). The LPAR1 expression was negatively correlated with the purity of tumor ($r = -0.475$, $P = 7.54e{-}25$), Furthermore, the LPAR1 expression was positively correlated with the abundance of several immune cell types, including CD4+ T cells ($r = 0.311$, $P = 1.21e{-}10$), CD8+ T cells ($r = 0.334$, $P = 2.84e{-}12$), neutrophils ($r = 0.362$, $P = 2.68e{-}14$), macrophages ($r = 0.435$, $P = 1.19e{-}20$), and dendritic cells ($r = 0.41$, $P = 2.95e{-}18$) in PRAD. To validate these findings, we used the MCPcounter method. We evaluated the association between LPAR1 and tumor-infiltrating immune cells from the mRNA expression data. A strong positive correlation between LPAR1 and myeloid dendritic cells, T cells, B lineage, monocytic lineage, cytotoxic lymphocytes, and natural killer (NK) cells was seen (**Figure 2B**). In addition, the ssGSEA analysis (**Figure 2C**) revealed that LPAR1 was positively correlated with the infiltration of γδ T cells, effective memory T cells, central memory T cells, type 1 T helper cells, CD8+ T cells, dendritic cells (DCs), M1 macrophages, and B cells and negatively correlated with CD56 bright NK cells and Treg cells. In addition, LPAR1 was also positively correlated with tumor-infiltrating immune cells based on the GSE6956 dataset (**Figure S2**). Hence, LPAR1 may play critical roles in regulating antitumor immunity.

LPAR1 Expression Level Was Associated With the Prognosis of Patients With Prostate Cancer

The downregulation of LPAR1 was validated by using the TCGA-PRAD dataset (**Figure 2D**). To gain deeper insights into the tumor mechanisms in human prostate cancer, we performed analyses to reveal the relevance between LPAR1 and the prognosis of patients with prostate cancer. Interestingly, as analyzed by Kaplan–Meier plot and log-rank tests, LPAR1 was

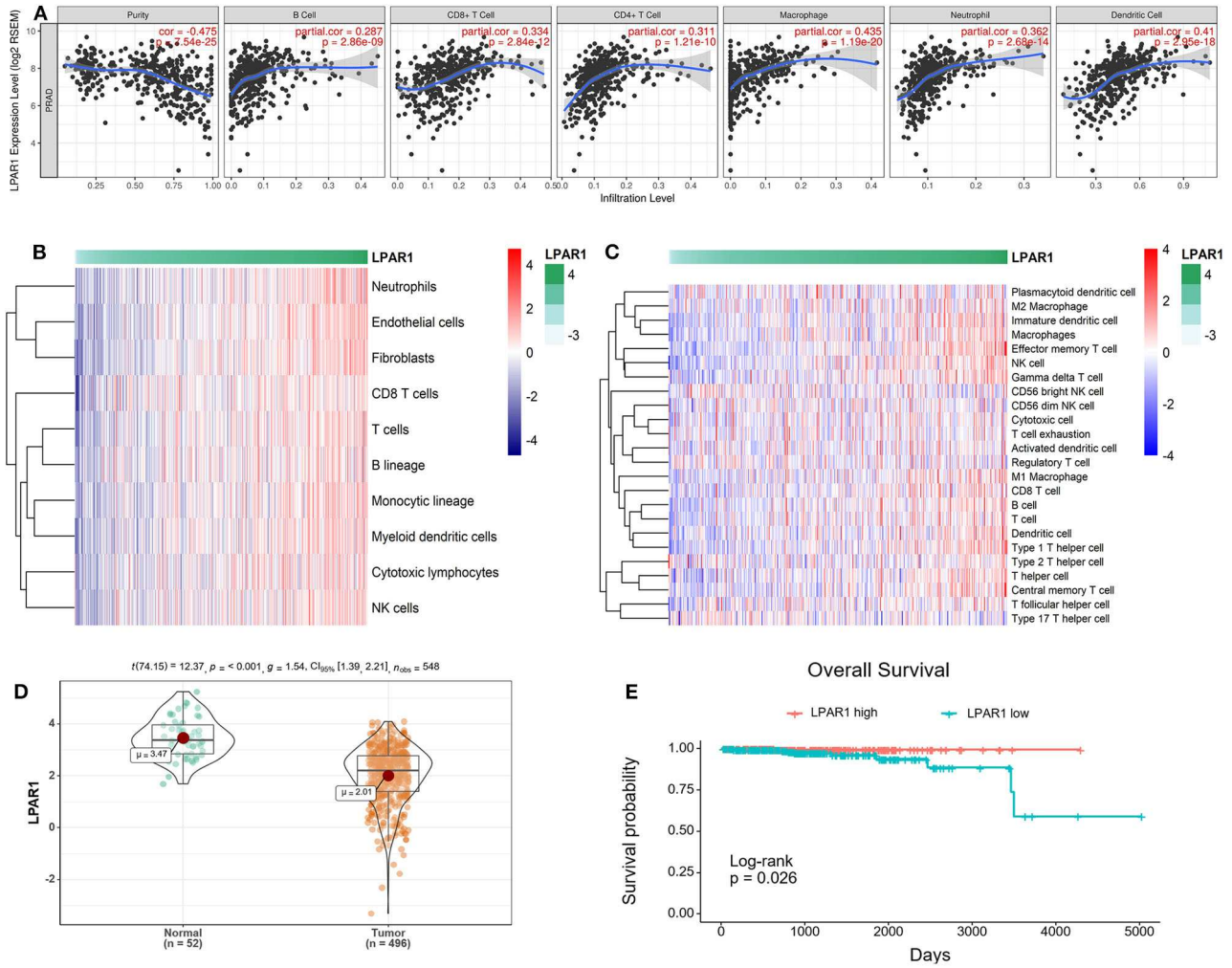

FIGURE 2 | Correlation of lysophosphatidic acid receptor 1 (LPAR1) expression and tumor-infiltrating immune cells and prognosis in prostate adenocarcinoma (PRAD). **(A)** LPAR1 expression was significantly negatively related to tumor purity and had a positive correlation with the abundance of several immune cell types in PRAD, including CD8+ T cells, CD4+ T cells, macrophages, B cells, neutrophils, and dendritic cells. **(B)** Heatmap of the correlation between LPAR1 and T cells, B lineage, monocytic lineage, myeloid dendritic cells, cytotoxic lymphocytes, and natural killer cells as performed by the MCPcounter R package. Higher LPAR1 expression was associated with higher abundance of immune infiltrates in PRAD. **(C)** Heatmap of the correlation between LPAR1 and several immune cells based on ssGSEA R package. **(D)** Violin plot comparing the LPAR1 expression for patients with highly expressed LPAR1 *vs*. those with lowly expressed LPAR1 in prostate cancer with p-value < 0.001. **(E)** Kaplan–Meier plot comparing the overall survival for patients with highly expressed LPAR1 *vs*. those with lowly expressed LPAR1 in prostate cancer using log-rank test with p-value < 0.05.

correlated with the patients' clinical outcome (**Figure 2E**). In addition, we did a univariate cox proportional hazards regression analysis and found that a high LPAR1 expression was correlated with a favorable overall survival (OS) (HR = 0.51, $P = 0.00462$) in prostate cancer, suggesting that LPAR1 expression can impact the prognosis of patients with prostate cancer.

LPAR1 Was Related to Several Immune-Related Pathways in Prostate Cancer

Patients with high LPAR1 expression had a prolonged OS time, suggesting that LPAR1 may be involved in the initiation and the progression of prostate cancer. Then, we analyzed the RNA sequencing data downloaded from TCGA and compared the tumor samples between samples with high LPAR1 expression and samples with low LPAR1 expression. The volcano plot was shown in **Figure 3A** and DEGs were shown in **Table S1**, including 595 upregulated genes and 269 downregulated genes. We used upregulated genes in high LPAR1 patients for GO analysis. The GO analysis showed that the DEGs were enriched in a set of pathways, including passive transmembrane transporter activity, cell motility, metal ion transport, cell differentiation, tube development, G protein-coupled receptor signaling pathway, and chemotaxis (**Figure 3B**). In addition, the downregulated genes were enriched in pathways, including the

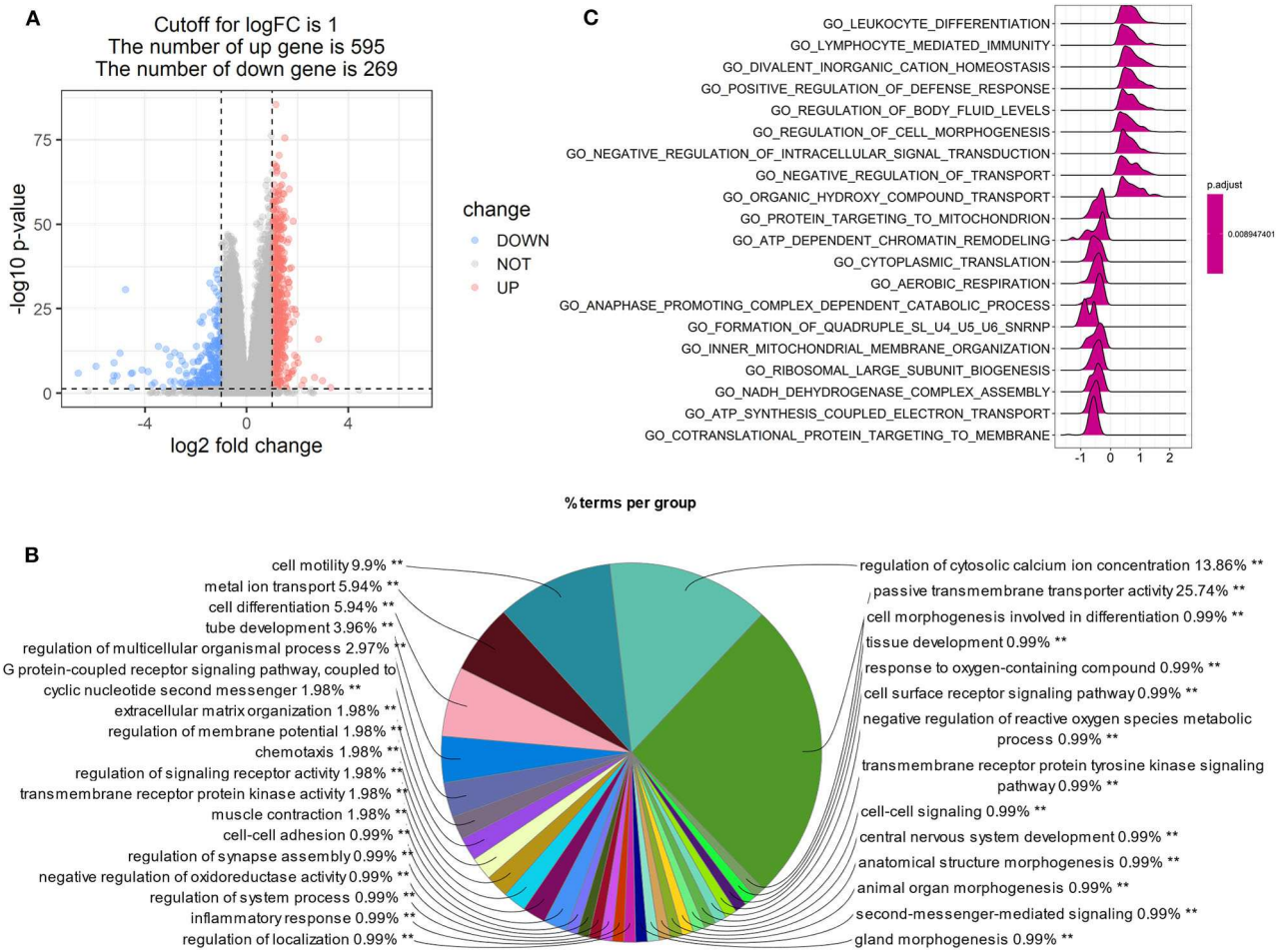

FIGURE 3 | Gene Ontology (GO) and Gene Set Enrichment Analysis (GSEA) of tumor samples with high expression of lysophosphatidic acid receptor 1 (LPAR1) *vs.* those with low expression of LPAR1. The analysis was based on the biological process category in GO. **(A)** Volcano plot showing the differentially expressed genes (DEGs) comparing tumor samples between samples with high LPAR1 expression and samples with low LPAR1 expression. **(B)** The pie plot only showed the pathways with p-value < 0.01 and the GO term network connectivity score is 0.6. The upregulated DEGs were enriched in a set of pathways, including passive transmembrane transporter activity, cell motility, metal ion transport, cell differentiation, tube development, and G protein-coupled receptor signaling pathway. **(C)** The plot shows the top 20 categories with p-value < 0.05 *via* GSEA, including leukocyte differentiation, lymphocyte-mediated immunity, divalent inorganic cation homeostasis, positive regulation of defense response, regulation of body fluid levels, regulation of cell morphogenesis, and so on.

detection of chemical stimulus, cell proliferation in the external granule layer, and telencephalon cell migration (**Figure S3**). The GSEA indicated the enrichment in many categories, such as leukocyte differentiation, lymphocyte-mediated immunity, divalent inorganic cation homeostasis, positive regulation of the defense response pathway, and regulation of cell morphogenesis (**Figure 3C**). We used the whole gene set after sorting for GSEA. The results of GSEA showed that LPAR1 participated in various functions and pathways, including antitumor immune responses.

Furthermore, we found that LPAR1 can take part in several immune-related pathways and influence many processes of immune cells. The results indicated that LPAR1 was associated with the activation (**Figure 4A**) of T cell, NK cell, B cell, DC, and macrophage, the proliferation (**Figure 4B**) of T cell, NK cell, and B cell, the differentiation (**Figure 4C**) of T cell, NK cell, B cell, DC, and macrophage, and the migration (**Figure 4D**) of T cell, DC, neutrophil, and macrophage.

Linear Correlation and PPI Network Between LPAR1, Chemokines, and Chemokine Receptors

To further clarify the association between LPAR1 and immune cell migration, we integrated chemokines and chemokine receptors in **Figures 5A–I**. As the figures show, LPAR1 expression was positively correlated with lymphocyte-associated chemokines and chemokine receptors, including CX3CL1, CX3CR1, CCL4, CCR5, CCL22, CCR4, CCL23, CCR1, XCL1, XCR1, CXCL9, CXCR3, CXCL1, CXCR2, CXCL16, CXCR6, CCL5, and CCR1. The correlation curves with two different y axes were performed by ggplot2 R package. Those chemokine and chemokine receptors that seemed to be upregulated with LPAR1 expression level increased. Hence, high LPAR1 expression may contribute to the migration of immune cells to the tumor tissues.

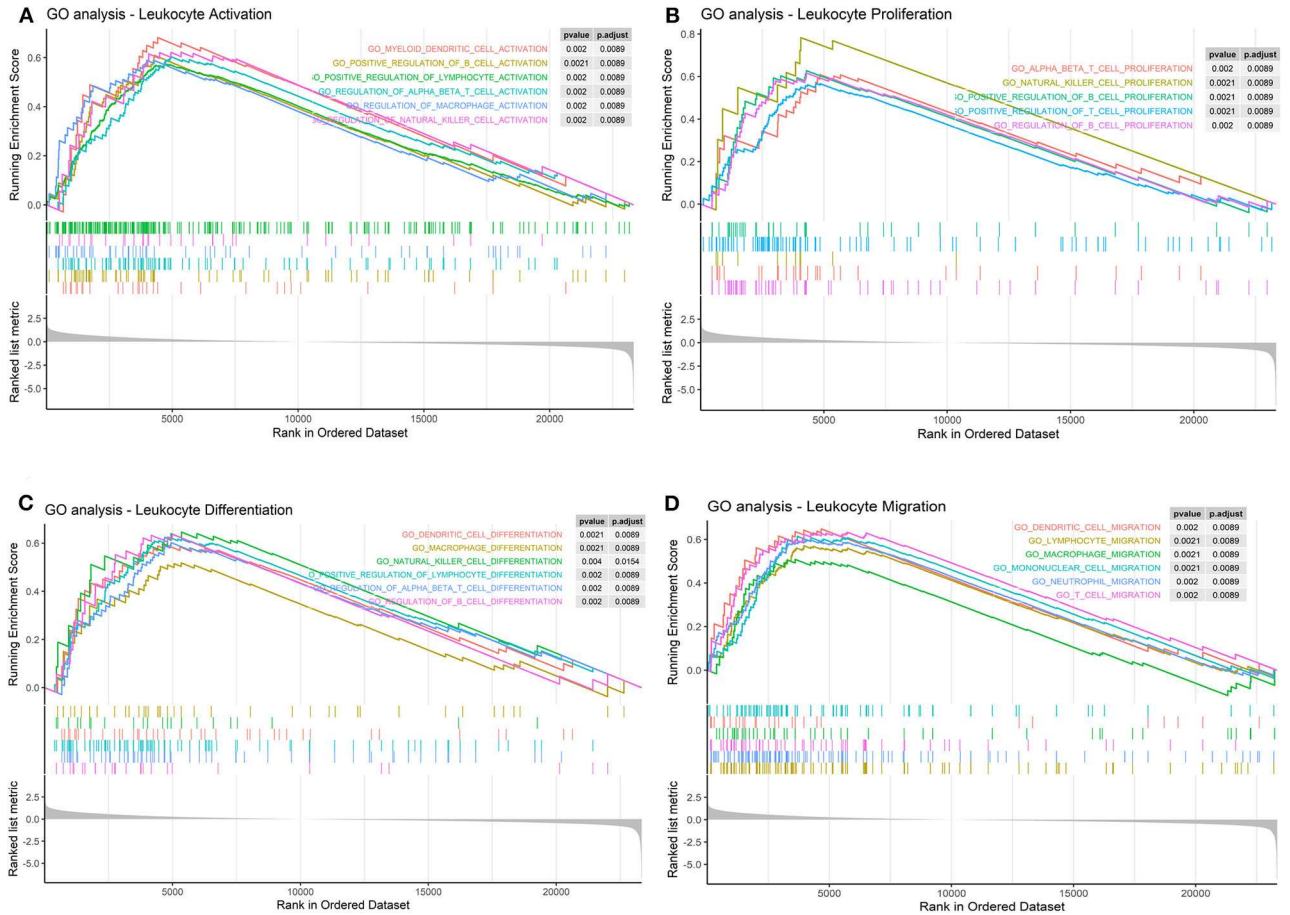

FIGURE 4 | Immune cell-related pathways based on the Gene Set Enrichment Analysis (GSEA). **(A)** Lysophosphatidic acid receptor 1 (LPAR1) was associated with the activation of T cell, natural killer (NK) cell, B cell, dendritic cell (DC), and macrophage in Gene Ontology (GO) terms. **(B)** LPAR1 was associated with the proliferation of T cell, NK cell, and B cell in GO terms. **(C)** LPAR1 was associated with the differentiation of T cell, NK cell, B cell, DC, and macrophage in GO terms. **(D)** LPAR1 was associated with the migration of T cell, DC, neutrophil, and macrophage in GO terms.

To better understand the interactions among LPAR1 and chemokines or chemokine receptors, the STRING database was utilized to generate and visualize a PPI network. The PPI network showed that LPAR1 had known or predicted interactions with the various chemokines studied above (**Figure 6A**), including 10 nodes and 38 edges. The LPAR1/CCL5, LPAR1/CCL4, and LPAR1/XCL1 interactions were experimentally determined. The interactions of CCL4, CCL5, CXCL1, CXCL9, CXCL16, CX3CL1, and XCL1 with LPAR1 were all extracted from the curated databases. The PPI network among LPAR1 and chemokine receptors (**Figure 6B**) showed that the chemokine receptors, including CCR1, CCR4, CCR5, CXCR2, CXCR3, CXCR6, CX3CR1, and XCR1, had known interactions with LPAR1.

DISCUSSION

The present study suggests, based on bioinformatics analysis, the importance of LPAR1 in prostate cancer. LPAR1 was lowly expressed in prostate cancer and was significantly related to patient survival. In addition, LPAR1 may be involved in the biological process when immune cells move into the tumor tissues and improve the TME of patients, which impact the development of prostate cancer and the prognosis of patients. Hence, LPAR1 is a potential immune-related biomarker in prostate cancer. Our findings offer deeper insights into the mechanisms of LPAR1 in the development of prostate cancer.

In this study, based on independent datasets in the Oncomine database and TCGA datasets, we examined the LPAR1 expression level in various types of cancer. The differential expression of LPAR1 was seen in a set of cancers between tumor and normal tissues. In the Oncomine database, the results showed that LPAR1 was highly expressed in lymphoma while lowly expressed in prostate, bladder, brain, colon, head and neck, kidney, leukemia, lung, melanoma, and ovarian cancers. The TCGA datasets showed that LPAR1 expression was significantly lowly expressed in PRAD, BLCA, BRCA, COAD, READ, ESCA, HNSC, KICH, KIRC, LIHC, STAD, THCA, and UCEC compared with normal tissues.

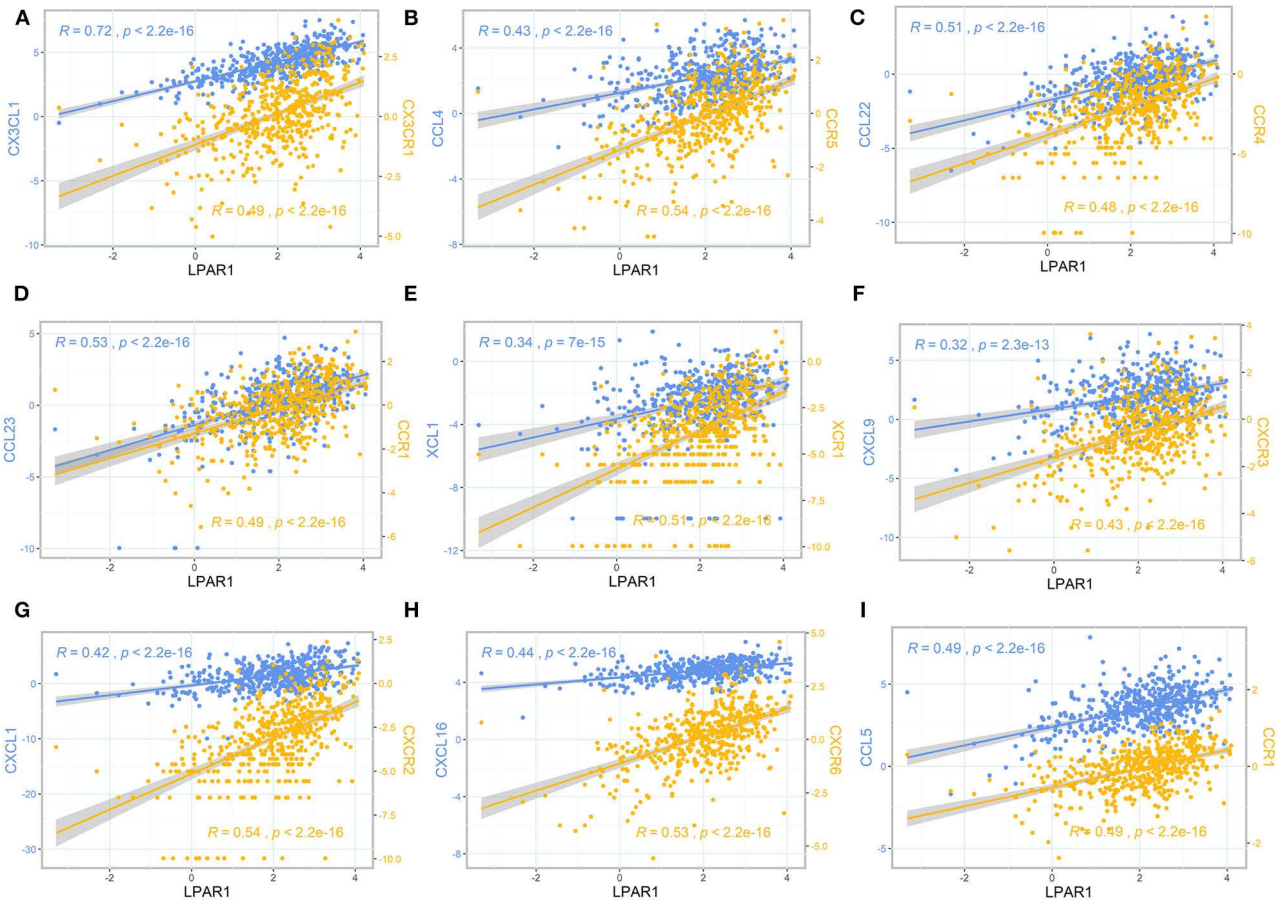

FIGURE 5 | The scatter plot and correlation curve of lysophosphatidic acid receptor 1 (LPAR1), chemokines, and chemokine receptors. **(A–I)** LPAR1 was positively associated with CX3CL1, CX3CR1, CCL4, CCR5, CCL22, CCR4, CCL23, CCR1, XCL1, XCR1, CXCL9, CXCR3, CXCL1, CXCR2, CXCL16, CXCR6, CCL5, and CCR1. CCL, CC chemokine ligand; CCR, CC chemokine receptor; CXCR, CXC chemokine receptor; CXCL, CXC chemokine ligand; XCL, C chemokine ligand; XCR, C chemokine receptor; CX3CL, CX3C chemokine ligand; CX3CR, CX3C chemokine receptor.

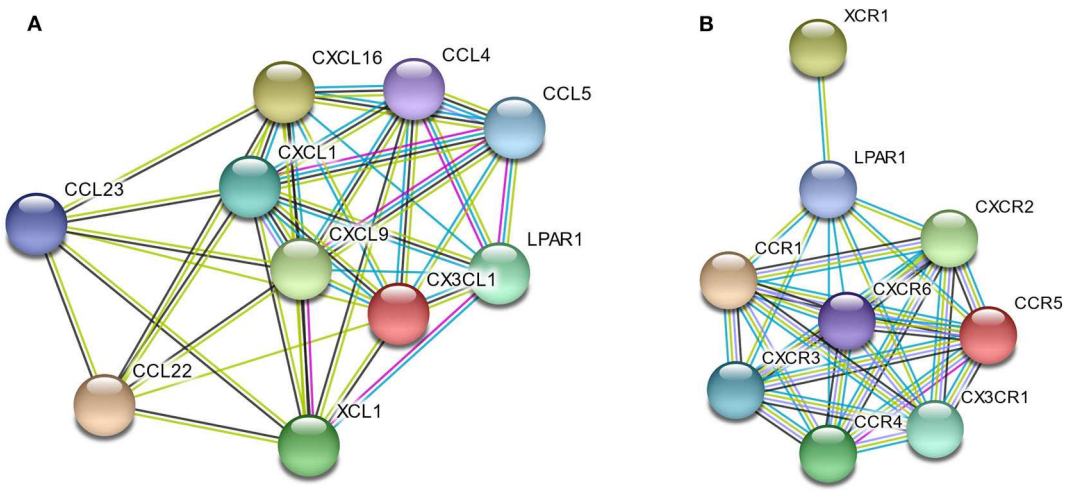

FIGURE 6 | Protein–protein interactions (PPI) network based on lysophosphatidic acid receptor 1 (LPAR1) and chemokines/chemokine receptors with a minimum required interaction score > 0.40. **(A)** PPI network among LPAR1 and nine chemokines. **(B)** PPI network among LPAR1 and eight chemokine receptors.

The TME has a great impact on the development of cancers (4–6, 31). Studies have shown that the TME, especially the immune microenvironment in tumor, can affect the prognosis of patients (32, 33). However, few reports elaborated the function of LPAR1 in the TME. Through the TIMER database, we found that LPAR1 impacted tumor-infiltrating immune cells in prostate cancer. The LPAR1 expression was significantly negatively related to tumor purity. It may contribute to the infiltration of various immune cells in prostate cancer, including B cells, dendritic cells, NK cells, CD8+ T cells, macrophages, and neutrophils. The MCPcounter and ssGSEA methods revealed that LPAR1 was positively correlated with the infiltration of various types of T cells (γδ T cells, effective memory T Cell, Th1 cells, central memory T cells, and CD8+ T cells), DCs, M1 macrophages, and B cells and negatively correlated with CD56 bright NK cells and Treg cells. The increase of NK cells and CD8+ T cells can help enhance the anti-tumor immunity by secreting various cytokines and releasing perforin and granzyme (34). The infiltration of DCs, the most powerful antigen-presenting cell, can help present antigenic peptides of tumor-associated or tumor-specific antigens to T cells (35). It has been reported that tumor-associated macrophages (36) have a double effect in tumor development. M1 macrophages secrete pro-inflammatory and chemokines, which participate in antigen presentation and immune surveillance, while M2 macrophages secrete inhibitory cytokines. With the LPAR1 upregulated, the M1 macrophages infiltrate into tumor sites and exert an anti-tumor function. The increasing infiltration of B cells helps to eliminate tumor by participating in antibody-dependent cell-mediated cytotoxicity. The CD56 bright NK cells, which are less cytotoxic compared with CD56 dim NK cells, decreased with the upregulation of LPAR1. LPAR1 also downregulates the infiltration of Treg cells, which protect the human body from tumor suppression. Consequently, LPAR1 may play a critical role in regulating TME in prostate cancer by participating in cellular and humoral immunity and motivating the anti-tumor function. Besides that, an analysis of TCGA revealed that the decreased LPAR1 expression was correlated with a poor prognosis in PRAD. A high LPAR1 expression has a correlation with a low HR for poor prognosis, suggesting that LPAR1 is a critical biomarker in prostate cancer.

Concerning biological function, LPAR1 participated in many signaling pathways in tumor cells through GO analysis, for example, passive transmembrane transporter activity, cell motility, metal ion transport, cell differentiation, tube development, G protein-coupled receptor signaling pathway, and chemotaxis. The GSEA results showed that the LPAR1 function was enriched in GO_Leukocyte_Differentiation and GO_Lymphocyte_Mediated_Immunity in prostate cancer. Furthermore, the GSEA on LPAR1 immune-related function indicates that LPAR1 influenced the activation, proliferation, differentiation, and migration of immune cells. It hints that LPAR1 improves the immune response of prostate cancer through various pathways.

LPAR1 has been proven to be associated with chemotaxis, which was also found in the present study. Studies had reported that LPAR1 played a critical role in the LPA-induced chemotactic migration of olfactory ensheathing cells (37). LPAR1-deficient rats showed decreased pulmonary influx of macrophages and neutrophils (38). A previous study showed that LPA promoted microglial migration and induced the secretion of chemokines and pro-inflammatory cytokines, as well as the expression of M1 markers (39, 40). LPA1 and LPA3 receptors play an important role in the synthesis of CXCL1 and its receptor CXCR2 and in the regulation of leukocyte recruitment (14). LPA can induce the chemotaxis of Th1 and Th2 cells (41), and it can promote T cell recruitment through CXCL13 synthesis (42). The chemotaxis of NK cells was also reported to be associated with LPA and LPA receptor (43). We integrated chemokines and chemokine receptors and analyzed the association between LPAR1 and immune cell migration to explore the potential immune-related mechanisms of LPAR1 in prostate cancer. Chemokines control the positioning and the migratory patterns of immune cells. Chemokines are critical for immune cell movement and homeostasis (44). The CX3CL1/CX3CR1 interaction functions in the recruitment of T cell, NK cell, and monocyte. The CX3CL1/CX3CR1 interaction is also associated with the activation of cytotoxic T lymphocytes and NK cell. The CCL4/CCR5 interaction promotes the recruitment of T cell, DC, monocyte, and NK cell, as well as T cell–DC interactions. The CCL22/CCR4 and XCL1/XCR1 interactions are associated with T cell and NK cell recruitment. CCL5/CCR1 takes part in macrophage and NK migration and T cell–DC interactions. The CCL23/CCR1 interaction is about monocyte, neutrophil, and T cell migration. CXCL9/CXCR3 promotes the recruitment of effector T cell. CXCL1/CXCR2 and CXCL16/CXCR6 are associated with neutrophil recruitment and natural killer T cell migration, respectively. In the present study, LPAR1 was not only positively correlated with those chemokine/chemokine receptors but also had known or predicted interactions with them based on the PPI network, indicating that LPAR1 may increase the immune infiltrates of tumor through regulating the migration of immune cells in prostate cancer.

As far as we know, this is the first study to elaborate the potential functions of LPAR1 and its association with tumor-infiltrating immune cells by using integrated bioinformatics analysis. However, this present study had limitations. Further molecular experiments are deserved to verify the mechanisms of LPAR1 and its effects on the clinical outcome in prostate cancer. Moreover, it is also important to integrate and elaborate the association between LPAR1 and chemokines/chemokine receptors, which can help us better understand the TME, especially the immune microenvironment in tumors.

DATA AVAILABILITY STATEMENT

All datasets were extracted from The Cancer Genome Atlas (https://tcga-data.nci.nih.gov/tcga/) and Oncomine (https://www.oncomine.org/) websites, so the ethical statement was already admitted and further evaluation of it was not necessary.

AUTHOR CONTRIBUTIONS

KY and JS conceived and designed the project. JS, DJ, SY, XZ, JW, YLi, YS, and YLu analyzed the data. JS wrote the manuscript with input from all the other authors.

FUNDING

This work was supported by the National Natural Science Foundation of China (No. 81772763).

SUPPLEMENTARY MATERIAL

The Supplementary Material for this article can be found online at: https://www.frontiersin.org/articles/10.3389/fonc.2020.00846/full#supplementary-material

REFERENCES

1. Siegel RL, Miller KD, Jemal A. Cancer statistics, 2019. *CA Cancer J Clin.* (2019) 69:7–34. doi: 10.3322/caac.21551
2. Hussain M, Fizazi K, Saad F, Rathenborg P, Shore N, Ferreira U, et al. Enzalutamide in men with nonmetastatic, castration-resistant prostate cancer. *N Eng J Med.* (2018) 378:2465–74. doi: 10.1056/NEJMoa1800536
3. James ND, Spears MR, Sydes MR. Abiraterone in metastatic prostate cancer. *N Eng J Med.* (2017) 377:1696–7. doi: 10.1056/NEJMc1711029
4. Casey SC, Amedei A, Aquilano K, Azmi AS, Benencia F, Bhakta D, et al. Cancer prevention and therapy through the modulation of the tumor microenvironment. *Semin Cancer Biol.* (2015) 35:S199–223. doi: 10.1016/j.semcancer.2015.02.007
5. Sfanos KS, Yegnasubramanian S, Nelson WG, De Marzo AM. The inflammatory microenvironment and microbiome in prostate cancer development. *Nat Rev Urol.* (2018) 15:11–24. doi: 10.1038/nrurol.2017.167
6. Pasero C, Gravis G, Guerin M, Granjeaud S, Thomassin-Piana J, Rocchi P, et al. Inherent and tumor-driven immune tolerance in the prostate microenvironment impairs natural killer cell antitumor activity. *Cancer Res.* (2016) 76:2153–65. doi: 10.1158/0008-5472.CAN-15-1965
7. Schepisi G, Cursano MC, Casadei C, Menna C, Altavilla A, Lolli C, et al. CAR-T cell therapy: a potential new strategy against prostate cancer. *J Immunother Cancer.* (2019) 7:258. doi: 10.1186/s40425-019-0741-7
8. Madan RA, Gulley JL. Prostate cancer: better VISTAs ahead? Potential and pitfalls of immunotherapy. *Nat Rev Urol.* (2017) 14:455–6. doi: 10.1038/nrurol.2017.75
9. Zhao SG, Lehrer J, Chang SL, Das R, Erho N, Liu Y, et al. The immune landscape of prostate cancer and nomination of PD-L2 as a potential therapeutic target. *J Natl Cancer Inst.* (2019) 111:301–10. doi: 10.1093/jnci/djy141
10. Taverna G, Giusti G, Seveso M, Hurle R, Colombo P, Stifter S, et al. Mast cells as a potential prognostic marker in prostate cancer. *Dis Markers.* (2013) 35:711–20. doi: 10.1155/2013/478303
11. Zhang Q, Helfand BT, Carneiro BA, Qin W, Yang XJ, Lee C, et al. Efficacy against human prostate cancer by prostate-specific membrane antigen-specific, transforming growth factor-beta insensitive genetically targeted CD8(+) T-cells derived from patients with metastatic castrate-resistant disease. *Eur Urol.* (2018) 73:648–52. doi: 10.1016/j.eururo.2017.12.008
12. Erlandsson A, Carlsson J, Lundholm M, Falt A, Andersson SO, Andren O, et al. M2 macrophages and regulatory T cells in lethal prostate cancer. *Prostate.* (2019) 79:363–9. doi: 10.1002/pros.23742
13. Choi JW, Herr DR, Noguchi K, Yung YC, Lee CW, Mutoh T, et al. LPA receptors: subtypes and biological actions. *Ann Rev Pharmacol Toxicol.* (2010) 50:157–86. doi: 10.1146/annurev.pharmtox.010909.105753
14. Zhao C, Sardella A, Chun J, Poubelle PE, Fernandes MJ, Bourgoin SG. TNF-alpha promotes LPA1- and LPA3-mediated recruitment of leukocytes *in vivo* through CXCR2 ligand chemokines. *J lipid Res.* (2011) 52:1307–18. doi: 10.1194/jlr.M008045
15. Ma X, Feng J, Lu M, Tang W, Han J, Luo X, et al. microRNA-501-5p promotes cell proliferation and migration in gastric cancer by downregulating LPAR1. *J Cell Biochem.* (2019) 121:1911–22. doi: 10.1002/jcb.29426
16. Sumitomo A, Siriwach R, Thumkeo D, Ito K, Nakagawa R, Tanaka N, et al. LPA Induces keratinocyte differentiation and promotes skin barrier function through the LPAR1/LPAR5-RHO-ROCK-SRF axis. *J Invest Dermatol.* (2019) 139:1010–22. doi: 10.1016/j.jid.2018.10.034
17. Guerrero JA, Rivera J, Quiroga T, Martinez-Perez A, Anton AI, Martinez C, et al. Novel loci involved in platelet function and platelet count identified by a genome-wide study performed in children. *Haematologica.* (2011) 96:1335–43. doi: 10.3324/haematol.2011.042077
18. He Z, Tang F, Lu Z, Huang Y, Lei H, Li Z, et al. Analysis of differentially expressed genes, clinical value and biological pathways in prostate cancer. *Am J Transl Res.* (2018) 10:1444–56. doi: 10.3892/mmr.2018.8711
19. Foj L, Filella X. Identification of potential miRNAs biomarkers for high-grade prostate cancer by integrated bioinformatics analysis. *Pathol Oncol Res.* (2019) 25:1445–56. doi: 10.1007/s12253-018-0508-3
20. Harma V, Knuuttila M, Virtanen J, Mirtti T, Kohonen P, Kovanen P, et al. Lysophosphatidic acid and sphingosine-1-phosphate promote morphogenesis and block invasion of prostate cancer cells in three-dimensional organotypic models. *Oncogene.* (2012) 31:2075–89. doi: 10.1038/onc.2011.396
21. Zhou C, Zhu C, Liu Q. Toward *in silico* Identification of tumor neoantigens in immunotherapy. *Trends Mol Med.* (2019) 25:980–92. doi: 10.1016/j.molmed.2019.08.001
22. Colaprico A, Silva TC, Olsen C, Garofano L, Cava C, Garolini D, et al. TCGAbiolinks: an R/Bioconductor package for integrative analysis of TCGA data. *Nucleic Acids Res.* (2016) 44:e71. doi: 10.1093/nar/gkv1507
23. Love MI, Huber W, Anders S. Moderated estimation of fold change and dispersion for RNA-seq data with DESeq2. *Genome Biol.* (2014) 15:550. doi: 10.1186/s13059-014-0550-8
24. Shannon P, Markiel A, Ozier O, Baliga NS, Wang JT, Ramage D, et al. Cytoscape: a software environment for integrated models of biomolecular interaction networks. *Genome Res.* (2003) 13:2498–504. doi: 10.1101/gr.1239303
25. Bindea G, Mlecnik B, Hackl H, Charoentong P, Tosolini M, Kirilovsky A, et al. ClueGO: a cytoscape plug-in to decipher functionally grouped gene ontology and pathway annotation networks. *Bioinformatics.* (2009) 25:1091–3. doi: 10.1093/bioinformatics/btp101
26. Yu G, Wang LG, Han Y, He QY. clusterProfiler: an R package for comparing biological themes among gene clusters. *J Integr Biol.* (2012) 16:284–7. doi: 10.1089/omi.2011.0118
27. Li T, Fan J, Wang B, Traugh N, Chen Q, Liu JS, et al. TIMER: a web server for comprehensive analysis of tumor-infiltrating immune cells. *Cancer Res.* (2017) 77:e108–10. doi: 10.1158/0008-5472.CAN-17-0307
28. Becht E, Giraldo NA, Lacroix L, Buttard B, Elarouci N, Petitprez F, et al. Estimating the population abundance of tissue-infiltrating immune and stromal cell populations using gene expression. *Genome Biol.* (2016) 17:218. doi: 10.1186/s13059-016-1070-5
29. Finotello F, Trajanoski Z. Quantifying tumor-infiltrating immune cells from transcriptomics data. *Cancer immunol Immunother.* (2018) 67:1031–40. doi: 10.1007/s00262-018-2150-z
30. Bindea G, Mlecnik B, Tosolini M, Kirilovsky A, Waldner M, Obenauf AC, et al. Spatiotemporal dynamics of intratumoral immune cells reveal the immune landscape in human cancer. *Immunity.* (2013) 39:782–95. doi: 10.1016/j.immuni.2013.10.003
31. Chiarugi P, Paoli P, Cirri P. Tumor microenvironment and metabolism in prostate cancer. *Semin Oncol.* (2014) 41:267–80. doi: 10.1053/j.seminoncol.2014.03.004
32. Mo RJ, Han ZD, Liang YK, Ye JH, Wu SL, Lin SX, et al. Expression of PD-L1 in tumor-associated nerves correlates with reduced CD8(+) tumor-associated lymphocytes and poor prognosis in prostate cancer. *Int J Cancer.* (2019) 144:3099–110. doi: 10.1002/ijc.32061
33. Anker JF, Naseem AF, Mok H, Schaeffer AJ, Abdulkadir SA, Thumbikat P. Multi-faceted immunomodulatory and tissue-tropic clinical bacterial isolate potentiates prostate cancer immunotherapy. *Nat Commun.* (2018) 9:1591. doi: 10.1038/s41467-018-03900-x
34. Andre P, Denis C, Soulas C, Bourbon-Caillet C, Lopez J, Arnoux T, et al. Anti-NKG2A mAb is a checkpoint inhibitor that promotes anti-tumor immunity by unleashing both T and NK cells. *Cell.* (2018) 175:1731–43.e13. doi: 10.1016/j.cell.2018.10.014

35. Gardner A, Ruffell B. Dendritic cells and cancer immunity. *Trends Immunol.* (2016) 37:855–65. doi: 10.1016/j.it.2016.09.006
36. Liang P, Henning SM, Guan J, Grogan T, Elashoff D, Cohen P, et al. Effect of dietary omega-3 fatty acids on castrate-resistant prostate cancer and tumor-associated macrophages. *Prostate Cancer Prostatic Dis.* (2019) 23:127–35 doi: 10.1038/s41391-019-0168-8
37. Zhong W, Bian K, Hu Y, Ji Z, Xu X, Li J, et al. Lysophosphatidic acid guides the homing of transplanted olfactory ensheathing cells to the lesion site after spinal cord injury in rats. *Exp Cell Res.* (2019) 379:65–72. doi: 10.1016/j.yexcr.2019.03.023
38. Chen X, Walther FJ, Laghmani EH, Hoogeboom AM, Hogen-Esch AC, van Ark I, et al. Adult lysophosphatidic acid receptor 1-deficient rats with hyperoxia-induced neonatal chronic lung disease are protected against lipopolysaccharide-induced acute lung injury. *Front Physiol.* (2017) 8:155. doi: 10.3389/fphys.2017.00155
39. Plastira I, Bernhart E, Goeritzer M, DeVaney T, Reicher H, Hammer A, et al. Lysophosphatidic acid via LPA-receptor 5/protein kinase D-dependent pathways induces a motile and pro-inflammatory microglial phenotype. *J Neuroinflam.* (2017) 14:253. doi: 10.1186/s12974-017-1024-1
40. Plastira I, Bernhart E, Goeritzer M, Reicher H, Kumble VB, Kogelnik N, et al. 1-Oleyl-lysophosphatidic acid (LPA) promotes polarization of BV-2 and primary murine microglia towards an M1-like phenotype. *J Neuroinflam.* (2016) 13:205. doi: 10.1186/s12974-016-0701-9
41. Wang L, Knudsen E, Jin Y, Gessani S, Maghazachi AA. Lysophospholipids and chemokines activate distinct signal transduction pathways in T helper 1 and T helper 2 cells. *Cell Signal.* (2004) 16:991–1000. doi: 10.1016/S0898-6568(04)00022-1
42. Hui W, Zhao C, Bourgoin SG. LPA promotes t cell recruitment through synthesis of CXCL13. *Mediat Inflam.* (2015) 2015:248492. doi: 10.1155/2015/248492
43. Maghazachi AA. G protein-coupled receptors in natural killer cells. *J Leukocyte Biol.* (2003) 74:16–24. doi: 10.1189/jlb.0103019
44. Balkwill F. Cancer and the chemokine network. *Nat Rev Cancer.* (2004) 4:540–50. doi: 10.1038/nrc1388

Conflict of Interest: The authors declare that the research was conducted in the absence of any commercial or financial relationships that could be construed as a potential conflict of interest.

Copyright © 2020 Shi, Jiang, Yang, Zhang, Wang, Liu, Sun, Lu and Yang. This is an open-access article distributed under the terms of the Creative Commons Attribution License (CC BY). The use, distribution or reproduction in other forums is permitted, provided the original author(s) and the copyright owner(s) are credited and that the original publication in this journal is cited, in accordance with accepted academic practice. No use, distribution or reproduction is permitted which does not comply with these terms.

frontiers in Oncology

ORIGINAL RESEARCH
published: 20 August 2020
doi: 10.3389/fonc.2020.01436

Apolipoprotein C1 (APOC1): A Novel Diagnostic and Prognostic Biomarker for Clear Cell Renal Cell Carcinoma

*Yankang Cui†, Chenkui Miao†, Chao Hou†, Zengjun Wang and Bianjiang Liu**

Department of Urology, The First Affiliated Hospital of Nanjing Medical University, Nanjing, China

Background: Apolipoprotein C1 (APOC1) has been proved to play a critical role in gastric, breast, lung, and pancreatic cancer. However, the relationship between APOC1 and urinary tumors remains unclear. This study aimed to assess the diagnostic and prognostic value of APOC1 in urinary tumors.

Methods: We performed a pan analysis of APOC1 mRNA expression in urinary cancer using the Gene Expression Profiling Interactive Analysis (GEPIA) database. To further investigate the prognostic value of APOC1 expression in urinary cancers, the Kaplan-Meier plotter database was used. Furthermore, we collected the tumor and adjacent normal samples of 32 ccRCC patients to perform qRT-PCR and western blotting assays. A total of 72 cases with ccRCC were analyzed using tissue microarrays (TMAs).

Results: Our results based on Kaplan-Meier plotter database indicated that a high expression of APOC1 may lead to poor overall survival (OS, $p = 0.0019$) in patients with ccRCC. Furthermore, the cancer stages and tumor grade of ccRCC appeared to be strongly linked with APOC1 expression according to UALCAN database. Hence, we reached a preliminary conclusion that APOC1 may play a key role in the tumorigenesis and progression of ccRCC. Furthermore, the Kaplan-Meier survival curve analyses of 72 clinical patients indicated that high expression of APOC1 was associated with poor progression-free survival (PFS, $p = 0.007$) and OS ($p = 0.022$). In addition, univariate Cox regression analysis confirmed the significant relationship between APOC1 expression and survival ($p = 0.038$). The TMAs analysis in combination with the patients' clinicopathological features was also performed. The expression of APOC1 was found to be significantly correlated with the tumor size ($p = 0.018$) and histological grade ($p = 0.016$).

Conclusions: In conclusion, the findings of our study suggest that APOC1 may serve as a novel diagnostic and prognostic biomarker for ccRCC. Further evidence on the mechanism of APOC1 promoting tumor progression may transform it to a new therapeutic target for the treatment of ccRCC.

Keywords: apolipoprotein C1 (APOC1), clear cell renal cell carcinoma (ccRCC), diagnosis, prognosis, biomarker

OPEN ACCESS

Edited by:
Xin Xu,
Zhejiang University, China

Reviewed by:
Jonas Busch,
Charité–Universitätsmedizin Berlin, Germany
Matteo Ferro,
European Institute of Oncology (IEO), Italy

****Correspondence:***
Bianjiang Liu
bjliu@njmu.edu.cn

†These authors have contributed equally to this work

Specialty section:
This article was submitted to Genitourinary Oncology, a section of the journal Frontiers in Oncology

Received: *15 February 2020*
Accepted: *07 July 2020*
Published: *20 August 2020*

Citation:
Cui Y, Miao C, Hou C, Wang Z and Liu B (2020) Apolipoprotein C1 (APOC1): A Novel Diagnostic and Prognostic Biomarker for Clear Cell Renal Cell Carcinoma. Front. Oncol. 10:1436. doi: 10.3389/fonc.2020.01436

INTRODUCTION

Kidney cancers account for ∼2.2% of the global burden of all cancers, with more than 400,000 new diagnoses and 175,098 deaths worldwide in 2018 (1). Renal cell carcinoma (RCC) is the most common type, representing 85% of all kidney cancers (2). RCC consists of a family of carcinomas derived from the epithelium of renal tubules. The most frequent forms are clear cell renal cell carcinoma (ccRCC), papillary renal cell carcinoma, and chromophobe renal cell carcinoma. Approximately 80–90% of all RCCs are ccRCC, which is signified by the appearance of tumor cells with abundant clear cytoplasm (3). Patients with early stage ccRCC will benefit from timely surgical treatment, but for advanced tumors the 5-year survival rate is only 23% (2). Hence, it's of great urgency to improve our understanding of this disease and identify novel therapeutic targets with a better diagnostic and prognostic value.

Apolipoprotein C1 (APOC1), the smallest of all apolipoproteins (Mr = 6.6 kDa), is a member of the apolipoprotein C family and located at position 19q13.32. APOC1 is primarily expressed in the liver and activated when monocytes differentiate into macrophages (4). The encoded protein plays a central role in the metabolism of high-density lipoprotein (HDL) and very low-density lipoprotein (VLDL). This protein has also been shown to inhibit cholesteryl ester transfer protein in the plasma (5). In recent years, APOC1 was also reported to play significant roles in some biological processes, such as cholesterol catabolism, dendritic reorganization, and membrane remodeling (6, 7). APOC1 is associated with the progression of multiple diseases, including Alzheimer's disease, glomerulosclerosis, type 1 or type 2 diabetes, and diabetic nephropathy (8–11). Additionally, some studies revealed that APOC1 acts as an oncogene in the progression of some malignant tumors, including breast, pancreatic, colorectal, and lung cancer (11–15). However, the role of APOC1 in renal cancer has not been elucidated. The findings of our study revealed that APOC1 may act as an oncogene with novel prognostic and therapeutic target potential in ccRCC.

METHODS

GEPIA Database Analysis

The transcription profiling of APOC1 gene expression in a variety of urinary cancers was performed using the Gene Expression Profiling Interactive Analysis (GEPIA) database (http://gepia.cancer-pku.cn/index.html). We used The Cancer Genome Atlas (TCGA) tumors vs. TCGA normal + The Genotype-Tissue Expression (GTEx) normal datasets to draw the expression box plots. The log2FC cutoff was set as 1, and p-value cutoff was 0.01. Genes with higher |log2FC| values and lower q values than preset thresholds are considered differentially expressed genes (15).

Kaplan-Meier Plotter Database Analysis

The Kaplan Meier plotter (http://kmplot.com/analysis/) is used to assess the effect of 54 k genes on survival in 21 cancer types. The system includes gene chip and RNA-seq data-sources for the databases include Gene Expression Omnibus (GEO) and TCGA. The correlation between APOC1 mRNA expression and survival in kidney chromophobe (KICH), kidney renal clear cell carcinoma (KIRC), kidney renal papillary cell carcinoma (KIRP), prostate adenocarcinoma (PRAD), testicular germ cell tumors (TGCT), and bladder urothelial carcinoma (BLCA) was analyzed using the Kaplan-Meier plotter database. We split patients of all cancer stages to high and low APOC1 expression by auto select best cutoff. All possible cutoff values between the upper and lower quartiles are computed, and the best performing threshold is used as a cutoff. The log-rank p-value and hazard ratio with 95% confidence interval were also calculated. The follow-up threshold contained all survival time.

UALCAN Database Analysis

UALCAN (http://ualcan.path.uab.edu/index.html) is an interactive web portal for in-depth analysis of TCGA gene expression data (16). Here, we used UALCAN to investigate the potential relationship between the APOC1 expression level and tumor malignancy including cancer stage and tumor grade.

Sample Collection

The ccRCC tumor and normal tissues were acquired from patients who were diagnosed with ccRCC and underwent surgery at The First Affiliated Hospital of Nanjing Medical University between 2010 and 2018. Patients who were diagnosed with ccRCC by pathology were included, and those who had any medical history of other neoplasms were excluded. Finally, a total of 72 pairs of tissues were included in the cohort; 1 patient had metastasis by the time of surgery. We collected the clinical data and pathological features of these patients who were included in these tissue microarrays (TMAs). The deadline date of follow-up was July 2018. Samples for RNA and protein extraction were freshly frozen in liquid nitrogen and stored at −80°C. Samples for immunohistochemical analysis were formalin fixed. The study design and protocol was approved by the ethics committee of The First Affiliated Hospital of Nanjing Medical University. All patients included in this study provided informed consent.

Cell Culture and Treatment

Human renal cancer cell lines (786-O, 769-P, CAKI-1, CAKI-2, and ACHN) and human renal tubular epithelial cells (HK-2) were purchased from the Chinese Academy of Sciences (Shanghai, China). All cell lines were cultured at 37°C with 5% CO2. CAKI-1 and CAKI-2 were cultured in McCoy's 5A Medium (Gibco, Waltham, MA, USA); 786-O and 769-P were cultured in RPMI-1640 medium (Gibco, Grand Island, NY, USA). HK-2 was cultured in DMEM. The medium was supplemented with 10% fetal bovine serum (FBS) (Gibco, Grand Island, NY, USA).

RNA Extraction, Reverse Transcription, and Quantitative RT-PCR

Total RNA was extracted from renal tissues and cell lines using TRIzol reagent (Invitrogen, Carlsbad, CA, USA), following the manufacturer's protocol. The total RNA was reverse transcribed into complementary DNA (cDNA) using HiScript II (Vazyme, Shanghai, China). qRT-PCR was performed

using SYBR Green I (Vazyme, Shanghai, China) on ABI 7900 system (Applied Biosystems, Carlsbad, CA, USA) and the primers for APOC1 were as follows: forward(F), 5′-AGGACAAGGCTCGGGAACTCAT-3′, and reverse(R), 5′-GATGTCACCCTTCAGGTCCTCA-3′. The primers for β-actin were as follows: (F), 5′-GAAGATCAAGATCATTGCTCCT-3′, and (R), 5′-TACTCCTGCTTGCTGATCCA-3′.

Western Blotting

Cell lines and renal tissues were lysed using RIPA Lysis Buffer (Beyotime biotechnology, Shanghai, China), and proteins were harvested and quantified using the bicinchoninic acid (BCA) kit (Beyotime biotechnology, Shanghai, China). Proteins were separated on a 15% gel using sodium dodecyl sulfate (SDS)-PAGE and transferred onto polyvinylidene fluoride (PVDF) membranes

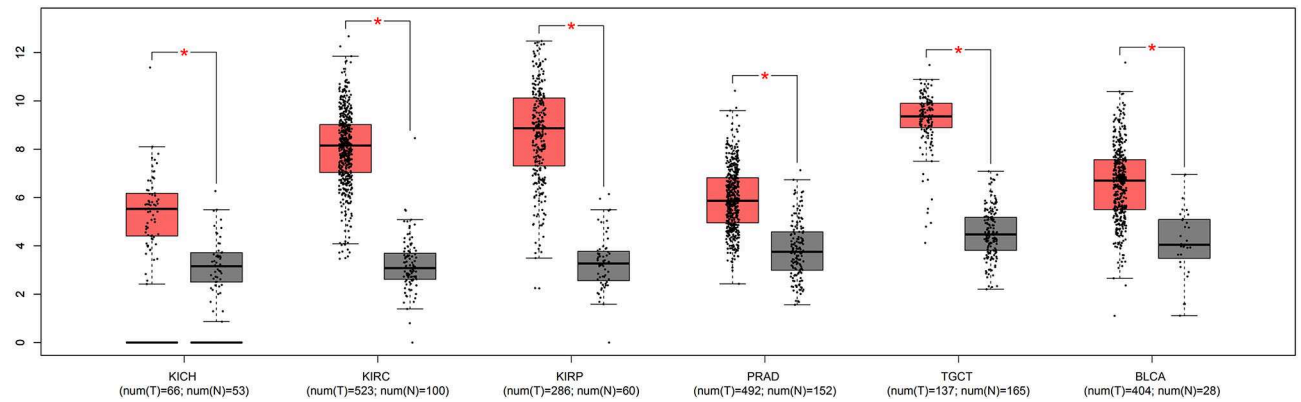

FIGURE 1 | The mRNA expression of APOC1 was significantly increased in urinary tumor tissues, compared to that in normal tissues (*p <0.05).

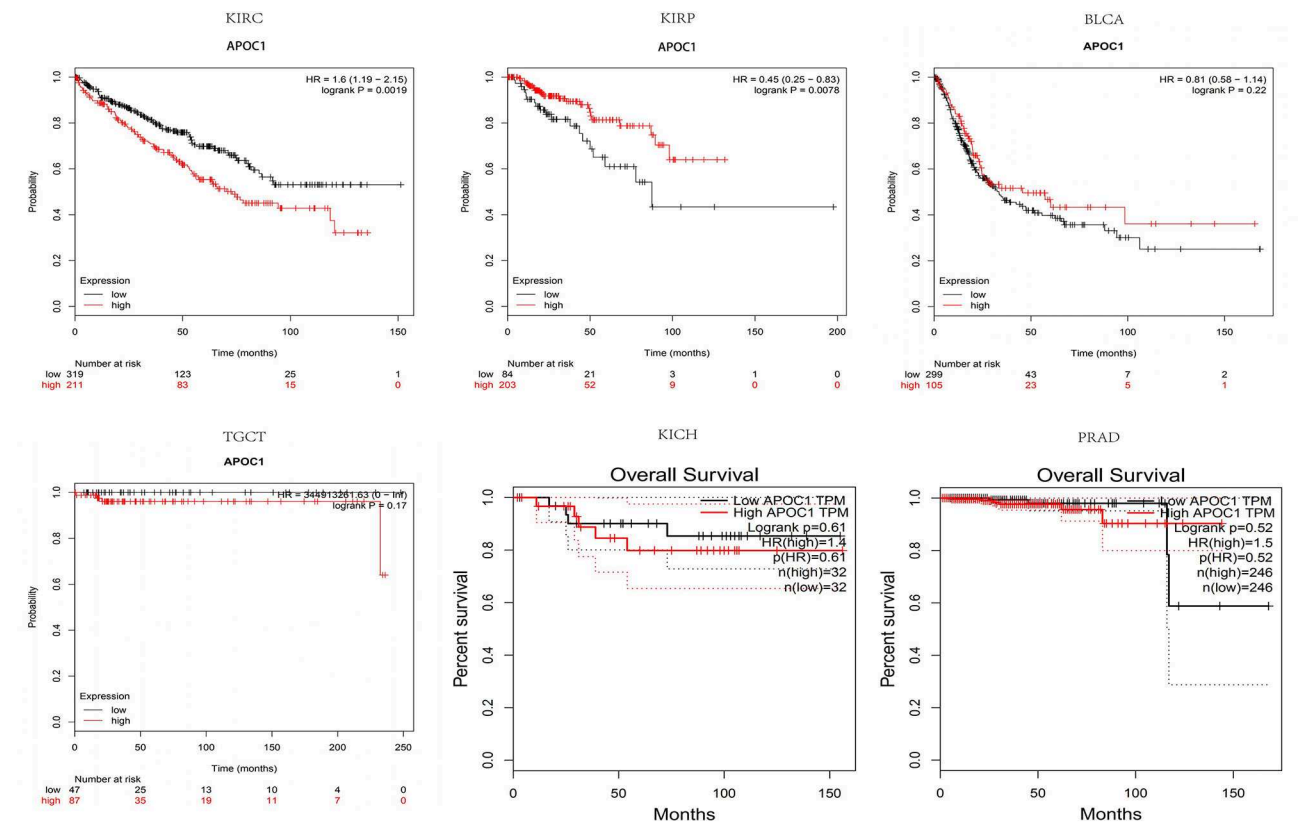

FIGURE 2 | Higher expression of APOC1 was significantly associated with shorter overall survival in KIRC (p = 0.0019). However, no such association was observed in KIRP (p = 0.0078), despite the high APOC1 levels. Additionally, high APOC1 had no significant association with the overall survival in other urinary tumors, including BLCA (p = 0.22), TGCT (p = 0.17), KICH (p = 0.61), and PRAD (p = 0.52).

(Sigma-Aldrich, St. Louis, MO, USA). The membranes were blocked in Tris-buffered saline (TBS) containing 5% non-fat milk for 2 h. After incubation with an anti-APOC1 antibody (1:1,000, ab198288, Abcam), and an anti-GAPDH antibody (1:2,500, ab9485, Abcam) overnight at 4°C, the membranes were washed three times with TBS-T (TBS containing 0.1% Tween-20). Subsequently, the membranes were incubated in a secondary antibody solution at room temperature for 2 h. After washes, the signals were detected using the chemiluminescence system and analyzed with Image Lab Software.

Immunohistochemistry (IHC)

IHC staining and evaluation of it was performed as in previously described methods (17). In brief, the protein expression of APOC1 in serial ccRCC tumor tissues from TMAs was detected by anti-APOC1 antibody (1:400, ab198288, Abcam) and a secondary antibody (1:5,000, L3012-2, SAB). Immunoreactive score of Remmele and Stegner (IRS) system was used to determine the protein expression level. From previous methods, a final score >1 was considered a high APOC1 expression; otherwise, it was considered as low APOC1 expression.

Statistical Analysis

Chi-square test or Fisher's exact test was used to assess the associations between the protein expression level and clinicopathological factors. Kaplan-Meier curve and log-rank test were used to compare the progression free survival (PFS; progression-free survival was defined as the time between the diagnosis and the first unequivocal clinical or radiological sign of disease progress) and overall survival (OS; overall survival was defined as the time from randomization until death from any cause) in the study cohort. Additionally, univariate Cox

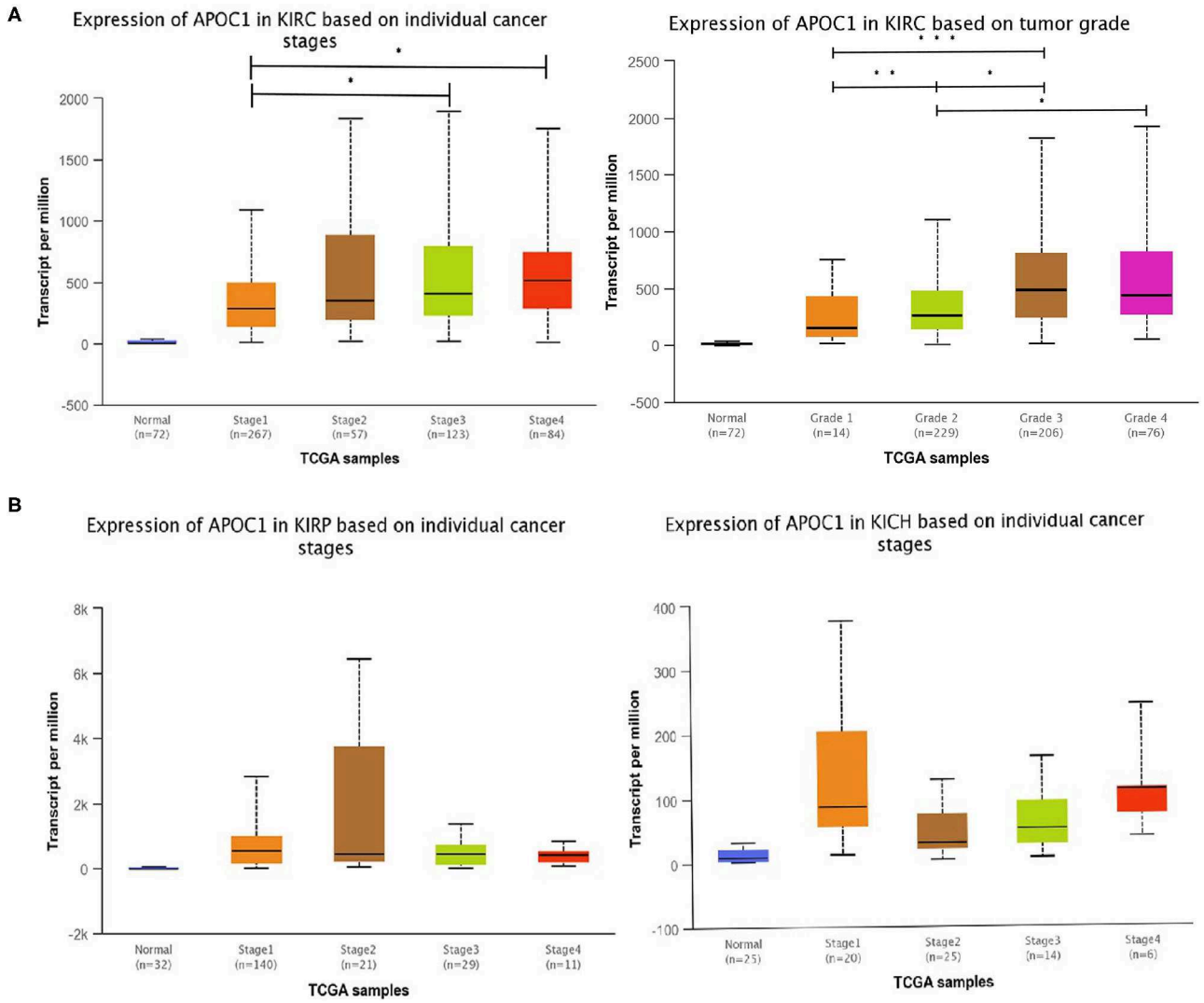

FIGURE 3 | (A) The transcript level of APOC1 in different stages of kidney cancers. The expression of APOC1 increased with the development of KIRC, but made no sense for KIRP and KICH. **(B)** Similarly, the significantly difference in APOC1 expression was also found in ccRCC tumor grades.

regression analysis was performed. The Student's *t*-test was used to compare differences between two or three groups, and $P < 0.05$ was considered statistically significant. The analyses were performed using the SPSS 16.0 software and GraphPad Prism 7.0.

RESULTS

APOC1 Is Increased in Urinary Tumors and Correlates With the Prognosis of ccRCC in Patients Based on the Public Databases

We first investigated whether the mRNA expression of APOC1 was altered in urinary tumors. The results from the GEPIA database revealed that the APOC1 level was significantly increased in tumor tissues compared to that in normal tissues (**Figure 1**).

To further explore the APOC1 expression pattern and its prognostic significance in urinary tumors, we used Kaplan-Meier plotter database to draw survival curves. As shown in **Figure 2**, high expression of APOC1 was significantly associated with shorter OS in ccRCC ($p = 0.0019$). However, longer overall survival was found in KIRP ($p = 0.0078$) with high level of APOC1. Additionally, high APOC1 had no statistical difference on the overall survival of other urinary tumors, including BLCA ($p = 0.22$), TGCT ($p = 0.17$), KICH ($p = 0.61$), and PRAD ($p = 0.52$).

APOC1 Promotes Tumor Progression in ccRCC

Given that APOC1 was upregulated in ccRCC tissues and its high expression led to shorter OS, we further investigated the role of APOC1 in the tumor progression of ccRCC based on the cancer stage and tumor grade. According to the analysis of UALCAN database (**Figure 3A**), we found that the expression of APOC1 increased with the development of KIRC, but no such observation was made in case of KIRP and KICH. Furthermore, higher expression of APOC1 was observed in higher tumor grade of KIRC (**Figure 3B**). Therefore, we speculated that APOC1 may act as an oncogene in ccRCC to promote tumor progression.

Aberrant Expression of APOC1 in RCC Tumor Specimens and Cell Lines

To verify the above results, we subsequently performed qRT-PCR and western blot for the ccRCC tumor samples. A total of 32

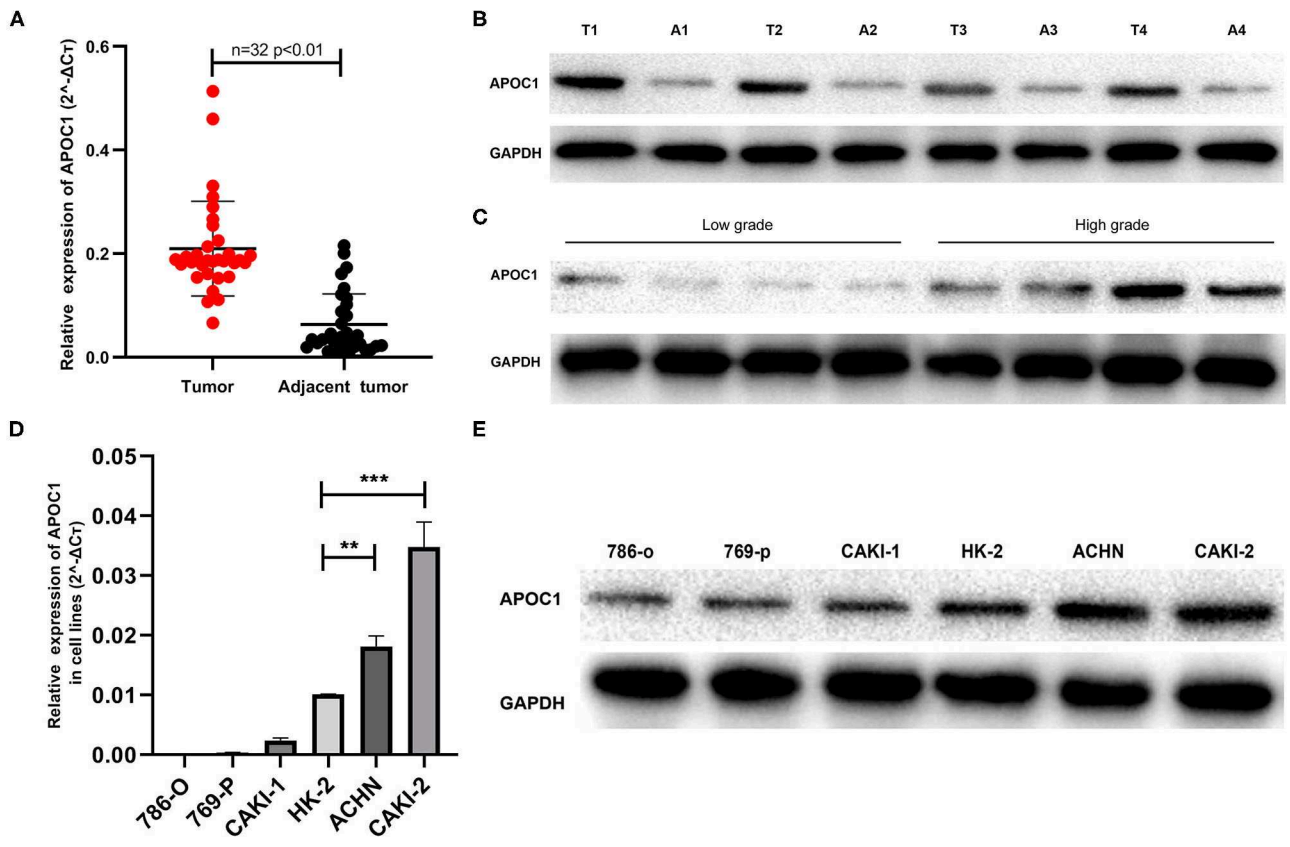

FIGURE 4 | (A) PCR results of the 32 ccRCC tumor tissues. The mRNA expression of APOC1 in tumor tissues was significantly higher than that in adjacent tissues ($p < 0.01$) **(B)** the APOC1 protein level was significantly higher in tumor tissues than that in adjacent tissues. **(C)** The western blot analysis of eight ccRCC patients with different tumor grades revealed higher protein expression of APOC1 in patients with higher tumor grade. **(D,E)** The mRNA and protein expression level of APOC1 was highest in CAKI-2. In addition to CAKI-2 and ACHN, all the other cell lines showed lower APOC1 expression than HK-2, which is considered as a normal tissue cell line (**$p < 0.01$, ***$p < 0.001$).

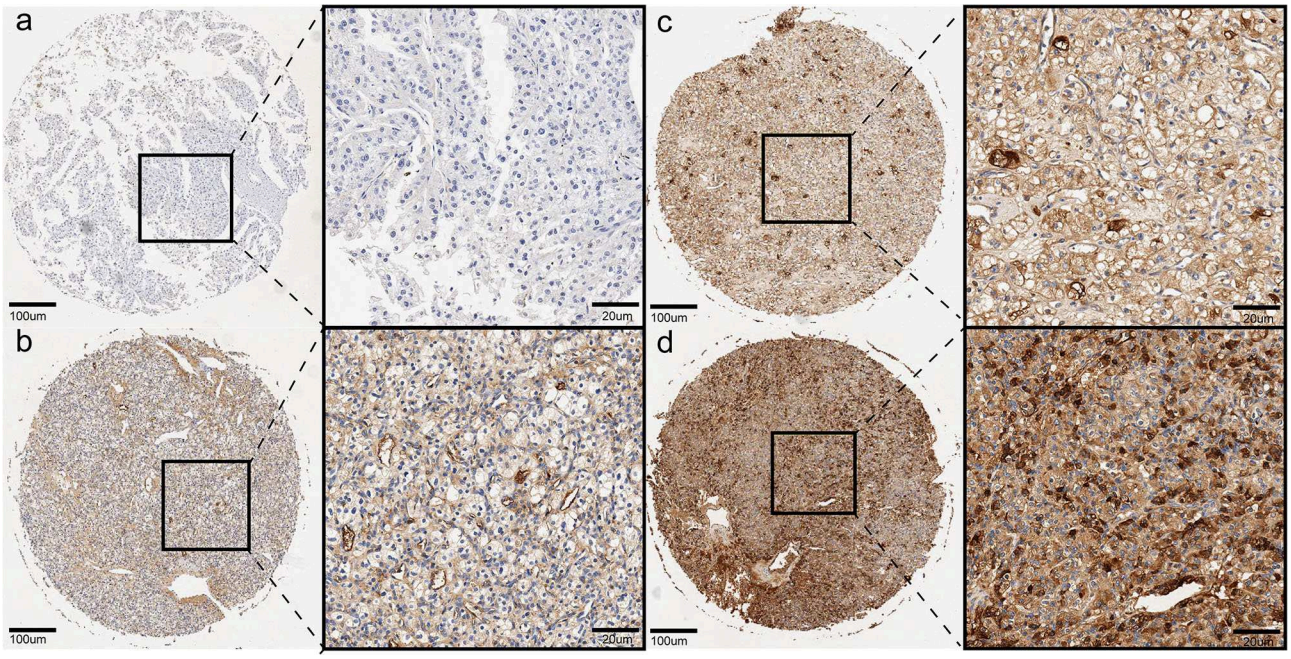

FIGURE 5 | Representative pictures of ccRCC in tissue microarray by IHC, **(a)** (negative), **(b)** (weak brown), **(c)** (moderate brown), **(d)** (strong brown).

TABLE 1 | Correlations between the expression of APOC1 and clinicopathological features in 72 ccRCC patients.

Characteristics	Case	APOC1 expression		*p*
		Low	High	
All cases	72	27	45	
Age(years)				0.219
<60	48	16	32	
≥60	24	11	13	
Gender				0.452
Male	46	18	28	
Female	26	9	17	
TNM stage				0.393
T1	61	22	39	
T2–T4	11	5	6	
Tumor size(cm)				0.018*
≤4	38	19	19	
>4	34	8	26	
Histological grade				0.016*
I and II	52	15	37	
III and IV	20	12	8	

*$P < 0.05$.

ccRCC tumor tissues and adjacent normal tissues (normal tissues adjacent to the tumor volume) were collected. The PCR result is shown in **Figure 4A**. The transcriptional expression of APOC1 in tumor tissues was significantly higher than that in the adjacent tissues ($p < 0.01$). Similarly, the APOC1 protein level was also found to be higher in tumor tissues (**Figure 4B**).

Subsequently, we investigated whether APOC1 was expressed in renal cancer cell lines (786-O, 769-P, CAKI-1, CAKI-2, and ACHN) and normal cell line HK-2. As displayed in **Figures 4D,E**, the mRNA and protein expression levels of APOC1 were highest in CAKI-2. In addition to CAKI-2 and ACHN, all the other cell lines showed a lower expression of APOC1 than HK-2.

The difference in the expression of APOC1 in the progression of ccRCC was also verified in this study. We collected eight ccRCC tumor tissue samples, half of which were with high Fuhrman grade (grade: 3–4) and half were with low Fuhrman grade (grade: 1–2), based on postoperative pathology. The western blot analysis revealed that higher protein expression of APOC1 could be found in patients of ccRCC with higher tumor grade (**Figure 4C**). These results were consistent with our current findings.

Expression Pattern of APOC1 in Clinical RCC Cohorts and Its Prognostic Validation

IHC staining assay was performed using TMAs tissues of our clinical cohort. As shown in **Figure 5**, a total of 72 ccRCC patients were classified into the low APOC1 expression group (IRS≤1) and high APOC1 expression group (IRS>1) based on the IHC staining score. Finally, 45 of the 72 (62.5%) samples showed high expression of APOC1, while 27 (37.5%) of tissues with relatively low APOC1 level. The association between the APOC1 expression and clinicopathological characteristics of patients were summarized in **Table 1**. We found that high expression of APOC1 was significantly associated with the larger tumor size (*p*

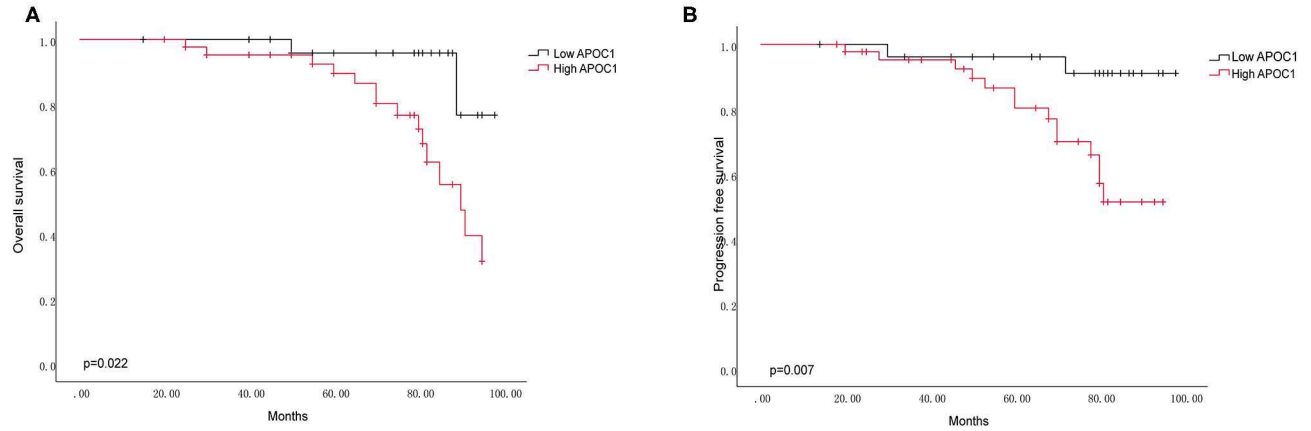

FIGURE 6 | The APOC1 high expression group was associated with decreased overall survival **(A)** and progression-free survival **(B)** in 72 ccRCC patients. Log-rank *p* value was 0.022 for OS, and 0.007 for PFS.

= 0.018) and advanced histological grade ($p = 0.016$). However, APOC1 expression status had no significant difference in the age, gender, and TNM stage of ccRCC patients.

In addition, we performed the outcome analysis of our clinical cohort to validate the prognostic significance of APOC1 expression in ccRCC. Kaplan-Meier curves revealed that the patients with high APOC1 expression had a shorter OS and PFS ($p = 0.022$ for OS and $p = 0.007$ for PFS, **Figures 6A,B**). Finally, univariate Cox regression analysis for the survival analysis was conducted to explore the significant value of APOC1 in prognosis (**Table 2**; HR, 0.209; 95% CI, 0.048–0.916 [$p = 0.038$]).

TABLE 2 | Univariate Cox regression for OS.

Variable	HR (95% CI)	*P*
APOC1 expression	0.209 (0.048–0.916)	0.038*

*HR (95% CI), hazard ratio, with 95% confidence interval; OS, overall survival; *P < 0.05.*

DISCUSSION

In this study, we first investigated the APOC1 expression profile in urinary tumors and its relevant prognostic value in ccRCC. We compared the expression level of APOC1 in the urinary tumor tissues and normal tissues using databases and found a general higher expression in tumors as compared to that in normal tissues. Besides, high expression of APOC1 made a significant difference in the overall survival of patients with ccRCC and KIRP. We further investigated the role of APOC1 in the tumor progression of ccRCC and KIRP. Our observation found higher APOC1 expression in advanced tumor malignancy characterized by tumor grade and cancer stage of ccRCC. To verify the results from the analysis of databases, we collected tissue samples from patients with ccRCC to perform subsequent validation using qRT-PCR, western blotting, and IHC staining assays. The obtained results were consistent with our previous findings using the databases. Moreover, by analyzing the associations between APOC1 expression and the clinicopathological characteristics of patients with ccRCC, we confirmed the correlation between APOC1 expression and tumor size, which reflects the tumor's aggressiveness.

It is known that ccRCC is highly aggressive and distant metastasis often occurs during advanced tumor stage. About 30% of all patients with ccRCC have metastases at the time of diagnosis, and another 30–40% will develop metastases at a later stage (18). Recently, despite the development of molecular targeted therapies, ccRCC patients' treatment is still challenging once metastasis is manifested, leading to a 5-year survival of only 23% (2, 19). Hence, it's of pressing requirement indeed to identify effective targets to diagnose and intervene ccRCC at an early stage.

The ccRCC cells have the aggregation characteristics of cholesterol, cholesterol ester, and other lipids (20), suggesting that the content of cholesterol and cholesterol ester in ccRCC tissues is higher than that in normal kidney tissue (21). Cholesterol has been demonstrated to slightly promote the ccRCC cell proliferation, but it significantly increases the capacities of invasion and migration by regulating the KLF5/miR-27a/FBXW7 axis (22). APOC1 is present in chylomicrons, VLDL, and HDL. APOC1 acts as an exchangeable apolipoprotein between these lipoprotein classes with an important role in lipid transport, metabolism, and homeostasis (23). *In vivo*, the overexpression of human APOC1 in mice led to hyperlipidemia owing to the reduced uptake of VLDL and post-lipolysis particles by inhibiting the binding of VLDL to VLDLR (24). This could be one of the contributing factors in the high APOC1 expression leading to poor clinical outcomes for patients with ccRCC. Therefore, targeting APOC1 to regulate cholesterol metabolism may be a novel treatment approach.

Recently, the relationship between APOC1 and malignant tumors has been highlighted. APOC1 was demonstrated to

promote cell proliferation in prostate cancer cells *in vitro* (25). In gastric cancer (GC), APOC1 revealed the value of diagnosing and prognosing for GC (17). In colorectal cancer, APOC1 played its proliferative activity by MAPK signaling (13), and in pancreatic cells it was found to inhibit apoptosis (12). Herein, our findings for the first time revealed that APOC1 could be considered as a potential diagnostic and prognostic biomarker for ccRCC. However, the limitation that cannot be ignored is the small sample scales in our study, which might weaken the statistical association between APOC1 expression and ccRCC progression. Nevertheless, analysis of ccRCC patients relying on TCGA datasets was also performed and further confirmed our results. Further research should be undertaken to uncover the potential mechanism of APOC1 promoting ccRCC tumor progression by regulating cholesterol metabolism. Better understanding of this may give a new hope for the treatment of advanced ccRCC patients.

CONCLUSIONS

In summary, this is the first study to investigate the role of APOC1 in ccRCC. APOC1 expression was much higher in ccRCC tumor tissues, and high expression of APOC1 correlated with a shorter OS, PFS, and poor clinical characters, including cancer stage, tumor grade, and tumor size. We speculate that APOC1 might act as a tumor promoter by regulating the cholesterol metabolism. However, further research should be carried out to reveal the underlying mechanism. Cumulatively, APOC1 may be a promising biomarker to diagnose ccRCC and predict prognostic outcomes in ccRCC patients.

DATA AVAILABILITY STATEMENT

The datasets generated for this study are available on request to the corresponding author.

ETHICS STATEMENT

The studies involving human participants were reviewed and approved by Medical ethics committee of The First Affiliated Hospital of Nanjing Medical University. The patients/participants provided their written informed consent to participate in this study.

AUTHOR CONTRIBUTIONS

YC and CM designed the study. YC collected the data and edited the manuscript. CH analyzed the data. CM and ZW sourced the literature. BL acquired the funding and supervised the whole study. All authors contributed to the article and approved the submitted version.

FUNDING

This study was supported by the Six Talent Peak Project of High-level Talents in Jiangsu Province (WSW-017); 333 High-level Talents Training Project in Jiangsu Province, Professional from Six-Pronged Top-Talent Program (LGY2018053); Qing Lan Project of Jiangsu University (JX2161015100); The Fifth Batch of Outstanding Young and Middle-aged Teachers Support Program of Nanjing Medical University; A Project Funded by the Priority Academic Program Development of Jiangsu Higher Education Institutions (JX10231802); Postgraduate Research & Practice Innovation Program of Jiangsu Province (KYCX19_1159) and International Exchange and Cooperation Program for Postgraduates of Nanjing Medical University.

ACKNOWLEDGMENTS

We thank all the participants who were involved in this study. We also thank the Cooperation Program between The First Affiliated Hospital of Nanjing Medical University and Brigham and Women's Hospital.

REFERENCES

1. Bray F, Ferlay J, Soerjomataram I, Siegel RL, Torre LA, Jemal A. Global cancer statistics 2018: GLOBOCAN estimates of incidence and mortality worldwide for 36 cancers in 185 countries. *CA Cancer J Clin*. (2018) 68:394–424. doi: 10.3322/caac.21492
2. Ljungberg B, Bensalah K, Canfield S, Dabestani S, Hofmann F, Hora M, et al. EAU guidelines on renal cell carcinoma: 2014 update. *Eur Urol*. (2015) 67:913–24. doi: 10.1016/j.eururo.2015.01.005
3. Motzer RJ, Jonasch E, Agarwal N, Bhayani S, Bro WP, Chang SS, et al. Kidney Cancer, Version 2.2017, NCCN clinical practice guidelines in oncology. *J Natl Compr Canc Netw*. (2017) 15:804–34. doi: 10.6004/jnccn.2017.0100
4. Frossard PM, Coleman RT, Malloy MJ, Kane JP, Levy-Wilson B, Appleby VA. Human apolipoprotein CI (apoC1) gene locus: DraI dimorphic site. *Nucleic Acids Res*. (1987) 15:1884. doi: 10.1093/nar/15.4.1884
5. Xu Y, Berglund L, Ramakrishnan R, Mayeux R, Ngai C, Holleran S, et al. A common Hpa I RFLP of apolipoprotein C-I increases gene transcription and exhibits an ethnically distinct pattern of linkage disequilibrium with the alleles of apolipoprotein E. *J Lipid Res*. (1999) 40:50–8.
6. Poirier J, Hess M, May PC, Finch CE. Cloning of hippocampal poly(A) RNA sequences that increase after entorhinal cortex lesion in adult rat. *Brain Res Mol Brain Res*. (1991) 9:191–5. doi: 10.1016/0169-328X(91)90002-F
7. Mooyaart AL, Valk EJ, van Es LA, Bruijn JA, de Heer E, Freedman BI, et al. Genetic associations in diabetic nephropathy: a meta-analysis. *Diabetologia*. (2011) 54:544–53. doi: 10.1007/s00125-010-1996-1
8. McKay GJ, Savage DA, Patterson CC, Lewis G, McKnight AJ, Maxwell AP. Association analysis of dyslipidemia-related genes in diabetic nephropathy. *PLoS ONE*. (2013) 8:e58472. doi: 10.1371/journal.pone.0058472
9. Ki CS, Na DL, Kim DK, Kim HJ, Kim JW. Genetic association of an apolipoprotein C-I (APOC1) gene polymorphism with late-onset Alzheimer's disease. *Neurosci Lett*. (2002) 319:75–8. doi: 10.1016/S0304-3940(01)02559-9
10. Bus P, Pierneef L, Bor R, Wolterbeek R, van Es LA, Rensen PC, et al. Apolipoprotein C-I plays a role in the pathogenesis of glomerulosclerosis. *J Pathol*. (2017) 241:589–99. doi: 10.1002/path.4859
11. Sun Y, Zhang J, Guo F, Zhao W, Zhan Y, Liu C, et al. Identification of apolipoprotein C-I peptides as a potential biomarker and its biological roles in breast cancer. *Med Sci Monit*. (2016) 22:1152–60. doi: 10.12659/MSM.896531

12. Takano S, Yoshitomi H, Togawa A, Sogawa K, Shida T, Kimura F, et al. Apolipoprotein C-1 maintains cell survival by preventing from apoptosis in pancreatic cancer cells. *Oncogene*. (2008) 27:2810–22. doi: 10.1038/sj.onc.1210951
13. Ren H, Chen Z, Yang L, Xiong W, Yang H, Xu K, et al. Apolipoprotein C1 (APOC1) promotes tumor progression via MAPK signaling pathways in colorectal cancer. *Cancer Manag Res*. (2019) 11:4917–30. doi: 10.2147/CMAR.S192529
14. Ko HL, Wang YS, Fong WL, Chi MS, Chi KH, Kao SJ. Apolipoprotein C1 (APOC1) as a novel diagnostic and prognostic biomarker for lung cancer: A marker phase I trial. *Thorac Cancer*. (2014) 5:500–8. doi: 10.1111/1759-7714.12117
15. Tang Z, Li C, Kang B, Gao G, Li C, Zhang Z. GEPIA: a web server for cancer and normal gene expression profiling and interactive analyses. *Nucleic Acids Res*. (2017) 45:W98–102. doi: 10.1093/nar/gkx247
16. Chandrashekar DS, Bashel B, Balasubramanya SAH, Creighton CJ, Ponce-Rodriguez I, Chakravarthi B, et al. UALCAN: a portal for facilitating tumor subgroup gene expression and survival analyses. *Neoplasia*. (2017) 19:649–58. doi: 10.1016/j.neo.2017.05.002
17. Yi J, Ren L, Wu J, Li W, Zheng X, Du G, et al. Apolipoprotein C1 (APOC1) as a novel diagnostic and prognostic biomarker for gastric cancer. *Ann Transl Med*. (2019) 7:380. doi: 10.21037/atm.2019.07.59
18. Lam JS, Shvarts O, Leppert JT, Figlin RA, Belldegrun AS. Renal cell carcinoma 2005: new frontiers in staging, prognostication and targeted molecular therapy. *J Urol*. (2005) 173:1853–62. doi: 10.1097/01.ju.0000165693.68449.c3
19. Ghatalia P, Zibelman M, Geynisman DM, Plimack ER. Checkpoint inhibitors for the treatment of renal cell carcinoma. *Curr Treat Options Oncol*. (2017) 18:7. doi: 10.1007/s11864-017-0458-0
20. Drabkin HA, Gemmill RM. Obesity, cholesterol, and clear-cell renal cell carcinoma (RCC). *Adv Cancer Res*. (2010) 107:39–56. doi: 10.1016/S0065-230X(10)07002-8
21. Lee CK, Marschner IC, Simes RJ, Voysey M, Egleston B, Hudes G, et al. Increase in cholesterol predicts survival advantage in renal cell carcinoma patients treated with temsirolimus. *Clin Cancer Res*. (2012) 18:3188–96. doi: 10.1158/1078-0432.CCR-11-3137
22. Liu Z, Liu X, Liu S, Cao Q. Cholesterol promotes the migration and invasion of renal carcinoma cells by regulating the KLF5/miR-27a/FBXW7 pathway. *Biochem Biophys Res Commun*. (2018) 502:69–75. doi: 10.1016/j.bbrc.2018.05.122
23. Fuior EV, Gafencu AV. Apolipoprotein C1: its pleiotropic effects in lipid metabolism and beyond. *Mol Sci*. (2019) 20:5939. doi: 10.3390/ijms20235939
24. Shachter NS, Ebara T, Ramakrishnan R, Steiner G, Breslow JL, Ginsberg HN, et al. Combined hyperlipidemia in transgenic mice overexpressing human apolipoprotein Cl. *J Clin Invest*. (1996) 98:846–55. doi: 10.1172/JCI118857
25. Su WP, Sun LN, Yang SL, Zhao H, Zeng TY, Wu WZ, et al. Apolipoprotein C1 promotes prostate cancer cell proliferation *in vitro*. (2018) 32:e22158. doi: 10.1002/jbt.22158

Conflict of Interest: The authors declare that the research was conducted in the absence of any commercial or financial relationships that could be construed as a potential conflict of interest.

Copyright © 2020 Cui, Miao, Hou, Wang and Liu. This is an open-access article distributed under the terms of the Creative Commons Attribution License (CC BY). The use, distribution or reproduction in other forums is permitted, provided the original author(s) and the copyright owner(s) are credited and that the original publication in this journal is cited, in accordance with accepted academic practice. No use, distribution or reproduction is permitted which does not comply with these terms.

frontiers in Oncology

ORIGINAL RESEARCH
published: 16 September 2020
doi: 10.3389/fonc.2020.01774

Phenotypic Analysis of Urothelial Exfoliated Cells in Bladder Cancer via Microfluidic Immunoassays: Sialyl-Tn as a Novel Biomarker in Liquid Biopsies

Sandra Carvalho[1], Catarina M. Abreu[1], Dylan Ferreira[2,3], Luís Lima[2,3,4], José A. Ferreira[2,3], Lúcio L. Santos[2,3], Ricardo Ribeiro[5,6,7], Vânia Grenha[8], Mónica Martínez-Fernández[9], Marta Duenas[10,11], Cristian Suárez-Cabrera[10,11], Jesus M. Paramio[10,11], Lorena Diéguez[1], Paulo P. Freitas[12] and Marta I. Oliveira[1]**

[1] International Iberian Nanotechnology Laboratory, Department of Life Sciences, Braga, Portugal, [2] Experimental Pathology and Therapeutics Group, Research Center of the Portuguese Institute of Oncology (CI-IPOP), Porto, Portugal, [3] Porto Comprehensive Cancer Center (P.ccc), Porto, Portugal, [4] School of Health, Polytechnic Institute of Porto, Porto, Portugal, [5] Tumor & Microenvironment Group, i3S/INEB, Instituto de Investigação e Inovação em Saúde/Instituto de Engenharia Biomédica, University of Porto, Porto, Portugal, [6] Faculty of Medicine, Environmental Health Institute, University of Lisbon, Lisbon, Portugal, [7] Departament of Clinical Pathology, Centro Hospitalar e Universitário de Coimbra, Coimbra, Portugal, [8] Department of Urology, Centro Hospitalar Do Alto Ave, Guimarães, Portugal, [9] Genomes and Disease Lab., Research Center of Molecular Medicine and Chronic Diseases (CIMUS), University of Santiago de Compostela, Santiago de Compostela, Spain, [10] Molecular Oncology Unit, CIEMAT, Madrid, Spain, [11] CIBERONC, Institute of Biomedical Research, University Hospital "12 de Octubre", Madrid, Spain, [12] International Iberian Nanotechnology Laboratory, Department of Nanoelectronics Engineering, Braga, Portugal

Bladder cancer is the most common malignancy of the urinary tract, having one of the highest recurrence rates and progression from non-muscle to muscle invasive bladder cancer that commonly leads to metastasis. Cystoscopy and urine cytology are the standard procedures for its detection but have limited clinical sensitivity and specificity. Herein, a microfluidic device, the UriChip, was developed for the enrichment of urothelial exfoliated cells from fresh and frozen urine, based on deformability and size, and the cancer-associated glycan Sialyl-Tn explored as a putative bladder cancer urinary biomarker. Spiking experiments with bladder cancer cell lines showed an isolation efficiency of 53%, while clinical sample analyses revealed retention of cells with various morphologies and sizes. *in situ* immunoassays demonstrated significantly higher number of Sialyl-Tn-positive cells in fresh and frozen voided urine from bladder cancer patients, compared to healthy individuals. Of note, urothelial exfoliated cells from cryopreserved urine sediments were also successfully isolated by the UriChip, and found to express significantly high levels of Sialyl-Tn. Remarkably, Sialyl-Tn expression is correlated with tumor stage and grade. Overall, our findings demonstrate the potential of UriChip and Sialyl-Tn to detect urothelial bladder cancer cells in follow-up and long-term retrospective studies.

Keywords: bladder cancer, microfluidics, liquid biopsy, urine, Sialyl-Tn

OPEN ACCESS

Edited by:
Paula Alexandra Quintela Videira, New University of Lisbon, Portugal

Reviewed by:
Pedro C. Barata, Tulane University, United States
Guru Sonpavde, Dana–Farber Cancer Institute, United States

****Correspondence:***
Sandra Carvalho
sandra.carvalho@inl.int
Marta I. Oliveira
martaioliveira@gmail.com

Specialty section:
This article was submitted to Genitourinary Oncology, a section of the journal Frontiers in Oncology

Received: *06 January 2020*
Accepted: *10 August 2020*
Published: *16 September 2020*

Citation:
Carvalho S, Abreu CM, Ferreira D, Lima L, Ferreira JA, Santos LL, Ribeiro R, Grenha V, Martínez-Fernández M, Duenas M, Suárez-Cabrera C, Paramio JM, Diéguez L, Freitas PP and Oliveira MI (2020) Phenotypic Analysis of Urothelial Exfoliated Cells in Bladder Cancer via Microfluidic Immunoassays: Sialyl-Tn as a Novel Biomarker in Liquid Biopsies. Front. Oncol. 10:1774. doi: 10.3389/fonc.2020.01774

INTRODUCTION

Bladder cancer (BC) is the most common malignancy of the urinary tract (1). Cystoscopy and urine cytology are the standard pathological procedures for its detection (2, 3). However, cystoscopy is an invasive and expensive method with limited and operator-dependent sensitivity (4). On the other hand, urine cytology has low sensitivity for low-grade papillary tumors, depends on the examiner's subjective opinion, and displays long turnaround times (5–7). Although most patients are diagnosed with non-muscle invasive BC (NMIBC), which has a 5-year survival rate of 90% (8, 9), high recurrence rates (30–80%) impose long-term cystoscopy and cytology-based follow-ups after transurethral resection of malignant lesions (10, 11). Thus, management of BC is a hurdle with extremely high costs to health care systems (12, 13). To circumvent this issue, distinct BC biomarker assays have been developed targeting tumor-derived proteins or genetic material in voided urine (14–16). A few have reached commercialization, like the Urovysion and Immunocyt kits, showing superior sensitivity when compared to cytology (17). Still, their implementation in clinical diagnosis has been hampered by their high false-positive rates, complexity and high cost (18). In turn, BTA stat and BTA trak tests, which detect urinary human complement factor H-related protein, and NMP22/BladderChek, another protein-based test, have shown to report with limited sensitivity and selectivity for the diagnosis of BC (19–21). Hence, novel platforms and urinary biomarkers that may assist in early detection and monitoring of BC, as a non-invasive and cost-effective strategy, are of outmost importance.

Due to their high throughput and low cost, microfluidic-based diagnostic tools hold the promise for improved patient care and outcomes considering the limitations of current screening and diagnostic techniques as well as the societal and economic impact of BC (22, 23). Microfluidics enables precise manipulation of biological samples and can potentially provide portability and automation, offering exceptional advantages for clinical application (24). A panoply of microfluidic chips have been developed for blood-based biopsies, i.e., isolation of circulating tumor cells (CTCs) and/or tumor-derived material from blood of cancer patients with outstanding results (25–27). In the context of BC, we have recently reported two distinct microfluidic devices for CTC isolation and analysis (28, 29), while Alva et al. evaluated CTCs captured by the commercial system Isoflux (30). Despite the prognostic significance of CTCs in BC, microfluidic analysis of putative cancer biomarkers in voided urine would be ideal, non-invasive and provide significant benefits for patient monitoring, particularly at early stages of the disease, when survival rates are higher and CTCs may not yet be present. Nevertheless, only a scarcity of studies have used microfluidic chips for urine-based BC detection, employing different detection principles, complex systems, and processing times (31–34).

Built on our previous work regarding the development of microfluidic platforms for the capture of BC CTCs (28, 29), we herein report a new microfluidic chip for exfoliated tumor cell (ETC) enrichment from voided urine of BC patients. Importantly, ETCs are valuable sources of information regarding tumor biology and dynamics throughout the course of BC and treatment-follow up (35). A schematic representation of the experimental design used in this study is shown in **Figure 1**. This label-free strategy, based on cell size and deformability, allowed unbiased retention of ETCs of various sizes and morphologies. Moreover, ETCs were successfully isolated from fresh voided urine samples as well as from cryopreserved urine sediments, which to the best of our knowledge had never been assessed, revealing the feasibility of the system for retrospective analyses. A double marker analysis was performed using pan-cytokeratin (pan-CK) and Sialyl-Tn (STn), a tumor associated antigen overexpressed in BC but absent in the healthy urothelium (36). Our experiments showed, for the first time, STn expression in ETCs from patients, which correlated with staging and grading of BC. Noteworthy, data resulted from two independent data sets, corroborating the versatility of this platform and the potential of STn as a novel biomarker in liquid biopsies.

MATERIALS AND METHODS

Design and Fabrication of the UriChip Microfluidic Device

Masters were designed in AutoCAD software (Autodesk, USA) and consist of five rows of posts with increasingly narrower gap widths (50, 20, 15, 10, and 5 μm) (**Figures 2A,B**), allowing for a wide size-range of urothelial exfoliated cells to be captured (37, 38). A set of square posts with 100 μm gaps were incorporated for structural support of the channels and to prevent the device from clogging with urinary debris and large cell clusters. The design was patterned by direct write laser lithography (DWL 2.0 Heidelberg, Germany) on 200 mm silicon wafers (P/Boron, <100>, Siegert Wafer, Germany). Features with 20 μm depth were defined by silicon deep reactive ion etching (DRIE, STPS Pegasus, United Kingdom) with sulfur hexafluoride (SF6, Sigma 366 Aldrich, USA), and exposed areas passivated with octafluorocyclobutane (C_4F_8, Sigma Aldrich, USA). The etching of the features was confirmed by SEM inspection. Photoresist residues were stripped by oxygen plasma (PVA Tepla GIGAbatch 360M, Germany) and the wafer was diced using a DAD 3350 Dicing Saw (Disco, Japan). Masters were then cleaned with isopropyl alcohol (IPA, Sigma- Aldrich, USA), rinsed with deionized water and dried at 150°C. Finally, masters were hydrophobized through treatment with trichloro(1H,1H,2H,2H-perfluorooctyl)silane (97%, Sigma-Aldrich, USA) and cured for 1 h at 65°C.

Devices were fabricated in polydimethylsiloxane (PDMS, Ellsworth Adhesives Iberica, Spain), which was prepared as a two-part system with mix ratio of 10:1 (w/w) base/curing agent, poured over the master, degassed and cured for 2 h at 65°C. Following that, the PDMS was unmolded and inlet and outlet made using a puncher. Irreversible bonding was achieved through surface activation of clean glass slides and PDMS replicas by low power oxygen plasma for 15 s (PDC-002-CE, Harrick Plasma, USA). Immediately after fabrication and bonding (**Figure 2C1**), microfluidic devices were connected to a multi-channel pressure controller which allows the simultaneous

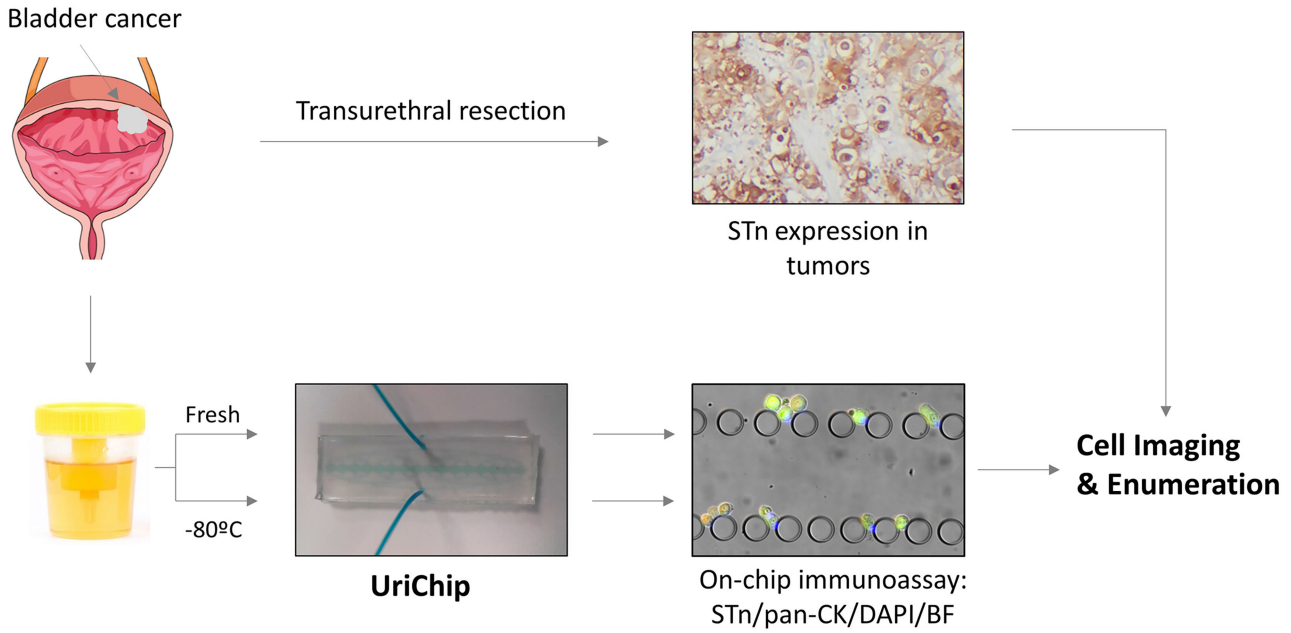

FIGURE 1 | Schematic representation of the enrichment and analysis of urothelial exfoliated cells from bladder washes and voided urine of BC patients using the UriChip. Bladder washes and voided urine from BC patients were collected, subjected or not to cryopreservation and run into the UriChip. A dual biomarker immunoassay was then performed, comprising pan-CK (epithelial marker), STn (tumor associated marker), and DAPI (nuclei staining). Trapped cells were next imaged by immunofluorescence microscopy and nucleated cells expressing STn and/or CK counted. In parallel, corresponding FFPE tissues were screened for STn by immunohistochemistry and results compared to clinicopathological information of patients.

run of up to four independent devices (MFCS^{TM}-EZ, Fluigent, France) (**Figure 2C2**), and channels firstly primed with ethanol 70% (v/v) at 100 mbar to enhance the wettability, then rinsed with 10 mM of Phosphate Buffered Saline (PBS, Sigma-Aldrich, USA) at 200 mbar and lastly treated with 1% (w/v) Pluronic F-127 (Sigma-Aldrich, USA) overnight at 4°C to avoid unspecific cell attachment.

Cell Culture

Human urinary BC cell lines HT1376 and MCR-STn [overexpressing the sialyl-Tn antigen (39)] were grown in monolayer culture and maintained at 37°C in an atmosphere of 5% CO_2 in RPMI 1640 GlutaMAX (Invitrogen, USA) and DMEM high glucose (Invitrogen, USA), respectively. Media were supplemented with 10% heat-inactivated fetal bovine serum and 1% penicillin-streptomycin (both from Invitrogen, USA). Cells were continuously monitored by microscopy to ensure they maintained their original morphology. Where appropriate, BC cells were harvested by incubation in 0.25% Trypsin-EDTA (Invitrogen, USA), washed with PBS and labeled with 12.5 μM calcein-AM (Sigma Aldrich, USA) according to the manufacturer's instructions.

Isolation of Human PBMCs

Peripheral blood (3 mL) was collected from healthy blood donors after informed consent, layered over histopaque-1077 (Sigma-Aldrich, USA) and centrifuged at room temperature for 10 min at 650 g, without active break. Peripheral blood mononuclear cells (PBMCs) were then gently collected from the gradient interface, washed twice and resuspended in PBS supplemented with 2% bovine serum albumin (BSA, Sigma-Aldrich, USA). Cell viability and concentration were determined using the Tuerk solution (Sigma-Aldrich, USA).

Collection and Processing of Patient Samples

BC patients were enrolled at the Urology department of Hospital da Senhora da Oliveira, Guimarães, Portugal ($n = 8$) and Hospital Universitario 12 de Ocubre, Madrid, Spain ($n = 6$). Voided urine samples (30–50 mL) from 14 patients were collected prior to transurethral resection of bladder tumor (TURBT). Bladder wash samples (10–30 mL) were obtained after flushing the bladder with saline buffer immediately before TURBT. **Table 1** summarizes clinicopathological information obtained from the patients' clinical records. Biological samples were processed within 3 h upon collection, being centrifuged at 1,200 rpm for 5 min and washed twice in PBS. Pellets were then resuspended in 500 μL of PBS-2%BSA for immediate microfluidic analysis or frozen at −80°C for later analysis. As a normal control group, voided urine samples ($n = 6$) from healthy subjects were obtained and subjected to the same protocol. Formalin-fixed paraffin-embedded (FFPE) tumor tissue sections were also included in the study. All procedures were performed after patient informed consent and approval by the Ethics Committee of both hospitals.

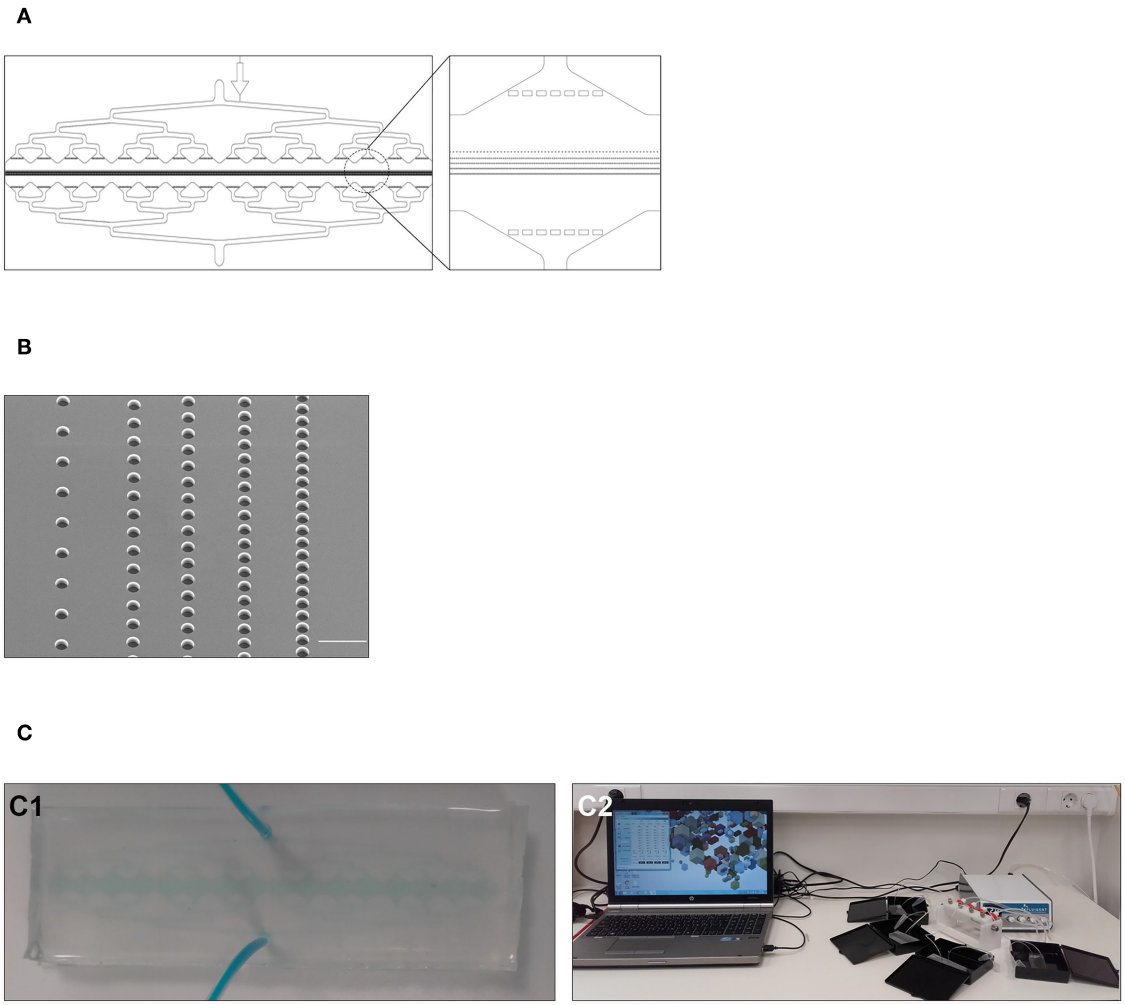

FIGURE 2 | Design and fabrication of the UriChip. **(A)** AutoCAD design of the UriChip. Design includes a circular inlet and outlet, square posts for structural support of the channels, pre-filtering system to prevent debris and large cell clusters, and five row of posts with increasingly narrower gap widths (50, 20, 15, 10, and 5 μm) to separate cells according to their size and deformability. **(B)** Scanning electron microscopy (SEM) image of the five rows of gaps in the master that will give rise to the posts of the UriChip. Scale bar, 100 μm. **(C1)** UriChip after fabrication with PDMS. **(C2)** Experimental setup for simultaneous analysis of four independent samples.

Analysis of Cell Entrapment in the UriChip Devices

HT1376 cells (1,000 cells in 500 μL of PBS) previously labeled with calcein-AM were injected into the UriChip microfluidic devices at two different inlet pressures (200 and 300 mbar) with the help of a pressure pump. Trapped cells were then fixed with 4% (w/v) formaldehyde solution (Sigma-Aldrich, USA) during 20 min and finally washed with PBS. Capture efficiency (CE) of HT1376 cells was determined by imaging and counting the number of calcein-AM-positive cells captured and comparing with the total input.

$$\text{CE}\ (\%) = (\text{captured HT1376 cells})/(\text{total input HT1376 cells}) \times 100$$

To determine cancer cell capture purity in the presence of leucocytes (which may be found in the urine due to cancer associated inflammation), calcein-AM-stained HT1376 cells were next spiked in 500 μL of PBS containing unlabeled PBMCs at a 1:10 ratio, run at 200 mbar and fixed with 4% (w/v) formaldehyde solution as described above. Cell purity and PBMC retention were determined according the following formulas:

$$\text{Purity}\ (\%) = [(\text{captured HT1376 cells})/(\text{captured HT1376 cells} + \text{captured PBMCs})] \times 100$$

$$\text{PBMC retention}\ (\%) = (\text{captured PBMCs})/(\text{total input PBMCs}) \times 100$$

Similarly, to evaluate the efficiency of isolating cancer cells from voided urine, MCR-STn cells were pre-stained with calcein-AM for 30 min at 37°C, spiked in 500 μL of PBS-2%BSA containing urine sediment from healthy subjects and run at 200 mbar. Cells were then fixed with 4% (w/v) formaldehyde solution and finally washed with PBS. The number of calcein-AM-positive MCR-STn cells captured in the device was compared to the total number of MCR-STn cells spiked, and CE determined.

TABLE 1 | Clinicopathological features of patients included in this study.

Patient variable	BC patient (%)
N	14
Invasiveness	
NMIBC	11 (78.57%)
MIBC	3 (21.43%)
Grading	
Low grade	11 (78.57%)
High grade	3 (21.43%)

NMIBC, non-muscle invasive bladder cancer; MIBC, muscle invasive bladder cancer; BC, bladder cancer.

Immunofluorescence Cell Staining and Detection

Patient samples (processed bladder washes or voided urine) were resuspended in PBS-2%BSA and injected into the chips at 200 mbar. After a 30 min incubation period with no flow to reduce unspecific binding, cells were fixed with 4% (w/v) formaldehyde for 20 min and further treated with 0.25% Triton X-100 in PBS for 5 min to induce cellular permeability. Subsequently, two washes with PBS were performed and mouse monoclonal anti-CK pan-FITC antibody (1:100 Clone C-11) and DAPI (1:1,000, both from Sigma-Aldrich, USA) diluted in PBS-2%BSA were loaded into the UriChips for 1 h in the dark. The immunostaining process ended by washing with PBS before imaging, with the flow rate set at 200 mbar during the entire procedure. Where appropriate, cells were also immunostained using the anti-STn mouse monoclonal antibody clone B72.3 (0.25 μg/mL in PBS-2%BSA, Abcam, UK) for 1 h and 30 min at room temperature, and labeled with a secondary goat anti-mouse IgG-TRITC antibody (1:1,000 in PBS-2%BSA, ThermoFisher Scientific, USA) for one additional hour, prior to cell fixation and permeabilization. Following sample processing, a fluorescence microscopy analysis of the captured cells was performed under an inverted fluorescence microscope (Ti-E, Nikon, Spain). A total of twenty-five fields (20x) per device were selected randomly and the number of captured cells counted. Only DAPI and STn-positive cells with identifiable cellular morphology and well-delimited cytoplasm were considered for cell enumeration, and count normalized to the total number of DAPI-positive cells.

Tissue Immunohistochemistry

FFPE tissue sections from patients with BC were screened for STn staining using the streptavidin/biotin peroxidase method with the anti-STn antibody, as previously described (29).

Neuraminidase Treatment

Samples were incubated with *Clostridium perfringens* neuraminidase (0.1 unit/mL, Sigma-Aldrich, USA) for 2 h at 37°C to cleave terminal sialic acid residues from glycoproteins on cell surfaces. The reaction was stopped with PBS washes.

Statistical Analysis

Statistical analysis was performed using GraphPad Prism, version 5 (GrapPad Software, Inc., La Jola, CA, USA). Data is presented as mean ± SD. Deviation from normality was tested using the D'Agostino and Pearson normality test. The Mann-Whitney test was used for unpaired samples and differences were considered to be significant when $p < 0.05$ ($^{*}p < 0.05$; $^{**}p < 0.01$; $^{***}p < 0.001$).

RESULTS

UriChip Performance With BC Cell Lines

The performance of the microfluidic device to capture BC cells was firstly investigated using HT1376 BC cells as a model, pre-stained with calcein-AM and spiked in PBS. As illustrated in **Figure 3A**, cells captured inside the chip were morphologically intact and remained mostly trapped in the rows of posts with 15–10 μm spacing, in agreement with their average cell size (15.5 μm, **Figure S1A**), and their higher ability to deform as compared to non-malignant counterparts (40).

To avoid the risk of device leaking and ensure the proper and intact morphology of urothelial exfoliated cells during the microfluidic capture, 300 mbar of inlet pressure was applied in the UriChip. On the other hand, to prevent squeezing of urothelial cells through the microposts under pressure and consequently their loss to the outlet, the minimum inlet pressure of 200 mbar was tested. By working on the range of 200–300 mbar, results revealed a higher CE of HT1376 cells at 200 mbar when compared to 300 mbar input pressure (**Figure 3B**). This result can be explained by increased hydrodynamic forces acting on the post-trapped cells at higher pressure values, causing cell loss. Hence, in all subsequent experiments the inlet pressure was set to 200 mbar.

Given that the urine of BC patients is heterogeneous and usually contains leucocytes due to cancer associated inflammation, we next investigated the CE of HT1376 cells pre-stained with calcein-AM in the presence of non-labeled PBMCs isolated from healthy donors, spiked in PBS. PBMC population comprises lymphocytes and monocytes that range between 7 and 15 μm in diameter with a high deformability capacity (41). Notably, CE of HT1376 cells increased up to 50% in comparison to single cell population suspensions, while PBMC retention was minimal (**Figure 3C**). In fact, a PBMC depletion of 96.1% was observed, hence maintaining high sample purity (62%).

Capture and Analysis of Human Urothelial Exfoliated Cells in the UriChip

Having confirmed the ability of the UriChip to isolate BC cells in single and mixed model samples, we further evaluated its potential for the capture and analysis of cells from clinical samples, known to be much more complex and heterogeneous. As such, we analyzed both bladder wash samples, which are highly cellular and contain well-preserved cells (42), as well as voided urine from BC patients and compared them to voided urine from healthy subjects. As expected, several types of urothelial exfoliated cells with distinct morphological features were observed either in healthy controls and patient

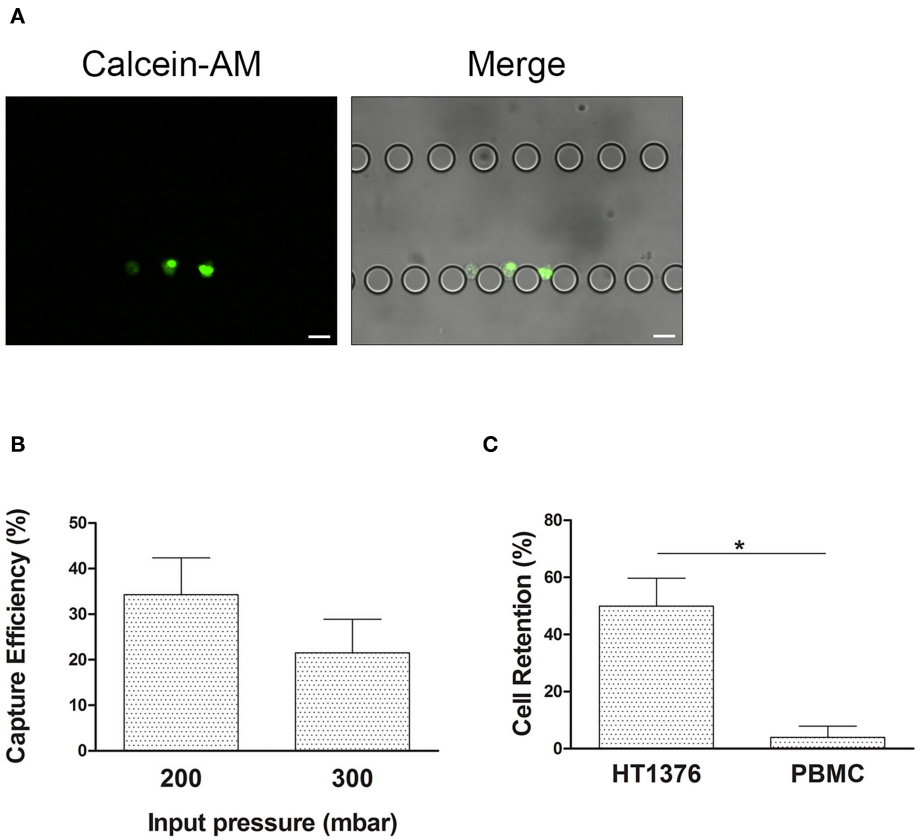

FIGURE 3 | UriChip performance with HT1376 bladder cancer cells. **(A)** HT1376 cells (pre-stained with calcein-AM) captured in the UriChip and visualized by fluorescence microscopy. Scale bar, 20 μm. **(B)** Capture efficiency (CE) of HT1376 cancer cells spiked in PBS and run at 200 and 300 mbar. **(C)** CE of HT1376 cells spiked in PBS solution containing PBMCs at 200 mbar input pressure (50%). Results are described as Mean ± S.D. of three independent experiments. * indicates statistical significance ($p < 0.05$).

samples (**Figure 4A**). Indeed, the urothelium is composed of multiple epithelial cell layers, namely basal, intermediate and umbrella cells (43, 44). Basal cells, which localize on the basal membrane of the bladder lining, are smaller (∼10 μm in diameter), mononucleated, and cuboidal-rounded shape (**Figure 4A1**). Intermediate cells are pyriform in shape, 10–25 μm in diameter, and constitute the majority of the urothelium (**Figure 4A2**). Umbrella cells, the most superficial cells of the bladder lining, display a very large cytoplasm (25–250 μm in diameter), large and rounded nucleus sometimes bi- or multinucleated, as well as prominent nucleoli (**Figure 4A3**) (45). In addition, in patient samples, we also identified cells with increased nuclear/cytoplasmic (N/C) ratio, irregular nuclear borders and irregular chromatin patterns. Cells were found either isolated or in clusters, exhibiting various shapes and sizes, including CMV-like atypical cells with an "eye-bird" appearance (**Figure 4A4**); cells with enlarged nucleus or multinucleated (**Figures 4A5,6**), clusters of atypical cells (**Figure 4A7**), spindle-like cells (**Figure 4A8**), and granular membrane atypical cells (**Figure 4A9**), as previously reported (46–48). We further evaluated the shape deformation of captured urothelial exfoliated cells as they squeeze through the posts of the UriChip. Large captured cells from healthy controls mostly localized within upper rows of posts (≥20 gap width), while similar sized cells from BC patients were able to deform more and squeeze through narrower posts (**Figure 4A10**). These observations are supported by the fact that malignant urothelial cells from voided urine present reduced cell stiffness as compared to their healthy counterparts (47).

Cytokeratins are highly expressed in intermediate filaments of normal and neoplastic epithelial cells (49). Hence, to validate the epithelial profile of captured cells from both healthy controls and BC patients, an on-chip immunoassay was performed using a pan-CK-FITC antibody. As illustrated in **Figure 4B**, the majority of the cells trapped inside the microfluidic device were nucleated and positive for cytokeratin expression, particularly in samples from healthy donors.

These results highlight the potential of the UriChip to retain cells of different sizes and shapes from voided urine, using a label-free approach. Moreover, morphological analysis of captured cells can be performed, and phenotypic characteristics identified via *in situ* immunofluorescence.

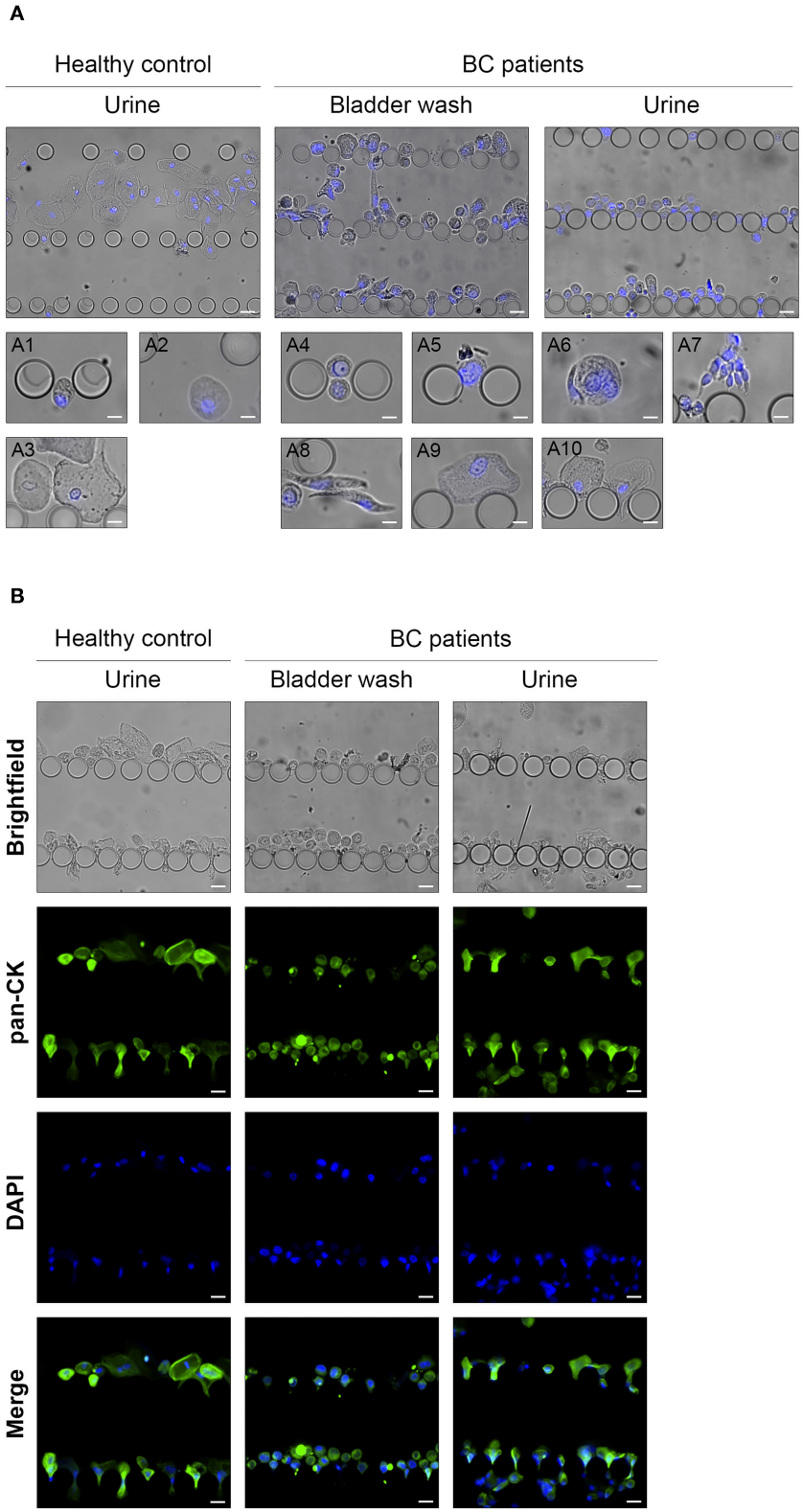

FIGURE 4 | Analysis of UriChip-captured urothelial exfoliated cells from biological samples. **(A)** Microscopy images showing different types of urothelial exfoliated cells from human voided urine and bladder washes retained along the UriChip and stained for the nuclear marker DAPI (blue): (**A1)** basal cell, **(A2)** intermediate cells, **(A3)** umbrella cells, (**A4)** CMV-like cell, **(A5)** cell with a large nucleus, **(A6)** multinucleated cells, **(A7)** cell clusters, **(A8)** spindle-shaped cells, **(A9)** membrane garrulous cells, **(A10)** cell deformability capacity. **(B)** Isolated cells trapped between pillars of the UriChip were stained *in situ* with the anti-pan cytokeratin-FITC antibody (green) and the nuclear marker DAPI (blue). Scale bar, 20 μm.

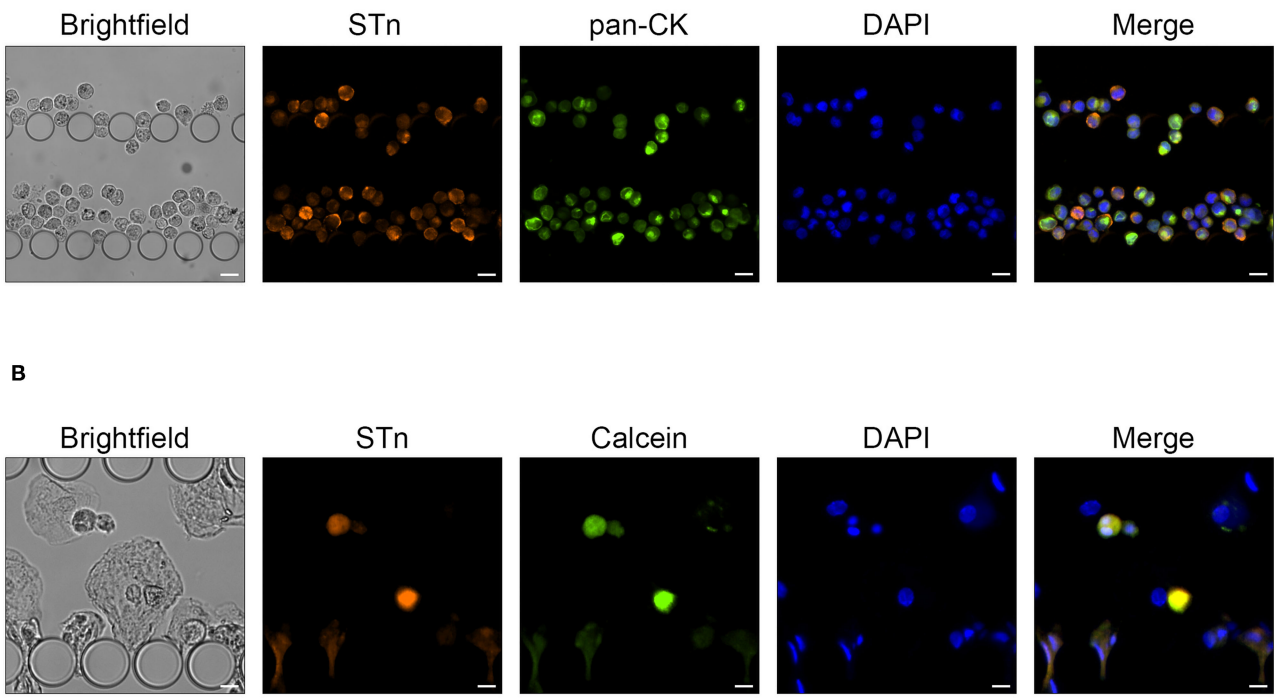

FIGURE 5 | MCR-STn bladder cancer cells captured in the UriChip. **(A)** Immunofluorescence analysis showing the pattern of STn (orange) and pan-CK (green) expression in UriChip-captured MCR-STn cells. STn is mostly expressed at the cell membrane and cytoplasm of cancer cells. Cell nuclei were stained with DAPI (blue). Scale bar, 25 μm. **(B)** MCR-STn cells pre-labeled with calcein-AM (green) spiked in urine from healthy controls. Cell nuclei were stained with DAPI (blue). A capture efficiency of 53% was achieved. Scale bar, 15 μm.

Rigorous Identification of Urothelial ETCs in Clinical Samples

In order to accurately identify urothelial ETCs and distinguish them from benign ones, we selected STn, a tumor associated antigen overexpressed in BC but absent in the healthy urothelium, as malignant biomarker (36). Indeed, STn has been directly associated with BC progression, metastatic potential of neoplastic cells, and decreased overall survival (28, 36). More importantly, we recently reported STn expression in microfluidic-isolated CTCs from BC patients (28, 29). For optimization purposes, we firstly used the invasive BC cell line MCR overexpressing STn antigen (MCR-STn), since STn levels in various non-transduced BC cells lines, including HT1376, are negligible (data not shown) (36). **Figure 5A** shows morphologically intact MCR-STn cells retained within UriChip and expressing high levels of STn mostly at the cell membrane but also intracellularly. Neuraminidase treatment confirmed STn labeling specificity, since after enzymatic release of STn no signal could be detected in captured cells (**Figure S2A**). Furthermore, MCR-STn cells were also immunostained for CK and found to be positive, corroborating their epithelial nature and further validating this dual marker microfluidic immunoassay (**Figure 5A**).

STn expression enhances the migration and invasive capacity of MCR cells (36), which are larger (average cell size of 20 μm) than HT1376 (**Figure S1B**). In addition, cancer cells become more deformable as they become more invasive. Hence, considering that UriChip captures cells based on their size and deformability, we next reassessed its performance, in even more complex and heterogeneous samples such as urine. For that purpose, MCR-STn cells were pre-labeled with calcein-AM, spiked in voided urine from healthy donors, and stained for STn antigen (**Figure 5B**). To perform an accurate quantification of the BC cells trapped within the UriChip and rule out possible variations of STn expression levels on MCR-STn cells, the number of calcein and DAPI-positive cells was compared with the total number of MCR-STn cells spiked. Remarkably, the CE was found to be very similar (53%) to that achieved when using HT1376 spiked in PBMCs, demonstrating the good consistency of the UriChip for biological and heterogeneous samples.

STn Expression of Urothelial Exfoliated Cells Correlates With Tumor Invasiveness and Grade

We next moved to the pre-clinical testing of the UriChip using both bladder washes and fresh voided urine from BC patients and a combination of two biomarkers, STn and CK

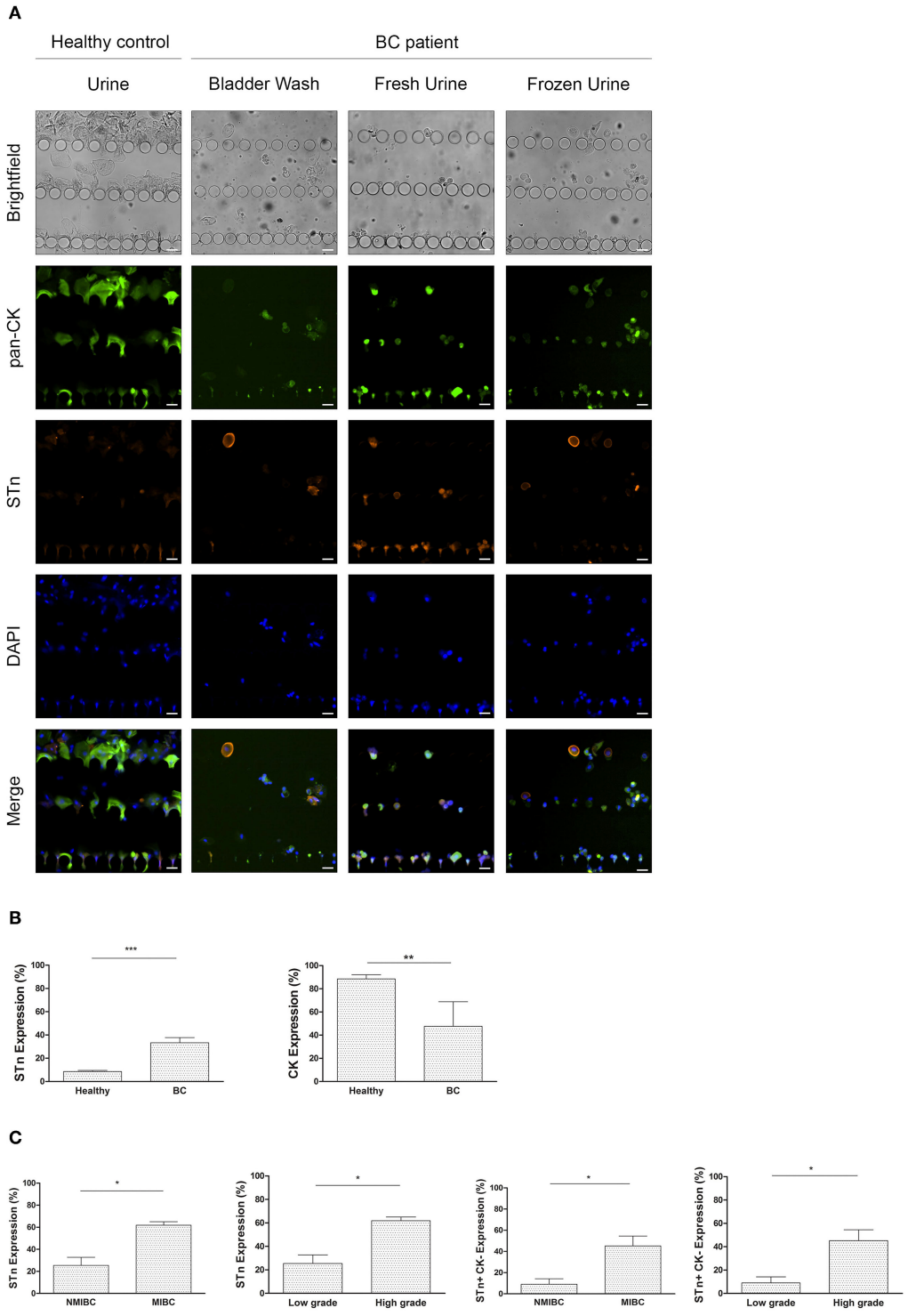

FIGURE 6 | STn expression in bladder urothelial ETC isolated by the UriChip. **(A)** Immunofluorescence staining pattern of urothelial exfoliated cells captured in the UriChip from healthy controls and BC patient samples, namely bladder washes and voided urine, subjected or not to cryopreservation. Cells were probed for STn antigen (orange), pan-CK (green), and DAPI (blue). ETCs were identified according to the following criteria: DAPI-positive, STn-positive, and pan-CK-positive or negative. Scale bar, 20 μm. **(B)** Percentage of STn and pan-CK-positive cells in BC patients vs. healthy controls. As expected, expression of STn is significantly higher in BC (33.28%) compared with healthy controls (8.57%). $p = 0.0006$. In contrast, CK expression decreases significantly in BC (from 8.55% in healthy controls to 47.62% in BC). $p = 0.0015$. **(C)** Correlation of STn-positive and STn-positive/CK-negative cell count with tumor invasiveness and grade. Capture of STn-positive cells and STn-positive/CK-negative cells in the UriChip are significantly higher in muscle invasive BC and high grade bladder tumors ($p = 0.0127$). Statistical significance $^{*}p < 0.05$, $^{**}p < 0.01$, $^{***}p < 0.001$.

to detect malignant cells. Of note, we extended this analysis and evaluated UriChip and STn/CK immunoassay feasibility to detect cells from cryopreserved samples, greatly relevant for retrospective studies. **Figure 6A** depicts representative images obtained for each condition tested and shows enhanced STn expression in cells from BC patients as compared to healthy controls. STn labeling was found to be specific as confirmed by the loss of signal upon sample treatment with neuraminidase (**Figure S2B**). Moreover, STn expression in corresponding tissue sections was evaluated and found to be lower in low-grade NMIBC in comparison to high-grade lesions (**Figure S3**), while absent in the normal urothelium, in accordance with previous reports (28, 36). CK-positive cells were also found in all samples tested, characteristic of their epithelial origin. Remarkably, results also demonstrated that it was possible to successfully entrap urothelial cells subjected to cryopreservation, which retained the morphologic features and the immunophenotypic markers observed in non-preserved samples (**Figure 6A**). A quantitative analysis of the captured cells from all fresh and cryopreserved urine samples from BC patients was then performed, revealing that patient urothelial exfoliated cells express significantly higher levels of STn compared to healthy controls (**Figure 6B**). On the other hand, a significant reduction in the number of CK-positive cells from BC patients was detected (**Figure 6B**) suggesting a distinct state of differentiation of these epithelial cells. More importantly, we found significant correlations between STn expression and tumor stage and grade, with STn-positive cells decreasing CK expression with higher grade and stage (**Figure 6C**).

DISCUSSION

The working principle of UriChip device is based on size-exclusion and cell deformability, which allows for the capture and characterization of urothelial ETCs. In fact, urothelial ETCs, which are shed directly by the growing tumor in the bladder, are known to reflect disease progression (24) and for this reason, they have been widely used as a diagnostic marker in urine cytology. However, the standard diagnostic techniques, are limited considering the requirements for early-cancer diagnosis (1, 50). UriChip has revealed to be a simple and easy-to-use microfluidic device with easy fabrication and cost-effective procedure having the potential to be produced on an industrial scale and thus applied for clinical detection in low-resource settings. Urothelial exfoliated cells of various sizes and intact cellular morphology are efficiently harvested by UriChip from large volumes of patient samples. In addition, the design of five rows of posts with increasingly narrower gap widths enables to handle a wide range of urothelial exfoliated cells, both single and clustered, to be captured and characterized by immunoassays. In addition, the spatially square posts incorporated prevent the built-up of cellular and non-cellular debris and the damage of trapped cells.

Optimization tests were conducted with two distinct BC cell models, prior to the analysis of clinical samples: bladder washes, which contain well-preserved cells when collected before TURBT (42), and voided urine from BC patients, both frequently used for cytological assessment with equivalent results (51, 52). Patient body fluids were then compared to voided urine from healthy subjects. By using a multi-channel pressure controller, which compensates the increase of flow resistance caused by the numerous components of the urine, we were able to efficiently process four independent samples in parallel without rupture or leakage of the system. A few additional studies have also exploited microfluidic chips for urinary cell-based BC detection. However, these involved intricate equipment (31), long incubation periods for surface functionalization and immune affinity selection (34) or lacked clinical validation (32).

Spiking experiments demonstrated that, using the UriChip, the CE of BC cells spiked in leukocytes and urine from healthy donors achieved 53%, typical for size-based filtration (53, 54). Higher efficiencies have recently been reported by Cheng et al., using a size-based microfluidic system, but with less complex model samples, i.e., with BC cells diluted in PBS which do not fully represent the cellular heterogeneity of biological samples (33). Accordingly, cells with different sizes and morphologies were found to be retained in the UriChip, with those originating from BC patients exhibiting higher shape deformation capacity and squeezing though narrower gaps in comparison to similar sized urothelial cells from urine of healthy donors. Consistent with our observations, previous reports using microfluidics and other methodologies confirmed the reduced stiffness of bladder and other cancerous cells compared to their non-malignant counterparts (47, 55–57).

In addition, we phenotypically characterized captured cells *in situ*, via a microfluidic immunoassay involving the epithelial marker, pan-CK, and the tumor-associated glycan, STn. On-chip immunostaining of CTCs isolated from blood samples by microfluidics with distinct biomarkers has been extensively performed (27, 58), and has also been tested with BC urothelial exfoliated cells with good detection accuracy (33), which demonstrates the potential of this approach for effective screening and diagnosis of BC. Based on our previous work showing that more than 90% of BC CTCs captured by a size-based microfluidic device were STn positive (28, 29), we explored the expression of STn in exfoliated cells present in voided urine. Importantly, this antigen is overexpressed in primary bladder tumors, lymph nodes, and distant metastasis, while absent or marginally present on normal urothelium (28, 36), and correlates with decreased overall survival (28). Moreover, STn has been directly associated with a more aggressive phenotype of tumor cells, conferring an invasive potential (59–61). Notably, we found, for the first time, significant high levels of STn in captured urothelial exfoliated cells from voided urine of BC patients. STn expression in corresponding primary tumors was also evaluated in all patients tested and found to be positive. Additionally, STn expression in urinary BC cells significantly correlated with tumor grade and invasiveness, in agreement with STn expression pattern in the tissue, further supporting previously reported findings (28, 29). Notably, a detailed analysis of the STn-positive cell population revealed that these cells display lower levels of CK, indicative of a more mesenchymal-like phenotype. This was

particularly evident in more advanced grade tumors, supportive of STn association with tumor aggressiveness. These results suggest that throughout BC progression, urothelial cells undergo an epithelial to mesenchymal transition, with increased potential to invade. Accordingly, we have previously reported that the percentage of CTCs expressing STn was three times higher than those expressing the epithelial marker EpCAM (29), thus linking STn to tumor progression and dissemination.

Parallel to the analysis of fresh clinical samples, we also evaluated cryopreserved patient samples in the UriChip. Results showed that cryopreserved BC cells were successfully isolated and maintained the morphologic features and phenotypic markers, evidencing the versatility of this low-cost system and its feasibility for multi-centric and retrospective analysis on archived samples. To the best of our knowledge, this is the first study evaluating cryopreserved urine sediments by microfluidics. Yet, a large-scale clinical trial is needed to validate the device, particularly for clinical implementation. Proper external regulatory approval would be also necessary. Increasing the cohort of patients with BC (from different grades and stages) will enable to assess the detection accuracy of UriChip. Additionally, further studies by combining UriChip immunoassay with traditional cytology and comparing with commercial available FDA-approved markers are warranted to validate the present findings. Furthermore, the capture and enrichment of intact urothelial exfoliated cells within UriChip provide the opportunity for downstream on-chip proteomic and off-chip single-cell genomic analyses for a precise diagnosis of BC.

Overall, UriChip microfluidic-based platform is able to efficiently capture and enrich urothelial exfoliated cells, from both fresh and frozen voided urine of BC patients, according to their size and deformability. Notably, STn expression in ETCs from patients from two independent data sets was demonstrated herein for the first time, which correlated with staging and grading of BC.

Combination with high-throughput processing and automation may constitute a first step toward a fully integrated system for rapid label-free capture, on-chip phenotypic characterization and enumeration of BC cells. In addition, exploring glycosylation of tumor cells in body fluids, namely STn expression, will offer a more selective malignant cell isolation, paving the way to downstream molecular analysis and fostering precision medicine applications in bladder cancer and other malignancies.

DATA AVAILABILITY STATEMENT

All datasets generated for this study are included in the article/**Supplementary Material**.

ETHICS STATEMENT

The studies involving human participants were reviewed and approved by the ethics committee of Hospital Senhora da Oliveira, Guimarães, Portugal. The patients/participants provided their written informed consent to participate in this study.

AUTHOR CONTRIBUTIONS

SC was responsible for the study design, patient samples processing, analytical measurements *in vitro*, data analysis, and manuscript writing. CA and LD were responsible for the design and fabrication of the UriChip microfluidic device and evaluation of its performance. DF performed tissue immunohistochemistry experiments. RR, VG, and MD selected and collected patient samples. LL, JF, LS, MM-F, MD, CS-C, JP, and PF contributed to the interpretation of the experimental data. MO was responsible for the project conception, study design, data interpretation, and manuscript writing. All authors discussed the results and commented on the manuscript.

ACKNOWLEDGMENTS

The authors would like to thank the patients participating in this study for providing samples and Professor Paula Videira (FCT-UNL, Portugal) for kindly providing the MCR-STn cell model used in this study. We wish to thank our funding source for this research, the Cancer: Advancing Cancer Research: From Basic Knowledge to Application (NORTE-01-0145-FEDER-000029), supported by the Norte Regional Operational Programme (NORTE2020), under the PORTUGAL 2020 Partnership Agreement, through the European Regional Development Fund (ERDF), partially by funds from Fondo Europeo de Desarrollo Regional (FEDER), by grants from the Spanish Government CB/16/00228, from Instituto de Salud Carlos III, and by funds from Fundação para a Ciência e Tecnologia (FCT) (POCI-01-0145-FEDER-031442-InNPeC, CEECIND/ 03186/2017 and PEst-OE/SAU/UI0776/201). FCT is co-financed by European Social Fund (ESF) under Human Potential Operation Programme (POPH) from National Strategic Reference Framework (NSRF).

SUPPLEMENTARY MATERIAL

The Supplementary Material for this article can be found online at: https://www.frontiersin.org/articles/10.3389/fonc.2020.01774/full#supplementary-material

REFERENCES

1. Kamat AM, Hahn NM, Efstathiou JA, Lerner SP, Malmström P-U, Choi W, et al. Bladder cancer. *Lancet.* (2016) 388:2796–810. doi: 10.1016/S0140-6736(16)30512-8
2. Antoni S, Ferlay J, Soerjomataram I, Znaor A, Jemal A, Bray F. Bladder cancer incidence and mortality: a global overview and recent trends. *Eur Urol.* (2017) 71:96–108. doi: 10.1016/j.eururo.2016.06.010
3. Ferlay J, Soerjomataram I, Ervik M, Dikshit R, Eser S, Mathers C, et al. *GLOBOCAN 2012v1.0, Cancer Incidence and Mortality Worldwide.* IARC Cancer Base No. 11. Lyon: International Agency for Research on Cancer (2013).
4. Kołodziej A, Krajewski W, Matuszewski M, Tupikowski K. Review of current optical diagnostic techniques for non-muscle-invasive bladder cancer. *Central Eur J Urol.* (2016) 69:150–6. doi: 10.5173/ceju.2016.780

5. Lotan Y, Roehrborn CG. Sensitivity and specificity of commonly available bladder tumor markers versus cytology: results of a comprehensive literature review and meta-analyses. *Urology.* (2003) 61:109–18. doi: 10.1016/S0090-4295(02)02136-2
6. Karakiewicz PI, Benayoun S, Zippe C, LÜDecke G, Boman H, Sanchez-Carbayo M, et al. Institutional variability in the accuracy of urinary cytology for predicting recurrence of transitional cell carcinoma of the bladder. *BJU Int.* (2006) 97:997–1001. doi: 10.1111/j.1464-410X.2006.06036.x
7. Reid MD, Osunkoya AO, Siddiqui MT, Looney SW. Accuracy of grading of urothelial carcinoma on urine cytology: an analysis of interobserver and intraobserver agreement. *Int J Clin Exp Pathol.* (2012) 5:882–91.
8. Siddiqui MR, Grant C, Sanford T, Agarwal PK. Current clinical trials in non-muscle invasive bladder cancer. *Urol Oncol.* (2017) 35:516–27. doi: 10.1016/j.urolonc.2017.06.043
9. Rayn KN, Hale GR, Grave GP-L, Agarwal PK. New therapies in nonmuscle invasive bladder cancer treatment. *Indian J Urol.* (2018) 34:11–9. doi: 10.4103/iju.IJU_296_17
10. Zieger K, Wolf H, Olsen PR, Højgaard K. Long-term follow-up of noninvasive bladder tumours(stage Ta): recurrence and progression. *BJU Int.* (2000) 85:824–8. doi: 10.1046/j.1464-410x.2000.00547.x
11. Olivier Bosset P, Neuzillet Y, Paoletti X, Molinie V, Botto H, Lebret T. Long-term follow-up of TaG1 non–muscle-invasive bladder cancer. *Urol Oncol Semin Orig Investig.* (2015) 33:20.e21–7. doi: 10.1016/j.urolonc.2014.09.001
12. Sloan FA, Yashkin AP, Akushevich I, Inman BA. The cost to medicare of bladder cancer care. *Eur Urol Oncol.* (2020) 3:515–22. doi: 10.1016/j.euo.2019.01.015
13. Svatek RS, Hollenbeck BK, Holmäng S, Lee R, Kim SP, Stenzl A, et al. The economics of bladder cancer: costs and considerations of caring for this disease. *Eur Urol.* (2014) 66:253–62. doi: 10.1016/j.eururo.2014.01.006
14. Villicana P, Whiting B, Goodison S, Rosser CJ. Urine-based assays for the detection of bladder cancer. *Biomark Med.* (2009) 3:265. doi: 10.2217/bmm.09.23
15. Leiblich A. Recent developments in the search for urinary biomarkers in bladder cancer. *Curr Urol Rep.* (2017) 18:100. doi: 10.1007/s11934-017-0748-x
16. Tan WS, Tan WP, Tan M-Y, Khetrapal P, Dong L, deWinter P, et al. Novel urinary biomarkers for the detection of bladder cancer: a systematic review. *Cancer Treat Rev.* (2018) 69:39–52. doi: 10.1016/j.ctrv.2018.05.012
17. Hajdinjak T. UroVysion FISH test for detecting urothelial cancers: meta-analysis of diagnostic accuracy and comparison with urinary cytology testing. *Urol Oncol Semin Orig Investig.* (2008) 26:646–51. doi: 10.1016/j.urolonc.2007.06.002
18. Chou R, Gore JL, Buckley D, Fu R, Gustafson K, Griffin JC, et al. Urinary biomarkers for diagnosis of bladder cancer: a systematic review and meta-analysisurinary biomarkers for diagnosis of bladder cancer. *Ann Int Med.* (2015) 163:922–31. doi: 10.7326/M15-0997
19. Sarosdy MF, Hudson MLA, Ellis WJ, Soloway MS, White Rd, Sheinfeld J, et al. Improved detection of recurrent bladder cancer using the bard bta stat test. *Urology.* (1997) 50:349–53. doi: 10.1016/S0090-4295(97)00292-6
20. Landman J, Chang Y, Kavaler E, Droller MJ, Liu BCS. Sensitivity and specificity of NMP-22, telomerase, and BTA in the detection of human bladder cancer. *Urology.* (1998) 52:398–402. doi: 10.1016/S0090-4295(98)00219-2
21. Malkowicz SB. The application of human complement factor H-related protein (bta trak) in monitoring patients with bladder cancer. *Urol Clin North Am.* (2000) 27:63–73. doi: 10.1016/S0094-0143(05)70235-4
22. Chiu DT, deMello AJ, Di Carlo D, Doyle PS, Hansen C, Maceiczyk RM, et al. Small but perfectly formed? successes, challenges, and opportunities for microfluidics in the chemical and biological sciences. *Chem.* (2017) 2:201–23. doi: 10.1016/j.chempr.2017.01.009
23. Han SJ, Park H-K, Kim KS. Applications of microfluidic devices for urology. *Int Neurourol J.* (2017) 21:S4–9. doi: 10.5213/inj.1734838.419
24. Streets AM, Huang Y. Chip in a lab: microfluidics for next generation life science research. *Biomicrofluidics.* (2013) 7:011302. doi: 10.1063/1.4789751
25. Nagrath S, Sequist LV, Maheswaran S, Bell DW, Irimia D, Ulkus L, et al. Isolation of rare circulating tumour cells in cancer patients by microchip technology. *Nature.* (2007) 450:1235–9. doi: 10.1038/nature06385
26. Kulasinghe A, Wu H, Punyadeera C, Warkiani ME. The use of microfluidic technology for cancer applications and liquid biopsy. *Micromachines.* (2018) 9:397. doi: 10.3390/mi9080397
27. Sun Y, Haglund TA, Rogers AJ, Ghanim AF, Sethu P. Review: microfluidics technologies for blood-based cancer liquid biopsies. *Anal Chim Acta.* (2018) 1012:10–29. doi: 10.1016/j.aca.2017.12.050
28. Lima L, Neves M, Oliveira MI, Dieguez L, Freitas R, Azevedo R, et al. Sialyl-Tn identifies muscle-invasive bladder cancer basal and luminal subtypes facing decreased survival, being expressed by circulating tumor cells and metastases. *Urol Oncol Semin Orig Investig.* (2017) 35:675. doi: 10.1016/j.urolonc.2017.08.012
29. Neves M, Azevedo R, Lima L, Oliveira MI, Peixoto A, Ferreira D, et al. Exploring sialyl-Tn expression in microfluidic-isolated circulating tumour cells: a novel biomarker and an analytical tool for precision oncology applications. *New Biotechnol.* (2019) 49:77–87. doi: 10.1016/j.nbt.2018.09.004
30. Alva A, Friedlander T, Clark M, Huebner T, Daignault S, Hussain M, et al. Circulating tumor cells as potential biomarkers in bladder cancer. *J Urol.* (2015) 194:790–8. doi: 10.1016/j.juro.2015.02.2951
31. Hirai Y, Takagi D, Anai S, Chihara Y, Tsuchiya T, Fujimoto K, et al. ALA-induced fluorescence detection with photoresist-based microfluidic cell sorter for bladder cancer diagnosis. *Sensors Actuators B Chem.* (2015) 213:547–57. doi: 10.1016/j.snb.2015.01.118
32. Hosseini SA, Zanganeh S, Akbarnejad E, Salehi F, Abdolahad M. Microfluidic device for label-free quantitation and distinction of bladder cancer cells from the blood cells using micro machined silicon based electrical approach; suitable in urinalysis assays. *J Pharm Biomed Anal.* (2017) 134:36–42. doi: 10.1016/j.jpba.2016.11.026
33. Chen A, Fu G, Xu Z, Sun Y, Chen X, Cheng KS, et al. Detection of urothelial bladder carcinoma via microfluidic immunoassay and single-cell DNA copy-number alteration analysis of captured urinary-exfoliated tumor cells. *Cancer Res.* (2018) 78:4073. doi: 10.1158/0008-5472.CAN-17-2615
34. Geng C, Li C, Li W, Yan W, Li J, Aziz AUR, et al. A simple fabricated microfluidic chip for urine sample-based bladder cancer detection. *J Micromech Microeng.* (2018) 28:115011. doi: 10.1088/1361-6439/aae016
35. Critelli R, Fasanelli F, Oderda M, Polidoro S, Assumma MB, Viberti C, et al. Detection of multiple mutations in urinary exfoliated cells from male bladder cancer patients at diagnosis and during follow-up. *Oncotarget.* (2016) 7:67435–48. doi: 10.18632/oncotarget.11883
36. Ferreira JA, Videira PA, Lima L, Pereira S, Silva M, Carrascal M, et al. Overexpression of tumour-associated carbohydrate antigen sialyl-Tn in advanced bladder tumours. *Mol Oncol.* (2013) 7:719–31. doi: 10.1016/j.molonc.2013.03.001
37. Sullivan PS, Chan JB, Levin MR, Rao J. Urine cytology and adjunct markers for detection and surveillance of bladder cancer. *Am J Transl Res.* (2010) 2:412–40.
38. Andersson E, Dahmcke CM, Steven K, Larsen LK, Guldberg P. Filtration device for on-site collection, storage and shipment of cells from urine and its application to DNA-based detection of bladder cancer. *PLoS ONE.* (2015) 10:e0131889. doi: 10.1371/journal.pone.0131889
39. Videira PA, Correia M, Malagolini N, Crespo HJ, Ligeiro D, Calais FM, et al. ST3Gal.I sialyltransferase relevance in bladder cancer tissues and cell lines. *BMC Cancer.* (2009) 9:357. doi: 10.1186/1471-2407-9-357
40. Lekka M. Discrimination between normal and cancerous cells using AFM. *BioNanoScience.* (2016) 6:65–80. doi: 10.1007/s12668-016-0191-3
41. Rodrigues RO, Pinho D, Faustino V, Lima R. A simple microfluidic device for the deformability assessment of blood cells in a continuous flow. *Biomed. Microdev.* (2015) 17:108. doi: 10.1007/s10544-015-0014-2
42. Kiliçarslan A, Süngü N, Balci S, Canda E, Altinova S, Güler G. The role of collecting bladder wash fluid before biopsy procedure to help the cytological diagnosis of residual tumor. *J Cytol.* (2015) 32:85–9. doi: 10.4103/0970-9371.160549
43. Keshtkar A, Keshtkar A, Lawford P. Cellular morphological parameters of the human urinary bladder (malignant and normal). *Int J Exp Pathol.* (2007) 88:185–90. doi: 10.1111/j.1365-2613.2006.00520.x

44. Khandelwal P, Abraham SN, Apodaca G. Cell biology and physiology of the uroepithelium. *Am J Physiol Renal Physiol.* (2009) 297:F1477–501. doi: 10.1152/ajprenal.00327.2009
45. Apodaca G. The uroepithelium: not just a passive barrier. *Traffic.* (2004) 5:117–28. doi: 10.1046/j.1600-0854.2003.00156.x
46. Bhatia A, Dey P, Kakkar N, Srinivasan R, Nijhawan R. Malignant atypical cell in urine cytology: a diagnostic dilemma. *CytoJournal.* (2006) 3:28. doi: 10.1186/1742-6413-3-28
47. Shojaei-Baghini E, Zheng Y, Jewett MAS, Geddie WB, Sun Y. Mechanical characterization of benign and malignant urothelial cells from voided urine. *Appl. Phys. Lett.* (2013) 102:123704. doi: 10.1063/1.4798495
48. Fogazzi GB, Pallotti F, Garigali G. Atypical/malignant urothelial cells in routine urinary sediment: worth knowing and reporting. *Clin Chim Acta.* (2015) 439:107–11. doi: 10.1016/j.cca.2014.10.021
49. Moll R, Achtstätter T, Becht E, Balcarova-Ständer J, Ittensohn M, Franke WW. Cytokeratins in normal and malignant transitional epithelium. Maintenance of expression of urothelial differentiation features in transitional cell carcinomas and bladder carcinoma cell culture lines. *Am J Pathol.* (1988) 132:123–44.
50. Sanli O, Dobruch J, Knowles MA, Burger M, Alemozaffar M, Nielsen ME, et al. Bladder cancer. *Nat Rev Dis Primers.* (2017) 3:17022. doi: 10.1038/nrdp.2017.22
51. Wiener HG, Mian CH, Haitel A, Pycha A, Schatzl G, Marberger M. Can urine bound diagnostic tests replace cystoscopy in the management of bladder cancer? *J Urol.* (1998) 159:1876–80. doi: 10.1016/S0022-5347(01)63184-7
52. Keller AK, Jensen JB. Voided urine versus bladder washing cytology for detection of urothelial carcinoma: which is better? *Scand J Urol.* (2017) 51:290–2. doi: 10.1080/21681805.2017.1310130
53. Xu L, Mao X, Imrali A, Syed F, Mutsvangwa K, Berney D, et al. Optimization and evaluation of a novel size based circulating tumor cell isolation system. *PLoS ONE.* (2015) 10:e0138032. doi: 10.1371/journal.pone.0138032
54. Renier C, Pao E, Che J, Liu HE, Lemaire CA, Matsumoto M, et al. Label-free isolation of prostate circulating tumor cells using Vortex microfluidic technology. *NPJ Precision Oncol.* (2017) 1:15. doi: 10.1038/s41698-017-0015-0
55. Hou HW, Li QS, Lee GYH, Kumar AP, Ong CN, Lim CT. Deformability study of breast cancer cells using microfluidics. *Biomed Microdev.* (2009) 11:557–64. doi: 10.1007/s10544-008-9262-8
56. Ramos JR, Pabijan J, Garcia R, Lekka M. The softening of human bladder cancer cells happens at an early stage of the malignancy process. *Beilstein J Nanotechnol.* (2014) 5:447–57. doi: 10.3762/bjnano.5.52
57. Raj A, Sen AK. Entry and passage behavior of biological cells in a constricted compliant microchannel. *RSC Adv.* (2018) 8:20884–93. doi: 10.1039/C8RA02763C
58. Jiang J, Zhao H, Shu W, Tian J, Huang Y, Song Y, et al. An integrated microfluidic device for rapid and high-sensitivity analysis of circulating tumor cells. *Sci Rep.* (2017) 7:42612. doi: 10.1038/srep42612
59. Stowell SR, Ju T, Cummings RD. Protein glycosylation in cancer. *Annu Rev Pathol.* (2015) 10:473–510. doi: 10.1146/annurev-pathol-012414-040438
60. Munkley J. The role of Sialyl-Tn in cancer. *Int J Mol Sci.* (2016) 17:275. doi: 10.3390/ijms17030275
61. Azevedo R, Peixoto A, Gaiteiro C, Fernandes E, Neves M, Lima L, et al. Over forty years of bladder cancer glycobiology: where do glycans stand facing precision oncology? *Oncotarget.* (2017) 8:91734–64. doi: 10.18632/oncotarget.19433

Conflict of Interest: The authors declare that the research was conducted in the absence of any commercial or financial relationships that could be construed as a potential conflict of interest.

Copyright © 2020 Carvalho, Abreu, Ferreira, Lima, Ferreira, Santos, Ribeiro, Grenha, Martínez-Fernández, Duenas, Suárez-Cabrera, Paramio, Diéguez, Freitas and Oliveira. This is an open-access article distributed under the terms of the Creative Commons Attribution License (CC BY). The use, distribution or reproduction in other forums is permitted, provided the original author(s) and the copyright owner(s) are credited and that the original publication in this journal is cited, in accordance with accepted academic practice. No use, distribution or reproduction is permitted which does not comply with these terms.

frontiers in Oncology

ORIGINAL RESEARCH
published: 08 February 2021
doi: 10.3389/fonc.2020.570819

CTHRC1 Is a Prognostic Biomarker and Correlated With Immune Infiltrates in Kidney Renal Papillary Cell Carcinoma and Kidney Renal Clear Cell Carcinoma

Fenfang Zhou[1†], Dexin Shen[1†], Yaoyi Xiong[1†], Songtao Cheng[1], Huimin Xu[1], Gang Wang[2,3,4], Kaiyu Qian[2,3,4], Lingao Ju[2,3] and Xinhua Zhang[1*]*

[1] Department of Urology, Zhongnan Hospital of Wuhan University, Wuhan, China, [2] Department of Biological Repositories, Zhongnan Hospital of Wuhan University, Wuhan, China, [3] Human Genetics Resource Preservation Center of Hubei Province, Wuhan, China, [4] Laboratory of Precision Medicine, Zhongnan Hospital of Wuhan University, Wuhan, China

OPEN ACCESS

Edited by:
Marco Borghesi, University of Genoa, Italy

Reviewed by:
Daniela Terracciano, University of Naples Federico II, Italy
Lothar Bergmann, University Hospital Frankfurt, Germany

***Correspondence:**
Xinhua Zhang
zhangxinhuad@163.com
Lingao Ju
julingao1990@whu.edu.cn

[†]These authors have contributed equally to this work

Specialty section:
This article was submitted to Genitourinary Oncology, a section of the journal Frontiers in Oncology

Received: *09 June 2020*
Accepted: *22 December 2020*
Published: *08 February 2021*

Citation:
Zhou F, Shen D, Xiong Y, Cheng S, Xu H, Wang G, Qian K, Ju L and Zhang X (2021) CTHRC1 Is a Prognostic Biomarker and Correlated With Immune Infiltrates in Kidney Renal Papillary Cell Carcinoma and Kidney Renal Clear Cell Carcinoma. Front. Oncol. 10:570819. doi: 10.3389/fonc.2020.570819

Kidney renal clear cell carcinoma (KIRC) and kidney renal papillary cell carcinoma (KIRP) are the most common RCC types. RCC has high immune infiltration levels, and immunotherapy is currently one of the most promising treatments for RCC. Collagen triple helix repeat containing 1 (CTHRC1) is an extracellular matrix protein that regulates tumor invasion and modulates the tumor microenvironment. However, the association of *CTHRC1* with the prognosis and tumor-infiltrating lymphocytes of KIRP and KIRC has not been reported. We examined the *CTHRC1* expression differences in multiple tumor tissues and normal tissues *via* exploring TIMER, Oncomine, and UALCAN databases. Then, we searched the Kaplan-Meier plotter database to evaluate the correlation of *CTHRC1* mRNA level with clinical outcomes. Subsequently, the TIMER platform and TISIDB website were chosen to assess the correlation of *CTHRC1* with tumor immune cell infiltration level. We further explored the causes of aberrant *CTHRC1* expression in tumorigenesis. We found that *CTHRC1* level was significantly elevated in KIRP and KIRC tissues relative to normal tissues. *CTHRC1* expression associates with tumor stage, histology, lymph node metastasis, and poor clinical prognosis in KIRP. The *CTHRC1* level correlates to tumor grade, stage, nodal metastasis, and worse survival prognosis. Additionally, *CTHRC1* is positively related to different tumor-infiltrating immune cells in KIRP and KIRC. Moreover, *CTHRC1* was closely correlated with the gene markers of diverse immune cells. Also, high *CTHRC1* expression predicted a worse prognosis in KIRP and KIRC based on immune cells. Copy number variations (CNV) and DNA methylation might contribute to the abnormal upregulation of *CTHRC1* in KIRP and KIRC. In conclusion, *CTHRC1* can serve as a biomarker to predict the prognosis and immune infiltration in KIRP and KIRC.

Keywords: collagen triple helix repeat containing 1 (CTHRC1), kidney renal clear cell carcinoma, kidney renal papillary cell carcinoma, prognosis, immune infiltration

INTRODUCTION

Kidney cancer is among the top ten causes of cancer-related deaths. There are various subtypes of kidney cancer based on mixed histology, clinical course, and gene course. Renal cell carcinoma (RCC) is the most important type of kidney cancer (1). Besides, kidney renal clear cell carcinoma (KIRC) and kidney renal papillary cell carcinoma (KIRP) account for almost 95% of all renal cell cancers (2). The diagnosis, examination, surgery, and drug therapy of RCC have been advanced. However, its clinical outcome remains unsatisfactory (3, 4). RCC is a heterogeneous tumor that requires useful molecular markers suitable for personalized therapy (5, 6).

During cancer tumorigenesis and progression, tumor cells are affected by the tumor-infiltrating immune cells (7, 8). The immune invasion of the tumor is closely associated with the clinical prognosis of RCC. Precious studies indicated that tumor-infiltrating macrophages, regulatory T Cells (Treg cells), and $CD8^+$ T cells influence RCC treatment outcomes (9–11). Besides, M1 macrophages are associated with better prognosis, while M2 macrophages predict poor outcome in KIRP. Immunoregulatory molecules CTLA-4 and LAG-3 associate with a poor prognosis in KIRC, while IDO1 and PD-L2 correlate with a poor prognosis in KIRP (12). These findings demonstrate that tumor infiltration of immune cells may be a useful drug target that improving clinical outcomes.

Tumor microenvironment comprises infiltrating immune cells, stromal cells, extracellular matrix, and tumor cells. Several studies have reported that tumor-infiltrating lymphocytes have different vital roles in tumor development. For example, tumor-associated macrophages (TAM) promotes cancer metastasis (13). CTHRC1 is a 30 kDa secreted protein, which is highly expressed in cartilage, developing bones, and myofibroblasts during skin wound healing and solid tumors (14, 15). Previous studies indicate that CTHRC1 promotes tumor cell progression *via* influencing specific pathways in various cancer types. CTHRC1 is elevated in cervical carcinoma and promotes metastasis through the Wnt/PCP pathway. In contrast, CTHRC1 modulates aggressiveness *via* GSK-3β/β-catenin pathway in human non-small cell lung cancer (16). Therefore, CTHRC1 is suggested to play an essential role in cancer progression. Current studies have found CTHRC1 function in modulating the tumor microenvironment *via* the E6/E7-p53-POU2F1 axis or focal adhesion kinase signal pathway (17, 18). In endometrial cancer, CTHRC1 promotes M2-like macrophage recruitment and myometrial invasion *via* the integrin-Akt signaling pathway (19). Thus, CTHRC1 has multifaceted functions in the tumor microenvironment. However, the underlying mechanisms of CTHRC1 in KIRP and KIRC progression and tumor-infiltrating lymphocytes remains unclear.

In this study, we used Oncomine, TIMER, UALCAN datasets, and Kaplan–Meier plotter web to analyze *CTHRC1* expression and its association with the prognosis. Furthermore, we used the TIMER web resource and TISIDB database to analyze the correlation between *CTHRC1* and tumor-infiltrated immune cells in the tumor microenvironment. Besides, we further explored the molecular mechanisms of CTHRC1 dysregulation, such as analysis of the CNV, DNA methylation, and somatic cell mutations. Our findings underline the vital role of CTHRC1 in KIRP and KIRC prognosis. Also, we provide an underlying mechanism of *CTHRC1* expression in potentially regulating the infiltration of immune cells, partly affecting the prognosis of KIRP and KIRC.

Abbreviations: RCC, Renal Cell Carcinoma; KIRC, Kidney Renal Clear Cell Carcinoma; KIRP, Kidney Renal Papillary Cell Carcinoma; LUAD, Lung Adenocarcinoma; THCA, Thyroid Carcinoma; CESC, Cervical and Endocervical Cancer; CTLA-4, Cytotoxic T - Lymphocyte Antigen 4; LAG-3, Lymphocyte-activation-gene-3; IDO1, Indoximod -1; PD-L2, Programmed death-2; NK cells, Natural Killer cells; NK T cells, Natural Killer T cells; Th 1 cells, Type I helper T cells; Th 2 cells, Type II helper T cells; Treg, Regulatory T cells; Th17 cells, Type 17 T helper cells; Tfh, T follicular helper cell; TAMs, Tumor-Associated Macrophages; TEMs, Tie2-expressing monocytes; TILs, Tumor infiltrating lymphocytes; OS, Overall Survival; RFS, Relapse-Free Survival; DSS, Disease-Specific Survival; DFI, Disease-Free Interval; PFI, Progression-Free Interval; CNV, Copy number variations.

MATERIALS AND METHODS

Oncomine Database Analysis

Oncomine database (https://www.oncomine.org/resource/main.html) integrates literature and databases of tumor microarray results and is mainly used for gene expression analysis, co-expression analysis, enrichment analysis, interaction networks (20). We used the Oncomine database to analyze *CTHRC1* expression in various cancer types.

TIMER Database Analysis

TIMER web server (https://cistrome.shinyapps.io/timer/) is a website for comprehensive analysis of gene expression and tumor-infiltrating immune cells of diverse cancer types. This web assesses the abundances of six tumor-infiltrating cells (B cells, $CD4^+$ T cells, $CD8^+$ T cells, neutrophils, macrophages, and dendritic cells), using the TIMER algorithm (21). TIMER website also enables the user to explore gene expression in tumor tissues and normal tissues in multiple cancers. We used the TIMER website to analyze the differential expression of CTHRC1 in tumor and normal tissues in various cancers. We evaluated the correlation of CTHRC1 with 6 tumor immune infiltrating cells and molecular markers of 16 immune cells. We also used this web to explore the relationship between immune infiltrating cells and gene expression that affects clinical prognosis in KIRP and KIRC. The levels of gene expression were expressed as log2 RSEM.

UALCAN Database Analysis

UALCAN database (http://ualcan.path.uab.edu/index.html) is available for online analysis of differential gene expression in cancer and normal tissue from the TCGA RNA sequencing data and clinical data of 31 malignancies (22). Besides, this website provides survival prognosis data based on gene expression differences in 31 cancer types. This study used the UALCAN database to validate the analysis results of the Oncomine database, and furtherly determined the correlation between *CTHRC1* gene expression and clinical features. Differences at $p<0.05$ were considered statistically significant.

Kaplan-Meier Plotter Database Analysis

Kaplan-Meier plotter (http://kmplot.com/analysis/) (23) is an open, intuitive portal tool for prognostic analysis. It contains 54,675 genes survival data from 10,461 cancer samples. Kaplan-Meier plotter database was used to assess the relationship between clinic outcomes and *CTHRC1* expression in different cancers. We performed a prognostic analysis based on *CTHRC1* expression levels in relevant immune cell subgroups using this web. We calculated hazard ratios (HRs) of 95% confidence intervals (CIs) and the log-rank p-value.

TISIDB

TISIDB database (http://cis.Hku.hk/TISIDB/) is a portal for analyzing tumor and immune cell interactions that integrates multiple heterogeneous data types (24). We analyze the correlation between *CTHRC1* expression and tumor-infiltrating lymphocytes *via* this platform.

UCSC Xena

UCSC Xena database (http://xena.ucsc.edu/) is a genome-related database, which brings approximately 200 public databases together, including TCGA, ICGC, TARGET, GTEx, CCL, etc. (25). The database is available to examine copy number and methylation, somatic mutation, gene expression, protein expression. This web also provides clinical information such as patient treatment and survival.

DiseaseMeth Version 2.0

The Human Disease Methylation Database (http://bioinfo.hrbmu.edu.cn/diseasemeth/) is an interactive database that provides annotation and analysis of abnormal DNA methylation in human diseases, especially cancers, which includes 32701 samples, 88 diseases, 679602 disease-gene associations (26).

Statistical Analysis

The *CTHRC1* expression was analyzed *via* the Oncomine, TIMER, and UALCAN database. Survival curves were generated using the Kaplan-Meier plotter database and R project using "survival" packages. We used Spearman's correlation analysis to evaluate the correlation of gene expression in the TIMER. $p<0.05$ were considered statistically significant.

RESULTS

The *Collagen Triple Helix Repeat Containing 1* mRNA Expression in Different Cancers

We analyzed the mRNA expression of *CTHRC1* using the Oncomine database. The results showed that *CTHRC1* was significantly high in various cancer tissues, compared to normal tissues (**Figure 1A**). Then, the mRNA level in the TIMER database was determined. We found that *CTHRC1* mRNA expression was significantly high in most human tumors, especially in KIRP and KIRC, compared with the corresponding normal tissues (**Figure 1B**). These results showed that *CTHRC1* was highly expressed in various cancers. Besides, we used the UALCAN database to validate the findings in Oncomine and TIMER web and reported higher expression of *CTHRC1* in KIRP and KIRC tissues than in normal tissues (**Figures 1C, G**). Notably, *CTHRC1* expression was associated with tumor histology, stage, lymph node metastasis in KIRP (**Figures 1D–F**). Meanwhile, the high *CTHRC1* level in KIRC was related to lymph node metastasis high grade and stage (**Figures 1H–J**).

Prognostic Significance of *Collagen Triple Helix Repeat Containing 1* Expression in Human Cancers

We investigated the Kaplan-Meier plotter database for the prognostic significance of *CTHRC1* expression in human cancers. High levels of *CTHRC1* predicted poor prognostic in KIRP (**Figures 2A, B**), KIRC (**Figures 2C, D**), THCA (**Figures 2E, F**), and LUAD (**Figures 2G, H**). As Kaplan-Meier plotter analyzes only OS and RFS value, we assessed the multiple clinical prognostic value of *CTHRC1* in a variety of cancers by R project using "survival" packages. Forest plot showed *CTHRC1* as a risk factor of different prognosis in KIRP and KIRC (**Figure 3**). Besides, we generated the Kaplan-Meier plot, which showed that high expression of *CTHRC1* had a poor prognosis in KIRP (**Supplementary Figures S1A–D**) and KIRC (**Supplementary Figures S1E–H**). These findings indicated that *CTHRC1* is a hazard for predicting worse prognostic in KIRP and KIRC.

Correlation of *Collagen Triple Helix Repeat Containing 1* Expression With Clinical Characteristics of Kidney Renal Papillary Cell Carcinoma and Kidney Renal Clear Cell Carcinoma Patients

Then, we investigated the association of *CTHRC1* expression with different clinical characteristics of KIRP and KIRC using the Kaplan-Meier Plotter database (**Table 1**). High *CTHRC1* level was associated with poorer OS and RFS in females (OS: HR=7.87, p=0.00021; RFS: HR=8.01, p=0.0022) and stage 3 (OS: HR=4.87, p=0.0028; RFS: HR=9.2, p=0.00021) in KIRP. Similarly, upregulated levels of *CTHRC1* was correlated with worse prognostic outcomes in males (OS: HR=1.71, p=0.0143; RFS: HR=5.44, p=0.0025), and stage 2 (OS: HR=13.51, p=0.0021), stage 3 (RFS: HR=4.65, p=0.0457), stage 4 (OS: HR=1.72, p=0.0345) in KIRC. These results illustrate that the prognostic value of the *CTHRC1* mRNA level, following their clinical characteristics, particularly in the advanced stage of KIRP and KIRC patients.

Collagen Triple Helix Repeat Containing 1 Expression is Correlated With Immune Infiltration in Kidney Renal Papillary Cell Carcinoma and Kidney Renal Clear Cell Carcinoma

Tumor-infiltrating lymphocytes can independently be used to predict sentinel lymph node status and prognosis in cancers

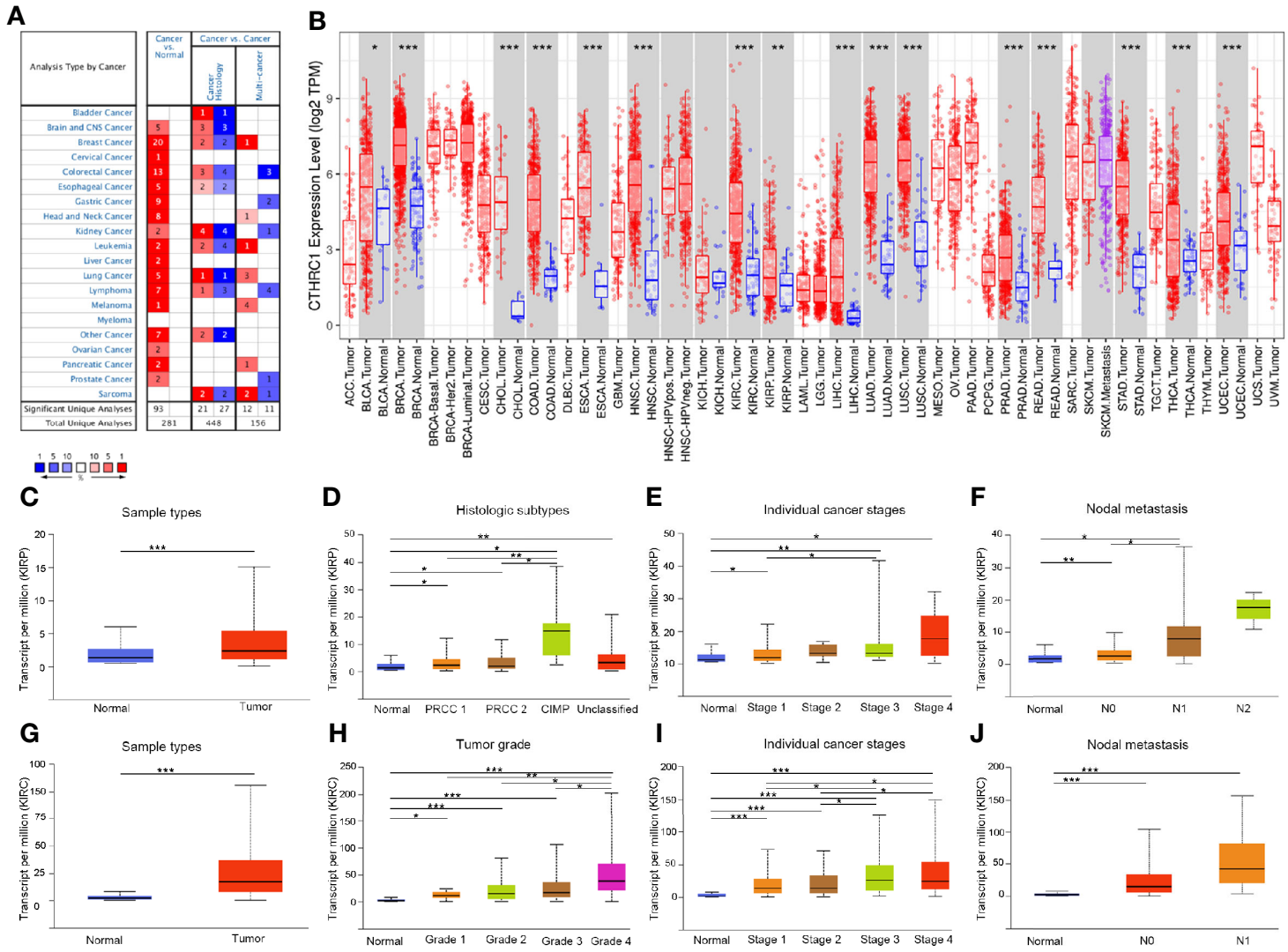

FIGURE 1 | The expression of *CTHRC1* in different cancers and its relationship with individual clinical parameters of KIRP and KIRC. **(A)** *CTHRC1* level in different cancers tissues compared to normal tissues in the Oncomine database. **(B)** *CTHRC1* expression of different tumor types in the TIMER database. **(C)** *CTHRC1* expression difference in KIRP samples. **(D–F)** *CTHRC1* mRNA expressions were remarkably correlated with KIRP patients' individual cancer histologic subtypes **(D)**, stages **(E)**, nodal metastasis **(F)**. **(G)** Differential expression of *CTHRC1* in KIRC tissues. **(H–J)** *CTHRC1* level were significantly associated with KIRC patients' individual cancer grade **(H)**, stages **(I)**, nodal metastasis **(J)**. N0: Metastases in 1 to 3 axillary lymph nodes, N1: Metastases in 1 to 3 axillary lymph nodes, N2: Metastases in 4 to 9 axillary lymph nodes. *p<0.05, **p<0.01, ***p<0.001.

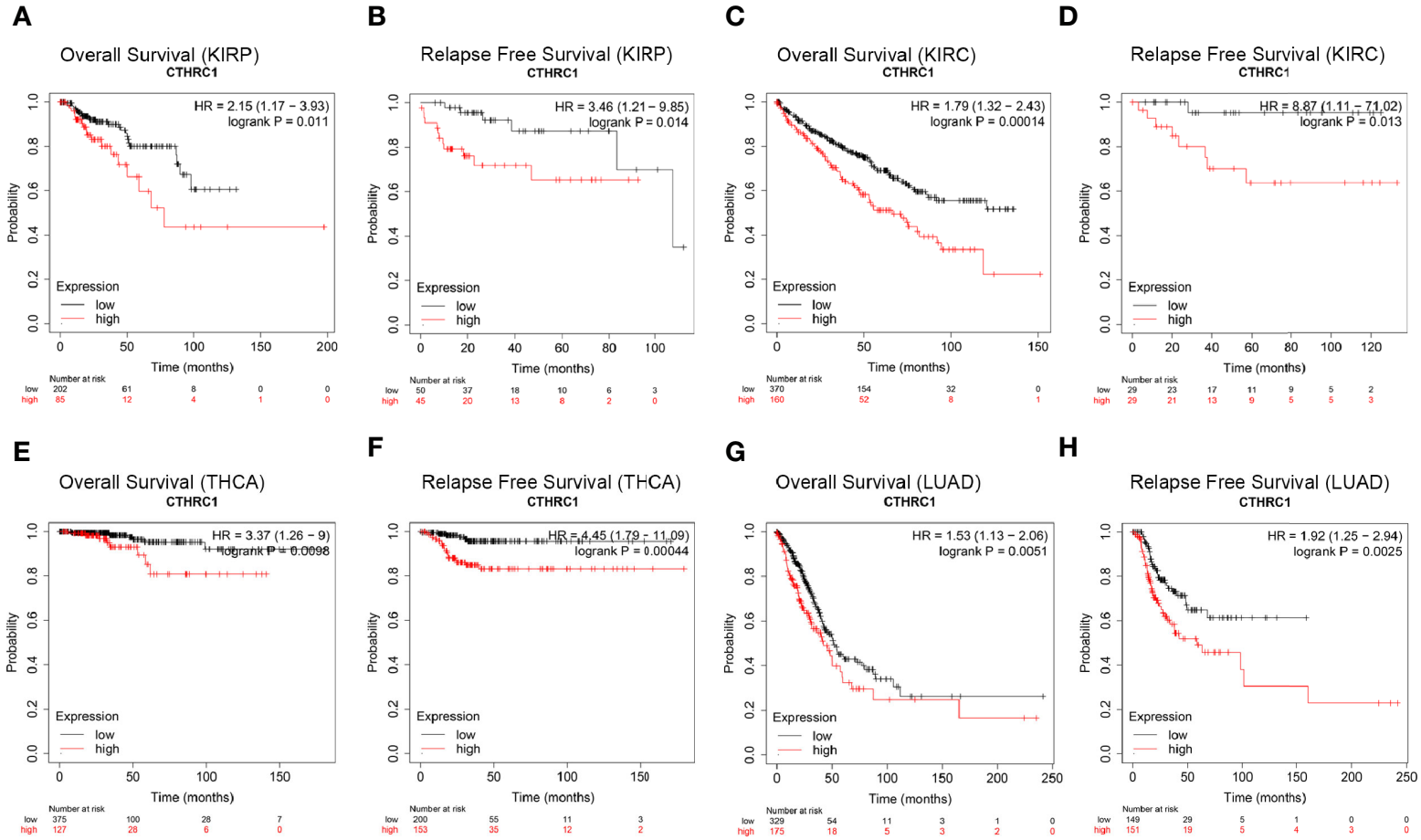

FIGURE 2 | Comparison of Kaplan-Meier survival curves of *CTHRC1* high and low expression in different cancers. **(A, B)** High *CTHRC1* expression had poor OS and RFS in KIRP (n=288). **(C, D)** Upregulated *CTHRC1* expression had worse OS and RFS in KIRC (n=530). **(E, F)** Difference in survival among high and low *CTHRC1* levels in THCA (n=502). **(G, H)** Survival differences of *CTHRC1* expression in LUAD (n=513).

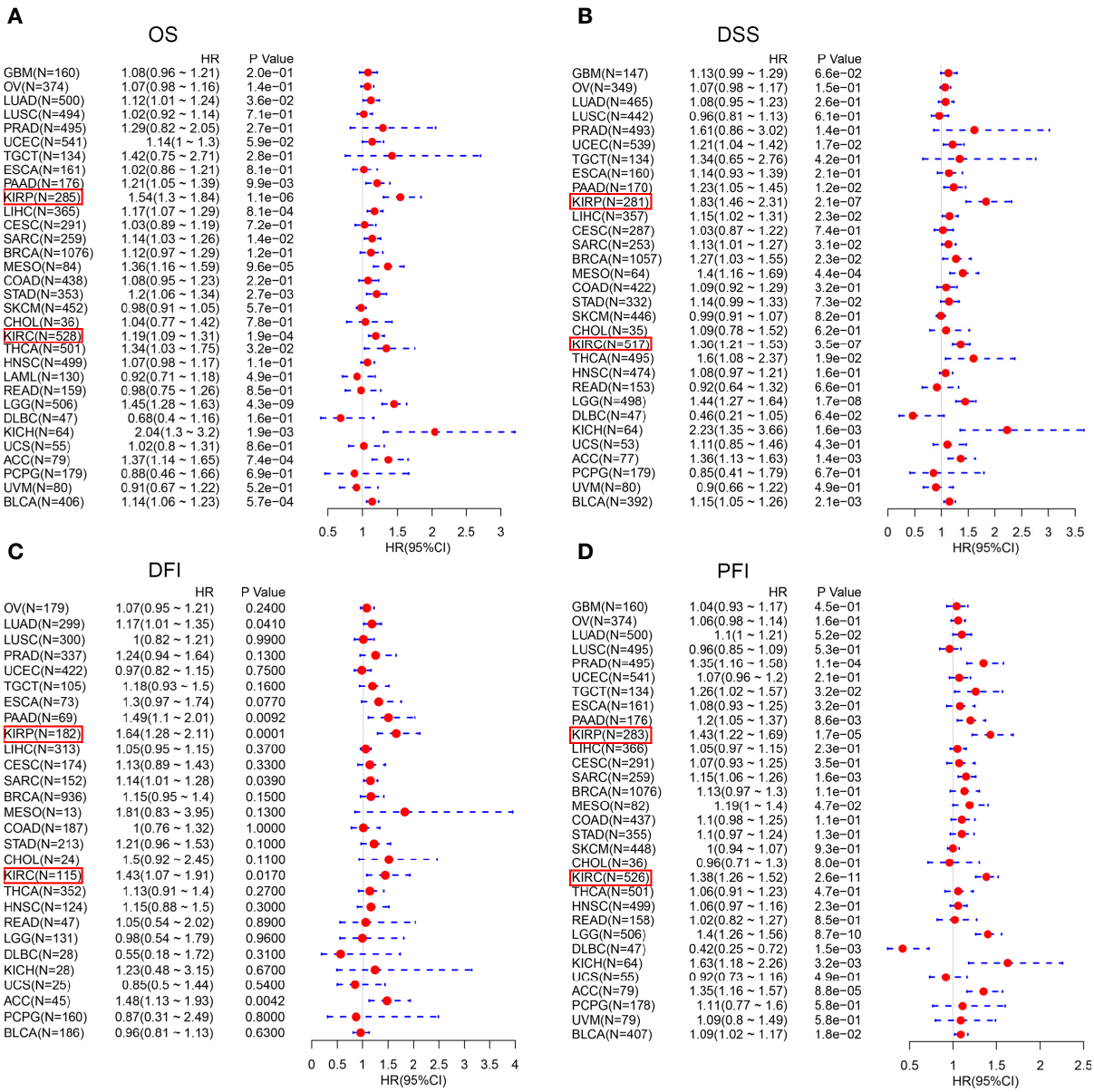

FIGURE 3 | Forest plot of the prognostic values in various cancer subgroups of *CTHRC1*. **(A–D)** Prognostic HR of *CTHRC1* in different cancers for OS **(A)**, DSS **(B)**, DFI **(C)**, PFI **(D)**.

(27, 28). Therefore, we used TIMER to analyze the correlation of *CTHRC1* level with immune infiltration levels in various cancer types. The results showed that *CTHRC1* expression is significantly positively correlated with B cells (r=0.311, p=3.66e-07), $CD4^+$ T cells (r=0.347, p=1.03e-08), $CD8^+$ T cells (r=0.324, p=1.03e-07), dendritic cells (r=0.463, p=4.98e-15) and neutrophils (r=0.464, p=3.66e-15) in KIRP (**Figure 4A**). Besides, the *CTHRC1* level showed a positive correlation with infiltrating levels of $CD4^+$ T cells (r=0.195, p=2.63e-05), neutrophils (r=0.214, p=3.89e-06), macrophage (r=0.187, p=6.54e-04), dendritic cell (r=0.152, p=1.12e-03) in KIRC (**Figure 4B**). However, *CTHRC1* was not correlated with B cells (r=−0.053, p=3.80e-01), $CD4^+$ T cells (r=0.021, p=7.27e-01), $CD8^+$ T cells (r=−0.063, p=2.98e-01), dendritic cells (r=0.041, p=4.98e-01), and neutrophils (r=−0.037, p=5.42e-01) in cervical and endocervical cancers (**Figure 4C**). In addition, we examined prognostic value of *CTHRC1* level and tumor infiltrating immune cells in KIRP and KIRC, using Cox proportional hazard model by TIMER. The result states that B cells (p=0.039), $CD8^+$ T cells (p=0.001), dendritic cells (p=0.018), *CTHRC1* expression (p<0.001) were significantly correlated with clinical prognosis in KIRP (**Table 2**). Besides, there is a strong correlation between Macrophage (p=0.020), *CTHRC1* expression (p<0.001) and clinical outcome of KIRC (**Table 2**). Then, we

TABLE 1 | Correlation of *CTHRC1* mRNA expression and prognosis in KIRP and KIRC with different clinicopathological factors by Kaplan-Meier plotter.

Clinicopathological factors	KIRP				KIRC			
	OS		RFS		OS		RFS	
	HR	p	HR	p	HR	p	HR	p
SEX								
Female	7.87(2.16–28.65)	0.00021	8.01(1.68–38.26)	0.0022	3.58(2.11–6.08)	5.00E-07	1.71(0.24–12.18)	0.587
Male	5.61(1.34–23.50)	0.0078	2.55(0.93–7.00)	0.06	1.71(1.11–2.65)	0.0143	5.44(1.59–18.67)	0.0025
Stage								
1	3.15(0.92–10.75)	0.054	1.8(0.58–5.587)	0.3	1.7(0.92–3.11)	0.085	2.97(0.31–28.72)	0.323
2	0(0-Inf)	0.36	–	–	13.51(1.69–107.66)	0.0021	–	–
3	4.87(1.55–15.37)	0.0028	9.2(2.25–37.59)	0.00021	1.51(0.75–3.02)	0.2451	4.65(0.89–24.47)	0.0457
4	–	–	–	–	1.72(1.13–2.87)	0.0345	–	–

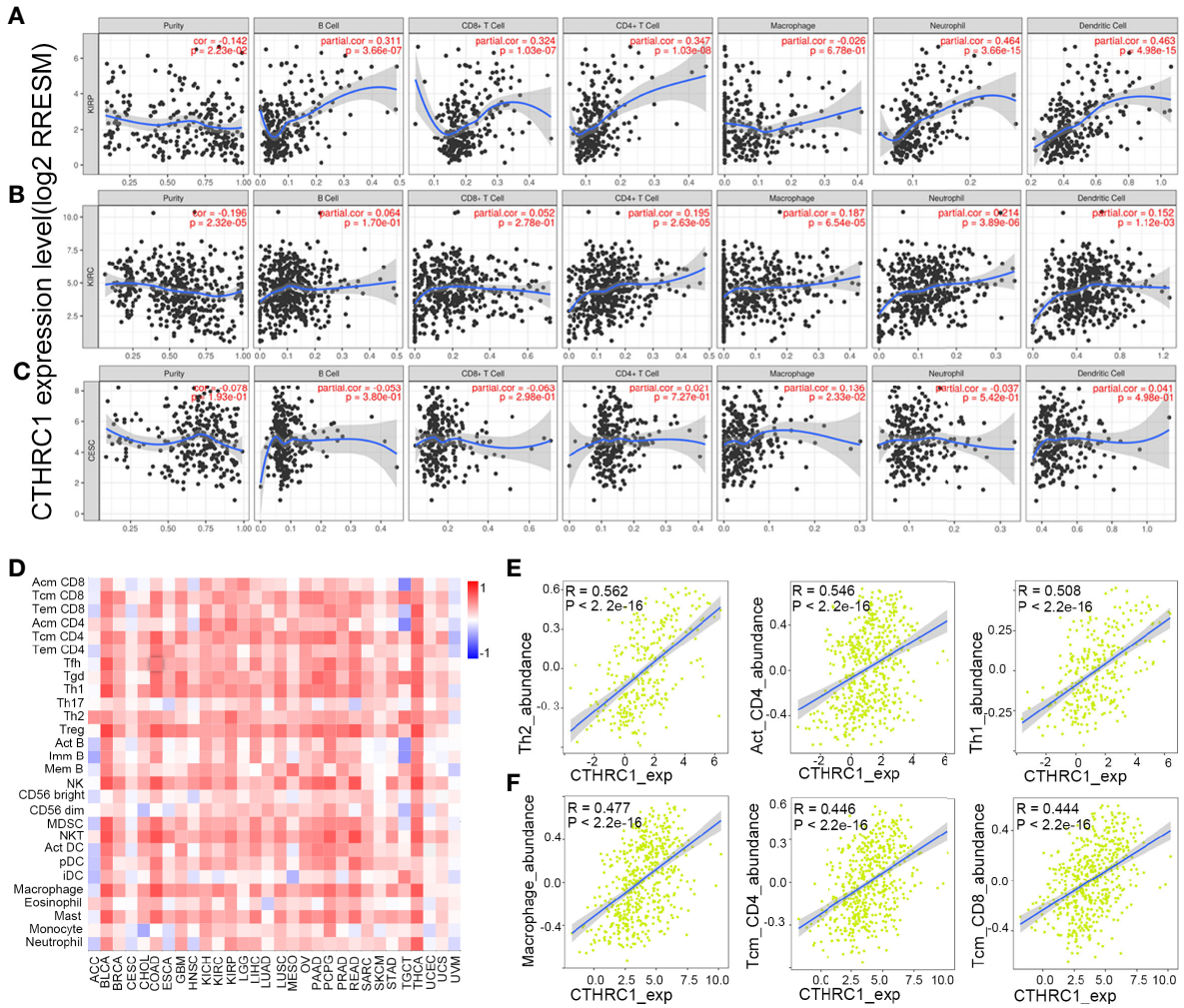

FIGURE 4 | Correlation analysis of *CTHRC1* level and immune cells infiltration levels across human cancers using the TIMER database and TISIDB database. **(A)** *CTHRC1* expression in KIRP tissues positive correlates with tumor immune infiltration levels of B cells, $CD8^+$ T cells, $CD4^+$ T cells, neutrophils, and dendritic cells. **(B)** *CTHRC1* level correlates with tumor immune infiltration in KIRC. **(C)** *CTHRC1* level weakly correlated with immune cells infiltration of CESC. **(D)** Relations between expression of *CTHRC1* and 28 types of TILs across human heterogeneous cancers. **(E)** Top 3 TILs were displaying the greatest Spearman's correlation with *CTHRC1* expression in KIRP. **(F)** *CTHRC1* significantly correlated with abundance of top 3 TILs in KIRC.

TABLE 2 | The cox proportional hazard model of CTHRC1 and six tumor-infiltrating immune cells in KIRP and KIRC (TIMER).

	KIRP					KIRC				
	coef	HR	95%CI_l	95%CI_u	p.value	coef	HR	95%CI_l	95%CI_u	p.value
B cell	5.238	188.256	1.311	27041.674	0.039	–0.496	0.609	0.027	13.546	0.754
CD8 T cell	9.748	17125.920	44.033	6660832.100	0.001	–1.126	0.324	0.065	1.629	0.171
CD4 T cell	–1.312	0.269	0.000	725.972	0.745	–0.615	0.541	0.037	7.928	0.654
Macrophage	–3.662	0.026	0.000	4.235	0.160	–2.793	0.061	0.006	0.644	0.020
Neutrophil	–9.450	0.000	0.000	63.944	0.173	2.477	11.910	0.209	679.922	0.230
Dendritic	–5.194	0.000	0.000	0.416	0.018	0.561	1.753	0.289	10.623	0.542
CTHRC1	0.649	1.913	1.435	2.551	0.000	0.205	1.228	1.110	1.359	0.000

used TISIDB database to furtherly explore the relationship between *CTHRC1* level and 28 tumor immune infiltrating cell subtypes. These results showed that *CTHRC1* is associated with twenty-seven immune cell subtypes in KIRP (**Figure 4D**, **Table 3**). Especially, effector memory $CD8^+$ T cell (r=0.414, p=1.81E-13), activated CD4 T cell (r=0.546, p<2.2e-16), Type 1 T helper cell (r=0.454, p<2.2e-16), Type 2 T helper cell (r=0.562, p<2.2e-16), regulatory T cell (r=0.435, p<2.2e-16), activated B cell (r=0.409, p=4.11e-13), natural killer cell (r=0.493, p<2.2e-16), natural killer T cell (r=0.508, p<2.2e-16), neutrophil (r=0.422, p=3.40E-14) and *CTHRC1* are moderately correlated (**Figure 4E**). In addition, *CTHRC1* showed a positive correlation with 24 immune cell (**Figure 4D**, **Table 3**). Notably, central memory $CD8^+$ T cell (r=0.444, p<2.2e-16), central memory $CD4^+$ T cell (r=0.446, p<2.2e-16), gamma delta T cell (r=0.43, p<2.2e-16), macrophage (r=0.477, p<2.2e-16) displayed a moderate correlation with *CTHRC1* expression (**Figure 4F**). These results strongly implicate that *CTHRC1* could serve as a major tumor immune infiltration regulator in KIRP and KIRC.

TABLE 3 | The correlation between CTHRC1 expression and tumor lymphocyte infiltration in human cancer (TISIDB).

	KIRP		KIRC	
	r	p	r	p
Activated CD8 T cell (Act _CD8)	0.358	4.39E-10	0.184	1.86E-05
Central memory CD8 T cell (Tcm _CD8)	0.355	5.96E-10	0.444	<2.2e-16
Effector memory CD8 T cell (Tem _CD8)	0.414	1.81E-13	0.19	1.01E-05
Activated CD4 T cell (Act _CD4)	0.546	<2.2e-16	0.328	1.00E-14
Central memory CD4T cell (Tcm _CD4)	0.340	3.45E-09	0.446	<2.2e-16
Effector memory CD4 T cell (Tem _CD4)	0.328	1.24E-08	0.259	1.47E-09
T follicular helper cell(Tfh)	0.210	9.73E-13	0.311	2.56E-13
Gamma delta T cell (Tgd)	0.336	<2.2e-16	0.430	<2.2e-16
Type 1 T helper cell (Th1)	0.454	<2.2e-16	0.360	3.54E-08
Type 17 T helper cell (Th17)	0.157	7.20E-03	0.072	9.55E-01
Type 2 T helper cell (Th2)	0.562	<2.2e-16	0.337	1.48E-15
Regulatory T cell (Treg)	0.435	<2.2e-16	0.349	1.15E-16
Activated B cell (Act _B)	0.409	4,11e-13	0.184	2.03E-05
Immature B cell (Imm _B)	0.387	1.09E-10	0.118	6.19E-03
Memory B cell (Mem _B)	0.353	7.88-10	0.303	1.09E-12
natural killer cell (NK)	0.493	<2.2e-16	0.324	2.31E-14
CD56bright natural killer cell (CD56bright)	0.206	4.23E-03	0.205	1.86E-06
CD56dim natural killer cell (CD56dim)	0.231	7.26E-05	0.142	1.02E-03
Myeloid derived suppressor cell (MDSC)	0.351	9.96-10	0.321	4.00E-14
Natural killer T cell (NKT)	0.508	<2.2e-16	0.380	<2.2e-16
Activated dendtritic cell (Act _DC)	0.357	4.49E-10	0.163	1.63E-03
Plasmacytoid dendtritic cell (pDC)	0.386	1.27E-11	0.285	2.38E-11
Immature dendtritic cell (iDC)	0.048	4.17E-01	-0.101	2.00E-02
Macrophage (Macrophage)	0.393	5.09E-12	0.477	<2.2e-16
Eosinophi (Eosinophil)	0.361	2.87E-10	0.053	2.24E-01
Mast (Mast)	0.344	2.15E-09	0.304	9.37E-13
Monocyte(Monocyte)	0.237	4.78E-05	0.213	7.37E-13
Neutrophil (Neutrophil)	0.422	3.40E-14	0.035	4.13E-01

Collagen Triple Helix Repeat Containing 1 Expressions Were Correlated With Immune Cell Type Markers

We assessed the correlation between *CTHRC1* expression and tumor-infiltrating immune cell gene marker levels in KIRP, KIRC, and CESC tissues by exploring the TIMER database. Our results showed that the *CTHRC1* level in KIRP tissues was strongly associated with immune markers of B cells, monocytes, and dendritic neutrophils, DCs, $CD8^+$ T cells, T helper, Tregs, and T exhaustion cells. Moreover, *CTHRC1* in KIRC positively correlates with the marker genes of B cells, macrophages, and neutrophils. However, there were only ten significant markers associated with *CTHRC1* in CESC.

Notably, we found that the *CTHRC1* level was significantly correlated with various subtypes of T cells marker levels, including $CD8^+$ T markers, CD8A, CD8B, cell T (general) markers, CD3D, CD3E, CD2, exhausted T cell marker, GZMB, LAG-3, PD-1, Th2 markers, GATA3, Th17 markers, STAT3, Treg markers, FOXP3, CCR8, TGF-β, Tfh marker, BCL6, and neutrophils markers, ITGAM, CCR7, DC markers, CD1C, NRP1, B cells markers, CD79A, CD19 in KIRP (**Table 4**). A significant correlation of *CTHRC1* level with the marker genes expression in different subsets of macrophage. M2 macrophage markers MS4A4A, VSIG4, CD163, monocyte markers, CSF1R, CD86, TAM markers, CD68, B cell markers, CD19, CD79A, was reported (**Table 4**). Furthermore, the expression of *CTHRC1* was not markedly related to marker genes for $CD8^+$ T cells, NK cells, Th2, and Th17 cells in KIRC. These findings reveal that CTHRC1 is involved in the regulation of tumor immune infiltration in KIRP and KIRC.

Prognostic Potential of *Collagen Triple Helix Repeat Containing 1* Expressions in Different Tumors Based on Immune Cells

This study showed that the *CTHRC1* level was associated with the immune infiltration of KIRP and KIRC. Also, upregulated *CTHRC1* has a worse prognosis in KIRP and KIRC patients.

TABLE 4 | Correlation analysis between CTHRC1 and relate genes and markers of immune cells in TIMER.

Description	Gene markers	KIRP				KIRC				CESC			
		None		Purity		None		Purity		None		Purity	
		cor	p	cor	p	cor	p	cor	p	cor	p	cor	p
B cell	CD19	0.375	***	0.392	***	0.295	***	0.301	***	−0.099	0.083	−0.106	0.078
	CD79A	0.489	***	0.489	***	0.246	***	0.260	***	−0.064	0.267	−0.061	0.311
$CD8^+$ T cell	CD8A	0.403	***	0.425	***	0.082	0.059	0.091	0.050	−0.062	0.276	−0.079	0.188
	CD8B	0.355	***	0.390	***	0.054	0.214	0.065	0.161	−0.044	0.441	−0.062	0.307
Dendritic cell	ITGAX	0.221	**	0.213	**	0.068	0.114	0.051	0.270	0.046	0.419	0.036	0.547
	NRP1	0.330	***	0.328	***	0.220	***	0.220	***	0.293	***	0.298	***
	CD1C	0.430	***	0.453	***	0.045	0.302	0.032	0.491	0.168	*	0.170	*
	HLA-DPA1	0.295	***	0.307	***	0.099	0.023	0.113	0.015	−0.085	0.136	−0.104	0.083
	HLA-DRA	0.302	***	0.313	***	0.126	*	0.141	*	−0.094	0.102	−0.116	0.054
	HLA-DQB1	0.235	***	0.275	***	0.019	0.660	0.022	0.638	−0.082	0.153	−0.112	0.062
	HLA-DPB1	0.285	***	0.307	***	0.106	0.015	0.119	0.010	−0.102	0.074	−0.120	0.046
M1 Macrophage	PTGS2	0.397	***	0.417	***	0.322	***	0.326	***	0.201	**	0.187	*
	IRF5	−0.124	0.030	−0.153	0.014	−0.112	*	−0.125	*	−0.023	0.688	−0.008	0.901
	NOS2	0.173	*	0.205	**	−0.005	0.900	−0.017	0.712	0.012	0.832	0.012	0.844
M2 Macrophage	MS4A4A	0.304	***	0.298	***	0.307	***	0.310	***	0.145	0.011	0.120	0.045
	VSIG4	0.337	***	0.342	***	0.352	***	0.350	***	0.128	0.025	0.118	0.049
	CD163	0.317	***	0.323	***	0.289	***	0.293	***	0.121	0.034	0.114	0.058
Monocyte	CSF1R	0.353	***	0.374	***	0.279	***	0.276	***	0.149	*	0.141	0.019
	CD86	0.351	***	0.363	***	0.256	***	0.263	***	0.132	0.021	0.101	0.093
Natural killer cell	KIR2DS4	0.236	***	0.300	***	0.044	0.312	0.072	0.124	−0.068	0.236	−0.068	0.260
	KIR3DL3	0.128	0.030	0.126	0.044	0.014	0.743	0.031	0.505	−0.111	0.052	−0.148	0.013
	KIR3DL2	0.309	***	0.345	***	0.079	0.069	0.116	0.012	−0.110	0.054	−0.127	0.035
	KIR3DL1	0.330	***	0.360	***	0.047	0.276	0.072	0.121	0.008	0.885	−0.010	0.866
	KIR2DL4	0.332	***	0.361	***	0.082	0.059	0.099	0.033	−0.141	0.013	−0.176	*
	KIR2DL3	0.293	***	0.334	***	0.047	0.280	0.072	0.122	−0.010	0.865	−0.047	0.436
	KIR2DL1	0.263	***	0.286	***	0.043	0.318	0.073	0.115	−0.076	0.187	−0.090	0.133
Neutrophils	CCR7	0.371	***	0.372	***	0.239	***	0.269	***	0.009	0.875	0.020	0.743
	ITGAM	0.404	***	0.424	***	0.195	***	0.180	**	0.064	0.261	0.053	0.382
	CEACAM8	0.049	0.410	0.061	0.331	−0.127	*	−0.112	0.016	−0.047	0.415	−0.024	0.693
T cell (general)	CD3D	0.392	***	0.413	***	0.131	*	0.136	*	−0.126	0.028	−0.150	0.012
	CD3E	0.411	***	0.446	***	0.140	0.001	0.146	*	−0.063	0.270	−0.079	0.187
	CD2	0.395	***	0.425	***	0.155	**	0.158	**	−0.061	0.286	−0.081	0.179
T cell exhaustion	CTLA4	0.272	***	0.290	***	0.151	**	0.153	**	−0.009	0.881	−0.033	0.582
	LAG3	0.411	***	0.424	***	0.103	0.018	0.105	0.024	−0.072	0.209	−0.102	0.090
	HAVCR2	0.013	0.832	0.004	0.951	−0.175	***	−0.175	**	0.069	0.228	0.047	0.434
	GZMB	0.446	***	0.472	***	0.135	*	0.159	**	−0.107	0.062	−0.133	0.026
	PDCD1	0.353	***	0.374	***	0.071	0.101	0.084	0.070	−0.074	0.196	−0.091	0.129
TAM	CCL2	0.313	***	0.317	***	−0.036	0.404	−0.052	0.263	0.202	**	0.202	**
	IL10	0.286	***	0.292	***	0.195	***	0.199	***	0.180	*	0.183	*
	CD68	0.070	0.234	0.057	0.361	0.260	***	0.277	***	−0.033	0.562	−0.065	0.277
Tfh	BCL6	0.390	***	0.384	***	0.290	***	0.297	***	0.227	***	0.210	**
	IL21	0.125	0.033	0.131	0.035	0.150	**	0.160	**	−0.027	0.636	−0.037	0.539
Th1	TBX21	0.345	***	0.397	***	0.080	0.065	0.093	0.045	−0.055	0.341	−0.083	0.169
	STAT4	0.271	***	0.286	***	0.191	***	0.211	***	0.042	0.459	0.008	0.897
	STAT1	0.380	***	0.396	***	0.125	*	0.119	0.011	0.106	0.065	0.068	0.260
	IFNG	0.284	***	0.313	***	0.108	0.013	0.116	0.013	−0.024	0.676	−0.059	0.323
	IL13	0.099	0.091	0.086	0.166	−0.034	0.429	−0.015	0.752	0.093	0.105	0.106	0.077
Th2	GATA3	0.453	***	0.474	***	0.099	0.022	0.061	0.192	0.155	*	0.146	0.015
	STAT6	0.162	*	0.153	0.014	−0.114	*	−0.102	0.028	0.044	0.447	0.061	0.312
	STAT5A	0.218	**	0.242	***	0.109	0.011	0.101	0.030	−0.110	0.055	−0.109	0.069
Th17	STAT3	0.425	***	0.441	***	0.110	0.011	0.095	0.042	0.067	0.242	0.075	0.210
	IL17A	0.126	0.033	0.111	0.073	0.108	0.012	0.118	0.011	−0.142	0.013	−0.137	0.023
Treg	FOXP3	0.415	***	0.438	***	0.329	***	0.340	***	0.151	*	0.130	0.031
	CCR8	0.362	***	0.373	***	0.259	***	0.272	***	0.221	***	0.192	*
	STAT5B	0.166	*	0.170	*	−0.124	*	−0.120	0.010	0.206	**	0.196	*
	TGFB1	0.516	***	0.563	***	0.444	***	0.423	***	0.337	***	0.315	***

*$p<0.01$; **$p<0.001$; ***$p<0.0001$.

Thus, we propose a hypothesis that CTHRC1 may affect the prognosis of KIRP and KIRC patients partly through immune infiltration.

We perform Kaplan-Meier plotter analyses of *CTHRC1* expression in KIRP and KIRC following B cells, CD4+ memory T cells, $CD8^+$ T cells, macrophages, NK T cells, Treg

T cells, Th1 cells, Th2 cells. We found that high *CTHRC1* levels in KIRP in enriched B cells (p=0.00017), B cells (p=4.6e-05), $CD4^+$ memory T cells (p=8.8e-03), $CD8^+$ T cells (p=8e-03), macrophages (p=2.6e-04), natural killer T cells (p=5.8e-03), regulatory T cells (p=1e-03), type 1 T helper cells (p=4.7e-03) cohort had a worse prognosis (**Figures 5A–G**). Unfortunately, clinical samples of Th2 cells enriched in renal cancer are too few to analyze. Similarly, the high expression of *CTHRC1* in KIRC had poor prognosis in enriched B cells (p=5.5e-03), $CD4^+$ memory T cells (p=1.9e-04), $CD8^+$ T cells (p=6.3e-04), macrophages (p=3.9e-05), regulatory T cells (p=4.7e-04), type 2 T-helper cells (p=3.5e-03) (**Figures 5H–K, M, O**). However, there was no significant difference between high and low *CTHRC1* expression groups overall survival in enriched NK cells (p=0.18) and Th1 cells (p=0.05) (**Figures 5L, N**). The above analysis suggested that immune infiltration may, in part, affect high *CTHRC1* expression prognosis of KIRC and KIRP patients.

Mutation, Copy Number Variation, and Methylation Analysis of *Collagen Triple Helix Repeat Containing 1*

CTHRC1 expression was significantly elevated in KIRP and KIRC. We assessed the cause of elevated *CTHRC1* levels. DNA methylation, gene mutation, CNV was critically involved in genetic and epigenetic regulation and were highly associated with the process of cancers. We verified the DNA methylation, gene mutation, CNV levels of the CTHRC1 in KIRP and KIRC *via* the UCSC Xena database. The heatmap indicates that the expression of *CTHRC1* mRNA was correlated with CNV and DNA methylation, but not with a somatic mutation in KIRP (**Figure 6A**) and KIRC (**Figure 6B**). The human disease methylation database was used to further validate the lower methylation level in KIRP (**Supplementary Figures S2A, B**) and KIRC (**Supplementary Figures S2C, D**), compared to normal tissues. Therefore, we suggested that CNV and DNA methylation might contribute to the elevated level of *CTHRC1* in KIRP and KIRC, respectively.

DISCUSSION

CTHRC1 is an extracellular matrix protein that regulates tumor metastasis and the extracellular microenvironment. In this study, we analyzed *CTHRC1* expression, prognostic value, genetic variations, and correlation with tumor immune cell infiltration in KIRP and KIRC for the first time.

In this study, we found that *CTHRC1* expression was highly elevated in KIRP and KIRC, compared to normal tissues. Moreover, *CTHRC1* expression has associations with tumor histology, stage, lymph node metastasis in KIRP (**Figures 1D–F**). Meanwhile, the high *CTHRC1* level was related to lymph node metastasis, high grade, and stage (**Figures 1H–J**). These results suggest that *CTHRC1* plays an important role in the progression and metastasis of KIRP and KIRC. Our findings are consistent with previous researches. *CTHRC1* was elevated in some tumor tissues and associated with clinicopathological features, including late T stage, lymph nodal metastasis, and TNM staging (17, 29).

Results from survival analysis showed that high *CTHRC1* expression was associated with poor OS, DSS, DFI, and PFI (**Figure S1**) in KIRP and KIRC, consistent with previous findings *CTHRC1* affects tumor growth and invasion and leads to a poor prognosis (30, 31). Ni et al. (32) reported that *CTHRC1* promotes metastasis through an epithelial-mesenchymal transformation in colorectal cancer, resulting in a poor prognosis. Our results strongly indicate that *CTHRC1* can be used as a prognostic biomarker for KIRP and KIRC.

CTHRC1 was previously reported to regulate tumor microenvironment. Through correlation analysis, we reported that *CTHRC1* expression is associated with several immune infiltrating cells in KIRP and KIRC (**Figure 4**, **Table 3**). These results suggest that CTHRC1 is involved in the regulation of tumor immune cells. Lee et al (33). study revealed that CTHRC1 recruits Tie2-expressing monocytes into tumor tissues by activating ERK-dependent AP-1 to promote angiogenesis. Besides, the use of CTHRC1 antibodies reduced tumor burden and TEMs infiltration in tumor tissue in xenograft mouse models. Another study demonstrated that *CTHRC1* expression has a role in tumor-associated macrophages infiltration by upregulating fractalkine chemokine receptor (CX3CR1) expression (19). Our analysis had the effect of mutual authentication with the results of this researches.

We further analyzed the immunotype markers in KIRP and KIRC. After cell purity correction, *CTHRC1* was positively correlated with many immune cell makers in KIRP and KIRC (**Table 4**). The results further imply that *CTHRC1* is associated with immune infiltration in KIRP and KIRC. Besides, our results suggest that *CTHRC1* can potentially modulate Tregs and results in T cell exhaustion. Notably, increased *CTHRC1* level was positively associates with Treg and T cells exhaustion markers, such as FOXP3. FOXP3 is a valid target for identifying Treg in the tumor microenvironment and contributes significantly to Treg cells differentiation and mediated tumor immune escape (34). There was a significant correlation between *CTHRC1* level and several T helper cells (Th1, Th2, Tfh, and Th17) markers in KIRP. These connections may indicate the underlying mechanisms for *CTHRC1* regulation of T cell function in KIRP. Therefore, it was potentially related to the poor prognosis of KIRP and KIRC by recruiting and regulating immune cells.

Through the Kaplan Meier-Plotter database analysis, high expression levels of *CTHRC1* enriched in a variety of immune cells cohort of KIRP and KIRC had a worse prognosis (**Figure 5**). Tregs can suppress anti-tumor responses, leading to tumor immune escape (35). DC can promote tumor metastasis by increasing Treg cells and decreasing the cytotoxicity of $CD8^+$ T cells (36). Myeloid origin suppressor cells (MDSC) contact with T cells, which rapidly depletes arginine from the microenvironment and leads to tumor-mediated immune escape (37). Previous studies also have proven that the proportion of macrophages, $CD8^+$ T cells, Tregs, and MDSC in RCC patients correlates with poor prognosis (9–11, 38, 39). These results may explain that high expression of *CTHRC1* partly affects the prognosis of KIRP and KIRC patients through immune infiltration.

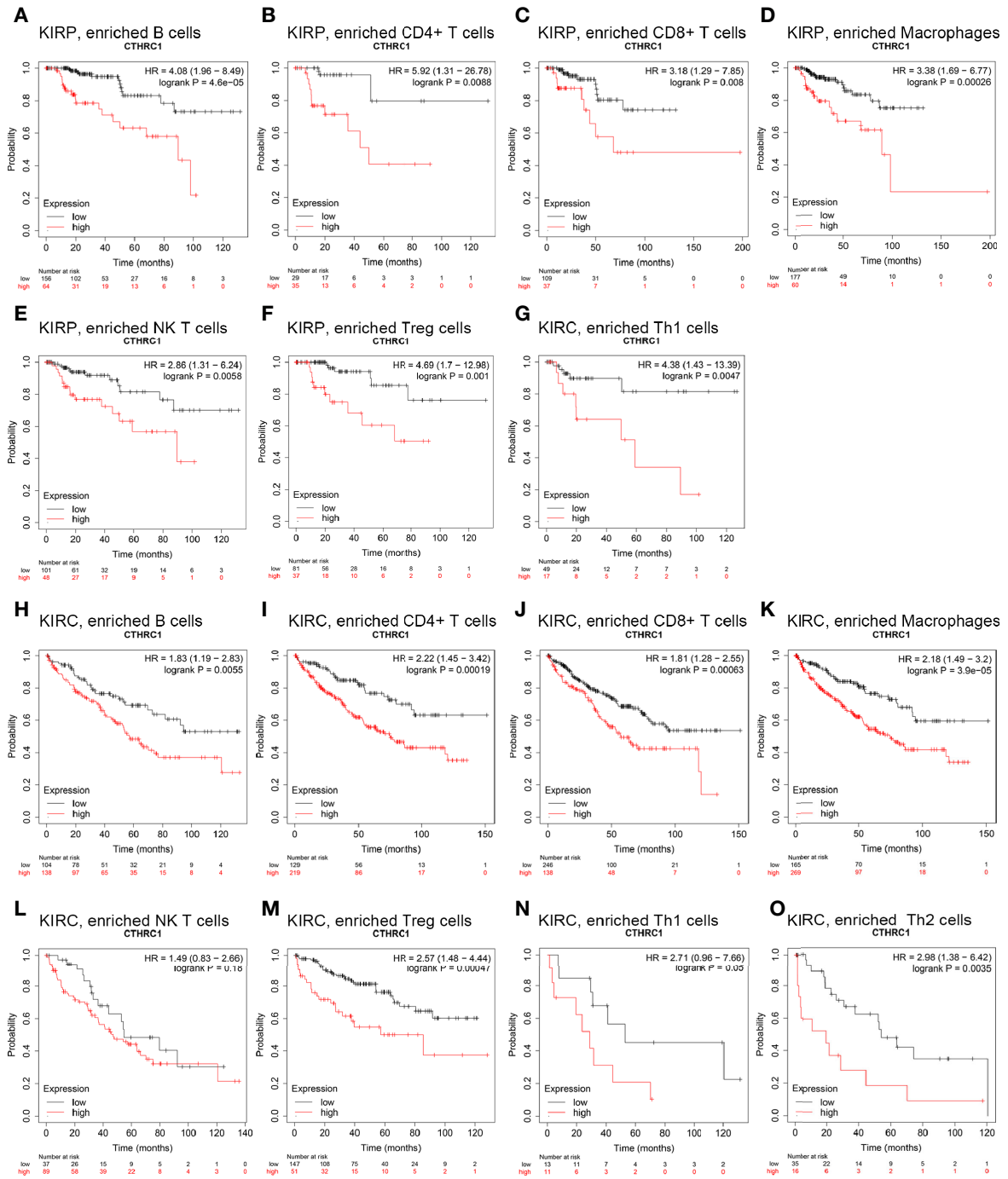

FIGURE 5 | Comparison of Kaplan-Meier survival curves of the high and low expression of CTHRC1 in KIRP and KIRC based on immune cells subgroups. **(A–G)** High *CTHRC1* level enriched in B cells, $CD4^+$ memory T cells, $CD8^+$ T cells, macrophages, NK T cells, Treg T cells, Th1 cells had worse OS in KIRP. **(H–O)** Relationships between *CTHRC1* of enriched in diverse immune and OS in KIRC.

Genetic and epigenetic phenomena play an essential role in regulating gene expression (40). In this study, we found that *CTHRC1* expression was strongly correlated with DNA methylation and CNV and not with somatic mutations. DNA methylation is the most common epigenetic phenotype that usually acts as a transcriptional repressor and plays an essential role in tumor progression (41, 42). Besides, *CTHRC1* is reported to be upregulated by promoter demethylation in

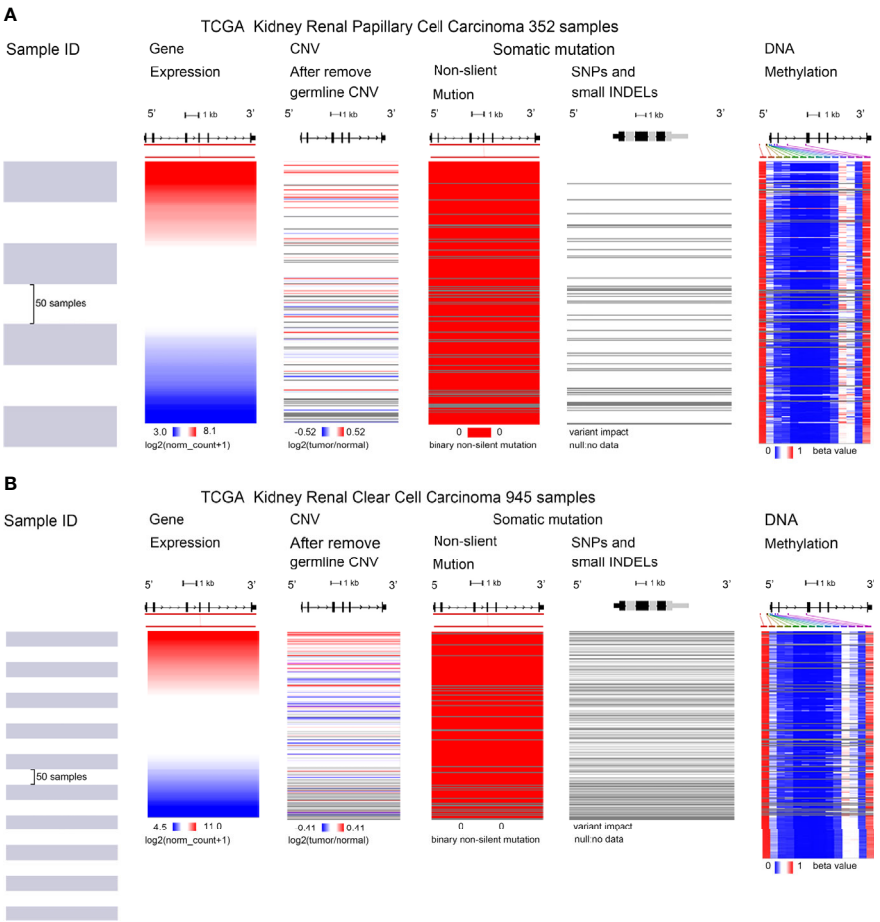

FIGURE 6 | Mutation, CNV, and methylation analysis of CTHRC1 in KIRP and KIRC. **(A, B)** Heatmap showing the correlations between *CTHRC1* mRNA and somatic mutations, CNV, and methylation in KIRP **(A)** and KIRC **(B)** *via* UCSC Xena.

gastric cancer and down-regulated by hypermethylation in hepatocellular carcinoma (43). DNA copy number variation, including gene amplification, gain, loss, and deletion. And CNV influences the gene expression in carcinogenesis (44). Wang et al. (45) presented the evidence that 5-aza-2'-deoxycytidine (the demethylating agent) can restore *CTHRC1* expression, and TGF-β1 led to an increase in levels of *CTHRC1* mRNA and protein. Therefore, DNA hypomethylation and CNV may be a cause for *CTHRC1* upregulated in KIRP and KIRC.

In conclusion, the upregulated *CTHRC1* is strongly associated with clinicopathological features, poor prognosis, and immune cell infiltration. DNA methylation and copy number variation may attribute to *CTHRC1* upregulated. Furthermore, our study provides a new mechanism that CTHRC1 may affect the prognosis of KIRP and KIRC through tumor immune infiltration. Therefore, this study offers insights for further studies on tumor immunotherapy of KIRP and KIRC. The current study is the preliminary part of a larger study, including validation in a study population prospectively enrolled. Undoubtedly, we will make further validation when there are available independent datasets and perform experiments in the future.

DATA AVAILABILITY STATEMENT

The datasets presented in this study can be found in online repositories. The names of the repository/repositories and accession number(s) can be found in the article.

AUTHOR CONTRIBUTIONS

FZ, DS, YX, LJ, and XZ conceived and designed the study. FZ, DS, YX, and LJ performed the analysis procedures. FZ, DS, SC, GW, and YX analyzed the results. YX, SC, KQ, and LJ contributed the analysis tools. FZ, DS, LJ, and XZ contributed to the writing of the manuscript. All authors reviewed the manuscript. All authors contributed to the article and approved the submitted version.

FUNDING

This work was supported by the National Natural Science Foundation of China (81770757, 31900902, and 81902603).

ACKNOWLEDGMENTS

We acknowledge the Oncomine, TIMER, UALCAN, Kaplan–Meier Plotter, TISIDB, UCSC Xena, and DiseaseMeth version 2.0 databases for free use.

SUPPLEMENTARY MATERIAL

The Supplementary Material for this article can be found online at: https://www.frontiersin.org/articles/10.3389/fonc.2020.570819/full#supplementary-material

REFERENCES

1. Ljungberg B, Bensalah K, Canfield S, Dabestani S, Hofmann F, Hora M, et al. EAU Guidelines on Renal Cell Carcinoma: 2014 Update. *Eur Urol* (2015) 67 (5):913–24. doi: 10.1016/j.eururo.2015.01.005
2. Hsieh J, Purdue M, Signoretti S, Swanton C, Albiges L, Schmidinger M, et al. Renal cell carcinoma. *Nat Rev Dis Primers* (2017) 3:17009. doi: 10.1038/nrdp.2017.9
3. Srigley J, Delahunt B, Eble J, Egevad L, Epstein J, Grignon D, et al. The International Society of Urological Pathology (ISUP) Vancouver Classification of Renal Neoplasia. *Am J Surg Pathol* (2013) 37(10):1469–89. doi: 10.1097/PAS.0b013e318299f2d1
4. Shuch B, Amin A, Armstrong A, Eble J, Ficarra V, Lopez-Beltran A, et al. Understanding Pathologic Variants of Renal Cell Carcinoma: Distilling Therapeutic Opportunities from Biologic Complexity. *Eur Urol* (2014) 67 (1):85–97. doi: 10.1016/j.eururo.2014.04.029
5. Garcia J, Rini B. Recent Progress in the Management of Advanced Renal Cell Carcinoma. *CA: Cancer J Clin* (2007) 57(2):112–25. doi: 10.3322/canjclin.57.2.112
6. Barata P, Rini B. Treatment of renal cell carcinoma: Current status and future directions. *CA: A Cancer J Clin* (2017) 67(6):507–24. doi: 10.3322/caac.21411
7. Matsushita H, Vesely M, Koboldt D, Rickert C, Uppaluri R, Magrini V, et al. Cancer Exome Analysis Reveals a T Cell Dependent Mechanism of Cancer Immunoediting. *Nature* (2012) 482:400–4. doi: 10.1038/nature10755
8. Hanahan D, Weinberg R. Hallmarks of Cancer: The Next Generation. *Cell* (2011) 144:646–74. doi: 10.1016/j.cell.2011.02.013
9. Cros J, Sbidian E, Posseme K, Letierce A, Guettier C, Benoît G, et al. Nestin expression on tumour vessels and tumour-infiltrating macrophages define a poor prognosis subgroup of pt1 clear cell renal cell carcinoma. *Virchows Archiv* (2016) 469(3):331–7. doi: 10.1007/s00428-016-1973-2
10. Desar I, Jacobs J, Hulsbergen-vandeKaa C, Oyen W, Mulders P, Van der Graaf W, et al. Sorafenib reduces the percentage of tumour infiltrating regulatory T cells in renal cell carcinoma patients. International journal of cancer. *J Int Du Cancer* (2011) 129:507–12. doi: 10.1002/ijc.25674
11. Zhu Q, Cai M-Y, Weng D-S, Zhao J-J, Pan Q-Z, Wang Q-J, et al. PD-L1 expression patterns in tumour cells and their association with CD8 + tumour infiltrating lymphocytes in clear cell renal cell carcinoma. *J Cancer* (2019) 10:1154–61. doi: 10.7150/jca.29052
12. Zhang S, Zhang E, Long J, Hu Z, Peng J, Liu L, et al. Immune Infiltration in Renal Cell Carcinoma. *Cancer Sci* (2019) 110(5):1564–72. doi: 10.1111/cas.13996
13. Coussens L, Werb Z. Matrix metalloproteinase and the development of cancer. *Chem Biol* (1996) 3:895–904. doi: 10.1016/S1074-5521(96)90178-7
14. Liu W, Fu X-L, Yang J-Y, Yang M, Tao L-Y, Liu D-J, et al. Elevated expression of CTHRC1 predicts unfavorable prognosis in patients with pancreatic ductal adenocarcinoma. *Am J Cancer Res* (2016) 6:1820–7. doi: 10.1002/cam4.1064
15. Tang L, Dai D, Su M, Martinka M, Yang F, Zhou Y. Aberrant expression of collagen triple helix repeat containing 1 in human solid cancers. *Clin Cancer Res* (2006) 12:3716–22. doi: 10.1158/1078-0432.CCR-06-0030
16. Ke Z, He W, Lai Y, Guo X, Chen S, Li S, et al. Overexpression of Collagen Triple Helix Repeat Containing 1 (CTHRC1) is associated with tumour aggressiveness and poor prognosis in human non-small cell lung cancer. *Oncotarget* (2014) 5:9410–24. doi: 10.18632/oncotarget.2421
17. Zhang R, Lu H, Lyu Y-Y, Yang X-M, Zhu L-Y, Yang G-D, et al. E6/E7-P53-POU2F1-CTHRC1 axis promotes cervical cancer metastasis and activates Wnt/PCP pathway. *Sci Rep* (2017) 7:44744. doi: 10.1038/srep44744
18. Guo B, Yan H, Li L, Yin K, Ji F, Zhang S. Collagen triple helix repeat containing 1 (CTHRC1) activates Integrin β3/FAK signaling and promotes metastasis in ovarian cancer. *J Ovarian Res* (2017) 10:69. doi: 10.1186/s13048-017-0358-8
19. Li L-Y, Yin K-M, Bai Y-H, Zhang Z-G, di W, Zhang S. CTHRC1 promotes M2-like macrophage recruitment and myometrial invasion in endometrial carcinoma by integrin-Akt signaling pathway. *Clin Exp Metastasis* (2019) 36 (4):351–63. doi: 10.1007/s10585-019-09971-4
20. Rhodes D, Kalyana-Sundaram S, Mahavisno V, Varambally R, Yu J, Briggs B, et al. Oncomine 3.0: Genes, Pathways, and Networks in a Collection of 18,000 Cancer Gene Expression Profiles. *Neoplasia (N Y NY)* (2007) 9:166–80. doi: 10.1593/neo.07112
21. Li T, Fan J, Traugh N, Chen Q, Liu J, Li B, et al. TIMER: A Web Server for Comprehensive Analysis of Tumor-Infiltrating Immune Cells. *Cancer Res* (2017) 77:e108–10. doi: 10.1158/0008-5472.CAN-17-0307
22. Sc D, Bashel B, Balasubramanya S, Creighton C, Ponce-Rodriguez I, Chakravarthi B, et al. UALCAN: A Portal for Facilitating Tumor Subgroup Gene Expression and Survival Analyses. *Neoplasia* (2017) 19:649–58. doi: 10.1016/j.neo.2017.05.002
23. Nagy Á., Lánczky A, Menyhart O, Győrffy B. Validation of miRNA prognostic power in hepatocellular carcinoma using expression data of independent datasets. *Sci Rep* (2018) 8(1):9227. doi: 10.1038/s41598-018-27521-y
24. Ru B, Wong C, Tong Y, Zhong J, Zhong S, Wu W, et al. TISIDB: an integrated repository portal for tumor-immune system interactions. *Bioinformatics* (2019) 35(20):4200–2. doi: 10.1093/bioinformatics/btz210
25. Goldman M, Craft B, Hastie M, Repečka K, McDade F, Kamath A, et al. Visualizing and interpreting cancer genomics data via the Xena platform. *Nat Biotechnol* (2020) 38(6):675–8. doi: 10.1038/s41587-020-0546-8
26. Xiong Y-C, Wei Y, Gu Y, Zhang S, Zhang B, Chen C, et al. DiseaseMeth version 2.0: a major expansion and update of the human disease methylation database. *Nucleic Acids Res* (2016) 45(D1):D888–95. doi: 10.1093/nar/gkw1123
27. Ohtani H. Focus on TILs: Prognostic significance of tumor infiltrating lymphocytes in human colorectal cancer. *Cancer Immun* (2007) 7:4.
28. Azimi F, Scolyer R, Rumcheva P, Moncrieff M, Murali R, McCarthy S, et al. Tumor-Infiltrating Lymphocyte Grade Is an Independent Predictor of Sentinel Lymph Node Status and Survival in Patients With Cutaneous Melanoma. *J Clin Oncol* (2012) 30:2678–83. doi: 10.1200/JCO.2011.37.8539
29. Chen Y-L, Wang T-H, Hsu H-C, Yuan R-H, Jeng Y-M. Overexpression of CTHRC1 in Hepatocellular Carcinoma Promotes Tumor Invasion and Predicts Poor Prognosis. *PLoS One* (2013) 8:e70324. doi: 10.1371/journal.pone.0070324
30. He W, Zhang H, Wang Y, Zhou Y, Luo Y, Cui Y, et al. CTHRC1 induces non-small cell lung cancer (NSCLC) invasion through upregulating MMP-7/MMP-9. *BMC Cancer* (2018) 18:400. doi: 10.1186/s12885-018-4317-6
31. Ye J, Chen W, Wu Z-Y, Zhang J-H, Fei H, Zhang L-W, et al. Upregulated CTHRC1 promotes human epithelial ovarian cancer invasion through activating EGFR signaling. *Oncol Rep* (2016) 36(6):3588–96. doi: 10.3892/or.2016.5198
32. Ni S, Ren F, Xu M-D, Tan C, Weiwei W, Huang Z, et al. CTHRC1 overexpression predicts poor survival and enhances epithelial-mesenchymal transition in colorectal cancer. *Cancer Med* (2018) 7(11):5643–54. doi: 10.1002/cam4.1807
33. Lee J, Song J, Kwon E-S, Jo S, Kang M, Kim Y, et al. CTHRC1 promotes angiogenesis by recruiting Tie2-expressing monocytes to pancreatic tumors. *Exp Mol Med* (2016) 48:e261. doi: 10.1038/emm.2016.87
34. Wang C, Li Z, Shao F, Yang X, Feng X, Shi S, et al. High expression of Collagen Triple Helix Repeat Containing 1 (CTHRC1) facilitates progression of oesophageal squamous cell carcinoma through MAPK/MEK/ERK/FRA-1 activation. *J Exp Clin Cancer Res CR* (2017) 36(1):84. doi: 10.1186/s13046-017-0555-8
35. Sakaguchi S, Miyara M, Costantino C, Hafler D. FOXP3+ regulatory T cells in the human immune system. *Nat Rev Immunol* (2010) 10:490–500. doi: 10.1038/nri2785

36. Sawant A, Hensel J, Chanda D, Harris B, Siegal G, Maheshwari A, et al. Depletion of Plasmacytoid Dendritic Cells Inhibits Tumor Growth and Prevents Bone Metastasis of Breast Cancer Cells. *J Immunol (Baltimore Md 1950)* (2012) 189:4258–65. doi: 10.4049/jimmunol.1101855
37. Ochoa A, Zea A, Hernandez C, Rodriguez P. Arginase, Prostaglandins, and Myeloid-Derived Suppressor Cells in Renal Cell Carcinoma. *Clin Cancer Res* (2007) 13:721s–6s. doi: 10.1158/1078-0432.CCR-06-2197
38. Shang B, Liu Y, Jiang SJ. Prognostic value of tumor-infiltrating FoxP3+ regulatory T cells in cancers: A systematic review and meta-analysis. *Sci Rep* (2015) 5:15179. doi: 10.1038/srep15179
39. Walter S, Weinschenk T, Stenzl A, Pluzanska A, Szczylik C, Staehler M, et al. Multipeptide immune response to cancer vaccine IMA901 after single-dose cyclophosphamide associates with longer patient survival. *Nat Med* (2012) 18 (8):1254–61. doi: 10.1038/nm.2883
40. Grewal S, Moazed D. Heterochromatin and Epigenetic Control of Gene Expression. *Science (New York NY)* (2003) 301:798–802. doi: 10.1126/science.1086887
41. Feinberg A, Tycko B. The history of cancer epigenetics. *Nat Rev Cancer* (2004) 4:143–53. doi: 10.1038/nrc1279
42. Ehrlich M. DNA methylation in cancer: too much, but also too little. *Oncogene* (2002) 21:5400–13. doi: 10.1038/sj.onc.1205651
43. Sun XJ, Wang MC, Zhang FH, Kong X. An integrated analysis of genome-wide DNA methylation and gene expression data in hepatocellular carcinoma. *FEBS Open Bio* (2018) 8(7):1093–103. doi: 10.1002/2211-5463.12433
44. Hudler P. Genetic Aspects of Gastric Cancer Instability. *Sci World J* (2012) 2012:761909. doi: 10.1100/2012/761909
45. Wang P, Wang Y-C, Chen X-Y, Shen Z-Y, Cao H, Zhang Y-J, et al. CTHRC1 is upregulated by promoter demethylation and transforming growth factor-β1 and may be associated with metastasis in human gastric cancer. *Cancer Sci* (2012) 103(7):1327–33. doi: 10.1111/j.1349-7006.2012.02292.x

Conflict of Interest: The authors declare that the research was conducted in the absence of any commercial or financial relationships that could be construed as a potential conflict of interest.

Copyright © 2021 Zhou, Shen, Xiong, Cheng, Xu, Wang, Qian, Ju and Zhang. This is an open-access article distributed under the terms of the Creative Commons Attribution License (CC BY). The use, distribution or reproduction in other forums is permitted, provided the original author(s) and the copyright owner(s) are credited and that the original publication in this journal is cited, in accordance with accepted academic practice. No use, distribution or reproduction is permitted which does not comply with these terms.

frontiers in Oncology

REVIEW
published: 19 March 2021
doi: 10.3389/fonc.2021.648968

Emerging Biomarkers for Predicting Bladder Cancer Lymph Node Metastasis

Chunyu Zhang[1], Jiao Hu[1], Huihuang Li[1], Hongzhi Ma[2], Belaydi Othmane[1], Wenbiao Ren[1,3], Zhenglin Yi[1], Dongxu Qiu[1], Zhenyu Ou[1], Jinbo Chen[1] and Xiongbing Zu[1]**

[1] Department of Urology, Xiangya Hospital, Central South University, Changsha, China, [2] Department of Radiation Oncology, Hunan Cancer Hospital, Central South University, Changsha, China, [3] George Whipple Lab for Cancer Research, University of Rochester Medical Institute, Rochester, NY, United States

Bladder cancer is one of the leading causes of cancer deaths worldwide. Early detection of lymph node metastasis of bladder cancer is essential to improve patients' prognosis and overall survival. Current diagnostic methods are limited, so there is an urgent need for new specific biomarkers. Non-coding RNA and m6A have recently been reported to be abnormally expressed in bladder cancer related to lymph node metastasis. In this review, we tried to summarize the latest knowledge about biomarkers, which predict lymph node metastasis in bladder cancer and their mechanisms. In particular, we paid attention to the impact of non-coding RNA on lymphatic metastasis of bladder cancer and its specific molecular mechanisms, as well as some prediction models based on imaging, pathology, and biomolecules, in an effort to find more accurate diagnostic methods for future clinical application.

Keywords: lymph node metastasis, bladder cancer, biomarkers, oncogenes, tumor suppressor genes

OPEN ACCESS

Edited by:
Matteo Ferro, European Institute of Oncology (IEO), Italy

Reviewed by:
Felice Crocetto, Federico II University Hospital, Italy
Ciro Imbimbo, University of Naples Federico II, Italy
Nicola Longo, Federico II University Hospital, Italy

***Correspondence:**
Xiongbing Zu
zuxbxyyy@126.com
Jinbo Chen
chenjinbo1989@yahoo.com

Specialty section:
This article was submitted to Genitourinary Oncology, a section of the journal Frontiers in Oncology

Received: *14 January 2021*
Accepted: *05 March 2021*
Published: *19 March 2021*

Citation:
Zhang C, Hu J, Li H, Ma H, Othmane B, Ren W, Yi Z, Qiu D, Ou Z, Chen J and Zu X (2021) Emerging Biomarkers for Predicting Bladder Cancer Lymph Node Metastasis. Front. Oncol. 11:648968. doi: 10.3389/fonc.2021.648968

INTRODUCTION

Bladder cancer (BCa) is the 10th most common cancer form, causing an estimated 549,000 new cases and 200,000 deaths in 2018. The incidence of BCa in men is four times that of women, and smoking is the most important risk factor for BCa in the population (1). More than 90% of bladder cancers are urothelial carcinoma, and the rest are squamous cell carcinoma and adenocarcinoma.

The most common metastatic manner of BCa is lymph node metastasis (LNM), which is more common in pelvic lymph nodes. LNM has a great influence on the prognosis and survival rate of BCa patients. For BCa patients with positive LNM, the 5-year CSS rate was 27.7%, which is significantly lower than that of patients without lymph node metastasis (2). CT or MRI is commonly used in clinical practice to diagnose pelvic LNM, but it is often difficult to accurately detect metastatic lymph nodes less than 6.8 mm in diameter (3). Many studies have recently reported the correlation between molecular markers and BCa metastasis, indicating a direct link between LNM and abnormal expression of specific biomarkers. Therefore, high-risk LNM patients can be diagnosed by detecting specific biomarkers to achieve early detection and early treatment, thereby achieving timely treatment and improving the survival rate.

Moreover, some predictive models, including imaging, pathology, and molecular markers, have been gradually developed and verified. In this review, we summarized the markers for LNM in BCa

from different aspects, including genes, non-coding RNA, and some predictive models (**Figure 1**). The downstream genes of non-coding RNA are specifically listed here (**Table 1**). Generally, mechanisms for LNM in cancers mainly include cell proliferation, cell invasion and migration, inhibition of cell apoptosis, and chemosensitivity. Based on this, we also elaborated on the regulation mechanism of these biomarkers.

THE MOLECULAR FUNCTION OF GENES IN BCA WITH LNM

There have been many studies on genes as markers for lymph node metastasis in bladder cancer. These genes act as oncogenes or tumor suppressor genes to influence the progression of cancer (**Figure 2**).

Genes as Oncogenes

VEGF-C (vascular endothelial growth factor C) is the first discovered lymphangiogenesis factor. It contains the mature form of the VEGF homology region. Our team's studies found that the expression of VEGF-C in BCa patients with LNM was significantly higher than that in BCa patients without LNM (57). Simultaneously, we also found that VEGF-C can promote proliferation, invasion, metastasis, and mitomycin C resistance of BCa cells. The mechanisms for that are thought to be related to the increased ratio of Bcl-2/Bax, inactivation of Caspase-3, and increased expression of MMP-9. Also, phosphorylated p38 MAPK and Akt, Keratin 8, Serpin B5, and Annexin A8 may be involved (58, 59). VEGF-C can promote the formation of tumor lymphatic vessels and the metastasis of tumor cells to regional lymph nodes. The combination of the activated VEGF-C and VEGFR-3 can induce phosphorylation of tyrosine kinase, causing the proliferation of lymphatic endothelial cells, thereby promoting the proliferation or expansion of lymphatic vessels (60). VEGF-C also positively affected primary tumor cells' invasiveness since it changed the adhesion of tumor cells to the extracellular matrix, thereby providing the necessary environmental conditions for tumor cells to more easily transfer to the surrounding extracellular matrix. VEGF-C can stimulate lymphatic endothelial cells to release proteolytic enzymes, such as uPA, which facilitate the invasion and infiltration of cancer cells into the matrix, making cancer cells more easily detached from the original tissue (61). The up-regulation of VEGF-C may be the reason for BCa cells' resistance to cisplatin, and the inhibition of VEGF-C reverses the resistance by increasing the expression level of maspin (62). Therefore, we suggest that VEGF-C and VEGFR-3 expression may serve as new indicators for early detection and diagnosis of BCa lymphatic metastasis in the future. Additionally, COX-2 may stimulate VEGF-C secretion to promote the formation of lymphatic vessels (63). COX-2, a subtype enzyme in the COX family, is an inducible enzyme. COX (Cyclooxygenase) is a rate-limiting enzyme in prostaglandin synthesis, which can catalyze arachidonic acid metabolites to prostaglandins. Previous

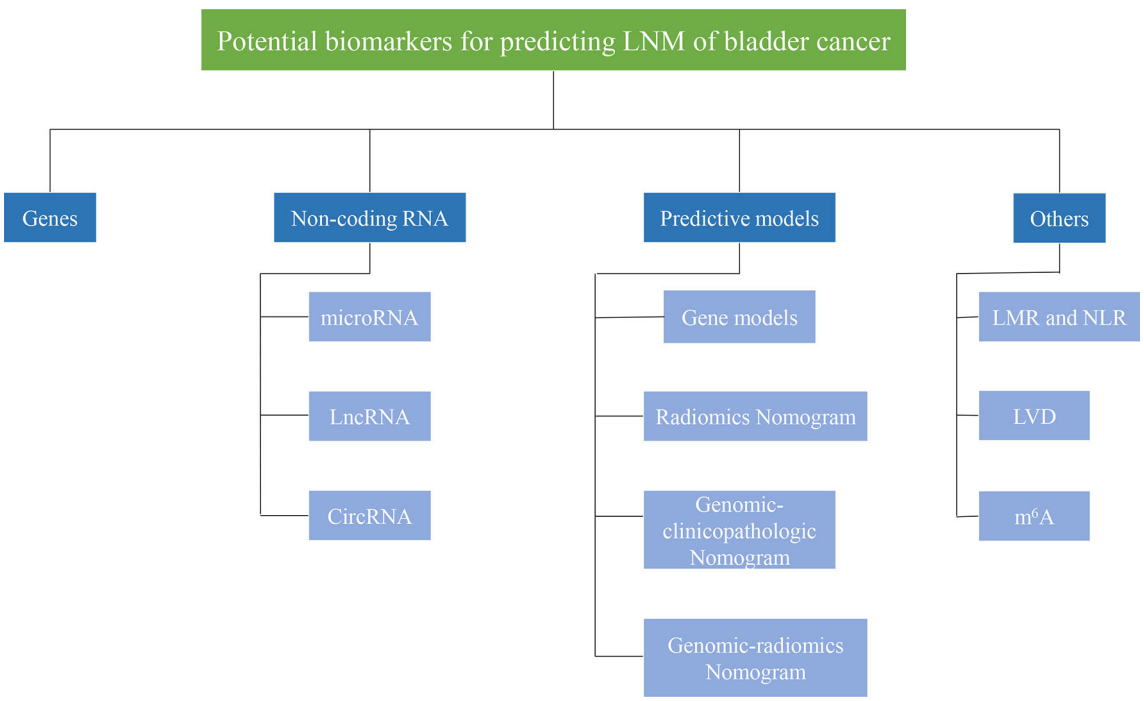

FIGURE 1 | Potential biomarkers for predicting lymph node metastasis of bladder cancer. Biomarkers for predicting lymphatic metastasis of bladder cancer can be divided into different categories, such asgenes, non-coding RNA, prediction models.

TABLE 1 | Downstream genes of non-coding RNA in bladder cancer.

Marker	Relationship with downstream genes	Downstream genes	Reference
miR-101	Negative	FZD4	(4)
		c-FOS	(5)
		c-Met	(6)
		VEGF-C	(7)
		COX-2	(8)
miR-143	Negative	COX-2	(9)
		MSI2	(10)
miR-133b	Positive	DUSP1	(11)
	Negative	Bcl-w、Akt1	(12)
		Epidermal growth factor receptor	(13)
		TAGLN2	(14)
miR-539	Negative	IGF-1R、AKT、ERK	(15)
miR-497	Positive	E-cadherin	(16)
	Negative	Vimentin	
		BIRC5、WNT7A	(17)
		E2F3	(18)
miR-154	Negative	RSF1、RUNX2	(19)
		ATG7	(20)
miR-223	Positive	Caspase-3/7	(21)
	Negative	WDR62	
		ANLN	(22)
		Nuclear receptor co-activator 1	(23)
miR-148a	Negative	DNMT1	(24)
miR-3658	Positive	LASS2	(25)
LncRNA MALAT1	Negative	E-cadherin	(26)
	Positive	ZEB1, ZEB2	
		VEGF-C	(27)
		Bcl-2、MMP-13	(28)
		Foxq1	(29)
		Cyclin D1	(30)
LncRNA PVT1	Positive	VEGF-C	(31)
		CDK1	(32)
LncRNA OXCT1-AS1	Positive	JAK1	(33)
LncRNA BLACAT2	Positive	VEGF-C	(34)
LncRNA LNMAT1	Positive	CCL-2、VEGF-C	(35)
LncRNA SNHG16	Positive	ZEB1、ZEB2	(36)
		TIMP3	(37)
		STAT3	(38)
LncRNA ZFAS1	Positive	ZEB1、ZEB2	(39)
	Negative	KLF2、NKD2	
LncRNA DLX6-AS1	Positive	HSP90B1	(40)
		Wnt/β-catenin	(41)
LINC01296	Positive	EMT	(42)
LncRNA DANCR	Positive	CCND1、PLAU	(43)
		MSI2	(44)
LncRNA SPRY4-IT1	Positive	EZH2	(45)
LncRNA NNT-AS1	Positive	HMGB1	(46)
		PODXL	(47)
LncRNA LNMAT2	Positive	PROX1	(48)
LncRNA HOXA-AS2	Positive	Smad2	(49)
LncRNA HNF1A-AS1	Positive	Bcl-2	(50)
CircHIPK3	Negative	HPSE、MMP-9、VEGF	(51)
CircFNDC3B	Negative	G3BP2/SRC/FAK	(52)
CircFUT8	Positive	KLF10	(53)
CircACVR2A	Positive	EYA4	(54)
CircPICALM	Positive	STEAP4、EMT	(55)
cTFRC	Positive	TFRC	(56)

studies have shown that COX-2 expression was significantly increased in BCa tissues and was associated with LNM (64).

Another well-known gene that functions as an oncogene in BCa is PCMT1. PCMTl gene is located at 6p22.3-6q24, about 60kb in length, and contains eight exons and seven introns. Studies have shown that the expression of PCMT1 in BCa tissue was higher than that in normal urothelial tissue, and its expression was significantly associated with LNM. PCMT1 regulated the migration and invasion of BCa cells by regulating the expression of epithelial-mesenchymal transition (EMT) related genes, such as E-cadherin, vimentin, Snail, and Slug (65). Sonic Hedgehog (Shh) also activated EMT to promote tumorigenicity and stemness in BCa (66). Shh is a member of the Hedgehog (HH) family. The study found that the expression of Shh protein was significantly correlated with LNM (67). Shh can promote the migration and invasion of BCa cells. The Shh pathway's activation through the binding of the Shh ligand to the transmembrane protein Patched1 eliminates the inhibitory effect on smoothened (SMO). The activation of SMO produced a downstream signaling cascade that led to the nuclear translocation of the transcription factor Gli1, which further induce the transcription of target genes (68).

The overexpression of CXCL5 can promote the progression of BCa. CXCL5, known as epithelial-derived neutrophil-activating peptide 78 (ENA78), is a small (8-14 kDa) protein belonging to the CXC-type chemokine family. CXCL5 (chemokine C-X-C motif ligand 5) was expressed higher in BCa tissues than normal tissues, which was associated with LNM (69). It is also related to promoting mitomycin resistance by activating EMT and NF-κB pathway (70). Moreover, CXCL5 increased BCa cells proliferation, migration, and decreased cell apoptosis through Snail, PI3K-AKT, and ERK1/2 signaling pathways. In addition, CXCL5 combined with CXCR2 induces the expression of MMP-2 and MMP-9 and activates the PI3K/AKT signaling pathway (71, 72). Matrix metalloproteinases (MMPs) are a family of structurally related zinc-dependent endopeptidases that can substantially degrade all components of the extracellular matrix (ECM). MMP2, MMP7, and MMP9 are important members of the matrix metalloproteinase family. MMP-2 can physiologically degrade type IV collagen. Mohammad et al. (73) found that the higher the MMP-2 activity level in BCa, the higher the positive rate of LNM. MMP-7, also known as matrilysin, is the smallest MMP. It is produced by the tumor cells themselves, unlike other MMPs which are solely produced by stromal cells. Studies have shown that high expression of MMP-7 was significantly associated with LNM of BCa (74). Studies have shown that MMP-9 genes and proteins' expression levels in urine and blood of patients with BCa were significantly increased (75). These genes can also decompose the extracellular matrix, make cancer cells easily pass through the extracellular matrix, and promote tumor metastasis.

In addition, Zhao et al. (76) identified a new oncogene candidate, IPO11, in BCa, which is located on chromosome 5q12. Importin-11, a 116 kD protein, is encoded by IPO11. It is a karyopherin family member, which mediates the nucleocytoplasmic transport of proteins and nucleic acids

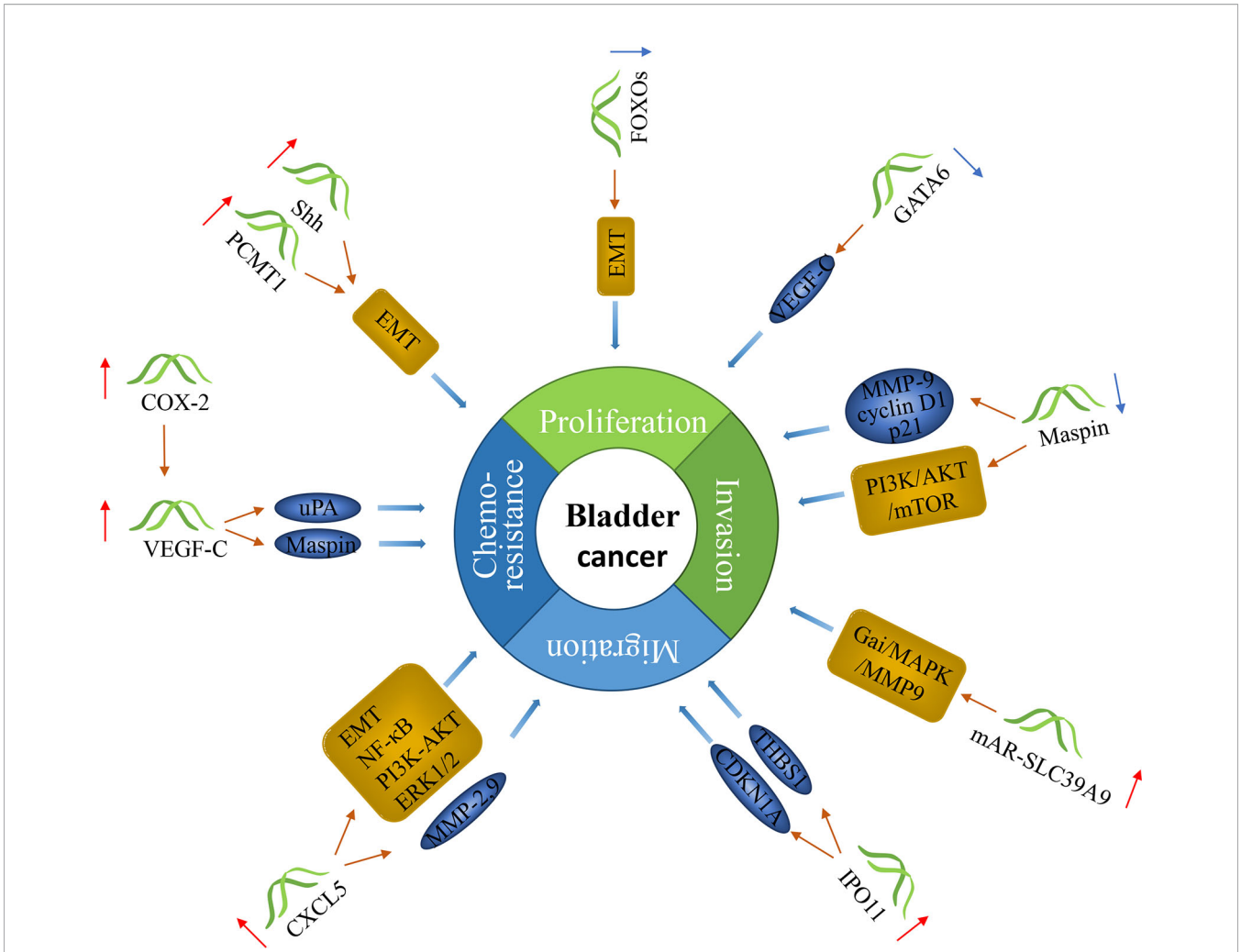

FIGURE 2 | The molecular function of genes in bladder cancer with lymph node metastasis. Genes can predict lymph node metastasis in bladder cancer. Some of them can promote the progression of cancer, and some can inhibit it.

through the nuclear pore complexes. Studies have shown that IPO11 mRNA was highly expressed in invasive BCa cell lines. The overexpression of importin-11 was positively correlated with LNM. Importin-11 can promote BCa cells' invasiveness, which may be related to the abnormal expression of CDKN1A and THBS1 (77). Presler et al. (78) found that SCD1 was overexpressed in BCa, which was related to LNM. SCD-1 (Stearoyl-CoA desaturase-1) can convert SFA (saturated fatty acids) to MUFA (monounsaturated fatty acids). It is located on chromosome 10q24.31. SCD inhibitors and SCD gene interference reduced the proliferation and invasion of BCa cells (79). FGFR3 (fibroblast growth factor receptor 3) stimulated SCD1 activity to promote tumor growth in BCa cells (80).

The studies of our team also found some new oncogenes. ISYNA1 (Inositol-3-phosphate synthase 1) was positively associated with tumor T stage and LNM of BCa patients. It is an important regulatory factor in promoting proliferation and inhibiting apoptosis in BCa cells (81). The high expression of mAR-SLC39A9 was directly associated with BCa pathological stage, pathological grade, and lymph node metastasis presence. It also increased BCa metastasis through Gαi/MAPK/MMP9 signaling (82).

Genes as Tumor Suppressors

Maspin (mammary sefine protease inhibitor) is an important member of the serin protease inhibitor (serpin) superfamily. It is located at 18q21.3-q23. Our team's previous studies found that Maspin expression in BCa tissue was significantly down-regulated in comparison with normal tissues adjacent to the cancer and was related also to LNM. The negative correlation between the protein expression level and VEGF-C is statistically significant (83, 84). Maspin can inhibit the invasion of BCa cells, and its growth-inhibiting properties were related to its localization in cells. The surface-bound Maspin directly controlled the adhesion of BCa cells to the blood vessel wall (85). The combination of nuclear-localized maspin and chromatin can effectively prevent cell migration. Mapsin mainly promoted the development of BCa through DNA

methylation and histone deacetylation to cause low expression of genes (86). Maspin modulated HDAC1 target genes, including cyclin D1, p21, MMP9, and vimentin (87). In our previous study, maspin could enhance Cisplatin chemosensitivity through the PI3K/AKT/mTOR signaling pathway in MIBC T24 and 5637 cell lines (88).

Another gene that functions as a tumor suppressor in BCa is GATA6. GATA6 (GATA-binding factor 6), a zinc-finger transcription factor, is located at 18q11.2. It regulates transcription cofactors and RNA polymerase II to the proximal promoter to regulate target genes' transcription. Wang et al. (89) found that GATA6 decreased in BCa, and further decreased in patients with positive LNM. GATA6 was significantly down-regulated in BCa through frequent promoter methylation. GATA6 mainly inhibited LNM of BCa by regulating VEGF-C. Down-regulation of GATA6 promoted VEGF-C transcription, which promoted lymphangiogenesis, resulting in an increased lymphatic spread of BCa. This increased spread shows that it is of great significance to check the methylation status of the GATA6 promoter in the urine of BCa patients. The low expression of FOXOs was also associated with LNM in BCa (90). FOXO (Forkhead box class O) is the subgroup O of forkhead box (FOX) transcription factors, which has four members, FOXO1, FOXO3, FOXO4 and FOXO6. FOXOs have a highly conserved forkhead DNA binding domain. FOXOs can inhibit the invasion of BCa cells by down-regulating Twist2 and YB-1 and up-regulating E-cadherin (91).

REGULATION OF MICRORNAS FOR BCA PATIENTS WITH LYMPH NODE METASTASIS

MiRNA is a type of 21-23nt small RNA, which can complement mRNA and either silence it or degrade it. Most miRNAs are down-regulated in bladder cancer. Moreover, they inhibit the lymph node metastasis of bladder cancer (**Figure 3**).

MiR-101 can suppress the progression of BCa. Studies have shown that the expression of miR-101 in BCa patients was down-regulated and significantly associated with LNM (92). Moreover, it can inhibit the proliferation, migration, and invasion of BCa cells by directly targeting FZD4 (frizzled class receptor 4), c-FOS, and c-Met (4–6). MiR-101 increased Cisplatin sensitivity by inhibiting the expression of VEGF-C and COX-2 in BCa cells (7, 8). MiR-143 also inhibited the growth and migration of BCa cells by targeting COX-2 (9). MiR-143 was reported to suppress the progression of BCa as well and it is located on chromosome 5q32. Liu et al. (93) found that miR-143 was down-expressed in the serum of BCa patients with LNM. It also directly affected the expression of MSI2 through its RNAi effect, which also effectively inhibited the KRAS network, thereby regulating BCa cells (10).

Another gene, miR-133b, is located on chromosome 6p12.2. Studies have shown that the expression level of miR-133b in BCa tissues is significantly reduced, which was significantly correlated with LNM (94). MiR-133b may inhibit the proliferation of BCa by up-regulating dual-specificity protein phosphatase 1 (DUSP1) (11). It inhibited angiogenesis and enhanced BCa cells' chemosensitivity to Gemcitabine by targeting transgelin 2 (TAGLN2) (14). MiR-133b can regulate the proliferation, migration, and invasion of BCa cells by down-regulating Bcl-w, Akt1, and epidermal growth factor receptor along with its downstream effector protein (12, 13). Liao et al. (15) found that miR-539 was down-regulated in BCa, and was related to LNM. MiR-539 is located on chromosome 14q32.31, and it can inhibit the proliferation and invasion of BCa cells by directly targeting IGF-1R and inactivating the AKT and ERK signaling pathways.

MiR-497 is also known as a tumor suppressor in BCa, and it is located on chromosome 17p13.1. Studies have revealed that the expression of miR-497 in BCa tissue was lower than that of adjacent non-cancer tissues, and it was correlated with LNM (16). MiR-497 can inhibit the proliferation, migration, and invasion of BCa by up-regulating E-cadherin and down-regulating vimentin, α-smooth muscle actin, BIRC5, WNT7A, and E2F3 (16–18). Previous studies have found that miR-154 was significantly down-regulated in BCa tissues and was associated with LNM. MiR-154 is located in the human imprinted 14q32 domain. MiR-154 inhibited the proliferation, migration, and invasion of BCa cells by regulating the expression of RSF1, RUNX2, and ATG7 (19, 20). MiR-223 is located on chromosome Xq12. Sugita et al. (21) found that the expression level of miR-223 was significantly reduced in BCa tissues, which was related to LNM. MiR-223 inhibited cell invasion and promoted cell apoptosis in BCa *via* caspase-3/7 activation and negatively regulating WDR62 (WD repeat domain 62), ANLN, and nuclear receptor coactivator 1 (21–23). MiR-148a, with 68 nucleotide sequences, locates to 7p15.2, and is confirmed by Ma et al. (95) that its expression level in BCa tissue is lower than that of adjacent normal tissues, and that its low expression level is associated with advanced tumor progression and LNM. Also, Lombard et al. (24) found that miR-148a increased the apoptosis of BCa cells by reducing the expression of DNA methyltransferase 1 (DNMT1).

MiR-3658 is known as an oncogene in BCa. The expression of miR-3658 in BCa tissue was up-regulated, and its expression was significantly related to the lymph node infiltration, distant metastasis, and TNM stage (96). It can also promote cell proliferation, migration, and invasion by targeting LASS2 (25).

LNCRNAS REGULATE LYMPH NODE METASTASIS IN BCA

LncRNA is a non-coding RNA with a length of more than 200 nucleotides and is closely related to cancer occurrence and development. It can directly bind to proteins to block its functions or change its cellular location, regulate mRNA translation and act as a miRNA sponge. Most lncRNAs act as oncogenes to promote lymphatic metastasis of bladder cancer (**Figure 4**).

Our team's studies found several lncRNAs as oncogenes, such as MALAT1, PVT1, and OXCT1-AS1. The expression of MALAT1 was positively associated with LNM in BCa. It

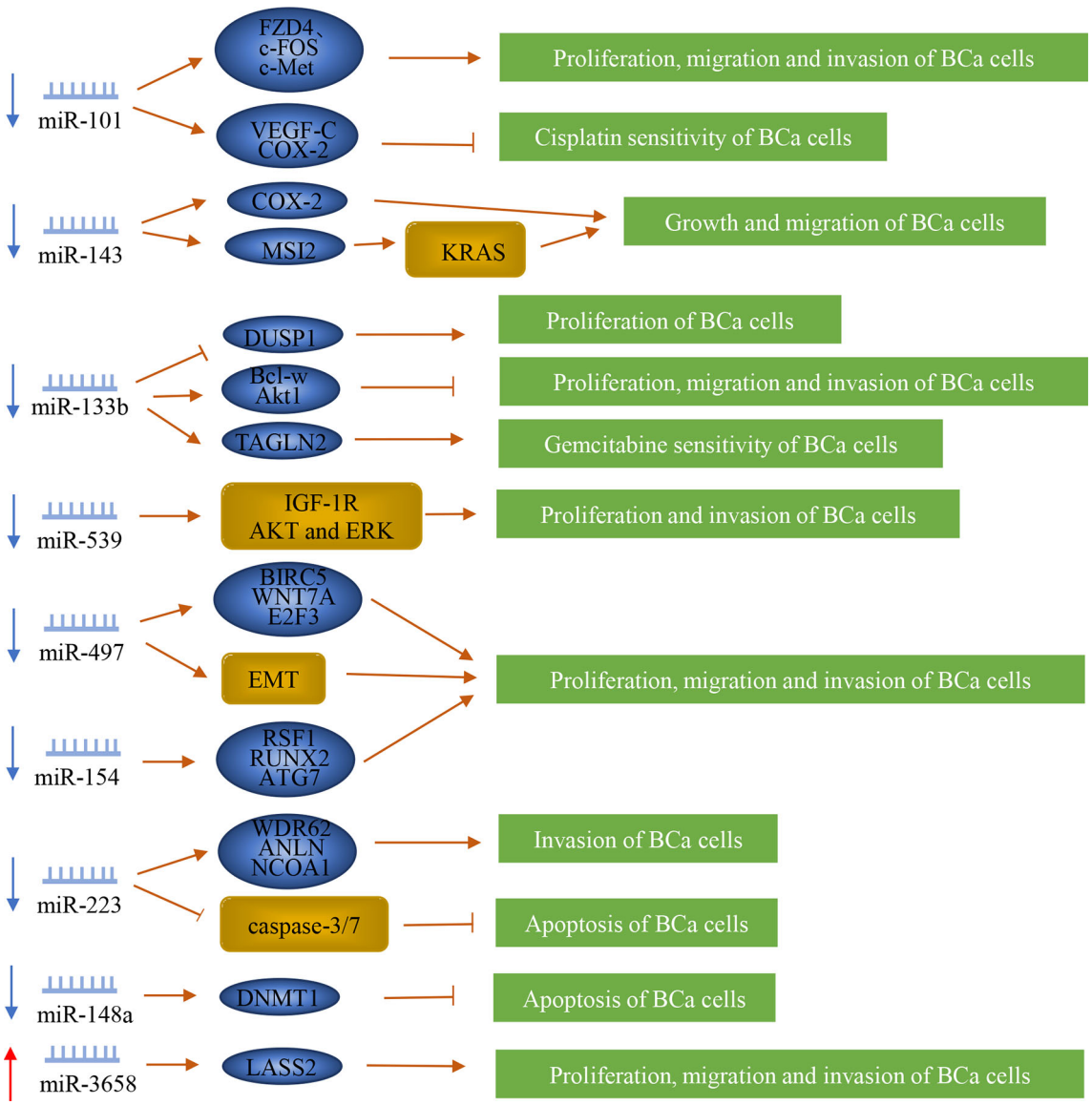

FIGURE 3 | Regulation of microRNAs in bladder cancer patients with lymph node metastasis. MiRNAs play a vital role in the lymph node metastasis of bladder cancer. They can promote or inhibit the metastasis of bladder cancer by regulating downstream genes or proteins.

enhanced the Cisplatin resistance of the BCa cells by regulating the miR-101-3p/VEGF-C pathway (27, 97). MALAT1 promoted proliferation and invasion by miR-125b-Bcl-2/MMP-13, miR-124/foxq1 and microRNA-34a/cyclin D1 in BCa cells (28–30). It also up-regulated EMT-associated ZEB1, ZEB2, and Slug and downregulated E-cadherin levels (26). LncRNA PVT1 is located at 8q24, downstream of MYC. High PVT1 expression is associated with higher tumor stage and positive lymph node metastasis (98). PVT1 directly interacted with miR-128, reducing the binding of miR-128 to VEGF-C, thereby inhibiting the degradation of VEGFC mRNA by miR-128 (31). Moreover, PVT1 down-regulated miR-31 to enhance CDK1 expression and promote the proliferation, migration, and invasion of BCa cells (32). LncRNA OXCT1-AS1 (OXCT1 antisense RNA 1) is located on chromosome 5p13.1 and was also significantly up-regulated in BCa cell lines with LNM and was found to be inhibiting miR-455-5p in order to up-regulate the expression of JAK1, thus promoting the invasion of BCa (33).

Some lncRNAs regulate VEGF-C to promote the progression of BCa. BLACAT2 (bladder cancer-associated transcript 2) was significantly overexpressed in BCa patients with LNM. It combines with the VEGF-C promoter by forming triplexes to up-regulate VEGF-C expression, thereby promoting lymphangiogenesis and lymphatic metastasis. BLACAT2

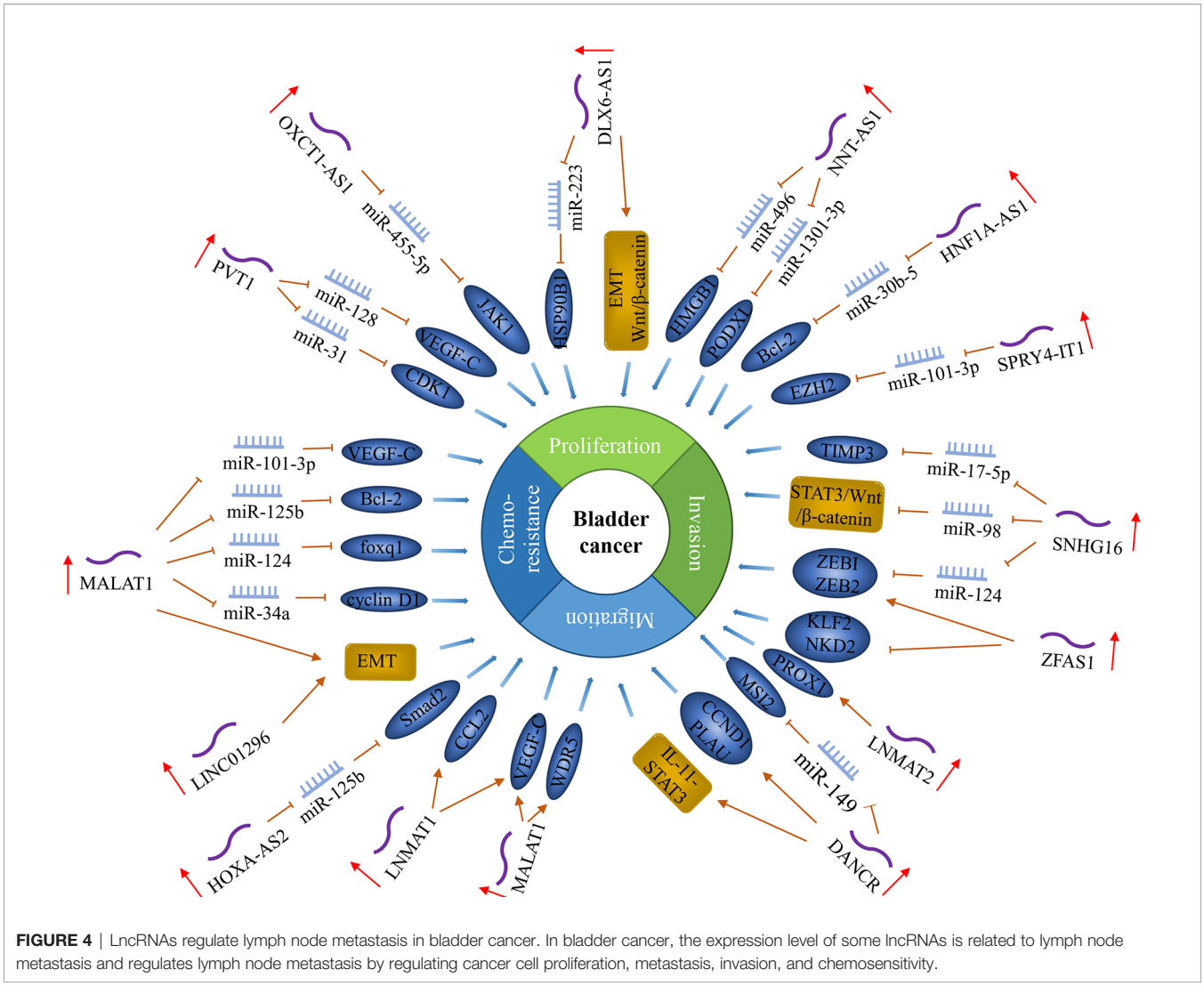

FIGURE 4 | LncRNAs regulate lymph node metastasis in bladder cancer. In bladder cancer, the expression level of some lncRNAs is related to lymph node metastasis and regulates lymph node metastasis by regulating cancer cell proliferation, metastasis, invasion, and chemosensitivity.

directly interacted with WDR5 (the core component of the histone H3K4 methyltransferase complex) to epigenetically induce lymphangiogenesis and invasion (34). LNMAT1 (lymph node metastasis-associated Transcript 1) was significantly up-regulated in BCa with LNM. LNMAT1 recruited hnRNPL to the CCL2 promoter to activate CCL2 expression, resulting in increased H3K4 trimethylation, thereby ensuring hnRNPL binding and enhancing transcription. In addition, LNMAT1-induced CCL2 regulated the tumor microenvironment in BCa tissues through tumor-associated macrophages (TAMs) infiltration and VEGF-C upregulation, which ultimately led to lymphangiogenesis and lymphatic metastasis (35).

Several lncRNAs promote the progression of BCa by regulating ZEB1 and ZEB2. LncRNA SNHG16 (small nucleolar RNA host gene 16) is encoded by a 7571-bp region at chromosome 17q25.1. Previous studies have found that SNHG16 was highly expressed in BCa tissues and was positively correlated with LNM (37). SNHG16 can regulate the proliferation, apoptosis, EMT, invasion, and migration of BCa by directly acting on the miR-17-5p/metalloproteinase 3 (TIMP3) axis, miR-200a-3p/ZEB1/ZEB2 axis, and miR-98/STAT3/Wnt/β-catenin pathway axis (36–38). LncRNA ZFAS1 (zinc finger antisense 1), located on the antisense strand of the ZNFX1 promoter region, is transcript antisense to the 5′- end of the gene zinc finger NFX1-type containing 1 (ZNFX1). Yang et al. (39) found that the expression level of ZFAS1 in BCa was increased and positively correlated with LNM. ZFAS1 can promote the proliferation, migration and invasion of BCa by down-regulating the expression of KLF2 and NKD2, and at the same time, up-regulating the expression of ZEB1 and ZEB2. It also promotes tumorigenesis of BCa through sponging miR-329 (99).

Also, some lncRNAs regulate EMT to promote BCa progression. LncRNA DLX6-AS1 (distal-less homeobox 6 antisense 1) is regulatory of members in the DLX gene family, which is localized on chromosome 7q21.3. DLX6-AS1 was

up-regulated in BCa, which was related to LNM. Overexpression of DLX6-AS1 promoted the proliferation, invasion, and migration of BCa cells by regulating EMT and Wnt/β-catenin signaling pathway activity (41). DLX6-AS1-mediated miR-223 silencing can promote the growth and invasion of BCa through the up-regulation of HSP90B1 (40). LINC01296 is a novel intergenic lncRNA located at 14q11.2. The expression of LINC01296 was positively correlated with lymph node-positive BCa, and its up-regulated expression can promote BCa cells metastasis by activating the EMT pathway (42).

Another lncRNA, DANCR (differentiation antagonizing non-protein coding RNA), is located on chromosome 4q12.5, which is mainly distributed in the cytoplasm. Chen et al. (43) found that DANCR was significantly up-regulated in BCa tissues and positively correlated with LNM. DANCR promoted the LNM and BCa cells' proliferation *via* DANCR guided LRPPRC (leucine-rich pentatricopeptide repeat containing) to stabilize its mRNA, then to activate IL-11-STAT3 signaling and increase CCND1 and PLAU expression. Zhan et al. (44) found that DANCR positively regulated the expression of MSI2 (musashi RNA binding protein 2) through sponging miR-149 to promote the malignant phenotype of BCa cells. Zhao et al. (100) found that the expression level of SPRY4-IT1 in BCa tissue was also higher than that of adjacent non-tumor tissues and was associated with LNM. SPRY4-IT1 is derived from the intron region of the SPRY4 gene and may contain several long hairpin secondary structures, which are located in 5q31.3. SPRY4-IT1 can promote proliferation and metastasis of BCa cells by sponging miR-101-3p to actively regulate the expression of EZH2 (45). Wu et al. (46) found that lncRNA NNT-AS1 was up-regulated in BCa, which was significantly associated with LNM. NNT-AS1 (nicotinamide nucleotide transhydrogenase antisense RNA 1) is located on chromosome 5p12 with 3 exons. NNT-AS1 promoted the proliferation, migration, and invasion of BCa cells by acting as a competing endogenous RNA for miR-496 to enhance the expression level of HMGB1. NNT-AS1 also targeted the miR-1301-3p/PODXL axis and activated the Wnt pathway, thereby enhancing BCa cells' growth (47). LncRNA LNMAT2 (lymph node metastasis-associated transcript 2) was overexpressed in urinary-EXO and serum-EXO of patients with BCa, which was related to LNM. LNMAT2 was found to bind to the prospero homeobox 1 (PROX1) promoter by inducing H3K4 trimethylation, which enhanced PROX1 transcription, thus promoting lymphangiogenesis and lymph node metastasis in bladder cancer (48).

Additionally, several lncRNAs positively correlated with LNM, including: (1) HOXA-AS2, which inhibited the expression of miR-125b to promote the expression of Smad2, thus promoting the migration and invasion of BCa cells (49); (2) HNF1A-AS1, which positively regulated the expression of Bcl-2 by sponging miR-30b-5 to promote the proliferation of bladder cancer and inhibited its apoptosis (50, 101); (3) ROR1-AS1, which promoted the growth and migration of bladder cancer by regulating miR-504 (102); (4) RMRP, which promoted the proliferation, migration, and invasion of bladder cancer cells by regulating miR-206 as a sponge (103).

THE ROLE OF CIRCRNAS FOR BCA LYMPH NODE METASTASIS

CircRNA is a type of non-coding RNA that forms a circular structure by covalent bonds but does not have a 5'-end cap and a 3'-end poly(A) tail. It is closely related to the occurrence and development of cancer. It can act as an mRNA 'sponge', regulate transcription and splicing, and interact with RNA-binding proteins (104). Most circRNA negatively regulates lymph node metastasis of bladder cancer, and some molecules positively regulate this process (**Figure 5**).

CircHIPK3 (circRNA ID: hsa_circ_0000284), also known as bladder cancer-related circular RNA-2 (BCRC-2), was significantly down-regulated in BCa and was negatively correlated with LNM. It originates from the second exon of the Homeodomain-interacting protein kinase 3 (HIPK3) gene. CircHIPK3 sponged miR-558 and prevented miR-558 from being transported into the nucleus to bind the promoter of heparanase (HPSE) gene in BCa cells, thereby down-regulating the expression of HPSE and its downstream targets such as MMP-9, and VEGF, thus weakening the migration, invasion and angiogenesis of BCa cells (51). Additionally, Liu et al. (52) confirmed that circFNDC3B was significantly down-regulated in BCa tissue, and its low expression was significantly correlated with LNM. It is originated from exons 5 and 6 of the FNDC3B gene. CircFNDC3B acted as a sponge of miR-1178-3p to inhibit G3BP2 and further inhibit the downstream SRC/FAK signaling pathway, thereby inhibiting the proliferation, migration, and invasion of BCa cells.

By screening RNA sequencing data generated from human BCa tissues and matched adjacent normal bladder tissues, two novel tumor suppressors were separately identified, which are circFUT8 and circACVR2A. CircFUT8 (circBase: hsa_circ_0003028) was originated from exon 3 of the FUT8 gene. CircACVR2A was derived from exons 3, 4, and 5 of the ACVR2A gene. These two tumor suppressors were down-regulated in BCa tissues and were related to LNM (53, 54). CircFUT8 regulated the expression of Slug by sponging miR-570-3p to promote the expression of Krüpple-like-factor 10 (KLF10), thus inhibiting the metastasis and invasion of BCa cells (54). CircACVR2A can inhibit the proliferation, migration, and invasion of BCa cells by directly interacting with miR-626 and acting as a miRNA sponge to regulate EYA4 expression (53). In addition, circPICALM was found to suppress cancer progression. It is generated from exons 9-12 of PICALM. It was down-regulated in BCa tissues and associated with LNM. CircPICALM acted as a miR-1265 sponge to regulate STEAP4 and further affect FAK phosphorylation and EMT, thereby inhibiting the metastasis of BCa (55).

Serval other circRNAs were found to be possibly promoting cancer progression by inducing the malignant proliferation or migration and invasion of cancer cells. Su et al. identified a novel circular RNA called cTFRC. His study has shown that cTFRC was up-regulated in BCa tissues and was associated with LNM. The study also revealed that cTFRC might act as a sponge for miR-107 to up-regulate the expression of TFRC (transferrin

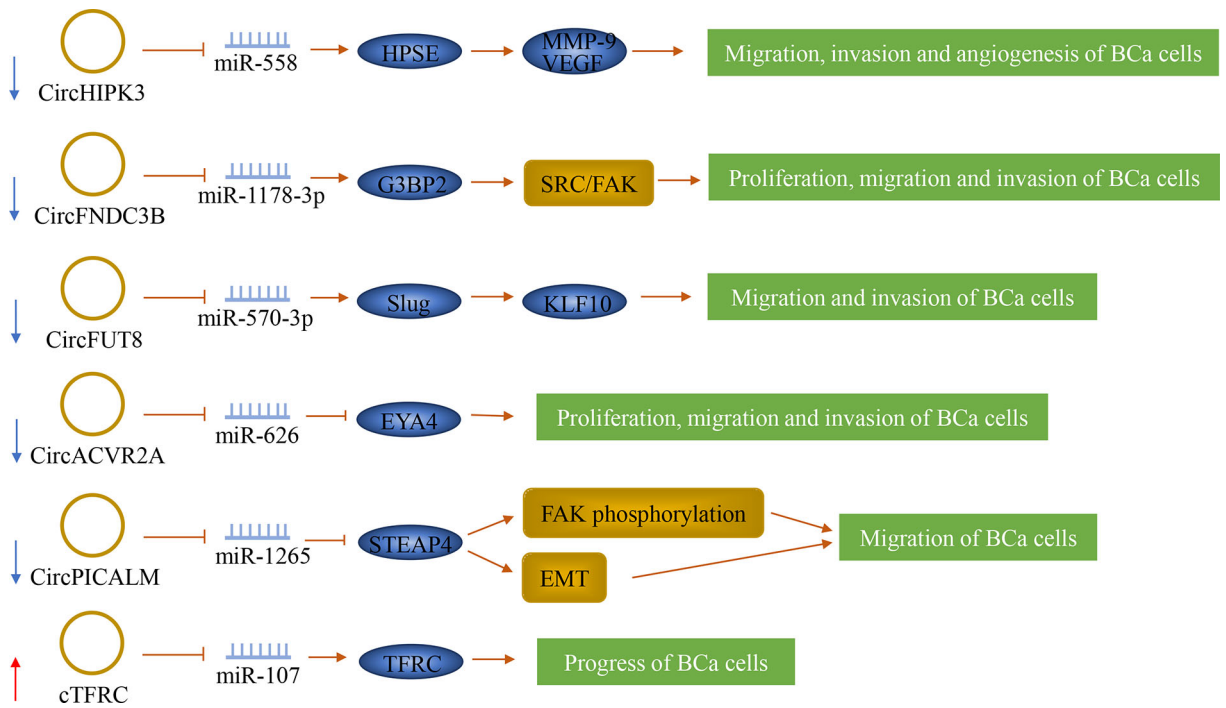

FIGURE 5 | The role of circRNAs in bladder cancer lymph node metastasis. CircRNAs can play a role in bladder cancer as oncogenes and tumor suppressor genes. They can also predict lymph node metastasis.

receptor), further promoting the transitional phenotype of BCa cells from epithelial to mesenchymal, thereby promoting the progress of BCa. (56) Another circRNA, circPTK2, was significantly increased in BCa, and its expression level is closely related to LNM. CircPTK2 can promote the proliferation and migration of BCa cells, but its specific mechanisms are still unclear (105).

OTHER MOLECULES AS PREDICTIVE BIOMARKERS

In addition to the molecules described above, studies on the tumor microenvironment and genetic modification can also help predict the lymphatic metastasis of bladder cancer.

Tumors often form a microenvironment that allows inflammatory cells to proliferate and produce large amounts of mediators. D'Andrea et al. (106) found that LMR (lymphocyte-to-monocyte ratio) and NLR (neutrophil-to-lymphocyte ratio) can be used as independent factors to predict the preoperative LNM and postoperative recurrence rate of BCa patients. Zhou et al. (107) found that lymphatic vessel density (LVD) within and around the tumor increases, and lymph node metastasis of bladder cancer also increase significantly. LVD is also related to the patient's prognosis.

m^6A (N6-methyladenosine) refers to methylation of the N6 position of adenosine bases. m6A RNA modification is a reversible posttranscriptional modification process maintained by a multicomponent methyltransferase 'writer' complex (KIAA1429, METTL3, METTL14, RBM15, WTAP, and ZC3H13) and removed by demethylases 'erasers' (FTO and ALKBH5). The function of m^6A in mRNA metabolism primarily depends on reader proteins, which include HNRNPC, YTHDC1, YTHDC2, YTHDF1, and YTHDF2. These regulators were differentially associated with different clinicopathological variables of BCa patients. The expression of WTAP was significantly correlated with LNM (108). Han et al. (109) found that METTL3 was significantly increased in bladder cancer and correlated with high histological grade and poor prognosis. METTL3 interacted with the microprocessor protein DGCR8 and positively modulated the pri-miR221/222 processes, resulting in the reduction of PTEN, which ultimately leads to the progression of bladder cancer.

PREDICTIVE MODELS AS BIOMARKERS FOR BCA LNM

The prediction model includes many aspects, such as molecules, imaging, and pathology. With the advent of models, the predictive results of bladder cancer lymphatic metastasis have become more and more reliable.

Gene Expression Model

Smith et al. (110) developed a 20-GEM (gene expression model) for predicting pathological node status, which is evaluable on

primary tumor tissue from clinically node-negative (cN0) patients. The predictive efficacy of the model is modest. Seiler et al. (111) invented a KNN51 (K-nearest neighbor classifier 51) to predict pathological lymph node metastases, but the lack of external validation limited its application. Lu et al. (112) presented a preoperative nomogram incorporating the LNM signature and a genomic mutation of MLL2. The LNM signature consists of 48 selected features. The model demonstrated good discrimination and good calibration. KNN51 included 24 non-coding features from the 51 gene signature, but the LN20 signature was based only on coding genes. Clinical factors were not incorporated into the predictive models for evaluation.

Radiomics Nomogram

Wu et al. (113, 114) developed and validated two types of radiomics nomograms incorporating the radiomics signature and CT/MRI-reported LN status for the preoperative prediction of LNM in patients with BCa, which was a non-invasive preoperative prediction tool. It shows favorable predictive accuracy, especially for cN0 patients. Multicenter validation should be performed to acquire high-level evidence for its clinical application.

Genomic-Clinicopathologic Nomogram

Wu et al. (115) constructed an inclusive nomogram that incorporated the five-mRNA-based classifier, image-based LN status, transurethral resection (TUR) T stage, and TUR lymphovascular invasion (LVI) to predict LNM in BCa patients. Five LN-status-related mRNAs include ADRA1D, COL10A1, DKK2, HIST2H3D, and MMP11. It shows favorable discriminatory ability and may aid in clinical decision-making, especially for cN-patients. However, it requires multicenter prospective clinical trials to provide high-level evidence for clinical application.

Genomic-Radiomics Nomogram

Chen et al. (116) validated a genomic-radiomics nomogram incorporating CCR7 and CT to predict LNM in patients with BCa. The combined evaluation of CCR7 and CT appeared to be a more reliable marker for lymph node metastasis in BCa than the diagnosis by CT or CCR7 alone. However, these results require further confirmation by large sample and multi-center prospective studies.

OTHER FACTORS AFFECTING THE PROGNOSIS OF BCA

Systemic Diseases

In recent years, studies have found that some systemic diseases were closely related to tumor occurrence and development. Metabolic syndrome (MetS) was defined as the presence of three of the following: hypertension, hyperlipidemia, diabetes, or body mass index >30. Previous studies have proved that MetS cannot predict higher pathological stages and the risks of LVI and LNM, but a single component of metabolic syndrome was related to them. Body mass index, waist circumference, and hypertension were positively correlated with the risk of higher pathological stages. And higher BMI value was related to lymphatic invasion and lymph node metastasis (117, 118). Obesity was significantly related to recurrence-free survival, cancer-specific survival, and overall mortality. Adipose tissue can produce a variety of inflammatory factors, including leptin, adiponectin, and cytokines. Leptin played an anti-tumor effect by promoting the proliferation and activation of natural killer cells (119, 120). Nonalcoholic fatty liver was positively correlated with

TABLE 2 | The relationship between biomarkers and prognosis in bladder cancer.

Reference	Marker	Relationship with LNM	Prognosis
57	VEGF-C	Positive	DFS
64	COX-2	Positive	OS
65	PCMT1	Positive	OS
67	Sonic Hedgehog	Positive	No
69	CXCL5	Positive	OS、PFS、RFS
75	MMPs	Positive	OS、RFS
76	IPO11	Positive	OS
79	SCD1	Positive	OS
–	ISYNA1	Positive	–
82	mAR-SLC39A9	Positive	OS、DFS
88	Maspin	Negative	OS、PFS
89	GATA6	Negative	OS
90	FOXO	Negative	OS
Chen et al. (4)	miR-101	Negative	OS
93	miR-143	Negative	OS
94	miR-133b	Negative	OS、PFS
–	miR-539	Negative	–
18	miR-497	Negative	OS
19	miR-154	Negative	OS
21	miR-223	Negative	No
95	miR-148a	Negative	OS
–	miR-3658	Positive	–
97	LncRNA MALAT1	Positive	OS
98	LncRNA PVT1	Positive	OS
–	LncRNA OXCT1-AS1	Positive	–
34	LncRNA BLACAT2	Positive	OS
35	LncRNA LNMAT1	Positive	OS、DFS
Peng et al. (37)	LncRNA SNHG16	Positive	OS
99	LncRNA ZFAS1	Positive	OS、PFS
–	LncRNA DLX6-AS1	Positive	–
42	LINC01296	Positive	OS
43	LncRNA DANCR	Positive	OS、DFS
100	LncRNA SPRY4-IT1	Positive	OS
46	LncRNA NNT-AS1	Positive	OS
	LncRNA LNMAT2	Positive	
–	LncRNA HOXA-AS2	Positive	–
Wang et al. (101)	LncRNA HNF1A-AS1	Positive	OS
Cheng et al. (102)	LncRNA ROR1-AS1	Positive	OS
103	LncRNA RMRP	Positive	OS
–	CircHIPK3	Negative	–
52	CircFNDC3B	Negative	OS
He et al. (53)	CircFUT8	Negative	OS
Dong et al. (54)	CircACVR2A	Negative	OS
55	CircPICALM	Negative	OS
56	cTFRC	Positive	OS
–	CircPTK2	Positive	–

OS, overall survival; DFS, disease free survival; PFS, progression-free survival; RFS, relapse free survival.

BCa, and it was a poor prognostic factor for BCa. Patients with nonalcoholic fatty liver disease had elevated vascular endothelial growth factor, interleukin 6, TNF-α, and IGF-1. These factors may increase the risk of BCa recurrence and lead to a poor prognosis (121). Studies have shown that patients with BCa had higher insulin resistance than those without cancer but with bladder disease (122). DM was associated with elevated BCa or cancer mortality risk, especially in men (123). Metformin is the most commonly used drug for patients with t2DM. Our team's study found that the intake of metformin was positively associated with RFS, which improved PFS and cancer-specific survival (124). Metformin targeted a YAP1-TEAD4 complex *via* AMPKα to regulate CCNE1/2 in BCa cells (125). It can suppress cyclin D1, cyclin-dependent kinase 4 (CDK4), E2F1, and mammalian target of rapamycin (mTOR) (126). The use of insulin can increase the risk of BCa progression (127). High-dose human insulin and insulin glargine similarly promoted T24 BCa cell proliferation *via* PI3K-independent activation of Akt (128).

Environmental Toxins

Environmental toxins are closely related to cancer occurrence and development, and arsenic is the most reported in BCa. Dimethylarsinic acid (DMAV) is a methylated metabolite of arsenicals found in most mammals, and long-term exposure to DMAV can lead to BCa. Previous studies have found that recurrent BCa with high arsenic levels in tissues was more aggressive and had a higher stage and grade, and recured earlier than people with low levels of arsenic (129). Zhou et al. found that chronic arsenic exposure can upregulate HER2 in human and rat bladder epithelial cells and promote the proliferation, migration, epithelial-mesenchymal transition, and angiogenesis of cancer cells by activating the MAPK, PI3K/AKT, and STAT3 pathways (130). Moreover, sodium arsenite can reduce the human urothelial WIF1 gene expression, increase its DNA methylation level, and promote cancer cells' migration. The WIF1 gene expression and its DNA methylation can be considered as potential biomarkers for the diagnosis of human BCa (131).

CONCLUSIONS

For the LNM in BCa, three mechanisms are mainly involved: tumor cell proliferation, tumor cell migration and invasion, and chemosensitivity. Most biomarkers are related to the proliferation, migration, and invasion of BCa cells. Several biomarkers are involved in chemosensitivity. MiR-143, miR-101, miR-133b, MALAT1, CXCL5, and VEGF-C are related to all three of the above mechanisms. These biomarkers are more likely to be prognostic factors for BCa with LNM, but a large number of retrospective studies are still needed for further verification. Previous studies have shown that most biomarkers have a clear relationship with the prognosis of BCa patients (**Table 2**). However, the relationship between these eight biomarkers: ISYNA1, miR-539, miR-3658, OXCT1-AS1, DLX6-AS1, HOXA-AS2, circHIPK3, and circPTK2 and prognosis is still unclear; therefore, further research is needed to tap into their potential for the prognosis of BCa patients. Many biological assessment methods are economical and accurate. For example, peripheral blood can detect MMP, LMR, and NLR. Urine can detect the methylation status of GATA6 promoter, CXCL5, and MMP. Genetic testing for LNM is more sensitive and specific than traditional pathological examinations and is particularly suitable for micrometastasis diagnosis. Those test samples are easy to obtain before surgery, with strong reproducibility and high clinical feasibility. Recently, the research on SNP and m6A is also a hot spot. The relationship between them and bladder cancer with lymph node metastasis is not yet clear, and further investigation is needed, but it provides new directions for our future research. As for imaging, pathology, and molecular composition models, they are more accurate in terms of predicting lymphatic metastasis for bladder cancer, which should be studied in-depth and applied to clinical practice.

AUTHOR CONTRIBUTIONS

CZ contributed to reading the literature, preparing figures and the table, and writing the manuscript. JH, HL, HM, BO, WR, ZY, DQ, ZO, JC, and XZ assisted with writing and revised the manuscript. All authors contributed to the article and approved the submitted version.

FUNDING

This work was supported by the National Natural Science Foundation of China (81873626, 81902592), Hunan Natural Science Foundation (2020JJ5884), Hunan Province Key R&D Program (2019SK2202), and Xiangya Hospital Youth Fund (2018Q09).

ACKNOWLEDGMENTS

We sincerely thank You-e He for editing the language of this article.

REFERENCES

1. Bray F, Ferlay J, Soerjomataram I, Siegel RL, Torre LA, Jemal A. Global cancer statistics 2018: GLOBOCAN estimates of incidence and mortality worldwide for 36 cancers in 185 countries. *CA Cancer J Clin* (2018) 68:394–424. doi: 10.3322/caac.21492
2. Zhang ZL, Dong P, Li YH, Liu ZW, Yao K, Han H, et al. Radical cystectomy for bladder cancer: oncologic outcome in 271 Chinese patients. *Chin J Cancer* (2014) 33:165–71. doi: 10.5732/cjc.012.10312
3. Li Y, Diao F, Shi S, Li K, Zhu W, Wu S, et al. Computed tomography and magnetic resonance imaging evaluation of pelvic lymph node metastasis in bladder cancer. *Chin J Cancer* (2018) 37:3. doi: 10.1186/s40880-018-0269-0

4. Hu Z, Lin Y, Chen H, Mao Y, Wu J, Zhu Y, et al. MicroRNA-101 suppresses motility of bladder cancer cells by targeting c-Met. *Biochem Biophys Res Commun* (2013) 435:82–7. doi: 10.1016/j.bbrc.2013.04.042
5. Long Y, Wu Z, Yang X, Chen L, Han Z, Zhang Y, et al. MicroRNA-101 inhibits the proliferation and invasion of bladder cancer cells *via* targeting c-FOS. *Mol Med Rep* (2016) 14:2651–6. doi: 10.3892/mmr.2016.5534
6. Chen L, Long Y, Han Z, Yuan Z, Liu W, Yang F, et al. MicroRNA-101 inhibits cell migration and invasion in bladder cancer *via* targeting FZD4. *Exp Ther Med* (2019a) 17:1476–85. doi: 10.3892/etm.2018.7084
7. Bu Q, Fang Y, Cao Y, Chen Q, Liu Y. Enforced expression of miR-101 enhances cisplatin sensitivity in human bladder cancer cells by modulating the cyclooxygenase-2 pathway. *Mol Med Rep* (2014) 10:2203–9. doi: 10.3892/mmr.2014.2455
8. Lei Y, Li B, Tong S, Qi L, Hu X, Cui Y, et al. miR-101 suppresses vascular endothelial growth factor C that inhibits migration and invasion and enhances cisplatin chemosensitivity of bladder cancer cells. *PloS One* (2015) 10:e0117809. doi: 10.1371/journal.pone.0117809
9. Song T, Zhang X, Wang C, Wu Y, Dong J, Gao J, et al. Expression of miR-143 reduces growth and migration of human bladder carcinoma cells by targeting cyclooxygenase-2. *Asian Pac J Cancer Prev* (2011) 12:929–33.
10. Tsujino T, Sugito N, Taniguchi K, Honda R, Komura K, Yoshikawa Y, et al. MicroRNA-143/Musashi-2/KRAS cascade contributes positively to carcinogenesis in human bladder cancer. *Cancer Sci* (2019) 110:2189–99. doi: 10.1111/cas.14035
11. Cai X, Qu L, Yang J, Xu J, Sun L, Wei X, et al. Exosome-transmitted microRNA-133b inhibited bladder cancer proliferation by upregulating dual-specificity protein phosphatase 1. *Cancer Med* (2020) 9:6009–19. doi: 10.1002/cam4.3263
12. Zhou Y, Wu D, Tao J, Qu P, Zhou Z, Hou J. MicroRNA-133 inhibits cell proliferation, migration and invasion by targeting epidermal growth factor receptor and its downstream effector proteins in bladder cancer. *Scand J Urol* (2013) 47:423–32. doi: 10.3109/00365599.2012.748821
13. Chen XN, Wang KF, Xu ZQ, Li SJ, Liu Q, Fu DH, et al. MiR-133b regulates bladder cancer cell proliferation and apoptosis by targeting Bcl-w and Akt1. *Cancer Cell Int* (2014) 14:70. doi: 10.1186/s12935-014-0070-3
14. Zhao F, Zhou LH, Ge YZ, Ping WW, Wu X, Xu ZL, et al. MicroRNA-133b suppresses bladder cancer malignancy by targeting TAGLN2-mediated cell cycle. *J Cell Physiol* (2019) 234:4910–23. doi: 10.1002/jcp.27288
15. Liao G, Chen F, Zhong J, Jiang X. MicroRNA−539 inhibits the proliferation and invasion of bladder cancer cells by regulating IGF−1R. *Mol Med Rep* (2018) 17:4917–24. doi: 10.3892/mmr.2018.8497
16. Wei Z, Hu X, Liu J, Zhu W, Zhan X, Sun S. MicroRNA-497 upregulation inhibits cell invasion and metastasis in T24 and BIU-87 bladder cancer cells. *Mol Med Rep* (2017) 16:2055–60. doi: 10.3892/mmr.2017.6805
17. Itesako T, Seki N, Yoshino H, Chiyomaru T, Yamasaki T, Hidaka H, et al. The microRNA expression signature of bladder cancer by deep sequencing: the functional significance of the miR-195/497 cluster. *PloS One* (2014) 9: e84311. doi: 10.1371/journal.pone.0084311
18. Zhang Y, Zhang Z, Li Z, Gong D, Zhan B, Man X, et al. MicroRNA-497 inhibits the proliferation, migration and invasion of human bladder transitional cell carcinoma cells by targeting E2F3. *Oncol Rep* (2016) 36:1293–300. doi: 10.3892/or.2016.4923
19. Zhao X, Ji Z, Xie Y, Liu G, Li H. MicroRNA-154 as a prognostic factor in bladder cancer inhibits cellular malignancy by targeting RSF1 and RUNX2. *Oncol Rep* (2017) 38:2727–34. doi: 10.3892/or.2017.5992
20. Zhang J, Mao S, Wang L, Zhang W, Zhang Z, Guo Y, et al. MicroRNA−154 functions as a tumor suppressor in bladder cancer by directly targeting ATG7. *Oncol Rep* (2019) 41:819–28. doi: 10.3892/or.2018.6879
21. Sugita S, Yoshino H, Yonemori M, Miyamoto K, Matsushita R, Sakaguchi T, et al. Tumor−suppressive microRNA−223 targets WDR62 directly in bladder cancer. *Int J Oncol* (2019) 54:2222–36. doi: 10.3892/ijo.2019.4762
22. Guo J, Cao R, Yu X, Xiao Z, Chen Z. MicroRNA-223-3p inhibits human bladder cancer cell migration and invasion. *Tumour Biol* (2017) 39:1010428317691678. doi: 10.1177/1010428317691678
23. Sugawara S, Yamada Y, Arai T, Okato A, Idichi T, Kato M, et al. Dual strands of the miR-223 duplex (miR-223-5p and miR-223-3p) inhibit cancer cell aggressiveness: targeted genes are involved in bladder cancer pathogenesis. *J Hum Genet* (2018) 63:657–68. doi: 10.1038/s10038-018-0437-8
24. Lombard AP, Mooso BA, Libertini SJ, Lim RM, Nakagawa RM, Vidallo KD, et al. miR-148a dependent apoptosis of bladder cancer cells is mediated in part by the epigenetic modifier DNMT1. *Mol Carcinog* (2016) 55:757–67. doi: 10.1002/mc.22319
25. Luan T, Zou R, Huang L, Li N, Fu S, Huang Y, et al. Hsa-miR-3658 Promotes Cell Proliferation, Migration and Invasion by Effecting LASS2 in Bladder Cancer. *Clin Lab* (2018) 64:515–25. doi: 10.7754/Clin.Lab.2017.171026
26. Ying L, Chen Q, Wang Y, Zhou Z, Huang Y, Qiu F. Upregulated MALAT-1 contributes to bladder cancer cell migration by inducing epithelial-to-mesenchymal transition. *Mol Biosyst* (2012) 8:2289–94. doi: 10.1039/c2mb25070e
27. Liu P, Li X, Cui Y, Chen J, Li C, Li Q, et al. LncRNA-MALAT1 mediates cisplatin resistance *via* miR-101-3p/VEGF-C pathway in bladder cancer. *Acta Biochim Biophys Sin (Shanghai)* (2019b) 51:1148–57. doi: 10.1093/abbs/gmz112
28. Xie H, Liao X, Chen Z, Fang Y, He A, Zhong Y, et al. LncRNA MALAT1 Inhibits Apoptosis and Promotes Invasion by Antagonizing miR-125b in Bladder Cancer Cells. *J Cancer* (2017) 8:3803–11. doi: 10.7150/jca.21228
29. Jiao D, Li Z, Zhu M, Wang Y, Wu G, Han X. LncRNA MALAT1 promotes tumor growth and metastasis by targeting miR-124/foxq1 in bladder transitional cell carcinoma (BTCC). *Am J Cancer Res* (2018) 8:748–60.
30. Liu Y, Gao S, Du Q, Zhao Q. Knockdown of long non-coding RNA metastasis associated lung adenocarcinoma transcript 1 inhibits the proliferation and migration of bladder cancer cells by modulating the microRNA-34a/cyclin D1 axis. *Int J Mol Med* (2019c) 43:547–56. doi: 10.3892/ijmm.2018.3959
31. Yu C, Longfei L, Long W, Feng Z, Chen J, Chao L, et al. LncRNA PVT1 regulates VEGFC through inhibiting miR-128 in bladder cancer cells. *J Cell Physiol* (2019) 234:1346–53. doi: 10.1002/jcp.26929
32. Tian Z, Cao S, Li C, Xu M, Wei H, Yang H, et al. LncRNA PVT1 regulates growth, migration, and invasion of bladder cancer by miR-31/CDK1. *J Cell Physiol* (2019) 234:4799–811. doi: 10.1002/jcp.27279
33. Chen JB, Zhu YW, Guo X, Yu C, Liu PH, Li C, et al. Microarray expression profiles analysis revealed lncRNA OXCT1-AS1 promoted bladder cancer cell aggressiveness *via* miR-455-5p/JAK1 signaling. *J Cell Physiol* (2019b) 234:13592–601. doi: 10.1002/jcp.28037
34. He W, Zhong G, Jiang N, Wang B, Fan X, Chen C, et al. Long noncoding RNA BLACAT2 promotes bladder cancer-associated lymphangiogenesis and lymphatic metastasis. *J Clin Invest* (2018) 128:861–75. doi: 10.1172/JCI96218
35. Chen C, He W, Huang J, Wang B, Li H, Cai Q, et al. LNMAT1 promotes lymphatic metastasis of bladder cancer *via* CCL2 dependent macrophage recruitment. *Nat Commun* (2018) 9:3826. doi: 10.1038/s41467-018-06152-x
36. Feng F, Chen A, Huang J, Xia Q, Chen Y, Jin X. Long noncoding RNA SNHG16 contributes to the development of bladder cancer *via* regulating miR-98/STAT3/Wnt/β-catenin pathway axis. *J Cell Biochem* (2018) 119:9408–18. doi: 10.1002/jcb.27257
37. Peng H, Li H. The encouraging role of long noncoding RNA small nuclear RNA host gene 16 in epithelial-mesenchymal transition of bladder cancer *via* directly acting on miR-17-5p/metalloproteinases 3 axis. *Mol Carcinog* (2019) 58:1465–80. doi: 10.1002/mc.23028
38. Chen W, Jiang T, Mao H, Gao R, Zhang H, He Y, et al. SNHG16 regulates invasion and migration of bladder cancer through induction of epithelial-to-mesenchymal transition. *Hum Cell* (2020b) 33:737–49. doi: 10.1007/s13577-020-00343-9
39. Yang H, Li G, Cheng B, Jiang R. ZFAS1 functions as an oncogenic long non-coding RNA in bladder cancer. *Biosci Rep* (2018) 38(3):BSR20180475. doi: 10.1042/BSR20180475
40. Fang C, Xu L, He W, Dai J, Sun F. Long noncoding RNA DLX6-AS1 promotes cell growth and invasiveness in bladder cancer *via* modulating the miR-223-HSP90B1 axis. *Cell Cycle* (2019) 18:3288–99. doi: 10.1080/15384101.2019.1673633
41. Guo J, Chen Z, Jiang H, Yu Z, Peng J, Xie J, et al. The lncRNA DLX6-AS1 promoted cell proliferation, invasion, migration and epithelial-to-mesenchymal transition in bladder cancer *via* modulating Wnt/β-catenin signaling pathway. *Cancer Cell Int* (2019b) 19:312. doi: 10.1186/s12935-019-1010-z

42. Wang X, Wang L, Gong Y, Liu Z, Qin Y, Chen J, et al. Long noncoding RNA LINC01296 promotes cancer-cell proliferation and metastasis in urothelial carcinoma of the bladder. *Onco Targets Ther* (2019a) 12:75–85. doi: 10.2147/OTT.S192809
43. Chen Z, Chen X, Xie R, Huang M, Dong W, Han J, et al. DANCR Promotes Metastasis and Proliferation in Bladder Cancer Cells by Enhancing IL-11-STAT3 Signaling and CCND1 Expression. *Mol Ther* (2019c) 27:326–41. doi: 10.1016/j.ymthe.2018.12.015
44. Zhan Y, Chen Z, Li Y, He A, He S, Gong Y, et al. Long non-coding RNA DANCR promotes malignant phenotypes of bladder cancer cells by modulating the miR-149/MSI2 axis as a ceRNA. *J Exp Clin Cancer Res* (2018) 37:273. doi: 10.1186/s13046-018-0921-1
45. Liu D, Li Y, Luo G, Xiao X, Tao D, Wu X, et al. LncRNA SPRY4-IT1 sponges miR-101-3p to promote proliferation and metastasis of bladder cancer cells through up-regulating EZH2. *Cancer Lett* (2017) 388:281–91. doi: 10.1016/j.canlet.2016.12.005
46. Wu D, Zhang T, Wang J, Zhou J, Pan H, Qu P. Long noncoding RNA NNT-AS1 enhances the malignant phenotype of bladder cancer by acting as a competing endogenous RNA on microRNA-496 thereby increasing HMGB1 expression. *Aging (Albany NY)* (2019a) 11:12624–40. doi: 10.18632/aging.102591
47. Liu Y, Wu G. NNT-AS1 enhances bladder cancer cell growth by targeting miR-1301-3p/PODXL axis and activating Wnt pathway. *Neurourol Urodyn* (2020) 39:547–57. doi: 10.1002/nau.24238
48. Chen C, Luo Y, He W, Zhao Y, Kong Y, Liu H, et al. Exosomal long noncoding RNA LNMAT2 promotes lymphatic metastasis in bladder cancer. *J Clin Invest* (2020c) 130:404–21. doi: 10.1172/JCI130892
49. Wang F, Wu D, Chen J, Chen S, He F, Fu H, et al. Long non-coding RNA HOXA-AS2 promotes the migration, invasion and stemness of bladder cancer *via* regulating miR-125b/Smad2 axis. *Exp Cell Res* (2019b) 375:1–10. doi: 10.1016/j.yexcr.2018.11.005
50. Wang YH, Liu YH, Ji YJ, Wei Q, Gao TB. Upregulation of long non-coding RNA HNF1A-AS1 is associated with poor prognosis in urothelial carcinoma of the bladder. *Eur Rev Med Pharmacol Sci* (2018c) 22:2261–5.
51. Li Y, Zheng F, Xiao X, Xie F, Tao D, Huang C, et al. CircHIPK3 sponges miR-558 to suppress heparanase expression in bladder cancer cells. *EMBO Rep* (2017b) 18:1646–59. doi: 10.15252/embr.201643581
52. Liu H, Bi J, Dong W, Yang M, Shi J, Jiang N, et al. Invasion-related circular RNA circFNDC3B inhibits bladder cancer progression through the miR-1178-3p/G3BP2/SRC/FAK axis. *Mol Cancer* (2018) 17:161. doi: 10.1186/s12943-018-0908-8
53. Dong W, Bi J, Liu H, Yan D, He Q, Zhou Q, et al. Circular RNA ACVR2A suppresses bladder cancer cells proliferation and metastasis through miR-626/EYA4 axis. *Mol Cancer* (2019) 18:95. doi: 10.1186/s12943-019-1025-z
54. He Q, Yan D, Dong W, Bi J, Huang L, Yang M, et al. circRNA circFUT8 Upregulates Krüpple-like Factor 10 to Inhibit the Metastasis of Bladder Cancer *via* Sponging miR-570-3p. *Mol Ther Oncolytics* (2020) 16:172–87. doi: 10.1016/j.omto.2019.12.014
55. Yan D, Dong W, He Q, Yang M, Huang L, Kong J, et al. Circular RNA circPICALM sponges miR-1265 to inhibit bladder cancer metastasis and influence FAK phosphorylation. *EBioMedicine* (2019) 48:316–31. doi: 10.1016/j.ebiom.2019.08.074
56. Su H, Tao T, Yang Z, Kang X, Zhang X, Kang D, et al. Circular RNA cTFRC acts as the sponge of MicroRNA-107 to promote bladder carcinoma progression. *Mol Cancer* (2019) 18:27. doi: 10.1186/s12943-019-0951-0
57. Zu X, Tang Z, Li Y, Gao N, Ding J, Qi L. Vascular endothelial growth factor-C expression in bladder transitional cell cancer and its relationship to lymph node metastasis. *BJU Int* (2006) 98:1090–3. doi: 10.1111/j.1464-410X.2006.06446.x
58. Zhang HH, Qi F, Shi YR, Miao JG, Zhou M, He W, et al. RNA interference-mediated vascular endothelial growth factor-C reduction suppresses malignant progression and enhances mitomycin C sensitivity of bladder cancer T24 cells. *Cancer Biother Radiopharm* (2012a) 27:291–8. doi: 10.1089/cbr.2010.0919
59. Zhang HH, Qi F, Zu XB, Cao YH, Miao JG, Xu L, et al. A proteomic study of potential VEGF-C-associated proteins in bladder cancer T24 cells. *Med Sci Monit* (2012b) 18:Br441–9. doi: 10.12659/MSM.883537
60. Mccoll BK, Baldwin ME, Roufail S, Freeman C, Moritz RL, Simpson RJ, et al. Plasmin activates the lymphangiogenic growth factors VEGF-C and VEGF-D. *J Exp Med* (2003) 198:863–8. doi: 10.1084/jem.20030361
61. Pepper MS, Mandriota SJ, Jeltsch M, Kumar V, Alitalo K. Vascular endothelial growth factor (VEGF)-C synergizes with basic fibroblast growth factor and VEGF in the induction of angiogenesis *in vitro* and alters endothelial cell extracellular proteolytic activity. *J Cell Physiol* (1998) 177:439–52. doi: 10.1002/(SICI)1097-4652(199812)177:3<439::AID-JCP7>3.0.CO;2-2
62. Zhu H, Yun F, Shi X, Wang D. VEGF-C inhibition reverses resistance of bladder cancer cells to cisplatin *via* upregulating maspin. *Mol Med Rep* (2015) 12:3163–9. doi: 10.3892/mmr.2015.3684
63. Liu J, Yu HG, Yu JP, Wang XL, Zhou XD, Luo HS. Overexpression of cyclooxygenase-2 in gastric cancer correlates with the high abundance of vascular endothelial growth factor-C and lymphatic metastasis. *Med Oncol* (2005) 22:389–97. doi: 10.1385/MO:22:4:389
64. Al-Maghrabi B, Gomaa W, Abdelwahed M, Al-Maghrabi J. Increased COX-2 Immunostaining in Urothelial Carcinoma of the Urinary Bladder Is Associated with Invasiveness and Poor Prognosis. *Anal Cell Pathol (Amst)* (2019) 2019:5026939. doi: 10.1155/2019/5026939
65. Dong L, Li Y, Xue D, Liu Y. PCMT1 is an unfavorable predictor and functions as an oncogene in bladder cancer. *IUBMB Life* (2018) 70:291–9. doi: 10.1002/iub.1717
66. Islam SS, Mokhtari RB, Noman AS, Uddin M, Rahman MZ, Azadi MA, et al. Sonic hedgehog (Shh) signaling promotes tumorigenicity and stemness *via* activation of epithelial-to-mesenchymal transition (EMT) in bladder cancer. *Mol Carcinog* (2016) 55:537–51. doi: 10.1002/mc.22300
67. Nedjadi T, Salem N, Khayyat D, Al-Sayyad A, Al-Ammari A, Al-Maghrabi J. Sonic Hedgehog Expression is Associated with Lymph Node Invasion in Urothelial Bladder Cancer. *Pathol Oncol Res* (2019) 25:1067–73. doi: 10.1007/s12253-018-0477-6
68. Syed IS, Pedram A, Farhat WA. Role of Sonic Hedgehog (Shh) Signaling in Bladder Cancer Stemness and Tumorigenesis. *Curr Urol Rep* (2016) 17:11. doi: 10.1007/s11934-015-0568-9
69. Zhu X, Qiao Y, Liu W, Wang W, Shen H, Lu Y, et al. CXCL5 is a potential diagnostic and prognostic marker for bladder cancer patients. *Tumour Biol* (2016) 37:4569–77. doi: 10.1007/s13277-015-4275-4
70. Wang C, Li A, Yang S, Qiao R, Zhu X, Zhang J. CXCL5 promotes mitomycin C resistance in non-muscle invasive bladder cancer by activating EMT and NF-κB pathway. *Biochem Biophys Res Commun* (2018a) 498:862–8. doi: 10.1016/j.bbrc.2018.03.071
71. Zheng J, Zhu X, Zhang J. CXCL5 knockdown expression inhibits human bladder cancer T24 cells proliferation and migration. *Biochem Biophys Res Commun* (2014) 446:18–24. doi: 10.1016/j.bbrc.2014.01.172
72. Gao Y, Guan Z, Chen J, Xie H, Yang Z, Fan J, et al. CXCL5/CXCR2 axis promotes bladder cancer cell migration and invasion by activating PI3K/AKT-induced upregulation of MMP2/MMP9. *Int J Oncol* (2015) 47:690–700. doi: 10.3892/ijo.2015.3041
73. Mohammad MA, Ismael NR, Shaarawy SM, El-Merzabani MM. Prognostic value of membrane type 1 and 2 matrix metalloproteinase expression and gelatinase A activity in bladder cancer. *Int J Biol Markers* (2010) 25:69–74. doi: 10.1177/172460081002500202
74. Szarvas T, Becker M, Vom Dorp F, Gethmann C, Tötsch M, Bánkfalvi A, et al. Matrix metalloproteinase-7 as a marker of metastasis and predictor of poor survival in bladder cancer. *Cancer Sci* (2010) 101:1300–8. doi: 10.1111/j.1349-7006.2010.01506.x
75. Vasala K, Pääkko P, Turpeenniemi-Hujanen T. Matrix metalloproteinase-9 (MMP-9) immunoreactive protein in urinary bladder cancer: a marker of favorable prognosis. *Anticancer Res* (2008) 28:1757–61.
76. Zhao J, Xu W, He M, Zhang Z, Zeng S, Ma C, et al. Whole-exome sequencing of muscle-invasive bladder cancer identifies recurrent copy number variation in IPO11 and prognostic significance of importin-11 overexpression on poor survival. *Oncotarget* (2016) 7:75648–58. doi: 10.18632/oncotarget.12315
77. Zhao J, Shi L, Zeng S, Ma C, Xu W, Zhang Z, et al. Importin-11 overexpression promotes the migration, invasion, and progression of bladder cancer associated with the deregulation of CDKN1A and THBS1. *Urol Oncol* (2018) 36:311.e311–13. doi: 10.1016/j.urolonc.2018.03.001

78. Presler M, Wojtczyk-Miaskowska A, Schlichtholz B, Kaluzny A, Matuszewski M, Mika A, et al. Increased expression of the gene encoding stearoyl-CoA desaturase 1 in human bladder cancer. *Mol Cell Biochem* (2018) 447:217–24. doi: 10.1007/s11010-018-3306-z
79. Piao C, Cui X, Zhan B, Li J, Li Z, Li Z, et al. Inhibition of stearoyl CoA desaturase-1 activity suppresses tumour progression and improves prognosis in human bladder cancer. *J Cell Mol Med* (2019) 23:2064–76. doi: 10.1111/jcmm.14114
80. Du X, Wang QR, Chan E, Merchant M, Liu J, French D, et al. FGFR3 stimulates stearoyl CoA desaturase 1 activity to promote bladder tumor growth. *Cancer Res* (2012) 72:5843–55. doi: 10.1158/0008-5472.CAN-12-1329
81. Guo X, Li HH, Hu J, Duan YX, Ren WG, Guo Q, et al. ISYNA1 is overexpressed in bladder carcinoma and regulates cell proliferation and apoptosis. *Biochem Biophys Res Commun* (2019a) 519:246–52. doi: 10.1016/j.bbrc.2019.08.129
82. Chen J, Chou F, Yeh S, Ou Z, Shyr C, Huang C, et al. Androgen dihydrotestosterone (DHT) promotes the bladder cancer nuclear AR-negative cell invasion *via a* newly identified membrane androgen receptor (mAR-SLC39A9)-mediated Gαi protein/MAPK/MMP9 intracellular signaling. *Oncogene* (2020a) 39:574–86. doi: 10.1038/s41388-019-0964-6
83. Tang Y, Zu X, Xiong Y, Zhang X. [Expression of Maspin in bladder carcinoma and the relationship between Maspin and lymph node metastasis]. *Zhong Nan Da Xue Xue Bao Yi Xue Ban* (2015) 40:1306–12. doi:10.11817/j.issn.1672-7347.2015.12.004
84. Zhang HH, Qi F, Cao YH, Zu XB, Chen MF. Expression and clinical significance of microRNA-21, maspin and vascular endothelial growth factor-C in bladder cancer. *Oncol Lett* (2015) 10:2610–6. doi: 10.3892/ol.2015.3540
85. Juengel E, Beecken WD, Mundiyanapurath S, Engl T, Jonas D, Blaheta RA. Maspin modulates adhesion of bladder carcinoma cells to vascular endothelium. *World J Urol* (2010) 28:465–71. doi: 10.1007/s00345-010-0539-1
86. Sugimoto S, Maass N, Takimoto Y, Sato K, Minei S, Zhang M, et al. Expression and regulation of tumor suppressor gene maspin in human bladder cancer. *Cancer Lett* (2004) 203:209–15. doi: 10.1016/j.canlet.2003.09.010
87. Lin YH, Tsui KH, Chang KS, Hou CP, Feng TH, Juang HH. Maspin is a PTEN-Upregulated and p53-Upregulated Tumor Suppressor Gene and Acts as an HDAC1 Inhibitor in Human Bladder Cancer. *Cancers (Basel)* (2019) 12(1):10. doi: 10.3390/cancers12010010
88. Chen J, Wang L, Tang Y, Gong G, Liu L, Chen M, et al. Maspin enhances cisplatin chemosensitivity in bladder cancer T24 and 5637 cells and correlates with prognosis of muscle-invasive bladder cancer patients receiving cisplatin based neoadjuvant chemotherapy. *J Exp Clin Cancer Res* (2016a) 35:2. doi: 10.1186/s13046-015-0282-y
89. Wang C, Liu Q, Huang M, Zhou Q, Zhang X, Zhang J, et al. Loss of GATA6 expression promotes lymphatic metastasis in bladder cancer. *FASEB J* (2020) 34:5754–66. doi: 10.1096/fj.201903176R
90. Zhang Y, Jia L, Zhang Y, Ji W, Li H. Higher expression of FOXOs correlates to better prognosis of bladder cancer. *Oncotarget* (2017) 8:96313–22. doi: 10.18632/oncotarget.22029
91. Shiota M, Song Y, Yokomizo A, Kiyoshima K, Tada Y, Uchino H, et al. Foxo3a suppression of urothelial cancer invasiveness through Twist1, Y-box-binding protein 1, and E-cadherin regulation. *Clin Cancer Res* (2010) 16:5654–63. doi: 10.1158/1078-0432.CCR-10-0376
92. Chen X. MiR-101 acts as a novel bio-marker in the diagnosis of bladder carcinoma. *Med (Baltimore)* (2019) 98:e16051. doi: 10.1097/MD.0000000000016051
93. Liu X, Zhao W, Wang X, Zhu Y, Zhou Z, Shi B. Expression of mir-143 in serum of bladder cancer patients and its correlation with clinical features and prognosis. *J Buon* (2019a) 24:791–6.
94. Chen X, Wu B, Xu Z, Li S, Tan S, Liu X, et al. Downregulation of miR-133b predict progression and poor prognosis in patients with urothelial carcinoma of bladder. *Cancer Med* (2016b) 5:1856–62. doi: 10.1002/cam4.777
95. Ma L, Xu Z, Xu C, Jiang X. MicroRNA-148a represents an independent prognostic marker in bladder cancer. *Tumour Biol* (2016) 37:7915–20. doi: 10.1007/s13277-015-4688-0
96. Chen YJ, Wang HF, Liang M, Zou RC, Tang ZR, Wang JS. Upregulation of miR-3658 in bladder cancer and tumor progression. *Genet Mol Res* (2016c) 15(4). doi: 10.4238/gmr15049048
97. Li C, Cui Y, Liu LF, Ren WB, Li QQ, Zhou X, et al. High Expression of Long Noncoding RNA MALAT1 Indicates a Poor Prognosis and Promotes Clinical Progression and Metastasis in Bladder Cancer. *Clin Genitourin Cancer* (2017a) 15:570–6. doi: 10.1016/j.clgc.2017.05.001
98. Li B, Guo LH, Ban ZQ, Liu L, Luo L, Cui TY. Upregulation of lncRNA plasmacytoma variant translocation 1 predicts poor prognosis in patients with muscle-invasive bladder cancer. *Med (Baltimore)* (2020) 99:e21059. doi: 10.1097/MD.0000000000021059
99. Wang JS, Liu QH, Cheng XH, Zhang WY, Jin YC. The long noncoding RNA ZFAS1 facilitates bladder cancer tumorigenesis by sponging miR-329. *BioMed Pharmacother* (2018b) 103:174–81. doi: 10.1016/j.biopha.2018.04.031
100. Zhao XL, Zhao ZH, Xu WC, Hou JQ, Du XY. Increased expression of SPRY4-IT1 predicts poor prognosis and promotes tumor growth and metastasis in bladder cancer. *Int J Clin Exp Pathol* (2015) 8:1954–60.
101. Zhan Y, Li Y, Guan B, Wang Z, Peng D, Chen Z, et al. Long non-coding RNA HNF1A-AS1 promotes proliferation and suppresses apoptosis of bladder cancer cells through upregulating Bcl-2. *Oncotarget* (2017) 8:76656–65. doi: 10.18632/oncotarget.20795
102. Chen Q, Fu L. Upregulation of long non-coding RNA ROR1-AS1 promotes cell growth and migration in bladder cancer by regulation of miR-504. *PloS One* (2020) 15:e0227568. doi: 10.1371/journal.pone.0227568
103. Cao HL, Liu ZJ, Huang PL, Yue YL, Xi JN. lncRNA-RMRP promotes proliferation, migration and invasion of bladder cancer *via* miR-206. *Eur Rev Med Pharmacol Sci* (2019) 23:1012–21.
104. Liang Z, Guo W, Fang S, Zhang Y, Lu L, Xu W, et al. CircRNAs: Emerging Bladder Cancer Biomarkers and Targets. *Front Oncol* (2020) 10:606485. doi: 10.3389/fonc.2020.606485
105. Xu ZQ, Yang MG, Liu HJ, Su CQ. Circular RNA hsa_circ_0003221 (circPTK2) promotes the proliferation and migration of bladder cancer cells. *J Cell Biochem* (2018) 119:3317–25. doi: 10.1002/jcb.26492
106. D'andrea D, Moschini M, Gust KM, Abufaraj M, Özsoy M, Mathieu R, et al. Lymphocyte-to-monocyte ratio and neutrophil-to-lymphocyte ratio as biomarkers for predicting lymph node metastasis and survival in patients treated with radical cystectomy. *J Surg Oncol* (2017) 115:455–61. doi: 10.1002/jso.24521
107. Zhou M, He L, Zu X, Zhang H, Zeng H, Qi L. Lymphatic vessel density as a predictor of lymph node metastasis and its relationship with prognosis in urothelial carcinoma of the bladder. *BJU Int* (2011) 107:1930–5. doi: 10.1111/j.1464-410X.2010.09725.x
108. Chen M, Nie ZY, Wen XH, Gao YH, Cao H, Zhang SF. m6A RNA methylation regulators can contribute to malignant progression and impact the prognosis of bladder cancer. *Biosci Rep* (2019d) 39(12): BSR20192892. doi: 10.1042/BSR20192892
109. Han J, Wang JZ, Yang X, Yu H, Zhou R, Lu HC, et al. METTL3 promote tumor proliferation of bladder cancer by accelerating pri-miR221/222 maturation in m6A-dependent manner. *Mol Cancer* (2019) 18:110. doi: 10.1186/s12943-019-1036-9
110. Smith SC, Baras AS, Dancik G, Ru Y, Ding KF, Moskaluk CA, et al. A 20-gene model for molecular nodal staging of bladder cancer: development and prospective assessment. *Lancet Oncol* (2011) 12:137–43. doi: 10.1016/S1470-2045(10)70296-5
111. Seiler R, Lam LL, Erho N, Takhar M, Mitra AP, Buerki C, et al. Prediction of Lymph Node Metastasis in Patients with Bladder Cancer Using Whole Transcriptome Gene Expression Signatures. *J Urol* (2016) 196:1036–41. doi: 10.1016/j.juro.2016.04.061
112. Lu X, Wang Y, Jiang L, Gao J, Zhu Y, Hu W, et al. A Pre-operative Nomogram for Prediction of Lymph Node Metastasis in Bladder Urothelial Carcinoma. *Front Oncol* (2019) 9:488. doi: 10.3389/fonc.2019.00488
113. Wu S, Zheng J, Li Y, Yu H, Shi S, Xie W, et al. A Radiomics Nomogram for the Preoperative Prediction of Lymph Node Metastasis in Bladder Cancer. *Clin Cancer Res* (2017) 23:6904–11. doi: 10.1158/1078-0432.CCR-17-1510
114. Wu S, Zheng J, Li Y, Wu Z, Shi S, Huang M, et al. Development and Validation of an MRI-Based Radiomics Signature for the Preoperative

Prediction of Lymph Node Metastasis in Bladder Cancer. *EBioMedicine* (2018a) 34:76–84. doi: 10.1016/j.ebiom.2018.07.029
115. Wu SX, Huang J, Liu ZW, Chen HG, Guo P, Cai QQ, et al. A Genomic-clinicopathologic Nomogram for the Preoperative Prediction of Lymph Node Metastasis in Bladder Cancer. *EBioMedicine* (2018b) 31:54–65. doi: 10.1016/j.ebiom.2018.03.034
116. Chen J, Cui YU, Liu L, Li C, Tang Y, Zhou XU, et al. CCR7 as a predictive biomarker associated with computed tomography for the diagnosis of lymph node metastasis in bladder carcinoma. *Oncol Lett* (2016d) 11:735–40. doi: 10.3892/ol.2015.3939
117. Cantiello F, Cicione A, Autorino R, Salonia A, Briganti A, Ferro M, et al. Visceral obesity predicts adverse pathological features in urothelial bladder cancer patients undergoing radical cystectomy: a retrospective cohort study. *World J Urol* (2014) 32:559–64. doi: 10.1007/s00345-013-1147-7
118. Garg T, Young AJ, O'keeffe-Rosetti M, Mcmullen CK, Nielsen ME, Murphy TE, et al. Association between metabolic syndrome and recurrence of nonmuscle-invasive bladder cancer in older adults. *Urol Oncol* (2020) 38:737.e717–23. doi: 10.1016/j.urolonc.2020.04.010
119. Chromecki TF, Cha EK, Fajkovic H, Rink M, Ehdaie B, Svatek RS, et al. Obesity is associated with worse oncological outcomes in patients treated with radical cystectomy. *BJU Int* (2013) 111:249–55. doi: 10.1111/j.1464-410X.2012.11322.x
120. Kwon T, Jeong IG, You D, Han KS, Hong S, Hong B, et al. Obesity and prognosis in muscle-invasive bladder cancer: the continuing controversy. *Int J Urol* (2014) 21:1106–12. doi: 10.1111/iju.12530
121. Chiang CL, Huang HH, Huang TY, Shih YL, Hsieh TY, Lin HH. Nonalcoholic Fatty Liver Disease Associated With Bladder Cancer. *Am J Med Sci* (2020) 360:161–5. doi: 10.1016/j.amjms.2020.04.031
122. Tarantino G, Crocetto F, Di Vito C, Creta M, Martino R, Pandolfo SD, et al. Association of NAFLD and Insulin Resistance with Non Metastatic Bladder Cancer Patients: A Cross-Sectional Retrospective Study. *J Clin Med* (2021) 10 (2):346. doi: 10.3390/jcm10020346
123. Xu Y, Huo R, Chen X, Yu X. Diabetes mellitus and the risk of bladder cancer: A PRISMA-compliant meta-analysis of cohort studies. *Med (Baltimore)* (2017) 96:e8588. doi: 10.1097/MD.0000000000008588
124. Hu J, Chen JB, Cui Y, Zhu YW, Ren WB, Zhou X, et al. Association of metformin intake with bladder cancer risk and oncologic outcomes in type 2 diabetes mellitus patients: A systematic review and meta-analysis. *Med (Baltimore)* (2018) 97:e11596. doi: 10.1097/MD.0000000000011596
125. Wu Y, Zheng Q, Li Y, Wang G, Gao S, Zhang X, et al. Metformin targets a YAP1-TEAD4 complex *via* AMPKα to regulate CCNE1/2 in bladder cancer cells. *J Exp Clin Cancer Res* (2019b) 38:376. doi: 10.1186/s13046-019-1346-1
126. Zhang T, Guo P, Zhang Y, Xiong H, Yu X, Xu S, et al. The antidiabetic drug metformin inhibits the proliferation of bladder cancer cells *in vitro* and *in vivo*. *Int J Mol Sci* (2013) 14:24603–18. doi: 10.3390/ijms141224603
127. Newton CC, Gapstur SM, Campbell PT, Jacobs EJ. Type 2 diabetes mellitus, insulin-use and risk of bladder cancer in a large cohort study. *Int J Cancer* (2013) 132:2186–91. doi: 10.1002/ijc.27878
128. Liu S, Li Y, Lin T, Fan X, Liang Y, Heemann U. High dose human insulin and insulin glargine promote T24 bladder cancer cell proliferation *via* PI3K-independent activation of Akt. *Diabetes Res Clin Pract* (2011) 91:177–82. doi: 10.1016/j.diabres.2010.11.009
129. Pal DK, Agrawal A, Ghosh S, Ghosh A. Association of arsenic with recurrence of urinary bladder cancer. *Trop Doct* (2020) 50:325–30. doi: 10.1177/0049475520930155
130. Zhou Q, Jin P, Liu J, Li S, Liu W, Xi S. Arsenic-induced HER2 promotes proliferation, migration and angiogenesis of bladder epithelial cells *via* activation of multiple signaling pathways *in vitro* and *in vivo*. *Sci Total Environ* (2021) 753:141962. doi: 10.1016/j.scitotenv.2020.141962
131. Jou YC, Wang SC, Dai YC, Chen SY, Shen CH, Lee YR, et al. Gene expression and DNA methylation regulation of arsenic in mouse bladder tissues and in human urothelial cells. *Oncol Rep* (2019) 42:1005–16. doi: 10.3892/or.2019.7235

Conflict of Interest: The authors declare that the research was conducted in the absence of any commercial or financial relationships that could be construed as a potential conflict of interest.

Copyright © 2021 Zhang, Hu, Li, Ma, Othmane, Ren, Yi, Qiu, Ou, Chen and Zu. This is an open-access article distributed under the terms of the Creative Commons Attribution License (CC BY). The use, distribution or reproduction in other forums is permitted, provided the original author(s) and the copyright owner(s) are credited and that the original publication in this journal is cited, in accordance with accepted academic practice. No use, distribution or reproduction is permitted which does not comply with these terms.

frontiers in Oncology

MINI REVIEW
published: 28 May 2021
doi: 10.3389/fonc.2021.676716

Tissue-Based Biomarkers for the Risk Stratification of Men With Clinically Localized Prostate Cancer

*Spyridon P. Basourakos[1], Michael Tzeng[1], Patrick J. Lewicki[1], Krishnan Patel[2], Bashir Al Hussein Al Awamlh[1], Siv Venkat[1], Jonathan E. Shoag[1,3], Michael A. Gorin[4,5], Christopher E. Barbieri[1] and Jim C. Hu[1]**

[1] Department of Urology, New York-Presbyterian Hospital, Weill Cornell Medicine, New York, NY, United States, [2] Radiation Oncology Branch, National Cancer Institute, Bethesda, MD, United States, [3] Department of Urology, University Hospitals Cleveland Medical Center, Case Western Reserve University School of Medicine, Cleveland, OH, United States, [4] Department of Urology, University of Pittsburg School of Medicine, Pittsburgh, PA, United States, [5] Urology Associates and UPMC Western Maryland, Cumberland, MD, United States

OPEN ACCESS

Edited by:
Eric A. Singer,
Rutgers Cancer Institute of New Jersey, United States

Reviewed by:
Shian Shiang Wang,
Taichung Veterans General Hospital, Taiwan
Andrew Leonard Laccetti,
Memorial Sloan Kettering Cancer Center, United States

***Correspondence:**
Jim C. Hu
jch9011@med.cornell.edu

Specialty section:
This article was submitted to Genitourinary Oncology, a section of the journal Frontiers in Oncology

Received: 05 March 2021
Accepted: 21 April 2021
Published: 28 May 2021

Citation:
Basourakos SP, Tzeng M, Lewicki PJ, Patel K, Al Hussein Al Awamlh B, Venkat S, Shoag JE, Gorin MA, Barbieri CE and Hu JC (2021) Tissue-Based Biomarkers for the Risk Stratification of Men With Clinically Localized Prostate Cancer. Front. Oncol. 11:676716. doi: 10.3389/fonc.2021.676716

Risk stratification of men with clinically localized prostate cancer has historically relied on basic clinicopathologic parameters such as prostate specific antigen level, grade group, and clinical stage. However, prostate cancer often behaves in ways that cannot be accurately predicted by these parameters. Thus, recent efforts have focused on developing tissue-based genomic tests that provide greater insights into the risk of a given patient's disease. Multiple tests are now commercially available and provide additional prognostic information at various stages of the care pathway for prostate cancer. Indeed, early evidence suggests that these assays may have a significant impact on patient and physician decision-making. However, the impact of these tests on oncologic outcomes remains less clear. In this review, we highlight recent advances in the use of tissue-based biomarkers in the treatment of prostate cancer and identify the existing evidence supporting their clinical use.

Keywords: prostate cancer, tissue biomarker, prognosis, genetic marker, decision making

INTRODUCTION

Until recently, the only available means for risk-stratifying men with clinically localized prostate cancer (PCa) was through the use of clinicopathologic variables such as prostate-specific antigen (PSA) level, histologic grade group, and clinical stage (1, 2). Based on these variables, several nomograms and risk calculators were developed to quantify the risk of disease aggressiveness and assist in patient counseling. The most widely used risk assessment tools include the Partin tables, the Memorial Sloan Kettering Cancer Center (MSKCC) nomogram (3), and the Cancer of the Prostate Risk Assessment (CAPRA) score (4). The Partin tables and MSKCC nomogram are used to predict pathologic tumor and nodal stage following radical prostatectomy (RP). Additionally, the MSKCC nomogram provides information on post-operative cancer-specific and progression-free survival. Likewise, the CAPRA score predicts post-operative pathology including the presences of high-risk features and lymph node involvement as well as recurrence free survival at 3 and 5 years (5–7).

Although these tools offer a reasonable degree of predictive ability, advances in molecular biology have given birth to a variety of urine, blood, and tissue-based tests that provide the physician and patient with additional information about a given patient's risk for a number of treatment outcomes (8–11). In this review, we aim to discuss tissue-based assays that have become commercially available over the past several years and appraise their utility for treatment planning in men with PCa (**Table 1**).

Decipher

The Decipher test (Decipher Biosciences, San Diego, CA, USA) uses a microarray platform to measure the expression levels of 22 genes (LASP1, IQGAP3, NFIB, S1PR4, THBS2, ANO7, PCDH7, MYBPC1, EPPK1, TSBP, PBX1, NUSAP1, ZWILCH, UBE2C, CAMK2N1, RABGAP1, PCAT-32, GLYATL1P4, PCAT-80, TNFRSF19) that participate in multiple biologic pathways, such as cell proliferation, differentiation, adhesion and cell cycle progression, and androgen receptor signaling (28). The test requires the extraction of RNA from formalin-fixed paraffin-embedded tissue and a tumor specimen measuring at least 0.5 mm (29). A Decipher Biopsy score is generated when the assay is performed on biopsy tissue, and a Decipher Radical Prostatectomy score is generated when the assay is performed on a RP specimen. Both scores are reported as a number ranging from 0 to 1. A score of 0 to 0.45 is defined as low-risk, 0.46 to 0.6 is average-risk, and above 0.61 is high-risk.

The Decipher Biopsy report provides an assessment of adverse pathology at time of RP, as well as the risk of metastasis and PCa-specific mortality at 5 and 15 years, respectively. The Decipher Radical Prostatectomy report provides similar information with respect to risk of metastasis and prostate-cancer specific mortality, with the goal of guiding decision-making regarding the use of adjuvant radiotherapy, however the clinical utility of this test has never been prospectively validated. Given the recent results of GETUG-AFU 17, RADICALS-RT, and RAVES summarized in the ARTISTIC meta-analysis, which suggest similar outcomes to a strategy of salvage radiotherapy when compared to adjuvant radiotherapy for patients with high-risk histopathologic findings, the utility of genomic classifiers (GCs) may now be somewhat limited in this clinical setting (30–33).

TABLE 1 | Summary of available tissue-based biomarkers and indications.

Test Name	Manufacturer	Genetic Material tested	Endpoint	Test Report	Target Population	Reference
Repeat Biopsy						
ConfirmMDx	MDxHealth	Methylation status of 3 genes (GSTP1, RASSF1, APC)	Risk of PCa on repeat biopsy	Likelihood of PCa in %	Men with negative biopsy and considering second one	Stewart et al. (12), Partin et al. (13), Van Neste et al. (14)
After Biopsy: Active Surveillance vs. Intervention						
Prolaris Biopsy	Myriad Genetics	Expression levels (RNA) of 31 cell-cycle progression genes	10-year risk of PCa-specific mortality	CCP Score: 0-6	Men with PCa on biopsy	Cuzick et al. (15, 16)
Decipher Biopsy	GenomeDx Biosciences	Expression levels (RNA) of 22 genes (LASP1, IQGAP3, NFIB, S1PR4, THBS2, ANO7, PCDH7, MYBPC1, EPPK1, TSBP, PBX1, NUSAP1, ZWILCH, UBE2C, CAMK2N1, RABGAP1, PCAT-32, GLYATL1P4, PCAT-80, TNFRSF19)	5-year risk metastasis Likelihood of high grade PCa on RP 10-year risk of PCa-specific mortality	GC Score: 0-1.0	Men with localized PCa	Cooperberg et al. (17), Klein et al. (18), Ross et al. (19)
Oncotype DX	Genomic Health	Expression levels (RNA) of 12 genes (AZGP1, KLK2, SRD5A2, FAM13C, FLNC, GSN, TPM2, GSTM2, TPX2, BGN, COL1A1, SFRP4)	Likelihood of GGG 1 or GGG2 on RP Likelihood of organ-confined PCa on RP	GPS Score: 0-100	Men with very low- and low-risk PCa*	Cullen et al. (20), Klein et al. (21)
ProMark	Metamark	Quantitative levels of 8 proteins (DERL1, CUL2, SMAD4, PDSS2, HSPA9, FUS, pS6, YBOX1)	Risk of GGG ≥ 3 or non-organ confined PCa on RP	ProMark Score: 0-100	Men with GGG 1 or 2 on biopsy	Shipitsin et al. (22), Blume-Jensen et al. (23)
PTEN/ TMPRSS2: ERG	Metamark	PTEN deletion and TMPRSS2:ERG fusion		Risk groups	Men with GGG 1 or 2 on biopsy	Yoshimoto et al. (24)
Management after RP: Further Treatment vs. Observation						
Prolaris	Myriad Genetics	Expression levels (RNA) of 31 cell-cycle progression genes	10-year risk of BCR	CCP Score: 0-6	Men after RP	Cuzick et al. (25), Cooperberg et al. (17)
Decipher	GenomeDx Biosciences	Expression levels (RNA) of 22 genes	5-year risk of metastasis 10-year risk of PCa specific mortality	GC Score: 0-1.0	Men with high-risk pathology or high-risk clinical features after RP	Karnes et al. (26), Den et al. (27)

PCa, prostate cancer; BCR, biochemical recurrence; CCP, cell cycle progression; GC, genomic classifier; GGG, Gleason grade group; GPS, genomic prostate score; RP, radical prostatectomy.
**based on NCCN risk group.*

Open questions include the clinical benefit of risk stratification with GCs for the selection of adjuvant radiotherapy in select patients with multiple risk factors (34), the possibility of GCs to identify a population unlikely to benefit from salvage radiotherapy (35), and the possible application of GCs in the selection of patients to undergo androgen deprivation therapy as an adjunct to salvage radiotherapy (36).

The expression signature of the genomic classifier that underlies the Decipher test was originally developed using RP specimens from a cohort of men treated at the Mayo Clinic (28). A panel of more than 1.4 million genomic markers, including coding and non-coding RNAs, were compared between 192 men with metastatic PCa and 353 controls. The area-under-curve (AUC) for the genomic classifier was 0.90 in the original cohort and was additionally validated in a second cohort of 186 patients where the AUC was 0.75. In this study, the genomic classifier was the strongest predictor of metastasis in a multivariable analysis ($P < 0.001$). After the initial validation, further studies expanded its use to predict metastasis (18, 19, 37) and prostate-cancer specific survival after RP (26, 38).

Most of the data to support Decipher Biopsy come from studies done on RP specimens. However, in 2016, Knudsen et al. demonstrated the applicability of the Decipher test in tissue derived from biopsy specimens (39). The authors were able to show that almost 95% of the transcriptomic information extracted from RP specimens could also be derived from biopsy tissue with high correlation ($r = 0.96$) (39). Several subsequent studies demonstrated the clinical efficacy of the Decipher Biopsy test (40–42). For example, Klein et al. found that Decipher score from prostate biopsy specimens was a significant predictor of metastasis within 10 years after RP with an AUC of 0.8 (43).

Multiple studies have evaluated the role of Decipher testing in clinical decision making (44–46). For example, PRO-ACT was a prospective study that evaluated the treatment decisions of 15 community urologists before and after exposure to the Decipher test results (47). In total, 60% of patients with high-risk disease were reclassified as low risk based on the results of this test and the decision to proceed with adjuvant radiation was changed in 30% of cases. Additionally, 42% of patients who were initially recommended to undergo adjuvant therapy were subsequently reassigned to observation following Decipher testing. In this study, the use of Decipher significantly changed urologists' adjuvant treatment recommendations for men who were at high risk of metastasis post-prostatectomy ($P < 0.001$) (47). PRO-IMPACT demonstrated similar results (45). This was a prospective study evaluating the impact of Decipher testing on decision making for adjuvant and salvage radiation therapy in 265 post-prostatectomy patients found to have either adverse pathology or a rising PSA. Prior to Decipher testing, observation was recommended for 89% of patients considering adjuvant radiation and 58% of patients considering salvage treatment. After Decipher testing, 18% of treatment recommendations changed in the adjuvant radiation arm and 32% in the salvage arm. In both groups, the Decipher test was associated with significant decrease in decisional conflict for both physicians and patients ($P < 0.001$). Finally, the role of Decipher has been evaluated as a guide for androgen deprivation therapy after adjuvant or salvage radiotherapy post-prostatectomy (48). In this setting, a low Decipher score predicts a more favorable prognosis and may change treatment intensification strategies (40). Recently, Jairath et al. performed a systematic review on the available evidence on Decipher and its role on PCa management (40). The authors concluded that in multiple studies Decipher was an independent prognostic factor for adverse pathology, biochemical failure, metastasis, and cancer-specific and overall survival. Decipher's utility seems to be more important for intermediate-risk PCa as well as post-prostatectomy decision-making.

According to the guidelines from the National Comprehensive Cancer Network (NCCN), the Decipher test may be offered to men with very-low, low- and intermediate-risk PCa on biopsy and a life expectancy of at least 10 years. The goal of the test in this context is to aid in the selection of candidates for active surveillance. Post-prostatectomy, the Decipher test may be offered to men with pT2 disease and positive surgical margins or any pT3 disease to aid in the decision whether to undergo adjuvant radiation therapy (49).

Prolaris

The Prolaris Molecular Score (Myriad Genetics, Salt Lake City, UT, USA) assay measures the expression of 31 cell cycle progression (CCP) genes related to cancer proliferation and can be performed on either a biopsy or RP specimen (25). The CCP score ranges from 0 to 10, with a high score indicating a more aggressive cancer and correlating with a high risk for disease progression (15, 16). Each 1-unit increase reflects a doubling in gene expression level, suggesting a more aggressive tumor. The CCP score has been used for men with newly diagnosed PCa (Prolaris biopsy test) as well as men who have already undergone prostatectomy (Prolaris post-prostatectomy test). The Prolaris biopsy test reports the risk of 10-year PCa-specific mortality and 10-year metastasis with definitive treatment, whereas the Prolaris post-prostatectomy test reports the risk of 10-year biochemical recurrence.

The Prolaris assay is comprised by an index of 31 genes which were felt most reliably to model the entirety of the identified set of CCP genes. The predictive utility of this gene signature was first reported in a retrospective study which showed a significant correlation between the CCP score and clinical outcomes in two separate cohorts, the first comprised of 366 patients who had undergone and the second 337 men with localized PCa diagnosed by a transurethral resection who were managed conservatively. The CCP score was associated with risk of biochemical recurrence (HR 1.77, 95%CI 1.40–2.22, $P < 0.001$) in the prostatectomy cohort and PCa specific mortality (HR 2.57, 95%CI 1.93–3.43, $P < 0.001$) in the conservatively managed cohort (16).

The predictive utility of the CCP score was first defined in a 2011 report in which the authors used two different patient cohorts for validation (16). The first cohort had 366 patients who had undergone RP, and the second cohort had 337 men with clinically localized PCa diagnosed by a transurethral resection (TURP) who were managed conservatively. In this study, the CCP score was associated with risk of biochemical recurrence (HR 1.77, 95%CI 1.40–2.22, $P < 0.001$) in the prostatectomy

cohort and PCa specific mortality (HR 2.57, 95%CI 1.93–3.43, P < 0.001) in the conservatively managed cohort (16).

The Prolaris post-prostatectomy test was subsequently validated on another independent cohort of 413 men by Cooperberg and co-workers (17). In this study the authors demonstrated that when controlling for clinicopathologic factors, CCP score was a strong predictor of biochemical recurrence with each increase in score (HR 2.1, 95%CI 1.6 to 2.9, P < 0.001) (17). Based on this finding, Prolaris may be used to select men who are candidates for post-prostatectomy adjuvant therapy. A later study by Koch et al. showed that men with increased CCP score who had biochemical recurrence after RP had increased risk of systematic disease, suggesting that this patient population could benefit from earlier adjuvant therapy (10, 50).

The Prolaris biopsy test can facilitate decision-making process for men considering active surveillance *versus* localized treatment (surgery or radiation). Bishoff et al. evaluated the CCP score in prostate biopsy specimens of 582 men who underwent radical prostatectomy and demonstrated that increased biopsy CCP score was associated with biochemical recurrence (HR per score unit 1.47, 95%CI 1.23–1.76, P < 0.001) and metastatic progression (HR per score unit 4.19, 95%CI 2.08–8.45, P < 0.001) (51). In 2015, Cuzick et al. demonstrated in a study of 585 men undergoing active surveillance that biopsy CCP score is an independent predictor of prostate-cancer specific mortality (HR per score unit 1.76, 95%CI 1.44–2.14, P < 0.001) after adjusting for Gleason score, PSA, extent of disease, and clinical stage (15).

The Prolaris biopsy test also provides a 10-year PCa specific mortality risk upon combining the patient's PSA, clinical stage, % of positive cores, biopsy grade group, and AUA risk group (52). The PROCEDE-1000, a large, prospective registry with almost 1,600 participants, showed that the CCP score resulted in a change in treatment for 47.8% of patients (53). More specifically, treatment was deescalated in 75% of cases and escalated in 25% of cases. In spite of CCP score's use as a means to help physicians and patients reach personalized treatment decisions, no prospective data have shown clinical superiority of the decisions that the test informs.

According to the NCCN guidelines (49), Prolaris biopsy test may be recommended to men with very-low, low-, and favorable intermediate-risk PCa on biopsy and a life expectancy of at least 10 years.

PTEN/TMPRSS2:ERG

The PTEN/TMPRSS2:ERG (Metamark, Cambridge, MA, USA) assay detects the presence of both *PTEN* and the fusion *TMPRSS2:ERG* genes in biopsy specimens. Deletion of *PTEN* and/or presence of *TMPRSS2:ERG* indicates more aggressive PCa (54).

PTEN is a tumor suppressor gene that helps regulate cell division by modifying other proteins and lipids *via* phosphatase action. *PTEN* loss results in deactivation of the PI3K signaling pathway which controls cell growth and proliferation (55). Loss of *PTEN* in PCa has been associated with high cancer grade group, tumor progression and poor outcomes (56, 57). Yoshimoto et al. demonstrated that men with homozygous *PTEN* deletion are more likely to develop late biochemical recurrence (P = 0.005) (24).

TMPRSS2:ERG fusion gene is a common chromosomal rearrangement in PCa. While TMPRSS2:ERG fusion gene has not been found to be a strong predictor of biochemical recurrence and PCa-specific mortality, its presence is associated with higher T-stage and higher risk of metastasis (58, 59). Ahearn et al. showed that loss of PTEN in the presence of TMPRSS2:ERG fusion is independently associated with PCa progression (60). Heterozygous or homozygous *PTEN* loss was associated with PCa specific mortality in the absence of ERG fusion. However, this association was not seen in patients with a loss of PTEN in the presence of ERG fusion. Therefore, the presence of TMPRSS2:ERG fusion may modulate the effects of PTEN loss on the disease biology (10, 60).

The impact of the PTEN/TMPRSS2:ERG tissue assay on the decision making process regarding therapy has not been studied yet. However, the MyProstateScore (LynxDx, Inc., Ann Arbor, Michigan, USA) test is a recent advancement that uses urinary TMPRSS2:ERG, urinary PCa antigen 3, and serum PSA to rule out grade group ≥2 cancer in biopsy naïve men (61). Currently, PTEN/TMPRSS2:ERG is available as a standalone test for men with atypical pathology, high-grade prostatic *in situ* neoplasia and those with grade group 1 or 2 PCa to provide risk stratification (10). However, both PTEN mutations and TMPRSS2:ERG fusions are regularly tested as part of commercially available next generation sequencing (NGS) panels such as FoundationOne CDx (62). The latter is the first FDA-approved tissue-based broad companion diagnostic (CDx) that is clinically and analytically validated for all solid tumors.

The PTEN/TMPRSS2:ERG assay is not recommended as standalone test for routine use in the most recent NCCN guidelines. However, germline genetic testing is now supported by NCCN guidelines for all men with high-risk, very-high-risk, regional or metastatic PCa as well as men with PCa who have Ashkenazi Jewish ancestry or family history of high-risk germline mutations (*e.g.* BRCA1/2, Lynch Syndrome). Furthermore, men with PCa and positive family history for cancer (brother or father or multiple family members with PCa under the age of 60 or more than three cancers on the same side of family) should also undergo germline genetic testing (49).

Oncotype DX

Oncotype DX (Genomic Health, Redwood City, CA, USA) is an assay that utilizes reverse transcriptase-PCR to measure the expression levels of 12 cancer genes and five housekeeping genes. The 12 cancer genes are components of four major cellular pathways: proliferation (TPX2), androgen receptor pathway (AZGP1, KLK2, SRD5A2, FAM13C) cellular organization (FLNC, GSN, TPM2, GSTM2) and stromal response (BGN, COL1A1, SFRP4). The combination of these genes is used to calculate the Genomic Prostate Score (GPS), which ranges from 0 to 100. GPS correlates with the probability of adverse pathology, such as primary grade group and/or non-organ confined disease at the time of prostatectomy (63).

Initially introduced for breast (64) and colon cancer (65), the Oncotype Dx test was approved for use in PCa in 2013. Klein et al. validated Oncotype DX using three cohorts of patients: prostatectomy discovery cohort, prostate biopsy cohort, and an independent prostate biopsy validation cohort (21). The authors first explored 732 candidate genes in the prostatectomy discovery cohort and identified 288 genes predictive of clinical recurrence and 198 genes predictive of aggressive disease after adjustment for PSA, grade group, and clinical stage. These genes were then evaluated in a prostate biopsy cohort to identify a subset that is associated with adverse pathology at prostatectomy. This analysis led to the development of current test's 17 gene panel which was independently validated in an unrelated 395 patients with available prostate biopsy and prostatectomy pathology. Notably, this cohort included only men with low-volume intermediate-risk PCa. GPS predicted high-grade and high-stage disease at RP. Another study by Cullen et al. showed that GPS score can predict adverse pathology at prostatectomy but also eventual post-treatment biochemical recurrence (HR 2.73, 95%CI 1.84–3.96, P < 0.001 per 20 GPS units increase) (20).

Regarding the role of Oncotype DX in clinical decision making, Badani et al. performed a prospective study in 158 men with very low to low-intermediate risk PCa to assess the impact of incorporating Oncotype DX on treatment recommendations (66). The authors found that the use of Oncotype DX resulted in an 18% overall change in treatment recommendation. More specifically, active surveillance increased from 41 to 51%, prostatectomy decreased from 21 to 19% and radiation therapy decreased by 33%.

Furthermore, while the predictive utility of the Oncotype DX score to prognosticate adverse pathologic or clinical outcomes has been well validated, its prospective utility as a decision aid to modify treatment recommendations still requires validation in PCa. However, based on advances in the field of breast cancer, it is hopeful that this translation will be fruitful. While the Oncotype DX score for breast cancer was initially validated in the NSABP B20 cohort as a predictive marker for distant metastases (67), a more recent prospective trial, TAILORx, has demonstrated prospective utility as a decision aid to identify a subgroup of women with higher risk, early stage node-negative disease in whom omission of chemotherapy is appropriate (68–70).

According to the NCCN guidelines, Oncotype DX may be offered to men with very-low, low- or favorable intermediate-risk PCa on biopsy and a life expectancy of at least 10 years (49).

ConfirmMDx

ConfirmMDx for PCa (MDxHealth, Inc., Irvine, CA, USA) is a tissue-based assay that can be used for risk stratification of men with negative prior prostate biopsies. This test involves quantifying the methylation of promoter regions of three tumor suppressor genes (*RASSF1*, *GSTP1*, and *APC*) in benign prostate biopsy tissue (14, 71). When the CpG islands expand in the promoter regions of these genes, there is an increased risk for PCa development. The concept behind this test is that the normal prostatic tissue surrounding an area of adenocarcinoma will undergo epigenetic changes (72).

The two major studies that validate the use of ConfirmMDx are the Methylation Analysis to Locate Occult Cancer (MATLOC) and Detection of Cancer Using Methylated Events in Negative Tissue (DOCUMENT) (12, 13). The MATLOC study demonstrated that ConfirmMDx has sensitivity and specificity of 68 and 64%, respectively, for identifying occult PCa, defined as having a negative biopsy followed by a positive biopsy within 30 months. Furthermore, it showed that ConfirmMDx decreased the number of unnecessary prostate biopsies by up to 64% (12). The DOCUMENT study showed that ConfirmMDx is an independent predictor for PCa when compared to other clinicopathologic parameters and has a negative predictive value of almost 90% (13). Furthermore, Van Neste et al. concluded that men with low DNA-methylation levels in benign biopsies had a negative predictive value of 96% for high-grade cancer (73). The most recent clinical trial on ConfirmMDx is PASCUAL (NCT02250313), which has yet to be reported after termination in 2018. Nevertheless, it's important to note that these trials were performed prior to the adoption of prostate MRI in the diagnostic algorithm of PCa. Therefore, the role of ConfirmMDx should be reevaluated in the era of MRI-targeted prostate biopsies.

Regarding the role of ConfirmMDx in clinical decision making, Wonju et al. found that only 4.4% of men with negative ConfirmMDx had repeat biopsy, compared to a 43% repeat biopsy rate in the PLCO trial (74). In this study, all the repeat biopsies of patients with negative ConfirmMDx were also negative. Moreover, Van Neste et al. demonstrated that if a probability threshold of 15% is applied, then 30 unnecessary repeat biopsies could be avoided per 100 patients (9, 73).

CONFIRMMDX has not been incorporated in the most recent NCCN guidelines.

ProMark

The ProMark test (Metamark, Cambridge, MA, USA) is a protein-based assay that measures the levels of eight proteins (DERL1, CUL2, SMAD4, PDSS2, HSPA9, FUS, pS6, and YBOX1) in a prostate biopsy specimen through quantitative immuno fluorescence. These proteins participate in cell signaling, stress response and cell proliferation (9). The concept behind evaluating protein levels is based on the significant intratumoral heterogeneity that characterizes PCa. Thus, a protein-based panel aims to provide information derived from the most aggressive cells that might exist in a tumor.

ProMark reports a score from 0 to 1 that reflects the probability of Gleason score ≥4 + 3 disease or non-organ confined disease on RP. The test is meant to be used by men who are NCCN very-low or low-risk and considering active surveillance.

Initially, Shipitsin et al. reported 12 protein biomarkers that predicted PCa aggressiveness and lethal outcome in both high- and low-Gleason areas (22). In 2015, Blume-Jensen et al. used eight of the 12 protein biomarkers in 381 matched prostate biopsy and prostatectomy specimens to validate the eight-biomarker assay as a predictor of prostate pathology (23). More specifically, they showed that a "favorable" score of ≤0.33 is predictive of favorable pathology in 95% of very low-risk and 81.5% of low-risk NCCN patients. The predictive value

for non-favorable pathology was 76.9% at biomarker risk scores >0.8 across all risk groups. The authors also performed a validation study in 276 cases and were able to show that the eight-protein biomarker separates favorable from non-favorable disease as well as Gleason score 6 disease *versus* non-Gleason score 6 disease (AUC 0.68 and 0.65, respectively).

According to the NCCN guidelines, ProMark is recommended for men with very-low or low-risk PCa on biopsy and a life expectancy of at least 10 years (49).

Limitations of Tissue-Based Biomarkers

Tissue biomarkers for PCa need to be used within the context of their limitations. First, the majority of the tissue-based biomarkers have been validated in cohorts primarily consisting of White Caucasian men. However, there are multiple reports demonstrating that the aggressiveness of PCa differs among races (75–78). This stands true especially for African American men in whom there is a higher incidence and mortality secondary to PCa (79). While there is emerging data suggesting that the mortality difference between African American and White males may be a product of unequal access to care rather than genetics, this is still an area of active research. Therefore, the use of genetic risk classifiers in African American men likely requires further validation. Second, most of the tissue-based biomarkers have inconsistent coverage from insurances in the United States. Thus, the financial burden may preclude their use for certain patient populations. Third, there is lack of data regarding cost-effectiveness. Lobo et al. demonstrated that a Decipher-based care model could lead to cost savings of approximately 25% without any significant change in life expectancy (80). However, the literature lacks similar reports on the other available tissue biomarkers Fourth, the heterogeneity and multifocality of primary PCa should not be ignored. As demonstrated by Salami et al. gene expression assays performed on low-grade PCa biopsy tissue may not provide meaningful information on the presence of coexisting unsampled aggressive disease (81). More specifically, multifocal, low-grade and high-grade PCa foci can exhibit distinct prognostic expression signatures within the same case. Recent studies have also characterized significant changes to the genomic classifier scores in some patients depending on the biopsy core or area of the prostatectomy specimen analyzed suggesting the challenges of genomic risk classification in tumors with clonal and genomic heterogeneity (81–83). Fifth, many of the tissue biomarker related studies were performed in the pre-MRI era. Thus, it remains unclear if biomarkers provide clinically useful information in the management of localized PCa beyond MRI-guided interventions and treatment decisions. Furthermore, given the lack of head-to-head comparative studies, there is no level 1 evidence to establish the superiority of a single tissue biomarker over another and thus the choice of biomarker falls to the patient or clinician and may be somewhat dependent on financial factors (49). Therefore, there is no tissue-based biomarker that is considered "better" than others and it is each individual clinician's decision after discussion with his patients which to choose. Moreover, as recommended by the American Society of Clinical Oncology and the European Association of Urology, while tissue-based biomarkers could aid in the decision-making process for some men with PCa, they should not be offered routinely to everyone (84, 85). Finally, it needs to be highlighted that the literature lacks prospective studies supporting the role of tissue biomarkers as means to guide specific therapies (e.g. salvage or adjuvant treatment) and impact PCa-specific outcomes. Trials similar to the TAILORx trial in breast cancer need to be performed for PCa tissue biomarkers to evaluate their impact in disease specific outcomes.

Conclusions and Future Directions

A multitude of tissue-based genomic tests have emerged in recent years, providing prognostic information beyond that of standard clinicopathologic variables. These assays are available at various stages in the care pathway of PCa and offer insight into the risk of high-grade disease, rate of metastasis, and cancer-specific survival. However, many challenges lie ahead. To date, Decipher and Prolaris have the most supporting data available but, again, neither has been proven superior in comparative studies. Although some tests have demonstrated an ability to significantly impact management—guiding the pursuit of active surveillance, definitive therapy, and adjuvant radiation post-prostatectomy, there is lack of prospective studies supporting their impact on disease specific outcomes. Given the multiple commercial options for tissue-based biomarkers, it is likely that market forces including industrial investments in direct-to-consumer and direct-to-provider advertising will be major drivers of assay uptake and usage in clinical practice. Representation in national guidelines has already begun and will likely continue to grow as more genomic markers of PCa are discovered. However, incorporation in the daily clinical practice and insurance coverage still constitute areas that more work needs to be done so physicians and patients can benefit. Such assays may soon claim a central role in the management of men with PCa and deserve recognition as facilitators of an individualized approach to patient care.

AUTHOR CONTRIBUTIONS

All authors contributed to data gathering and manuscript drafting and review. All authors contributed to the article and approved the submitted version.

FUNDING

JH receives research support from the Frederick J. and Theresa Dow Wallace Fund of the New York Community Trust. JH also receives salary support from NIH R01 CA241758, PCORI CER-2019C1-15682 and CER-2019C2-17372. JS is supported by the Frederick J. and Theresa Dow Foundation of the New York Community Trust and a Damon Runyon Cancer Research Foundation Physician Scientist Training Award.

REFERENCES

1. Epstein JI, Walsh PC, Carmichael M, Brendler CB. Pathologic and Clinical Findings to Predict Tumor Extent of Nonpalpable (Stage T1c) Prostate Cancer. *JAMA* (1994) 271(5):368–74. doi: 10.1001/jama.1994.03510290050036
2. Stephenson AJ, Scardino PT, Eastham JA, Bianco FJJr., Dotan ZA, DiBlasio CJ, et al. Postoperative Nomogram Predicting the 10-Year Probability of Prostate Cancer Recurrence After Radical Prostatectomy. *J Clin Oncol* (2005) 23(28):7005–12. doi: 10.1200/JCO.2005.01.867
3. Memorial Sloan Kettering Cancer Center. *Pre-Prostatectomy Nomogram* (2021). Availble at: https://www.mskcc.org/nomograms/prostate/pre_o [Retrieved January, 21 2021].
4. University of California San Francisco. *Prostate Cancer Risk Assessment and the UCSF-CAPRA Score* (2021). Available at: https://urology.ucsf.edu/research/cancer/prostate-cancer-risk-assessment-and-the-ucsf-capra-score [Retrieved January, 21 2021].
5. Cooperberg MR. Prostate Cancer Risk Assessment: Choosing the Sharpest Tool in the Shed. *Cancer* (2008) 113(11):3062–6. doi: 10.1002/cncr.23920
6. Zhao KH, Hernandez DJ, Han M, Humphreys EB, Mangold LA, Partin AW. External Validation of University of California, San Francisco, Cancer of the Prostate Risk Assessment Score. *Urology* (2008) 72(2):396–400. doi: 10.1016/j.urology.2007.11.165
7. May M, Knoll N, Siegsmund M, Fahlenkamp D, Vogler H, Hoschke B, et al. Validity of the CAPRA Score to Predict Biochemical Recurrence-Free Survival After Radical Prostatectomy. Results From a European Multicenter Survey of 1,296 Patients. *J Urol* (2007) 178(5):1957–62; discussion 1962. doi: 10.1016/j.juro.2007.07.043
8. Cooperberg MR, Cowan JE, Lindquist KJ, Kobayashi Y, Simko JP, Bengtsson H, et al. Multiple Tissue Biomarkers Independently and Additively Predict Prostate Cancer Pathology Outcomes. *Eur Urol* (2021) 79(1):141–9. doi: 10.1016/j.eururo.2020.09.003
9. Alford AV, Brito JM, Yadav KK, Yadav SS, Tewari AK, Renzulli J. The Use of Biomarkers in Prostate Cancer Screening and Treatment. *Rev Urol* (2017) 19 (4):221–34. doi: 10.3909/riu0772
10. Clinton TN, Bagrodia A, Lotan Y, Margulis V, Raj GV, Woldu SL. Tissue-Based Biomarkers in Prostate Cancer. *Expert Rev Precis Med Drug Dev* (2017) 2(5):249–60. doi: 10.1080/23808993.2017.1372687
11. Cucchiara V, Cooperberg MR, Dall'Era M, Lin DW, Montorsi F, Schalken JA, et al. Genomic Markers in Prostate Cancer Decision Making. *Eur Urol* (2018) 73(4):572–82. doi: 10.1016/j.eururo.2017.10.036
12. Stewart GD, Van Neste L, Delvenne P, Delree P, Delga A, McNeill SA, et al. Clinical Utility of an Epigenetic Assay to Detect Occult Prostate Cancer in Histopathologically Negative Biopsies: Results of the MATLOC Study. *J Urol* (2013) 189(3):1110–6. doi: 10.1016/j.juro.2012.08.219
13. Partin AW, Van Neste L, Klein EA, Marks LS, Gee JR, Troyer DA, et al. Clinical Validation of an Epigenetic Assay to Predict Negative Histopathological Results in Repeat Prostate Biopsies. *J Urol* (2014) 192 (4):1081–7. doi: 10.1016/j.juro.2014.04.013
14. Van Neste L, Bigley J, Toll A, Otto G, Clark J, Delree P, et al. A Tissue Biopsy-Based Epigenetic Multiplex PCR Assay for Prostate Cancer Detection. *BMC Urol* (2012) 12:16. doi: 10.1186/1471-2490-12-16
15. Cuzick J, Stone S, Fisher G, Yang ZH, North BV, Berney DM, et al. Validation of an RNA Cell Cycle Progression Score for Predicting Death From Prostate Cancer in a Conservatively Managed Needle Biopsy Cohort. *Br J Cancer* (2015) 113(3):382–9. doi: 10.1038/bjc.2015.223
16. Cuzick J, Swanson GP, Fisher G, Brothman AR, Berney DM, Reid JE, et al. Prognostic Value of an RNA Expression Signature Derived From Cell Cycle Proliferation Genes in Patients With Prostate Cancer: A Retrospective Study. *Lancet Oncol* (2011) 12(3):245–55. doi: 10.1016/S1470-2045(10)70295-3
17. Cooperberg MR, Simko JP, Cowan JE, Reid JE, Djalilvand A, Bhatnagar S, et al. Validation of a Cell-Cycle Progression Gene Panel to Improve Risk Stratification in a Contemporary Prostatectomy Cohort. *J Clin Oncol* (2013) 31(11):1428–34. doi: 10.1200/JCO.2012.46.4396
18. Klein EA, Yousefi K, Haddad Z, Choeurng V, Buerki C, Stephenson AJ, et al. A Genomic Classifier Improves Prediction of Metastatic Disease Within 5 Years After Surgery in Node-Negative High-Risk Prostate Cancer Patients Managed by Radical Prostatectomy Without Adjuvant Therapy. *Eur Urol* (2015) 67 (4):778–86. doi: 10.1016/j.eururo.2014.10.036
19. Ross AE, Johnson MH, Yousefi K, Davicioni E, Netto GJ, Marchionni L, et al. Tissue-Based Genomics Augments Post-prostatectomy Risk Stratification in a Natural History Cohort of Intermediate- and High-Risk Men. *Eur Urol* (2016) 69(1):157–65. doi: 10.1016/j.eururo.2015.05.042
20. Cullen J, Rosner IL, Brand TC, Zhang N, Tsiatis AC, Moncur J, et al. A Biopsy-based 17-Gene Genomic Prostate Score Predicts Recurrence After Radical Prostatectomy and Adverse Surgical Pathology in a Racially Diverse Population of Men With Clinically Low- and Intermediate-risk Prostate Cancer. *Eur Urol* (2015) 68(1):123–31. doi: 10.1016/j.eururo.2014.11.030
21. Klein EA, Cooperberg MR, Magi-Galluzzi C, Simko JP, Falzarano SM, Maddala T, et al. A 17-Gene Assay to Predict Prostate Cancer Aggressiveness in the Context of Gleason Grade Heterogeneity, Tumor Multifocality, and Biopsy Undersampling. *Eur Urol* (2014) 66(3):550–60. doi: 10.1016/j.eururo.2014.05.004
22. Shipitsin M, Small C, Choudhury S, Giladi E, Friedlander S, Nardone J, et al. Identification of Proteomic Biomarkers Predicting Prostate Cancer Aggressiveness and Lethality Despite Biopsy-Sampling Error. *Br J Cancer* (2014) 111(6):1201–12. doi: 10.1038/bjc.2014.396
23. Blume-Jensen P, Berman DM, Rimm DL, Shipitsin M, Putzi M, Nifong TP, et al. Development and Clinical Validation of an in Situ Biopsy-Based Multimarker Assay for Risk Stratification in Prostate Cancer. *Clin Cancer Res* (2015) 21(11):2591–600. doi: 10.1158/1078-0432.CCR-14-2603
24. Yoshimoto M, Cunha IW, Coudry RA, Fonseca FP, Torres CH, Soares FA, et al. FISH Analysis of 107 Prostate Cancers Shows That PTEN Genomic Deletion is Associated With Poor Clinical Outcome. *Br J Cancer* (2007) 97 (5):678–85. doi: 10.1038/sj.bjc.6603924
25. Sommariva S, Tarricone R, Lazzeri M, Ricciardi W, Montorsi F. Prognostic Value of the Cell Cycle Progression Score in Patients With Prostate Cancer: A Systematic Review and Meta-Analysis. *Eur Urol* (2016) 69(1):107–15. doi: 10.1016/j.eururo.2014.11.038
26. Karnes RJ, Choeurng V, Ross AE, Schaeffer EM, Klein EA, Freedland SJ, et al. Validation of a Genomic Risk Classifier to Predict Prostate Cancer-Specific Mortality in Men With Adverse Pathologic Features. *Eur Urol* (2018) 73 (2):168–75. doi: 10.1016/j.eururo.2017.03.036
27. Den RB, Santiago-Jimenez M, Alter J, Schliekelman M, Wagner JR, Renzulli Ii JF, et al. Decipher Correlation Patterns Post Prostatectomy: Initial Experience From 2 342 Prospective Patients. *Prostate Cancer Prostatic Dis* (2016) 19 (4):374–9. doi: 10.1038/pcan.2016.38
28. Erho N, Crisan A, Vergara IA, Mitra AP, Ghadessi M, Buerki C, et al. Discovery and Validation of a Prostate Cancer Genomic Classifier That Predicts Early Metastasis Following Radical Prostatectomy. *PLoS One* (2013) 8(6):e66855. doi: 10.1371/journal.pone.0066855
29. Decipher Biosciences. (2021). Available at: from https://decipherbio.com/wp-content/themes/decipher/assets/pdf/decipher-prostate-specimen-preparation-shipping-Instructions.pdf [Retrieved January 21, 2021].
30. Kneebone A, Fraser-Browne C, Duchesne GM, Fisher R, Frydenberg M, Herschtal A, et al. Adjuvant Radiotherapy Versus Early Salvage Radiotherapy Following Radical Prostatectomy (TROG 08.03/ANZUP RAVES): A Randomised, Controlled, Phase 3, non-Inferiority Trial. *Lancet Oncol* (2020) 21(10):1331–40. doi: 10.1016/S1470-2045(20)30456-3
31. Sargos P, Chabaud S, Latorzeff I, Magne N, Benyoucef A, Supiot S, et al. Adjuvant Radiotherapy Versus Early Salvage Radiotherapy Plus Short-Term Androgen Deprivation Therapy in Men With Localised Prostate Cancer After Radical Prostatectomy (GETUG-AFU 17): A Randomised, Phase 3 Trial. *Lancet Oncol* (2020) 21(10):1341–52. doi: 10.1016/S1470-2045(20)30454-X
32. Parker CC, Clarke NW, Cook AD, Kynaston HG, Petersen PM, Catton C, et al. Timing of Radiotherapy After Radical Prostatectomy (RADICALS-RT): A Randomised, Controlled Phase 3 Trial. *Lancet* (2020) 396(10260):1413–21. doi: 10.1016/S0140-6736(20)31553-1
33. Vale CL, Fisher D, Kneebone A, Parker C, Pearse M, Richaud P, et al. Adjuvant or Early Salvage Radiotherapy for the Treatment of Localised and Locally Advanced Prostate Cancer: A Prospectively Planned Systematic Review and Meta-Analysis of Aggregate Data. *Lancet* (2020) 396 (10260):1422–31. doi: 10.1016/S0140-6736(20)31952-8
34. Dalela D, Santiago-Jimenez M, Yousefi K, Karnes RJ, Ross AE, Den RB, et al. Genomic Classifier Augments the Role of Pathological Features in Identifying Optimal Candidates for Adjuvant Radiation Therapy in Patients With Prostate Cancer: Development and Internal Validation of a Multivariable

Prognostic Model. *J Clin Oncol* (2017) 35(18):1982–90. doi: 10.1200/JCO.2016.69.9918
35. Zhao SG, Chang SL, Spratt DE, Erho N, Yu M, Ashab HA, et al. Development and Validation of a 24-Gene Predictor of Response to Postoperative Radiotherapy in Prostate Cancer: A Matched, Retrospective Analysis. *Lancet Oncol* (2016) 17(11):1612–20. doi: 10.1016/S1470-2045(16)30491-0
36. Karnes RJ, Sharma V, Choeurng V, Ashab HA, Erho N, Alshalalfa M, et al. Development and Validation of a Prostate Cancer Genomic Signature That Predicts Early ADT Treatment Response Following Radical Prostatectomy. *Clin Cancer Res* (2018) 24(16):3908–16. doi: 10.1158/1078-0432.CCR-17-2745
37. Spratt DE, Yousefi K, Deheshi S, Ross AE, Den RB, Schaeffer EM, et al. Individual Patient-Level Meta-Analysis of the Performance of the Decipher Genomic Classifier in High-Risk Men After Prostatectomy to Predict Development of Metastatic Disease. *J Clin Oncol* (2017) 35(18):1991–8. doi: 10.1200/JCO.2016.70.2811
38. Cooperberg MR, Davicioni E, Crisan A, Jenkins RB, Ghadessi M, Karnes RJ. Combined Value of Validated Clinical and Genomic Risk Stratification Tools for Predicting Prostate Cancer Mortality in a High-Risk Prostatectomy Cohort. *Eur Urol* (2015) 67(2):326–33. doi: 10.1016/j.eururo.2014.05.039
39. Knudsen BS, Kim HL, Erho N, Shin H, Alshalalfa M, Lam LLC, et al. Application of a Clinical Whole-Transcriptome Assay for Staging and Prognosis of Prostate Cancer Diagnosed in Needle Core Biopsy Specimens. *J Mol Diagn* (2016) 18(3):395–406. doi: 10.1016/j.jmoldx.2015.12.006
40. Jairath NK, Dal Pra A, Vince RJr., Dess RT, Jackson WC, Tosoian JJ, et al. A Systematic Review of the Evidence for the Decipher Genomic Classifier in Prostate Cancer. *Eur Urol* (2021) 79(3):374–83. doi: 10.1016/j.eururo.2020.11.021
41. Nguyen PL, Haddad Z, Ross AE, Martin NE, Deheshi S, Lam LLC, et al. Ability of a Genomic Classifier to Predict Metastasis and Prostate Cancer-Specific Mortality After Radiation or Surgery Based on Needle Biopsy Specimens. *Eur Urol* (2017) 72(5):845–52. doi: 10.1016/j.eururo.2017.05.009
42. Nguyen PL, Martin NE, Choeurng V, Palmer-Aronsten B, Kolisnik T, Beard CJ, et al. Utilization of Biopsy-Based Genomic Classifier to Predict Distant Metastasis After Definitive Radiation and Short-Course ADT for Intermediate and High-Risk Prostate Cancer. *Prostate Cancer Prostatic Dis* (2017) 20(2):186–92. doi: 10.1038/pcan.2016.58
43. Klein EA, Haddad Z, Yousefi K, Lam LL, Wang Q, Choeurng V, et al. Decipher Genomic Classifier Measured on Prostate Biopsy Predicts Metastasis Risk. *Urology* (2016) 90:148–52. doi: 10.1016/j.urology.2016.01.012
44. Lobo JM, Dicker AP, Buerki C, Daviconi E, Karnes RJ, Jenkins RB, et al. Evaluating the Clinical Impact of a Genomic Classifier in Prostate Cancer Using Individualized Decision Analysis. *PLoS One* (2015) 10(3):e0116866. doi: 10.1371/journal.pone.0116866
45. Gore JL, du Plessis M, Santiago-Jimenez M, Yousefi K, Thompson DJS, Karsh L, et al. Decipher Test Impacts Decision Making Among Patients Considering Adjuvant and Salvage Treatment After Radical Prostatectomy: Interim Results From the Multicenter Prospective PRO-IMPACT Study. *Cancer* (2017) 123(15):2850–9. doi: 10.1002/cncr.30665
46. Marascio J, Spratt DE, Zhang J, Trabulsi EJ, Le T, Sedzorme WS, et al. Prospective Study to Define the Clinical Utility and Benefit of Decipher Testing in Men Following Prostatectomy. *Prostate Cancer Prostatic Dis* (2020) 23(2):295–302. doi: 10.1038/s41391-019-0185-7
47. Michalopoulos SN, Kella N, Payne R, Yohannes P, Singh A, Hettinger C, et al. Influence of a Genomic Classifier on Post-Operative Treatment Decisions in High-Risk Prostate Cancer Patients: Results From the PRO-ACT Study. *Curr Med Res Opin* (2014) 30(8):1547–56. doi: 10.1185/03007995.2014.919908
48. Berlin A, Murgic J, Hosni A, Pintilie M, Salcedo A, Fraser M, et al. Genomic Classifier for Guiding Treatment of Intermediate-Risk Prostate Cancers to Dose-Escalated Image Guided Radiation Therapy Without Hormone Therapy. *Int J Radiat Oncol Biol Phys* (2019) 103(1):84–91. doi: 10.1016/j.ijrobp.2018.08.030
49. National Comprehensive Cancer Network. *Prostate Cancer (Version 2.2021).* (2021). Available at: https://www.nccn.org/professionals/physician_gls/pdf/prostate.pdf [Retrieved August 25, 2020].
50. Koch MO, Cho JS, Kaimakliotis HZ, Cheng L, Sangale Z, Brawer M, et al. Use of the Cell Cycle Progression (CCP) Score for Predicting Systemic Disease and Response to Radiation of Biochemical Recurrence. *Cancer Biomark* (2016) 17(1):83–8. doi: 10.3233/CBM-160620
51. Bishoff JT, Freedland SJ, Gerber L, Tennstedt P, Reid J, Welbourn W, et al. Prognostic Utility of the Cell Cycle Progression Score Generated From Biopsy in Men Treated With Prostatectomy. *J Urol* (2014) 192(2):409–14. doi: 10.1016/j.juro.2014.02.003
52. "Understanding the Prolaris Report". In: *Myriad Prolaris*. Available at: https://prolaris.com/understanding-the-prolaris-report/ [Retrieved Feb 28,2021].
53. Shore ND, Kella N, Moran B, Boczko J, Bianco FJ, Crawford ED, et al. Impact of the Cell Cycle Progression Test on Physician and Patient Treatment Selection for Localized Prostate Cancer. *J Urol* (2016) 195(3):612–8. doi: 10.1016/j.juro.2015.09.072
54. Jamaspishvili T, Berman DM, Ross AE, Scher HI, De Marzo AM, Squire JA, et al. Clinical Implications of PTEN Loss in Prostate Cancer. *Nat Rev Urol* (2018) 15(4):222–34. doi: 10.1038/nrurol.2018.9
55. Cairns P, Okami K, Halachmi S, Halachmi N, Esteller M, Herman JG, et al. Frequent Inactivation of PTEN/MMAC1 in Primary Prostate Cancer. *Cancer Res* (1997) 57(22):4997–5000.
56. Bertram J, Peacock JW, Fazli L, Mui AL, Chung SW, Cox ME, et al. Loss of PTEN is Associated With Progression to Androgen Independence. *Prostate* (2006) 66(9):895–902. doi: 10.1002/pros.20411
57. Koksal IT, Dirice E, Yasar D, Sanlioglu AD, Ciftcioglu A, Gulkesen KH, et al. The Assessment of PTEN Tumor Suppressor Gene in Combination With Gleason Scoring and Serum PSA to Evaluate Progression of Prostate Carcinoma. *Urol Oncol* (2004) 22(4):307–12. doi: 10.1016/j.urolonc.2004.01.009
58. Pettersson A, Graff RE, Bauer SR, Pitt MJ, Lis RT, Stack EC, et al. The TMPRSS2:ERG Rearrangement, ERG Expression, and Prostate Cancer Outcomes: A Cohort Study and Meta-Analysis. *Cancer Epidemiol Biomarkers Prev* (2012) 21(9):1497–509. doi: 10.1158/1055-9965.EPI-12-0042
59. Song C, Chen H. Predictive Significance of TMRPSS2-ERG Fusion in Prostate Cancer: A Meta-Analysis. *Cancer Cell Int* (2018) 18:177. doi: 10.1186/s12935-018-0672-2
60. Ahearn TU, Pettersson A, Ebot EM, Gerke T, Graff RE, Morais CL, et al. A Prospective Investigation of PTEN Loss and ERG Expression in Lethal Prostate Cancer. *J Natl Cancer Inst* (2016) 108(2):djv346. doi: 10.1093/jnci/djv346
61. Tosoian JJ, Trock BJ, Morgan TM, Salami SS, Tomlins SA, Spratt DE, et al. Use of the MyProstateScore Test to Rule Out Clinically Significant Cancer: Validation of a Straightforward Clinical Testing Approach. *J Urol* (2021) 205(3):732–9. doi: 10.1097/JU.0000000000001430
62. U.S. Food and Drug Administration. *Foundationone CDx - P170019*. (2017). Available at: https://www.fda.gov/medical-devices/recently-approved-devices/foundationone-cdx-p17001.
63. Kornberg Z, Cooperberg MR, Cowan JE, Chan JM, Shinohara K, Simko JP, et al. A 17-Gene Genomic Prostate Score as a Predictor of Adverse Pathology in Men on Active Surveillance. *J Urol* (2019) 202(4):702–9. doi: 10.1097/JU.0000000000000290
64. Albain KS, Barlow WE, Shak S, Hortobagyi GN, Livingston RB, Yeh IT, et al. Prognostic and Predictive Value of the 21-Gene Recurrence Score Assay in Postmenopausal Women With Node-Positive, Oestrogen-Receptor-Positive Breast Cancer on Chemotherapy: A Retrospective Analysis of a Randomised Trial. *Lancet Oncol* (2010) 11(1):55–65. doi: 10.1016/S1470-2045(09)70314-6
65. Gray RG, Quirke P, Handley K, Lopatin M, Magill L, Baehner FL, et al. Validation Study of a Quantitative Multigene Reverse Transcriptase-Polymerase Chain Reaction Assay for Assessment of Recurrence Risk in Patients With Stage II Colon Cancer. *J Clin Oncol* (2011) 29(35):4611–9. doi: 10.1200/JCO.2010.32.8732
66. Badani KK, Kemeter MJ, Febbo GF, Jeffrey Lawrence H, Denes BS, Rothney MP, et al. The Impact of a Biopsy Based 17-Gene Genomic Prostate Score on Treatment Recommendations in Men With Newly Diagnosed Clinically Prostate Cancer Who are Candidates for Active Surveillance. *Urol Pract* (2015) 2(4):181–9. doi: 10.1016/j.urpr.2014.10.010
67. Paik S, Shak S, Tang G, Kim C, Baker J, Cronin M, et al. A Multigene Assay to Predict Recurrence of Tamoxifen-Treated, Node-Negative Breast Cancer. *N Engl J Med* (2004) 351(27):2817–26. doi: 10.1056/NEJMoa041588
68. Sparano JA, Gray RJ, Makower DF, Pritchard KI, Albain KS, Hayes DF, et al. Adjuvant Chemotherapy Guided by a 21-Gene Expression Assay in Breast Cancer. *N Engl J Med* (2018) 379(2):111–21. doi: 10.1056/NEJMoa1804710

69. Sparano JA, Gray RJ, Ravdin PM, Makower DF, Pritchard KI, Albain KS, et al. Clinical and Genomic Risk to Guide the Use of Adjuvant Therapy for Breast Cancer. *N Engl J Med* (2019) 380(25):2395–405. doi: 10.1056/NEJMoa1904819
70. Sparano JA, Gray RJ, Makower DF, Pritchard KI, Albain KS, Hayes DF, et al. Prospective Validation of a 21-Gene Expression Assay in Breast Cancer. *N Engl J Med* (2015) 373(21):2005–14. doi: 10.1056/NEJMoa1510764
71. Trock BJ, Brotzman MJ, Mangold LA, Bigley JW, Epstein JI, McLeod D, et al. Evaluation of GSTP1 and APC Methylation as Indicators for Repeat Biopsy in a High-Risk Cohort of Men With Negative Initial Prostate Biopsies. *BJU Int* (2012) 110(1):56–62. doi: 10.1111/j.1464-410X.2011.10718.x
72. Heichman KA, Warren JD. DNA Methylation Biomarkers and Their Utility for Solid Cancer Diagnostics. *Clin Chem Lab Med* (2012) 50(10):1707–21. doi: 10.1515/cclm-2011-0935
73. Van Neste L, Partin AW, Stewart GD, Epstein JI, Harrison DJ, Van Criekinge W. Risk Score Predicts High-Grade Prostate Cancer in DNA-methylation Positive, Histopathologically Negative Biopsies. *Prostate* (2016) 76(12):1078–87. doi: 10.1002/pros.23191
74. Wojno KJ, Costa FJ, Cornell RJ, Small JD, Pasin E, Van Criekinge W, et al. Reduced Rate of Repeated Prostate Biopsies Observed in ConfirmMDx Clinical Utility Field Study. *Am Health Drug Benefits* (2014) 7(3):129–34.
75. Chornokur G, Dalton K, Borysova ME, Kumar NB. Disparities At Presentation, Diagnosis, Treatment, and Survival in African American Men, Affected by Prostate Cancer. *Prostate* (2011) 71(9):985–97. doi: 10.1002/pros.21314
76. Moses KA, Orom H, Brasel A, Gaddy J, Underwood W3rd3rd. Racial/ethnic Differences in the Relative Risk of Receipt of Specific Treatment Among Men With Prostate Cancer. *Urol Oncol* (2016) 34(9):415.e7–12. doi: 10.1016/j.urolonc.2016.04.002
77. Hoffman RM, Gilliland FD, Eley JW, Harlan LC, Stephenson RA, Stanford JL, et al. Racial and Ethnic Differences in Advanced-Stage Prostate Cancer: The Prostate Cancer Outcomes Study. *J Natl Cancer Inst* (2001) 93(5):388–95. doi: 10.1093/jnci/93.5.388
78. Deka R, Courtney PT, Parsons JK, Nelson TJ, Nalawade V, Luterstein E, et al. Association Between African American Race and Clinical Outcomes in Men Treated for Low-Risk Prostate Cancer With Active Surveillance. *JAMA* (2020) 324(17):1747–54. doi: 10.1001/jama.2020.17020
79. DeSantis CE, Miller KD, Goding Sauer A, Jemal A, Siegel RL. Cancer Statistics for African Americans, 2019. *CA Cancer J Clin* (2019) 69(3):211–33. doi: 10.3322/caac.21555
80. Lobo JM, Trifiletti DM, Sturz VN, Dicker AP, Buerki C, Davicioni E, et al. Cost-Effectiveness of the Decipher Genomic Classifier to Guide Individualized Decisions for Early Radiation Therapy After Prostatectomy for Prostate Cancer. *Clin Genitourin Cancer* (2017) 15(3):e299–309. doi: 10.1016/j.clgc.2016.08.012
81. Salami SS, Hovelson DH, Kaplan JB, Mathieu R, Udager AM, Curci NE, et al. Transcriptomic Heterogeneity in Multifocal Prostate Cancer. *JCI Insight* (2018) 3(21):e123468. doi: 10.1172/jci.insight.123468
82. Punnen S, Stoyanova R, Kwon D, Reis IM, Soodana-Prakash N, Ritch CR, et al. Heterogeneity in Genomic Risk Assessment From Tissue Based Prognostic Signatures Used in the Biopsy Setting and the Impact of Magnetic Resonance Imaging Targeted Biopsy. *J Urol* (2021) 205(5):1344–51. doi: 10.1097/JU.0000000000001559
83. Wei L, Wang J, Lampert E, Schlanger S, DePriest AD, Hu Q, et al. Intratumoral and Intertumoral Genomic Heterogeneity of Multifocal Localized Prostate Cancer Impacts Molecular Classifications and Genomic Prognosticators. *Eur Urol* (2017) 71(2):183–92. doi: 10.1016/j.eururo.2016.07.008
84. Eggener SE, Rumble RB, Beltran H. Molecular Biomarkers in Localized Prostate Cancer: Asco Guideline Summary. *JCO Oncol Pract* (2020) 16(6):340–3. doi: 10.1200/JOP.19.00752
85. Mottet N, van den Bergh RCN, Briers E, Van den Broeck T, Cumberbatch MG, De Santis M, et al. Eau-Eanm-Estro-Esur-Siog Guidelines on Prostate Cancer-2020 Update. Part 1: Screening, Diagnosis, and Local Treatment With Curative Intent. *Eur Urol* (2021) 79(2):243–62. doi: 10.1016/j.eururo.2020.09.042

Conflict of Interest: The authors declare that the research was conducted in the absence of any commercial or financial relationships that could be construed as a potential conflict of interest.

Copyright © 2021 Basourakos, Tzeng, Lewicki, Patel, Al Hussein Al Awamlh, Venkat, Shoag, Gorin, Barbieri and Hu. This is an open-access article distributed under the terms of the Creative Commons Attribution License (CC BY). The use, distribution or reproduction in other forums is permitted, provided the original author(s) and the copyright owner(s) are credited and that the original publication in this journal is cited, in accordance with accepted academic practice. No use, distribution or reproduction is permitted which does not comply with these terms.

frontiers in Oncology

ORIGINAL RESEARCH
published: 30 September 2021
doi: 10.3389/fonc.2021.726655

Identification of Hub Genes Associated With Clear Cell Renal Cell Carcinoma by Integrated Bioinformatics Analysis

Hao Huang[1,2,3], *Ling Zhu*[2,3], *Chao Huang*[3,4], *Yi Dong*[2,3], *Liangliang Fan*[2,3], *Lijian Tao*[1,3], *Zhangzhe Peng*[1,3*] *and Rong Xiang*[2,3*]

[1] Department of Nephrology, Xiangya Hospital Central South University, Changsha, China, [2] Department of Cell Biology, School of Life Sciences, Central South University, Changsha, China, [3] Hunan Key Laboratory of Organ Fibrosis, Central South University, Changsha, China, [4] Department of Otolaryngology-Head and Neck Surgery, Second Xiangya Hospital Central South University, Changsha, China

OPEN ACCESS

Edited by:
Marco Borghesi,
University of Genoa, Italy

Reviewed by:
Shaolong Cao,
University of Texas MD Anderson Cancer Center, United States
Pasquale Ditonno,
University of Bari, Italy

***Correspondence:**
Zhangzhe Peng
pengzhangzhe@csu.edu.cn
Rong Xiang
shirlesmile@csu.edu.cn

Specialty section:
This article was submitted to Genitourinary Oncology, a section of the journal Frontiers in Oncology

Received: 17 June 2021
Accepted: 06 September 2021
Published: 30 September 2021

Citation:
Huang H, Zhu L, Huang C, Dong Y, Fan L, Tao L, Peng Z and Xiang R (2021) Identification of Hub Genes Associated With Clear Cell Renal Cell Carcinoma by Integrated Bioinformatics Analysis. Front. Oncol. 11:726655. doi: 10.3389/fonc.2021.726655

Background: Clear cell renal cell carcinoma (ccRCC) is a common genitourinary cancer type with a high mortality rate. Due to a diverse range of biochemical alterations and a high level of tumor heterogeneity, it is crucial to select highly validated prognostic biomarkers to be able to identify subtypes of ccRCC early and apply precision medicine approaches.

Methods: Transcriptome data of ccRCC and clinical traits of patients were obtained from the GSE126964 dataset of Gene Expression Omnibus and The Cancer Genome Atlas Kidney Renal Clear Cell Carcinoma (TCGA-KIRC) database. Weighted gene co-expression network analysis (WGCNA) and differentially expressed gene (DEG) screening were applied to detect common differentially co-expressed genes. Gene Ontology, Kyoto Encyclopedia of Genes and Genomes analysis, survival analysis, prognostic model establishment, and gene set enrichment analysis were also performed. Immunohistochemical analysis results of the expression levels of prognostic genes were obtained from The Human Protein Atlas. Single-gene RNA sequencing data were obtained from the GSE131685 and GSE171306 datasets.

Results: In the present study, a total of 2,492 DEGs identified between ccRCC and healthy controls were filtered, revealing 1,300 upregulated genes and 1,192 downregulated genes. Using WGCNA, the turquoise module was identified to be closely associated with ccRCC. Hub genes were identified using the maximal clique centrality algorithm. After having intersected the hub genes and the DEGs in GSE126964 and TCGA-KIRC dataset, and after performing univariate, least absolute shrinkage and selection operator, and multivariate Cox regression analyses, *ALDOB*, *EFHD1*, and *ESRRG* were identified as significant prognostic factors in patients diagnosed with ccRCC. Single-gene RNA sequencing analysis revealed the expression profile of *ALDOB*, *EFHD1*, and *ESRRG* in different cell types of ccRCC.

Conclusions: The present results demonstrated that *ALDOB*, *EFHD1*, and *ESRRG* may act as potential targets for medical therapy and could serve as diagnostic biomarkers for ccRCC.

Keywords: clear cell renal cell carcinoma, weighted gene co-expression network analysis, differentially expressed genes, prognostic genes, single-cell analysis

INTRODUCTION

Renal cell carcinoma (RCC) is one of the most common genitourinary cancer types worldwide, and it has a number of heterogeneous histological subtypes, with clear cell RCC (ccRCC) accounting for ~85% of all cases (1). In total, 431,288 new patients were diagnosed with renal cancer, and 179,368 of these patients succumbed to the disease worldwide in 2020 (2). ccRCC is not susceptible to chemoradiotherapy (3). Although ccRCC is curable at an early localized stage by partial or total surgical nephrectomy, advanced or metastatic ccRCC remains a clinical challenge (4). Over the past years, antiangiogenic treatment, inhibitors of the mammalian target of rapamycin (mTOR) pathway, or immune checkpoint inhibition therapy have considerably evolved (5). However, due to diverse biochemical alterations and a high level of tumor heterogeneity, it is important to select highly validated prognostic biomarkers to identify subtypes of ccRCC early and apply precision medicine approaches (6).

The molecular mechanism of ccRCC is characterized by genetic diversity and chromosomal complexity. Loss of the heterozygosity of chromosome 3p, where the von Hippel–Lindau (*VHL*) gene is located, is found in over 90% of ccRCC cases, and it is considered the critical genetic event (7–9). A loss-of-function mutation in the *VHL* gene induces the aberrant regulation of a number of *VHL*-mediated targets, pathways, and processes, which is a significant step in the development of ccRCC (10, 11). The VHL protein, as an E3 ubiquitin ligase, is notably involved in the ubiquitylation of the prolyl hydroxylated transcription factors, hypoxia-inducible factor 1 α (HIF1 α) and HIF2 α, under normoxic conditions. HIF1 α and HIF2 α have an important role in the regulation of angiogenesis, erythropoiesis, glycolysis, and apoptosis (12–14). Moreover, next-generation sequencing technologies have provided evidence that *PBRM1*, *SETD2*, or *BAP1* mutations are the drivers of tumor evolution (15, 16). Although the molecular features of ccRCC have been increasingly defined by previous studies (17–19), there remain numerous subtypes of ccRCC the pathogenic mechanisms of which have yet to be clearly determined at the genetic and molecular levels. Thus, it is important to identify more additional disease-related genes.

Benefiting from the rapid development of genome sequencing technology, bioinformatics can be used to study gene expression profiles in order to examine the molecular mechanism of tumors and identify tumor-specific indicators. Weighted gene co-expression network analysis (WGCNA) was developed by Horvath and Zhang in 2005 (20). At present, WGCNA is becoming a powerful approach to detecting gene modules, exploring the correlation of the modules and phenotypes, and discovering hub genes that regulate critical biological processes (21, 22).

In the present study, a gene expression profile of ccRCC from the Gene Expression Omnibus (GEO) was downloaded. WGCNA and differentially expressed gene (DEG) screening were applied to detect common differentially co-expressed genes. Then, The Cancer Genome Atlas Kidney Renal Clear Cell Carcinoma (TCGA-KIRC) data were used to establish the prognostic model of ccRCC. Single-cell RNA sequencing (RNA-seq) data from GEO were used to verify the expression profile of the prognostic genes in different cell types. This study aimed not only to understand ccRCC pathogenesis but also to determine its molecular mechanisms and provide insights into novel therapeutic targets for drugs.

METHODS

Data Collection and Single-Cell RNA Sequencing Data Processing

The workflow for the current study is presented in **Figure 1**. Original data were collected from the GSE126964 dataset, which contained 55 ccRCC tumor tissues and 11 matched normal tissues (23). The GEO expression matrix was annotated with gene symbols using the information from the GPL20795 HiSeq X Ten platform file, as well as $\log_2$ transformed in R (version 4.0.4) and RStudio (version 1.2.5033) if necessary. Principal component analysis (PCA) was performed, and the outliers of GSM3619137 and GSM3619152 were excluded (**Figure S1**). In total, only 53 ccRCC sample and 11 normal sample data were used for subsequent analysis.

RNA-seq data of TCGA-KIRC and corresponding clinical information were obtained from TCGA (https://portal.gdc.cancer.gov/).

Single-cell RNA-seq data from GSE131685 and GSE171306 were downloaded through GEO website. R package "Seurat" (version 4.0.2) was used to process the data (24). Three healthy kidney samples from GSE131685 (25) and two ccRCC samples from GSE171306 (26) were merged for further analysis. The single-cell RNA-seq data processing was described previously (27). The cell clusters were annotated manually based on previous knowledge and information from literatures (28, 29). Expression profiling of the genes were depicted by heatmap and violin plot using the function "FeaturePlot" and "VlnPlot."

Differentially Expressed Gene Identification

The "limma" software package (version 3.48.0) (30) was used to conduct the DEG analysis between ccRCC and normal sample data from the GSE126964 dataset (30). An adjusted p-value <0.05

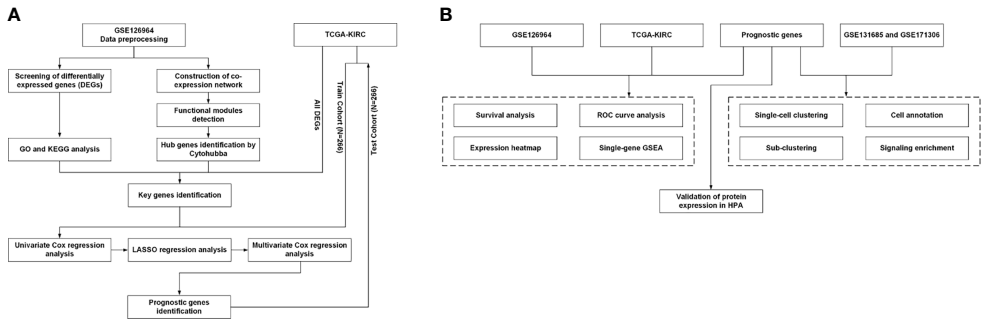

FIGURE 1 | Workflow of the present study. **(A)** Identification workflow. **(B)** Verification workflow. DEG, differentially expressed gene; GO, Gene Ontology; KEGG, Kyoto Encyclopedia of Genes and Genomes; TCGA, The Cancer Genome Atlas; LASSO, least absolute shrinkage and selection operator; ROC, receiver operating characteristic; HPA, Human Protein Atlas; GSEA, gene set enrichment analysis.

and a $|\log_2$fold change$|$ of ≥2.0 were selected as the cutoff criteria. The volcano and heatmap plots were generated using ggplot2 (version 3.3.3) and pheatmap (version 1.0.12) packages, respectively. The DEGs of TCGA-KIRC dataset (https://portal.gdc.cancer.gov/) were obtained *via* Gene Expression Profiling Interactive Analysis (GEPIA2; http://gepia2.cancer-pku.cn/) (31) using the same aforementioned threshold.

Gene Ontology Enrichment and Kyoto Encyclopedia of Genes and Genomes Analysis of Differentially Expressed Genes

The "clusterProfiler" (version 3.18.1) R package was used for GO and KEGG enrichment analyses (http://www.bioconductor.org/packages/release/bioc/html/clusterProfiler.html) (32). The three main processes in GO analysis are as follows: biological process (BP), molecular function (MF), and cellular component (CC). The p-value was conventionally set at 0.05. A circle plot was generated by "Goplot" R package (version 1.0.2).

Weighted Gene Co-Expression Network Construction

The "WGCNA" package (version 1.70-3) of R (20) was used to construct the co-expression networks. Genes with mean counts of over 5 were selected. A total of 64 samples were used to calculate the Pearson's correlation matrices. The matrices of adjacency were created based on the Pearson's correlation matrices. Then, the clinical trait data were uploaded, and the scale independence and mean connectivity were estimated. Subsequently, the topological overlap measure (TOM) matrix, which was created from the adjacency matrix, was used to estimate the network's connectivity property. A hierarchical clustering dendrogram of the TOM matrix was constructed using the average distance with a minimum size threshold of 50 to classify the similar gene expression profiles into different gene modules. Finally, similar gene modules were merged, with a threshold of 0.20.

Co-Expression Network Construction and Hub Gene Identification

The Cytoscape software v3.7.2 was used to visualize the co-expression network in the turquoise module (33). The data were imported into Cytohubba, a Cytoscape plug-in for hub gene identification, and the maximal clique centrality (MCC) algorithm was used to calculate the scores of all nodes of the network. The top 30 nodes with the highest MCC scores were selected as the hub genes associated with ccRCC. The "real" key genes were identified as those intersecting between the top 30 nodes in turquoise module, DEGs from GSE126964 and DEGs from TCGA-KIRC.

Identification and Verification of Prognostic Gene Signatures

Univariate Cox regression analysis was performed to screen the genes significantly associated with overall survival (OS) in the TCGA-KIRC dataset. The OS-related genes with $p < 0.1$ were included in the least absolute shrinkage and selection operator (LASSO) regression analysis by using the R package "glmnet" (version 4.1-2). Then, a multivariate Cox regression model analysis was performed to establish a Cox proportional hazards regression prognostic model. We used the following formula to calculate the risk score of each patient:

$$\text{Risk Score} = \sum_{i=1}^{n} \beta_i \times x_i$$

In this formula, β is coefficient and x is the expression level of each prognostic gene i. The samples were divided into a high-risk group and a low-risk group according to the median risk score of the training cohort from TCGA-KIRC. Receiver operating characteristic (ROC) analysis and Kaplan–Meier analysis were conducted between the high-risk group and the low-risk group.

Validation of the Protein Expression Levels of Prognostic Genes in the Human Protein Atlas Database

The Human Protein Atlas (HPA) is a database that aims to map all the human proteins in cells, tissues, and organs using an integration of various omics technologies (https://www.proteinatlas.org/). We also verified the protein expression levels of the survival-related hub genes based on immunohistochemistry using the HPA database.

Gene Set Enrichment Analysis of Prognostic Genes

Gene set enrichment analysis (GSEA) was also used to detect the potential molecular mechanisms of the prognostic genes. Enriched terms predicted to be associated with the KEGG pathway in c2.cp.v7.2.symbols.gmt were screened by GSEA. Images were generated by "ggplot2" (version 3.3.3) package. The p-value of <0.05 was considered statistically significant.

Prognostic Gene Expression Profiles

The prognostic gene expression profiles were obtained from the GTEx Portal (https://gtexportal.org/home/).

RESULTS

Differentially Expressed Gene Screening

The "limma" package was utilized to analyze DEGs in the GSE126964 dataset, with the threshold of $|\log_2(\text{fold-change})|>2.0$ and adjusted $p < 0.05$. A total of 2,492 DEGs between ccRCC and normal control samples were filtered, revealing 1,300 upregulated genes and 1,192 downregulated genes (**Figures 2A, B**).

The DEGs were mostly enriched in "T cell activation," "leukocyte cell–cell adhesion," "apical part of cell," "external side of plasma membrane," "collagen-containing extracellular matrix (ECM)," and "ion transmembrane transporter activity" in the GO analysis (**Figure 2C**). In the KEGG analysis, DEGs were enriched in "cytokine–cytokine receptor interaction," "hematopoietic cell lineage," "viral protein interaction with cytokine and cytokine receptor," "cell adhesion molecules," and "protein digestion and absorption" (**Figure 2C**).

We also evaluated the metabolic shift between ccRCC tissues and normal control tissues in the GSE126964 dataset. Similar to the finding of Clark et al. (19), glycolysis-associated genes were found to be significantly upregulated, and most oxidative phosphorylation (OXPHOS) and tricarboxylic acid (TCA) cycle-associated genes were significantly downregulated in the GSE126964 dataset (**Figure S2**).

Weighted Co-Expression Network Construction and Analysis

The sample clustering dendrograms of the ccRCC and normal samples are shown in **Figure S3A**. The soft-power threshold β was selected as 5 to ensure that both the scale-free topology model fit index (R^2) and mean connectivity reached steady status (**Figure 3A**). Then, gene modules were detected based on the TOM matrix. A total of 25 modules were identified *via* average linkage hierarchical clustering, and each module was represented by a different color (**Figure 3B**). Among the modules, the turquoise module had the highest correlation with ccRCC traits (r = -0.97, p = 1e-39) (**Figure 3C**). A set of 400 selected genes were identified for the network heatmap construction (**Figure S3B**).

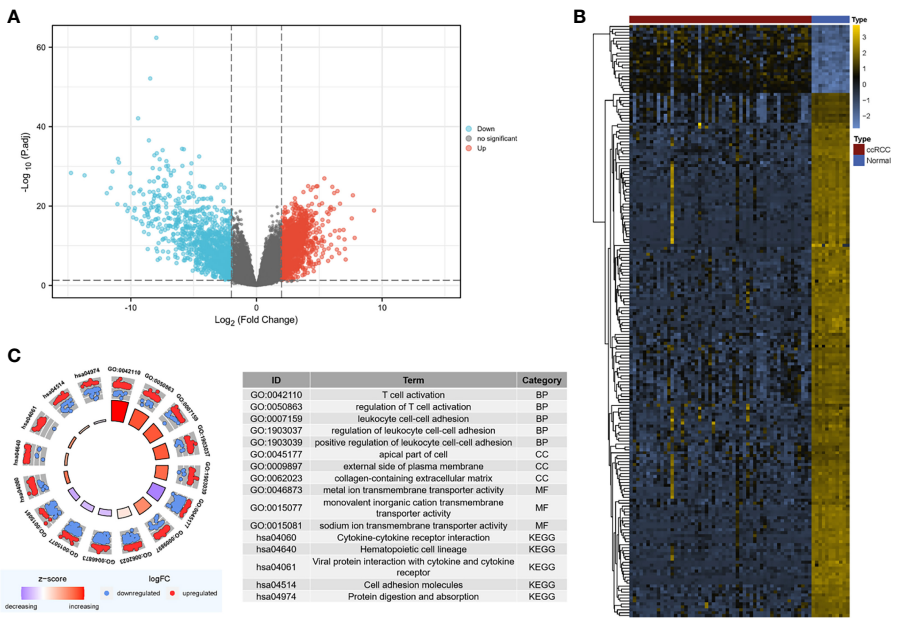

ID	Term	Category
GO:0042110	T cell activation	BP
GO:0050863	regulation of T cell activation	BP
GO:0007159	leukocyte cell-cell adhesion	BP
GO:1903037	regulation of leukocyte cell-cell adhesion	BP
GO:1903039	positive regulation of leukocyte cell-cell adhesion	BP
GO:0045177	apical part of cell	CC
GO:0009897	external side of plasma membrane	CC
GO:0062023	collagen-containing extracellular matrix	CC
GO:0046873	metal ion transmembrane transporter activity	MF
GO:0015077	monovalent inorganic cation transmembrane transporter activity	MF
GO:0015081	sodium ion transmembrane transporter activity	MF
hsa04060	Cytokine-cytokine receptor interaction	KEGG
hsa04640	Hematopoietic cell lineage	KEGG
hsa04061	Viral protein interaction with cytokine and cytokine receptor	KEGG
hsa04514	Cell adhesion molecules	KEGG
hsa04974	Protein digestion and absorption	KEGG

FIGURE 2 | Screening for DEGs. **(A)** Volcano map of DEGs between ccRCC and normal samples in the GSE126964 dataset. The red plots in the volcano represent upregulated genes, and the blue points represent downregulated genes. **(B)** Heatmap of the 200 selected DEGs. The color in heatmaps from blue to yellow shows the progression from low expression to high expression, respectively. **(C)** GO and KEGG analyses of the DEGs. The outer circle shows the scatter plot of the assigned gene $\log_2$fold change for all terms: red points show genes that exhibited increased expression, whereas the blue points represent genes that exhibited decreased expression. The inner circle indicates the Z-score value and the number of genes. Red represents a higher z-score value, and purple represents a lower Z-score value. DEG, differentially expressed gene; BP, biological process; CC, cell component; MF, molecular function; GO, Gene Ontology; KEGG, Kyoto Encyclopedia of Genes and Genomes; ccRCC, clear cell renal cell carcinoma.

Identification of Key Genes

An intramodular analysis of gene significance (GS) and module membership (MM) of the genes in the module turquoise was subsequently conducted. A high correlation coefficient of GS and MM was found in the turquoise module (cor = 0.97, p < 1e-200) (**Figure 3D**). The co-expression network of the turquoise module was constructed using Cytoscape software. Then, the module net was analyzed with the "Cytohubba" plug-in, and a network of the top 30 hub genes was constructed using the MCC algorithm (**Figure 3E**).

In order to identify the "real" key genes, we then obtained 796 DEGs, using a cohort of KIRC, from TCGA *via* GEPIA2, with the same threshold values. After comparing the DEGs in the GSE126964 dataset, TCGA-KIRC data and the top 30 hub genes from the turquoise module, a set of 13 key genes was identified (**Figure 4A**).

Validation of Key Genes *via* Survival Analysis

We randomly divided the patients in TCGA-KIRC into two cohorts, a training cohort (N = 266) and a testing cohort (N = 266). The univariate Cox regression analyses of 13 key genes with regard to OS of samples from the training cohort were performed (**Table 1**). Eight genes with p < 0.1 (*GGT6*, *SLC22A8*, *FAM3B*, *PTH1R*, *ALDOB*, *ESRRG*, *SLC34A1*, and *EFHD1*) were included in LASSO analysis (**Figures 4B, C**). Following the cross validation, seven genes achieved the minimum partial likelihood deviance. Then, we performed a multivariate Cox regression with these seven genes (*GGT6*, *FAM3B*, *PTH1R*, *ALDOB*, *ESRRG*, *SLC34A1*, and *EFHD1*) as covariants. We finally got three genes, including *ALDOB*, *ESRRG*, and *EFHD1* without collinearity, and each of them could be an independent prognostic marker for ccRCC (**Figure 4D**). A prognostic model based on the three genes was established. The risk score for each individual patient was calculated with the following formula: risk score = (-0.105197) * *ALDOB* + (-0.275676) * *ESRRG* + (-0.269554) * *EFHD1*.

Then, the Kaplan–Meier analysis was performed. As shown in **Figure 4E**, the survival rate of patients in the high-risk group was significantly lower than that in the low-risk group in either training cohort (p < 5.81e-4) or testing cohort (p < 5.48e-20). The ROC curve was then used to evaluate the accuracy of the

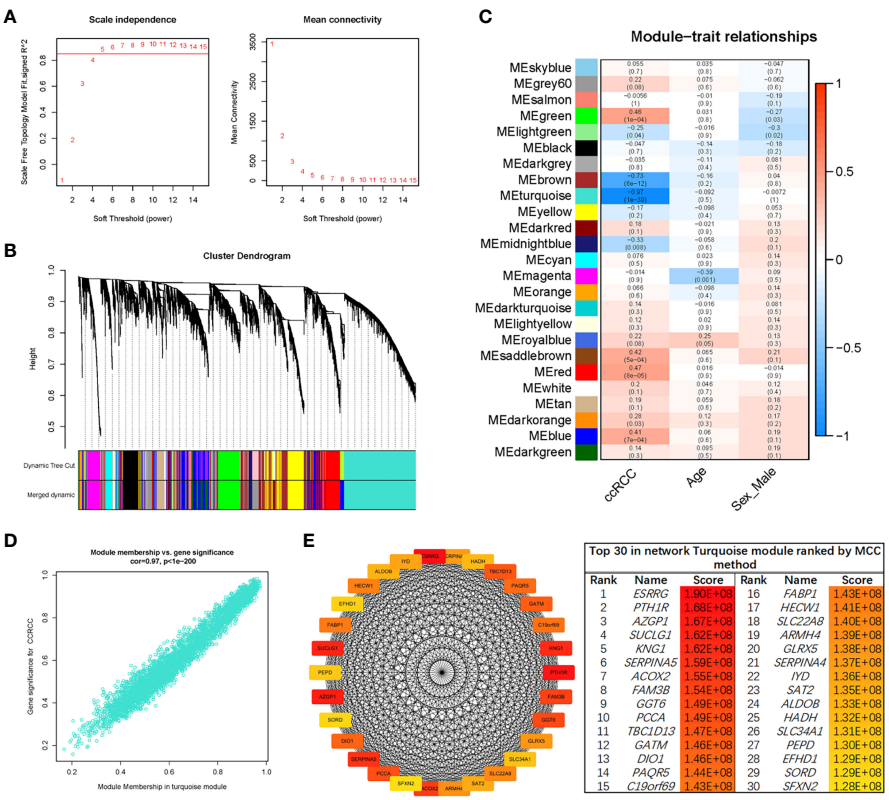

Top 30 in network Turquoise module ranked by MCC method

Rank	Name	Score	Rank	Name	Score
1	*ESRRG*	1.90E+08	16	*FABP1*	1.43E+08
2	*PTH1R*	1.68E+08	17	*HECW1*	1.41E+08
3	*AZGP1*	1.67E+08	18	*SLC22A8*	1.40E+08
4	*SUCLG1*	1.62E+08	19	*ARMH4*	1.39E+08
5	*KNG1*	1.62E+08	20	*GLRX5*	1.38E+08
6	*SERPINA5*	1.59E+08	21	*SERPINA4*	1.37E+08
7	*ACOX2*	1.55E+08	22	*IYD*	1.36E+08
8	*FAM3B*	1.54E+08	23	*SAT2*	1.35E+08
9	*GGT6*	1.49E+08	24	*ALDOB*	1.33E+08
10	*PCCA*	1.49E+08	25	*HADH*	1.32E+08
11	*TBC1D13*	1.47E+08	26	*SLC34A1*	1.31E+08
12	*GATM*	1.46E+08	27	*PEPD*	1.30E+08
13	*DIO1*	1.46E+08	28	*EFHD1*	1.29E+08
14	*PAQR5*	1.44E+08	29	*SORD*	1.29E+08
15	*C19orf69*	1.43E+08	30	*SFXN2*	1.28E+08

FIGURE 3 | WGCNA of the ccRCC samples. **(A)** Analysis of the network topology for various soft-thresholding powers. The left plot shows the scale-free fit index (y-axis) as a function of the soft-thresholding power (x-axis). The horizontal red line shows x-axis = 0.85. The right plot displays the mean connectivity (degree, y-axis) as a function of the soft-thresholding power (x-axis). The power was set as 5 for further analysis. **(B)** Hierarchical cluster analysis was conducted to detect co-expression clusters with corresponding color assignments. Each color represents a module in the constructed gene co-expression network, as assessed *via* WGCNA. **(C)** Module–trait relationships. Each row represents a color module, and every column represents a clinical trait. Each cell contains the corresponding correlation and p-value. **(D)** A scatter plot of GS for ccRCC *vs.* the MM in the turquoise module. **(E)** Identification of hub genes using the MCC method. Genes with the top 30 MCC values were colored red to yellow. Red refers to a relatively large MCC value, and yellow refers to relatively smaller MCC values. WGCNA, weighted gene co-expression network analysis; ccRCC, clear cell renal cell carcinoma; GS, gene significance; MM, module membership; MCC, maximal clique centrality.

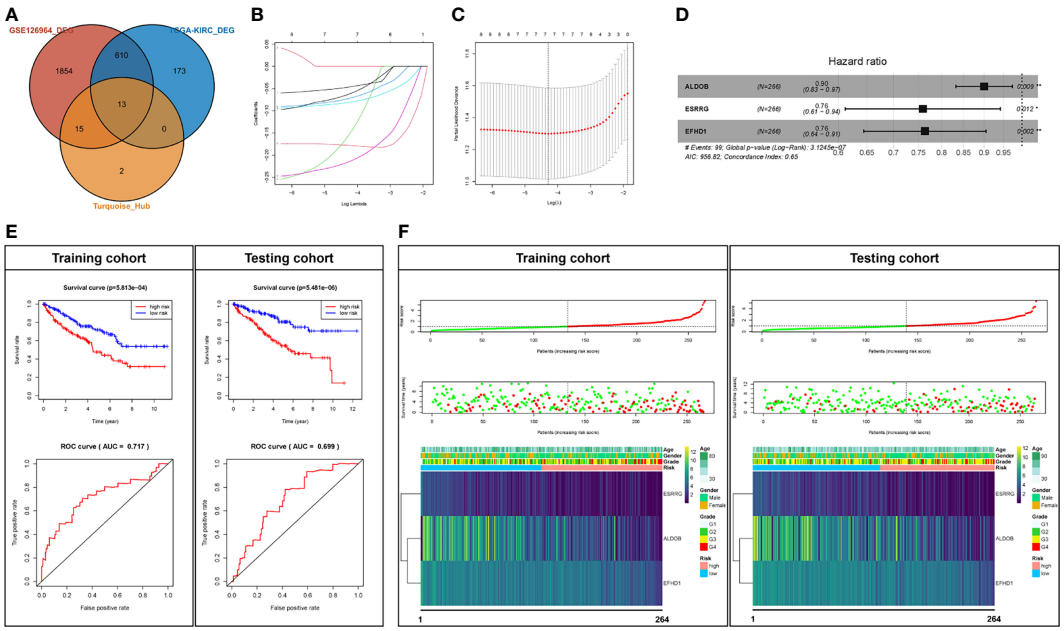

FIGURE 4 | Prognostic analysis of the key genes. **(A)** Key genes belonging to both the hub genes and DEGs of the GSE126964 and TCGA-KIRC datasets. **(B, C)** LASSO regression complexity was controlled by lambda using the glmnet R package. **(D)** The multivariate analysis of risk factors in ccRCC. **(E)** Overall survival and ROC analysis between high-risk score and low-risk score groups in the training cohort and testing cohort. **(F)** The overall survival stratified by the high- and low-risk score groups was plotted for the training cohort and testing cohort. Detailed risk scores, survival information, and heat maps of gene expression are also included for each dataset. *p < 0.05; **p < 0.01; DEG, differentially expressed gene; TCGA-KIRC, The Cancer Genome Atlas Kidney Renal Clear Cell Carcinoma; ROC, receiver operating characteristic; AUC, area under the curve; ccRCC, clear cell renal cell carcinoma; LASSO, least absolute shrinkage and selection operator.

survival analysis. The areas under the curves (AUCs) were 0.717 and 0.699 in the training cohort and testing cohort, respectively (**Figure 4E**), which indicate that the prediction effect was good. We also plotted the distribution of risk scores in patients with ccRCC and the correlation between survival time and risk scores in the training cohort and testing cohort (**Figure 4F**). In addition, all of the three genes (*ALDOB*, *ESRRG*, and *EFHD1*) were significantly downregulated and associated with poor pathologic stages in the training cohort, testing cohort, or GSE126964 dataset (**Figure 4F** and **Figure S4**). Moreover, *ALDOB*, *ESRRG*, and *EFHD1* were highly expressed in renal tissues among the different normal tissues, which indicated a critical regulatory function of these genes in the normal kidney (**Figure S5**).

Validation of Protein Expressions of Prognostic Genes

Immunohistochemistry staining results obtained from the HPA database revealed the protein expression levels of the key survival-related genes (**Figure 5**). The results showed the downregulation of ALDOB, EFHD1, and ESRRG protein in ccRCC samples compared with normal controls.

TABLE 1 | Univariate Cox regression analysis in the train cohort.

Characteristics	HR	95% CI	*p*-value
GGT6 (High *vs.* Low)[#]	0.702	0.535-0.922	0.011*
KNG1 (High *vs.* Low)	0.995	0.856-1.157	0.952
DIO1 (High *vs.* Low)	0.938	0.744-1.181	0.584
SLC22A8 (High *vs.* Low)	0.706	0.531-0.937	0.016*
FAM3B (High *vs.* Low)	0.738	0.519-1.049	0.090
SERPINA5 (High *vs.* Low)	1.047	0.932-1.175	0.440
FABP1 (High *vs.* Low)	0.920	0.776-1.091	0.340
PTH1R (High *vs.* Low)	0.795	0.693-0.911	0.001*
ARMH4 (High *vs.* Low)	0.783	0.570-1.075	0.131
ALDOB (High *vs.* Low)	0.873	0.809-0.942	<0.001***
ESRRG (High *vs.* Low)	0.685	0.557-0.843	<0.001***
SLC34A1 (High *vs.* Low)	0.825	0.700-0.973	0.022*
EFHD1 (High *vs.* Low)	0.700	0.594-0.825	<0.001***

*HR, hazard ratio; CI, confidence interval; [#]Samples were classified into high and low gene expression according to a cut-off of 50%; *p < 0.05; ***p < 0.001.*

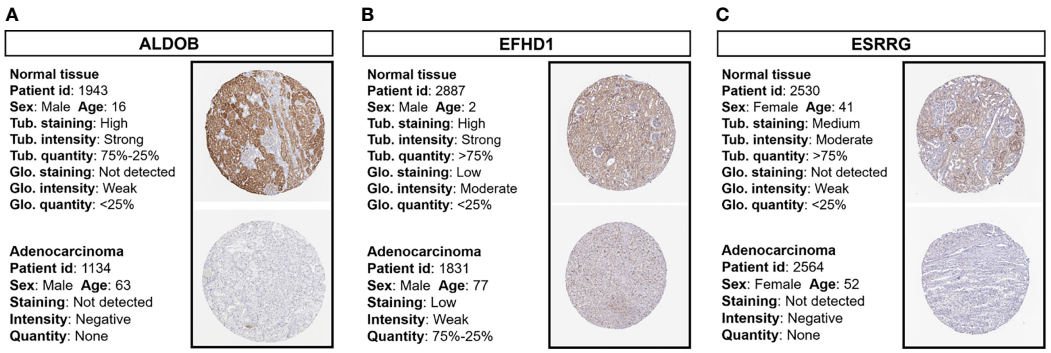

FIGURE 5 | Immunohistochemistry staining of prognostic proteins based on the HPA. Protein expression levels of **(A)** ALDOB, **(B)** EFHD1, and **(C)** ESRRG in tumor tissues and normal tissues. HPA, Human Protein Atlas; Tub., tubules; Glo., glomeruli.

Gene Set Enrichment Analysis of Prognostic Genes

GSEA was conducted to search the KEGG pathways in which the prognostic genes and risk scores were enriched in the samples with high expression or high-risk levels from TCGA-KIRC. "Oxidative phosphorylation" and "Fatty acid metabolism" pathways were enriched with low-risk score and high expression of *ALDOB*, *ESRRG*, and *EFHD1*, while immune-related pathways, including "Cytokine–cytokine receptor interaction," "Chemokine signaling pathway," and "Primary immunodeficiency" were significantly enriched with high-risk score and low expression of the prognostic genes (**Figures 6A–D**).

Single-Cell Transcriptomic Context of the Prognostic Genes

To further verify the relationship among *ALDOB*, *ESRRG*, and *EFHD1* in ccRCC, single-cell RNA-seq data from GSE131685 and GSE171306 were employed (25, 26). After quality control, a total of 34,371 cells from two ccRCC samples and three normal kidney samples were profiled (**Figure 7A**). We identified 27 different cell clusters and five cell groups, including immune cells, epithelial cells, endothelial cells, mesenchymal cells, and tumor cells (**Figures 7B, C**). Consistent with previous research (28), proximal tubular epithelial cells account for over 90% of a normal renal cortical sample, while in ccRCC, over 50% was accounted for immune cells and approximate 20% for tumor cells (**Figure 7D**). Except the clusters of macrophage 1 (MC1) and T cell 2 (T2), most kinds of immune cells were identified from ccRCC patients, which depicted a tumor immune microenvironment of ccRCC (**Figure 7E**). We also identified four tumor cell clusters. Analysis of KEGG pathway in tumor cells suggested the increased glycolysis gluconeogenesis, cancer, and focal adhesion-associated metabolism in ccRCC, while oxidative phosphorylation-associated pathways were negatively enriched with tumor cells (**Figures S6**, **S7**).

We then explored the expression profile of *ALDOB*, *ESRRG*, and *EFHD1* in different types of cells. Similar with results from TCGA-KIRC and GSE126964, the expression of *ALDOB*, *ESRRG*, and *EFHD1* were much lower in tumor cells than that in other intrinsic renal cells (**Figures 7F–I**).

DISCUSSION

ccRCC is a common genitourinary cancer with a high mortality rate (3). There is an urgent requirement to identify additional potential targets for drugs and biomarkers for early diagnosis of ccRCC. In the present study, a novel prognostic model based on three genes (*ALDOB*, *EFHD1*, and *ESRRG*) for ccRCC was established. *ALDOB*, *EFHD1*, and *ESRRG* were also identified as novel independent prognostic markers for ccRCC in different datasets *via* integrated bioinformatics analysis, including DEG analysis, WGCNA, and single-cell analysis.

Metabolic Shift in Clear Cell Renal Cell Carcinoma

Metabolic disorder is a hallmark in different types of cancer, since sufficient energy and metabolite production are required for the malignant proliferation of cancer cells (34). Gebhard et al. (35) reported that ccRCC tissues were overloaded with glycogen and lipid compared with normal tissues, which suggested that the metabolism of lipids and glucose may be altered in ccRCC (36). In particular, a mutation in *VHL* is considered to be closely associated with metabolic reprogramming in ccRCC (37). Subsequent accumulation of HIF1 α leads to the expression of glucose transporter-1, thereby promoting cellular glucose uptake. In addition, it can induce lactate dehydrogenase, which promotes the conversion of pyruvate to lactate and switches energy production from the TCA to lactate fermentation (38). This phenomenon is widely known as the Warburg effect. Despite the well-known VHL–HIF axis, there are a number of altered levels of the biochemical enzymes, substrates, and metabolic intermediates or products that are involved in the metabolic reprogramming waiting to be discovered. Our analysis of the GSE126964 data and single-cell RNA-seq data from GSE131685 and GSE171306 supported the observations of the metabolic shift in ccRCC and demonstrated the upregulation of

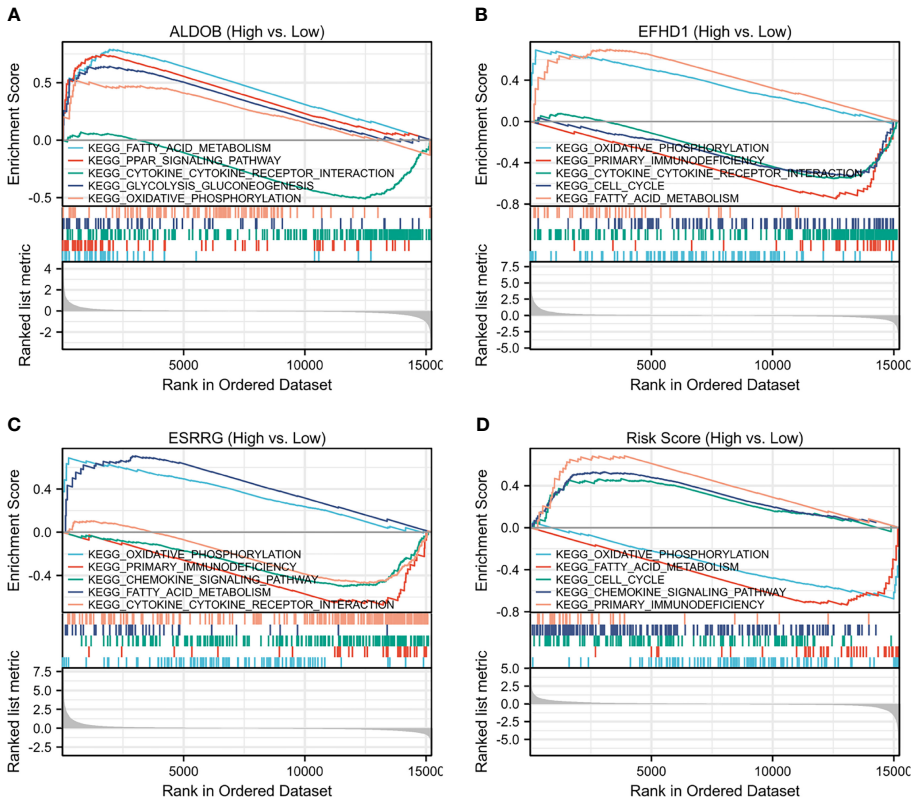

FIGURE 6 | Single-gene GSEA of **(A)** ALDOB, **(B)** EFHD1, **(C)** ESRRG and **(D)** risk score based on TCGA-KIRC. GSEA, gene set enrichment analysis; KEGG, Kyoto Encyclopedia of Genes and Genomes; TCGA-KIRC, The Cancer Genome Atlas Kidney Renal Clear Cell Carcinoma.

glycolysis-associated genes and downregulation of OXPHOS and TCA-associated genes at the transcriptome level (**Figure 6** and **Figures S2**, **S6**, **S7**). Although a metabolic shift is advantageous for tumor progression, altered metabolic pathways in ccRCC may also be exploited as therapeutic targets and may be an important future research direction.

ALDOB, *EFHD1*, and *ESRRG* Can Be Novel Independent Prognostic Markers for Clear Cell Renal Cell Carcinoma

ALDOB encodes aldolase B, an enzyme that is expressed in the liver and kidneys and is involved in glycolysis process and fructolysis process. The function of which can cleave fructose-1,6-bisphosphate to yield glyceraldehyde and dihydroxyacetone phosphate (39). A research found that declined *ALDOB* expression was associated with multiple malignant characteristics of HCC and indicate a poor prognosis (40). Moreover, Bu et al. (41) shows that *ALDOB* upregulation is commonly found in the metastatic cell in liver during primary colon cancer proliferation by enhancing fructose metabolism and central carbon metabolism. A study by Wang et al. (42) found that the low expression of *ALDOB* is also important in ccRCC and predicts poor prognosis, which is consistent with our research results. It leads to a high level of fructose 1,6-bisphosphate (FBP) and protects ccRCC from oxidative stress (42). However, the mechanism and prognostic value of accumulated FBP remain unknown.

EFHD1 encodes a mitochondrial inner membrane protein, acted as a calcium sensor for mitochondrial flash activation (43), and induced metabolic changes during the development of pro-/pre-B cells (44). A recent report suggested that EFHD1 may interact with β-actin for its involvement in the Ca^{2+}-dependent regulation of mitochondrial morphology (45). *EFHD1* was significantly downregulated in both the GSE126964 and TCGA-KIRC cohorts (**Figure 4**) and may also have an impact on mitochondrial energy metabolism in ccRCC. However, the detailed mechanism of how EFHD1 regulates ccRCC pathogenesis is currently unknown.

ESRRG encodes a member of nuclear receptor superfamily of transcription factors and has been shown to be a tumor suppressor in different types of cancer (46–48). A study by Huang et al. (49) also identified *ESRRG* as a co-expressed DEG in different datasets of hypertension-related RCC. Moreover, an experimental study on the mechanism of *ESRRG* conducted by Nam et al. (50) demonstrated that ESRRG suppressed the migratory and invasive abilities of behaviors in RCC cells. Our analysis and previous studies have all suggested that lower *ESRRG* expression may be a reliable predictor of a poor clinical outcome.

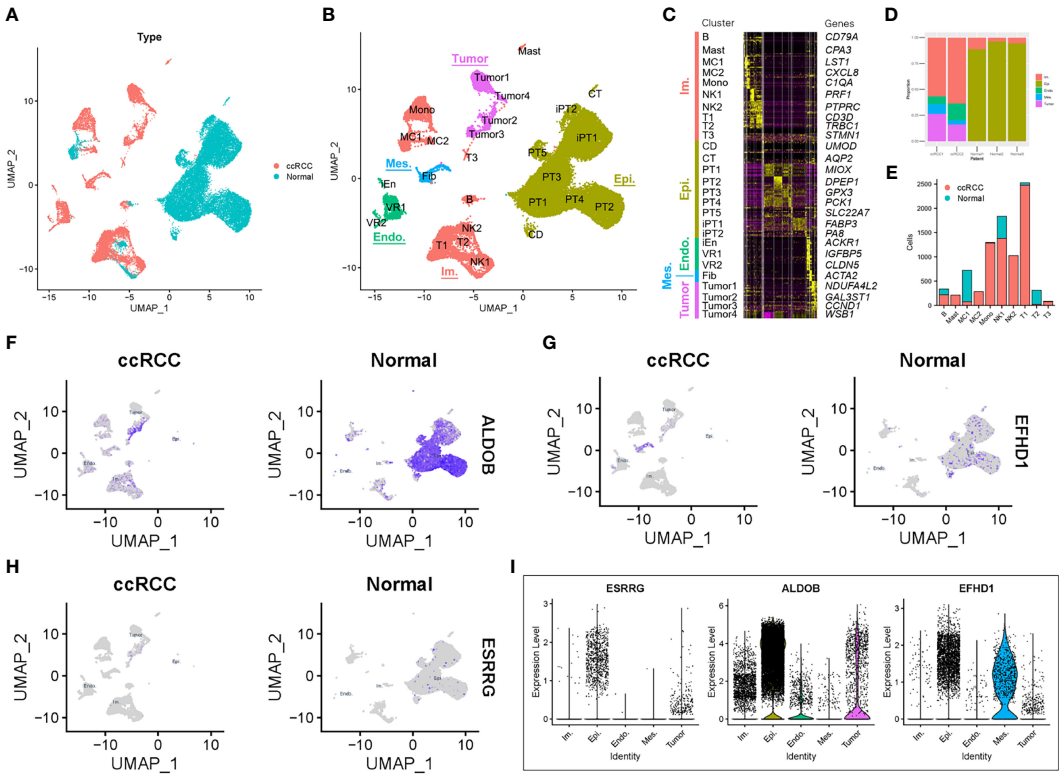

FIGURE 7 | Prognostic expression profile based on single-cell sequencing analysis. **(A)** Composition and distribution of single cells from GSE131685 and GSE171306. **(B)** UMAP embedding of 34,371 single cells from three human normal kidneys and two ccRCC samples. Labels refer to 27 clusters identified. **(C)** Scaled gene expression of the top 10 specific genes in each cluster. Each column is the average expression of all cells in a cluster. **(D)** Composition of different cell types in the five single-cell RNA-seq samples. **(E)** Number of cells per immune cell type and clinical parameter. The expression profile of **(F)** *ALDOB*, **(G)** *EFHD1*, and **(H)** *ESRRG* for each cell and the **(I)** violin plot. UMAP, Uniform Manifold Approximation and Projection; ccRCC, clear cell renal cell carcinoma; Im., immune; Epi., epithelial; Endo., endothelial; Mes, mesenchymal; CD, collecting duct; CT, connecting tubule; iEn, injured endothelial cells; Fib, fibroblast; Mast, mast cell; MC, macrophage; Mono, monocyte; PT, proximal tubule; iPT, injured proximal tubule; VR, vasa recta.

Hub Genes Including *ARMH4*, PTH1R, *SLC22A8*, and *SLC34A1* Were Correlated With Cancer

ARMH4, also named *C14ORF37*, encodes a protein that contains an armadillo-like helical domain. It has been shown that ARMH4 can interact with and inhibit the function of mTOR complex 2 kinase activity and function as a tumor suppressor in hematological malignancies, which is driven by interleukin 6 (IL-6)–signal transducer and activator of transcription 3 (STAT3) signaling pathways (51, 52). Wang et al. (53) also predicted that ARMH4 may act as a modulator for QKI, KH domain containing RNA binding, one of the key RNA-binding proteins shown in TCGA-KIRC dataset, and may change its splicing regulation in kidney cancer (53). Our analysis further confirmed the importance of *ARMH4* in ccRCC. However, the specific mechanism remains to be explored.

PTH1R encodes a G protein-coupled receptor of parathyroid hormone (PTH) and PTH-related protein and plays a central role in calcium homeostasis (54). Recently, the structure and dynamics of the active PTH1R have been shown by cryo-electron microscopy (55). Studies from different research groups have reported that the decreased expression of PTH1R was a poor prognosis factor in multiple types of cancer (56–59). Although PTH1R was found to be highly expressed in normal kidney samples (**Figure 5** and **Figure S4**), the detailed mechanism of PTH1R in renal function and ccRCC has yet to be fully elucidated and requires further study.

SLCs are a superfamily of membrane proteins responsible for the cellular uptake of a diverse range of substances. Among the SLCs, SLC22A8 and SLC34A1 both show kidney-specific expression. SLC22A8 is involved in the sodium-independent transport and excretion of organic anions, while SLC34A1 is a sodium-phosphate co-transporter that controls proximal tubule phosphate reabsorption (60, 61). Although defects in SLCs can lead to serious diseases (62–64), there is lack of research in cancer, especially ccRCC. Kang et al. (65) examined the expression patterns and prognostic values of SLCs in the development of ccRCC using different bioinformatics methods. These authors demonstrated that the low expression levels of a cluster of SLCs, including SLC34A1, were correlated with ccRCC

progression and poor prognosis (65). Since ccRCC shows a prominent metabolic shift effect, the production and accumulation of metabolites are also different from those in normal tissues. Therefore, SLCs may be critical in ccRCC.

CONCLUSION

Through a series of comprehensive bioinformatics analyses, including DEG screening, WGCNA, and single-cell analysis, a prognostic model based on *ALDOB*, *EFHD1*, and *ESRRG* was established, and these three genes were also identified as independent prognostic markers for ccRCC. The aforementioned prognostic genes have the potential to become therapeutic targets and biomarkers for ccRCC. However, these key survival-related genes should be tested in a large cohort of ccRCC cases and should be analyzed and validated in additional *in vivo* and *in vitro* experiments.

DATA AVAILABILITY STATEMENT

The original contributions presented in the study are included in the article/**Supplementary Material**. Further inquiries can be directed to the corresponding authors.

ETHICS STATEMENT

The review board of the Xiangya Hospital of Central South University approved the present study.

AUTHOR CONTRIBUTIONS

ZP, RX, and LT conceived and directed the project. HH and LZ collected the data and information. HH, CH, YD, and LF analyzed and interpreted the data. HH wrote the manuscript with the help of all the other authors. All authors contributed to the article and approved the submitted version.

FUNDING

This study was supported by the project funded by China Postdoctoral Science Foundation (2020TQ0363 and 2020M682598), the National Natural Science Foundation of China (82073918, 82090020, and 82090024), the Natural Science Foundation of Hunan, China (2021JJ40992), and the Fundamental Research Funds for the Central Universities of Central South University (2021zzts0078).

ACKNOWLEDGMENTS

We would like to acknowledge the reviewers for their helpful comments on this paper.

SUPPLEMENTARY MATERIAL

The Supplementary Material for this article can be found online at: https://www.frontiersin.org/articles/10.3389/fonc.2021.726655/full#supplementary-material

Supplementary Figure 1 | PCA based on the whole gene list. PCA, principal component analysis.

Supplementary Figure 2 | Schematic of metabolic pathways and their selected genes for glycolysis, TCA and electron transport chain, with the log_2FC level between ccRCC and control samples in the GSE126964 dataset. *$p<0.05$; **$p<0.01$; ***$p<0.001$. FC, fold change; ccRCC, clear cell renal cell carcinoma; TCA, tricarboxylic acid cycle.

Supplementary Figure 3 | (A) Sample clustering was conducted to detect outliers. All samples are located in the clusters and pass the cutoff thresholds after removing outliers. **(B)** Heatmap depicting the TOM of genes selected for weighted co-expression network analysis. The light color represents lower overlap, and red represents higher overlap. TOM, Topological Overlap Matrix.

Supplementary Figure 4 | The overall survival stratified by the high and low-risk score groups was plotted for the GSE126964 dataset. Detailed risk scores, survival information and heat maps of gene expression are also included.

Supplementary Figure 5 | Prognostic genes expression profiles in different normal tissues.

Supplementary Figure 6 | Single-gene GSEA of four tumor clusters for KEGG pathway enrichment. GSEA, gene set enrichment analysis; KEGG, Kyoto Encyclopedia of Genes and Genomes; FC, fold change.

Supplementary Figure 7 | The expression profile of **(A)** OXPHOS-associated and **(B)** glycolysis-associated genes for each cell. OXPHOS, oxidative phosphorylation.

Supplementary Figure 8 | The expression profile of other key genes for each cell.

REFERENCES

1. Jonasch E, Gao J, Rathmell WK. Renal Cell Carcinoma. *BMJ* (2014) 349: g4797. doi: 10.1136/bmj.g4797
2. Sung H, Ferlay J, Siegel RL, Laversanne M, Soerjomataram I, Jemal A, et al. Global Cancer Statistics 2020: GLOBOCAN Estimates of Incidence and Mortality Worldwide for 36 Cancers in 185 Countries. *CA Cancer J Clin* (2021) 71:209–49. doi: 10.3322/caac.21660
3. Hsieh JJ, Purdue MP, Signoretti S, Swanton C, Albiges L, Schmidinger M, et al. Renal Cell Carcinoma. *Nat Rev Dis Primers* (2017) 3:17009. doi: 10.1038/nrdp.2017.9
4. Angulo JC, Manini C, Lopez JI, Pueyo A, Colas B, Ropero S. The Role of Epigenetics in the Progression of Clear Cell Renal Cell Carcinoma and the Basis for Future Epigenetic Treatments. *Cancers (Basel)* (2021) 13:2071. doi: 10.3390/cancers13092071
5. Kotecha RR, Motzer RJ, Voss MH. Towards Individualized Therapy for Metastatic Renal Cell Carcinoma. *Nat Rev Clin Oncol* (2019) 16:621–33. doi: 10.1038/s41571-019-0209-1
6. The Cancer Genome Atlas Research Network. Comprehensive Molecular Characterization of Clear Cell Renal Cell Carcinoma. *Nature* (2013) 499:43–9. doi: 10.1038/nature12222

7. Latif F, Tory K, Gnarra J, Yao M, Duh FM, Orcutt ML, et al. Identification of the Von Hippel-Lindau Disease Tumor Suppressor Gene. *Science* (1993) 260:1317–20. doi: 10.1126/science.8493574
8. Yao X, Tan J, Lim KJ, Koh J, Ooi WF, Li Z, et al. VHL Deficiency Drives Enhancer Activation of Oncogenes in Clear Cell Renal Cell Carcinoma. *Cancer Discov* (2017) 7:1284–305. doi: 10.1158/2159-8290.CD-17-0375
9. Zhang J, Wu T, Simon J, Takada M, Saito R, Fan C, et al. VHL Substrate Transcription Factor ZHX2 as an Oncogenic Driver in Clear Cell Renal Cell Carcinoma. *Science* (2018) 361:290–5. doi: 10.1126/science.aap8411
10. Choueiri TK, Kaelin WJ. Targeting the HIF2-VEGF Axis in Renal Cell Carcinoma. *Nat Med* (2020) 26:1519–30. doi: 10.1038/s41591-020-1093-z
11. Zhang J, Zhang Q. VHL and Hypoxia Signaling: Beyond HIF in Cancer. *Biomedicines* (2018) 6:35. doi: 10.3390/biomedicines6010035
12. Majmundar AJ, Wong WJ, Simon MC. Hypoxia-Inducible Factors and the Response to Hypoxic Stress. *Mol Cell* (2010) 40:294–309. doi: 10.1016/j.molcel.2010.09.022
13. Krieg M, Haas R, Brauch H, Acker T, Flamme I, Plate KH. Up-Regulation of Hypoxia-Inducible Factors HIF-1alpha and HIF-2alpha Under Normoxic Conditions in Renal Carcinoma Cells by Von Hippel-Lindau Tumor Suppressor Gene Loss of Function. *Oncogene* (2000) 19:5435–43. doi: 10.1038/sj.onc.1203938
14. Ferraro E, Germano M, Mollace R, Mollace V, Malara N. HIF-1, the Warburg Effect, and Macrophage/Microglia Polarization Potential Role in COVID-19 Pathogenesis. *Oxid Med Cell Longev* (2021) 2021:8841911. doi: 10.1155/2021/8841911
15. Brugarolas J. PBRM1 and BAP1 as Novel Targets for Renal Cell Carcinoma. *Cancer J* (2013) 19:324–32. doi: 10.1097/PPO.0b013e3182a102d1
16. Hakimi AA, Ostrovnaya I, Reva B, Schultz N, Chen YB, Gonen M, et al. Adverse Outcomes in Clear Cell Renal Cell Carcinoma With Mutations of 3p21 Epigenetic Regulators BAP1 and SETD2: A Report by MSKCC and the KIRC TCGA Research Network. *Clin Cancer Res* (2013) 19:3259–67. doi: 10.1158/1078-0432.CCR-12-3886
17. Krishna C, DiNatale RG, Kuo F, Srivastava RM, Vuong L, Chowell D, et al. Single-Cell Sequencing Links Multiregional Immune Landscapes and Tissue-Resident T Cells in ccRCC to Tumor Topology and Therapy Efficacy. *Cancer Cell* (2021) 39:662–77. doi: 10.1016/j.ccell.2021.03.007
18. Du W, Zhang L, Brett-Morris A, Aguila B, Kerner J, Hoppel CL, et al. HIF Drives Lipid Deposition and Cancer in ccRCC *via* Repression of Fatty Acid Metabolism. *Nat Commun* (2017) 8:1769. doi: 10.1038/s41467-017-01965-8
19. Clark DJ, Dhanasekaran SM, Petralia F, Pan J, Song X, Hu Y, et al. Integrated Proteogenomic Characterization of Clear Cell Renal Cell Carcinoma. *Cell* (2020) 180:207. doi: 10.1016/j.cell.2019.12.026
20. Langfelder P, Horvath S. WGCNA: An R Package for Weighted Correlation Network Analysis. *BMC Bioinf* (2008) 9:559. doi: 10.1186/1471-2105-9-559
21. Yu J, Mao W, Sun S, Hu Q, Wang C, Xu Z, et al. Identification of an M6a-Related lncRNA Signature for Predicting the Prognosis in Patients With Kidney Renal Clear Cell Carcinoma. *Front Oncol* (2021) 11:663263. doi: 10.3389/fonc.2021.663263
22. Zhou Z, Bai J, Zhong S, Zhang R, Kang K, Zhang X, et al. Downregulation of ATP6V1A Involved in Alzheimer's Disease *via* Synaptic Vesicle Cycle, Phagosome, and Oxidative Phosphorylation. *Oxid Med Cell Longev* (2021) 2021:5555634. doi: 10.1155/2021/5555634
23. Zhao Q, Xue J, Hong B, Qian W, Liu T, Fan B, et al. Transcriptomic Characterization and Innovative Molecular Classification of Clear Cell Renal Cell Carcinoma in the Chinese Population. *Cancer Cell Int* (2020) 20:461. doi: 10.1186/s12935-020-01552-w
24. Hao Y, Hao S, Andersen-Nissen E, Mauck WR, Zheng S, Butler A, et al. Integrated Analysis of Multimodal Single-Cell Data. *Cell* (2021) 184:3573–87. doi: 10.1016/j.cell.2021.04.048
25. Liao J, Yu Z, Chen Y, Bao M, Zou C, Zhang H, et al. Single-Cell RNA Sequencing of Human Kidney. *Sci Data* (2020) 7:4. doi: 10.1038/s41597-019-0351-8
26. Yu Z, Lu W, Su C, Lv Y, Ye Y, Guo B, et al. Single-Cell RNA-Seq Identification of the Cellular Molecular Characteristics of Sporadic Bilateral Clear Cell Renal Cell Carcinoma. *Front Oncol* (2021) 11:659251. doi: 10.3389/fonc.2021.659251
27. Wang Z, Su G, Dai Z, Meng M, Zhang H, Fan F, et al. Circadian Clock Genes Promote Glioma Progression by Affecting Tumour Immune Infiltration and Tumour Cell Proliferation. *Cell Prolif* (2021) 54:e12988. doi: 10.1111/cpr.12988
28. Kuppe C, Ibrahim MM, Kranz J, Zhang X, Ziegler S, Perales-Paton J, et al. Decoding Myofibroblast Origins in Human Kidney Fibrosis. *Nature* (2021) 589:281–6. doi: 10.1038/s41586-020-2941-1
29. Borcherding N, Vishwakarma A, Voigt AP, Bellizzi A, Kaplan J, Nepple K, et al. Mapping the Immune Environment in Clear Cell Renal Carcinoma by Single-Cell Genomics. *Commun Biol* (2021) 4:122. doi: 10.1038/s42003-020-01625-6
30. Ritchie ME, Phipson B, Wu D, Hu Y, Law CW, Shi W, et al. Limma Powers Differential Expression Analyses for RNA-Sequencing and Microarray Studies. *Nucleic Acids Res* (2015) 43:e47. doi: 10.1093/nar/gkv007
31. Tang Z, Li C, Kang B, Gao G, Li C, Zhang Z. GEPIA: A Web Server for Cancer and Normal Gene Expression Profiling and Interactive Analyses. *Nucleic Acids Res* (2017) 45:W98–102. doi: 10.1093/nar/gkx247
32. Yu G, Wang LG, Han Y, He QY. ClusterProfiler: An R Package for Comparing Biological Themes Among Gene Clusters. *Omics* (2012) 16:284–7. doi: 10.1089/omi.2011.0118
33. Otasek D, Morris JH, Boucas J, Pico AR, Demchak B. Cytoscape Automation: Empowering Workflow-Based Network Analysis. *Genome Biol* (2019) 20:185. doi: 10.1186/s13059-019-1758-4
34. Coller HA. Is Cancer a Metabolic Disease? *Am J Pathol* (2014) 184:4–17. doi: 10.1016/j.ajpath.2013.07.035
35. Gebhard RL, Clayman RV, Prigge WF, Figenshau R, Staley NA, Reesey C, et al. Abnormal Cholesterol Metabolism in Renal Clear Cell Carcinoma. *J Lipid Res* (1987) 28:1177–84. doi: 10.1016/S0022-2275(20)38606-5
36. Hakimi AA, Reznik E, Lee CH, Creighton CJ, Brannon AR, Luna A, et al. An Integrated Metabolic Atlas of Clear Cell Renal Cell Carcinoma. *Cancer Cell* (2016) 29:104–16. doi: 10.1016/j.ccell.2015.12.004
37. Nickerson ML, Jaeger E, Shi Y, Durocher JA, Mahurkar S, Zaridze D, et al. Improved Identification of Von Hippel-Lindau Gene Alterations in Clear Cell Renal Tumors. *Clin Cancer Res* (2008) 14:4726–34. doi: 10.1158/1078-0432.CCR-07-4921
38. Weidemann A, Johnson RS. Biology of HIF-1alpha. *Cell Death Differ* (2008) 15:621–7. doi: 10.1038/cdd.2008.12
39. Chang YC, Yang YC, Tien CP, Yang CJ, Hsiao M. Roles of Aldolase Family Genes in Human Cancers and Diseases. *Trends Endocrinol Metab* (2018) 29:549–59. doi: 10.1016/j.tem.2018.05.003
40. Tao QF, Yuan SX, Yang F, Yang S, Yang Y, Yuan JH, et al. Aldolase B Inhibits Metastasis Through Ten-Eleven Translocation 1 and Serves as a Prognostic Biomarker in Hepatocellular Carcinoma. *Mol Cancer* (2015) 14:170. doi: 10.1186/s12943-015-0437-7
41. Bu P, Chen KY, Xiang K, Johnson C, Crown SB, Rakhilin N, et al. Aldolase B-Mediated Fructose Metabolism Drives Metabolic Reprogramming of Colon Cancer Liver Metastasis. *Cell Metab* (2018) 27:1249–62. doi: 10.1016/j.cmet.2018.04.003
42. Wang J, Wu Q, Qiu J. Accumulation of Fructose 1,6-Bisphosphate Protects Clear Cell Renal Cell Carcinoma From Oxidative Stress. *Lab Invest* (2019) 99:898–908. doi: 10.1038/s41374-019-0203-3
43. Hou T, Jian C, Xu J, Huang AY, Xi J, Hu K, et al. Identification of EFHD1 as a Novel Ca(2+) Sensor for Mitoflash Activation. *Cell Calcium* (2016) 59:262–70. doi: 10.1016/j.ceca.2016.03.002
44. Stein M, Dutting S, Mougiakakos D, Bosl M, Fritsch K, Reimer D, et al. A Defined Metabolic State in Pre B Cells Governs B-Cell Development and is Counterbalanced by Swiprosin-2/Efhd1. *Cell Death Differ* (2017) 24:1239–52. doi: 10.1038/cdd.2017.52
45. Mun SA, Park J, Park KR, Lee Y, Kang JY, Park T, et al. Structural and Biochemical Characterization of EFhd1/Swiprosin-2, an Actin-Binding Protein in Mitochondria. *Front Cell Dev Biol* (2020) 8:628222. doi: 10.3389/fcell.2020.628222
46. Kang MH, Choi H, Oshima M, Cheong JH, Kim S, Lee JH, et al. Estrogen-Related Receptor Gamma Functions as a Tumor Suppressor in Gastric Cancer. *Nat Commun* (2018) 9:1920. doi: 10.1038/s41467-018-04244-2
47. Tiraby C, Hazen BC, Gantner ML, Kralli A. Estrogen-Related Receptor Gamma Promotes Mesenchymal-to-Epithelial Transition and Suppresses Breast Tumor Growth. *Cancer Res* (2011) 71:2518–28. doi: 10.1158/0008-5472.CAN-10-1315
48. Kang MH, Eyun SI, Park YY. Estrogen-Related Receptor-Gamma Influences Helicobacter Pylori Infection by Regulating TFF1 in Gastric Cancer. *Biochem Biophys Res Commun* (2021) 563:15–22. doi: 10.1016/j.bbrc.2021.05.076

49. Huang W, Wu K, Wu R, Chen Z, Zhai W, Zheng J. Bioinformatic Gene Analysis for Possible Biomarkers and Therapeutic Targets of Hypertension-Related Renal Cell Carcinoma. *Transl Androl Urol* (2020) 9:2675–87. doi: 10.21037/tau-20-817
50. Nam HY, Chandrashekar DS, Kundu A, Shelar S, Kho EY, Sonpavde G, et al. Integrative Epigenetic and Gene Expression Analysis of Renal Tumor Progression to Metastasis. *Mol Cancer Res* (2019) 17:84–96. doi: 10.1158/1541-7786.MCR-17-0636
51. Conway SJ, McConnell R, Simmons O, Snider PL. Armadillo-Like Helical Domain Containing-4 is Dynamically Expressed in Both the First and Second Heart Fields. *Gene Expr Patterns* (2019) 34:119077. doi: 10.1016/j.gep.2019.119077
52. Lee D, Wang YH, Kalaitzidis D, Ramachandran J, Eda H, Sykes DB, et al. Endogenous Transmembrane Protein UT2 Inhibits Pstat3 and Suppresses Hematological Malignancy. *J Clin Invest* (2016) 126:1300–10. doi: 10.1172/JCI84620
53. Wang Y, Chen SX, Rao X, Liu Y. Modulator-Dependent RBPs Changes Alternative Splicing Outcomes in Kidney Cancer. *Front Genet* (2020) 11:265. doi: 10.3389/fgene.2020.00265
54. Bastepe M, Turan S, He Q. Heterotrimeric G Proteins in the Control of Parathyroid Hormone Actions. *J Mol Endocrinol* (2017) 58:R203–24. doi: 10.1530/JME-16-0221
55. Zhao LH, Ma S, Sutkeviciute I, Shen DD, Zhou XE, de Waal PW, et al. Structure and Dynamics of the Active Human Parathyroid Hormone Receptor-1. *Science* (2019) 364:148–53. doi: 10.1126/science.aav7942
56. Wang HJ, Wang L, Song SS, He XL, Pan HY, Hu ZM, et al. Decreased Expression of PTH1R is a Poor Prognosis in Hepatocellular Carcinoma. *Cancer Biomark* (2018) 21:723–30. doi: 10.3233/CBM-170823
57. Li S, Chen P, Zheng K, Wang W, Pei Y, Qiu E, et al. Beta-Alanine Mediated Inhibition of PTHR1suppresses the Proliferation, Invasion and Tumorigenesis in Metastatic Human Osteosarcoma U2OS Cells. *Int J Biol Macromol* (2018) 111:1255–63. doi: 10.1016/j.ijbiomac.2018.01.106
58. Ho PW, Goradia A, Russell MR, Chalk AM, Milley KM, Baker EK, et al. Knockdown of PTHR1 in Osteosarcoma Cells Decreases Invasion and Growth and Increases Tumor Differentiation *In Vivo*. *Oncogene* (2015) 34:2922–33. doi: 10.1038/onc.2014.217
59. Garcia M, Rodriguez-Hernandez CJ, Mateo-Lozano S, Perez-Jaume S, Goncalves-Alves E, Lavarino C, et al. Parathyroid Hormone-Like Hormone Plays a Dual Role in Neuroblastoma Depending on PTH1R Expression. *Mol Oncol* (2019) 13:1959–75. doi: 10.1002/1878-0261.12542
60. Bush KT, Singh P, Nigam SK. Gut-Derived Uremic Toxin Handling *In Vivo* Requires OAT-Mediated Tubular Secretion in Chronic Kidney Disease. *JCI Insight* (2020) 5:e133817. doi: 10.1172/jci.insight.133817
61. Janiec A, Halat-Wolska P, Obrycki L, Ciara E, Wojcik M, Pludowski P, et al. Long-Term Outcome of the Survivors of Infantile Hypercalcaemia With CYP24A1 and SLC34A1 Mutations. *Nephrol Dial Transplant* (2020) 36:1484–92. doi: 10.1093/ndt/gfaa178
62. McNeill A, Iovino E, Mansard L, Vache C, Baux D, Bedoukian E, et al. SLC12A2 Variants Cause a Neurodevelopmental Disorder or Cochleovestibular Defect. *Brain* (2020) 143:2380–7. doi: 10.1093/brain/awaa176
63. Preising MN, Gorg B, Friedburg C, Qvartskhava N, Budde BS, Bonus M, et al. Biallelic Mutation of Human SLC6A6 Encoding the Taurine Transporter TAUT is Linked to Early Retinal Degeneration. *FASEB J* (2019) 33:11507–27. doi: 10.1096/fj.201900914RR
64. Hu C, Tao L, Cao X, Chen L. The Solute Carrier Transporters and the Brain: Physiological and Pharmacological Implications. *Asian J Pharm Sci* (2020) 15:131–44. doi: 10.1016/j.ajps.2019.09.002
65. Kang W, Zhang M, Wang Q, Gu D, Huang Z, Wang H, et al. The SLC Family Are Candidate Diagnostic and Prognostic Biomarkers in Clear Cell Renal Cell Carcinoma. *BioMed Res Int* (2020) 2020:1932948. doi: 10.1155/2020/1932948

Conflict of Interest: The authors declare that the research was conducted in the absence of any commercial or financial relationships that could be construed as a potential conflict of interest.

Publisher's Note: All claims expressed in this article are solely those of the authors and do not necessarily represent those of their affiliated organizations, or those of the publisher, the editors and the reviewers. Any product that may be evaluated in this article, or claim that may be made by its manufacturer, is not guaranteed or endorsed by the publisher.

Copyright © 2021 Huang, Zhu, Huang, Dong, Fan, Tao, Peng and Xiang. This is an open-access article distributed under the terms of the Creative Commons Attribution License (CC BY). The use, distribution or reproduction in other forums is permitted, provided the original author(s) and the copyright owner(s) are credited and that the original publication in this journal is cited, in accordance with accepted academic practice. No use, distribution or reproduction is permitted which does not comply with these terms.

frontiers in Oncology

ORIGINAL RESEARCH
published: 07 October 2021
doi: 10.3389/fonc.2021.740985

Development and Validation of Prognostic Model in Transitional Bladder Cancer Based on Inflammatory Response-Associated Genes

Zhiwen Xie[1†], Jinming Cai[1†], Wenlan Sun[2†], Shan Hua[1†], Xingjie Wang[1], Anguo Li[3] and Juntao Jiang[1*]*

[1] Department of Urology, Shanghai General Hospital, Shanghai Jiao Tong University School of Medicine, Shanghai, China,
[2] Department of Geriatrics, Shanghai General Hospital, Shanghai Jiao Tong University, School of Medicine, Shanghai, China,
[3] Department of Urology, The Fifth Peoples Hospital of Zunyi, Guizhou, China

OPEN ACCESS

Edited by:
Paula Alexandra Quintela Videira, New University of Lisbon, Portugal

Reviewed by:
Angelo Porreca, Veneto Institute of Oncology (IRCCS), Italy
Xavier Maldonado, Vall d'Hebron University Hospital, Spain

***Correspondence:**
Anguo Li
lianguo92099@126.com
Juntao Jiang
jjturologist@126.com

[†]These authors have contributed equally to this work

Specialty section:
This article was submitted to Genitourinary Oncology, a section of the journal Frontiers in Oncology

Received: 14 July 2021
Accepted: 16 September 2021
Published: 07 October 2021

Citation:
Xie Z, Cai J, Sun W, Hua S, Wang X, Li A and Jiang J (2021) Development and Validation of Prognostic Model in Transitional Bladder Cancer Based on Inflammatory Response-Associated Genes. Front. Oncol. 11:740985. doi: 10.3389/fonc.2021.740985

Background: Bladder cancer is a common malignant type in the world, and over 90% are transitional cell carcinoma. While the impact of inflammatory response on cancer progression has been reported, the role of inflammatory response-associated genes (IRAGs) in transitional bladder cancer still needs to be understood.

Methods: In this study, IRAGs were download from Molecular Signature Database (MSigDB). The transcriptional expression and matched clinicopathological data were separately obtained from public databases. The TCGA-BLCA cohort was used to identify the differentially expressed IRAGs, and prognostic IRAGs were filtrated by univariate survival analysis. The intersection between them was displayed by Venn diagram. Based on least absolute shrinkage and selection operator (LASSO) regression analysis method, the TCGA-BLCA cohort was used to construct a risk signature. Survival analysis was conducted to calculate the overall survival (OS) in TCGA and GSE13507 cohort between two groups. We then conducted univariate and multivariate survival analyses to identify independently significant indicators for prognosis. Relationships between the risk scores and age, grade, stage, immune cell infiltration, immune function, and drug sensitivity were demonstrated by correlation analysis. The expression level of prognostic genes *in vivo* and *in vitro* were determined by qRT-PCR assay.

Results: Comparing with normal tissues, there were 49 differentially expressed IRAGs in cancer tissues, and 12 of them were markedly related to the prognosis in TCGA cohort for transitional bladder cancer patients. Based on LASSO regression analysis, a risk model consists of 10 IRAGs was established. Comparing with high-risk groups, survival analysis showed that patients in low-risk groups were more likely to have a better survival time in TCGA and GSE13507 cohorts. Besides, the accuracy of the model in predicting prognosis is acceptable, which is demonstrated by receiver operating characteristic curve (ROC) analysis. Age, stage, and risk scores variables were identified as the

independently significant indicators for survival in transitional bladder cancer. Correlation analysis represented that the risk score was identified to be significantly related to the above variables except gender variable. Moreover, the expression level of prognostic genes *in vivo* and *in vitro* was markedly upregulated for transitional bladder cancer.

Conclusions: A novel model based on the 10 IRAGs that can be used to predict survival time for transitional bladder cancer. In addition, this study may provide treatment strategies according to the drug sensitivity in the future.

Keywords: transitional bladder carcinoma, inflammatory response, prognostic model, risk score, drug sensitive, qRT-PCR

INTRODUCTION

Bladder cancer is a common malignant type in the world, and over 90% are transitional cell carcinoma, namely, bladder urothelial carcinoma (BUC), which accounts for the majority of primary bladder cancer (1). In addition to the type of non-muscle invasive tumor, muscle-invasive tumor is the other type of bladder cancer, which is categorized by the extent of tumor infiltration (2). Although 80% of bladder cancer are first diagnosed as non-muscle invasive tumor, up to 80% of them progress into muscle-invasive tumor after initial treatment within 5 years (2). However, metastasis in patients with muscle-invasive bladder cancer is easier to happen and has poor prognosis (3). Thus, it is imperative for us to determine practical biomarkers to predict BUC in patients at an early stage.

The connection between inflammation and cancer has been well established (4). Inflammation could not only inhibit tumors but also promote cancers (5). Recently, numerous studies indicated that inflammatory response regulates the development and progression of cancer, which has attracted increasing attention from researchers (6).

Since inflammatory biomarkers in the blood are easy to detect, researchers can explore their role in cancers (7). The indicators of inflammatory response, such as thrombocytosis, leukemoid, hypercalcemia, plasma fibrinogen, and D-dimer, as prognostic biomarkers for bladder cancer have been demonstrated (8, 9). In addition, the value of inflammatory indexes including lymphocyte-to-monocyte ratio, platelet-to-lymphocyte ratio, and neutrophil-to-lymphocyte ratio were estimated in new bladder cancer cases. Moreover, studies showed that these markers were the independent predictors for OS in bladder cancer (10–12). In the Glasgow prognosis model, C-reactive protein and albumin were independent prognostic factors in tumors (13). To develop a comprehensive prognostic model, increasing studies suggested that it would be a good choice for researchers to combine various acute phase proteins and inflammatory indexes. Furthermore, some IRAGs playing an important role in the metastasis of bladder cancer have been reported (14). However, the correlation between IRAGs and the prognosis of transitional bladder cancer still needs to be elucidated.

We first retrieved transcriptional expression and matched clinicopathological data of patients with transitional bladder cancer from TCGA and GEO databases in this study. Based on differentially expressed IRAGs, we then established and validated the risk model by TCGA and GSE13507 cohorts. Next, the possible mechanisms, which they were involved in, were explored by single sample gene set enrichment analysis (ssGSEA). Besides, associations between cancer stemness, tumor chemoresistance, immune infiltrate types, and the risk score were analyzed. Finally, qRT-PCR assay was performed to determine the levels of prognostic genes *in vivo* and *in vitro*.

Abbreviations: IRAGs, inflammatory response-associated genes; MSigDB, Molecular Signature Database; TCGA, The Cancer Genome Atlas; BLCA, bladder urothelial carcinoma; LASSO, least absolute shrinkage and selection operator; OS, overall survival; qRT-PCR, quantitative reverse transcription polymerase chain reaction; ROC, receiver operating characteristic; BUC bladder urothelial carcinoma; GEO, Gene Expression Omnibus; ssGSEA, single sample Gene Set Enrichment Analysis; ANOVA, analysis of variance; RNAss, RNA stemness score; DNAss, DNA stemness score.

MATERIAL AND METHODS

Data Collection and Preparation

Transcriptional expression profile and matched clinicopathological data were obtained from The Cancer Genome Atlas (TCGA) database, which was made up of 409 transitional bladder cancers and 19 normal adjacent tissues, to establish the model. One hundred sixty-five transitional cell carcinoma samples were used to validate the model, which were download from GSE13507 cohort (http://www.ncbi.nlm.gov/geo/query/acc.cgi?acc=GSE13507). Apart from the above, 200 inflammatory response-associated genes were acquired from Molecular Signature Database (http://gsea-msigdb.org) (**Supplementary Table S1**).

Identification of Differentially Expressed and Prognostic Inflammatory-Response-Associated Genes in TCGA Cohort

Limma R package was used to identify differentially expressed IRAGs in TCGA cohort, which were defined as those with a false discovery rate <0.05 and a |fold change| > 2. After eliminating the patient data with no survival time, the IRAGs with prognosis in TCGA cohort was determined by univariate Cox analysis, and

Benjamini–Hochberg (BH) correction method was used to adjust the p-value.

Establishment and Validation of a Prognostic Model

To avoid overfitting and to construct a novel gene signature in the study, LASSO regression analysis was used, the algorithm of which was conducted with glmnet R package to select and shrink variables for excluding the variables with a regression coefficient equal to 0. Then, an interpretable model was established according to the non-zero regression coefficients in TCGA cohort, and the optimum λ was selected in 10-fold cross-validation. We calculated the risk scores for each patient by summarizing the product of the expression level of each IRAGs and its corresponding regression coefficient and split BUC patients into two groups on the basis of risk scores in TCGA and GSE13507 cohort. We then conducted survival analysis to determine their different OS by using the R Survminer package and time-dependent ROC analysis by using the survival and timeROC R package to assess prediction accuracy.

Prognostic Implication of the Risk Score in TCGA Cohort

For tumor stage, age, gender, and risk scores variables, multivariate Cox analyses, after the initial screening by univariate cox analysis, were conducted to assess the implication of prognosis. Moreover, the relationship between risk scores and other variables were determined by correlation analysis.

Immune Infiltration and Tumor Immune Microenvironment

We calculated the immune and stromal scores to evaluate the cell infiltration levels in transitional bladder cancer. The relationships between risk score and those cells were analyzed by Spearman correlation analysis. To assess the difference in immune infiltration subtype in the two groups, two-way ANOVA analysis was performed. In addition, the feature of tumor stemness cell were downloaded from TCGA tumor samples. To analyze the links between the feature of tumor stemness and risk score, Spearman correlation analysis was conducted.

ssGSEA of the Gene Signatures

To explore the related pathways of the gene signatures in the TCGA cohort, ssGSEA was conducted in high and low scores, and BH method was used to calculate the adjusted p-value with the GSVA R package.

Drug-Sensitive Analysis of the Gene Signatures

After logging into the CellMiner project page (https://discover.nci.nih.gov/cellminer), the transcriptional expression of NCI-60 human cancer cell lines was downloaded. The association between prognostic genes and drug sensitivity was determined by Pearson correlation analysis.

qRT-PCR

Total RNAs of transitional bladder cancer tissues, adjacent normal tissues, T24, 5637, and SVHUC-1 cells were extracted by TRIzol (Novabio, China). Moreover, we obtained total RNAs of T24 and 5637 cells after treatment by 1 μm Dasatinib (15). We purchased these cell lines from Shanghai Chinese Academy of Sciences cell bank (Shanghai, China). RNA (1 μg) and PrimeScript RT kit (Novabio, China) were used to synthesize complementary DNA (cDNA). According to the manufacturer's protocol, the amplification of cDNA was conducted by using SYBR Green reagent and ddH_2O and analyzed by an ABI 7500 Real-Time PCR system (Applied Biosystems). All experiments were performed for three independent measures. Their primer sequences are shown in **Supplementary Table S3**.

Statistical Analysis

We used R version 4.0.4 to conduct statistical analyses, and statistical significance was assumed at two-sided p-value below 0.05.

RESULTS

Identification of Differentially Expressed Prognostic IRAGs in the TCGA Cohort

Figure 1 shows the flow chart of this study. There are 404 BLCA patients with survival statistics in the TCGA cohort. In addition, 200 IRAGs were downloaded from the Molecular Signature database. There were 49 IRAGs differentially expressed in tumor and normal tissues (**Supplementary Table S2**). Univariate regression analysis demonstrated that 31 IRAGs are correlated with OS (**Supplementary Figure S1**). Then, Venn diagram was used to screen the prognosis-related differentially expressed IRAGs (**Figure 2A**). Heatmap revealed their expression status in tumor and adjacent tissues (**Figure 2B**). **Figure 2C** represents the interactions of these signatures.

Development of a Prognostic Model

As shown in **Figure 2C**, there are 12 candidate genes that were associated with prognosis.

Then, a novel model consisting of 10 prognostic genes was developed through LASSO–Cox regression analysis (**Figures 3A, B**). The formula, risk score = (−0.166 * CXCL11) + 0.006 * INHBA + 0.166 * LDLR + 0.069 * MMP14 + 0.115 * MYC + (−0.09 * PTGER4) + (−0.150 * RIPK2) + 0.055 * SGMS2 + 0.029 * SPHK1 + 0.092 * TNFAIP6, was used to compute the risk score of each patient (**Figure 3C**). We then divided patients in the TCGA cohort into two groups by using the median risk scores (**Figure 3C**). Besides, scatter chart presented that patient in high-risk groups may have a worse outcome (**Figure 3D**).

Prognostic Implication of the Risk Score

Figures 4A, B demonstrate that patients with higher risk scores were more likely to suffer a markedly shorter OS than that of their counterpart in TCGA and GSE13507 cohorts, respectively. To investigate the predictive ability of the risk score for BUC

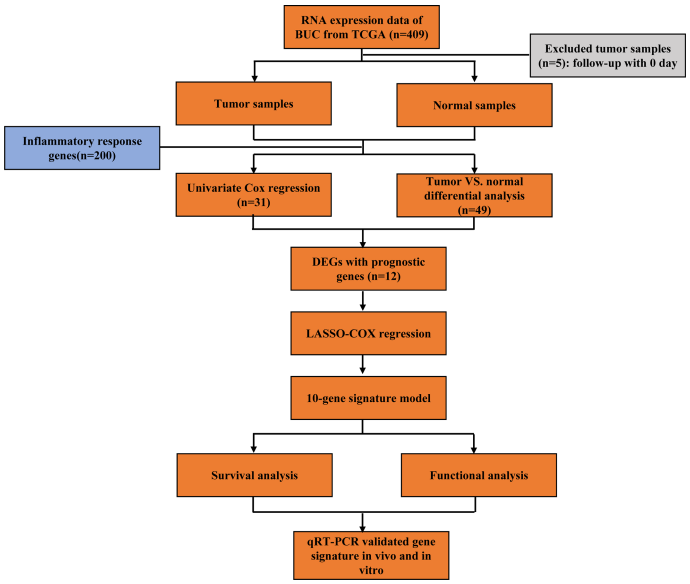

FIGURE 1 | Flow chart of data collection, analysis, and experiment.

patients, time-dependent ROC analysis was used, and the area under ROC (AUC) at 1, 2, and 3 years was 0.711, 0.670, and 0.655, respectively, in TCGA cohort (**Figure 4C**). In addition, the AUC at 1, 2, and 3 years was 0.669, 0.573, and 0.563, respectively, in GSE13507 cohort (**Supplementary Figure S2**). Moreover, our findings demonstrated that the risk score would be a significant variable for predicting prognosis by the univariate Cox regression analyses (HR = 3.369; CI = 2.354–4.822; $p < 0.001$) (**Figure 4D**). After eliminating the factors with $p > 0.05$, accompanying with stage and age, multivariate survival analyses showed that the risk score was negatively related to OS (HR = 2.696; CI = 1.851–3.925; $p < 0.001$) (**Figure 4E**).

Clinical Implication of the Risk Score

To elucidate the clinical implication of the risk score, clinical variables such as age, gender, grade, and stage variables were enrolled into the correlation analysis. Boxplot showed that patient with age >65, high grade, and stage III–IV are more likely have a high-risk score (**Figures 5A–C**). However, the relationship between gender variable and the risk score was not significant (**Figure 5D**).

Immune Status and Tumor Microenvironment

Enrichment scores were calculated in different immune cell subpopulations of these two groups by ssGSEA. Compared with the low-risk group, we found that there are significant enrichment of mast cells, natural killer (NK) cells, and macrophages in the high-risk group (**Figure 6A**). Furthermore, the scores of immune functions between them were not significant except CCR (**Figure 6B**, $p < 0.05$).

Six types of immune infiltration types were added to determine the association with risk score, namely, wound healing (C1), interferon gamma (IFN-γ) dominant (C2), inflammatory (C3), lymphocyte depleted (C4), immunologically quiet (C5), and transforming growth factor beta (TGF-b) dominant (C6), were studied in our work, which may function as tumor promoting or repressing. There is no BLCA patient belonging to C5 and C6, which were not studied in our work. As shown in **Figure 6C**, infiltration of wound healing may happen in patients in the high-risk group, while the infiltrations of lymphocyte depleted, inflammatory, and IFN-γ dominant are more likely to appear in those with low-risk score ($p < 0.05$).

To measure the tumor stemness, RNA stemness score (RNAss) and DNA methylation pattern (DNAss) were calculated in this study. Correlation analysis represented that the risk score has negative correlation with RNAss (**Figure 6D**, $p < 0.001$), while there is no association with DNAss (**Figure 6E**, $p > 0.05$)

In addition, correlation analysis demonstrated that the risk score was positively associated with stromal score ($p < 0.01$), Nevertheless, no significant difference was observed in immune score ($p > 0.05$) (**Figures 6F, G**).

Signaling Pathways in High- and Low-Risk Groups

In TCGA cohorts, ssGSEA showed that signaling pathways, such as AXON GUIDANCE (normalized enrichment score NES = 2.20, $p < 0.01$), WNT_SIGNALING_PATHWAY [(NES) = 2.31, $p < 0.01$], ARRHYTHMOGENIC_RIGHT_VENTRICULAR_CARDIOMYOPATHY_ARVC (NES = 2.25, $p < 0.01$), FOCAL ADHESION (NES = 2.26, $p < 0.01$), and ECM_RECEPTOR_INTERACTION (NES = 2.22, $p < 0.01$), in the high-risk group were markedly enriched, while in the low-risk group, signaling pathways, such as FATTY_ACID_METABOLISM

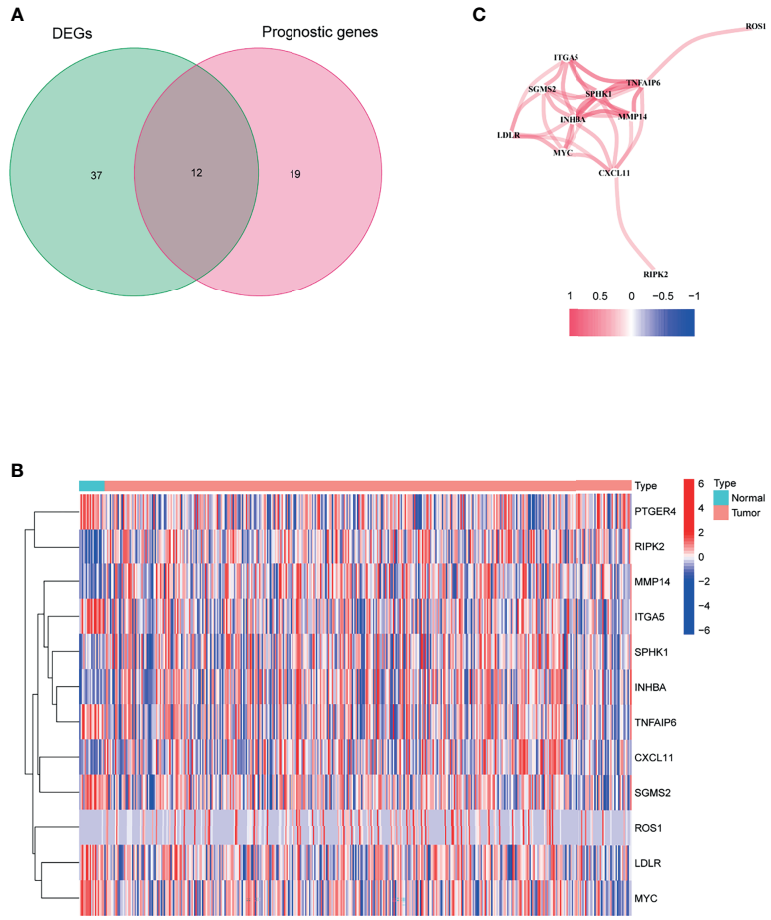

FIGURE 2 | Identification of the candidate inflammatory response-associated genes in the TCGA cohort. **(A)** Venn diagram to identify DEGs between BLCA tissues and adjacent normal tissues. **(B)** The 13 overlapping genes expression between BLCA tissues and adjacent normal tissues. **(C)** The correlation network of candidate genes.

(NES = −1.71, p = 0.023), ALPHA_LINOLENIC_ACID_METABOLISM (NES = −1.61, p = 0.022), and PEROXISOME (NES = −1.62, p = 0.026) were significantly enriched (**Figure 7**).

The Sensitivity of Prognostic Gene Expression to Chemotherapy

To study the relationship between these prognostic genes and drug sensitivity, we determined their level in NCI-60, a public database of human cancer cell lines. The results showed the top 16 correlation analysis according to the p-value. **Figure 8** demonstrates that MYC is sensitive to Palbociclib, Carmustine, Ifosfamide, Lomustine, Hydroxyurea, Oxaliplatin, Dromostanolone Propionate ($p < 0.001$), and INHBA is sensitive to Zoledronate and Dasatinib ($p < 0.001$), while it is insensitive to Tyrothricin and Tamoxifen ($p < 0.001$). Besides, the expression of LDLR is insensitive to Oxaliplatin ($p < 0.001$), and RIPK2 is insensitive to Decitabine. Moreover, SGMS2 is sensitive to Dasatinib, while it is insensitive to Pipamperone and Tamoxifen (all $p < 0.001$).

Verification of the Prognostic Gene Expression by qRT-PCR

To validate the different expressions of these prognostic genes, qRT-PCR was implemented to analyze the mRNA expression *in vivo* and *in vitro*. The results of qRT-PCR showed that the mRNA expression of INHBA and SPHK1 were significantly increased in cancer than in normal tissues and cells (**Figures 9A–D**). In addition, we observed that the mRNA expression of INHBA was significantly upregulated in T24 and 5637 cells when treated by Dasatinib (**Figures 9E, F**).

DISCUSSION

In the era of personalized precision medicine, high-throughput sequencing technology had been widely used for treating cancer including bladder cancer (16). Nevertheless, due to the lack of useful biomarkers, it is difficult for us to make early diagnosis and evaluate the efficacy of treatment on BUC patients (17). Recent

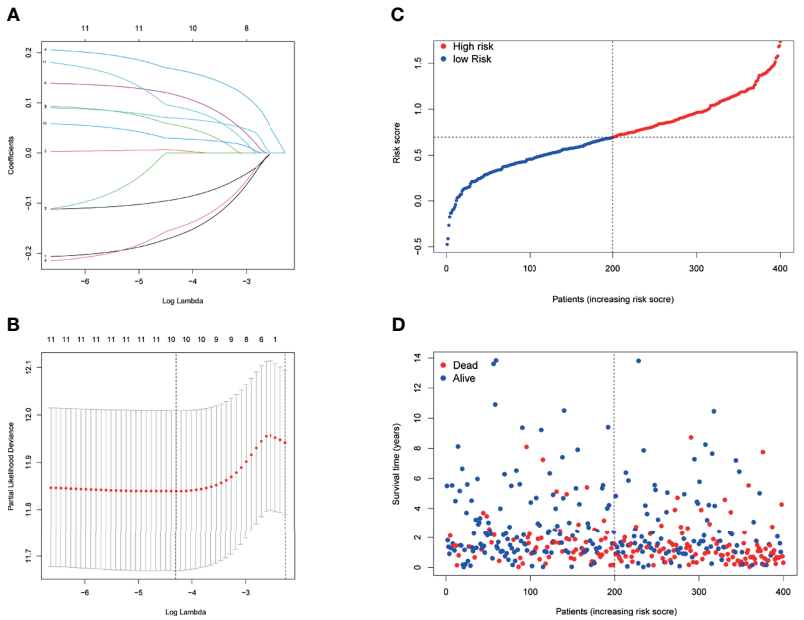

FIGURE 3 | Prognostic analysis of the 10-gene signature model in the TCGA cohort. **(A)** LASSO coefficient expression profiles of 13 candidate genes. **(B)** The penalty parameter (λ) in the LASSO model was selected through 10 cross-validation. **(C)** The median value and distribution of the risk scores. **(D)** The distribution of OS status.

studies suggested that some serum biomarkers, such as circulating tumor cells, vitamin D, and circulating tumor DNA, have good accuracy of BUC diagnosis and prognosis (18–20). Moreover, in addition to early diagnosis, inflammatory indexes can also contribute to predict prognosis of BUC (10, 21, 22). Nevertheless, the IRAGs has not yet been reported as a prognostic marker for BUC. Recent studies have demonstrated that ferroptosis, EMT, glycolysis, m6A, and hypoxia-associated gene signatures had been used for predicting OS of BUC, which were consistent with our study (23–26). In addition, comparing with risk gene signatures above, the IRAGs model constructed in our study had more advantages. For example, our study proved that the prognostic IRAGs were related to drug sensitivity and resistance.

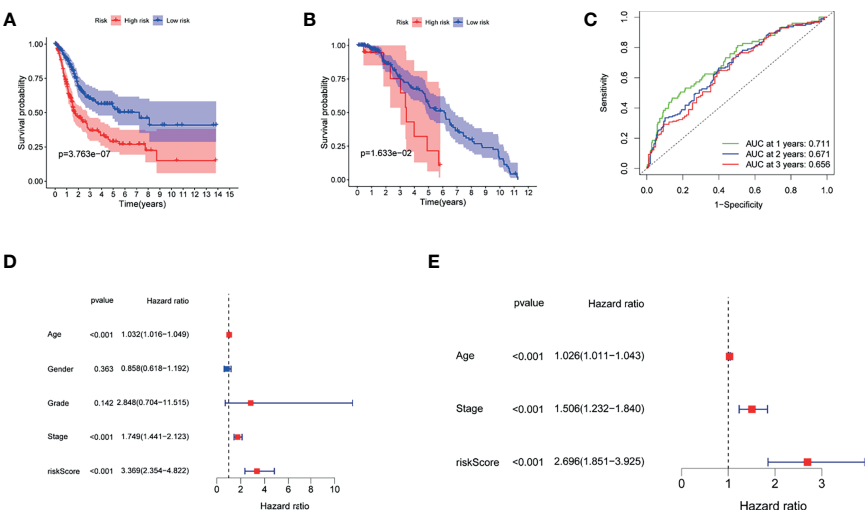

FIGURE 4 | The role of the risk score in overall survival. **(A)** Kaplan–Meier curves for OS of patients in the high- and low-risk groups of TCGA. **(B)** Kaplan–Meier curves for OS of patients in the high- and low-risk groups of GEO13507 cohort. **(C)** AUC time-dependent ROC curves for OS in TCGA. **(D)** OS-related factors were screened by univariate cox regression analyses in TCGA. **(E)** OS-related factors were screened by multivariate cox regression analyses in TCGA.

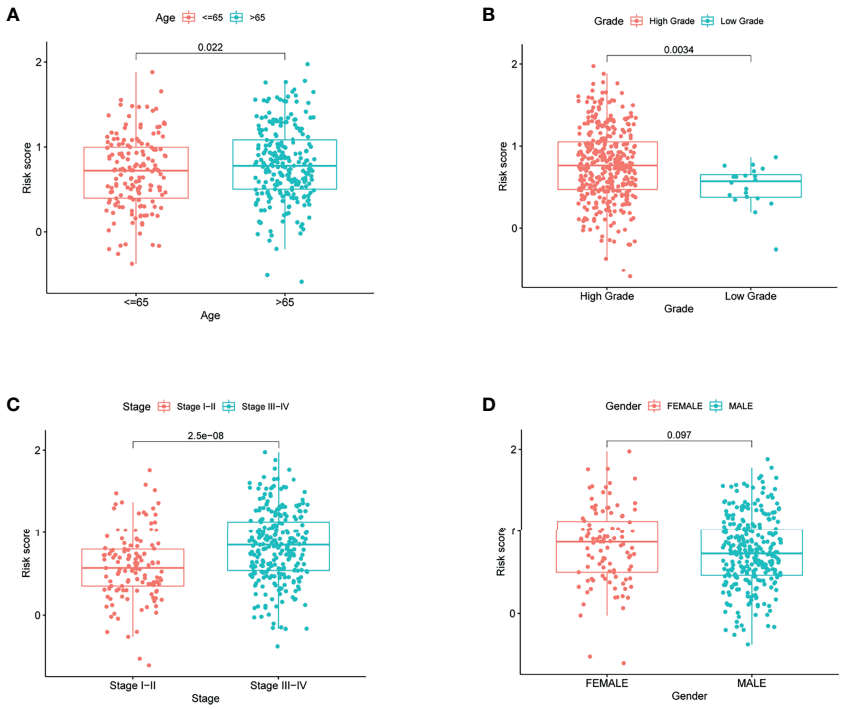

FIGURE 5 | The risk score in different groups divided by clinical characteristics in TCGA. **(A)** Age, **(B)** grade, **(C)** stage, and **(D)** gender.

Two hundred IRAGs were enrolled into the current study to determine the expression level of BUC patients and the association with prognosis. Forty-nine differentially expressed IRAGs were filtrated from the TCGA cohort. Twelve of these genes were related to the prognosis in BUC patients by univariate Cox regression analysis. We used TCGA cohort to develop a novel risk model based on 10 prognostic IRAGs and GSE 13507 cohort to validate the reliability. Based on the risk score, we split

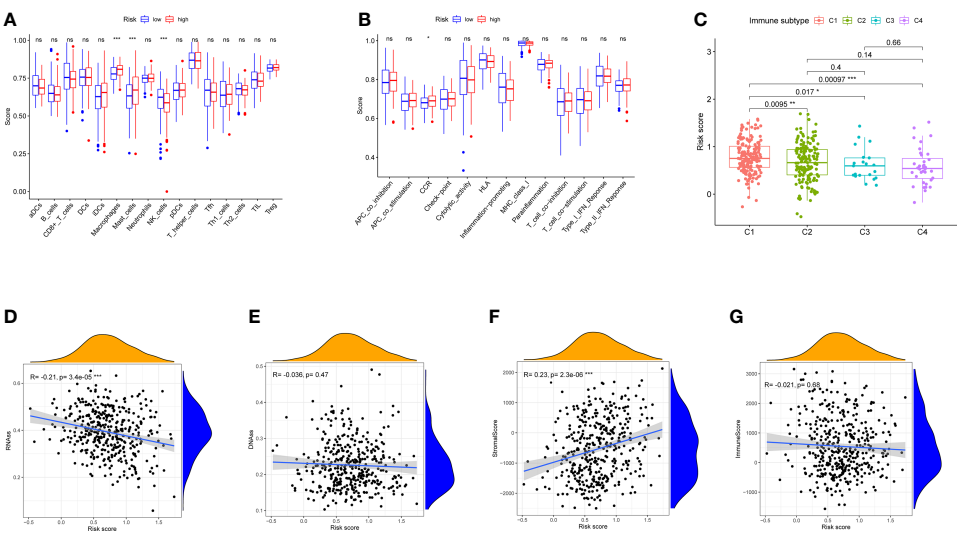

FIGURE 6 | Immune status between different risk groups and the association between risk score and tumor microenvironment in TCGA cohort. **(A)** The scores of 16 immune cells are shown in boxplots. **(B)** Thirteen immune-related functions are shown in boxplots. **(C)** Comparison of the risk score in different immune infiltration subtypes. **(D–G)** The relationship between risk score and RNAss, DNAss, stromal score, and immune score. p-values are shown as ns, not significant, *p < 0.05, **p < 0.01, and ***p < 0.001.

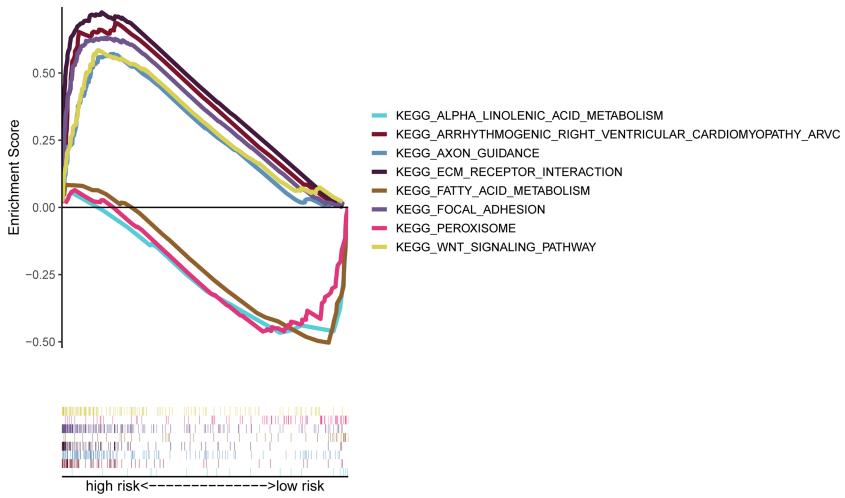

FIGURE 7 | Gene set enrichment analysis of biological functions and pathways.

BUC patients in TCGA or GSE 13507 cohort into two groups. Patients with low-risk score are more likely to have a lower tumor grade, tumor stage, and longer survival time. Univariate and multivariate survival analysis demonstrated that the risk score was an independent prognostic indicator for BUC patients.

Ten IRAGs were included in the model (CXCL11, INHBA, LDLR, MMP14, MYC, PTGER4, RIPK2, SGMS2, SPHK1, and TNFAIP6). C-X-C motif chemokine 11 (CXCL11) has been reported to contribute to the progression of tumors. In our study, we demonstrated that the expression of CXCL11 was negatively correlated with prognosis of BUC, which was consistent with the result of Vollmer Tino et al. In addition, they also found that the expression of CXCL11 was predictive of chemotherapy response in human bladder cancer (27). We also demonstrated the correlation between CXCL11 and chemotherapy drugs in this study, which was consistent with previous studies. Inhibin subunit beta A (INHBA) is highly expressed in various tumors. In our study, we also observed that the expression of INHBA was significantly increased in BUC than in normal tissues or cells. Moreover, our study showed that the high expression of INHBA was significantly associated with poor prognosis of BUC, which was also demonstrated by Sugawara Sho et al. (28). In terms of drug sensitivity, we observed that the expression of INHBA was positively correlated with Dasatinib.

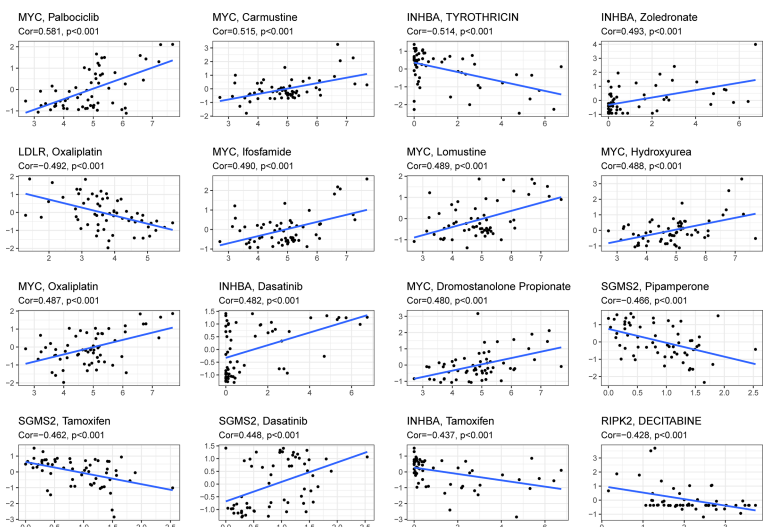

FIGURE 8 | Scatter plot of relationship between prognostic gene expression and drug sensitivity.

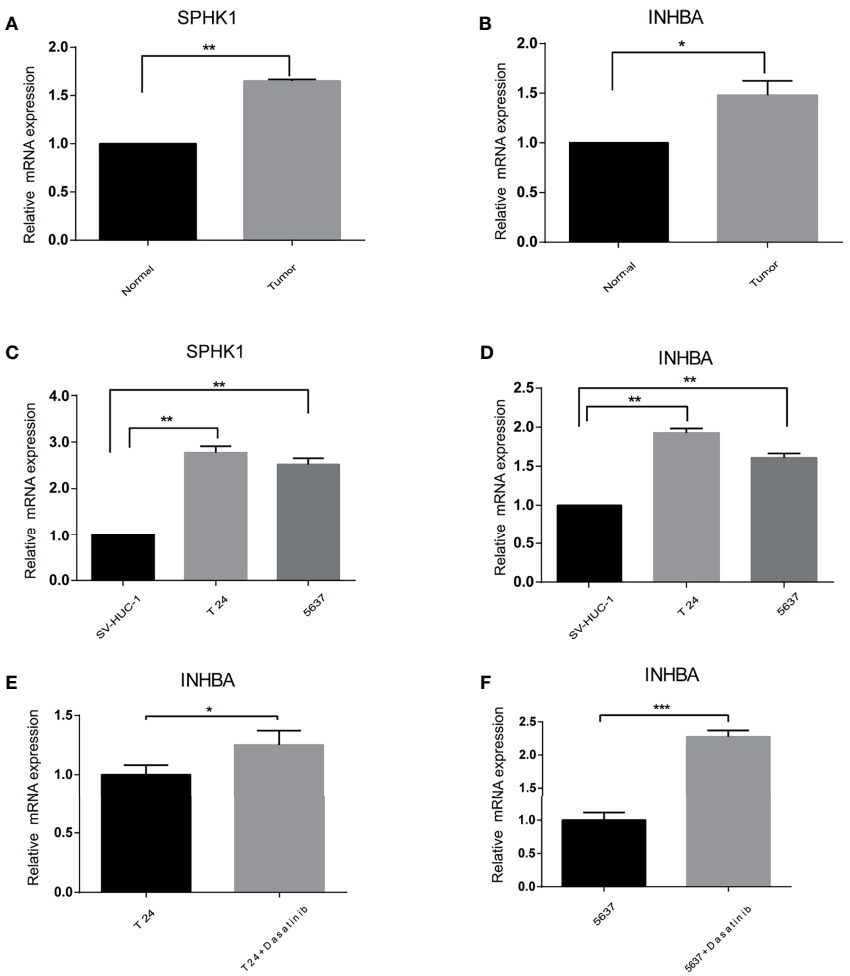

FIGURE 9 | The difference of the prognostic gene expression was confirmed by qRT-PCR. **(A, B)** *In vivo*. **(C, D)** *In vitro*. **(E, F)** Presence or absence with Dasatinib *in vitro*. *p < 0.05, **p < 0.01, ***p < 0.001.

Besides, we also observed the increased expression of INHBA after treatment with Dasatinib *in vitro*.

Low-density lipoprotein receptor (LDLR) is differentially expressed in bladder cancer. We observed that the expression of LDLR was negatively correlated with the sensitivity of Oxaliplatin. Moreover, Hamm et al. revealed cholesterol biosynthesis as an important resistance mechanism in T24 cells after archazolid B treatment (29). Our results demonstrated that the expression of MMP14 was associated with the prognosis in transitional bladder cancer. In addition, Wang et al. demonstrated the downregulation of MMP14-suppressed BC cell invasion and migration abilities *in vitro* (30). Moreover, our study demonstrated the expression of MMP14 was related to many chemotherapeutic drugs. A previous study has demonstrated that MMP was sensitive to the DNA demethylation molecule 5-aza-2′-deoxycytidine in T24 and 5637 cells (31). Therefore, MMP14 may be the therapeutic target for BUC patients in the future.

MYC is a proto-oncogene. Comparing with normal tissues, the expression of MYC in mRNA level was significantly increased, which may promote the development for BUC patients. Our results also demonstrated that the expression of MYC was related to the prognosis in BUC patients. In addition, we observed that the expression of MYC was positively associated with drug sensitivity. It has been reported that thymoquinone can inhibit the expression of MYC gene and then suppress invasion and metastasis in bladder cancer cells (32). Prostaglandin E receptor 4 (PTGER4) is one of the receptors of prostaglandin E2. Musser et al. demonstrated that the transitional cell carcinoma tissues displayed significantly less mRNA EP4R expression when compared to normal bladder mucosa, which was consistent with our result (33). Besides, we demonstrated that PTGER4 is a protector in BUC patients. However, previous studies have illustrated that the expression of PPTGER4 was associated with the development of malignancy and a poor prognosis in multiple human cancers (pathological function of prostaglandin E2 receptors in transitional cell carcinoma of the upper urinary tract). Therefore, the role of PTGER4 in bladder cancer needs further investigation.

Receptor-interacting serine/threonine-protein kinase 2 (RIPK2) was markedly increased in bladder cancer and a protector as demonstrated by univariate Cox analysis. However, RIPK2 polymorphism was also involved in the development of bladder cancer (34). Sphingomyelin synthase 2 (SGMS2) is a transferase that regulates the synthesis of sphingomyelin from ceramide. In our study, we observed the decreased expression of SGMS2 in BUC. Zheng et al. have demonstrated that the high expression of SGMS2 was associated with breast cancer metastasis (35). In addition, we observed that SGMS2 was a risk factor by univariate Cox analysis, and the expression of SGSM2 was negatively correlated with drug sensitivity to Tamoxifen. Sphingosine kinase 1 (SPHK1) can phosphorylate sphingosine to form sphingosine-1-phosphate, which plays critical roles in the regulation of cancer cell proliferation and survival in different types of cancer (36). Our study demonstrated that the increased expression of SPHK1 and SPHK1 was a prognostic biomarker in bladder cancer. miR163 and miRNA 125b can inhibit bladder cancer proliferation and migration through targeting SPHK1. Our results demonstrated that tumor necrosis factor (TNF) alpha-induced protein 6 (TNFAIP6) was one of the differentially expressed genes. It has been reported that TNFAIP6 high-expression predicted poor OS in patients with urothelial carcinoma (37). Likewise, we demonstrated that TNFAIP6 was a risk factor by survival analysis in our study.

To have a better understanding of the role of risk score in immune infiltration, six were involved in this study. The results showed that patients in high-risk group may happen with the enrichment of C1 in their microenvironment, while those with low-risk score usually happened with C2, C3, and C4 enrichment, which means that C1 is a risk factor and the other types can inhibit the genesis and progression of transitional bladder cancer. Since a high cytotoxicity can suppress the genesis and progression of tumor, the results of our study were in accordance with these previous findings (38). In relation to clinical implication, patients in high-risk groups are more likely to have higher tumor stage, which was a risk factor for cancer.

According to the results of GSEA, mitogen-activated protein kinase (MAPK), and Wnt signaling pathways were markedly enriched, which had been proven to be correlated with cancer, and they may be the potential therapeutic target in the future. Moreover, signal pathways such as melanoma, pathways in cancer, basal cell carcinoma, and colorectal cancer were enriched in high-risk groups, which demonstrated the important role of these IRAGs in cancer. Furthermore, patients are more likely to have a higher score of mast cells and macrophages, while they had lower scores of NK cells than the low-risk group. Interestingly, previous studies suggested that NK cells are a potent class of antitumor cell in bladder cancer, which was similar to our results (39). Besides, the risk score was markedly associated with stromal score, which means that tumor environment may contribute to the aggression of bladder cancer and negatively relate with RNAss that may be a protector for bladder cancer.

By analyzing the data of 60 different cell lines, the elevated expression of these prognostic genes cannot only enhance the drug sensitivity but also increase the resistance of chemotherapy drugs approved by the Food and Drug Administration (FDA). For example, cancer cells were sensitive to Tyrothricin with the increased expression of INHBA genes, while they were insensitive to Zoledronate. Moreover, cells with increased expression of MYC genes were susceptible to Oxaliplatin, which had been approved by FDA for bladder cancer. Therefore, these data may provide a new sight for precision therapy in the future.

To further verify the reliability of our results, qRT-PCR was performed *in vivo* and *in vitro* for INHBA and SPHK1 genes. The expression levels of INHBA and SPHk1 were all markedly upregulated for bladder cancer both *in vivo* and *in vitro*. In addition, when treated by Dasatinib, the expression of INHBA was significantly increased in T24 and 5637 cells, which was consistent with the correlation between INHBA and Dasatinib.

A good predictive ability of the risk model and differential expression of prognostic genes have been demonstrated in transitional bladder cancer. Nevertheless, there are two limitations in our study. First, to achieve a comprehensive understanding of these prognostic IRAGs, we should conduct multi-omics analysis. Second, a large-sample multicenter study is required to demonstrate the findings of our study.

CONCLUSIONS

Our prognostic model can accurately discriminate the transitional bladder cancer patients. Patients that have a worse survival time in high-risk groups can be identified by this model before the disease progression and obtained appropriate therapies immediately. In addition, cancer cells with these prognostic genes are sensitive or insensitive to FDA-approved antitumor drugs, which may contribute to the targeted therapies in transitional bladder cancer in the future.

DATA AVAILABILITY STATEMENT

The original contributions presented in the study are included in the article/**Supplementary Material**. Further inquiries can be directed to the corresponding authors.

ETHICS STATEMENT

The studies involving human participants were reviewed and approved by the Ethics Committee of Shanghai General Hospital. The patients/participants provided their written informed consent to participate in this study.

AUTHOR CONTRIBUTIONS

JJ and AL conducted research and conceived the design. ZX and JC performed data collection and article writing. SH performed

data analysis. WS revised the manuscript. All authors contributed to the article and approved the submitted version.

FUNDING

This work was supported by The National Natural Science Foundation of China (No. 81771564) and Zunyi Municipal Science and technology Bureau [No. 2018(192)].

SUPPLEMENTARY MATERIAL

The Supplementary Material for this article can be found online at: https://www.frontiersin.org/articles/10.3389/fonc.2021.740985/full#supplementary-material

Supplementary Figure 1 | Forest plots showing the results of the association between IRAGs and OS.

Supplementary Figure 2 | AUC time-dependent ROC curves for OS in GSE13507 cohort.

Supplementary Table 1 | The 200 inflammatory response-related genes.

Supplementary Table 2 | Differentially expressed genes between HCC tissues and adjacent non-tumorous tissues in TCGA.

Supplementary Table 3 | The primer sequences of the prognostic genes.

Supplementary Table 4 | The level of prognostic genes in NCI 60 human cancer cell lines.

Supplementary Table 5 | Marker genes for immune cell types.

REFERENCES

1. Potts KG, Irwin CR, Favis NA, Pink DB, Vincent KM, Lewis JD, et al. Deletion of (Ribonucleotide Reductase) in Vaccinia Virus Produces a Selective Oncolytic Virus and Promotes Anti-Tumor Immunity With Superior Safety in Bladder Cancer Models. *EMBO Mol Med* (2017) 9(5):638–54. doi: 10.15252/emmm.201607296
2. Lu Q, Liu T, Feng H, Yang R, Zhao X, Chen W, et al. Circular RNA circSLC8A1 Acts as a Sponge of miR-130b/miR-494 in Suppressing Bladder Cancer Progression *via* Regulating PTEN. *Mol Cancer* (2019) 18(1):111. doi: 10.1186/s12943-019-1040-0
3. Galsky MD, Stensland K, Sfakianos JP, Mehrazin R, Diefenbach M, Mohamed N, et al. Comparative Effectiveness of Treatment Strategies for Bladder Cancer With Clinical Evidence of Regional Lymph Node Involvement. *J Clin Oncol* (2016) 34(22):2627–35. doi: 10.1200/JCO.2016.67.5033
4. Fehniger TA, Suzuki K, Ponnappan A, VanDeusen JB, Cooper MA, Florea SM, et al. Fatal Leukemia in Interleukin 15 Transgenic Mice Follows Early Expansions in Natural Killer and Memory Phenotype CD8+ T Cells. *J Exp Med* (2001) 193(2):219–31. doi: 10.1084/jem.193.2.219
5. Lin Z, Xu Q, Miao D, Yu F. An Inflammatory Response-Related Gene Signature Can Impact the Immune Status and Predict the Prognosis of Hepatocellular Carcinoma. *Front Oncol* (2021) 11:644416. doi: 10.3389/fonc.2021.644416
6. Walter RB, Milano F, Brasky TM, White E. Long-Term Use of Acetaminophen, Aspirin, and Other Nonsteroidal Anti-Inflammatory Drugs and Risk of Hematologic Malignancies: Results From the Prospective Vitamins and Lifestyle (VITAL) Study. *J Clin Oncol* (2011) 29 (17):2424–31. doi: 10.1200/JCO.2011.34.6346
7. Drescher CW, Shah C, Thorpe J, O'Briant K, Anderson GL, Berg CD, et al. Longitudinal Screening Algorithm That Incorporates Change Over Time in CA125 Levels Identifies Ovarian Cancer Earlier Than a Single-Threshold Rule. *J Clin Oncol* (2013) 31(3):387–92. doi: 10.1200/JCO.2012.43.6691
8. Bennett JK, Wheatley JK, Walton KN, Watts NB, McNair O, O'Brien DP. Nonmetastatic Bladder Cancer Associated With Hypercalcemia, Thrombocytosis and Leukemoid Reaction. *J Urol* (1986) 135(1):47–8. doi: 10.1016/S0022-5347(17)45510-8
9. Li X, Shu K, Zhou J, Yu Q, Cui S, Liu J, et al. Preoperative Plasma Fibrinogen and D-Dimer as Prognostic Biomarkers for Non-Muscle-Invasive Bladder Cancer. *Clin Genitourin Cancer* (2020) 18(1):11–19.e1. doi: 10.1016/j.clgc.2019.10.025
10. Marchioni M, Primiceri G, Ingrosso M, Filograna R, Castellan P, De Francesco P, et al. The Clinical Use of the Neutrophil to Lymphocyte Ratio (NLR) in Urothelial Cancer: A Systematic Review. *Clin Genitourin Cancer* (2016) 14(6):473–84. doi: 10.1016/j.clgc.2016.04.008
11. Masson-Lecomte A, Rava M, Real FX, Hartmann A, Allory Y, Malats N. Inflammatory Biomarkers and Bladder Cancer Prognosis: A Systematic Review. *Eur Urol* (2014) 66(6):1078–91. doi: 10.1016/j.eururo.2014.07.033
12. Schuettfort VM, D'Andrea D, Quhal F, Mostafaei H, Laukhtina E, Mori K, et al. A Panel of Systemic Inflammatory Response Biomarkers for Outcome Prediction in Patients Treated With Radical Cystectomy for Urothelial Carcinoma. *BJU Int* (2021). doi: 10.1111/bju.15379
13. Guo Y, Cai K, Mao S, Zhang J, Wang L, Zhang Z, et al. Preoperative C-Reactive Protein/Albumin Ratio Is a Significant Predictor of Survival in Bladder Cancer Patients After Radical Cystectomy: A Retrospective Study. *Cancer Manag Res* (2018) 10:4789–804. doi: 10.2147/CMAR.S180301
14. Chen Z-L, Qin L, Peng X-B, Hu Y, Liu B. INHBA Gene Silencing Inhibits Gastric Cancer Cell Migration and Invasion by Impeding Activation of the TGF-β Signaling Pathway. *J Cell Physiol* (2019) 234(10):18065–74. doi: 10.1002/jcp.28439
15. Gabig TG, Waltzer WC, Whyard T, Romanov V. Clostridium Perfringens Enterotoxin as a Potential Drug for Intravesical Treatment of Bladder Cancer. *Biochem Biophys Res Commun* (2016) 478(2):887–92. doi: 10.1016/j.bbrc.2016.08.046
16. Flaig TW, Spiess PE, Agarwal N, Bangs R, Boorjian SA, Buyyounouski MK, et al. Bladder Cancer, Version 3.2020, NCCN Clinical Practice Guidelines in Oncology. *J Natl Compr Canc Netw* (2020) 18(3):329–54. doi: 10.6004/jnccn.2020.0011
17. Batista R, Vinagre N, Meireles S, Vinagre J, Prazeres H, Leão R, et al. Biomarkers for Bladder Cancer Diagnosis and Surveillance: A Comprehensive Review. *Diagnostics (Basel)* (2020) 10(1): 39. doi: 10.3390/diagnostics10010039
18. Alva A, Friedlander T, Clark M, Huebner T, Daignault S, Hussain M, et al. Circulating Tumor Cells as Potential Biomarkers in Bladder Cancer. *J Urol* (2015) 194(3):790–8. doi: 10.1016/j.juro.2015.02.2951
19. Dudley JC, Schroers-Martin J, Lazzareschi DV, Shi WY, Chen SB, Esfahani MS, et al. Detection and Surveillance of Bladder Cancer Using Urine Tumor DNA. *Cancer Discov* (2019) 9(4):500–9. doi: 10.1158/2159-8290.CD-18-0825
20. Mondul AM, Weinstein SJ, Männistö S, Snyder K, Horst RL, Virtamo J, et al. Serum Vitamin D and Risk of Bladder Cancer. *Cancer Res* (2010) 70 (22):9218–23. doi: 10.1158/0008-5472.CAN-10-0985
21. Adamkiewicz M, Bryniarski P, Kowalik M, Burzyński B, Rajwa P, Paradysz A. Lymphocyte-To-Monocyte Ratio Is the Independent Prognostic Marker of Progression in Patients Undergoing BCG-Immunotherapy for Bladder Cancer. *Front Oncol* (2021) 11:655000. doi: 10.3389/fonc.2021.655000
22. Wang X, Ni X, Tang G. Prognostic Role of Platelet-To-Lymphocyte Ratio in Patients With Bladder Cancer: A Meta-Analysis. *Front Oncol* (2019) 9:757. doi: 10.3389/fonc.2019.00757
23. Cao R, Yuan L, Ma B, Wang G, Qiu W, Tian Y. An EMT-Related Gene Signature for the Prognosis of Human Bladder Cancer. *J Cell Mol Med* (2020) 24(1):605–17. doi: 10.1111/jcmm.14767
24. Jiang W, Zhu D, Wang C, Zhu Y. An Immune Relevant Signature for Predicting Prognoses and Immunotherapeutic Responses in Patients With Muscle-Invasive Bladder Cancer (MIBC). *Cancer Med* (2020) 9(8):2774–90. doi: 10.1002/cam4.2942

25. Yang L, Roberts D, Takhar M, Erho N, Bibby BAS, Thiruthaneeswaran N, et al. Development and Validation of a 28-Gene Hypoxia-Related Prognostic Signature for Localized Prostate Cancer. *EBioMedicine* (2018) 31:182–9. doi: 10.1016/j.ebiom.2018.04.019
26. Zhang C, Gou X, He W, Yang H, Yin H. A Glycolysis-Based 4-mRNA Signature Correlates With the Prognosis and Cell Cycle Process in Patients With Bladder Cancer. *Cancer Cell Int* (2020) 20:177. doi: 10.1186/s12935-020-01255-2
27. Vollmer T, Schlickeiser S, Amini L, Schulenberg S, Wendering DJ, Banday V, et al. The Intratumoral CXCR3 Chemokine System is Predictive of Chemotherapy Response in Human Bladder Cancer. *Sci Transl Med* (2021) 13(576):eabb3735. doi: 10.1126/scitranslmed.abb3735
28. Sugawara S, Yamada Y, Arai T, Okato A, Idichi T, Kato M, et al. Dual Strands of the miR-223 Duplex (miR-223-5p and miR-223-3p) Inhibit Cancer Cell Aggressiveness: Targeted Genes are Involved in Bladder Cancer Pathogenesis. *J Hum Genet* (2018) 63(5):657–68. doi: 10.1038/s10038-018-0437-8
29. Hamm R, Chen YR, Seo E-J, Zeino M, Wu C-F, Müller R, et al. Induction of Cholesterol Biosynthesis by Archazolid B in T24 Bladder Cancer Cells. *Biochem Pharmacol* (2014) 91(1):18–30. doi: 10.1016/j.bcp.2014.06.018
30. Wang JF, Gong YQ, He YH, Ying WW, Li XS, Zhou XF, et al. High Expression of MMP14 is Associated With Progression and Poor Short-Term Prognosis in Muscle-Invasive Bladder Cancer. *Eur Rev Med Pharmacol Sci* (2020) 24 (12):6605–15. doi: 10.26355/eurrev_202006_21646
31. Li H, Li Q, Ma Z, Zhou Z, Fan J, Jin Y, et al. AID Modulates Carcinogenesis Network *via* DNA Demethylation in Bladder Urothelial Cell Carcinoma. *Cell Death Dis* (2019) 10(4):251. doi: 10.1038/s41419-019-1472-x
32. Zhang M, Du H, Wang L, Yue Y, Zhang P, Huang Z, et al. Thymoquinone Suppresses Invasion and Metastasis in Bladder Cancer Cells by Reversing EMT Through the Wnt/β-Catenin Signaling Pathway. *Chem Biol Interact* (2020) 320:109022. doi: 10.1016/j.cbi.2020.109022
33. Musser ML, Viall AK, Phillips RL, Hostetter JM, Johannes CM. Gene Expression of Prostaglandin EP4 Receptor in Three Canine Carcinomas. *BMC Vet Res* (2020) 16(1):213. doi: 10.1186/s12917-020-02431-2
34. Guirado M, Gil H, Saenz-Lopez P, Reinboth J, Garrido F, Cozar JM, et al. Association Between C13ORF31, NOD2, RIPK2 and TLR10 Polymorphisms and Urothelial Bladder Cancer. *Hum Immunol* (2012) 73(6):668–72. doi: 10.1016/j.humimm.2012.03.006
35. Zheng K, Chen Z, Feng H, Chen Y, Zhang C, Yu J, et al. Sphingomyelin Synthase 2 Promotes an Aggressive Breast Cancer Phenotype by Disrupting the Homoeostasis of Ceramide and Sphingomyelin. *Cell Death Dis* (2019) 10 (3):157. doi: 10.1038/s41419-019-1303-0
36. Tang C, Wu Y, Wang X, Chen K, Tang Z, Guo X. LncRNA MAFG-AS1 Regulates miR-125b-5p/SphK1 Axis to Promote the Proliferation, Migration, and Invasion of Bladder Cancer Cells. *Hum Cell* (2021) 34(2):588–97. doi: 10.1007/s13577-020-00470-3
37. Zhang X, Xue J, Yang H, Zhou T, Zu G. TNFAIP6 Promotes Invasion and Metastasis of Gastric Cancer and Indicates Poor Prognosis of Patients. *Tissue Cell* (2021) 68:101455. doi: 10.1016/j.tice.2020.101455
38. Tamborero D, Rubio-Perez C, Muiños F, Sabarinathan R, Piulats JM, Muntasell A, et al. A Pan-Cancer Landscape of Interactions Between Solid Tumors and Infiltrating Immune Cell Populations. *Clin Cancer Res* (2018) 24 (15):3717–28. doi: 10.1158/1078-0432.CCR-17-3509
39. Feyisetan O, Tracey C, Hellawell GO. Probiotics, Dendritic Cells and Bladder Cancer. *BJU Int* (2012) 109(11):1594–7. doi: 10.1111/j.1464-410X.2011.10749.x

Conflict of Interest: The authors declare that the research was conducted in the absence of any commercial or financial relationships that could be construed as a potential conflict of interest.

Publisher's Note: All claims expressed in this article are solely those of the authors and do not necessarily represent those of their affiliated organizations, or those of the publisher, the editors and the reviewers. Any product that may be evaluated in this article, or claim that may be made by its manufacturer, is not guaranteed or endorsed by the publisher.

Copyright © 2021 Xie, Cai, Sun, Hua, Wang, Li and Jiang. This is an open-access article distributed under the terms of the Creative Commons Attribution License (CC BY). The use, distribution or reproduction in other forums is permitted, provided the original author(s) and the copyright owner(s) are credited and that the original publication in this journal is cited, in accordance with accepted academic practice. No use, distribution or reproduction is permitted which does not comply with these terms.

frontiers in Oncology

ORIGINAL RESEARCH
published: 25 October 2021
doi: 10.3389/fonc.2021.726671

Risk Scores Based on Six Survival-Related RNAs in a Competing Endogenous Network Composed of Differentially Expressed RNAs Between Clear Cell Renal Cell Carcinoma Patients Carrying Wild-Type or Mutant Von Hippel–Lindau Serve Well to Predict Malignancy and Prognosis

Rui Zhu[†], *Xiezhao Li*[†], *Zhiduan Cai*[†], *Siyang Liang*, *Yaoji Yuan*, *Yuyu Xu*, *Dehui Lai*, *Haibo Zhao*, *Weiqing Yang*, *Jun Bian*, *Leyuan Liu*[*] *and Guibin Xu*[*]

Department of Urology, The Fifth Affiliated Hospital of Guangzhou Medical University, Guangzhou, China

Clear cell renal cell carcinoma (ccRCC) carrying wild-type Von Hippel–Lindau (VHL) tumor suppressor are more invasive and of high morbidity. Concurrently, competing endogenous RNA (ceRNA) network has been suggested to play an important role in ccRCC malignancy. In order to understand why the patients carrying wild-type VHL gene have high degrees of invasion and morbidity, we applied bioinformatics approaches to identify 861 differentially expressed RNAs (DE-RNAs) between patients carrying wild-type and patients carrying mutant VHL from The Cancer Genome Atlas (TCGA) database, established a ceRNA network including 122 RNAs, and elected six survival-related DE-RNAs including Linc00942, Linc00858, RP13_392I16.1, hsa-miR-182-5p, hsa-miR-183-5p, and PAX3. Examining clinical samples from our hospital revealed that patients carrying wild-type VHL had significantly higher levels of all six RNAs than those carrying mutant VHL. Patients carrying wild-type VHL had significantly higher risk scores, which were calculated based on expression levels of all six RNAs, than those carrying mutant VHL. Patients with higher risk scores had significantly shorter survival times than those with lower risk scores. Therefore, the risk scores serve well to predict malignancy and prognosis.

Keywords: ccRCC, ceRNA network, prognosis, risk score, VHL

OPEN ACCESS

Edited by:
Marijo Bilusic,
University of Miami Health System,
United States

Reviewed by:
Elena Cherkasova,
National Institutes of Health (NIH),
United States
Claudia A. S. Lage,
Federal University of Rio de Janeiro,
Brazil

***Correspondence:**
Guibin Xu
gyxgb@163.com
Leyuan Liu
liuleyuan@hotmail.com

[†]*These authors have contributed equally to this work*

Specialty section:
This article was submitted to Genitourinary Oncology, a section of the journal Frontiers in Oncology

Received: *17 June 2021*
Accepted: *01 October 2021*
Published: *25 October 2021*

Citation:
Zhu R, Li X, Cai Z, Liang S, Yuan Y, Xu Y, Lai D, Zhao H, Yang W, Bian J, Liu L and Xu G (2021) Risk Scores Based on Six Survival-Related RNAs in a Competing Endogenous Network Composed of Differentially Expressed RNAs Between Clear Cell Renal Cell Carcinoma Patients Carrying Wild-Type or Mutant Von Hippel–Lindau Serve Well to Predict Malignancy and Prognosis. Front. Oncol. 11:726671. doi: 10.3389/fonc.2021.726671

INTRODUCTION

Kidney cancer is one of the top 10 most common tumors, the second-ranked malignant tumor in urologic system, and contributes 2% to 3% of the human malignant tumors worldwide (1, 2). There are 400,000 new cases of kidney malignant tumors of which 175,000 lead to death per year (3). Among patients with renal cancer at early stage and even some of renal cancer patients who do not have any specific symptom regardless of the stage of the disease, only about 30% of patients diagnosed with renal cancer was found to be at initial stage of malignancy, but the other 70% were found to be already at late stage of malignancy (4, 5). About 90% of the cases with kidney cancers are those with renal cell carcinomas, of which 70% are with clear cell renal cell carcinomas (ccRCCs), which are either hereditary or sporadic (6). Among many genetic factors that were found to be related to ccRCC, the inactivation of Von Hippel–Lindau (VHL) tumor suppressor gene occurs in 80% of patients and is the most common event (7–9), leading to the interruption of both vascular endothelial growth factor (VEGF) and mammalian target of rapamycin (mTOR) signaling pathways, which serve as the targets of most of the drugs currently used in clinical practice (10, 11). Although the inactivation of VHL gene alone is not sufficient to cause tumors (12, 13), a study of ccRCC patients from Germany suggested that low expression of VHL was identified as a risk factor for worse overall survival (OS) (14). However, it was reported that there is no difference in survival between patients carrying wild-type or mutant VHL or between patients with different levels of either VHL protein or messenger RNA (mRNA), and patients with nonsense mutations in exon 1 have a worse prognosis based on a study of ccRCC patients from Brazil (15), suggesting that loss of VHL function is directly related to the prognosis of ccRCC patients. A recent study indicated that about 40%–60% of patients with sporadic ccRCC carry wild-type VHL, and such tumors are more invasive and lead to a dramatic reduction of survival rates as compared with those carrying mutant VHL (16, 17). Therefore, it is more urgent to identify other factors that are closely associated with patients' survival in addition to VHL mutation.

Long non-coding RNA (lncRNA) is a type of transcript with more than 200 nucleotides that does not encode a protein (18). It was initially considered to be "noise" generated by genome transcription without biological functions. More and more evidences show that lncRNA is involved not only in various physiological processes, such as cell proliferation, differentiation, and apoptosis, but also in pathological processes of various diseases (18). The long intergenic non-coding RNA (lincRNA) is the most common form of lncRNA. LncRNA is reported to be related to a variety of tumor diseases such as liver cancer (19), gastric cancer (20), oral squamous cell carcinoma (21), bladder cancer (22), prostate cancer (23), and kidney cancer (24). MicroRNAs (miRNAs) are small single-stranded non-coding molecules of about 22 nucleotides long and target the 3′UTR or CDS of mRNAs to form RNA-Induced Silencing Complexes (RISCs) to induce the degradation of the correspondent mRNA (25). Circular RNA (circRNA) is homologous to its target gene sequence and may act as a molecular sponge. Since lncRNA and mRNA share sequence homology, it is also possible to combine miRNA with lncRNA or circRNA to change expression levels of their downstream target genes. Therefore, miRNAs, lncRNAs, mRNAs, and other non-coding RNAs form a large-scale network of competing endogenous RNAs (ceRNAs), which are currently considered to be involved in the regulation of a variety of tumor diseases and play an important role in different stages of tumorigenesis (26).

Here, we constructed a ceRNA network after the sets of differentially expressed lncRNAs (DE-lncRNAs), miRNAs (DE-miRNAs), and mRNAs (DE-mRNAs) between patients carrying wild-type and those carrying mutant VHL, which were common in multiple database, were identified. Further identification of six survival-related RNAs including Linc00942, Linc00858, RP13_392I16.1, hsa-miR-182-5p, hsa-miR-183-5p, and PAX3, in the ceRNA network led to the building of a model in which risk scores were successfully applied to predict malignancy and prognosis of ccRCC.

MATERIALS AND METHODS

Selection of Patient Data in The Cancer Genome Atlas Database

The selection of patient data in The Cancer Genome Atlas (TCGA) database was performed following the workflow as shown (**Figure 1A**). The expression data (read count) of ccRCC patients in TCGA were downloaded and integrated using R's GDCRNATools package. The sample size for mRNA and lncRNA was 530, and miRNA was 516. The information about mutation of those samples was from cBioPortal (http://www.cbioportal.org/). The information about OS of those samples was from xenabrowser (https://xenabrowser.net/). Since RNA sequencing data were obtained directly from TCGA, approval by any ethics committee was not required.

Identification of Differentially Expressed Long Non-Coding RNAs, Differentially Expressed MicroRNAs, and Differentially Expressed Messenger RNAs Between Clear Cell Renal Cell Carcinoma Patients Carrying Wild-Type or Mutant Von Hippel–Lindau

Among the 530 ccRCC samples with information of mRNA and lncRNA expression, samples of 446 patients were genotyped as either wild type (223 samples) or mutant (223 samples). Among the 516 samples with information of miRNA, samples of 220 patients were genotyped as wild-type, and 221 patients were genotyped as mutant VHL. The RNA read count of samples carrying wild-type and mutant VHL was standardized and analyzed with the DESeq2 package. DE-lncRNAs, DE-miRNAs, and DE-mRNAs were elected with $|\log2foldchange| > 1$ and Adj.*p*.val < 0.05 as a threshold according to the method of Benjamini–Hochberg.

Construction of Competing Endogenous RNA Regulation Network

The interaction between lncRNA and miRNA came from miRcode database (http://www.mircode.org/). The interaction between miRNA and mRNA came from miRDB (http://mirdb.org/), miRTarBase (http://mirtarbase.mbc.nctu.edu.tw/php/index.

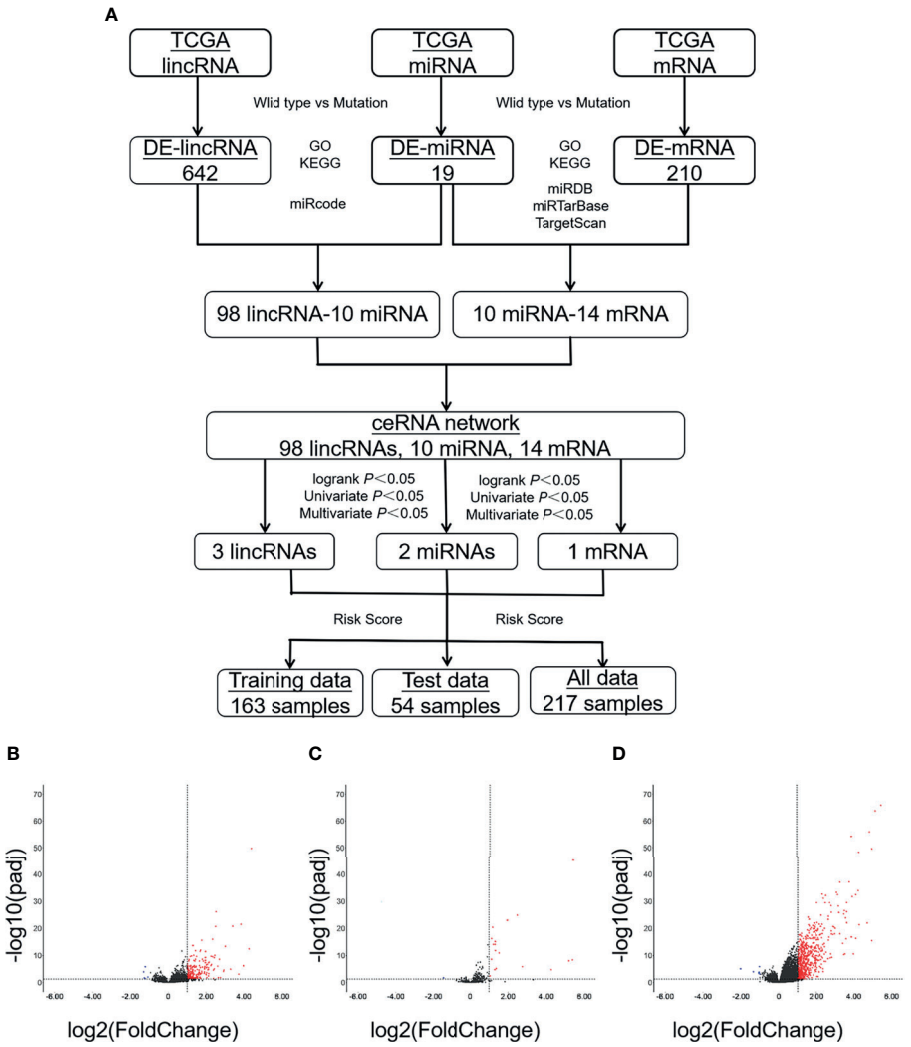

FIGURE 1 | A large number of DE-RNAs are identified between patients carrying either wild-type or mutant VHL. **(A)** A diagram showing the workflow of the study. **(B–D)** Volcanic maps showing the distribution of DE-lncRNAs **(B)**, DE-miRNAs **(C)**, or DE-mRNAs **(D)**. Red, blue, and black dots represent those RNAs that are significantly upregulated, significantly downregulated, and not significantly changed, respectively. VHL, Von Hippel–Lindau; DE-RNAs, differentially expressed RNAs; DE-lncRNAs, differentially expressed long non-coding RNAs; DE-miRNAs, differentially expressed microRNAs; DE-mRNAs, differentially expressed messenger RNAs.

php), and TargetScan (http://www.targetscan.org/vert_72/) databases. In order to improve the reliability of the results, we selected the intersection of DE-miRNA–DE-mRNA interaction pairs found in the three databases as candidate genes to construct the ceRNA network. Finally, we used Cytoscape software to visualize the ceRNA network.

Enrichment Analyses of the Competing Endogenous RNAs

The Gene Ontology (GO) molecular function enrichment and Kyoto Encyclopedia of Genes and Genomes (KEGG) pathway enrichment of DE-mRNA in the ceRNA network were analyzed with R's ClusterProfiler package. $p < 0.05$ was considered statistically significant.

Survival Analysis of Differential RNAs in the Competing Endogenous RNA Regulation Network

The expression level of each DE-lncRNA, DE-miRNA, and DE-mRNA in the ceRNA network in each patient was classified into either high- or low-expression group with their median as a threshold. The survival curve for each group was plotted through the Kaplan–Meier (K–M) survival analysis. $p < 0.05$ was considered statistically significant.

Univariate and Multivariate Cox Regression Analyses

Univariate and multivariate Cox regression analyses were used to screen the survival-related differentially expressed RNAs (DE-

RNAs) between patients carrying wild-type and those carrying mutant VHL to eliminate confounding factors, reduce the number of DE-RNAs, and calculate a hazard ratio (HR) and a 95% confidence interval (95% CI) for each variable. Genotypes with an HR greater than 1 or less than 1 and a Wald test *p*-value less than 0.05 were considered to be the ones that significantly affected patient survival.

External Verification of Survival-Related RNAs With Clinical Tissue Samples

Tissue samples were collected from 21 postoperative ccRCC patients who underwent surgery but did not receive any anti-tumor radiotherapy or chemotherapy before surgery at The Fifth Affiliated Hospital of Guangzhou Medical University from January 2018 to May 2020. All samples were frozen and stored in liquid nitrogen immediately after sampling and subjected to DNA sequencing to determine if their VHL gene was wild type or mutant. The expression levels of VHL protein in the samples were determined by immunohistochemistry analyses with a polyclonal antibody against VHL protein (Cat# 16538-1-AP, from ProteinTech®). The expression levels of target RNAs in the samples were verified by qRT-RCR. Tumor samples were staged according to the 2010 American Joint Committee on Cancer (AJCC) TNM stage and clinical stage system, and their histopathological grades were determined with the Furman grade method. The study was approved by the Ethics Committee of The Fifth Affiliated Hospital of Guangzhou Medical University. Patients and their family members had been fully informed, and signed consent forms indicated that their samples would be used for scientific research.

Establishment of a Prognostic Risk Score System and Clinical Correlation Analysis for Differentially Expressed RNAs in the Competing Endogenous RNA Regulation Network

A risk score system was established using the DE-RNAs selected by multivariate Cox regression analysis. To predict the patient's prognosis, risk scores were calculated with the formula "Risk score = $\Sigma(\beta i * Xi)$" in which "i" was the number of characteristic genes, "β" the correlation coefficient of mRNA in the multivariate Cox regression analysis, and X the levels of gene expression after log2 conversion. Pearson's chi-squared test and Fisher's exact test were applied to analyze the correlation between patient's risk score and clinicopathological characteristics in TCGA data set. $p < 0.05$ was considered to be statistically significant. The t-test was used to compare the difference of risk scores between clinical features that were significantly related to OS. $p < 0.05$ was considered to be statistically significant.

Gene Set Enrichment Analysis (GSEA) was applied to analyze the signaling pathways associated with patients carrying wild-type VHL and high risk score. The gene expression data from patients carrying high risk score and low risk score in the c2.cp.kegg.v7.0.symbols.gmt database were subjected to estimate the normalized enrichment scores (NESs), *p*-values, and *q*-values after false discovery rates (FDRs) were adjusted for each signal pathway with the GSEA software.

RESULTS

Multiple Differentially Expressed Long Non-Coding RNAs, Differentially Expressed MicroRNAs, and Differentially Expressed Messenger RNAs Are Identified Between Patients Carrying Either Wild-Type or Mutant Von Hippel–Lindau

We analyzed the levels of lncRNAs, miRNAs, and mRNAs between ccRCC patients carrying wild-type and those carrying mutant VHL in TCGA database; displayed the distribution of those DE-RNAs in form of volcano map; and defined those RNAs with $|\log2foldchange| > 1$ and Adj.*p*.val < 0.05 as DE-RNAs. A total of 642 DE-mRNAs (635 upregulated and seven downregulated), 210 DE-lncRNAs (205 upregulated and five downregulated), and 19 DE-miRNAs (18 upregulated and one downregulated) were identified (**Figures 1B–D**).

A Competing Endogenous RNA Network Is Established

We searched the miRcode database, identified 210 miRNAs that were targeted by DE-lncRNAs, and found interactions between 10 DE-miRNAs and 98 DE-lncRNAs. We searched the miRDB, miRTarBase, and TargetScan databases to identify interactions between miRNA–mRNA interaction and found 10 DE-miRNA and 14 DE-mRNA interactions (**Figure 2A**). Eventually, a ceRNA regulation network including 290 edges and 122 nodes (98 lncRNAs, 10 miRNAs, and 14 mRNAs) was established between patients carrying wild-type or mutant VHL as shown in **Figure 2B**.

The Signaling Pathways Affected by Genes in Competing Endogenous RNA Network Are Predicted

We performed GO enrichment and pathway enrichment analysis on 14 differential genes in the ceRNA network and displayed the top 10 candidate signaling pathways based on the rich factors (the number of differential genes in the GO term divided by the total number of genes in the GO term). The biological processes were mainly related to some kinase activity, growth factor receptor binding, receptor regulatory activity, and so on; cell components were mainly involved in the formation of cell adhesion, synapses and axon membrane structures, and mast cell granules; and molecular functions were mostly related to the kidney functions such as renal vesicle development, epithelial cell differentiation during kidney development, kidney capsule morphogenesis, and renal vesicle morphogenesis (**Figure 3A**).

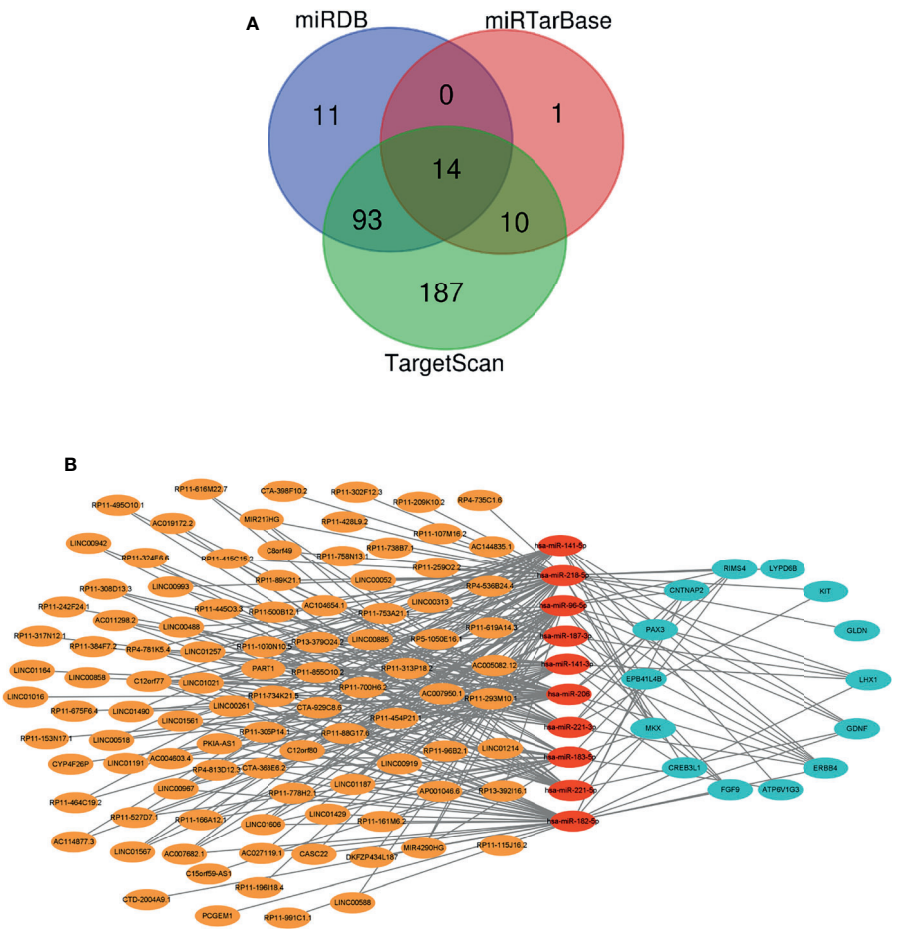

FIGURE 2 | A ceRNA network is created. **(A)** A Venn diagram showing the miRNA–mRNA interaction as predicted based on three databases. **(B)** A diagram showing the established ceRNA network. Orange, red, and blue circles represent DE-lncRNAs, DE-miRNAs, and DE-mRNAs, respectively. Gray lines represent interactions among lncRNAs, miRNAs, and mRNAs. ceRNA, competing endogenous RNA; DE-lncRNAs, differentially expressed long non-coding RNAs; DE-miRNAs, differentially expressed microRNAs; DE-mRNAs, differentially expressed messenger RNAs.

KEGG enrichment search identified not only some kidney-related pathways such as collecting duct acid secretion and vasopressin-regulated water absorption but also some cancer-related pathways such as PI3K-AKT signaling pathway and MAPK signal pathway as shown in the bubble chart (**Figure 3B**).

Survival-Related RNAs in Competing Endogenous RNA Network Are Identified Through Univariate and Multivariate Cox Regression Analyses

We estimated the significance of 98 lncRNAs, 10 miRNAs, and 14 mRNAs in the ceRNA network with OS of patients and identified 18 lncRNAs, four miRNAs, and three mRNAs, which significantly impacted OS either positively or negatively (**Table 1**). Univariate regression analysis found that these RNAs were significantly related to the aggressiveness of disease. Multivariate Cox regression analysis found that LINC00942, LINC00858, RP13_392I16.1, hsa-miR-183-5p, hsa-miR-182-5p, and PAX3 were considered as independent factors that impacted the prognosis of patients (**Table 1**). Therefore, these six RNAs were selected to build the risk score system.

The Survival-Related RNAs Detected in Databases Are Verified With External Clinical Samples

A total of 21 ccRCC tissue samples were collected in our hospital and subjected to gene sequencing and immunohistochemistry analysis. Using three sets of primers covering the three exons of VHL gene (**Figures 4A, B**), we identified 18 samples carrying wild-type VHL and three samples carrying mutant VHL as shown in **Figure 4C**. The identification of high percentage of patients carrying wild-type VHL gene was a surprise to us and triggered us to investigate if the wild-type gene has been suppressed due to other epigenetic modifications. Patients carrying wild-type VHL

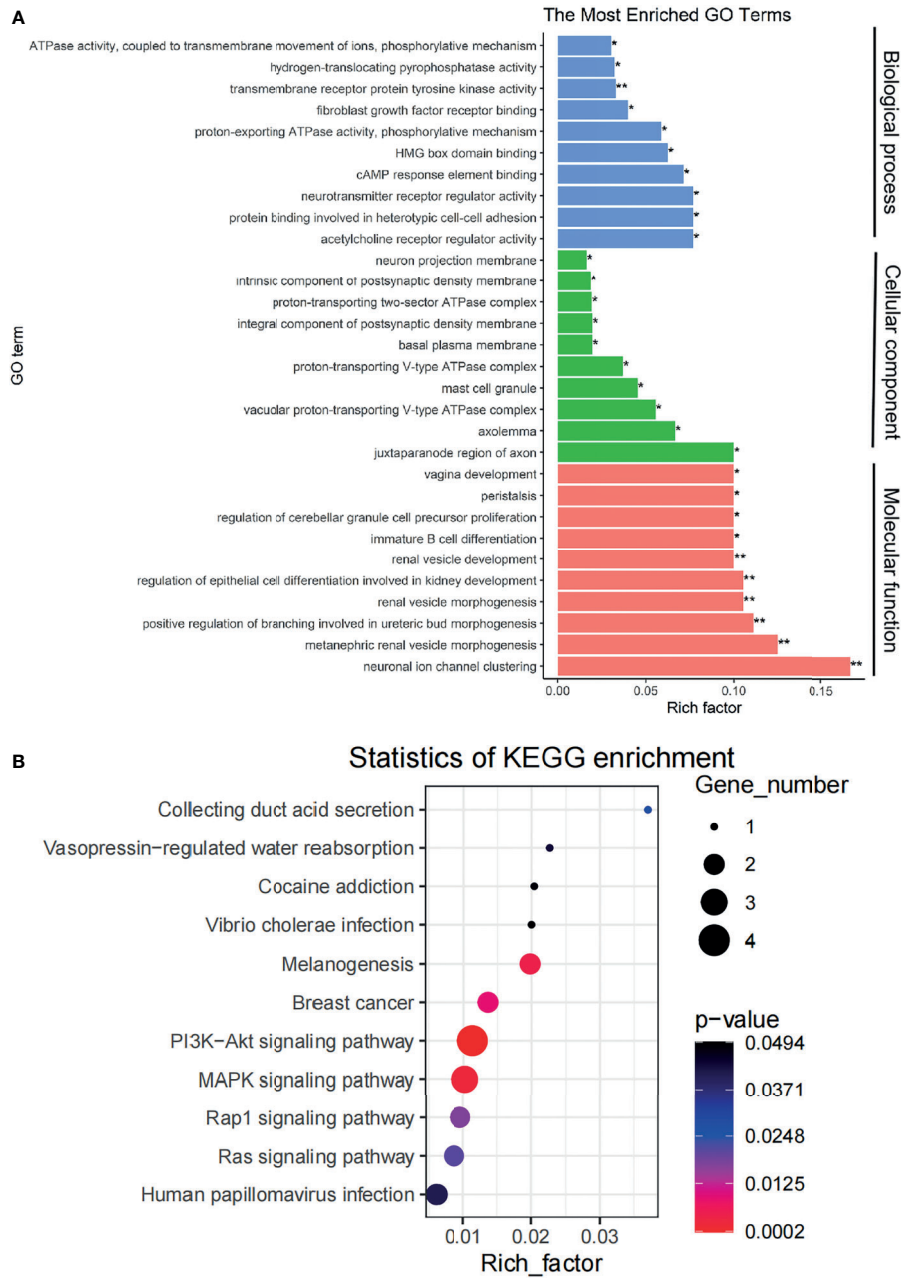

FIGURE 3 | The signaling pathways affected by genes in the ceRNA network are identified. **(A)** A plot showing the signaling pathways affected by genes in the ceRNA network as detected *via* GO enrichment analyses. **(B)** A bubble chart showing the signaling pathways affected by genes in the ceRNA network as detected *via* KEGG pathways analysis. ceRNA, competing endogenous RNA; GO, Gene Ontology; KEGG, Kyoto Encyclopedia of Genes and Genomes. *p < 0.05, **p < 0.01.

gene expressed higher levels of VHL protein than those carrying mutant VHL (**Figures 4D–G**), suggesting that the expression of wild-type gene was not suppressed in general by other epigenetic events such as DNA methylation. The qRT-PCR analyses using primer sets listed (**Figure 5A**) demonstrated that levels of LINC00942, LINC00858, RP13_392I16.1, hsa-miR-183-5p, hsa-miR-182-5p, and PAX3 were significantly higher in patients carrying wild-type VHL than in patients carrying mutant VHL (**Figures 5B–G**). Therefore, the results obtained from databases were verified with external clinical samples.

Risk Scores Are Significantly Different Between Patients with Different Clinical Characteristics

Based on a ratio of 3 to 1, we divided 217 ccRCC patients carrying wild-type VHL into a training set (163 cases) and a test

TABLE 1 | Univariate and multivariate cox regression analysis of survival-related lncRNAs, miRNAs, and mRNAs.

CeRNA	Impact	LogrankP	Univariate				Multivariate			
			Beta	HR	95% CI	*p* Value	Beta	HR	95% CI	*p* Value
LncRNA										
Linc00313	–	0.02	0.55	1.70	1.10–2.70	0.02	0.30	1.35	0.75–2.44	0.31
Linc00488	–	0.02	0.57	1.80	1.10–2.80	0.02	–0.01	0.99	0.57–1.73	0.97
CYP4F26P	–	0.04	0.48	1.60	1.00–2.60	0.04	–0.15	0.86	0.49–1.51	0.60
Linc00858	–	0.00	0.73	2.10	1.30–3.30	0.00	0.61	1.83	1.04–3.23	**0.04**
AC007682	–	0.01	0.65	1.90	1.20–3.00	0.01	–0.22	0.80	0.45–1.45	0.47
RP13-392I16.1	+	0.01	–0.64	0.52	0.32–0.86	0.01	–0.70	0.50	0.27–0.90	**0.02**
RP11-302F12.3	–	0.00	0.65	1.90	1.20–3.00	0.01	0.29	1.34	0.78–2.29	0.29
RP11-259O2.2	–	0.03	0.52	1.70	1.00–2.80	0.04	–0.10	0.90	0.48–1.69	0.75
Linc01016	–	0.00	0.70	2.00	1.20–3.30	0.00	0.34	1.41	0.77–2.58	0.27
Linc00942	–	0.00	0.96	2.60	1.60–4.30	0.00	0.74	2.09	1.09–4.01	**0.03**
CTD-2004A9.1	+	0.00	–0.71	0.49	0.31–0.79	0.00	0.13	1.14	0.60–2.17	0.69
RP11-96B2.1	–	0.00	0.68	2.00	1.20–3.10	0.00	0.06	1.06	0.58–1.94	0.85
RP11-619A14.3	–	0.03	0.52	1.70	1.10–2.70	0.03	–0.08	0.92	0.50–1.70	0.79
C8orf49	–	0.02	0.62	1.90	1.10–3.10	0.02	–0.01	0.99	0.55–1.77	0.96
AC144835	–	0.01	0.64	1.90	1.20–3.10	0.01	0.05	1.05	0.58–1.90	0.87
Linc00261	–	0.03	0.51	1.70	1.00–2.60	0.03	0.20	1.22	0.69–2.17	0.49
RP4-536B24.4	–	0.00	0.67	2.00	1.20–3.10	0.01	0.33	1.40	0.76–2.56	0.28
RP13-379O24.2	–	0.01	0.62	1.90	1.20–2.90	0.01	0.22	1.24	0.70–2.22	0.46
miRNA										
hsa-miR-182-5p	–	0.03	0.51	1.70	1.00–2.60	0.03	–1.31	0.27	0.12–0.63	**0.00**
hsa-miR-183-5p	–	0.00	1.10	2.90	1.70–4.80	0.00	1.52	4.58	1.97–10.62	**0.00**
hsa-miR-218-5p	–	0.03	0.52	1.70	1.10–2.70	0.03	0.41	1.51	0.79–2.89	0.21
hsa-miR-221-3p	–	0.00	1.00	2.80	1.70–4.50	0.00	0.65	1.91	0.99–3.69	0.05
mRNA										
RIMS4	–	0.01	1.90	1.90	1.20–3.10	0.01	0.11	1.12	0.63–1.98	0.70
PAX3	–	0.00	2.00	2.00	1.30–3.20	0.00	0.65	1.92	1.11–3.34	**0.02**
CREB3L1	–	0.02	1.70	1.70	1.10–2.70	0.02	–0.52	0.60	0.30–1.19	0.14

HR, hazard ratio; CI, confidence interval; lncRNAs, long non-coding RNAs; miRNAs, microRNAs; mRNAs, messenger RNAs; ceRNA, competing endogenous RNA. Values in bold are with p < 0.05.

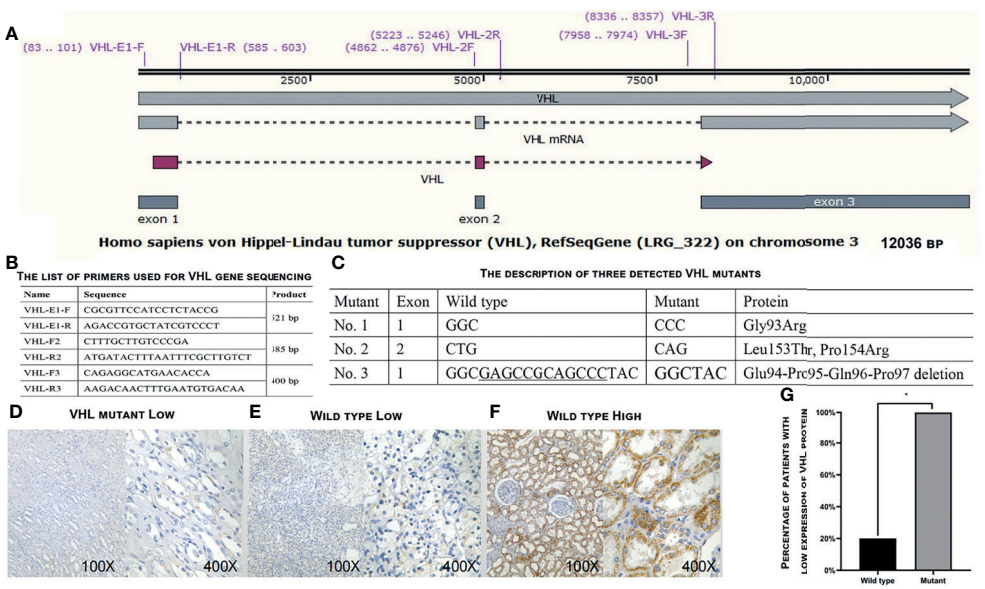

FIGURE 4 | Determination of VHL gene expression in the 21 patients. **(A)** A diagram showing the structure of VHL gene and positions of primers used for gene sequencing. **(B)** The list of primers used to sequence VHL gene. **(C)** The description of three detected VHL mutants. **(D–F)** Representative images showing the low expression levels of VHL protein in patients carrying mutant VHL **(D)** or wild-type VHL **(E)** and high expression levels of VHL protein in patients carrying wild-type VHL as detected by immunohistochemical staining in ccRCC patients enrolled in our hospital. **(G)** A plot showing the percentage of patients with low expression levels of VHL protein in patients carrying wild-type or mutant VHL gene. VHL, Von Hippel–Lindau; ccRCC, clear cell renal cell carcinoma. *p < 0.05.

A

The sequences of primer sets used to determine the expression levels of six RNAs

Gene	Product (bp)	Primer sequences
LINC00942	235	Forward：5'-TACAGCCACACAACCTGACT-3'
		Reverse：5'-CTCCGTGTAGCATTACCCCAA-3'
LINC00858	206	Forward：5'-AGTCCTTATAGTTACTGGCAT-3'
		Reverse：5'-CTTAAAGTGCCCACCTCC-3'
RP13_392I16.1	144	Forward：5'-CTGATGCCTCTTGACCCACA-3'
		Reverse：5'-ACTTTCTGCCTCTGATGTTGC-3'
hsa-miR-183-5p	112	Forward： 5'-CCTATGGCACTGGTAGAATTCACT-3'
		Reverse：5'- GGCCAACCGCGAGAAGATGTTTTTTTTT-3'
hsa-miR-182-5p	112	Forward: 5'-TTTGGCAATGGTAGAACTCACACT-3'
		Reverse：5'- GGCCAACCGCGAGAAGATGTTTTTTTTT-3'
PAX3	129	Forward：5'-GCCGTCAGTGAGTTCCATCA-3'
		Reverse：5'-ATGCCGTCGATGCTGTGTTT-3'
β-actin-ck	185	Forward：5'-AGCGAGCATCCCCCAAAGTT-3'
		Reverse：5'-GGGCACGAAGGCTCATCATT-3'
U6-F	112	Forward：5'-GCAAATTCGTGAAGCGTTCC-3'
		Reverse： 5'- GGCCAACCGCGAGAAGATGTTTTTTTTT-3'

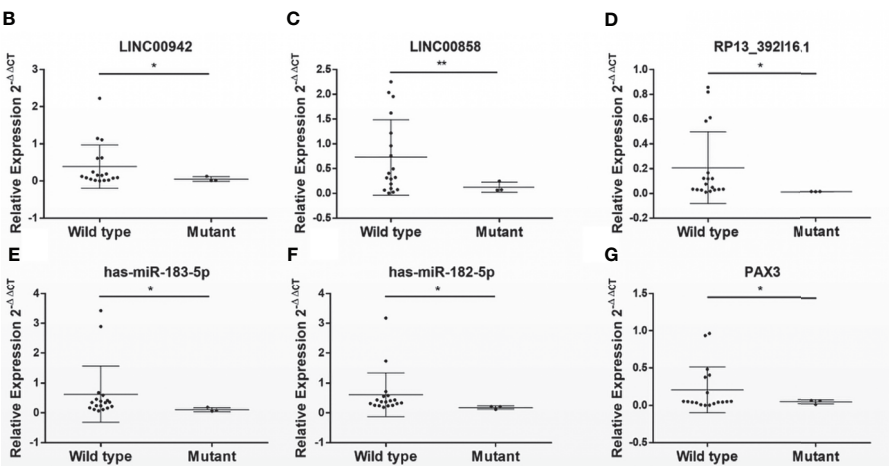

FIGURE 5 | The survival-related RNAs detected in databases are verified with external clinical samples. **(A–G)** A list of primers used to determine **(A)** and scatter diagrams showing **(B–G)** the expression levels of survival-related RNAs LINC00942 **(B)**, LINC00858 **(C)**, RP13.392I16.1 **(D)**, hsa-miR-183-5p, hsa-miR-182-5p **(F)**, and PAX3 **(G)** as detected by qRT-PCR in 21 clinical patients (wild-type n = 18 and mutant n = 3). *p < 0.05, *p < 0.01.

set (54 cases), attributed each patient in the training set with a risk score, and separated patients into a high-risk group (81 patients) and a low-risk group (82 patients) with the median of risk scores 1.77 as the threshold. Patients in the high-risk group exhibited significantly worse prognosis than those in the low-risk group in both training set and test set as well as in all patients (**Figure 6A–C**). Receiver operating characteristic (ROC) curve analysis detected an area under the curve (AUC) value of 0.79, 0.77, or 0.78 and further confirmed the results from survival analyses (**Figures 6D–F**). Patients carrying wild-type VHL had significantly higher risk scores than those carrying mutant VHL (**Figure 6G**). There was no significant difference in risk scores between different age groups, but patients at higher and advanced ccRCC classification stages exhibited significantly higher risk scores (**Table 2**).

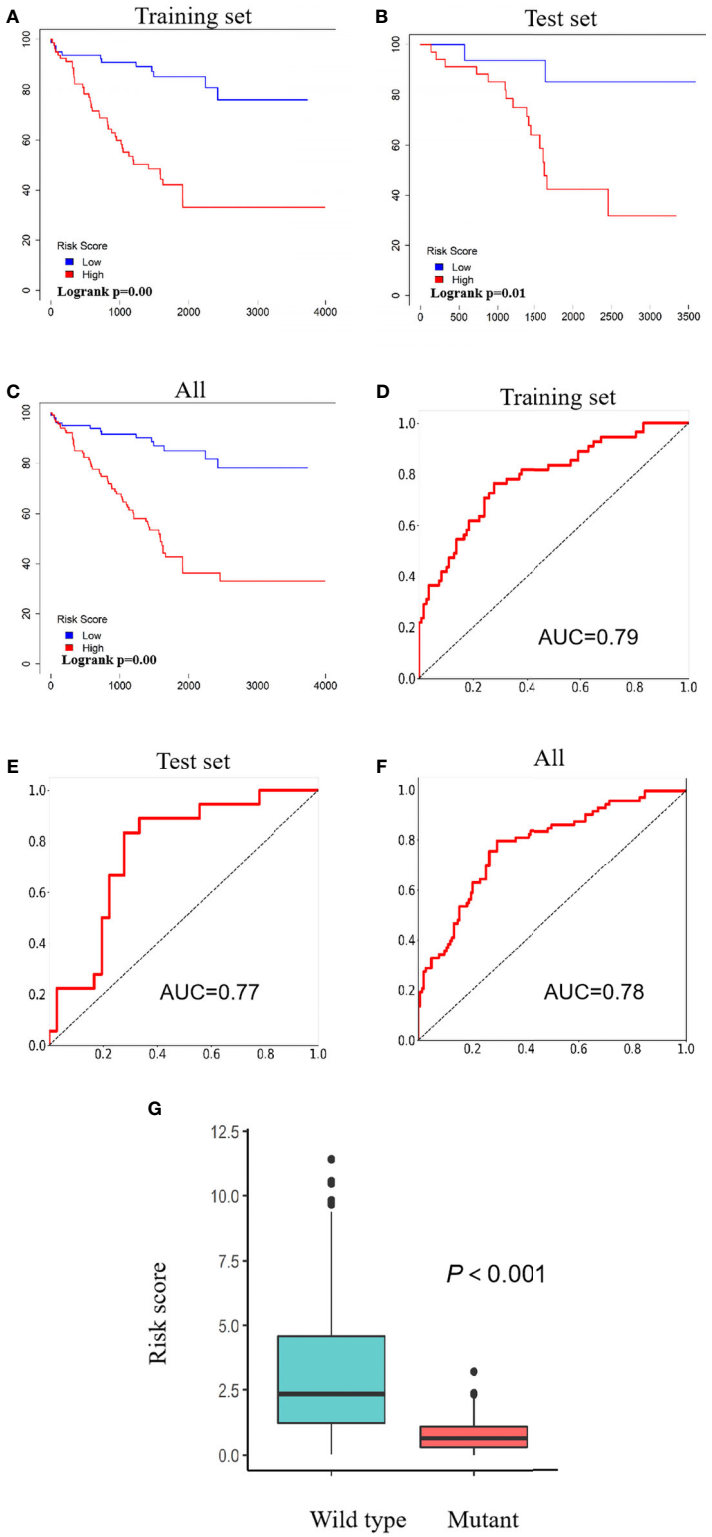

FIGURE 6 | Risk scores predict patients' survival. **(A–C)** Kaplan–Meier curves showing the relationship between risk scores and patients' survival in the training set **(A)**, test set **(B)**, and all patients **(C)**. **(D–F)** ROC curves showing AUC values of the training set **(D)**, test set **(E)**, and all patients **(F)**. **(G)** A scatter diagram showing differences of risk scores between patients carrying wild type and those carrying mutant VHL. ROC, receiver operating characteristic; AUC, area under the curve; VHL, Von Hippel–Lindau.

TABLE 2 | The analyses of correlation between risk scores and clinicopathological characteristics of patients in TCGA data set.

Clinical features	Case	Low risk	High risk	*p*	X ± S	*p*
Age						
<55	107	46	61		2.37 ± 2.91	
≥55	110	55	55	0.37	2.34 ± 3.02	0.94
Pathological T						
T1–T2	131	73	58		1.62 ± 2.61	
T2–T4	86	28	58	**0.00**	3.46 ± 3.13	**0.00**
Pathological M						
M0	179	91	88		2.03 ± 2.88	
M1	38	10	28	**0.01**	3.89 ± 2.88	**0.00**
Pathological N						
N0	105	56	49		1.98 ± 3.12	
N1	9	2	7	0.09	4.93 ± 3.94	**0.01**
Grade						
Grade 1–2	95	58	37		1.20 ± 2.33	
Grade 3–4	118	39	79	**0.00**	3.38 ± 3.07	**0.00**
Overall status						
Alive	144	87	57		1.35 ± 2.31	
Dead	73	14	59	**0.00**	4.33 ± 3.13	**0.00**
Neoplasm status						
Tumor free	128	75	53		1.49 ± 2.37	
With tumor	74	17	57	**0.00**	4.01 ± 3.08	**0.00**
Tumor stage						
I–II	120	70	50		1.43 ± 2.53	
III–IV	96	30	66	**0.00**	3.55 ± 3.04	**0.00**

TCGA, The Cancer Genome Atlas.
Values in bold are with p < 0.05.

Analysis of Signaling Pathway in Clear Cell Renal Cell Carcinoma Patients Carrying Wild-Type Von Hippel–Lindau and High Risk Scores

We conducted GSEA and identified 24 signaling pathways such as the "OLFACTORY_TRANSDUCTION" and "INTESTINAL _IMMUNE_NETWORK_FOR_IGA_PRODUCTION," which were enriched in the group of patients with high risk scores (**Table 3**).

DISCUSSION

A ceRNA network has been proposed to play important roles in ccRCC tumorigenesis and aggressiveness. Previous studies have revealed that the LINC01094 enhances the expression of miR-184 and inhibits the expression of SLC2A3, which suppresses the development of ccRCC (27). LINC01426 interacts with insulin-like growth factor 2 mRNA binding protein 1 (IGF2BP1) to enhance expression of CTBP1 in cytoplasm and promote the binding of CTBP1 to the promoter of miR-423-5p in the nucleus to recruit HDAC2 to synergistically inhibit the expression levels of miR-423-5p, leading to an elevation of expression levels of FOXM1 and a promotion of proliferation and migration of ccRCC cells (28). The ceRNA network constructed in this study yielded 98 DE-lncRNAs, 10 DE-miRNAs, and 14 DE-mRNAs. Analyses of the 14 DE-mRNAs revealed their involvement in functions related to kidney. Further analysis of the relationship of DE-RNAs in the ceRNA network with patients' survival rates led to the identification of LINC00942, LINC00858, RP13_392I16.1, hsa-miR-182-5p, hsa-miR-183-5p, and PAX3, which were used to calculate risk scores for each individual patient as independent factors to successfully predict the malignancy and prognosis of patients.

Three lncRNAs was identified to be survival-related ceRNAs. Currently, there is no report related to any role of RP13_392I16.1 yet, so this lncRNA needs to be further studied. LINC00942 was reported to promote METT14-mediated M6A methylation and regulate the expression and stability of its target gene CXCR4 and CYP1B1 during the initiation and progression of breast cancer (29). In another report, LINC00942 was identified as one of seven lncRNAs in an lncRNA signature related to immune cell infiltration and immune checkpoint blockade of immunotherapy-related molecules and may serve as a prognostic biomarker of hepatocellular carcinoma (30). Similarly, LINC00942 was identified as one of four immune-related lncRNAs to predict prognosis and immunotherapy efficiency in bladder cancer patients (31). It also reported that LINC00942 was identified as one of the two components in a ceRNA network associated with gene number copy variation, which can be used to predict tumor response to drug treatment in patients with lung adenocarcinomas (32). Initially, LINC00858 was identified as a ceRNA impacting miR-422a to control the expression of kallikrein-related peptidase 4, and its high expression was found to be closely correlated to tumor progression of non-small cell lung carcinomas (33). It was reported to be one of the four lncRNAs delivered from database search that were further validated with clinical samples (34) and able to promote colorectal cancer by sponging miR-4766-5p (35) or miR-22-3P (36). Literatures published recently revealed that LINC00858 was found

TABLE 3 | GSEA analysis of signaling pathways associated with patients with high risk scores.

Names of signaling pathways	NES	NOM *p*-Val	FDR *q*-Val
OLFACTORY_TRANSDUCTION	2.22	0.00	0.00
INTESTINAL_IMMUNE_NETWORK_FOR_IGA_PRODUCTION	2.12	0.00	0.00
P53_SIGNALING_PATHWAY	2.11	0.00	0.00
GLYCOSAMINOGLYCAN_BIOSYNTHESIS_CHONDROITIN_SULFATE	2.04	0.00	0.00
TASTE_TRANSDUCTION	2.00	0.00	0.00
CYTOKINE_CYTOKINE_RECEPTOR_INTERACTION	1.92	0.00	0.01
HOMOLOGOUS_RECOMBINATION	1.91	0.00	0.01
CELL_CYCLE	1.80	0.00	0.02
ECM_RECEPTOR_INTERACTION	1.76	0.00	0.02
DNA_REPLICATION	1.67	0.01	0.05
BASE_EXCISION_REPAIR	1.67	0.01	0.04
BASAL_CELL_CARCINOMA	1.62	0.01	0.06
SYSTEMIC_LUPUS_ERYTHEMATOSUS	1.61	0.01	0.06
HEMATOPOIETIC_CELL_LINEAGE	1.61	0.00	0.06
DILATED_CARDIOMYOPATHY	1.58	0.00	0.07
GLYCOSAMINOGLYCAN_DEGRADATION	1.56	0.03	0.08
HYPERTROPHIC_CARDIOMYOPATHY_HCM	1.54	0.01	0.09
HEDGEHOG_SIGNALING_PATHWAY	1.53	0.02	0.08
PATHOGENIC_ESCHERICHIA_COLI_INFECTION	1.52	0.02	0.09
NEUROACTIVE_LIGAND_RECEPTOR_INTERACTION	1.51	0.00	0.09
ARRHYTHMOGENIC_RIGHT_VENTRICULAR_CARDIOMYOPATHY_ARVC	1.48	0.02	0.10
PRIMARY_IMMUNODEFICIENCY	1.45	0.04	0.13
LEISHMANIA_INFECTION	1.45	0.03	0.12
JAK_STAT_SIGNALING_PATHWAY	1.34	0.03	0.23

GSEA takes NOM less than 0.05 and FDR q-val less than 0.25 to filter the results.
NES, normalized enrichment score; NOM p-val, credibility of the enrichment result; FDR q-val: p-value after multiple hypothesis correction; GSEA, Gene Set Enrichment Analysis; FDR, false discovery rate.

to play key roles in multiple types of cancers including Wilms' tumor (37), ovarian cancer (38), colon cancer (39), gastric cancer (40), hepatocellular carcinomas (41), and osteosarcomas (42).

Both hsa-miR-182-5p and hsa-miR-183-5p belong to the miR-183/96/182 family because of their sequence homology and function similarity (43). They were found to be among the 10 miRNA signatures that significantly distinguish cancer tissues from adjacent normal tissues from patients with ovarian cancer (44), the five miRNAs associated with tumorigenesis in lung adenocarcinomas (45), the top three miRNAs that target the largest number of genes in atypical endometrial hyperplasia (46), and the five miRNAs that show optimal diagnostic biomarkers for hepatocellular carcinomas (47). The levels of hsa-miR-182-5p are elevated in tumor tissues from patients with ovarian cancer and may predict poor prognosis (48). hsa-miR-182-5p was reported to be associated with resistance of breast cancer cell lines to anti-tumor drug veliparib (49). The significance of hsa-miR-183-5p with additional 10 genes in survival of ccRCC patients has been reported, and high expression of hsa-miR-183-5p predicts a reduced OS rate and poor prognosis (50). It was reported that hsa-miR-182-5p is reduced in renal cancer tissues and cell lines and regulates the expression of *DLL4* gene, which causes change of tumor microenvironment and tumor inhibition (51).

PAX3 gene (paired box gene 3) encodes a member of PAX family of transcription factors whose target genes impact proliferation, survival, differentiation, and motility (52). Rhabdomyosarcoma is one of the typical tumors in children and adolescence with a poor prognosis and an OS rate of only 20%–40% (53). PAX3-FOXO1 or PAX3-FKHR, a specific fusion gene that resulted from chromosomal translocation, is an important factor in the occurrence and development of rhabdomyosarcoma (54, 55). Such fusion gene was also reported to be associated with other types of cancers such as melanoma (56) and biphenotypic sinonasal sarcoma, a low-grade spindle cell sarcoma that affects middle-aged adults (57). PAX3 is highly expressed in prostate cancer tissues and cell lines and promotes the progression of prostate cancer by inhibiting the TGF-β/SMAD signal axis (58). Although there is no report about PAX3 in ccRCC, PAX3 gene is differentially hyper-methylated in chromophobe renal cell carcinomas compared with renal oncocytomas, a benign kidney neoplasm (59).

As discussed above, the relation between VHL mutation and patient survival is different in different reports. We identified LINC00942, LINC00858, RP13_392I16.1, hsa-miR-182-5p, hsa-miR-183-5p, and PAX3 as survival-related DE-RNAs between patients carrying wild-type or mutant VHL and were further used to calculate risk scores for each individual patient. The identified RNAs may not directly impact the VHL function. Because each of these DE-RNAs has already been shown to play significant roles in the tumorigenesis and aggressiveness of other types of cancers as discussed above, it is predicted that the risk scores may serve well as factors independent to VHL gene status to predict the malignancy and prognosis of ccRCC patients in the future.

DATA AVAILABILITY STATEMENT

The raw data supporting the conclusions of this article will be made available by the authors, without undue reservation.

ETHICS STATEMENT

The studies involving human participants were reviewed and approved by The Ethics Committee of The Fifth Affiliated Hospital of Guangzhou Medical University. The patients/participants provided their written informed consent to participate in this study.

AUTHOR CONTRIBUTIONS

RZ, XL, ZC, LL, and GX have full access to all of the data in the study, take responsibility for the integrity of the data and the accuracy of the data analysis, and wrote the manuscript. SL, YY, YX, DL, HZ, WY, and JB contributed the reagents. All authors contributed to the article and approved the submitted version.

FUNDING

This study is partially supported by the National Natural Science Foundation of China 81974392 and Natural Science Foundation of Guangdong Province 2018A030313087 to GX, the National Natural Science Foundation of China 82103359 to ZC, the Health Technology Project of Guangzhou City 20201A011106 and 20211A011103 to JB, and the National Natural Science Foundation of China 81772931 to LL.

REFERENCES

1. Clark DJ, Dhanasekaran SM, Petralia F, Pan J, Song X, Hu Y, et al. Integrated Proteogenomic Characterization of Clear Cell Renal Cell Carcinoma. *Cell* (2020) 180(1):207. doi: 10.1016/j.cell.2019.12.026
2. Ljungberg B, Campbell SC, Choi HY, Jacqmin D, Lee JE, Weikert S, et al. The Epidemiology of Renal Cell Carcinoma. *Eur Urol* (2011) 60(4):615–21. doi: 10.1016/j.eururo.2011.06.049
3. Bray F, Ferlay J, Soerjomataram I, Siegel RL, Torre LA, Jemal A. Global Cancer Statistics 2018: GLOBOCAN Estimates of Incidence and Mortality Worldwide for 36 Cancers in 185 Countries. *CA Cancer J Clin* (2018) 68 (6):394–424. doi: 10.3322/caac.21492
4. Jiang Z, Chu PG, Woda BA, Liu Q, Balaji KC, Rock KL, et al. Combination of Quantitative IMP3 and Tumor Stage: A New System to Predict Metastasis for Patients With Localized Renal Cell Carcinomas. *Clin Cancer Res* (2008) 14 (17):5579–84. doi: 10.1158/1078-0432.CCR-08-0504
5. Hsieh JJ, Purdue MP, Signoretti S, Swanton C, Albiges L, Schmidinger M, et al. Renal Cell Carcinoma. *Nat Rev Dis Primers* (2017) 3:17009. doi: 10.1038/nrdp.2017.9
6. Muglia VF, Prando A. Renal Cell Carcinoma: Histological Classification and Correlation With Imaging Findings. *Radiol Bras* (2015) 48(3):166–74. doi: 10.1590/0100-3984.2013.1927
7. Cancer Genome Atlas Research, N. Comprehensive Molecular Characterization of Clear Cell Renal Cell Carcinoma. *Nature* (2013) 499 (7456):43–9. doi: 10.1038/nature12222
8. Hsieh JJ, Chen D, Wang PI, Marker M, Redzematovic A, Chen YB, et al. Genomic Biomarkers of a Randomized Trial Comparing First-Line Everolimus and Sunitinib in Patients With Metastatic Renal Cell Carcinoma. *Eur Urol* (2017) 71(3):405–14. doi: 10.1016/j.eururo.2016.10.007
9. Haase VH. The VHL Tumor Suppressor in Development and Disease: Functional Studies in Mice by Conditional Gene Targeting. *Semin Cell Dev Biol* (2005) 16(4-5):564–74. doi: 10.1016/j.semcdb.2005.03.006
10. Leung JY, Kim WY. Bap1 and Pbrm1: Determinants of Tumor Grade and mTOR Activation in VHL-Deficient Mouse Models of Renal Cell Carcinoma. *Cancer Discovery* (2017) 7(8):802–4. doi: 10.1158/2159-8290.CD-17-0610
11. Kaelin WGJr. The Von Hippel-Lindau Tumor Suppressor Protein and Clear Cell Renal Carcinoma. *Clin Cancer Res* (2007) 13(2 Pt 2):680s–4s. doi: 10.1158/1078-0432.CCR-06-1865
12. Haase VH, Glickman JN, Socolovsky M, Jaenisch R. Vascular Tumors in Livers With Targeted Inactivation of the Von Hippel-Lindau Tumor Suppressor. *Proc Natl Acad Sci U.S.A.* (2001) 98(4):1583–8. doi: 10.1073/pnas.98.4.1583
13. Mandriota SJ, Turner KJ, Davies DR, Murray PG, Morgan NV, Sowter HM, et al. HIF Activation Identifies Early Lesions in VHL Kidneys: Evidence for Site-Specific Tumor Suppressor Function in the Nephron. *Cancer Cell* (2002) 1(5):459–68. doi: 10.1016/s1535-6108(02)00071-5
14. Hogner A, Krause H, Jandrig B, Kasim M, Fuller TF, Schostak M, et al. PBRM1 and VHL Expression Correlate in Human Clear Cell Renal Cell Carcinoma With Differential Association With Patient's Overall Survival. *Urol Oncol* (2018) 36(3):94 e1–94 e14. doi: 10.1016/j.urolonc.2017.10.027
15. Alves MR, Carneiro FC, Lavorato-Rocha AM, da Costa WH, da Cunha IW, de Cassio Zequi S, et al. Mutational Status of VHL Gene and its Clinical Importance in Renal Clear Cell Carcinoma. *Virchows Arch* (2014) 465 (3):321–30. doi: 10.1007/s00428-014-1629-z
16. Dagher J, Kammerer-Jacquet SF, Brunot A, Pladys A, Patard JJ, Bensalah K, et al. Wild-Type VHL Clear Cell Renal Cell Carcinomas Are a Distinct Clinical and Histologic Entity: A 10-Year Follow-Up. *Eur Urol Focus* (2016) 1 (3):284–90. doi: 10.1016/j.euf.2015.06.001
17. Herman JG, Latif F, Weng Y, Lerman MI, Zbar B, Liu S, et al. Silencing of the VHL Tumor-Suppressor Gene by DNA Methylation in Renal Carcinoma. *Proc Natl Acad Sci U.S.A.* (1994) 91(21):9700–4. doi: 10.1073/pnas.91.21.9700
18. Goodall GJ, Wickramasinghe VO. RNA in Cancer. *Nat Rev Cancer* (2021) 21 (1):22–36. doi: 10.1038/s41568-020-00306-0
19. Yuan JH, Yang F, Wang F, Ma JZ, Guo YJ, Tao QF, et al. A Long Noncoding RNA Activated by TGF-Beta Promotes the Invasion-Metastasis Cascade in Hepatocellular Carcinoma. *Cancer Cell* (2014) 25(5):666–81. doi: 10.1016/j.ccr.2014.03.010
20. Teng F, Zhang JX, Chen Y, Shen XD, Su C, Guo YJ, et al. LncRNA NKX2-1-AS1 Promotes Tumor Progression and Angiogenesis via Upregulation of SERPINE1 Expression and Activation of the VEGFR-2 Signaling Pathway in Gastric Cancer. *Mol Oncol* (2021) 15(4):1234–55. doi: 10.1002/1878-0261.12911
21. Wu C, Chen W, Yu F, Yuan Y, Chen Y, Hurst DR, et al. Long Noncoding RNA HITTERS Protects Oral Squamous Cell Carcinoma Cells From Endoplasmic Reticulum Stress-Induced Apoptosis via Promoting MRE11-RAD50-NBS1 Complex Formation. *Adv Sci (Weinh)* (2020) 7(22):2002747. doi: 10.1002/advs.202002747
22. Miao L, Liu HY, Zhou C, He X. LINC00612 Enhances the Proliferation and Invasion Ability of Bladder Cancer Cells as ceRNA by Sponging miR-590 to Elevate Expression of PHF14. *J Exp Clin Cancer Res* (2019) 38(1):143. doi: 10.1186/s13046-019-1149-4
23. Wu X, Xiao Y, Zhou Y, Zhou Z, Yan W. LncRNA FOXP4-AS1 is Activated by PAX5 and Promotes the Growth of Prostate Cancer by Sequestering miR-3184-5p to Upregulate FOXP4. *Cell Death Dis* (2019) 10(7):472. doi: 10.1038/s41419-019-1699-6
24. Yang W, Zhang K, Li L, Xu Y, Ma K, Xie H, et al. Downregulation of lncRNA ZNF582-AS1 Due to DNA Hypermethylation Promotes Clear Cell Renal Cell Carcinoma Growth and Metastasis by Regulating the N(6)-Methyladenosine Modification of MT-Rnr1. *J Exp Clin Cancer Res* (2021) 40(1):92. doi: 10.1186/s13046-021-01889-8
25. Gregory PA, Bert AG, Paterson EL, Barry SC, Tsykin A, Farshid G, et al. The miR-200 Family and miR-205 Regulate Epithelial to Mesenchymal Transition by Targeting ZEB1 and SIP1. *Nat Cell Biol* (2008) 10(5):593–601. doi: 10.1038/ncb1722
26. Salmena L, Poliseno L, Tay Y, Kats L, Pandolfi PP. A ceRNA Hypothesis: The Rosetta Stone of a Hidden RNA Language? *Cell* (2011) 146(3):353–8. doi: 10.1016/j.cell.2011.07.014
27. Jiang Y, Zhang H, Li W, Yan Y, Yao X, Gu W. FOXM1-Activated LINC01094 Promotes Clear Cell Renal Cell Carcinoma Development via MicroRNA 224-5p/CHSY1. *Mol Cell Biol* (2020) 40(3):e00357–19. doi: 10.1128/MCB.00357-19

28. Jiang Y, Zhang H, Li W, Yan Y, Yao X, Gu W. LINC01426 Contributes to Clear Cell Renal Cell Carcinoma Progression by Modulating CTBP1/miR-423-5p/FOXM1 Axis via Interacting With IGF2BP1. *J Cell Physiol* (2021) 236 (1):427–39. doi: 10.1002/jcp.29871
29. Sun T, Wu Z, Wang X, Wang Y, Hu X, Qin W, et al. LNC942 Promoting METTL14-Mediated M(6)A Methylation in Breast Cancer Cell Proliferation and Progression. *Oncogene* (2020) 39(31):5358–72. doi: 10.1038/s41388-020-1338-9
30. Xu Q, Wang Y, Huang W. Identification of Immune-Related lncRNA Signature for Predicting Immune Checkpoint Blockade and Prognosis in Hepatocellular Carcinoma. *Int Immunopharmacol* (2021) 92:107333. doi: 10.1016/j.intimp.2020.107333
31. Zhang L, Li L, Zhan Y, Wang J, Zhu Z, Zhang X. Identification of Immune-Related lncRNA Signature to Predict Prognosis and Immunotherapeutic Efficiency in Bladder Cancer. *Front Oncol* (2020) 10:542140. doi: 10.3389/fonc.2020.542140
32. Hu H, Xu H, Lu F, Zhang J, Xu L, Xu S, et al. Exploring the Effect of Differentially Expressed Long Non-Coding RNAs Driven by Copy Number Variation on Competing Endogenous RNA Network by Mining Lung Adenocarcinoma Data. *Front Cell Dev Biol* (2020) 8:627436. doi: 10.3389/fcell.2020.627436
33. Zhu SP, Wang JY, Wang XG, Zhao JP. Long Intergenic non-Protein Coding RNA 00858 Functions as a Competing Endogenous RNA for miR-422a to Facilitate the Cell Growth in non-Small Cell Lung Cancer. *Aging (Albany NY)* (2017) 9(2):475–86. doi: 10.18632/aging.101171
34. Yamada A, Yu P, Lin W, Okugawa Y, Boland CR, Goel A. A RNA-Sequencing Approach for the Identification of Novel Long non-Coding RNA Biomarkers in Colorectal Cancer. *Sci Rep* (2018) 8(1):575. doi: 10.1038/s41598-017-18407-6
35. Zhan W, Liao X, Chen Z, Li L, Tian T, Yu L, et al. LINC00858 Promotes Colorectal Cancer by Sponging miR-4766-5p to Regulate PAK2. *Cell Biol Toxicol* (2020) 36(4):333–47. doi: 10.1007/s10565-019-09506-3
36. Sha QK, Chen L, Xi JZ, Song H. Long non-Coding RNA LINC00858 Promotes Cells Proliferation, Migration and Invasion by Acting as a ceRNA of miR-22-3p in Colorectal Cancer. *Artif Cells Nanomed Biotechnol* (2019) 47(1):1057–66. doi: 10.1080/21691401.2018.1544143
37. Zhou D, Wang J, Xu S, Li Z, Kou D. LINC00858 Facilitates the Malignant Development of Wilms' Tumor by Targeting miR-653-5p. *Minerva Med* (2020). doi: 10.23736/S0026-4806.20.06566-0
38. Xue H, Wu Z, Rao D, Zhuo B, Chen Q. Long non-Coding RNA LINC00858 Aggravates the Oncogenic Phenotypes of Ovarian Cancer Cells Through miR-134-5p/RAD18 Signaling. *Arch Gynecol Obstet* (2020) 302(5):1243–54. doi: 10.1007/s00404-020-05722-z
39. Xu T, Wu K, Zhang L, Zheng S, Wang X, Zuo H, et al. Long non-Coding RNA LINC00858 Exerts a Tumor-Promoting Role in Colon Cancer via HNF4alpha and WNK2 Regulation. *Cell Oncol (Dordr)* (2020) 43(2):297–310. doi: 10.1007/s13402-019-00490-8
40. Qin L, Yao F, Yu H, Xu Y, Jin Y, Dong W. Up-Regulated lncRNA LINC00858 Facilitates Proliferation and Migration of Gastric Cancer Cells. *Pol J Pathol* (2020) 71(3):236–43. doi: 10.5114/pjp.2020.99790
41. Qi WY, Mao XB, He YB, Xiao CH. Long non-Coding RNA LINC00858 Promotes Cells Proliferation and Invasion Through the miR-153-3p/Rabl3 Axis in Hepatocellular Carcinoma. *Eur Rev Med Pharmacol Sci* (2020) 24 (18):9343–52. doi: 10.26355/eurrev_202009_23017
42. Gu Z, Hou Z, Zheng L, Wang X, Wu L, Zhang C. Long Noncoding RNA LINC00858 Promotes Osteosarcoma Through Regulating miR-139-CDK14 Axis. *Biochem Biophys Res Commun* (2018) 503(2):1134–40. doi: 10.1016/j.bbrc.2018.06.131
43. Dambal S, Shah M, Mihelich B, Nonn L. The microRNA-183 Cluster: The Family That Plays Together Stays Together. *Nucleic Acids Res* (2015) 43 (15):7173–88. doi: 10.1093/nar/gkv703
44. Wang L, Zhu MJ, Ren AM, Wu HF, Han WM, Tan RY, et al. A ten-microRNA Signature Identified From a Genome-Wide microRNA Expression Profiling in Human Epithelial Ovarian Cancer. *PloS One* (2014) 9(5):e96472. doi: 10.1371/journal.pone.0096472
45. Hsu YL, Hung JY, Lee YL, Chen FW, Chang KF, Chang WA, et al. Identification of Novel Gene Expression Signature in Lung Adenocarcinoma by Using Next-Generation Sequencing Data and Bioinformatics Analysis. *Oncotarget* (2017) 8 (62):104831–54. doi: 10.18632/oncotarget.21022
46. Tang S, Dai Y. RNA Sequencing Reveals Significant miRNAs in Atypical Endometrial Hyperplasia. *Eur J Obstet Gynecol Reprod Biol* (2018) 225:129–35. doi: 10.1016/j.ejogrb.2018.03.025
47. Zhao X, Dou J, Cao J, Wang Y, Gao Q, Zeng Q, et al. Uncovering the Potential Differentially Expressed miRNAs as Diagnostic Biomarkers for Hepatocellular Carcinoma Based on Machine Learning in The Cancer Genome Atlas Database. *Oncol Rep* (2020) 43(6):1771–84. doi: 10.3892/or.2020.7551
48. Li Y, Li L. Prognostic Values and Prospective Pathway Signaling of MicroRNA-182 in Ovarian Cancer: A Study Based on Gene Expression Omnibus (GEO) and Bioinformatics Analysis. *J Ovarian Res* (2019) 12 (1):106. doi: 10.1186/s13048-019-0580-7
49. Uhr K, Prager-van der Smissen WJC, Heine AAJ, Ozturk B, van Jaarsveld MTM, Boersma AWM, et al. MicroRNAs as Possible Indicators of Drug Sensitivity in Breast Cancer Cell Lines. *PloS One* (2019) 14(5):e0216400. doi: 10.1371/journal.pone.0216400
50. Qin S, Shi X, Wang C, Jin P, Ma F. Transcription Factor and miRNA Interplays Can Manifest the Survival of ccRCC Patients. *Cancers (Basel)* (2019) 11(11):1668. doi: 10.3390/cancers11111668
51. Wang W, Hu W, Wang Y, An Y, Song L, Shang P, et al. Long non-Coding RNA UCA1 Promotes Malignant Phenotypes of Renal Cancer Cells by Modulating the miR-182-5p/DLL4 Axis as a ceRNA. *Mol Cancer* (2020) 19 (1):18. doi: 10.1186/s12943-020-1132-x
52. Boudjadi S, Chatterjee B, Sun W, Vemu P, Barr FG. The Expression and Function of PAX3 in Development and Disease. *Gene* (2018) 666:145–57. doi: 10.1016/j.gene.2018.04.087
53. Sultan I, Qaddoumi I, Yaser S, Rodriguez-Galindo C, Ferrari A. Comparing Adult and Pediatric Rhabdomyosarcoma in the Surveillance, Epidemiology and End Results Program, 1973 to 2005: An Analysis of 2,600 Patients. *J Clin Oncol* (2009) 27(20):3391–7. doi: 10.1200/JCO.2008.19.7483
54. Pappo AS, Shapiro DN, Crist WM, Maurer HM. Biology and Therapy of Pediatric Rhabdomyosarcoma. *J Clin Oncol* (1995) 13(8):2123–39. doi: 10.1200/JCO.1995.13.8.2123
55. Crose LE, Galindo KA, Kephart JG, Chen C, Fitamant J, Bardeesy N, et al. Alveolar Rhabdomyosarcoma-Associated PAX3-FOXO1 Promotes Tumorigenesis via Hippo Pathway Suppression. *J Clin Invest* (2014) 124(1):285–96. doi: 10.1172/JCI67087
56. Medic S, Ziman M. PAX3 Across the Spectrum: From Melanoblast to Melanoma. *Crit Rev Biochem Mol Biol* (2009) 44(2-3):85–97. doi: 10.1080/10409230902755056
57. Wong WJ, Lauria A, Hornick JL, Xiao S, Fletcher JA, Marino-Enriquez A. Alternate PAX3-FOXO1 Oncogenic Fusion in Biphenotypic Sinonasal Sarcoma. *Genes Chromosomes Cancer* (2016) 55(1):25–9. doi: 10.1002/gcc.22295
58. Zeng K, Xie W, Huang J, Yang J, Deng K, Luo X. PAX3 Silencing Inhibits Prostate Cancer Progression Through the Suppression of the TGF-Beta/Smad Signaling Axis. *Cell Biol Int* (2020) 44(10):2131–9. doi: 10.1002/cbin.11421
59. Slater AA, Alokail M, Gentle D, Yao M, Kovacs G, Maher ER, et al. DNA Methylation Profiling Distinguishes Histological Subtypes of Renal Cell Carcinoma. *Epigenetics* (2013) 8(3):252–67. doi: 10.4161/epi.23817

Conflict of Interest: The authors declare that the research was conducted in the absence of any commercial or financial relationships that could be construed as a potential conflict of interest.

Publisher's Note: All claims expressed in this article are solely those of the authors and do not necessarily represent those of their affiliated organizations, or those of the publisher, the editors and the reviewers. Any product that may be evaluated in this article, or claim that may be made by its manufacturer, is not guaranteed or endorsed by the publisher.

Copyright © 2021 Zhu, Li, Cai, Liang, Yuan, Xu, Lai, Zhao, Yang, Bian, Liu and Xu. This is an open-access article distributed under the terms of the Creative Commons Attribution License (CC BY). The use, distribution or reproduction in other forums is permitted, provided the original author(s) and the copyright owner(s) are credited and that the original publication in this journal is cited, in accordance with accepted academic practice. No use, distribution or reproduction is permitted which does not comply with these terms.

frontiers in Oncology

ORIGINAL RESEARCH
published: 19 November 2021
doi: 10.3389/fonc.2021.772182

Prostate Health Index Density Outperforms Prostate Health Index in Clinically Significant Prostate Cancer Detection

Shih-Ting Chiu[1], Yung-Ting Cheng[2], Yeong-Shiau Pu[1], Yu-Chuan Lu[1], Jian-Hua Hong[1], Shiu-Dong Chung[3,4], Chih-Hung Chiang[1,5,6] and Chao-Yuan Huang[1*]*

[1] Department of Urology, National Taiwan University Hospital, Taipei, Taiwan, [2] Department of Urology, National Taiwan University Hospital Hsin-Chu Branch, Hsinchu, Taiwan, [3] Division of Urology, Department of Surgery, Far-Eastern Memorial Hospital, New Taipei City, Taiwan, [4] Graduate Program in Biomedical Informatics, College of Informatics, Yuan-Ze University, Chung-Li, Taiwan, [5] Department of Urology, Taipei Veterans General Hospital, Yuan-Shan/Su-Ao Branch, Yi-Lan, Taiwan, [6] Department of Medical Research and Education, Taipei Veterans General Hospital, Yuan-Shan/Su-Ao Branch, Yi-Lan, Taiwan

OPEN ACCESS

Edited by:
Marco Borghesi, University of Genoa, Italy

Reviewed by:
Daniela Terracciano, University of Naples Federico II, Italy
Francesco Del Giudice, Sapienza University of Rome, Italy

****Correspondence:***
Chih-Hung Chiang
guchiang@gmail.com
Chao-Yuan Huang
cyh540909@gmail.com

Specialty section:
This article was submitted to Genitourinary Oncology, a section of the journal Frontiers in Oncology

Received: *07 September 2021*
Accepted: *29 October 2021*
Published: *19 November 2021*

Citation:
Chiu S-T, Cheng Y-T, Pu Y-S, Lu Y-C, Hong J-H, Chung S-D, Chiang C-H and Huang C-Y (2021) Prostate Health Index Density Outperforms Prostate Health Index in Clinically Significant Prostate Cancer Detection. Front. Oncol. 11:772182. doi: 10.3389/fonc.2021.772182

Background: Prostate-specific antigen (PSA) is considered neither sensitive nor specific for prostate cancer (PCa). We aimed to compare total PSA (tPSA), percentage of free PSA (%fPSA), the PSA density (PSAD), Prostate Health Index (PHI), and the PHI density (PHID) to see which one could best predict clinically significant prostate cancer (csPCa): a potentially lethal disease.

Methods: A total of 412 men with PSA of 2–20 ng/mL were prospectively included. Serum biomarkers for PCa was collected before transrectal ultrasound guided prostate biopsy. PHI was calculated by the formula: (p2PSA/fPSA) x √tPSA. PHID was calculated as PHI divided by prostate volume measured by transrectal ultrasound.

Results: Of the 412 men, 134 (32.5%) and 94(22.8%) were diagnosed with PCa and csPCa, respectively. We used the area under the receiver operating characteristic curve (AUC) and decision curve analyses (DCA) to compare the performance of PSA related parameters, PHI and PHID in diagnosing csPCa. AUC for tPSA, %fPSA, %p2PSA, PSAD, PHI and PHID were 0.56、0.63、0.76、0.74、0.77 and 0.82 respectively for csPCa detection. In the univariate analysis, the prostate volume, tPSA, %fPSA, %p2PSA, PHI, PSAD, and PHID were all significantly associated with csPCa, and PHID was the most important predictor (OR 1.41, 95% CI 1.15–1.72). Besides, The AUC of PHID was significantly larger than PHI in csPCa diagnosis (p=0.004). At 90% sensitivity, PHID had the highest specificity (54.1%) for csPCa and could reduce the most unnecessary biopsies (43.7%) and miss the fewest csPCa (8.5%) when PHID ≥ 0.67. In addition to AUC, DCA re-confirmed the clinical benefit of PHID over all PSA-related parameters and PHI in csPCa diagnosis. The PHID cut-off value was positively correlated with the csPCa ratio in the PHID risk table, which is useful for evaluating csPCa risk in a clinical setting.

Conclusion: The PHID is an excellent predictor of csPCa. The PHID risk table may be used in standard clinical practice to pre-select men at the highest risk of harboring csPCa.

Keywords: prostate health index density, risk table, clinically significant prostate cancer, save unnecessary prostate biopsy, predict lethal disease

INTRODUCTION

Prostate cancer (PCa) is one of the most common malignancies in both Western and Asian countries. The introduction of the prostate-specific antigen (PSA) test in 1987 is one of the reasons for the growing incidence of PCa. Produced by prostate epithelial cells, PSA is regarded as an organ-specific rather than a disease-specific marker. The correlation between PSA and benign prostate hyperplasia, prostate inflammation, and PCa makes it a marker with broad clinical utility; however, it is a complex tool in terms of confirming the cancer diagnosis, with a 60%–70% false positive rate (1–3).

About 2% of patients have post-biopsy complications, such as infection, bleeding, or voiding difficulty (3). Moreover, overdiagnosis of low-risk tumors possibly leads to overtreatment and the possibility of subsequent harm (4). Thus, when to perform a prostate biopsy should be individualized and well discussed.

Prostate Health Index (PHI), a novel PCa screening alternative, is calculated with total PSA (tPSA), free PSA (fPSA), and [-2]pro-PSA (p2PSA) using the following formula: (p2PSA/fPSA) x √tPSA. PHI is proved to be better at predicting the presence of PCa and its aggressiveness than tPSA, fPSA, and PSA density (PSAD) in multiple studies in both Western and Asian countries (5–9). Current guidelines suggest considering PHI testing before prostate biopsy to increase specificity and to avoid unnecessary biopsy (10).

In recent years, PHI density (PHID) has been a focus of research for its clinical utility. One prospective study of 118 men in Western society receiving prostate biopsy showed PHID is associated with clinically significant prostate cancer (csPCa) and outperformed PHI in the area under the receiver operating characteristic curve (AUC) analysis (11). PHID is found to predict cancer aggressiveness in post-radical prostatectomy pathologies, such as high-grade cancer or extracapsular prostatic invasion (12). CsPCa [defined as a Gleason score (GS) of 6 with ≥3 positive cores and/or a maximum core participation of ≥50%, or GS ≥7 as the Epstein criteria (13)] is a potentially lethal disease that requires early diagnosis and active treatment. However, very few studies discuss the role of PHID in detecting csPCa, or how many unnecessary prostate biopsies could be avoided with PHID. Thus, this study aims to evaluate the performance PHID in csPCa detection.

MATERIAL AND METHODS

Study Population

This single-center prospective study was conducted in line with National Taiwan University Hospital guidelines. The study was approved by the institutional review board at the National Taiwan University Hospital (approval code: 201612091RIPD), and informed consent was obtained from all individual participants included in the study. Initially, 542 consecutive men undergoing prostate biopsy for suspected PCa were enrolled in the study. Inclusion criteria were as follows, adult patients with a total PSA between 2 and 20 ng/ml or abnormal digital rectal examination (DRE), who received transrectal ultrasound guided prostate (TRUS-P) biopsy for at least systemic 12 cores at one single tertiary center between February 2017 and January 2020. Patients underwent TRUS-P biopsy with a standardized protocol for at least 12 biopsy cores (range: 12-22). Additional finger-guided biopsy was decided by the physicians if palpable prostate nodules.

Exclusion criteria were as follows: 1) patients with untreated urinary tract infection or bacterial acute prostatitis; 2) patients who had transurethral resection of the prostate previously; 3) patients with prior history of prostate cancer; 4) patients who were treated with 5-alpha reductase inhibitors, such as finasteride or dutasteride. A total number of 412 patients with written informed consent were included in the final analysis.

Laboratory Analysis

After obtaining informed consent, blood samples were collected in ethylenediaminetetraacetic acid tubes before prostate biopsy and stored at -80°C after centrifugation. Serum samples were centrifuged at 1500 g for 15 min within 3 h of blood collection and stored at -20°C until analysis. The tPSA, fPSA, and p2PSA levels were analyzed with a Beckman Coulter Access 2 immunoassay analyzer (Beckman Coulter, Taiwan Inc.) with Beckman Coulter Access Hybritech reagent. The technology of chemiluminescent immunoenzymatic with Hybrithech PSA standardization was used. PHI was calculated according to the formula: PHI = (p2PSA/fPSA) x √tPSA. %fPSA was defined as (fPSA/tPSA) x 100; and %p2PSA was defined as [(p2PSA pg/mL)/(fPSA ng/mL x 1000)] x 100. Prostate volume was estimated with transrectal ultrasound with the standard ellipsoid formula: width x height x length x 0.52. PSA density (PSAD) was calculated with (tPSA/prostate volume), and PHI density (PHID) was calculated with (PHI/prostate volume).

Biopsy specimens were graded according to the updated Gleason grading system of the International Society of Urological Pathology (14). The specimens were examined by experienced genitourinary pathologists, who were blinded to the serum test results. csPCa Epstein criteria was defined as a Gleason score ≥7, or a Gleason score of 6 but with ≥3 positive cores and/or a maximum core involvement of ≥50% (13).

Study End Points

The primary end point was to evaluate the sensitivity, specificity, diagnostic accuracy, and clinical benefit of %fPSA, PSAD, %p2PSA, PHI and PHID (index tests) in determining the

presence of PCa and csPCa at prostate biopsy in comparison to tPSA (standard tests).

Statistical Analysis

The primary outcome was csPCa found on biopsy. Continuous variables were reported as median and interquartile range (IQR). Statistical differences were assessed with Mann–Whitney U test for continuous variables and Chi-square test for categorical variables. Univariable logistic regression was used to determine the association between measured covariates and prostate cancer and clinically significant prostate cancer. The area under the receiver operating characteristic curve (AUC) was used to examine the diagnostic ability of each PSA derivative. Difference between AUCs were evaluated with DeLong test. Decision curve analysis (DCA) was applied to compare different diagnostic strategies with regards to maximizing clinical net benefit at different threshold probability (15). Statistical analyses were performed with SPSS version 22.0 (IBM Corp, Inc) and R software. A two-sided p value of <0.05 was considered significant.

RESULTS

Of the 412 men included, 134 (32.5%) were diagnosed with PCa and 57 (42.5%) had a GS of 6 PCa. 94 of 412 men (22.8%) were diagnosed with csPCa, of which 77 (81.9%) were GS ≥7 and the rest 17 men (18.1%) had a GS of 6 fulfilling the Epstein criteria. (**Table 1**). In the baseline characteristics, men with csPCa were significantly older, had a higher proportion of abnormal DRE, and a smaller prostate volume than the non-csPCa group. As regards biomarkers, the tPSA level was similar between the two groups, while men with csPCa had a significantly lower %fPSA, and higher %p2PSA, PHI, PSAD, and PHID.

The univariable logistic regression (**Table 2**) showed that age, abnormal DRE, and prostate volume were significant predictors for both PCa and csPCa. However, tPSA failed to demonstrate significance in predicting PCa (OR 1.04, P=0.129) but was a predictor for csPCa (OR 1.09, P=0.005). Contrarily, biomarkers such as %fPSA, %p2PSA, PHI, PSAD, and PHID were all significantly associated with both PCa and csPCa. The prostate volume factor plus PSA-related serum markers demonstrated that PSAD and PHID were the most important predictors of PCa (OR 1.42, 95% CI 1.21–1.67, and OR 2.27, 95% CI 1.73–2.97, respectively) and csPCa (OR 1.24, 95% CI 1.07–1.44, and OR 1.41, 95% CI 1.15–1.72, respectively).

AUC was used to examine the ability of each diagnostic marker to indicate PCa (**Figure 1A**) and csPCa (**Figure 1B**). The predictors of PCa and csPCa in order from the worst to the best are as follows: tPSA (AUC= 0.53 and 0.56), %fPSA (AUC= 0.59 and 0.63), PSAD (AUC= 0.68 and 0.74), %p2PSA (AUC= 0.72 and 0.76), PHI (AUC= 0.72 and 0.77), and PHID (AUC= 0.77 and 0.82). The AUC of PHID was still significantly better than PHI in PCa or csPCa diagnosis (p=0.007 and 0.004, respectively). Among the tested biomarkers, PHID showed the highest discriminative ability for PCa and csPCa.

With a 90% sensitivity for detecting csPCa, PHID had the highest specificity at 54.1%, while tPSA only demonstrated a specificity of 17.9% (**Table 3**). At the cut-off value of ≥0.67 for PHID, it could reduce the most unnecessary biopsies (43.7%) and missed the least cases of csPCa (8.5%). On the other hand, at the given cut-off values with tPSA of ≥4.43 ng/mL, %fPSA ≤0.26, %p2PSA ≥1.12, PHI ≥31.0, and PSAD ≥0.11 ng/mL/cc, the avoidable biopsy percentages were 15.5%, 14.8%, 32.8%, 37.4% and 26.9% respectively. In summary, PHID is the best marker for csPCa in all PSA-related parameters.

DCA is an analytic method for comparing different diagnostic strategies with regards to maximizing clinical net benefit against different given threshold probability. DCA curves for different biopsy scenarios indicated by various PSA-related parameters, PHI and PHID were plotted in **Figure 2**. The models of each biomarker for csPCa diagnosis were listed in the order from the most net benefit to the least as follows: PHID, PHI, %p2PSA, PSAD, %fPSA and tPSA at probability threshold range 20% to

TABLE 1 | Characteristics of the study cohort.

	Overall (N = 412) (100%)		Benign (N = 278) (67.5%)		PCa (N = 134) (32.5%)		P value (*vs* benign)	csPCa (N = 94) (22.8%)		P value (*vs* non-csPCa)
Age, years	66	(60,71)	64	(58,69)	68	(63,74)	<0.001	68	(63,74)	<0.001
Abnormal DRE, n (%)	75	(18.2%)	33	(11.97%)	42	(31.34%)	<0.001	31	(32.9%)	<0.001
Prostate volume, ml	45	(34,61)	49	(38,67)	36	(27,47)	0.406	33	(25,43)	<0.001
Total PSA, ng/mL	7.2	(5.2,9.7)	7.2	(5.2,9.4)	7.4	(5.1,10)	0.002	7.7	(5.5,11.4)	0.064
%fPSA	16.6	(11.7,22.4)	17.6	(12.8,23.2)	14.3	(10.7,20.4)	<0.001	13.9	(10.1,19.1)	<0.001
%p2PSA	1.36	(1.01,1.81)	1.18	(0.94,1.57)	1.64	(1.36,2.16)	<0.001	1.73	(1.41,2.29)	<0.001
PHI	35.9	(25.8,47.9)	31.4	(24.6,42.2)	44.7	(34.5,58.6)	<0.001	47.8	(38.3,65.5)	<0.001
PSA density	0.15	(0.11,0.22)	0.14	(0.1,0.19)	0.20	(0.13,0.34)	<0.001	0.22	(0.15,0.39)	<0.001
PHI density	0.74	(0.48,1.32)	0.62	(0.41,0.95)	1.31	(0.78,2.01)	<0.001	1.49	(1.0,2.21)	<0.001
Gleason score, n(%) 3+3					57*	(42.5)		17	(18.1)	
3+4					39	(29.1)		39	(41.5)	
4+3					25	(18.7)		25	(26.6)	
8					6	(4.5)		6	(6.4)	
9					7	(5.2)		7	(7.4)	

PCa, prostate cancer; cs, clinically significant; DRE, digital rectal examination; PSA, prostate-specific antigen; %fPSA, percentage of free to total PSA; %p2PSA, percentage of p2PSA to free PSA ratio; PHI, Prostate Health Index; Data are median [interquartile range (IQR)] unless otherwise indicated.

**40 patients demonstrated insignificant PCa, and 17 patients demonstrated csPCa, according to the Epstein criteria.*

TABLE 2 | Univariable logistic regression models for the prediction of PCa and csPCa.

Variable	PCa		csPCa	
	Odds ratio (95%CI)	*P* value	Odds ratio (95%CI)	*P* value
Age	1.07 (1.04, 1.1)	<0.001	1.07 (1.04, 1.1)	<0.001
Abnormal DRE	3.39 (2.02, 5.67)	<0.001	3.06 (1.8,5.23)	<0.001
Prostate volume	0.96 (0.95, 0.97)	<0.001	0.94 (0.93,0.96)	<0.001
Total PSA	1.04 (0.99, 1.1)	0.129	1.09 (1.03-1.16)	0.005
%fPSA*	0.96 (0.93, 0.99)	0.004	0.94 (0.91,0.97)	<0.001
%p2PSA*	1.01 (1.01, 1.02)	<0.001	1.01 (1.01, 1.02)	<0.001
PHI	1.04 (1.03, 1.06)	<0.001	1.05 (1.03-1.06)	<0.001
PSA density†	1.42 (1.21, 1.67)	<0.001	1.24 (1.07,1.44)	0.005
PHI density	2.27 (1.73, 2.97)	<0.001	1.41 (1.15,1.72)	0.001

*PCa, prostate cancer; cs, clinically significant; DRE, digital rectal examination; PSA, prostate specific antigen; %fPSA, percentage of free to total PSA; %p2PSA, percentage of p2PSA to free PSA ratio; PHI, Prostate Health Index; CI, confidence interval; *per unit change of 1 percent; †per unit change of 0.1.*

30% (**Figure 2B**). As for the diagnosis of PCa (**Figure 2A**), there was an order almost similar to that of csPCa. Consistently with the AUC results, PHID had the most improvement in clinical net benefit at initiating biopsy for both PCa and csPCa.

In addition, a risk table was made to evaluate the positive chances of PCa, csPCa and high-grade PCa (GS ≥7) under different PHID values (**Table 4**). We found the PHID cut-off value was positively correlated with the PCa, csPCa, and HGPCa ratio. For the PHID cut-off value of 0.5–0.75, the risks of PCa, csPCa, and HGPCa were 17.2%, 10.1%, and 7.1%, respectively. If an individual had a PHID value of 1–1.5, it was assumed that they had about a one-third chance of having csPCa; if the PHID value was over 1.5, they had a nearly 50% chance of having csPCa. In summary, the PHID risk table may be used in standard clinical practice to pre-select men at the highest risk of harboring csPCa.

DISCUSSION

In our prospective cohort, we compared the performance of tPSA, %fPSA, %p2PSA, PSAD, PHI, and PHID in terms of predicting csPCa without missing the diagnosis. We found PHID was the best predictor of csPCa and could greatly reduce the number of unnecessary biopsies. We also found that the PHID cut-off value was positively correlated with the ratio of csPCa. We could further evaluate the patient's csPCa risks based on this PHID risk table to decide whether to arrange a prostate biopsy. In our understanding, this is the first time a PHID risk table to evaluate the csPCa risk has been established.

PSA is neither sensitive nor specific in csPCa prediction, leading to many unnecessary biopsies and indolent cancer detected (1–3). There are several proteomic and genomic tools being studied to better diagnose csPCa, including PHI, 4K score and Stockholm3 as blood tests, and Mi-prostate score, Exo DX Prostate, and Select MD-X as urinary biomarker-based tests (16). Besides, liquid biopsy using circulating tumor cells (CTC) play an emerging and promising role in genitourinary oncology (17, 18). CTC may act as tools for pre-diagnosis screening, post-diagnosis risk stratification, and treatment response evaluation in PCa (19, 20).

There is no denying that multiparametric magnetic resonance imaging (mpMRI) is the best tool for predicting csPCa (21–23), but mpMRI may not be the case in terms of cost-effectiveness. We try to make a trade-off between diagnostic accuracy and cost-effectiveness among these tests and examinations. In previous

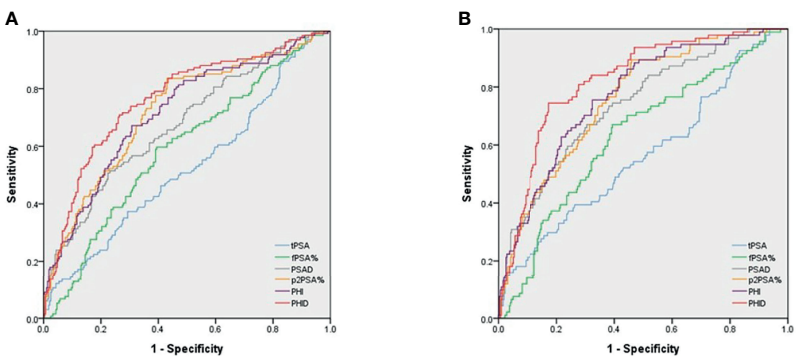

FIGURE 1 | Area under the receiver operating characteristic (AUC) curves for predicting **(A)** PCa and **(B)** csPCa. **(A)** AUC for PCa detection were as follows: PSA 0.53, %fPSA 0.59, PSAD0.68, %p2PSA 0.72, PHI 0.72 and PHID 0.77, respectively. **(B)** AUC for csPCa detection were as follows: PSA 0.56, %fPSA 0.63, PSAD 0.74, %p2PSA 0.76, PHI 0.77 and PHID 0.82, respectively. The AUC diagnostic effect of PHID is still significantly better than PHI in PCa or csPCa (p = 0.007 and 0.004, respectively).

TABLE 3 | Specificity, reduction of unnecessary biopsy, and missing positive cases at 90% sensitivity at predicting csPCa.

Biomarkers	Cut-off value	Specificity (%)	Avoidable biopsies (% of all biopsies, N = 412)		Missed biopsies (% of csPCa, N = 94)	
Total PSA	≥4.43	17.9%	64	(15.5%)	9	(9.6%)
%fPSA	≤0.26	16.7%	61	(14.8%)	10	(10.6%)
%p2PSA	≥1.12	39.9%	135	(32.8%)	9	(9.6%)
PHI	≥31.0	45.3%	154	(37.4%)	10	(10.6%)
PSA density	≥0.11	31.8%	111	(26.9%)	10	(10.6%)
PHI density	≥0.67	54.1%	180	(43.7%)	8	(8.5%)

csPCa, clinically significant prostate cancer; PSA, prostate specific antigen; %fPSA, percentage of free to total PSA; %p2PSA, percentage of p2PSA to free PSA ratio; PHI, Prostate Health Index.

study, mpMRI could indeed provide higher diagnostic accuracy in identifying csPCa than PHI (23). However, there are high rates of interobserver disagreements in reading prostate MRIs between different radiologists (24). mpMRI is also a resource-intensive and time-consuming examination. The costs of a prostate MRI are estimated to be €300–€500 in Europe and $700–$3000 in regions outside of Europe (25). In terms of cost-effectiveness, Kim et al. suggest that PHI as a triaging test may be an effective way to reduce mpMRI and biopsies without compromising the detection of csPCa (26). The cost-effectiveness of PHI testing is explored in both Western and Eastern world. The PHI-based strategy is more cost-effective than the PSA-based strategy for PCa regardless of what willingness-to-pay threshold by reducing biopsy costs and biopsy-related adverse events (27–30). The results may be applied not only in developed regions but also in developing countries (31).

To make up for the shortcomings of the low specificity and low sensitivity of PSA, PHI was developed. The first prospective PCa screening study in 2010 found PHI and %p2PSA (AUC= 0.77 and 0.76) could distinguish PCa from benign diseases more accurately than tPSA (AUC= 0.50) (32). Afterwards, many studies (5–8, 33–36) and our previous study (9) found that using PHI would detect PCa more accurately than tPSA, avoiding a considerable degree of unnecessary prostate biopsies. More importantly, PHI has shown promise in being able to differentiate csPCa more accurately from clinically insignificant PCa than tPSA, improving PCa cancer death rates and reducing unnecessary overdiagnoses and overtreatment of insignificant PCa (37). Furthermore, Fossati et al. (38) and our previous study (39) found that PHI can significantly improve the prediction of unfavorable PCa characteristics, larger tumor volume, and csPCa at final radical prostatectomy pathology (40).

PHI shows an excellent ability to accurately diagnose csPCa in different races. Our previous study (7) shows that for PSA 2–10 ng/ml, when we set the PHI threshold to 35, the PCa positive rate of Europeans and Asians can be increased from 52.1% and 13.1% to 66.6% and 29.4%, respectively. More importantly, in both Europeans and Asians, we can diagnose GS≥7 PCa more accurately, which increased from 28.8% and 8.1% to 40.2% and 21.5%, respectively. PHI (cut-off 35) can help avoid 32.6% and 71.1% of unnecessary biopsies in Europeans and Asians. In summary, although the PHI threshold of different races should be adjusted, the excellent diagnostic ability of PHI is the same.

Larger prostate volume is associated with increased PSA levels (41). Benson et al. first demonstrated that PSAD helped differentiate between benign prostate hypertrophy and PCa in PSA levels 4–20 ng/mL (42). Numerous following studies had similar results of the PSAD superiority over PSA in detecting PCa and adverse pathology (43–46). Similar to the conclusions of other articles, we found that PSAD was one of the top predictors

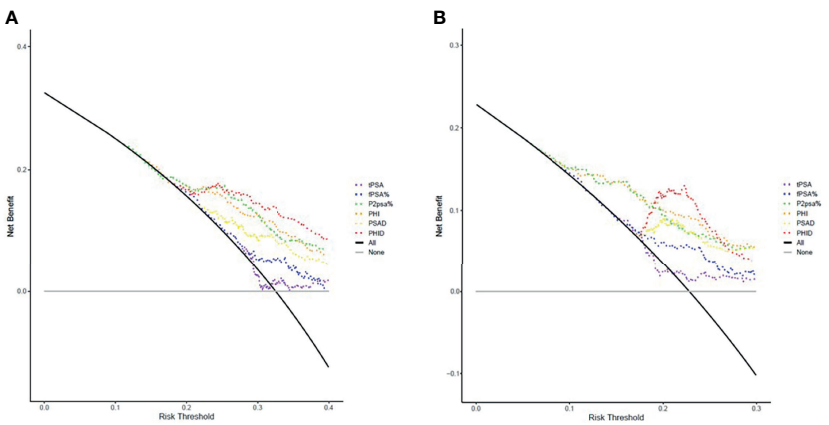

FIGURE 2 | Decision curve analysis (DCA) of various models on **(A)** PCa detection and **(B)** csPCa detection in comparison to biopsy-all (black curve line) and biopsy-none strategies (grey horizontal line). The markers of the best clinical benefit in the diagnosis of PCa and csPCa are list in order as follows: PHID, PHI, %p2PSA, PSAD, %fPSA and tPSA. Model of PHID (red dotted line) resulted in greater net benefit in overall PCa and csPCa detection at probability threshold range 20% to 30%.

TABLE 4 | Percentage of PCa, csPCa, and high-grade PCa (HGPCa) diagnosed at different PHI density values.

	PHI density cut-off value					Total
	<0.5	0.5-0.75	0.75-1	1-1.5	>1.5	
PCa	12.8% (14/109)	17.2% (17/99)	30.9% (17/55)	48.5% (32/66)	65.1% (54/83)	32.5% (134/412)
csPCa	3.7% (4/109)	10.1% (10/99)	16.4% (9/55)	37.9% (25/66)	55.4% (46/83)	22.8% (94/412)
HGPCa (GS≥7)	2.8% (3/109)	7.1% (7/99)	12.7% (7/55)	28.8% (19/66)	49.4% (41/83)	18.7% (77/412)

PHI, Prostate Health Index; PCa, prostate cancer; cs, clinically significant; HG, high-grade; GS, Gleason score.

of csPCa. PSAD also improved the diagnostic accuracy in patients with Prostate Imaging Reporting & Data System (PI-RADS) score ≤3 lesions in MRI, and the combination of PSAD and MRI was advocated to individualize prostate biopsy strategy (47–49).

Prostate volume is an important factor for csPCa and should be added to PSA-related factors to improve PCa detection. Filella et al. found PHI to be associated with prostate volume. The AUCs of PHI in patients with small, medium, and large prostate volumes were 0.818, 0.716, and 0.654, respectively, suggesting that a larger prostate size would decrease PHI diagnostic ability (50). Recently, studies have found that PHID is more significantly related to csPCa than other PSA-related parameters. In a prospective study by Tosoian et al., which consisted of 118 men with PSA>2 ng/mL and negative DRE, the median PHID value was 0.70 in the negative biopsy group, 0.53 in the clinically insignificant PCa group, and 1.21 in the csPCa group (p< 0.001). A higher PHID value is also significantly associated with more csPCa (3.6%, 36.7%, and 80.0% csPCa in PHID <0.43, 0.43–1.21, and >1.21, respectively, p<0.001). PHID was found to have the highest discriminative ability to detect csPCa (AUC 0.84) as compared to PSA, PSAD, %fPSA, and PHI. Moreover, PHID could be used to avoid 38% of unnecessary biopsies, while failing to detect only 2% of csPCa cases (11). Likewise, Barisiene et al. demonstrated that PHID best detected csPCa (AUC 0.80) and could help avoid 30% of prostate biopsies (51). Schulze et al. showed that PHID had a better performance in predicting PCa than PHI, PSAD, %fPSA, and tPSA. Only one csPCa case would have been missed in 50 csPCa cases (sensitivity 98%), and 20% of prostate biopsies could have been avoided with a combined use of PHID >0.9 and PHI >40 (52). Garrido et al. found PHID had the highest AUC in predicting overall PCa and csPCa (AUC 0.82 and 0.85, respectively) but there were no significant differences between the AUCs of PHID and PHI or between PHID and PSAD (53). A large retrospective cohort study demonstrated that PHID had similar AUC as PHI and had a small advantage on decision curve analysis than PHI alone in predicting overall PCa (54). Stephan et al. found PHID had significantly larger AUC than PHI in predicting overall PCa but no significant difference from PHI if aiming for csPCa (55). In our study, the AUC of PHID is significantly better than PHI in predicting csPCa (p=0.004, **Figure 1B**). Our study concluded that PHID is the best predictor of PCa and csPCa among various PSA-related biomarkers consistently both with AUC analysis and DCA.

The optimal PHID cut-off value was still not determined in as a result of the scarcity of the related studies. Tosoian et al. proposed a cut-off value 0.43 to detect Epstein significant disease with a 97.9% sensitivity and a 38.0% specificity (11). Barisiene et al. suggested a cut-off value of 0.61 to detect Epstein significant PCa at a 90% sensitivity, which had a resemblance to our PHID cut-off of 0.67 (51). Garrido et al. proposed PHID ≥ 0.49 as cut-off for csPCa, sparing 26.3% biopsies at 90% sensitivity (53). Besides, in men with initial negative prostate biopsy, those with initial PHID≥ 1.2 may have 21% risk developing csPCa at 6-year follow up, while those with PHID <0.4 had lowest risk and may not need intensive follow-up, depicted in a recent study by Liu et al. (56). In our study, at 90% sensitivity, PHID had the highest specificity (54.1%) for csPCa and could reduce the most unnecessary biopsies (43.7%) and miss the least csPCa (8.5%) when PHID > 0.67 (**Table 3**). We constructed a comprehensive table consisting of different PHID ranges and the corresponding risk for both PCa and csPCa (**Table 4**); for instance, the median PHID was 0.62 (0.41–0.95), 1.31 (0.78–2.01), and 1.49(1.0–2.21) in men with negative biopsy, PCa, and csPCa (p<0.001). The risk values for csPCa were 3.7%, 20.0%, and 55.4% for PHID <0.50, 0.5–1.5, and >1.50, respectively. We can avoid 43.7% of unnecessary biopsies and only miss 8.5% of csPCa cases for PHID > 0.67. The PHID and PHID risk tables may be used in standard clinical practice to pre-select men at a higher risk of harboring csPCa.

Association of different PCa biomarkers with mpMRI findings is another interesting topic worth researching. The combination of biomarkers and mpMRI may result in more clinical benefit than PSA plus mpMRI, especially in those who had equivocal PI-RADS scores (49, 57, 58). Druskin et al. recommended that prostate biopsy be performed in patients with PI-RADS ≥3 lesions in MRI or PHID ≥ 0.44 if PI-RADS score ≤2; this was 100% sensitive for csPCa detection (59). Similarly, in patients with at least one PI-RADS≥ 3 lesion in MRI, PHID added the greatest diagnostic value when fusion targeted biopsy methods were performed (60). We believe that the incorporation of PHID and MRI findings is a promising avenue and warrants further larger scale studies.

Our study had several limitations. First, the study cohort was heterogenous with biopsy-naïve subjects and those with biopsy histories. This may have confounded the results, as less PCa was detected in those who had prior biopsies. Secondly, the sample size of our study was relatively small. The PHID results and PHID risk table for csPCa need further external verification by other studies focused on different ethnicities. Third, mpMRI was not routinely performed in our entire cohort. We are incorporating PHI and mpMRI data from our cohort database. Further study results will be analyzed when more subjects are enrolled in the coming future.

CONCLUSIONS

In our prospective cohort, we found that PHID had the best performance, could reduce the most unnecessary biopsies, and missed the fewest csPCa cases. The PHID cut-off value is positively correlated with the csPCa ratio in the PHID risk table. In conclusion, the PHID has excellent ability to predict csPCa before biopsy. The PHID risk table may be used in standard clinical practice to pre-select men at a higher risk of harboring csPCa.

DATA AVAILABILITY STATEMENT

The original contributions presented in the study are included in the article/supplementary material. Further inquiries can be directed to the corresponding authors.

ETHICS STATEMENT

The studies involving human participants were reviewed and approved by National Taiwan University Hospital (approval code: 201612091RIPD). The patients/participants provided their written informed consent to participate in this study. Written informed consent was obtained from the individual(s) for the publication of any potentially identifiable images or data included in this article.

AUTHOR CONTRIBUTIONS

Study design and conceptualization: C-YH, C-HC, Y-TC. Data collection: Y-TC and S-TC. Formal analysis: Y-CL, J-HH, and S-DC. Writing—original draft preparation: Y-TC and S-TC. Writing—review and editing: Y-SP, C-YH, and C-HC. All authors contributed to the article and approved the submitted version.

ACKNOWLEDGMENTS

We thank C-YH, Chung-Hsin Chen, J-HH, Y-SP, Shih-Ping Liu, Y-CL, Yi-Kai Chang, Hong-Chiang Chang, Kuo-How Huang, Yuan-Ju Lee, Po-Ming Chow, I-Ni Chiang, Shih-Chun Hung and Shuo-Meng Wang for providing clinical data for analysis. We thank the research assistants I-Ting Teng and Pei-Yu Hsu for blood specimen collection and analysis. Beckman Coulter, Inc. provided the PHI testing kit.

REFERENCES

1. Martin RM, Donovan JL, Turner EL, Metcalfe C, Young GJ, Walsh EI, et al. Effect of a Low-Intensity PSA-Based Screening Intervention on Prostate Cancer Mortality: The CAP Randomized Clinical Trial. *JAMA* (2018) 319 (9):883–95. doi: 10.1001/jama.2018.0154
2. Schröder FH, Hugosson J, Roobol MJ, Tammela TLJ, Zappa M, Nelen V, et al. Screening and Prostate Cancer Mortality: Results of the European Randomised Study of Screening for Prostate Cancer (ERSPC) at 13 Years of Follow-Up. *Lancet* (2014) 384(9959):2027–35. doi: 10.1016/S0140-6736 (14)60525-0
3. Pinsky PF, Parnes HL, Andriole G. Mortality and Complications After Prostate Biopsy in the Prostate, Lung, Colorectal and Ovarian Cancer Screening (PLCO) Trial. *BJU Int* (2014) 113(2):254–9. doi: 10.1111/bju.12368
4. Loeb S, Bjurlin MA, Nicholson J, Tammela TL, Penson DF, Carter HB, et al. Overdiagnosis and Overtreatment of Prostate Cancer. *Eur Urol* (2014) 65 (6):1046–55. doi: 10.1016/j.eururo.2013.12.062
5. Yu G-P, Na R, Ye D-W, Qi J, Liu F, Chen H-T, et al. Performance of the Prostate Health Index in Predicting Prostate Biopsy Outcomes Among Men With a Negative Digital Rectal Examination and Transrectal Ultrasonography. *Asian J Androl* (2016) 18(4):633–8. doi: 10.4103/1008-682X.172823
6. Sriplakich S, Lojanapiwat B, Chongruksut W, Phuriyaphan S, Kitirattakarn P, Jun-Ou J, et al. Prospective Performance of the Prostate Health Index in Prostate Cancer Detection in the First Prostate Biopsy of Men With a Total Prostatic Specific Antigen of 4-10 Ng/mL and Negative Digital Rectal Examination. *Prostate Int* (2018) 6(4):136–9. doi: 10.1016/j.prnil.2018.02.002
7. Chiu PK, Ng CF, Semjonow A, Zhu Y, Vincendeau S, Houlgatte A, et al. A Multicentre Evaluation of the Role of the Prostate Health Index (PHI) in Regions With Differing Prevalence of Prostate Cancer: Adjustment of PHI Reference Ranges Is Needed for European and Asian Settings. *Eur Urol* (2019) 75(4):558–61. doi: 10.1016/j.eururo.2018.10.047
8. Loeb S, Sanda MG, Broyles DL, Shin SS, Bangma CH, Wei JT, et al. The Prostate Health Index Selectively Identifies Clinically Significant Prostate Cancer. *J Urol* (2015) 193(4):1163–9. doi: 10.1016/j.juro.2014.10.121
9. Cheng YT, Chiang CH, Pu YS, Liu SP, Lu YC, Chang YK, et al. The Application of P2psa% and Prostate Health Index in Prostate Cancer Detection: A Prospective Cohort in a Tertiary Medical Center. *J Formosan Med Assoc Taiwan Yi Zhi* (2019) 118(1 Pt 2):260–7. doi: 10.1016/j.jfma.2018.05.001
10. Carroll PH, Mohler JL. NCCN Guidelines Updates: Prostate Cancer and Prostate Cancer Early Detection. *J Natl Compr Canc Netw* (2018) 16(5s):620–3. doi: 10.6004/jnccn.2018.0036
11. Tosoian JJ, Druskin SC, Andreas D, Mullane P, Chappidi M, Joo S, et al. Prostate Health Index Density Improves Detection of Clinically Significant Prostate Cancer. *BJU Int* (2017) 120(6):793–8. doi: 10.1111/bju.13762
12. Huang Y-P, Lin T-P, Cheng W-M, Wei T-C, Huang I-S, Fan Y-H, et al. Prostate Health Index Density Predicts Aggressive Pathological Outcomes After Radical Prostatectomy in Taiwanese Patients. *J Chin Med Assoc* (2019) 82(11):835–9. doi: 10.1097/JCMA.0000000000000169
13. Epstein JI, Walsh PC, Carmichael M, Brendler CB. Pathologic and Clinical Findings to Predict Tumor Extent of Nonpalpable (Stage T1c) Prostate Cancer. *JAMA* (1994) 271(5):368–74. doi: 10.1001/jama.1994.03510290050036
14. Epstein JI, Allsbrook WC Jr, Amin MB, Egevad LL. The 2005 International Society of Urological Pathology (ISUP) Consensus Conference on Gleason Grading of Prostatic Carcinoma. *Am J Surg Pathol* (2005) 29(9):1228–42. doi: 10.1097/01.pas.0000173646.99337.b1
15. Vickers AJ, Elkin EB. Decision Curve Analysis: A Novel Method for Evaluating Prediction Models. *Med Decis Making* (2006) 26(6):565–74. doi: 10.1177/0272989X06295361
16. Ferro M, De Cobelli O, Lucarelli G, Porreca A, Busetto GM, Cantiello F, et al. Beyond PSA: The Role of Prostate Health Index (Phi). *Int J Mol Sci* (2020) 21 (4):1184. doi: 10.3390/ijms21041184
17. Cimadamore A, Aurilio G, Nolé F, Massari F, Scarpelli M, Santoni M, et al. Update on Circulating Tumor Cells in Genitourinary Tumors With Focus on Prostate Cancer. *Cells* (2020) 9(6):1495. doi: 10.3390/cells9061495
18. Nicolazzo C, Busetto GM, Gradilone A, Sperduti I, Del Giudice F, Loreni F, et al. Circulating Tumor Cells Identify Patients With Super-High-Risk Non-Muscle-Invasive Bladder Cancer: Updated Outcome Analysis of a Prospective Single-Center Trial. *Oncologist* (2019) 24(5):612–6. doi: 10.1634/theoncologist.2018-0784
19. Xu L, Mao X, Grey A, Scandura G, Guo T, Burke E, et al. Noninvasive Detection of Clinically Significant Prostate Cancer Using Circulating Tumor Cells. *J Urol* (2020) 203(1):73–82. doi: 10.1097/JU.0000000000000475

20. Rangel-Pozzo A, Liu S, Wajnberg G, Wang X, Ouellette RJ, Hicks GG, et al. Genomic Analysis of Localized High-Risk Prostate Cancer Circulating Tumor Cells at the Single-Cell Level. *Cells* (2020) 9(8):1863. doi: 10.3390/cells9081863
21. Eklund M, Jäderling F, Discacciati A, Bergman M, Annerstedt M, Aly M, et al. MRI-Targeted or Standard Biopsy in Prostate Cancer Screening. *N Engl J Med* (2021) 385(10):908–20. doi: 10.1016/S0302-2838(21)01388-9
22. van der Leest M, Cornel E, Israël B, Hendriks R, Padhani AR, Hoogenboom M, et al. Head-To-Head Comparison of Transrectal Ultrasound-Guided Prostate Biopsy Versus Multiparametric Prostate Resonance Imaging With Subsequent Magnetic Resonance-Guided Biopsy in Biopsy-Naïve Men With Elevated Prostate-Specific Antigen: A Large Prospective Multicenter Clinical Study. *Eur Urol* (2019) 75(4):570–8. doi: 10.1016/j.eururo.2018.11.023
23. Porpiglia F, Russo F, Manfredi M, Mele F, Fiori C, Bollito E, et al. The Roles of Multiparametric Magnetic Resonance Imaging, PCA3 and Prostate Health Index-Which Is the Best Predictor of Prostate Cancer After a Negative Biopsy? *J Urol* (2014) 192(1):60–6. doi: 10.1016/j.juro.2014.01.030
24. Rosenzweig B, Laitman Y, Zilberman DE, Raz O, Ramon J, Dotan ZA, et al. Effects of "Real Life" Prostate MRI Inter-Observer Variability on Total Needle Samples and Indication for Biopsy. *Urol Oncol* (2020) 38(10):793.e13–.e18. doi: 10.1016/j.urolonc.2020.03.015
25. Osses DF, Roobol MJ, Schoots IG. Prediction Medicine: Biomarkers, Risk Calculators and Magnetic Resonance Imaging as Risk Stratification Tools in Prostate Cancer Diagnosis. *Int J Mol Sci* (2019) 20(7):1637. doi: 10.3390/ijms20071637
26. Kim L, Boxall N, George A, Burling K, Acher P, Aning J, et al. Clinical Utility and Cost Modelling of the Phi Test to Triage Referrals Into Image-Based Diagnostic Services for Suspected Prostate Cancer: The PRIM (Phi to RefIne Mri) Study. *BMC Med* (2020) 18(1):95. doi: 10.1186/s12916-020-01548-3
27. Teoh JY, Leung CH, Wang MH, Chiu PK, Yee CH, Ng CF, et al. The Cost-Effectiveness of Prostate Health Index for Prostate Cancer Detection in Chinese Men. *Prostate Cancer Prostatic Dis* (2020) 23(4):615–21. doi: 10.1038/s41391-020-0243-1
28. Heijnsdijk EA, Denham D, de Koning HJ. The Cost-Effectiveness of Prostate Cancer Detection With the Use of Prostate Health Index. *Value Health* (2016) 19(2):153–7. doi: 10.1016/j.jval.2015.12.002
29. Bouttell J, Teoh J, Chiu PK, Chan KS, Ng CF, Heggie R, et al. Economic Evaluation of the Introduction of the Prostate Health Index as a Rule-Out Test to Avoid Unnecessary Biopsies in Men With Prostate Specific Antigen Levels of 4-10 in Hong Kong. *PLoS One* (2019) 14(4):e0215279. doi: 10.1371/journal.pone.0215279
30. Nichol MB, Wu J, Huang J, Denham D, Frencher SK, Jacobsen SJ. Cost-Effectiveness of Prostate Health Index for Prostate Cancer Detection. *BJU Int* (2012) 110(3):353–62. doi: 10.1111/j.1464-410X.2011.10751.x
31. Huang D, Yang X, Wu Y, Lin X, Xu D, Na R, et al. Cost-Effectiveness Analysis of Prostate Health Index in Decision Making for Initial Prostate Biopsy. *Front Oncol* (2020) 10:565382. doi: 10.3389/fonc.2020.565382
32. Le BV, Griffin CR, Loeb S, Carvalhal GF, Kan D, Baumann NA, et al. [-2] Proenzyme Prostate Specific Antigen Is More Accurate Than Total and Free Prostate Specific Antigen in Differentiating Prostate Cancer From Benign Disease in a Prospective Prostate Cancer Screening Study. *J Urol* (2010) 183 (4):1355–9. doi: 10.1016/j.juro.2009.12.056
33. Jansen FH, van Schaik RH, Kurstjens J, Horninger W, Klocker H, Bektic J, et al. Prostate-Specific Antigen (PSA) Isoform P2psa in Combination With Total PSA and Free PSA Improves Diagnostic Accuracy in Prostate Cancer Detection. *Eur Urol* (2010) 57(6):921–7. doi: 10.1016/j.eururo.2010.02.003
34. Guazzoni G, Nava L, Lazzeri M, Scattoni V, Lughezzani G, Maccagnano C, et al. Prostate-Specific Antigen (PSA) Isoform P2psa Significantly Improves the Prediction of Prostate Cancer at Initial Extended Prostate Biopsies in Patients With Total PSA Between 2.0 and 10 Ng/Ml: Results of a Prospective Study in a Clinical Setting. *Eur Urol* (2011) 60(2):214–22. doi: 10.1016/j.eururo.2011.03.052
35. Lazzeri M, Haese A, de la Taille A, Palou Redorta J, McNicholas T, Lughezzani G, et al. Serum Isoform [-2]proPSA Derivatives Significantly Improve Prediction of Prostate Cancer at Initial Biopsy in a Total PSA Range of 2-10 Ng/Ml: A Multicentric European Study. *Eur Urol* (2013) 63(6):986–94. doi: 10.1016/j.eururo.2013.01.011
36. Lughezzani G, Lazzeri M, Haese A, McNicholas T, de la Taille A, Buffi NM, et al. Multicenter European External Validation of a Prostate Health Index-Based Nomogram for Predicting Prostate Cancer at Extended Biopsy. *Eur Urol* (2014) 66(5):906–12. doi: 10.1016/j.eururo.2013.12.005
37. Tosoian JJ, Druskin SC, Andreas D, Mullane P, Chappidi M, Joo S, et al. Use of the Prostate Health Index for Detection of Prostate Cancer: Results From a Large Academic Practice. *Prostate Cancer Prostatic Dis* (2017) 20(2):228–33. doi: 10.1038/pcan.2016.72
38. Fossati N, Buffi NM, Haese A, Stephan C, Larcher A, McNicholas T, et al. Preoperative Prostate-Specific Antigen Isoform P2psa and Its Derivatives, % P2psa and Prostate Health Index, Predict Pathologic Outcomes in Patients Undergoing Radical Prostatectomy for Prostate Cancer: Results From a Multicentric European Prospective Study. *Eur Urol* (2015) 68(1):132–8. doi: 10.1016/j.eururo.2014.07.034
39. Cheng YT, Huang CY, Chen CH, Chiu ST, Hong JH, Pu YS, et al. Preoperative %P2psa and Prostate Health Index Predict Pathological Outcomes in Patients With Prostate Cancer Undergoing Radical Prostatectomy. *Sci Rep* (2020) 10 (1):776. doi: 10.1038/s41598-020-57618-2
40. Friedersdorff F, Groß B, Maxeiner A, Jung K, Miller K, Stephan C, et al. Does the Prostate Health Index Depend on Tumor Volume?-A Study on 196 Patients After Radical Prostatectomy. *Int J Mol Sci* (2017) 18(3):488. doi: 10.3390/ijms18030488
41. Pinsky PF, Kramer BS, Crawford ED, Grubb RL, Urban DA, Andriole GL, et al. Prostate Volume and Prostate-Specific Antigen Levels in Men Enrolled in a Large Screening Trial. *Urology* (2006) 68(2):352–6. doi: 10.1016/j.urology.2006.02.026
42. Benson MC, McMahon DJ, Cooner WH, Olsson CA. An Algorithm for Prostate Cancer Detection in a Patient Population Using Prostate-Specific Antigen and Prostate-Specific Antigen Density. *World J Urol* (1993) 11 (4):206–13. doi: 10.1007/BF00185070
43. Wolff JM, Scholz A, Boeckmann W, Jakse G. Differentiation of Benign Prostatic Hyperplasia and Prostate Cancer Employing Prostatic-Specific Antigen Density. *Eur Urol* (1994) 25(4):295–8. discussion 304. doi: 10.1159/000475304
44. Stephan C, Stroebel G, Heinau M, Lenz A, Roemer A, Lein M, et al. The Ratio of Prostate-Specific Antigen (PSA) to Prostate Volume (PSA Density) as a Parameter to Improve the Detection of Prostate Carcinoma in PSA Values in the Range of < 4 Ng/Ml. *Cancer* (2005) 104(5):993–1003. doi: 10.1002/cncr.21267
45. Elliott CS, Shinghal R, Presti JCJr. The Performance of Prostate Specific Antigen, Prostate Specific Antigen Density and Transition Zone Density in the Era of Extended Biopsy Schemes. *J Urol* (2008) 179(5):1756–61. discussion 61. doi: 10.1016/j.juro.2008.01.033
46. Omri N, Kamil M, Alexander K, Alexander K, Edmond S, Ariel Z, et al. Association Between PSA Density and Pathologically Significant Prostate Cancer: The Impact of Prostate Volume. *Prostate* (2020) 80(16):1444–9. doi: 10.1002/pros.24078
47. Knaapila J, Jambor I, Perez IM, Ettala O, Taimen P, Verho J, et al. Prebiopsy IMPROD Biparametric Magnetic Resonance Imaging Combined With Prostate-Specific Antigen Density in the Diagnosis of Prostate Cancer: An External Validation Study. *Eur Urol Oncol* (2020) 3(5):648–56. doi: 10.1016/j.euo.2019.08.008
48. Boesen L, Nørgaard N, Løgager V, Balslev I, Bisbjerg R, Thestrup KC, et al. Prebiopsy Biparametric Magnetic Resonance Imaging Combined With Prostate-Specific Antigen Density in Detecting and Ruling Out Gleason 7-10 Prostate Cancer in Biopsy-Naïve Men. *Eur Urol Oncol* (2019) 2(3):311–9. doi: 10.1016/j.euo.2018.09.001
49. Falagario UG, Jambor I, Lantz A, Ettala O, Stabile A, Taimen P, et al. Combined Use of Prostate-Specific Antigen Density and Magnetic Resonance Imaging for Prostate Biopsy Decision Planning: A Retrospective Multi-Institutional Study Using the Prostate Magnetic Resonance Imaging Outcome Database (PROMOD). *Eur Urol Oncol* (2020) S2588–9311 (20):30142–5. doi: 10.1016/j.euo.2020.08.014
50. Filella X, Foj L, Alcover J, Augé JM, Molina R, Jiménez W. The Influence of Prostate Volume in Prostate Health Index Performance in Patients With Total PSA Lower Than 10 μg/L. *Clin Chim Acta* (2014) 436:303–7. doi: 10.1016/j.cca.2014.06.019
51. Barisiene M, Bakavicius A, Stanciute D, Jurkeviciene J, Zelvys A, Ulys A, et al. Prostate Health Index and Prostate Health Index Density as Diagnostic Tools

for Improved Prostate Cancer Detection. *BioMed Res Int* (2020) 2020:9872146. doi: 10.1155/2020/9872146
52. Schulze A, Christoph F, Sachs M, Schroeder J, Stephan C, Schostak M, et al. Use of the Prostate Health Index and Density in 3 Outpatient Centers to Avoid Unnecessary Prostate Biopsies. *Urol Int* (2020) 104(3-4):181–6. doi: 10.1159/000506262
53. Garrido MM, Ribeiro RM, Pinheiro LC, Holdenrieder S, Guimarães JT. The Prostate Health Index (PHI) Density: Are There Advantages Over PHI or Over the Prostate-Specific Antigen Density? *Clin Chim Acta* (2021) 520:133–8. doi: 10.1016/j.cca.2021.06.006
54. Peters R, Stephan C, Jung K, Lein M, Friedersdorff F, Maxeiner A. Comparison of PHI and PHI Density for Prostate Cancer Detection in a Large Retrospective Caucasian Cohort. *Urol Int* (2021) 25:1–6.
55. Stephan C, Jung K, Lein M, Rochow H, Friedersdorff F, Maxeiner A. PHI Density Prospectively Improves Prostate Cancer Detection. *World J Urol* (2021) 39(9):3273–9. doi: 10.1007/s00345-020-03585-2
56. Liu AQ, Remmers S, Lau SY, Yip SY, Leung CH, Mak CW, et al. Initial Prostate Health Index (Phi) and Phi Density Predicts Future Risk of Clinically Significant Prostate Cancer in Men With Initial Negative Prostate Biopsy: A 6-Year Follow-Up Study. *Prostate Cancer Prostatic Dis* (2021). doi: 10.1038/s41391-021-00444-y
57. Busetto GM, Del Giudice F, Maggi M, De Marco F, Porreca A, Sperduti I, et al. Prospective Assessment of Two-Gene Urinary Test With Multiparametric Magnetic Resonance Imaging of the Prostate for Men Undergoing Primary Prostate Biopsy. *World J Urol* (2021) 39(6):1869–77. doi: 10.1007/s00345-020-03359-w
58. Hsieh PF, Li WJ, Lin WC, Chang H, Chang CH, Huang CP, et al. Combining Prostate Health Index and Multiparametric Magnetic Resonance Imaging in the Diagnosis of Clinically Significant Prostate Cancer in an Asian Population. *World J Urol* (2020) 38(5):1207–14. doi: 10.1007/s00345-019-02889-2
59. Druskin SC, Tosoian JJ, Young A, Collica S, Srivastava A, Ghabili K, et al. Combining Prostate Health Index Density, Magnetic Resonance Imaging and Prior Negative Biopsy Status to Improve the Detection of Clinically Significant Prostate Cancer. *BJU Int* (2018) 121(4):619–26. doi: 10.1111/bju.14098
60. Lopes Vendrami C, McCarthy RJ, Chatterjee A, Casalino D, Schaeffer EM, Catalona WJ, et al. The Utility of Prostate Specific Antigen Density, Prostate Health Index, and Prostate Health Index Density in Predicting Positive Prostate Biopsy Outcome Is Dependent on the Prostate Biopsy Methods. *Urology* (2019) 129:153–9. doi: 10.1016/j.urology.2019.03.018

Conflict of Interest: The authors declare that the research was conducted in the absence of any commercial or financial relationships that could be construed as a potential conflict of interest.

Publisher's Note: All claims expressed in this article are solely those of the authors and do not necessarily represent those of their affiliated organizations, or those of the publisher, the editors and the reviewers. Any product that may be evaluated in this article, or claim that may be made by its manufacturer, is not guaranteed or endorsed by the publisher.

Copyright © 2021 Chiu, Cheng, Pu, Lu, Hong, Chung, Chiang and Huang. This is an open-access article distributed under the terms of the Creative Commons Attribution License (CC BY). The use, distribution or reproduction in other forums is permitted, provided the original author(s) and the copyright owner(s) are credited and that the original publication in this journal is cited, in accordance with accepted academic practice. No use, distribution or reproduction is permitted which does not comply with these terms.

frontiers in Oncology

ORIGINAL RESEARCH
published: 25 November 2021
doi: 10.3389/fonc.2021.787835

Prognostic Value of Thyroid Hormone Ratio in Patients With Advanced Metastatic Renal Cell Carcinoma: Results From the Threefour Study (Meet-URO 14)

Marco Maruzzo[1], Elena Verzoni[2], Maria Giuseppa Vitale[3], Michele Dionese[1,4], Sebastiano Buti[5], Luca Galli[6], Andrea Zivi[7], Sara Watutantrige-Fernando[8], Teresa Zielli[5], Elisa Zanardi[9], Roberto Sabbatini[3], Umberto Basso[1], Vittorina Zagonel[1] and Giuseppe Procopio[2]*

[1] Oncology Unit 1, Istituto Oncologico Veneto, IOV - Istituto di Ricovero e Cura a Carattere Scientifico (IRCCS), Padova, Italy, [2] Genito-Urinary (GU) Oncology, Istituto di Ricovero e Cura a Carattere Scientifico (IRCCS) Fondazione Istituto Nazionale dei Tumori, Milano, Italy, [3] Oncology Unit, Azienda Ospedaliera Universitaria di Modena, Modena, Italy, [4] Dipartimento di Scienze Chirurgiche Oncologiche e Gastroenterologiche, Università degli Studi di Padova, Padova, Italy, [5] Oncology Unit, Azienda Ospedaliero-Universitaria di Parma, Parma, Italy, [6] Oncology Unit, Azienda Ospedaliera Universitaria Pisana, Pisa, Italy, [7] Oncology Unit, Azienda Ospedaliera Universitaria Integrata di Verona, Verona, Italy, [8] Hereditary Tumor Unit, Istituto Oncologico Veneto, IOV - Istituto di Ricovero e Cura a Carattere Scientifico (IRCCS), Padova, Italy, [9] Academic Unit of Medical Oncology, Istituto di Ricovero e Cura a Carattere Scientifico (IRCCS) San Martino Hospital, Genova, Italy

OPEN ACCESS

Edited by:
Elena Ranieri, University of Foggia, Italy

Reviewed by:
Daniela Esposito, University of Gothenburg, Sweden
Giovanni Vitale, University of Milan, Italy

***Correspondence:**
Marco Maruzzo
marco.maruzzo@iov.veneto.it

Specialty section:
This article was submitted to Genitourinary Oncology, a section of the journal Frontiers in Oncology

Received: *01 October 2021*
Accepted: *03 November 2021*
Published: *25 November 2021*

Citation:
Maruzzo M, Verzoni E, Vitale MG, Dionese M, Buti S, Galli L, Zivi A, Watutantrige-Fernando S, Zielli T, Zanardi E, Sabbatini R, Basso U, Zagonel V and Procopio G (2021) Prognostic Value of Thyroid Hormone Ratio in Patients With Advanced Metastatic Renal Cell Carcinoma: Results From the Threefour Study (Meet-URO 14). Front. Oncol. 11:787835. doi: 10.3389/fonc.2021.787835

Background: Thyroid hormone impairment, represented as an alteration in levels of thyroid hormones and a lower fT3/fT4 ratio, has been correlated with a worse prognosis for both cancer and non-cancer patients. The role of baseline thyroid function in patients with metastatic renal cell carcinoma (mRCC) however, has not been studied yet.

Materials and Methods: We recorded clinical data, baseline biochemical results, and oncological outcomes from 10 Oncology Units in Italy. We stratified patients into three groups according to the fT3/fT4 ratio value and subsequently analyzed differences in progression-free survival (PFS) and overall survival (OS) in the three groups. We also performed univariate and multivariate analyses to find prognostic factors for PFS and OS.

Results: We analyzed 134 patients treated with systemic treatment for mRCC. Median PFS in the low, intermediate, and high fT3/fT4 ratio group were 7.5, 12.1, and 21.7 months respectively ($p<0.001$); median OS in the three groups were 36.5, 48.6, and 70.5 months respectively ($p=0.006$). The low fT3/fT4 ratio maintained its prognostic role at the multivariate analysis independently from IMDC and other well-established prognostic factors. The development of iatrogenic hypothyroidism was not associated with a better outcome.

Conclusion: We found that baseline thyroid hormone impairment, represented by a low fT3/fT4 ratio, is a strong prognostic factor in patients treated for mRCC in first line setting and is independent of other parameters currently used in clinical practice.

Keywords: renal cell carcinoma, FT3/FT4, deiodination, tyrosine kinase inhibitors, immunotherapy, progression, survival

INTRODUCTION

In the last decades, the prognosis of patients affected with metastatic renal cell carcinoma (mRCC) progressively improved thanks to the development of new drugs that target tumor neoangiogenesis (tyrosine-kinase inhibitors of Vascular Endothelial Growth Factor Receptor, VEGFR) or promote the host immune response against tumoral cells (immune checkpoint inhibitors, ICI) (1, 2).

Despite the newest treatment options, however, some patients do not respond to systemic treatment or rapidly progress and die. Many prognostic scores were established over the years; the Memorial Sloan Kettering Cancer Center (MSKCC) and International Metastatic RCC Database Consortium (IMDC) risk score classification, the most commonly used in clinical practice, stratify patients into three risk groups taking into account clinical characteristics and biochemical examinations (3, 4). Those prognostic scores are currently used in daily clinical practice and clinical trials testing new drugs.

Thyroid hormone levels recently emerged as a prognostic factor in frail or elderly patients hospitalized for acute illness (5, 6). The presence of low levels of free triiodothyronine (fT3) in the absence of abnormalities in the thyroid function (defined as "euthyroid sick syndrome" or "non-thyroidal illness syndrome", NTIS) has been shown as an independent prognostic factor for patients hospitalized for many different diseases (end-stage kidney disease, heart failure, acute coronary syndrome, etc.) (6–8). Levels of the active forms of thyroid hormones are due to deiodinases, a family of enzymes that can transform the biological precursor into the "active" or "inactive" forms (8).

In cancer patients, low fT3 levels have been correlated with a worse prognosis in patients affected by different solid malignancies (9–11).

The use of the fT3/fT4 ratio instead of the mean values of the two single hormones could be a better marker of peripheral deiodination activity and can even help stratify patients with normal fT3 levels. TSH is not usually used because its level usually remains within the normal range for several and different reasons (pituitary dysfunction, lower hypothalamic THR production, and reduced TSH pulsatility) and is thus less reliable (7).

Pasqualetti et al. found that a low fT3/fT4 ratio in non-cancer patients was strongly associated with frailty and was able to predict prognosis even in the case of normal fT3 levels in hospitalized elderly patients (6).

Recently, two papers showed that a low fT3/fT4 ratio predicts shorter overall survival (OS) and progression-free survival (PFS) in patients affected by metastatic colorectal cancer, independently of other established prognostic factors (12, 13).

In mRCC, the development of hypothyroidism during treatment with anti-VEGF tyrosine kinase inhibitors is a well-known favorable prognostic factor (14). However, the role of baseline thyroid values (and especially the fT3/fT4 ratio) has not been appropriately studied to date.

We, therefore, designed a multicentre retrospective trial to evaluate the correlation between the baseline fT3/fT4 ratio and outcomes of systemic treatments for mRCC.

MATERIAL AND METHODS

The ThreeFour Study – Meet-URO 14 is a multicentre, retrospective, observational study. This study analyzed the clinical data of all consecutive mRCC patients treated from January 2007 to December 2014 at 10 Italian Oncology Units, within the Meet-URO cooperative group.

The study included patients aged 18 years or older with histologically confirmed mRCC who received first-line systemic treatment for metastatic disease and whose values of thyroid hormones were available. Patient data were collected retrospectively from clinical charts locally and imputed in a common, anonymized database. Demographic data, histological details (histological type, staging according to TMN, and grading), the risk group according to IMDC criteria, drugs used as first-line treatment, the values of thyroid hormones and the blood count were recorded for all patients, both at the baseline and at the time of the first radiological restaging, PFS and OS and best response to first-line treatment according to RECIST 1.1.

All the blood test was performed locally in the participant centres, in hospital certified laboratories. The ratio of fT3 and fT4 was calculated for each patient.

OS and PFS were evaluated with the Kaplan-Meier method from the start of the first-line treatment to the event of death for any cause or disease progression, respectively. All patients with no events were censored at the last follow-up. The OS and PFS in different groups were compared with the log-rank test and Cox's proportional hazards method. Univariate and multivariate analyses were performed with a Wald test.

The study coordinated by the Istituto Oncologico Veneto (IOV) was approved by the Ethics Committee on 28 January 2019 and conducted according to the Declaration of Helsinki. Given the retrospective design and the fact that the majority of patients were dead at the time of analysis, the signed informed consent was not required from patients.

RESULTS

One hundred and ninety patients were included in the ThreeFour Study but only 134 had complete data available on thyroid hormones, since it is not a standard practice the baseline assessment of fT3 and fT4. Therefore, only patients with complete data and the possibility to calculate fT3/fT4 ratio were eligible for the analyses. Patients' demographic data and principal clinical characteristics are reported in **Table 1**.

The median age of the cohort was 63.4 years, with approximately one-third of patients older than 70 years. The vast majority of patients were affected by clear cell carcinoma with a prevalence of intermediate IMDC risk category (61.2%). The preferred option as first-line treatment was single-agent tyrosine kinase inhibitor (TKI) (sunitinib, pazopanib, tivozanib, lenvatinib plus everolimus; 78.4%) followed by a combination of immunotherapy and antiangiogenic therapy (11.2%) and immunotherapy alone (10.4%).

TABLE 1 | Patient characteristics (N = 134).

Characteristics	Number of patients (%)
Gender:	
M	97 (72.4%)
F	37 (27.6%)
Age (years)	
Median (range)	63.4 (26.7-84.5)
>70 years (%)	44 (32.8%)
Prior Nephrectomy	
Yes	107 (79.9%)
No	27 (20.1%)
Histology	
Clear Cell	118 (88.1%)
Other histologies	16 (11.9%)
Sarcomatoid features	
Absent	130 (97.1%)
Present	4 (2.9%)
Metastatic Sites	
Lung	85 (63.4%)
Bone	17 (12.7%)
Liver	32 (23.9%)
CNS	5 (3.7%)
Lymph nodes	48 (35.8%)
Others	52 (38%)
Number of metastatic sites	
1	19 (14%)
2	62 (46%)
≥3	53 (40%)
Baseline thyroid hormone levels	
fT3 (median, range), pmol/l	3,81 (1,20-11,09)
fT4 (median, range), pmol/l	12,08 (4,04-21,10)
IMDC risk classification	
Good	38 (28.4%)
Intermediate	82 (61.2%)
Poor	13 (9.7%)
NA	1 (0.7%)
Time from diagnosis to treatment	
>12 months	62 (46.3%)
≤12 months	72 (53.7%)
First-line treatment	
TKI	105 (78.4%)
TKI + IT	15 (11.2%)
IT	14 (10.4%)

CNS, central nervous system; TKI, tyrosine kinase inhibitors; IT, immunotherapy; NA, not available.

The best response reported by investigators during first-line treatment was stable disease in 62 cases (46%), partial response in 52 cases (39%), and disease progression in 16 cases (12%); complete response was only detected in 3 patients (2%).

One-hundred and six patients (79.1%) progressed and 62 (46.3%) died after a median follow-up of 29.4 months.

The median PFS and the median OS were 20.3 months (95% CI: 15-23.3 months) and 49.4 months (95% CI: 40.9 – 66.8 months) respectively, in the whole population.

The baseline fT3/fT4 ratio ranged from 0.13 to 4.87. In the whole cohort the higher fT3/fT4 ratio, considered as a continuous variable, was associated with better PFS (HR 0.819, 95% CI: 0.679-0.988) and OS (HR 0.672, 95% CI: 0.492-0.916) (**Table 2**).

We subsequently stratified patients into three groups according to fT3/fT4 tertiles; 0.266 was the limit value between the low and intermediate group and 0.342 between the intermediate and high group.

The median PFS in the low, intermediate and high fT3/fT4 ratio group was 7.5, 12.1 and 21.7 months, respectively (p<0.001) (HR 0.54 for intermediate *vs* low fT3/fT4, 95% CI: 0.333-0.877; HR 0.43 for high *vs* low fT3/fT4, 95% CI: 0.263-0.693). The median OS in the low, intermediate and high fT3/fT4 groups was 6.5, 48.6 and 70.5 months, respectively (p =0.006) (HR 0.64 for intermediate *vs* low fT3/fT4, 95% CI: 0.357-1.149; HR 0.33 for high *vs* low fT3/fT4, 95% CI: 0.171-0.625) (**Figure 1**).

In the univariate analysis, the characteristics associated with PFS were the time from diagnosis to systemic treatment, the fT3/fT4 ratio, and the IMDC risk classification. A high neutrophil-to-lymphocyte ratio (NLR), a low fT3/fT4 ratio and, intermediate and poor risk according to the IMDC were associated with worse OS. Data on the type of treatment were not considered, given the heterogeneous variety of choice in the first-line treatment (**Table 2**).

In the multivariate analysis, the fT3/fT4 ratio was the only item that maintained a statistically significant association with PFS; a high fT3/fT4 ratio and a poor risk score based on the IMDC were factors associated with OS (**Table 3**).

The disease control rate (represented by patients achieving stability, partial or complete response as the best response, DCR) was associated with the baseline fT3/fT4 ratio (DCR of 77.8%, 91.1% and 95.5% in the low, intermediate and high fT3/fT4 group, respectively; p=0.027).

During the treatment, the patients undergo thyroid function test at the time of radiological assessments; 69 of them developed clinical or subclinical hypothyroidism. PFS and OS did not significantly differ in those patients who developed hypothyroidism compared with patients without this complication (median PFS 11.9 *vs* 13.3 months, p NS; median OS 48.6 *vs* 54.9 months, p NS).

DISCUSSION

This study's results cast new light on an interesting key connection of peripheral thyroid hormone metabolism with tumor progression and, thus, the survival of mRCC patients. The rationale of our analysis took inspiration from clinical situations that are different from cancer but with common features, such as cachexia or sarcopenia (15). Moreover, recent data were reported on the same topic for patients with colorectal carcinoma (12, 13).

The Italian cooperative group on urological oncology within the Meet-URO collected a robust dataset of patients diagnosed with mRCC and who were candidates to receive first-line treatment in accordance with clinical practice.

Our work shows that thyroid hormone dysfunction, represented by a lower fT3/fT4 ratio, is a strong prognostic factor for mRCC patients who underwent systemic treatment, confirming reported data for other neoplasms (11, 12).

The alteration of thyroid hormone values during acute or chronic illness (the so-called non-thyroidal illness syndrome [NTIS] which is not caused by an intrinsic dysfunction of the

TABLE 2 | Univariate analysis of characteristics associated with PFS and OS.

Characteristics	PFS HR (95% CI)	p	OS HR (95% CI)	p
Gender				
F	–	–	–	–
M	0.874 (0.57-1.34)	0.536	0.598 (0.35-1.01)	0.0534
Age (years)	1.006 (0.99-1.02)	0.481	1.003 (0.98-1.01)	0.802
Time from diagnosis to treatment				
>12 months	–	–	–	–
≤12 months	1.661 (1.109-2.487)	**0.014**	1.461 (0.86-2.484)	0.161
IMDC risk group				
Good	–	–	–	–
Intermediate	1.579 (1.024-2.435)	**0.0389**	1.563 (0.868-2.814)	0.136
Poor	2.522 (1.189-5.347)	**0.0159**	3.617 (1.513-8.647)	**0.00384**
Number of metastatic sites	1.212 (0.967-1.519)	0.0943	1.252 (0.945-1.658)	0.118
NLR				
<3	–	–	–	–
≥3	1.511 (0.993-2.301)	0.054	1.933 (1.145-3.262)	**0.0136**
fT3/fT4 ratio	0.819 (0.679-0.988)	**0.0367**	0.672 (0.492-0.916)	**0.0119**
fT3/fT4 ratio				
low	–	–	–	–
intermediate	0.541 (0.333-0.877)	**0.0123**	0.640 (0.357-1.149)	0.135
high	0.427 (0.263-0.693)	**0.00057**	0.327 (0.171-0.624)	**0.000712**

The bold values are p significant values.

thyroid gland) is a common phenomenon that has been correlated with a worse prognosis in patients with active disease from many different causes (5–8).

It is currently unclear if those alterations represent a form of adaptive response to sickness or if those changes must be considered as real tissue hypothyroidism that needs to be corrected with hormone replacement therapy (8). The pathophysiology of NTIS takes into account various mechanisms ranging from alterations in the expression of the thyroid hormone receptor and thyroid hormone-binding protein, abnormal activity of the hypothalamic-pituitary axis (important in the initial phase of acute illness), and alteration in the thyroid hormone metabolism (8).

The levels of the active forms of thyroid hormones are in fact due to iodothyronine deiodinases, a family of enzymes that can transform the biological precursor T4 (produced by the thyroid) into the "active" form T3 (by deiodinases 1 and 2, or D1 and D2) or the inactive forms rT3 (from T4) and T2 (from T3) (by deiodinase 3, D3) (6, 8). The three deiodinases involved in the metabolic pathway, apart from their role, differ because of the tissue of expression: in particular, D1 is expressed in the liver and kidney and D2 in the skeletal muscle, where it is located within the cells and gives rise to most of the T3; D3 is considered an inactivating enzyme and it is important for placental and fetal tissues (8).

Chronic illness, cachexia, liver or renal impairment, and chronic systemic inflammation can lead to lower activity of D1 and D2 and overactivity of D3, thus leading to reduced levels of fT3 (16, 17). Those clinical situations are common in cancer patients, particularly in the end stages of the disease, and are typically associated with poor prognosis. Indirect markers of systemic inflammation (for example neutrophil and platelet count, NLR) are well-known negative prognostic factors (4, 18).

Therefore, NTIS and thyronine deiodinases impairment could be considered as an indirect marker of chronic systemic inflammation, cachexia, sarcopenia, or organ dysfunction, all characteristics that are associated with more advanced disease, a worse response to systemic therapy, and a worse prognosis.

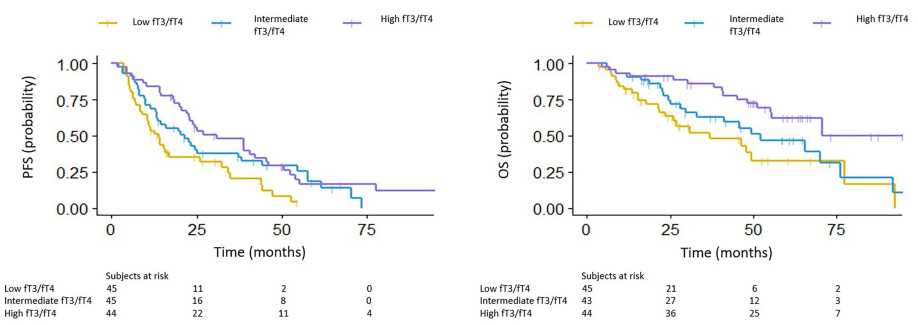

FIGURE 1 | PFS (left) and OS (right) in the low, intermediate and high fT3/fT4 ratio groups.

TABLE 3 | Multivariate analysis for PFS and OS.

Characteristic	HR for PFS (95% CI)	p	HR for OS (95% CI)	p
Time from diagnosis to treatment				
>12 months	–	–	–	–
≤12 months	1.351 (0.774-2.358)	0.289	0.923 (0.424-2.01)	0.840
Number of sites	1.005 (0.779-1.296)	0.967	1.026 (0.757-1.391)	0.867
NLR				
<3	–	–	–	–
≥3	1.061 (0.654 - 1.722)	0.812	1.461 (0.819- 2.604)	0.198
fT3/fT4 ratio				
low	–	–	–	–
intermediate	0.494 (0.281-0.867)	**0.0141**	0.524 (0.268-1.027)	0.0597
high	0.355 (0.199-0.635)	**0.0005**	0.293 (0.141-0.608)	**0.00097**
IMDC risk group				
Good	–	–	–	–
Intermediate	1.340 (0.745-2.413)	0.329	1.774 (0.762-4.130)	0.183
Poor	1.836 (0.821-4.05)	0.139	3.527 (1.291-9.632)	**0.0139**

The bold values are p significant values.

However, the pathophysiological mechanism in cancer patients remains debatable, as does the role of the thyroid hormone and the activity of the deiodinases on cancer cell proliferation and differentiation (19). Besides, it is unclear if the administration of substitutive thyroid hormone therapy with triiodothyronine can lead to an improvement in the oncological outcome or, at least, in clinical symptoms, while it does not appear to be effective in non-cancer diseases (8, 16, 20).

In an oncological setting, many authors found a correlation between low fT3 levels and a worse prognosis in patients affected by advanced solid malignancies such as lung cancer and lymphomas (9, 11). Interestingly, elevated fT4 levels in hepatocarcinoma were correlated with a worse prognosis (10).

The use of the fT3/fT4 ratio was first proposed by Pasqualetti et al. as an indirect marker of deiodination impairment in their analysis of a cohort of hospitalized elderly patients (6). A low fT3/fT4 ratio correlated with frailty and worse survival, even in patients who had normal T3 values (6).

The fT3/fT4 ratio was studied in colorectal cancer patients, where it was identified as a strong prognostic factor in heavily pre-treated patients (12, 13). In their analysis, the prognostic role of the T3/T4 ratio was also independent of other well-known, established prognostic factors (12, 13).

In our cohort, contrary to what was previously reported (14), the development of treatment-induced hypothyroidism during treatment did not correlate with a better outcome in terms of PFS and OS (14). Apart from bias selection, one possible explanation could be the heterogeneity of treatment choices applied to patients followed in 10 different Institutions, where the development of hypothyroidism correlated with the outcome in patients treated with TKI monotherapy (14).

This study has many limitations, including the retrospective design with bias selection. Moreover, patients were restaged at different time points according to local practice. This probably led to a selection bias for patients with longer OS and PFS, thus resulting in survival curves that were far better than historical data. The sample size, albeit not small in absolute terms given the rarity of the disease, does not allow us to perform a subgroup analysis of the prognostic value of the fT3/fT4 ratio according to the type of systemic therapy (antiangiogenic, immunotherapy, or combination regimes) proposed. For the same reason, we could not test the predictive effect of the fT3/fT4 ratio in terms of response to different treatment options. Finally, the role of patients' baseline iodine status and the possible presence of deiodinase polymorphisms were not studied in our cohort.

CONCLUSION

In mRCC patients undergoing first-line systemic treatment, we identified the presence of baseline thyroid hormone impairment, quantified by a low fT3/fT4 ratio, as a strong prognostic factor for both PFS and OS. The role of the fT3/fT4 ratio in mRCC patients warrants validation in prospective cohorts to introduce it as a recognized prognostic factor for clinical practice as well as for clinical trials.

Moreover, additional studies are warranted to assess if the supplementation of thyroid hormones and correction of reduced deiodination of fT4 can improve the patient prognosis, and to also assess whether the changes in the levels of free thyroid hormones (binding proteins) play a role in cancer patients.

DATA AVAILABILITY STATEMENT

The raw data supporting the conclusions of this article will be made available by the authors, without undue reservation.

ETHICS STATEMENT

The studies involving human participants were reviewed and approved by Comitato Etico dell'Istituto Oncologico Veneto. The patients/participants provided their written informed consent to participate in this study.

AUTHOR CONTRIBUTIONS

MM, conceptualization, methodology, formal analysis, supervision, and validation. EV, MV, SB, EZ, and RS, data curation, investigation, validation. MD, formal analysis, investigation, validation. LG, AZ, and TZ, data curation, investigation. SW-F, methodology, investigation, validation. UB, data curation, methodology, supervision, validation. VZ, supervision and validation. GP, methodology, supervision, validation. All authors contributed to the article and approved the submitted version.

REFERENCES

1. Escudier B, Porta C, Schmidinger M, Rioux-Leclercq N, Bex A, Khoo V, et al. Renal Cell Carcinoma: ESMO Clinical Practice Guidelines for Diagnosis, Treatment and Follow-Up. *Ann Oncol* (2019) 30(5):706–20. doi: 10.1093/annonc/mdz056
2. Choueiri TK, Motzer RJ. Systemic Therapy for Metastatic Renal-Cell Carcinoma. *N Engl J Med* (2017) 376(4):354–66. doi: 10.1056/NEJMra1601333
3. Motzer RJ, Mazumdar M, Bacik J, Berg W, Amsterdam A, Ferrara J. Survival and Prognostic Stratification of 670 Patients With Advanced Renal Cell Carcinoma. *J Clin Oncol* (1999) 17:2530–40. doi: 10.1200/JCO.1999.17.8.2530
4. Heng DY, Xie W, Regan MM, Harshman LC, Bjarnason GA, Vaishampayan UN, et al. External Validation and Comparison With Other Models of the International Metastatic Renal-Cell Carcinoma Database Consortium Prognostic Model: A Population-Based Study. *Lancet Oncol* (2013) 14:141–8. doi: 10.1016/S1470-2045(12)70559-4
5. De Alfieri W, Nistico F, Borgogni T, Riello F, Cellai F. Mori C Et Al: Thyroid Hormones as Predictors of Short-And Long-Term Mortality in Very Old Hospitalized Patients. *J Gerontol A Biol Sci Med Sci* (2013) 68(9):1122–8. doi: 10.1093/gerona/glt012
6. Pasqualetti G, Calsolaro V, Bernardini S, Linsalata G, Bigazzi R, Caraccio N, et al. Degree of Peripheral Thyroxin Deiodination, Frailty, and Long-Term Survival in Hospitalized Older Patients. *J Clin Endocrinol Metab* (2018) 103(5):1867–76. doi: 10.1210/jc.2017-02149
7. Fragidis S, Sombolos K, Thodis E, Panagoutsos S, Mourvati E, Pikilidou M, et al. Low T3 Syndrome and Long Term Mortality in Chronic Hemodialysis Patients. *World J Nephrol* (2015) 4(3):415–22. doi: 10.5527/wjn.v4.i3.415
8. Warner MH, Beckett GJ. Mechanism Behind the non-Thyroidal Illness Syndrome: An Update. *J Endocrinol* (2010) 205:1–13. doi: 10.1677/JOE-09-0412
9. Gao R, Liang JH, Wang L, Zhu HY, Wu W, Wu JZ, et al. Low T3 Syndrome Is a Strong Prognostic Predictor in Diffuse Large B Cell Lymphoma. *Br J Haematol* (2017) 177(1):95–105. doi: 10.1111/bjh.14528
10. Pinter M, Haupt L, Hucke F, Bota S, Bucsics T, Trauner M, et al. The Impact of Thyroid Hormones on Patients With Hepatocellular Carcinoma. *PLoS One* (2017) 12(8):e0181878. doi: 10.1371/journal.pone.0181878
11. Yasar ZA, Kirakli C, Yilmaz U, Ucar ZZ, Talay F. Can Nonthyroid Illness Syndrome Predict Mortality in Lung Cancer Patients? A Prospective Cohort Study. *Horm Cancer* (2014) 5(4):240–6. doi: 10.1007/s12672-014-0183-0
12. Schirripa M, Pasqualetti G, Giampieri R, Scartozzi M, Lonardi S, Rumano L, et al. Prognostic Value of Thyroid Hormone Ratios in Patients With Advanced Metastatic Colorectal Cancer Treated With Regorafenib: The TOREADOR Study. *Clin Colorectal Canc* (2018) 17(3):e601–15. doi: 10.1016/j.clcc.2018.05.013
13. Pasqualetti G, Schirripa M, Dochy E, Fassan M, Ziranu P. Puzzoni M Et Al: Thyroid Hormones Ratio Is a Major Prognostic Marker in Advanced Metastatic Colorectal Cancer: Results From the Phase III Randomised CORRECT Trial. *Eur J Cancer* (2020) 133:66–73. doi: 10.1016/j.ejca.2020.04.023
14. Buda-Nowak A, Kucharz J, Dumnicka P, Kuzniewski M, Herman RM, Zygulska AL, et al. Sunitinib-Induced Hypothyroidism Predicts Progression-Free Survival in Metastatic Renal Cell Carcinoma Patients. *Med Oncol* (2017) 34(4):68. doi: 10.1007/s12032-017-0928-z
15. Shyh-Chang Ng. Metabolic Changes During Cancer Cachexia Pathogenesis. *Adv Exp Med Biol* (2017) 1026:233–49. doi: 10.1007/978-981-10-6020-5_11
16. Mancini A, Di Segni C, Raimondo S, Olivieri G, Silvestrini A, Meucci E, et al. Thyroid Hormones, Oxidative Stress, and Inflammation. *Mediators Inflamm* (2016) 2016:6757154. doi: 10.1155/2016/6757154
17. De Luca R, Davis PJ, Lin HY, Gionfra F, Percario ZA, Affabris E, et al. Thyroid Hormones Interaction With Immune Response, Inflammation and Non-Thyroidal Illness Syndrome. *Front Cell Dev Biol* (2021) 21;8:614030. doi: 10.3389/fcell.2020.614030
18. Maruzzo M, Basso U, Diminutto A, Roma A, Zustovich F, Brunello A, et al. Role of Dose Exposure and Inflammatory Status in a Single Center, Real-World Analysis of Sunitinib in Patients With Metastatic Renal Cell Carcinoma. *Future Oncol* (2016) 12(7):909–19. doi: 10.2217/fon.16.14
19. Dentice M, Antonini D, Salvatore D. Type 3 Deiodinase and Solid Tumors: An Intriguing Pair. *Expert Opin Ther Targets* (2013) 17(11):1369–79. doi: 10.1517/14728222.2013.833189
20. Farwell A. Thyroid Hormone Therapy Is Not Indicated in the Majority of Patients With the Sick Euthyroid Syndrome. *Endocr Pract* (2008) 14(9):1180–7. doi: 10.4158/EP.14.9.1180

Conflict of Interest: The authors declare that the research was conducted in the absence of any commercial or financial relationships that could be construed as a potential conflict of interest.

Publisher's Note: All claims expressed in this article are solely those of the authors and do not necessarily represent those of their affiliated organizations, or those of the publisher, the editors and the reviewers. Any product that may be evaluated in this article, or claim that may be made by its manufacturer, is not guaranteed or endorsed by the publisher.

Copyright © 2021 Maruzzo, Verzoni, Vitale, Dionese, Buti, Galli, Zivi, Watutantrige-Fernando, Zielli, Zanardi, Sabbatini, Basso, Zagonel and Procopio. This is an open-access article distributed under the terms of the Creative Commons Attribution License (CC BY). The use, distribution or reproduction in other forums is permitted, provided the original author(s) and the copyright owner(s) are credited and that the original publication in this journal is cited, in accordance with accepted academic practice. No use, distribution or reproduction is permitted which does not comply with these terms.

frontiers in Oncology

CASE REPORT
published: 07 December 2021
doi: 10.3389/fonc.2021.782166

Case Report: Early ^{68}Ga-PSMA-PET Metabolic Assessment and Response to Systemic Treatment for First-Line Metastatic Clear Cell Renal Cell Carcinoma; About Two Clinical Cases

Emmanuel Seront[1]*, *Renaud Lhommel*[2] *and Bertrand Tombal*[3]

[1] Division of Medical Oncology, Institut de Recherche Clinique (IREC), Cliniques Universitaires Saint Luc, Brussels, Belgium,
[2] Division of Nuclear Medicine, Institut de Recherche Clinique (IREC), Cliniques Universitaires Saint Luc, Brussels, Belgium,
[3] Division of Urology, Institut de Recherche Clinique (IREC), Cliniques Universitaires Saint Luc, Brussels, Belgium

OPEN ACCESS

Edited by:
Matthew Zibelman,
Fox Chase Cancer Center,
United States

Reviewed by:
Cedric Poyet,
University Hospital Zürich, Switzerland
Katy Beckermann,
Vanderbilt University, United States

***Correspondence:**
Emmanuel Seront
emmanuel.seront@
saintluc.uclouvain.be

Specialty section:
This article was submitted to Genitourinary Oncology, a section of the journal Frontiers in Oncology

Received: 23 September 2021
Accepted: 16 November 2021
Published: 07 December 2021

Citation:
Seront E, Lhommel R and Tombal B (2021) Case Report: Early ^{68}Ga-PSMA-PET Metabolic Assessment and Response to Systemic Treatment for First-Line Metastatic Clear Cell Renal Cell Carcinoma; About Two Clinical Cases. Front. Oncol. 11:782166. doi: 10.3389/fonc.2021.782166

Early evaluation of response to anticancer treatment in metastatic renal cell carcinoma (RCC) is challenging as responses are sometimes delayed, as mixed responses can occur, and as conventional imaging have some limitations. As PSMA has been previously identified in neovasculature of clear cell RCC (ccRCC), ^{68}Ga-PSMA-Positron Emitted Tomography (PET) could appear as an interesting tool to evaluate therapeutic response. We describe the association of an early decrease in ^{68}Ga metabolism (at 8 weeks after treatment onset) and further radiological response (at 12 weeks after treatment onset) to treatment in two patients with different sensitivity to axitinib–pembrolizumab combination. Interestingly, one of these patients presented an initial progressive disease on pembrolizumab alone and a subsequent response to axitinib alone in the disease course; these response profiles were associated with absence of decrease and subsequent decrease in the ^{68}Ga metabolism, respectively. Even if further prospective trials are needed, ^{68}Ga-PSMA-PET may appear as a promising way for early prediction of response to ccRCC systemic treatment.

Keywords: renal cell carcinoma, axitinib, pembrolizumab, gallium, metastatic disease, PSMA

INTRODUCTION

Renal cell carcinoma (RCC) is the 7th most common malignancy with 338,000 new cases and 144,000 related deaths worldwide yearly; clear cell histology (ccRCC) accounts for 80% of the cases. One-third of RCC patients present at diagnosis with metastatic disease, and among patients with initially localized disease, a significant proportion will develop metastases (1–3). Antiangiogenic Tyrosine Kinase Inhibitors (TKI) and Immune Checkpoint Inhibitors (ICI) are widely used in

therapeutic strategy for metastatic RCC; however, efficacy remains modest, with a response rate not exceeding 30% and a 5-year survival rate not exceeding 20% (4–6). More recently, the association of ICI (pembrolizumab or avelumab) and TKI (axitinib) or the combination of two ICIs (nivolumab + ipilimumab) have been established as the new first-line standard treatment, increasing the response rate to 50–60% and improving the progression free survival and the overall survival compared to sunitinib (7–9).

Imaging evaluation is challenging in RCC; standard modalities such as computed tomography (CT) and bone scan are sometimes unable to detect metastatic dissemination or characterize suspect distant lesions. Furthermore, radiological response on anticancer treatment can be difficult to evaluate; response pattern observed with TKI or ICIs can include a prolonged disease stabilization before an ultimate tumor shrinkage, an initial increase in the tumor burden or a mixed response with new lesions. In addition, an early identification of therapeutic inefficacy could prevent the continuation of this treatment (10).

^{68}Gallium (^{68}Ga)-Prostate-Specific Membrane Antigen (PSMA)-Positron Emitted Tomography (PET) has been shown to be more sensitive and specific than CT and bone scan in prostate cancer. Since PSMA expression has been previously identified in the neovasculature of benign and malignant tumors including RCC, we have investigated ^{68}Ga-PSMA-PET in two ccRCC metastatic patients treated with TKI + ICI combination (11–17). To our knowledge, whether an early change in ^{68}Ga metabolism could predict response to these treatments remains unknown.

CASE DESCRIPTION

First case: an early decrease of ^{68}Gallium metabolism and further partial response on CT scan (**Figure 1**).

A 52-year-old male patient was diagnosed in January 2021 with a 10-centimeter left renal tumor. Baseline imaging work-up showed 3 millimetric bilateral lung lesions. Nephrectomy was performed, confirming a 11-centimeter ccRCC with tumor necrosis, grade ISUP 3 (International Society of Urological Pathology), and renal vein thrombus; the final staging was pT3a based on TNM classification (8th edition). No adjuvant treatment was started. In May 2021, a thoraco-abdominal CT showed an increase in size and number of lesions. ^{68}Ga-PSMA-PET showed 10 metabolic bilateral pulmonary lesions, ranging from 6 to 14 mm in size, and from 2.3 to 9.2 in SUVmax; there was no other detected lesion. Blood test was normal, namely, hemoglobin, calcium, and lactate deshydrogenase (LDH). This patient was classified as an intermediate risk group following the International Metastatic RCC Database Consortium (IMDC) risk group classification as the interval between diagnosis and treatment onset was inferior to 12 months. We started at this time association of pembrolizumab (200 mg every three weeks) + axitinib (5 mg bid). Eight weeks after treatment onset, a new ^{68}Ga-PSMA-PET CT showed disappearance of ^{68}Ga metabolism in pulmonary lesions and a decrease in the size of all lesions (partial response following RECIST criteria). This response was maintained on the CT scan performed 12 weeks after treatment onset (**Figure 1**).

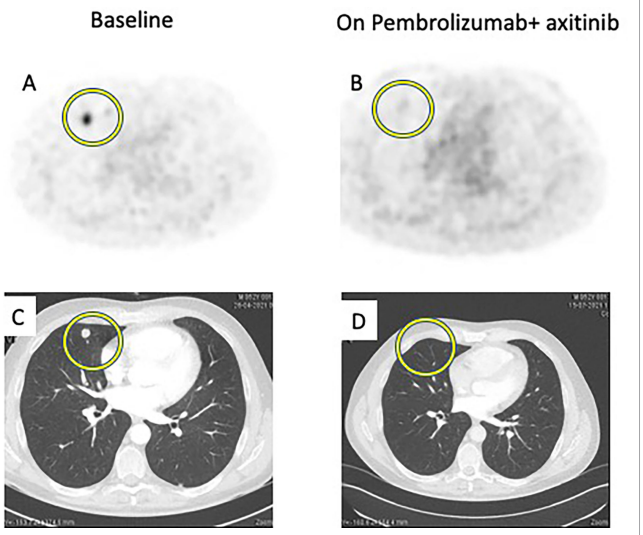

FIGURE 1 | Comparison between baseline imaging and on-treatment imaging. ^{68}GaPSMA-PET at baseline **(A)** and at 8-week **(B)** showing decrease of metabolism (yellow circle). Thoracic CT Scan at baseline **(C)** and at 12-week **(D)** showing disappearance of pulmonary lesions (yellow circle).

Second case: An absence of decrease of ^{68}Gallium metabolism and further radiological progression on CT scan (**Figure 2**).

A 72-year-old male patient was treated in 2018 with nephrectomy for a 6-centimeter ISUP 2 ccRCC with renal vein thrombus, classified as pT3a N0M0. In February 2021, a resurgence of the disease was diagnosed with a 26-millimeter tumor lesion in the nephrectomy site and three infra-centimetric lesions in the left inferior pulmonary lobe. ^{68}Ga-PSMA-PET showed intense metabolism of the local lesion (SUVmax 21.8) and moderate metabolism of the three pulmonary lesions (SUVmax ranging from 2.6 to 4.7). Blood tests (renal function, calcium, LDH, and liver tests) were normal except a grade 1 anemia. This patient was thus classified as an IMDC intermediate risk group. Systemic treatment with pembrolizumab (200 mg every three weeks) plus axitinib (5 mg bid) was started but axitinib had to be interrupted after 3 weeks due to the Common Terminology Criteria for Adverse Events (CTCAE v6) grade 3 nephrotic syndrome. Eight weeks after treatment onset, ^{68}Ga-PSMA-PET-CT showed an absence of decrease in ^{68}Ga metabolism in both local lesion and pulmonary lesions and the absence of decrease in lesions size (stable disease based on the RECIST criteria). The 12-week CT scan confirmed a disease progression following the RECIST criteria with an increase in the size of the pulmonary lesions (from 5 to 8 mm, from 4.5 to 9 mm and from 8 to 15 mm) and of the lesion in the nephrectomy site (from 2 to 38 mm). At this time, pembrolizumab alone was stopped and axitinib was reintroduced at 5 mg daily. Four weeks later (16 weeks after treatment initiation), ^{68}Ga-PSMA-PET-CT showed a disappearance of ^{68}Ga metabolism in all metastatic lesions; that was associated with a significant decrease

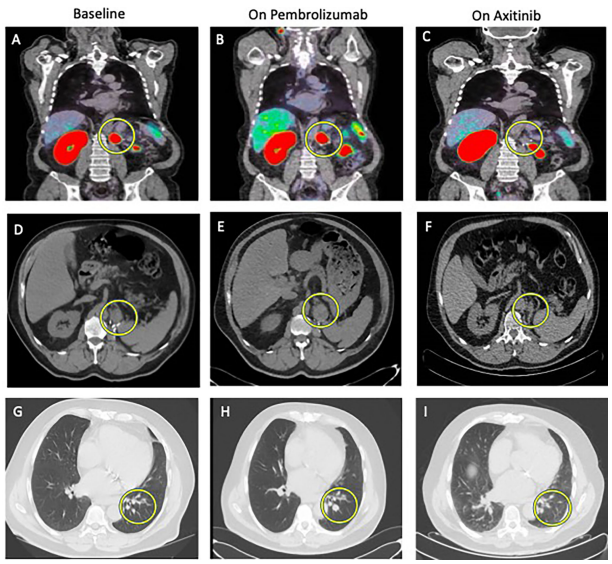

FIGURE 2 | Comparison between baseline imaging and on-treatment imaging. ^{68}GaPSMA-PET at baseline **(A)** and at 8-week on pembrolizumab alone **(B)** showing absence of metabolism decrease (yellow circle) and at 16-week on axitinib alone **(C)** showing disappearance of metabolism (yellow circle). Other metabolic lesion was not cancer lesion, but normal kidney (left) and physiological bowel metabolism (right on the picture). Abdominal CT Scan at baseline **(D)**, at 12-week **(E)** showing increase in size of the lesion at the nephrectomy site (yellow circle) and at 16-week **(F)** showing partial response. Thoracic CT Scan at baseline **(G)**, at 12-week **(H)** showing increase in size of pulmonary lesions (yellow circle) and at 16-week **(I)** showing partial response.

in size of the local lesions (from 38 to 25 mm) and of the pulmonary lesions (from 8 to 4 mm, from 9 to 2 mm and from 15 to 6 mm) (**Figure 2**).

Figure showcasing a timeline with imaging and response to treatment in the two clinical cases (**Figure 3**).

DISCUSSION

The type II transmembrane glycoprotein PSMA is significantly overexpressed in most prostate cancer cells and is associated with increasing tumor grade and stage. ^{68}Ga-PSMA PET-CT imaging demonstrated superior sensitivity and specificity compared to conventional imaging (thoraco-abdominal CT and bone scan) in primary, metastatic, and biochemically recurrent prostate cancer (18–20).

Interestingly, the increasing use of PSMA PET-CT imaging in prostate cancer has revealed PSMA ligand uptake in multiple non-prostatic benign and malignant diseases (21). Renal cell carcinoma (RCC) is a heavily vascularized tumor with well-documented PSMA expression in the neovasculature (22)

^{68}Ga-PSMA-PET-CT is an emerging imaging modality in the ccRCC management. Different retrospective studies showed that ^{68}Ga-PSMA-PET-CT was able to identify aggressive pathological features (high grade or sarcomatoid features) of ccRCC in the preoperative setting (23, 24) and to identify metastatic lesions or synchronous primary that were not detected on standard imaging (25). Furthermore, Rhee et al. prospectively showed in 10 RCC patients that the ^{68}Ga-PSMA-PET-CT had a stronger detection rate of metastases compared to CT scan, with less false negative lesions; this resulted in a change in the therapeutic management in the two patients (26). However, the role of ^{68}Ga-PSMA-PET-CT in early evaluation of response to treatment (TKI and ICI) remains unknown.

We report two types of radiological responses in the two ccRCC patients treated with TKI-ICI association on the 12-week standard imaging: a partial response and a progression disease based on the RECIST criteria. Interestingly, we showed that the 8-week ^{68}Ga metabolism change may be correlated with the 12-week radiological response. In the first patient, the decrease of ^{68}Ga metabolism was associated with the decrease in size and number of lesions. In the second patient, the absence of decrease in ^{68}Ga metabolism on pembrolizumab was associated with the further progression in size of described lesions. Importantly, in this last patient, the

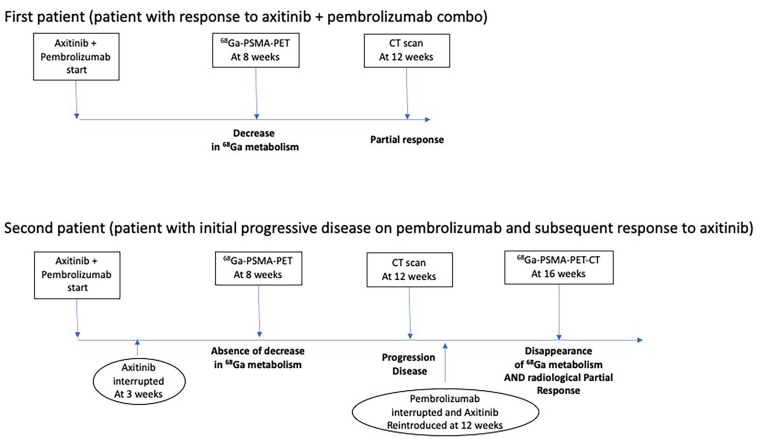

FIGURE 3 | Timeline with imaging and response to therapies in the two clinical cases.

introduction of a more effective treatment (axitinib), resulted in the early disappearance of ^{68}Ga metabolism, confirming the association between ^{68}Ga metabolism and response to treatment.

These associations between metabolic and radiological responses appear as promising in the early evaluation of response to ICI-combined treatments; radiological responses are sometimes delayed, appearing in some cases after many months, which renders the therapeutic evaluation challenging. Interpretation of mixed response, pseudo-progression and bone lesions evolution appears also difficult for clinicians and radiologists in the assessment of response.

Early assessment of ^{68}Ga metabolism of ccRCC lesions could be helpful in management of these patients; early detection of non-responding patients could prevent continuation of inefficient and potentially toxic treatment. In the era of combinations (TKI + ICI or ICI + ICI), the absence of predictive biomarker leads clinicians to start association of treatments; early prediction of response could help to adapt our management by starting monotherapy and assessing rapidly the metabolic response. Furthermore, this could also open new strategies including Lutetium-based treatment, particularly in patients with low tumor burden in which close surveillance attitude is adopted.

This report is only a description of two ccRCC patients that were treated with a similar combination. Even if TKI had to be stopped early in one of these patients, its further reintroduction allowed this patient to be the control of himself in terms of treatment efficacy assessment. Further prospective trials should be done with higher number of patients, similar characteristics (treatment schemes, IMDC risk group).

If 68Ga-PSMA-PET appears as a promising method for staging and characterizing RCC, it may also have a role in the early assessment of treatment efficacy in metastatic setting.

PATIENT PERSPECTIVE

The first patient: "having a good tool for rapidly predicting response to the treatment prevents the stress for waiting during three months whether there is a response or not to treatment". Of course, starting a treatment with potential toxicities in patients remains a challenge for clinicians. Having early tools to confirm efficacy will help the clinician to continue the same treatment or change towards another subsequent treatment.

The second patient: "choosing a treatment is challenging for the practician as we don't know whether this treatment will be efficient. In my case, after failure of pembrolizumab, it was important for me to rapidly known whether axitinib was efficient". In this case, pembrolizumab was not continued as PSMA-PET did not show any activity of this agent, which was confirmed later by CT scan.

DATA AVAILABILITY STATEMENT

The original contributions presented in the study are included in the article/supplementary material. Further inquiries can be directed to the corresponding author.

ETHICS STATEMENT

Written informed consent was obtained from the patient for the publication of any potentially identifiable images or data included in this article.

AUTHOR CONTRIBUTIONS

ES followed the patient, administered treatment, and wrote the manuscript. RL followed the patient, evaluated response with PSMA-PET and wrote the manuscript. BT followed the patient, administered treatment, and wrote the manuscript. All authors contributed to the article and approved the submitted version.

REFERENCES

1. Znaor A, Lortet-Tieulent J, Laversanne MJ, Jemal A, Bray F. International Variations and Trends in Renal Cell Carcinoma Incidence and Mortality. *Eur Urol* (2015) 67:519–30. doi: 10.1016/j.eururo.2014.10.002
2. Dabestani S, Thorstenson A, Lindblad P, Harmenberg U, Ljungberg B, Lundstam S. Renal Cell Carcinoma Recurrences and Metastases in Primary Non-Metastatic Patients: A Population-Based Study. *World J Urol* (2016) 34:1081–6. doi: 10.1007/s00345-016-1773-y
3. Thompson R, Hill J, Babayev Y, Cronin A, Kaag M, Kundu S, et al. Metastatic Renal Cell Carcinoma Risk According to Tumor Size. *J Urol* (2009) 182:41–5. doi: 10.1016/j.juro.2009.02.128
4. Motzer RJ, Hutson TE, Tomczak P, Michaelson MD, Bukowski RM, Rixe O, et al. Sunitinib Versus Interferon Alfa in Metastatic Renal-Cell Carcinoma. *N Engl J Med* (2007) 356(2):115–24. doi: 10.1056/NEJMoa065044
5. Sternberg CN, Davis ID, Mardiak J, Szczylik C, Lee E, Wagstaff J, et al. Pazopanib in Locally Advanced or Metastatic Renal Cell Carcinoma: Results of a Randomized Phase III Trial. *J Clin Oncol* (2010) 28(6):1061–8. doi: 10.1200/JCO.2009.23.9764
6. Motzer RJ, Escudier B, McDermott DF, George S, Hammers HJ, Srinivas S, et al. Nivolumab Versus Everolimus in Advanced Renal-Cell Carcinoma. *N Engl J Med* (2015) 373(19):1803–13. doi: 10.1056/NEJMoa1510665
7. Motzer RJ, Tannir NM, McDermott DF, Arén Frontera O, Melichar B, Choueiri TK, et al. Nivolumab Plus Ipilimumab Versus Sunitinib in Advanced Renal-Cell Carcinoma. *N Engl J Med* (2018) 378:1277–90. doi: 10.1056/NEJMoa1712126
8. Rini BI, Plimack ER, Stus V, Gafanov R, Hawkins R, Nosov D, et al. Pembrolizumab Plus Axitinib Versus Sunitinib for Advanced Renal-Cell Carcinoma. *N Engl J Med* (2019) 380:1116–27. doi: 10.1056/NEJMoa1816714
9. Motzer RJ, Penkov K, Haanen J, Rini B, Albiges L, Campbell MT, et al. Avelumab Plus Axitinib Versus Sunitinib for Advanced Renal-Cell Carcinoma. *N Engl J Med* (2019) 380:1103–15. doi: 10.1056/NEJMoa1816047
10. de Velasco G, Krajewski KM, Albiges L, Awad MM, Bellmunt J, Hodi FS, et al. Radiologic Heterogeneity in Responses to Anti-PD-1/PD-L1 Therapy in Metastatic Renal Cell Carcinoma. *Cancer Immunol Res* (2016) 4:12–7. doi: 10.1158/2326-6066.CIR-15-0197
11. Spatz S, Tolkach Y, Jung K, Stephan C, Busch J, Ralla B, et al. Comprehensive Evaluation of Prostate Specific Membrane Antigen Expression in the

Vasculature of Renal Tumors: Implications for Imaging Studies and Prognostic Role. *J Urol* (2018) 199(2):370–7. doi: 10.1016/j.juro.2017.08.079
12. Chang SS, Reuter VE, Heston WD, Gaudin PB. Metastatic Renal Cell Carcinoma Neovasculature Expresses Prostate-Specific Membrane Antigen. *Urology* (2001) 57(4):801–5. doi: 10.1016/S0090-4295(00)01094-3
13. Li G, Lambert C, Gentil-Perret A, Genin C, Tostain J. Molecular and Cytometric Analysis of Renal Cell Carcinoma Cells. Concepts, Techniques and Prospects. *Prog Urol* (2003) 13:1.
14. Al-Ahmadie HA, Olgac S, Gregor PD, Tickoo SK, Fine SW, Kondagunta GV, et al. Expression of Prostate-Specific Membrane Antigen in Renal Cortical Tumors. *Mod Pathol* (2008) 21:727–32. doi: 10.1038/modpathol.2008.42
15. Evangelista L, Basso U, Maruzzo M, Novara G. The Role of Radiolabeled Prostate-Specific Membrane Antigen Positron Emission Tomography/Computed Tomography for the Evaluation of Renal Cancer. *Eur Urol Focus* (2020) 6:146–50. doi: 10.1016/j.euf.2018.08.004
16. Ahn T, Roberts MJ, Abduljabar A, Joshi A, Perera M, Rhee H, et al. A Review of Prostate-Specific Membrane Antigen (PSMA) Positron Emission Tomography (PET) in Renal Cell Carcinoma (RCC). *Mol Imaging Biol* (2019) 21:799–807. doi: 10.1007/s11307-018-01307-0
17. Demirci E, Ocak M, Kabasakal L, Decristoforo C, Talat Z, Halaç M, et al. (68)Ga-PSMA PET/CT Imaging of Metastatic Clear Cell Renal Cell Carcinoma. *Eur J Nucl Med Mol Imaging* (2014) 41:1461–62. doi: 10.1007/s00259-014-2766-y
18. Perera M, Papa N, Christidis D, Wetherell D, Hofman MS, Murphy DG, et al. Sensitivity, Specificity, and Predictors of Positive 68Ga-Prostate-Specific Membrane Antigen Positron Emission Tomography in Advanced Prostate Cancer: A Systematic Review and Meta-Analysis. *Eur Urol* (2016) 70:926–37. doi: 10.1016/j.eururo.2016.06.021
19. Perera M, Papa N, Roberts M, Williams M, Udovicich C, Vela I, et al. Gallium-68 Prostate-Specific Membrane Antigen Positron Emission Tomography in Advanced Prostate Cancer-Updated Diagnostic Utility, Sensitivity, Specificity, and Distribution of Prostate Specific Membrane Antigen-Avid Lesions: A Systematic Review and Meta-Analysis. *Eur Urol* (2020) 77(4):403–17. doi: 10.1016/j.eururo.2019.01.049
20. Hofman MS, Lawrentschuk N, Francis RJ, Tang C, Vela I, Thomas P, et al. Prostate-Specific Membrane Antigen PET-CT in Patients With High-Risk Prostate Cancer Before Curative-Intent Surgery or Radiotherapy (Propsma): A Prospective, Randomised, Multicentre Study. *Lancet* (2020) 395 (10231):1208–16. doi: 10.1016/S0140-6736(20)30314-7
21. de Galiza Barbosa F, Queiroz MA, Nunes RF, Costa LB, Zaniboni EC, Marin J, et al. Nonprostatic Diseases on PSMA PET Imaging: A Spectrum of Benign and Malignant Findings. *Cancer Imaging* (2020) 20(1):23. doi: 10.1186/s40644-020-00300-7
22. Bychkov A, Vutrapongwatana U, Tepmongkol S, Keelawat S. PSMA Expression by Microvasculature of Thyroid Tumors - Potential Implications for PSMA Theranostics. *Sci Rep* (2017) 7(1):5202. doi: 10.1038/s41598-017-05481-z
23. Siva S, Callahan J, Pryor D, Martin J, Lawrentschuk N, Hofman MS. Utility of 68 Ga Prostate Specific Membrane Antigen - Positron Emission Tomography in Diagnosis and Response Assessment of Recurrent Renal Cell Carcinoma. *J Med Imaging Radiat Oncol* (2017) 61(3):372–8. doi: 10.1111/1754-9485.12590
24. Gao J, Xu Q, Fu Y, He K, Zhang C, Zhang Q, et al. Comprehensive Evaluation of 68Ga-PSMA-11 PET/CT Parameters for Discriminating Pathological Characteristics in Primary Clear-Cell Renal Cell Carcinoma. *Eur J Nucl Med Mol Imaging* (2021) 48(2):561–9. doi: 10.1007/s00259-020-04916-6
25. Raveenthiran S, Esler R, Yaxley J, Kyle S. The Use of 68Ga-PET/CT PSMA in the Staging of Primary and Suspected Recurrent Renal Cell Carcinoma. *Eur J Nucl Med Mol Imaging* (2019) 46(11):2280–8. doi: 10.1007/s00259-019-04432-2
26. Rhee H, Blazak J, Tham CM, Ng KL, Shepherd B, Lawson M, et al. Pilot Study: Use of Gallium-68 PSMA PET for Detection of Metastatic Lesions in Patients With Renal Tumour. *EJNMMI Res* (2016) 6(1):76. doi: 10.1186/s13550-016-0231-6

Conflict of Interest: The authors declare that the research was conducted in the absence of any commercial or financial relationships that could be construed as a potential conflict of interest.

Publisher's Note: All claims expressed in this article are solely those of the authors and do not necessarily represent those of their affiliated organizations, or those of the publisher, the editors and the reviewers. Any product that may be evaluated in this article, or claim that may be made by its manufacturer, is not guaranteed or endorsed by the publisher.

Copyright © 2021 Seront, Lhommel and Tombal. This is an open-access article distributed under the terms of the Creative Commons Attribution License (CC BY). The use, distribution or reproduction in other forums is permitted, provided the original author(s) and the copyright owner(s) are credited and that the original publication in this journal is cited, in accordance with accepted academic practice. No use, distribution or reproduction is permitted which does not comply with these terms.

frontiers in Oncology

ORIGINAL RESEARCH
published: 08 December 2021
doi: 10.3389/fonc.2021.744107

CD146 as a Prognostic-Related Biomarker in ccRCC Correlating With Immune Infiltrates

Zheng Lv[1,2], *Hua-Yi Feng*[2,3], *Wang Tao*[2,3], *Hong-Zhao Li*[2] *and Xu Zhang*[1,2*]

[1] School of Medicine, Nankai University, Tianjin, China, [2] Department of Urology, The Third Medical Center, Chinese People Liberation Army (PLA) General Hospital, Beijing, China, [3] Medical School of Chinese People Liberation Army (PLA), Beijing, China

Backgrounds: CD146 is highly expressed in various malignant tumors and associated with the poor prognosis. However, the role of CD146 in clear cell renal cell carcinoma (ccRCC) is still unknown. This study aimed to identify the role of CD146 in ccRCC by integrated bioinformatics analysis.

Methods: CD146 mRNA expression and methylation data in ccRCC was examined using the TIMER, UALCAN, and MethSurv databases. CD146 expression in paraffin-embedded tissues (140 cancer samples and 140 paracancer tissues) from our cohort were examined by immunohistochemistry assay. The LinkedOmics database was used to study the signaling pathways related to CD146 expression. TIMER and TISIDB were used to analyze the correlations among CD146, CD146-coexpressed genes, tumor-infiltrating immune cells, and immunomodulators. The relationship between CD146 and drug response in renal cancer cell lines was analyzed by the CTRP and CCLE databases.

Results: The mRNA and protein levels of CD146 were elevated in ccRCC tissues than that in paracancer tissues. The DNA methylation of CD146 in ccRCC tissues were lower than that in normal tissues. Importantly, high CD146 expression was associated with poor prognosis in patients with ccRCC. Furthermore, multivariate Cox regression analysis showed that CD146 was an independent prognostic factor in ccRCC. GO and KEGG pathway analyses indicated the co-expressed genes of CD146 were mainly related to a variety of immune-related pathways, including Th1 and Th2 cell differentiation, Th17 cell differentiation, and leukocyte transendothelial migration. Our data demonstrated that the expression and methylation status of CD146 were strongly correlated with immune infiltration levels, immunomodulators, and chemokines. Further, the sensitivity and resistance of renal cancer cell lines to some drugs were related to CD146 expression.

Conclusions: Our study highlights the clinical significance of CD146 in ccRCC and provides novel insights into the immune function of CD146 in the tumor microenvironment.

Keywords: CD146, ccRCC, prognosis, methylation, tumor microenvironment

OPEN ACCESS

Edited by:
Fabio Grizzi,
Humanitas Research Hospital, Italy

Reviewed by:
Ugo Giovanni Falagario,
University of Foggia, Italy
Maria Helena Ornellas,
Universidade Estadual do Rio de Janeiro, Brazil

****Correspondence:***
Xu Zhang
xzhang301@163.com

Specialty section:
This article was submitted to Genitourinary Oncology, a section of the journal Frontiers in Oncology

Received: *19 July 2021*
Accepted: *17 November 2021*
Published: *08 December 2021*

Citation:
Lv Z, Feng H-Y, Tao W, Li H-Z and Zhang X (2021) CD146 as a Prognostic-Related Biomarker in ccRCC Correlating With Immune Infiltrates. Front. Oncol. 11:744107. doi: 10.3389/fonc.2021.744107

INTRODUCTION

Clear renal cell carcinoma (ccRCC) is the most common subtype of renal cell carcinoma (1). Despite substantial advancement in ccRCC target therapies, such as tyrosine kinases inhibitors and mTOR inhibitors, the prognosis for advanced and metastatic ccRCC patients remains poor (2, 3). ccRCC is a highly immune-infiltrated tumor (4). In patients with metastatic RCC, immunotherapy-based combinations have become the standard of care and show an efficacy and overall survival benefit in the first-line metastatic setting (5, 6). The interaction between tumor cells and the tumor microenvironment (TME) provides new insights into the molecular drivers underlying ccRCC occurrence, metastasis, and recurrence (7, 8). However, the molecular mechanisms underlying ccRCC carcinogenesis remain unclear.

CD146, also known as MUC18, is a highly glycosylated type I transmembrane protein. Normal expression of CD146 is restricted to certain cell types, including endothelial cells (9), fibroblasts (10), smooth muscle cells (11), and lymphocytes (12). CD146 is weakly expressed or not detected in normal adult tissues but is strongly upregulated under various pathological conditions such as atherosclerosis (13), inflammation (14), and tumorigenesis (15). Accumulating evidence confirmed that CD146 was highly expressed on advanced primary and metastatic cancers including gastric cancer (16), melanoma (17), and lung cancer (18). The overexpression of CD146 could promote tumor progression and metastasis by altering the expression of genes in cancer cell proliferation, apoptosis, and angiogenesis (19, 20). While the expression of CD146 and clinical significance in ccRCC is still unknown.

Growing evidence suggested that CD146 could promote the tissue-infiltrative potential and augment inflammatory response in several inflammatory diseases, including systemic sclerosis (21), rheumatoid arthritis (22), and inflammatory bowel disease (23). CD146 participates in the regulation of local immunity by recruiting mononuclear cells from the peripheral blood to the site of inflammation (24). CD146 also induces the formation of cytoplasmic protrusions and acts as an endothelial adhesion receptor, thereby mediating lymphocyte adhesion, transmigration, and lymphocyte homing (25). Previous studies have shown that inflammation affects the progression of cancer, as the chronic inflammation persists, the risk of carcinogenesis increases (26). Netti GS et al. reported that the expression of PTX3 can affect immunoflogosis in the ccRCC microenvironment, by activating the classical pathway of CS (C1q) and releasing pro-angiogenic factors (C3a, C5a), thus playing an effect on resident cells to sustain carcinogenesis (27). Detection of these markers can provide information on early diagnosis, treatment effect, and prognosis of related malignant tumors (28, 29). Krishna Y et al. show that M2 type macrophages dominate in metastatic uveal melanoma and contribute to an immunosuppressive TME by upregulation of CD146 (30). Nevertheless, the role of CD146 in affecting the components in TME in ccRCC is still poorly understood.

Here, we present a comprehensive analysis of CD146 in ccRCC using multiple available databases. We found that CD146 is significantly overexpressed in ccRCC, and CD146 expression is associated with tumor stage, tumor grade, and prognosis in ccRCC patients. The co-expressed genes of CD146 were enriched in pathways involved in endothelium development, response to virus, T cell activation, and adaptive immune response. Both CD146 expression and its methylation status were correlated with tumor infiltrating immune cells and immunomodulators in ccRCC. More importantly, we also explored the potential of using CD146 as a possible therapeutic target in ccRCC treatment. Our study indicated that CD146 may be used as a prognostic biomarker and new immune-associated therapeutic target for ccRCC patients.

MATERIALS AND METHODS

Tumor Immune Estimation Resource Analysis

The Tumor Immune Estimation Resource (TIMER) (https://cistrome.shinyapps.io/timer/) web server is a resource that systematically analyzes immune infiltrates across different cancer types (31). To evaluate the expression difference of CD146 between tumor and adjacent normal tissues, we used the TIMER database to study the RNA sequence data of different cancer types in TCGA (The Cancer Genome Atlas). The immune cell abundance was estimated by the TIMER algorithm. Correlation modules were used to determine the relationship between the RNA-seq expression profile data of CD146 in ccRCC and immune cells, including CD4+ T cells, CD8+ T cells, regulatory T (Treg) cells, T follicular helper (Tfh) cells, Type 1 T helper (Th1) cells, Type 2 T helper (Th2) cells, natural killer (NK) cells, myeloid dendritic cells, monocyte, neutrophils, M1 macrophages, and M2 macrophages. The gene markers of immune cells were also correlated with CD146 expression using gene modules. These gene markers referenced are cited in previous publications (32–34).

DNA Methylation Analysis

DNA methylation during carcinogenesis has an impact on not only gene expression, but also the prognosis of cancer patients (35). MethSurv (https://biit.cs.ut.ee/methsurv/) is a web portal that provides survival analysis based on DNA methylation biomarkers using TCGA data. DNA methylation of CD146 at CpG sites and the prognostic value of these CpG sites in ccRCC were analyzed by MethSurv.

Patients and Clinical Materials

Tumor specimens were collected from 140 ccRCC patients diagnosed with ccRCC treated with radical or partial nephrectomy at the Department of Urology of the Chinese People's Liberation Army (PLA) General Hospital (Beijing, China) from January 2013 to December 2019. The medical records of clinic-pathologic data from our institutional database, including age, gender, T stage, N stage, M stage, and Fuhrman grade, were retrospectively reviewed. All patients were staged according to the eighth edition of the AJCC-UICC TNM classification (36). Fuhrman classification was used to attribute

nuclear grade (37). The clinic-pathologic data are reported in **Table 1**. All samples of cancer tissue had been pathologically confirmed as ccRCC by two pathologists. All patients were informed and signed a consent for the use of clinical data for scientific purposes. The present study was approved by the ethics committee of the Chinese PLA General Hospital.

Immunohistochemistry

To determine CD146 protein expression in ccRCC, IHC staining of CD146 was conducted on cancer and paracancer tissues for 140 ccRCC cases from our cohort. For IHC staining, a tissue microarray (TMA) was obtained from the tissue bank at the Department of Urology of the Chinese PLA General Hospital. IHC staining of TMA tissues was performed with antibodies against CD146 (Abcam, ab75769). The standard protocols were followed as previously described (38). Slides were scanned using an Axio Image Z2 Microscope (Zeiss) and the TissueFAXS imaging system (TissueGnostics GmbH, Austria). All images were analyzed by TissueQuest and StrataQuest software (TissueGnostics GmbH, Austria). Staining intensity was scored 0 (negative), 1 (weak), 2 (moderate), and 3 (strong). Staining range was scored on a 4-point scale (0 = 0%, 1 = 1%∼24%, 2 = 25%∼49%, and 3 = 50%∼100%). The final IHC score was obtained by multiplying the intensity scores with the staining range. ccRCC patients with a final IHC score ≥4 were included in the high CD146 group, whereas those with a final IHC score<4 were included in the low CD146 group (39).

Western Blot

Western blot assays were used according to standard techniques as previously reported (40). Antibodies against CD146 (ab75769; Abcam) and β-actin (#3700; CST) were used.

UALCAN Analysis

UALCAN (http://ualcan.path.uab.edu/) is a web resource for online analysis of gene transcriptional data and clinical data of cancers from TCGA (41). We obtained differential expression of CD146 mRNA and protein of CD146 in ccRCC tumor tissues and adjacent normal tissues in the UALCAN database. DNA hypermethylation at promoters can lead to gene silencing (42). To further identify the mechanisms underlying the upregulation of CD146 in ccRCC, the methylation levels of CD146 in the ccRCC dataset were also analyzed by the UALCAN database. The differential expression of CD146 and its promoter methylation status in patients with various tumor grade (grades 1, 2, 3, and 4), tumor stage (stages 1, 2, 3, and 4) and ccRCC subtype (ccA and ccB) were also compared.

LinkedOmics Database Analysis

The LinkedOmics database (http://www.linkedomics.org/login.php) is acknowledged as a web portal that analyses multi-omics data from TCGA datasets (43). We searched for the differentially expressed genes related to CD146 in ccRCC using the LinkFinder module. The correlation results were analyzed by the Pearson correlation coefficient and were visualized by volcano plot and heat maps. To obtain description information, the differentially expressed genes related to CD146 were annotated using Gene Ontology (GO) analysis, Kyoto Encyclopedia of Genes and Genomes (KEGG) pathway enrichment analysis, and gene set enrichment analysis (GSEA) *via* the LinkInterpreter module.

TISIDB Database Analysis

The TISIDB database (http://cis.hku.hk/TISIDB) is a web server for the interplay between the tumor and immune system, which can assist in the prediction of immunotherapy responses (44). In our study, the associations between CD146 expression and lymphocytes, immunomodulators, and chemokines were analyzed by the TISIDB database. A 'rho' value greater than 0.2 and less than −0.2 was considered as a significant correlation at $p < 0.05$ (45).

Correlation Between CD146 and Drug Response

To explore whether CD146 could be used as a therapeutic target in cancer patients, we investigated the correlation between

TABLE 1 | Relationship between CD146 expression and clinicopathological features in patients with ccRCC.

Variable	No. of patients (%)			χ^2	*p*-value
	Patients	CD146 high	CD146 low		
Age (years)					
≤60	104	50(48.1)	54(51.9)	1.126	0.289
> 60	36	21(58.3)	15(41.7)		
Gender					
Male	108	53(49.1)	55(50.9)	0.509	0.476
Female	32	18(56.3)	14(43.8)		
T stage					
T1+T2	106	49(46.2)	57(53.8)	3.517	0.061
T3+T4	34	22(64.7)	12(35.3)		
N stage					
N0	128	64(50.0)	64(50.0)	0.305	0.581
N1	12	7(58.3)	5(41.7)		
M stage					
M0	134	66(49.3)	68(50.7)	2.668	0.102
M1	6	5(83.3)	1(16.7)		
Fuhrman grade					
Grade 1 + 2	100	39(59.6)	61(40.4)	19.215	0.000
Grade 3 + 4	40	32(83.7)	8(16.3)		

CD146 expression and drug response. CD146 gene expression levels in 30 cancer cell lines were obtained from the Cancer Cell Line Encyclopedia (CCLE; https://portals.broadinstitute.org/ccle/). Drug response data in cancer cell lines were downloaded from the Cancer Therapy Response Portal (CTRP, https://portals.broadinstitute.org/ctrp.v2.2/) (46). The correlation between CD146 expression and drug response area under the curve (AUC) was analyzed by Pearson correlation coefficient analysis in each cancer cell type. The percentage of drugs significantly correlated with CD146 was obtained. The ratio of drugs related to CD146 in 10 different cancer types with 30 cell lines was represented by histogram. The correlation between CD146 and 545 drug responses under the curve in 21 renal cancer cell lines were analyzed by SangerBox and shown by volcanic plots. We considered a p-value of less than 0.05 as statistically significant.

Statistical Analysis

Statistical analysis was performed using the GraphPad Prism version 8.0 (GraphPad software, USA) and Statistical Package for Social Sciences (SPSS 17.0 for Windows, SPSS, Chicago, IL). The measurement data are presented as mean ± SD. An independent samples t test was used to analyze the differential expression levels of CD146 mRNA between the ccRCC tissues and the adjacent normal tissues from TCGA databases. Correlations between CD146 expression and clinicopathological characteristics were analyzed by the Pearson's Chi squared test. Overall survival (OS) analysis and progression-free survival (PFS) analysis were performed by Kaplan–Meier plots and the differences were compared using the log-rank test. Univariate and multivariable analyses were performed using the Cox proportional hazards regression models. A two-tailed P value of 0.05 was considered statistically significant.

RESULTS

CD146 Is Upregulated in ccRCC

Compared with normal tissues, CD146 was upregulated in cholangiocarcinoma, head and neck squamous cell carcinoma, kidney renal clear cell carcinoma, liver hepatocellular carcinoma, pheochromocytoma and paraganglioma, prostate adenocarcinoma, and thyroid carcinoma cancers, while CD146 was downregulated in bladder urothelial carcinoma, breast invasive carcinoma, cervical squamous cell carcinoma and endocervical adenocarcinoma, kidney chromophobe, lung adenocarcinoma, lung squamous cell carcinoma, and uterine corpus endometrial carcinoma cancers (**Figures 1A, B**). Consistent with the mRNA expression data, we found that CD146 protein was highly expressed in the ccRCC cancer tissues compared with paracancer tissues (**Figure 1C**). The positive staining of CD146 was mainly located in the plasma and membrane (**Figure 1C**). The results of UALCAN database analysis further confirmed that CD146 protein expression was higher in primary ccRCC cancer tissues than that in paracancer tissues (**Figure 1D**). The western blot assay also confirmed that CD146 is higher in ccRCC tumor tissues than that in paracancer tissues (**Figure 1E**). This evidence strongly indicated that the mRNA and protein expressions of CD146 were significantly upregulated in ccRCC.

The Prognostic Value of CD146 and Its Correlation With Clinicopathological Parameters in ccRCC

As is shown in **Table 1**, CD146 was more expressed in higher grade cancers compared to lower grades cancers (**Table 1**). Kaplan-Meier analysis demonstrated that high expression of CD146 was significantly associated with poor OS [hazard ratio (HR) = 3.677, p = 0.0028] and PFS (HR = 3.493, p = 0.0009) in ccRCC patients (**Figures 2A, B**). Univariate Cox regression analyses showed an association between OS with age, T stage, N stage, M stage, Fuhrman grade, and CD146 expression. Moreover, multivariate Cox regression analysis showed that CD146 expression (HR = 4.655, p = 0.007), Fuhrman grade (HR = 3.472, p = 0.005), and M stage (HR = 3.625, p = 0.004) were independent prognostic factors for ccRCC patients (**Table 2**). Univariate Cox regression analysis indicated that T stage, N stage, M stage, Fuhrman grade, and CD146 expression were correlated with PFS. Furthermore, multivariate Cox regression revealed that CD146 expression (HR = 5.829, p = 0.001), Fuhrman grade (HR = 2.927, p = 0.007), and M stage (HR = 3.028, p = 0.005) were independent prognostic indicators for ccRCC patients (**Table 3**). These results suggest that CD146 was upregulated in ccRCC and associated with worse prognosis.

DNA Methylation of CD146 and Its Prognostic Value in ccRCC

DNA methylation levels of CD146 were significantly lower in ccRCC cancer tissues compared with normal samples (**Figure 3A**). The methylation status of CD146 was high in late-stage and high-grade tumors (**Figures 3B, C**). Furthermore, correlation analysis indicated that expression of CD146 mRNA was significantly negatively correlated with its methylation status (**Figure 3D**). Among 18 predicted CpG sites of CD146, 15 CpG sites, including cg08187057, cg09042577, cg25484790, cg081861493, cg21096399, cg18890215, cg24827784, cg18165196, cg14976391, cg17466841, and cg11287851, were significantly correlated with the prognosis of ccRCC (**Table 4**). Consistently, CpG sites of CD146, including cg08187057, cg09042577, cg25484790, cg18890215, cg24827784, cg14976391, and cg17466841, showed higher methylation levels in ccRCC, indicating that the CD146 methylation in these CpG sites was correlated with poor prognosis in ccRCC patients (**Figure 3E**). These results revealed that the methylation levels of CD146 act as an effective prognostic biomarker for ccRCC, demonstrating that CD146 may have a pivotal role in tumor progression.

CD146 Co-Expression Network in ccRCC

The results of the co-expression pattern of CD146 showed that 1904 genes were positively correlated with CD146, while 1696 genes were negatively correlated with CD146 (**Figure 4A**). Heat maps displayed the top 50 genes positively and negatively

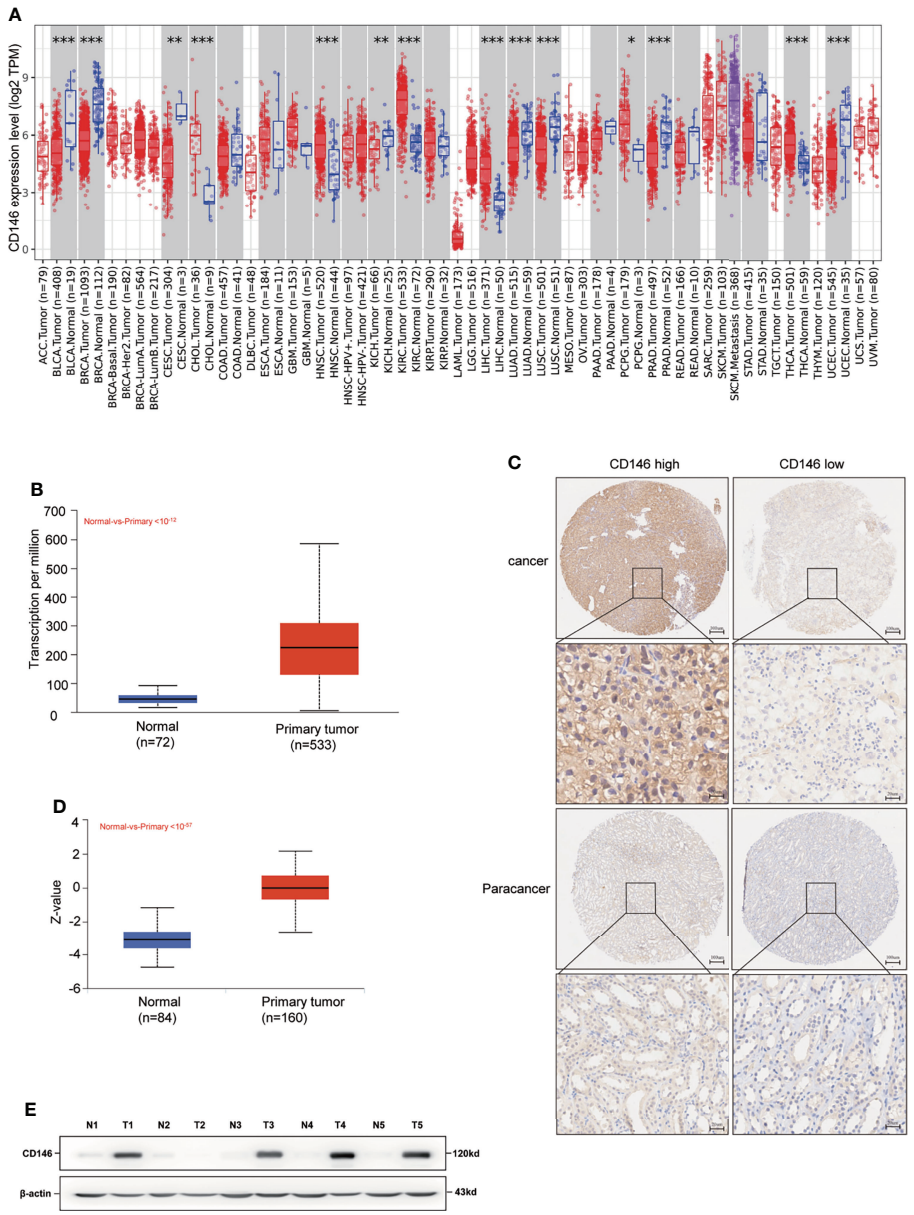

FIGURE 1 | High Expression of CD146 in ccRCC. **(A)** Human expression levels of CD146 in various malignant tumor types from The Cancer Genome Atlas (TCGA) database were analyzed by the Tumor Immune Estimation Resource (TIMER). CD146 was upregulated in cholangiocarcinoma (CHOL), head and neck squamous cell carcinoma (HNSC), kidney renal clear cell carcinoma (KIRC), liver hepatocellular carcinoma(LIHC), pheochromocytoma and paraganglioma (PCPG), prostate adenocarcinoma (PRAD), and thyroid carcinoma (THCA) cancers, and downregulated in bladder urothelial carcinoma (BLCA), breast invasive carcinoma (BRCA), cervical squamous cell carcinoma and endocervical adenocarcinoma (CESC), kidney chromophobe (KICH), lung adenocarcinoma (LUAD), lung squamous cell carcinoma (LUSC), and uterine corpus endometrial carcinoma (UCEC) cancers. *$p < 0.05$. **$p < 0.01$. ***$p < 0.001$. **(B)** Gene Expression Profiling Interaction Analysis (UALCAN) for the expression of CD146 mRNA in tumor tissues and normal tissues based on TCGA samples. **(C)** Representative immunohistochemistry images of CD146 in ccRCC cancer tissues and corresponding normal tissues. **(D)** Protein level of CD146 in normal tissues and ccRCC cancer tissues using CPTAC samples by the UALCAN database. **(E)** Protein expressions of CD146 in five pairs of ccRCC and adjacent normal tissues samples were determined by western blot assay (N: normal tissues, T: ccRCC cancer tissues).

associated with CD146 (**Figures 4B, C**). GO term annotation showed that co-expressed genes of CD146 join mainly in endothelium development, response to virus, T cell activation, adaptive immune response, extracellular structure organization, angiogenesis, regulation of immune effector process, negative regulation of defense response, regulation of innate immune response, leukocyte differentiation, etc. (**Figure 4D**). KEGG pathway analysis indicated enrichment in the Notch signaling pathway, Th1 and Th2 cell differentiation, microRNAs in cancer, Th17 cell differentiation, leukocyte transendothelial migration,

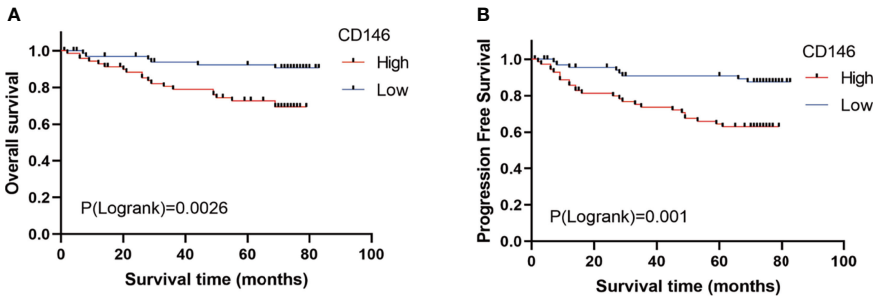

FIGURE 2 | The prognostic value of CD146 in patients with ccRCC. **(A, B)** Kaplan–Meier survival analysis revealed that ccRCC patients with high CD146 expression exhibited a shorter overall survival **(A)** and progression-free survival **(B)** than that in patients with low CD146 expression.

and the Rap1 signaling pathway (**Figure 4E**). These results indicate that the CD146 expression network influences the immune microenvironment greatly in ccRCC.

CD146 Is Correlated With Immune Infiltration in ccRCC

CD146 was positively correlated with infiltrating levels of neutrophils (rho = 0.312, p = 7.44e-12), myeloid dendritic cells (rho = 0.533, p = 3.36e-35), active CD4+ T cells (rho = 0.377, p = 5.63e-17), CD8+ T cells (rho = 0.203, p = 1.14e-05), Treg cells (rho = 0.316, p = 3.78e-12), Tfh cells (rho = -0.251, p = 4.58e-08), NK cells (rho = 0.308, p = 1.38e-11), activated mast cells (rho = 0.307, p = 1.49e-11), monocytes (rho = 0.256, p = 2.59e-08), macrophages (rho = 0.229, p = 6.56e-07), M1 macrophages (rho = 0.189, p = 4.46e-05), and M2 macrophages (rho = -0.333, p = 2.01e-13) (**Figure 5A**). In addition, CD146 was significantly correlated with the gene markers of monocytes, macrophages, M1 macrophages, M2 macrophages, neutrophils, NK cells, dendritic cells, Th1 cells, Th2 cells, Tfh cells, and Treg cells (**Table 5**). CD146 was significantly correlated with immune stimulators, such as TNFRSF4 (rho = 0.618, p < 2.2e-16), ENTPD1 (rho = 0.616, p < 2.2e-16), TMEM173 (rho = 0.505, p < 2.2e-16), and RAET1E (rho = 0.389, p < 2.2e-16) (**Figure 5B**). The expression of CD146 was also associated with immune inhibitors, including KDR (rho = 0.523, p < 2.2e-16), TGFB1 (rho = 0.424, p = 2.2e-16), ADORA2A (rho = 0.352, p < 4.97e-17), and IDO1 (rho = 0.303, p < 1.03e-12) (**Figure 5C**). CD146 expression was significantly correlated with CCL14 (rho = 0.566, p < 2.2e-16), CCL26 (rho = 0.300, p < 1.82e-12), CCL28 (rho = 0.214, p < 6.64e-7), and CX3CL1 (rho = 0.232, p < 6.21e-8) (**Figure 5D**). Meanwhile, CD146 expression was significantly associated with chemokine receptors, including CCR10 (rho = 0.443, p < 2.2e-16), CXCR4 (rho = 0.388, p < 2.2e-16), CCR6 (rho = 0.183, p < 2.14e-5), and CCR7 (rho = 0.180, p < 2.88e-5) (**Figure 5E**). These results support the findings that CD146 may function as an immunoregulatory factor in ccRCC.

TABLE 2 | Univariate and multivariable Cox regression of CD146 expression for overall survival in ccRCC patients.

Variable	Univariate Cox regression			Multivariable Cox regression		
	HR	95%CI	*p*-value	HR	95%CI	*p*-value
Age: >60 vs ≤60	0.431	0.212~0.874	0.020	0.739	0.335~1.632	0.455
Gender: male vs female	0.967	0.416~2.244	0.967			
T stage: T3+T4 vs T1+T2	3.668	1.761~7.638	0.001	1.252	0.502~3.123	0.630
N stage: N1 vs N0	4.416	1.680~11.609	0.003	3.136	0.859~11.444	0.084
M stage: M1 vs M0	8.994	4.146~19.510	0.000	3.625	1.495~8.789	0.004
Fuhrman grade: G3+G4 vs G1+G2	7.456	3.423~16.245	0.000	3.472	1.455~8.284	0.005
CD146: high vs low	8.117	2.833~23.255	0.000	4.655	1.525~14.207	0.007

TABLE 3 | Univariate and multivariable Cox regression of CD146 expression for progression-free survival in ccRCC patients.

Variable	Univariate Cox regression			Multivariable Cox regression		
	HR	95%CI	*p*-value	HR	95%CI	*p*-value
Age: >60 vs ≤60	0.730	0.366~1.453	0.370			
Gender: male vs female	1.227	0.539~2.793	0.626			
T stage: T3+T4 vs T1+T2	3.816	1.967~7.400	0.000	1.360	0.605~3.060	0.457
N stage: N1 vs N0	4.255	1.759~10.295	0.001	2.397	0.809~7.104	0.115
M stage: M1 vs M0	7.891	3.841~16.213	0.000	3.028	1.393~6.581	0.005
Fuhrman grade: G3+G4 vs G1+G2	6.302	3.140~12.648	0.000	2.927	1.341~6.390	0.007
CD146: high vs low	8.897	3.405~23.245	0.000	5.829	2.110~16.103	0.001

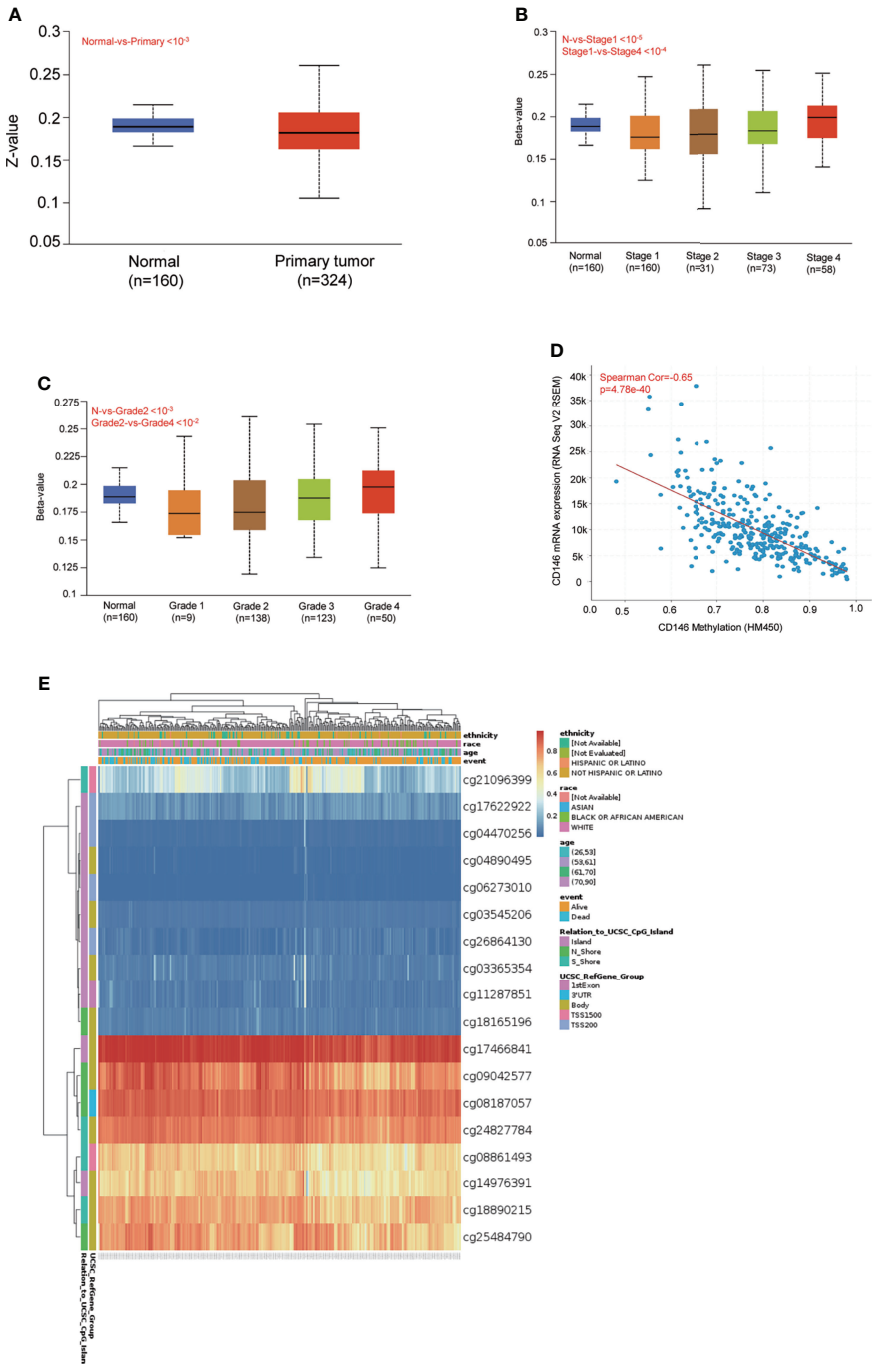

FIGURE 3 | DNA methylation levels of CD146 and its prognostic value in ccRCC. **(A)** Promoter methylation level of CD146 in normal tissues and primary ccRCC tissues by the UALCAN database. **(B, C)** Promoter methylation level of CD146 in ccRCC cancer tissues of various tumor stage **(B)** and tumor grade **(C)** by the UALCAN database. **(D)** Correlation analysis of CD146 mRNA expression with CD146 promoter methylation status by the UALCAN database. **(E)** The heat map of DNA methylation at CpG sites in the CD146 gene by the MethSurv database.

CD146 Methylation Is Associated With Immunosuppressive Status in ccRCC

As presented in the previous results, CD146 methylation in ccRCC correlates with prognosis in ccRCC. To elucidate the effect of CD146 methylation on the progression of ccRCC, we assessed the correlation of CD146 methylation with immune infiltration using TISIDB platforms. The result revealed that the methylation status of CD146 was negatively correlated with NK cells (rho = -0.153, p = 0.006), Th1 cells (rho = -0.119, p = 0.034), Th2 cells (rho = -0.242, p = 1.27e-5), and γδT cells (rho = -0.134,

TABLE 4 | The significant prognostic values of CpG in CD146.

Gene symbol	CpG Name	Hazard ratio	CI	LR test P value	UCSC Ref Gene Group	Relation to UCSC CpG Island
CD146	cg08187057	2.124	(1.444; 3.123)	1.6 e-04	3′UTR	N_Shore
	cg09042577	3.364	(1.944; 5.821)	7.6e-07	Body	N_Shore
	cg18165196	1.487	(0.913; 2.421)	0.097	Body	N_Shore
	cg25484790	2.848	(1.711; 4.740)	8.1e-06	Body	N_Shore
	cg08861493	1.959	(1.150; 3.337)	0.008	TSS1500	S_Shore
	cg21090399	1.794	(1.096; 2.905)	0.014	TSS1500	S_Shore
	cg18890215	1.898	(1.127; 3.196)	0.009	Body	S_Shore
	cg24827784	1.933	(1.224; 3.053)	0.003	Body	S_Shore
	cg03365354	1.236	(0.815; 1.874)	0.330	Body	Island
	cg03545206	0.437	(0.259; 0.738)	0.001	Body	Island
	cg04890495	0.658	(0.437; 0.989)	0.040	Body	Island
	cg14976391	1.895	(1.249; 2.873)	0.002	Body	Island
	cg17466841	2.482	(1.360; 4.530)	9e-04	Body	Island
	cg04470256	0.501	(0.340; 0.739)	4.6e-04	TSS200	Island
	cg02673010	0.329	(0.197; 0.549)	2.2e-06	TSS200	Island
	cg17622922	1.660	(1.131; 2.436)	0.096	TSS200	Island
	cg26864130	0.390	(0.225; 0.676)	2e-04	TSS200	Island
	cg11287851	1.824	(1.240; 2.682)	0.002	1stExon	Island

p = 0.0166) (**Figure 6A**). Similarly, the methylation status of CD146 was negatively associated with immune stimulators, such as C10orf54 (rho = -0.248, p = 8.13e-06), CD276 (rho = -0.296, p = 8.58e-08), CXCR4 (rho = -0.149, p = 0.0078), and ENTPD1 (rho = -0.287, p =2.04e-07) (**Figure 6B**), while being positively associated with immune inhibitors, such as CD274 (rho = 0.220, p = 7.84e-05), CTLA4 (rho = 0.134, p = 7.84e-05), HAVCR2 (rho = 0.122, p = 0.0289), and KDR (rho = 0.287, p = 2.11e-07) (**Figure 6C**). The methylation status of CD146 was also negatively associated with chemokines and receptors, such as CCL14 (rho = 0.341, p = 5.46e-10), CCR6 (rho = -0.122, p = 0.03), CCR10 (rho = -0.311, p = 1.73e-08), and CXCR4 (rho = -0.149, p = 0.0078) (**Figure 6D**). These results indicated that the methylation status of CD146 is positively associated with immunosuppressive status in ccRCC.

CD146 Expression and Drug Response in Renal Cancer Cell Lines

As is shown in **Figure 7A**, the ratio of drugs significantly correlated with CD146 expression in 10 different cancer cell

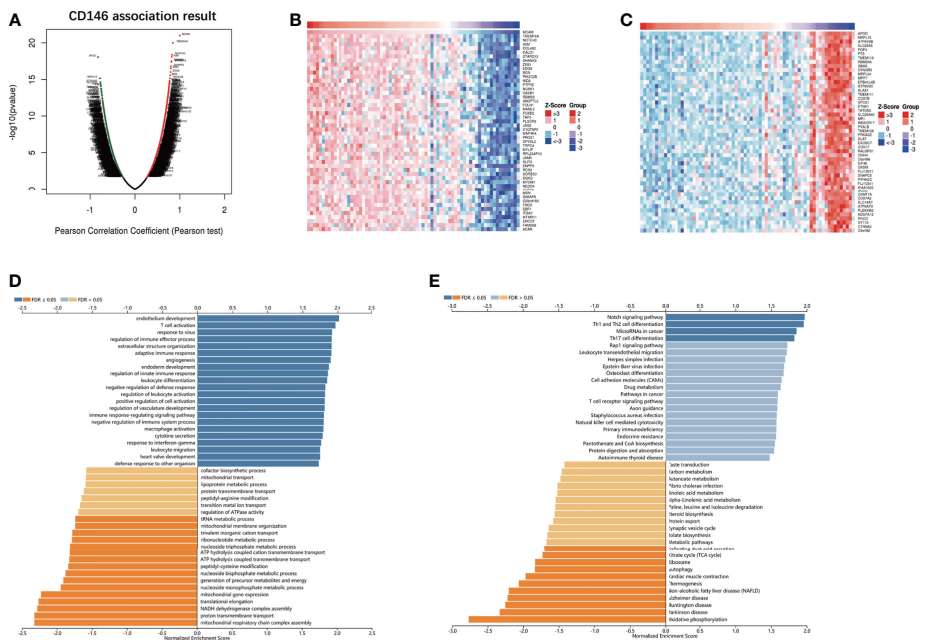

FIGURE 4 | CD146 co-expressed genes and functional enrichment analysis. **(A)** Volcano map of co-expressed profiling of CD146 in ccRCC by the LinkedOmics database. **(B, C)** Heat map of top 50 positively **(B)** and 50 negatively **(C)** correlated genes with CD146 are displayed. **(D, E)** CD146 co-expression genes were annotated by Gene Ontology (GO) analysis **(D)** and Kyoto Encyclopedia of Genes and Genomes (KEGG) pathway analysis **(E)** available at LinkedOmics.

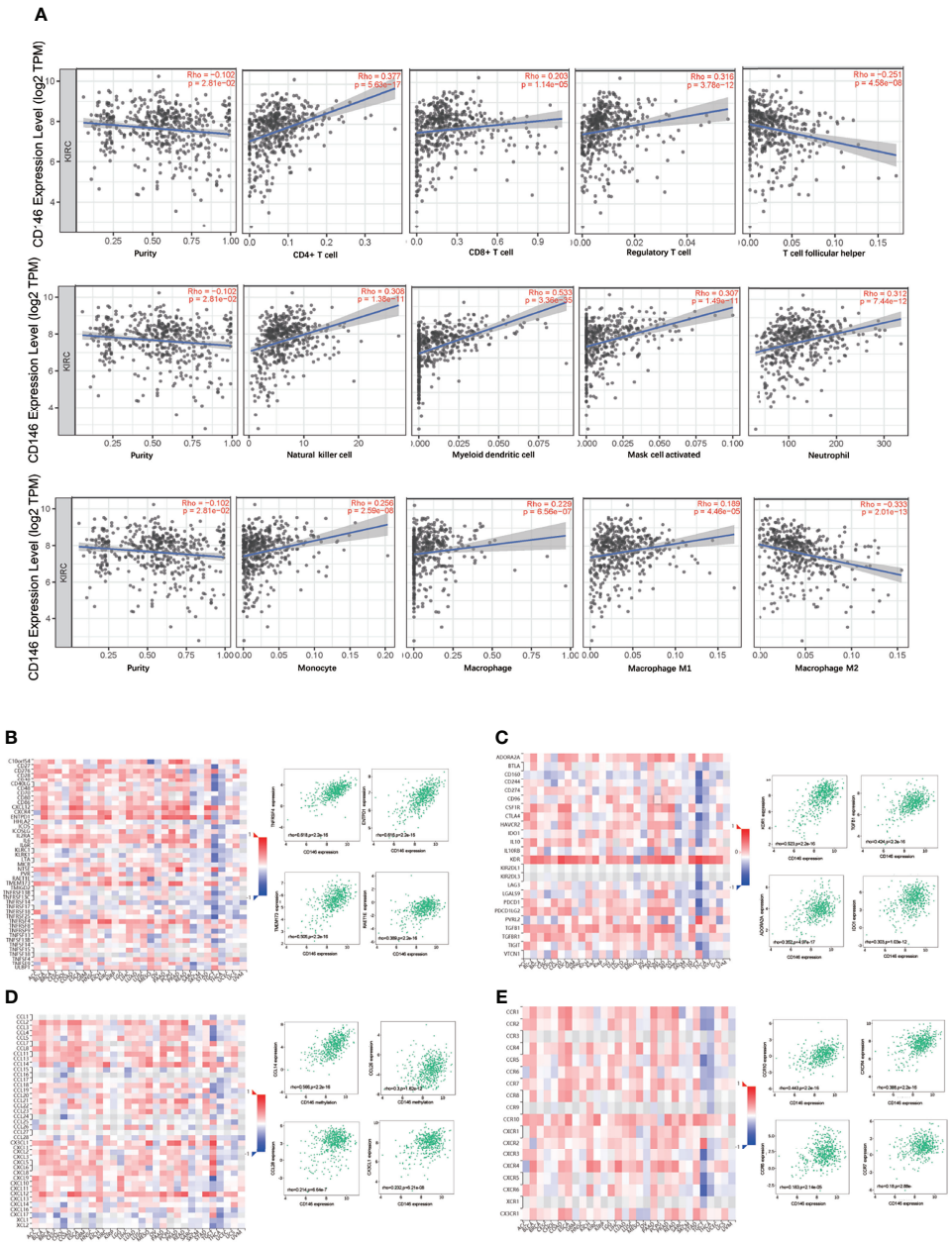

FIGURE 5 | Correlation between CD146 with immune infiltration in ccRCC. **(A)** Correlation between CD146 expression and the abundance of tumor infiltrating immune cells in ccRCC available from the TIMER2.0 database. **(B, C)** Correlation between CD146 expression and immunostimulators **(B)** and immunoinhibitors **(C)** in ccRCC available from the TISIDB database. **(D, E)** Correlation between CD146 expression and chemokines **(D)** and chemokine receptors **(E)** in ccRCC available from the TISIDB database.

line types is presented. The percentage of drugs significantly related with CD146 in renal cancer cell lines accounted for 5.5%. As is shown in **Figure 7B**, the relationship between CD146 and 545 drug response AUCs in renal cancer cell lines is presented. The drugs associated with CD146 in renal cancer cell lines are shown in **Table 6**. High CD146 expression was significantly correlated with a better response of inhibitors of topoisomerase I+II, including topotecan, SN-38, and etoposide. In addition, brivanib, inhibitor of VEGFR1/2, was also confirmed to be related to CD146 expression. Besides, inhibitors of DNA replication, including gemcitabine and clofarabine, were correlated with CD146 expression. Moreover, high CD146 expression was related to drug resistance of quizartinib, GSK1059615, BRD-K92856060, and AC55649. Overall, CD146 has the potential to become a therapeutic target for clinical treatment of ccRCC.

TABLE 5 | The correlations between CD146 and gene markers of immune cells in ccRCC and normal cells by GEPIA.

Description	Gene markers	None Cor	*p*-Value	Purity Cor	*p*-Value
CD8+T cell	CD8A	-0.005	0.910	-0.033	0.475
	CD8B	-0.028	0.521	-0.058	0.217
T cell (general)	CD3D	-0.001	0.973	-0.053	0.260
	CD3E	0.053	0.221	0.011	0.810
	CD2	0.024	0.584	-0.024	0.611
B cell	CD19	0.022	0.618	-0.006	0.904
	CD79A	0.026	0.542	-0.011	0.806
Monocyte	CD86	0.016	0.717	-0.034	0.466
	CD115(CSF1R)	0.165	***	0.124	**
TAM	CCL2	0.125	**	0.122	**
	CD68	-0.020	0.641	-0.052	0.267
	IL10	0.083	0.055	0.054	0.243
M1 macrophage	INOS(NOS2)	0.554	***	0.537	***
	IRF5	-0.214	***	-0.266	***
	COX2(PTGS2)	0.227	***	0.245	***
M2 macrophage	CD163	0.191	***	0.156	***
	VSIG4	0.079	0.069	0.024	0.610
	MS4A4A	0.154	***	0.120	*
Neutrophils	CD66b(CEACAM8)	0.087	*	0.095	0.041
	CD11b(ITGAM)	0.093	*	0.055	0.240
	CCR7	0.239	***	0.195	***
NK	KIR2DL1	0.316	***	0.305	***
	KIR2DL3	0.230	***	0.214	***
	KIR2DL4	0.061	0.161	0.045	0.339
	KIR3DL1	0.309	***	0.309	***
	KIR3DL2	0.275	***	0.254	***
	KIR3DL3	0.130	**	0.109	*
	KIR2DS4	0.274	***	0.265	***
Dendritic cell	HLA-DPB1	0.080	0.066	0.032	0.499
	HLA-DQB1	0.120	**	0.087	0.062
	HLA-DRA	0.048	0.264	0.001	0.984
	HLA-DPA1	0.094	*	0.048	0.302
	BDCA-1(CD1C)	0.245	***	0.214	***
	BDCA-4(NRP1)	0.683	***	0.668	***
	CD11c	-0.032	0.455	-0.053	0.259
Th1	T-bet (TBX21)	0.338	***	0.330	***
	STAT4	0.224	***	0.181	***
	STAT1	0.027	0.533	-0.013	0.779
	IFN-γ(IFNG)	-0.066	0.128	-0.109	*
	TNF-α(TNF)	0.032	0.454	-0.003	0.950
Th2	GATA3	0.043	0.326	0.053	0.259
	STAT6	0.228	***	0.226	*
	STAT5A	0.061	0.157	0.009	0.848
	IL13	0.101	*	0.125	**
Tfh	BCL6	0.303	***	0.306	***
	IL21	0.005	0.901	0.000	1.000
Th17	STAT3	0.437	***	0.437	***
	IL17A	0.024	0.577	0.003	0.942
Treg	FOXP3	0.004	0.919	-0.042	0.369
	CCR8	0.040	0.363	0.007	0.879
	STAT5B	0.452	***	0.458	***
	TGFβ(TGFB1)	0.506	***	0.504	***
T cell exhaustion	PD-1(PDCD1)	-0.076	0.078	-0.110	*
	CTLA4	-0.075	0.083	-0.124	**
	LAG3	-0.094	*	-0.133	**
	TIM3(HAVCR2)	0.024	0.578	-0.002	0.965
	GZMB	0.213	***	0.209	***

*$p < 0.05$. **$p < 0.01$. ***$p < 0.001$.

DISCUSSION

Although surgical resection is the first-line therapy for clinically localized RCC, mortality after surgical treatment for RCC cannot be ignored. Elder patients and patients at high stage tend to have a higher 30-day mortality risk after surgery (47). Recent advances in understanding the molecular background of ccRCC have led to unprecedented progress in the diagnosis, prognosis, and therapy of

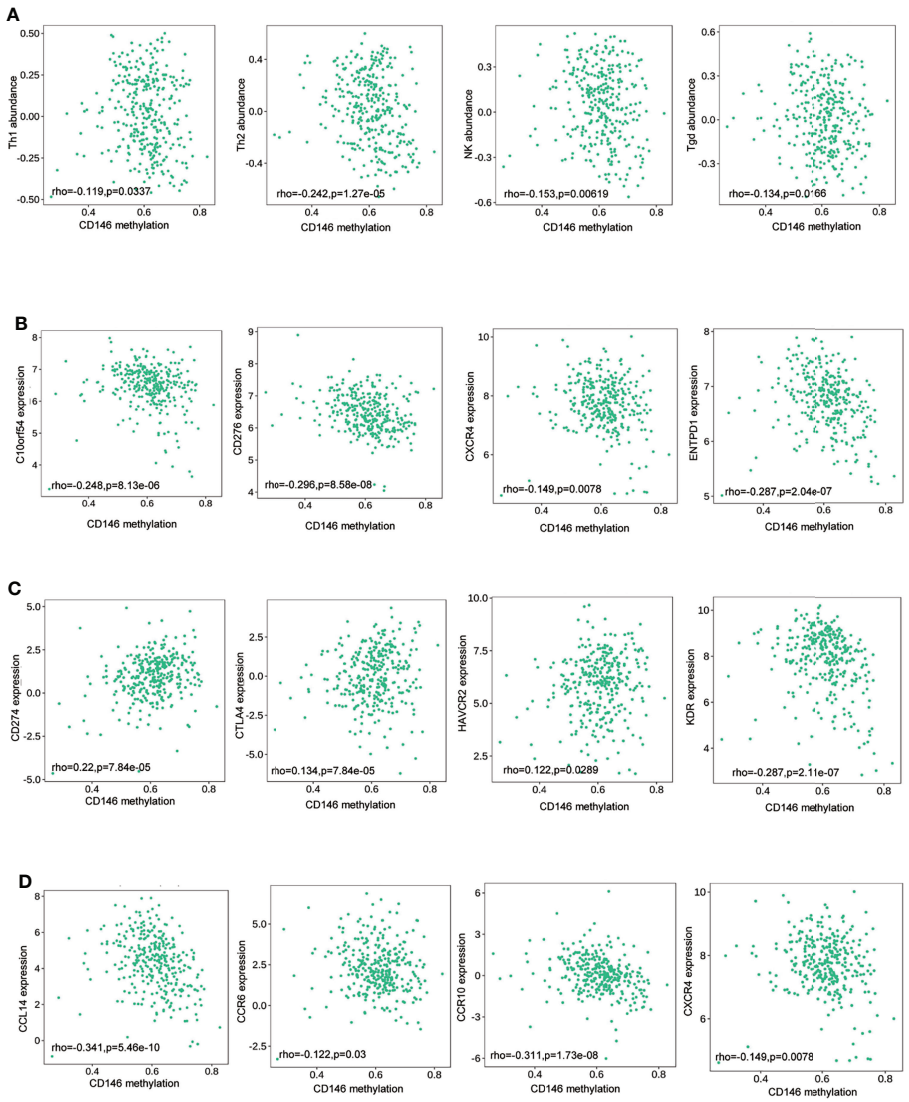

FIGURE 6 | Association between the methylation status of CD146 with immune infiltrates in ccRCC. **(A)** Correlation of the methylation status of CD146 with NK cells, Type 1 T helper cells, Type 2 T helper cells, and γδT helper cells in ccRCC available from the TISIDB database. **(B–D)** Correlation of the methylation status of CD146 with immunostimulators **(B)** and immunoinhibitors **(C)** and chemokines/receptors **(D)** in ccRCC available from the TISIDB database.

ccRCC (48). Immunotherapies targeting the PD-L1/PD1 pathway have shown benefits in advanced ccRCC patients (49). However, patients that are on immunotherapy will eventually develop treatment resistance due to the immune evasion mechanism (50). In addition to the PD-L1/PD1 pathway, ample evidence supports the fact that many other molecules, such as siglec-15 and FGL1, also contribute to dysfunctional immunity in the TME (51, 52). Therefore, exploring the potential immune-related factors responsible for tumor immune escape may help to improve the prognosis of ccRCC patients. CD146, originally identified as a cell adhesion molecule, is widely involved in immune response, cell migration, and angiogenesis (15). Recent evidence also indicates that CD146 is overexpressed in malignant tumors and is associated with tumor progression (18, 53, 54). While the role of CD146 in ccRCC is unclear, we aimed at exploring the clinical significance and biological functions of CD146 in ccRCC by employing open-access databases for a comprehensive analysis.

According to the analysis of TCGA data and our IHC analysis, ccRCC showed a remarkable high expression of CD146 as mRNA and protein. The mechanism of CD146 upregulation in ccRCC is unclear. Luo Y. et al. reported that CD146 expression and the HIF-1α transcriptional program reinforce each other to physiologically enable pulmonary artery smooth muscle cells to adopt a more synthetic phenotype (11). As ccRCC is well elucidated for its VHL/HIF dysregulation and downstream signal abnormalities (55), we may speculate that the VHL/HIF pathway is the key upstream regulator of CD146 in ccRCC, which needs further verification. Researchers demonstrated that aberrant CpG island methylation of

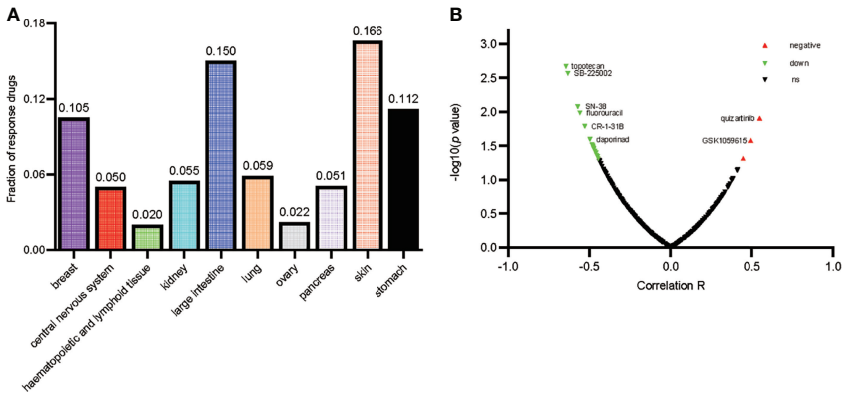

FIGURE 7 | Drug response analysis of CD146. **(A)** The ratio of drugs correlated with CD146 expression in 10 various cancer cell line types including 30 cell lines is shown by histogram. **(B)** The correlation between CD146 expression and drug response in renal cancer cell lines is shown by volcano plot.

the CD146 gene promoter in breast cancer cells lines is involved in the expression control of CD146 (56). So, we investigated the promoter methylation level of CD146 in ccRCC using the UALCAN database. We found that the DNA methylation levels of CD146 in cancer tissues were significantly lower than that in normal samples, indicating that a low level of promoter methylation status of CD146 is responsible for the overexpression of CD146 in ccRCC. CD146 was reported to promote tumor progression, and elevated expression of CD146 predicted poor prognosis in cancer patients. To determine whether CD146 could be used as a prognostic marker in ccRCC, we investigated the prognosis of ccRCC patients with different CD146 expression levels. In our cohort. we observed that high CD146 expression in ccRCC tissues was associated with a poor prognosis in ccRCC patients. Multivariate Cox regression further confirmed that high CD146 expression is an independent adverse prognosis factor for ccRCC patients, suggesting that CD146 is a novel prognostic biomarker in ccRCC.

The genes in the same clique tend to be co-expressed and synergistically co-regulated. To unravel the biological functions of CD146, co-expression analysis and functional enrichment analysis were performed. Importantly, we identified genes involved in various immune-related processes, including T cell activation, adaptive immune response, regulation of immune effector process,

TABLE 6 | Drug response related to CD146 expression in renal cancer cell lines.

Gene symbol	Compound	p-value	Correlation	Compound status	Target or activity of compound
CD146	gemcitabine	<0.000	-0.071	approved	inhibitor of DNA replication; inhibitor of ribonucleotide reductase, thymidylate synthetase, and cytidine monophosphate (UMP-CMP) kinase
	ML162	0.001	-0.703	probe	selectively kills engineered cells expressing mutant HRAS
	topotecan	0.002	-0.645	approved	inhibitor of topoisomerase I
	SB-225002	0.003	-0.633	probe	inhibitor of chemokine receptor 2
	SN-38	0.008	-0.572	probe	metabolite of irinotecan; inhibitor of topoisomerase I
	fluorouracil	0.010	-0.559	approved	pyrimidine analog; inhibitor of thymidylate synthase
	CR-1-31B	0.016	-0.530	probe	silvestrol analog; inhibits translation by modulating the eIF4F complex
	daporinad	0.025	-0.498	experimental	inhibitor of nicotinamide phosphoribosyltransferase
	GSK525762A	0.030	-0.485	probe	inhibitor of bromodomain (BRD) and extra-C terminal domain (BET) proteins
	BRD4132	0.031	-0.482	probe	screening hit
	clofarabine	0.032	-0.480	approved	inducer of DNA damage
	SNX-2112	0.033	-0.478	probe	inhibitor of HSP90alpha and HSP90beta
	WP1130	0.035	-0.474	probe	inhibitor of the deubiquitinase activity of USP9X, USP5, USP14, and UCH37
	I-BET151	0.035	-0.474	probe	inhibitor of bromodomain (BRD) and extra-C terminal domain (BET) proteins
	brivanib	0.038	-0.467	experimental	inhibitor of VEGFR 1/2
	serdemetan	0.040	-0.462	experimental	inhibitor of MDM2
	obatoclax	0.043	-0.456	experimental	inhibitor of MCL1, BCL2, and BCL-xL
	etoposide	0.046	-0.451	approved	inhibitor of topoisomerase II
	BIBR-1532	0.049	-0.446	probe	inhibitor of telomerase reverse transcriptase
	quizartinib	0.012	0.548	experimental	inhibitor of VEGFR3
	GSK1059615	0.027	0.495	experimental	inhibitor of PI3K and mTOR kinase activity
	BRD-K92856060	0.027	0.494	probe	screening hit
	AC55649	0.048	0.447	probe	agonist of retinoic acid receptor beta

regulation of innate immune response, regulation of leukocyte activation, macrophage activation, cytokine secretion, Th17 cell differentiation, Th1 and Th2 cell differentiation, and leukocyte transendothelial migration. These results indicate that CD146 may have complex regulatory roles in immune-related processes. To elucidate the role of CD146 in the TME, the relationships between CD146 and immune infiltration in ccRCC were analyzed by TIMER and TISIDB databases. Our results demonstrated that CD146 expression is not only significantly positively correlated with immune infiltration of the immune cell populations including neutrophil cells, monocytes, CD4+ T cells, CD8+ T cells, macrophages, myeloid dendritic cells, and NK cells, but also positively correlated with immunoinhibitors, such as KDR1, TGFB1, IDO1, and ADORA2A. Correlations between CD146 expression and gene markers of immune cells further revealed that CD146 has interactions with M2 macrophage cells and various functional T cells, such as Treg cells and exhausted T cells. These findings indicate that CD146 has dual inflammatory functions in ccRCC. High CD146 expression could enhance anti-tumor immunity by recruiting CD8+ T cells and NK cells to the TME, meanwhile, it induces exhausted phenotype T cells, Treg cells, and M2 type macrophages to accumulate in the TME, causing the inefficiency of anti-tumor immunity. Recent studies provided some insights that may explain the dual role of CD146 in ccRCC. Although CD146 could recruit neutrophils, macrophages, or activated T cells to the inflammatory microenvironment and exert a proinflammatory function (25, 57), the dynamic interaction between tumor cells and the TME could induce a chronic inflammation milieu that drives cancer development and progression (58, 59). The accumulation of Treg cells in tumors could inhibit anti-tumor immune responses. Our results showed that CD146 may be an important inducer of canonical features of T cell exhaustion. We observed that CD146 is positively correlated with key genes of exhausted T cells, including PD-1, LAG-3, TIM3, and GZMB. These genes are important immune checkpoint and immunotherapy targets in cancer therapy. Therefore, CD146 plays critical but different roles on the regulation of the TME, which is needed for identification at specific stages.

Dysregulation of DNA methylation of the epigenome will affect tumor immunogenicity and immune cells in the TME (60). Our study revealed that high methylation status of CD146 was often more frequently in high-grade and late-stage ccRCC, which may suggest that the pattern of methylation changes of CD146 promotes ccRCC progression. A previous study reported that aberrant methylation of the CD146 gene could potently induce the process of epithelial mesenchymal transition in cancer cells, thus contributing to tumor progression (56). To unravel the mechanism of CD146 methylation in promoting ccRCC progression, we analyzed the relationship between the methylation status of CD146 and immune infiltration. Our data showed that the methylation status of CD146 is negatively correlated with immune cells and immunostimulatory factors, while positively correlated with the immunoinhibitors. The methylation of CD146 may contribute to an immunosuppressive TME and promote tumor progression in ccRCC, which help to explain the high methylation status in late-stage and high-grade ccRCC tumors. The methylation of CD146 may be used as indicators of cancer immune infiltration and potential predictors of ccRCC patient response to immunotherapeutic drugs. In addition, we also found that CD146 methylation at certain CpG sites was correlated with poor prognosis in ccRCC patients, indicating that methylation levels of CD146 act as an effective prognostic biomarker for ccRCC.

Based on clinical and pathophysiological data, CD146 is a promising therapeutic target in ccRCC. The results of drug sensitivity analysis demonstrated that high CD146 expression in renal cancer cell lines was significantly correlated with a better response to brivanib, an inhibitor of VEGFR1/2. Previous studies showed that CD146, as a coreceptor of VEGFR2, participates in the angiogenesis of cancer *via* VEGF-induced VEGFR-2 phosphorylation (61, 62). Anti-CD146 and anti-VEGF therapy have a cumulative inhibitory effect on tumor angiogenesis, which may be new therapeutic models in ccRCC treatment. Besides, high CD146 expression was significantly correlated with a better response to inhibitors of topoisomerase, such as topotecan and SN-38. We speculate the expression of CD146 in ccRCC may be a new marker for increased sensitivity to topoisomerase inhibitors, which needs further validation. Importantly, we demonstrated a significant correlation of CD146 and drug resistance. For example, CD146 was significantly correlated with the resistance of GSK1059615. GSK1059615, an inhibitor of PI3K kinase activity, inhibited cancer cell growth, survival, proliferation, and cell cycle progression (63). The reason of the ineffectiveness of GSK1059615 in CD146 high expressing renal cancer cells may be that CD146 mediates mTORC2 activation, with no intervention of the PI3K and mTORC1 pathways, and promotes cell proliferation and survival (64). These results showed that CD146 may be a new therapeutic target for treating ccRCC patients.

In conclusion, this mining study revealed that CD146 is a prognosis-related biomarker for ccRCC. CD146 expression and methylation status of CD146 not only correlates with immune cell infiltration, but also correlates with immunomodulators and chemokines. Our study has certain limitations as follows: Firstly, gene expression analysis in our study, based on open-source databases, might not be sufficiently accurate. This calls for further experiments using *in vitro* and vivo models to explore the potential biological mechanisms of CD146 as well as tumor-immune interactions in ccRCC. Secondly, the role of CD146 in determining the clinical outcome to immunotherapy is still in need of further investigation. Thirdly, the scenario of methylation changes in the CD146 gene during development of ccRCC progression needs further study, as we cannot exclude the fact that CD146 acts as a tumor suppressor at the initial stage of carcinogenesis, as suggested by the study of Shih and others (65), and turns into an oncogene in the advanced stage. Therefore, our study highlights the novel immunomodulation function of CD146 in ccRCC.

DATA AVAILABILITY STATEMENT

The datasets presented in this study can be found in online repositories. The names of the repository/repositories and accession number(s) can be found in the article/supplementary material.

ETHICS STATEMENT

Written informed consent was obtained from the individual(s) for the publication of any potentially identifiable images or data included in this article.

AUTHOR CONTRIBUTIONS

XZ and ZL designed the study. HY-F performed the experiment and data analysis. WT and HY-F performed clinical data analysis. ZL conducted the IHC and western blot assay. ZL and XZ contributed to manuscript writing, reviewing, and revision. HZ-L and XZ supervised the study. All authors contributed to the article and approved the submitted version.

FUNDING

This study was financially supported by the National Natural Science Foundation of China (grant nos. 81972389 and 81770790).

REFERENCES

1. Siegel RL, Miller KD, Jemal A. Cancer Statistics, 2019. *CA Cancer J Clin* (2019) 69:7–34. doi: 10.3322/caac.21551
2. Choueiri TK, Halabi S, Sanford BL, Hahn O, Michaelson MD, Walsh MK, et al. Cabozantinib Versus Sunitinib As Initial Targeted Therapy for Patients With Metastatic Renal Cell Carcinoma of Poor or Intermediate Risk: The Alliance A031203 CABOSUN Trial. *J Clin Oncol* (2017) 35:591–7. doi: 10.1200/JCO.2016.70.7398
3. Motzer RJ, Barrios CH, Kim TM, Falcon S, Cosgriff T, Harker WG, et al. Phase II Randomized Trial Comparing Sequential First-Line Everolimus and Second-Line Sunitinib Versus First-Line Sunitinib and Second-Line Everolimus in Patients With Metastatic Renal Cell Carcinoma. *J Clin Oncol* (2014) 32:2765–72. doi: 10.1200/JCO.2013.54.6911
4. Yoshihara K, Shahmoradgoli M, Martínez E, Vegesna R, Kim H, Torres-Garcia W, et al. Inferring Tumour Purity and Stromal and Immune Cell Admixture From Expression Data. *Nat Commun* (2013) 4:2612. doi: 10.1038/ncomms3612
5. Motzer RJ, Penkov K, Haanen J, Rini B, Albiges L, Campbell MT, et al. Avelumab Plus Axitinib Versus Sunitinib for Advanced Renal-Cell Carcinoma. *N Engl J Med* (2019) 380:1103–15. doi: 10.1056/NEJMoa1816047
6. Rini BI, Plimack ER, Stus V, Gafanov R, Hawkins R, Nosov D, et al. Pembrolizumab Plus Axitinib Versus Sunitinib for Advanced Renal-Cell Carcinoma. *N Engl J Med* (2019) 380:1116–27. doi: 10.1056/NEJMoa1816714
7. Turajlic S, Xu H, Litchfield K, Rowan A, Horswell S, Chambers T, et al. Deterministic Evolutionary Trajectories Influence Primary Tumor Growth: TRACERx Renal. *Cell* (2018) 173:595–610. doi: 10.1016/j.cell.2018.03.043
8. Mitchell TJ, Turajlic S, Rowan A, Nicol D, Farmery JHR, O'Brien T, et al. Timing the Landmark Events in the Evolution of Clear Cell Renal Cell Cancer: TRACERx Renal. *Cell* (2018) 173:611–623.e17. doi: 10.1016/j.cell.2018.02.020
9. Brahmer A, Neuberger E, Esch-Heisser L, Haller N, Jorgensen MM, Baek R, et al. Platelets, Endothelial Cells and Leukocytes Contribute to the Exercise-Triggered Release of Extracellular Vesicles Into the Circulation. *J Extracell Vesicles* (2019) 8:1615820. doi: 10.1080/20013078.2019.1615820
10. Zheng B, Ohuchida K, Chijiiwa Y, Zhao M, Mizuuchi Y, Cui L, et al. CD146 Attenuation in Cancer-Associated Fibroblasts Promotes Pancreatic Cancer Progression. *Mol Carcinog* (2016) 55:1560–72. doi: 10.1002/mc.22409
11. Luo Y, Teng X, Zhang L, Chen J, Liu Z, Chen X, et al. CD146-HIF-1α Hypoxic Reprogramming Drives Vascular Remodeling and Pulmonary Arterial Hypertension. *Nat Commun* (2019) 10:3551. doi: 10.1038/s41467-019-11500-6
12. Dagur PK, Tatlici G, Gourley M, Samsel L, Raghavachari N, Liu P, et al. CD146+ T Lymphocytes Are Increased in Both the Peripheral Circulation and in the Synovial Effusions of Patients With Various Musculoskeletal Diseases and Display Pro-Inflammatory Gene Profiles. *Cytometry B Clin Cytom* (2010) 78:88–95. doi: 10.1002/cyto.b.20502
13. Luo Y, Duan H, Qian Y, Feng L, Wu Z, Wang F, et al. Macrophagic CD146 Promotes Foam Cell Formation and Retention During Atherosclerosis. *Cell Res* (2017) 27:352–72. doi: 10.1038/cr.2017.8
14. Sun Z, Ji N, Ma Q, Zhu R, Chen Z, Wang Z, et al. Epithelial-Mesenchymal Transition in Asthma Airway Remodeling Is Regulated by the IL-33/CD146 Axis. *Front Immunol* (2020) 11:1598. doi: 10.3389/fimmu.2020.01598
15. Wang Z, Yan X. CD146, a Multi-Functional Molecule Beyond Adhesion. *Cancer Lett* (2013) 330:150–62. doi: 10.1016/j.canlet.2012.11.049
16. Liu WF, Ji SR, Sun JJ, Zhang Y, Liu ZY, Liang AB, et al. CD146 Expression Correlates With Epithelial-Mesenchymal Transition Markers and a Poor Prognosis in Gastric Cancer. *Int J Mol Sci* (2012) 13:6399–406. doi: 10.3390/ijms13056399
17. Rapanotti MC, Campione E, Spallone G, Orlandi A, Bernardini S, Bianchi L. Minimal Residual Disease in Melanoma: Circulating Melanoma Cells and Predictive Role of MCAM/MUC18/MelCAM/Cd146. *Cell Death Discovery* (2017) 3:17005. doi: 10.1038/cddiscovery.2017.5
18. Zhang F, Wang J, Wang X, Wei N, Liu H, Zhang X. CD146-Mediated Acquisition of Stemness Phenotype Enhances Tumour Invasion and Metastasis After EGFR-TKI Resistance in Lung Cancer. *Clin Respir J* (2019) 13:23–33. doi: 10.1111/crj.12976
19. Chen Y, Sumardika IW, Tomonobu N, Kinoshita R, Inoue Y, Iioka H, et al. Critical Role of the MCAM-ETV4 Axis Triggered by Extracellular S100A8/A9 in Breast Cancer Aggressiveness. *Neoplasia* (2019) 21:627–40. doi: 10.1016/j.neo.2019.04.006
20. Wang P, Luo Y, Duan H, Xing S, Zhang J, Lu D, et al. MicroRNA 329 Suppresses Angiogenesis by Targeting CD146. *Mol Cell Biol* (2013) 33:3689–99. doi: 10.1128/MCB.00343-13
21. Kaspi E, Heim X, Granel B, Guillet B, Stalin J, Nollet M, et al. Identification of CD146 as a Novel Molecular Actor Involved in Systemic Sclerosis. *J Allergy Clin Immunol* (2017) 140:1448–51.e6. doi: 10.1016/j.jaci.2017.04.046
22. Neidhart M, Wehrli R, Brühlmann P, Michel BA, Gay RE, Gay S. Gay Synovial Fluid CD146 (MUC18), a Marker for Synovial Membrane Angiogenesis in Rheumatoid Arthritis. *Arthritis Rheum* (1999) 42:622–30. doi: 10.1002/1529-0131(199904)42:4<622:AID-ANR4>3.0.CO;2-Y
23. Tsiolakidou G, Koutroubakis IE, Tzardi M, Kouroumalis EA. Increased Expression of VEGF and CD146 in Patients With Inflammatory Bowel Disease. *Dig Liver Dis* (2008) 40:673–9. doi: 10.1016/j.dld.2008.02.010
24. Bardin N, Blot-Chabaud M, Despoix N, Kebir A, Harhouri K, Arsanto JP, et al. CD146 and its Soluble Form Regulate Monocyte Transendothelial Migration. *Arterioscler Thromb Vasc Biol* (2009) 29:746–53. doi: 10.1161/ATVBAHA.108.183251
25. Guezguez B, Vigneron P, Lamerant N, Kieda C, Jaffredo T, Dunon D. Dual Role of Melanoma Cell Adhesion Molecule (MCAM)/CD146 in Lymphocyte Endothelium Interaction: MCAM/CD146 Promotes Rolling *via* Microvilli Induction in Lymphocyte and Is an Endothelial Adhesion Receptor. *J Immunol* (2007) 179:6673–85. doi: 10.4049/jimmunol.179.10.6673
26. Murata M. Inflammation and Cancer. *Environ Health Prev Med* (2018) 23:50. doi: 10.1186/s12199-018-0740-1
27. Netti GS, Lucarelli G, Spadaccino F, Castellano G, Gigante M, Divella C, et al. PTX3 Modulates the Immunoflogosis in Tumor Microenvironment and Is a Prognostic Factor for Patients With Clear Cell Renal Cell Carcinoma. *Aging* (2020) 12:7585–602. doi: 10.18632/aging.103169
28. Falagario UG, Busetto GM, Netti GS, Sanguedolce F, Selvaggio O, Infante B, et al. Prospective Validation of Pentraxin-3 as a Novel Serum Biomarker to Predict the Risk of Prostate Cancer in Patients Scheduled for Prostate Biopsy. *Cancers* (2021) 13:1611–20. doi: 10.3390/cancers13071611
29. Lee A, Lee HJ, Huang HH, Tay KJ, Lee LS, Sim SPA, et al. Prognostic Significance of Inflammation-Associated Blood Cell Markers in

Nonmetastatic Clear Cell Renal Cell Carcinoma. *Clin Genitourin Cancer* (2020) 18:304–13. doi: 10.1016/j.clgc.2019.11.013
30. Krishna Y, Acha-Sagredo A, Sabat-Pośpiech D, Kipling N, Clarke K, Figueiredo CR, et al. Transcriptome Profiling Reveals New Insights Into the Immune Microenvironment and Upregulation of Novel Biomarkers in Metastatic Uveal Melanoma. *Cancers* (2020) 12:2832–54. doi: 10.3390/cancers12102832
31. Li T, Fan J, Wang B, Traugh N, Chen Q, Liu JS, et al. TIMER: A Web Server for Comprehensive Analysis of Tumor-Infiltrating Immune Cells. *Cancer Res* (2017) 77:e108–10. doi: 10.1158/0008-5472.Can-17-0307
32. Sousa S, Määttä J. The Role of Tumour-Associated Macrophages in Bone Metastasis. *J Bone Oncol* (2016) 5:135–8. doi: 10.1016/j.jbo.2016.03.004
33. Danaher P, Warren S, Dennis L, D'Amico L, White A, Disis ML, et al. Gene Expression Markers of Tumor Infiltrating Leukocytes. *J Immunother Cancer* (2017) 5:18. doi: 10.1186/s40425-017-0215-8
34. Siemers NO, Holloway JL, Chang H, Chasalow SD, Ross-MacDonald PB, Voliva CF, et al. Genome-Wide Association Analysis Identifies Genetic Correlates of Immune Infiltrates in Solid Tumors. *PloS One* (2017) 12: e0179726. doi: 10.1371/journal.pone.0179726
35. Győrffy B, Bottai G, Fleischer T, Munkácsy G, Budczies J, Paladini L, et al. Aberrant DNA Methylation Impacts Gene Expression and Prognosis in Breast Cancer Subtypes. *Int J Cancer* (2016) 138:87–97. doi: 10.1002/ijc.29684
36. Paner GP, Stadler WM, Hansel DE, Montironi R, Lin DW, Amin MB. Updates in the Eighth Edition of the Tumor-Node-Metastasis Staging Classification for Urologic Cancers. *Eur Urol* (2018) 73:560–9. doi: 10.1016/j.eururo.2017.12.018
37. Fuhrman SA, Lasky LC, Limas C. Limas Prognostic Significance of Morphologic Parameters in Renal Cell Carcinoma. *Am J Surg Pathol* (1982) 6:655–63. doi: 10.1097/00000478-198210000-00007
38. Zhao T, Ren H, Li J, Chen J, Zhang H, Xin W, et al. LASP1 Is a HIF1α Target Gene Critical for Metastasis of Pancreatic Cancer. *Cancer Res* (2015) 75:111–9. doi: 10.1158/0008-5472.CAN-14-2040
39. Gao Y, Li H, Ma X, Fan Y, Ni D, Zhang Y, et al. KLF6 Suppresses Metastasis of Clear Cell Renal Cell Carcinoma *via* Transcriptional Repression of E2F1. *Cancer Res* (2017) 77:330–42. doi: 10.1158/0008-5472.CAN-16-0348
40. Huang QB, Ma X, Li HZ, Ai Q, Liu SW, Zhang Y, et al. Endothelial Delta-Like 4 (DLL4) Promotes Renal Cell Carcinoma Hematogenous Metastasis. *Oncotarget* (2014) 5:3066–75. doi: 10.18632/oncotarget.1827
41. Chandrashekar DS, Bashel B, Balasubramanya SAH, Creighton CJ, Ponce-Rodriguez I, Chakravarthi BVSK, et al. UALCAN: A Portal for Facilitating Tumor Subgroup Gene Expression and Survival Analyses. *Neoplasia* (2017) 19:649–58. doi: 10.1016/j.neo.2017.05.002
42. Klutstein M, Nejman D, Greenfield R, Cedar H. DNA Methylation in Cancer and Aging. *Cancer Res* (2016) 76:3446–50. doi: 10.1158/0008-5472.CAN-15-3278
43. Vasaikar SV, Straub P, Wang J, Zhang B. LinkedOmics: Analyzing Multi-Omics Data Within and Across 32 Cancer Types. *Nucleic Acids Res* (2018) 46: D956–d963. doi: 10.1093/nar/gkx1090
44. Ru B, Wong CN, Tong Y, Zhong JY, Zhong SSW, Wu WC, et al. TISIDB: An Integrated Repository Portal for Tumor-Immune System Interactions. *Bioinformatics* (2019) 35:4200–2. doi: 10.1093/bioinformatics/btz210
45. Mukaka MM. Statistics Corner: A Guide to Appropriate Use of Correlation Coefficient in Medical Research. *Malawi Med J* (2012) 24:69–71.
46. Rees MG, Seashore-Ludlow B, Cheah JH, Adams DJ, Price EV, Gill S, et al. Correlating Chemical Sensitivity and Basal Gene Expression Reveals Mechanism of Action. *Nat Chem Biol* (2016) 12:109–16. doi: 10.1038/nchembio.1986
47. Falagario UG, Veccia A, Cormio L, Simeone C, Carbonara U, Crocerossa F, et al. Nomogram Predicting 30-Day Mortality After Nephrectomy in the Contemporary Era: Results From the SEER Database. *Int J Urol* (2021) 28:309–14. doi: 10.1111/iju.14461
48. Miao D, Margolis CA, Gao W, Voss MH, Li W, Martini DJ, et al. Genomic Correlates of Response to Immune Checkpoint Therapies in Clear Cell Renal Cell Carcinoma. *Science* (2018) 359:801–6. doi: 10.1126/science.aan5951
49. Dong H, Strome SE, Salomao DR, Tamura H, Hirano F, Flies DB, et al. Tumor-Associated B7-H1 Promotes T-Cell Apoptosis: A Potential Mechanism of Immune Evasion. *Nat Med* (2002) 8:793–800. doi: 10.1038/nm730
50. Sharma P, Hu-Lieskovan S, Wargo JA, Ribas A. Primary, Adaptive, and Acquired Resistance to Cancer Immunotherapy. *Cell* (2017) 168:707–23. doi: 10.1016/j.cell.2017.01.017
51. Wang J, Sun J, Liu LN, Flies DB, Nie X, Toki M, et al. Siglec-15 as an Immune Suppressor and Potential Target for Normalization Cancer Immunotherapy. *Nat Med* (2019) 25:656–66. doi: 10.1038/s41591-019-0374-x
52. Wang J, Sanmamed MF, Datar I, Su TT, Ji L, Sun J, et al. Fibrinogen-Like Protein 1 Is a Major Immune Inhibitory Ligand of LAG-3. *Cell* (2019) 176:334–47.e12. doi: 10.1016/j.cell.2018.11.010
53. Zoni E, Astrologo L, Ng CKY, Piscuoglio S, Melsen J, Grosjean J, et al. Therapeutic Targeting of CD146/MCAM Reduces Bone Metastasis in Prostate Cancer. *Mol Cancer Res* (2019) 17:1049–62. doi: 10.1158/1541-7786.MCR-18-1220
54. Chen J, Dang Y, Feng W, Qiao C, Liu D, Zhang T, et al. SOX18 Promotes Gastric Cancer Metastasis Through Transactivating MCAM and CCL7. *Oncogene* (2020) 39:5536–52. doi: 10.1038/s41388-020-1378-1
55. Schödel J, Grampp S, Maher ER, Moch H, Ratcliffe PJ, Russo P, et al. Hypoxia, Hypoxia-Inducible Transcription Factors, and Renal Cancer. *Eur Urol* (2016) 69:646–57. doi: 10.1016/j.eururo.2015.08.007
56. Dudzik P, Trojan SE, Ostrowska B, Lasota M, Dulińska-Litewka J, Laidler P, et al. Aberrant Promoter Methylation may be Responsible for the Control of CD146 (MCAM) Gene Expression During Breast Cancer Progression. *Acta Biochim Pol* (2019) 66:619–25. doi: 10.18388/abp.2019-2907
57. Stevenson C, Jiang D, Schaefer N, Ito Y, Berman R, Sanchez A, et al. MUC18 Regulates IL-13-Mediated Airway Inflammatory Response. *Inflammation Res* (2017) 66:691–700. doi: 10.1007/s00011-017-1050-6
58. Fridlender ZG, Sun J, Kim S, Kapoor V, Cheng G, Ling L, et al. Polarization of Tumor-Associated Neutrophil Phenotype by TGF-Beta: "N1" Versus "N2" TAN. *Cancer Cell* (2009) 16:183–94. doi: 10.1016/j.ccr.2009.06.017
59. Mehla K, Singh PK. Singh Metabolic Regulation of Macrophage Polarization in Cancer. *Trends Cancer* (2019) 5:822–34. doi: 10.1016/j.trecan.2019.10.007
60. Hogg SJ, Beavis PA, Dawson MA, Johnstone RW. Johnstone Targeting the Epigenetic Regulation of Antitumour Immunity. *Nat Rev Drug Discovery* (2020) 19:776–800. doi: 10.1038/s41573-020-0077-5
61. Jiang T, Zhuang J, Duan H, Luo Y, Zeng Q, Fan K, et al. CD146 Is a Coreceptor for VEGFR-2 in Tumor Angiogenesis. *Blood* (2012) 120:2330–9. doi: 10.1182/blood-2012-01-406108
62. Zeng Q, Wu Z, Duan H, Jiang X, Tu T, Lu D, et al. Impaired Tumor Angiogenesis and VEGF-Induced Pathway in Endothelial CD146 Knockout Mice. *Protein Cell* (2014) 5:445–56. doi: 10.1007/s13238-014-0047-y
63. Bei S, Li F, Li H, Li J, Zhang X, Sun Q, et al. Inhibition of Gastric Cancer Cell Growth by a PI3K-mTOR Dual Inhibitor GSK1059615. *Biochem Biophys Res Commun* (2019) 511:13–20. doi: 10.1016/j.bbrc.2019.02.032
64. Xu W, Hua H, Chiu YH, Li G, Zhi H, Yu Z, et al. CD146 Regulates Growth Factor-Induced Mtorc2 Activity Independent of the PI3K and Mtorc1 Pathways. *Cell Rep* (2019) 29:1311–22.e5. doi: 10.1016/j.celrep.2019.09.047
65. Shih LM, Hsu MY, Palazzo JP, Herlyn M. The Cell-Cell Adhesion Receptor Mel-CAM Acts as a Tumor Suppressor in Breast Carcinoma. *Am J Pathol* (1997) 151:745–51.

Conflict of Interest: The authors declare that the research was conducted in the absence of any commercial or financial relationships that could be construed as a potential conflict of interest.

Publisher's Note: All claims expressed in this article are solely those of the authors and do not necessarily represent those of their affiliated organizations, or those of the publisher, the editors and the reviewers. Any product that may be evaluated in this article, or claim that may be made by its manufacturer, is not guaranteed or endorsed by the publisher.

Copyright © 2021 Lv, Feng, Tao, Li and Zhang. This is an open-access article distributed under the terms of the Creative Commons Attribution License (CC BY). The use, distribution or reproduction in other forums is permitted, provided the original author(s) and the copyright owner(s) are credited and that the original publication in this journal is cited, in accordance with accepted academic practice. No use, distribution or reproduction is permitted which does not comply with these terms.

frontiers in Oncology

ORIGINAL RESEARCH
published: 09 December 2021
doi: 10.3389/fonc.2021.756843

FGL1 as a Novel Mediator and Biomarker of Malignant Progression in Clear Cell Renal Cell Carcinoma

Zheng Lv[1†], Bo Cui[2,3†], Xing Huang[2,3], Hua-Yi Feng[2,3], Tao Wang[2,3], Han-Feng Wang[2,3], Yun-Dong Xuan[2,3], Hong-Zhao Li[3], Xin Ma[3], Yan Huang[3] and Xu Zhang[1,3*]*

[1] School of Medicine, Nankai University, Tianjin, China, [2] Medical School of Chinese PLA, Beijing, China, [3] Department of Urology, The Third Medical Center, Chinese PLA General Hospital, Beijing, China

OPEN ACCESS

Edited by:
Antonio Augusto Ornellas, National Cancer Institute (INCA), Brazil

Reviewed by:
Jun Pang, Sun Yat-Sen University, China
Hongkai Wang, Shanghai Medical College of Fudan University, China

***Correspondence:**
Xu Zhang
xzhang@163.com
Yan Huang
dr.huangyan301@foxmail.com

[†]These authors have contributed equally to this work

Specialty section:
This article was submitted to Genitourinary Oncology, a section of the journal Frontiers in Oncology

Received: *11 August 2021*
Accepted: *22 November 2021*
Published: *09 December 2021*

Citation:
Lv Z, Cui B, Huang X, Feng H-Y, Wang T, Wang H-F, Xuan Y-D, Li H-Z, Ma X, Huang Y and Zhang X (2021) FGL1 as a Novel Mediator and Biomarker of Malignant Progression in Clear Cell Renal Cell Carcinoma. Front. Oncol. 11:756843. doi: 10.3389/fonc.2021.756843

Clear cell renal cell carcinoma (ccRCC), which is the most prevalent renal cell carcinoma subtype, has a poor prognosis. Emerging strategies for enhancing the immune response in ccRCC therapy are currently being investigated. Fibrinogen-like Protein 1(FGL1) is a novel mechanism that tumors may use to evade the immune system by binding LAG-3 and negatively regulating T cells. In this study, we aimed at investigating the underlying mechanism of FGL1 in ccRCC, and its expression and prognostic value. We found that FGL1 was upregulated in tumor tissues and plasma specimens of ccRCC patients. High FGL1 expression predicted a poor prognosis for ccRCC patients. We also discovered that overexpression of FGL1 enhances RCC cell migration, invasion, and metastasis by activating the epithelial-to-mesenchymal transition (EMT). Consistent with these results, we identified a significant positive correlation between expression of FGL1 and EMT-related genes through tissue microarray analysis. Gene-expression analysis revealed that FGL1-deficient ccRCC cell lines had altered transcriptional output in inflammatory response, cell-cell signaling, negative regulation of T cell activation, and intracellular signal transduction. Depletion of FGL1 significantly inhibited tumor growth and lung metastasis in orthotopic xenograft mouse model. Infiltration of myeloid-derived CD11b+ and Ly6G+ immune cells in tumor microenvironment (TME) was strikingly decreased when FGL1 expression reduced. Therefore, increased FGL1 expression in ccRCC is positively correlated with poor prognosis. Mechanistically, FGL1 facilitates the EMT process and modulates TME, which promotes ccRCC progression and metastasis. Consequently, targeting FGL1 can potentially improve clinical outcome of ccRCC patients.

Keywords: epithelial to mesenchymal transition, fibrinogen-like protein 1, progression, clear cell renal cell carcinoma, biomarker

Abbreviations: FGL1, Fibrinogen-like Protein 1; ccRCC, clear cell renal cell carcinoma; EMT, Epithelial-mesenchymal transition; TME, tumor microenvironment.

INTRODUCTION

Renal cell carcinoma (RCC) is the sixth most common type of neoplasm in men and the tenth in women worldwide (1). Clear cell renal cell carcinoma (ccRCC) is the dominant histological subtype of RCC, accounting for 70~80% of the cases (2). Approximately 30% of ccRCC patients have metastasis at the time of diagnosis, implying that the capacity of ccRCC to metastasize is high (3). Metastatic RCC (mRCC) has a poor prognosis, with a 5-year survival rate of only 5~10% after diagnosis (4). Besides, conventional chemotherapy and radiotherapy are often ineffective against mRCC (5). In the last decade, the availability of targeted therapies, such as tyrosine kinases inhibitors and mTOR inhibitors has improved the prognosis of mRCC patients (6, 7). However, the initial response rates of targeted therapies in ccRCC is only 10% ~30%, and nearly all patients treated with targeted agents eventually experience tumor progression due to acquired resistance (8–10).

Improved understanding of tumor microenvironment has led to the development of immunotherapy in RCC (11). The clinical success of immune checkpoint inhibitors (ICIs) that target programmed death 1 (PD-1)/programmed death ligand 1 (PD-L1) and cytotoxic T-lymphocyte associated protein 4 (CTLA-4) have revolutionized the treatment of ccRCC patients. Immunotherapy-based combinations have become standard of care in patients with advanced RCC, and have shown efficacy and overall survival benefits in the first-line metastatic setting (12, 13). Besides targeting PD-1/PD-L1 pathway, many other molecular mechanisms can help repress immunity in the tumor microenvironment (TME). Wang et al. (14), recently discovered that FGL1, a major LAG3 ligand, is responsible for the inhibitory function of T cells in TME. Therefore, we speculate that FGL1 is also essential in ccRCC.

Epithelial mesenchymal-transition (EMT), the process whereby epithelial cells transform into mesenchymal cells, has been considered to be a key mechanism in tumor invasion and metastasis (15). Cancer cells acquire motile features during EMT when mesenchymal markers such as vimentin, fibronectin, and N-cadherin are upregulated and epithelial markers like E-cadherin are downregulated (16, 17). A recent study showed that FGL1 promotes the progression of gastric cancer by facilitating the EMT process (18), whereas another study had suggested that loss of FGL1 could induce EMT in lung cancer (19). These conflicting results seem to mirror a double-sided role for FGL1 in regulating EMT during cancer progression. However, the specific role and mechanism of FGL1 in the process of EMT remain to be elucidated.

Fibrinogen-like Protein 1 (FGL1), also known as hepatocyte-derived fibrinogen-related protein, is structurally similar to angiopoietin-like proteins. It is mainly secreted by the liver and acts as an autocrine growth factor during liver regeneration by activating the EGFR/ERK cascade (20). It has been discovered that overexpression of FGL1 in gastric cancer is correlated with tumor progression and poor prognosis (18). In addition, the upregulation of FGL1 confers Gefitinib resistance by inhibiting apoptosis in non-small cell lung cancer (21). However, to the best of our knowledge, the expression, biological function, prognostic significance, and molecular mechanism of FGL1 in ccRCC is unclear. In addition, the role of FGL1 in modulating the TME is still largely undefined.

In this study, we determined that FGL1 expression was upregulated in ccRCC resulting in significant correlation with a poor prognosis for ccRCC patients. Besides, FGL1 promoted the migration, invasion, and metastasis of ccRCC cells by facilitating the EMT process. Finally, we revealed that FGL1 stimulated tumor growth *in vivo* by increasing myeloid-derived CD11b+ and Ly6G+ immune cell infiltration in TME. Collectively, these findings provided insights into the functions of FGL1 in tumor progression, suggesting that targeting FGL1 can be a potential therapeutic strategy for ccRCC.

MATERIALS AND METHODS

Patients and Clinical Materials

Tumor specimens were collected from 211 ccRCC patients who underwent surgery at the Urology Department of the Chinese People's Liberation Army (PLA) General Hospital (Beijing, China) from January 2012 to December 2019. Clinic-pathologic data of ccRCC patients were reported in **Supplementary Table 1**. Cancer tissue samples were pathologically confirmed as ccRCC according to the 2011 Union for International Cancer Control TNM classification of malignant tumors. Forty-three preoperative blood samples of ccRCC patients and 26 blood samples from healthy donors were collected between January and March 2021. The patients signed for consent after being informed about the use of their clinical specimens for scientific research. This study was approved by the ethics committee of the Chinese People's Liberation Army (PLA) General Hospital.

Plasmid Constructs

Oligonucleotides targeting human and mouse FGL1 were designed using short hairpin RNA (shRNA) sequences, and synthesized by BGI (Shenzhen, China). Double stranded oligonucleotides targeting FGL1 (shFGL1) and NC shRNA (shNC) were cloned into Plko.1, after annealing. The 1 puro lentiviral vector was digested with EcoRI and BstHI. The sequences of primers used for the shNC, FGL1-sh1, and FGL1-sh2 are listed in **Supplementary Table 2**.

Cell Culture, Transfection and Infection

Fetal bovine serum (FBS) was purchased from EVERY GREEN (Hangzhou, China). Different types of media including high glucose-DMEM, MEM, RPMI-1640, and McCoy's 5A were purchased from VIVICUM bioscience (Beijing, China). Similarly, various cell lines including the human embryonic kidney derived cell line HEK293T, human renal tubular epithelial cell line HKC, human ccRCC cell lines SN12, A498, 786O, ACHN, OS-RC-2, Caki-1, and Caki-2 were originally purchased from American Type Culture Collection. All the cells were cultured in medium containing 10% FBS and 1% penicillin/streptomycin in 5% CO_2 at 37°C. Cell lines HEK293T

and SN12 were cultured in high glucose-DMEM medium, A498 and ACHN in MEM medium, 786O and OS-RC-2 in RPMI-1640 medium, and Caki-1 and Caki-2 in McCoy's 5A medium, respectively.

Transient co-transfection of packing DNA yielded lentivirus in HEK293T cells. Cells were transfected with 6 μg vector plasmids along with 4.5μg psPAX2 and 1.5 μg pMD2-VSVG using the standard calcium chloride transfection method. The calcium transfection kit was purchased from Macgene Biotech (Beijing, China). Viral supernatant containing released viruses was collected at 48h and 72h after transfection, and filtered through a 0.45 μm filter. Target cells were infected at a multiplicity of infection (MOI) of 5 in the presence of 8 μg/mL polybrene for 24h. The infected cells were then selected with 2 μg/mL puromycin (Sigma, USA) for three days. A plasmid overexpressing human FGL1 was purchased from SinoBiological (Beijing, China). Overexpression of FGL1 in SN12 and A498 cells was carried out by transient transfection using Lipofectamine2000.

MTS Assay

The cells were seeded into 96-well plates (1000 cells/well) and cultured for 12h, 24h, 48h, and 72h. The viability of the cells was assessed using a CellTiter-Blue® (CTB) cell viability assay (CTB169, Promega, Beijing, China). At varying points in time, 20 μl of [3-(4,5-dimethylthiazol-2-yl) -5- (3-carboxymethoxyphenyl)-2-(4-sulfophenyl)-2H-tetrazolium (MTS) reagent was added to each well, and incubated for 2 h at 37°C. The absorbance was measured at a wavelength of 490 nm to detect the OD values. All experiments were performed in triplicate.

Cell Migration and Invasion Assay

Cell migration and invasion were gauged using transwell migration assay, wound healing assay, and Matrigel invasion assay. For transwell migration assay and Matrigel invasion assay, 5×10^4 cells suspended in 200 μl of medium without FBS were seeded on the upper chamber (8 μm pore size, 3422, Costar) with Matrigel-uncoated or coated membrane (356224, BD Biosciences). The lower chamber was filled with 500 μl medium containing 20% FBS. Cells were fixed with 4% paraformaldehyde after 16h of incubation at 37°C in 5% CO_2. The non-migrated cells on the top surface of the membrane were gently removed with a cotton swab, whereas the migrated cells were stained using 0.5% crystal violet (C8470, Solarbio, China), photographed, and counted under a light microscope (200x magnification).

In wound healing assay, cells were seeded in the six-well plate and cultured for 24h at 37°C in 5% CO_2. A scratch was made using a 200 μl pipette tip when the cells were grown to 90% confluence. The cells were washed with PBS for three times and then incubated in FBS-free medium at 37°C in 5% CO_2. The gaps between the wound edges were monitored and photographed using an IX2-UCB phase contrast microscope (Olympus, Tokyo, Japan) at 0 and 48 h (200x magnification).

Western Blot Analysis

Western blot assays were performed using standard techniques as previously reported (22). The information of antibodies was listed in **Supplementary Table 3**. The results of FGL1 protein expression were quantified by the relative gray value, which was calculated as "the gray value of FGL1 protein bands/the gray value of internal control β-tubulin bands".

ELISA Analysis

The concentration of FGL1 in the plasma of ccRCC patients and healthy controls was measured using commercially available sandwich ELISA kits (Wuhan Colorful Gene Biological Technology, China).

Immunohistochemistry (IHC) Staining

Tissue microarray for FGL1 IHC staining was obtained from the tissue bank at Urology Department of the Chinese PLA General Hospital, Beijing, China. The standard protocols were followed as previously described (23). Slides were scanned using Axio Image Z2 Microscope (Zeiss) and TissueFAXS imaging system (TissueGnostics GmbH, Austria). All images were analyzed by TissueQuest and StrataQuest software (TissueGnostics GmbH, Austria). As previously described (24), staining intensity was scored as follows: 0 (negative), 1 (weak), 2 (moderate), and 3 (strong), whereas the staining range was scored as: 0 (0%), 1 (1%–24%), 2 (25%–49%), and 3 (50%–100%). The IHC staining score was obtained by multiplying the intensity scores with staining range. The IHC staining score ranged from 0 to 9. Scores less than two were considered as negative staining, 2–3 indicated weak staining, 4–6 was moderate staining, and >6 was strong staining. Patients with an IHC staining score ≥4 were included in the high expression group, whereas those with an IHC staining score <4 were included in the low expression group.

Immunofluorescence Staining

Cells from different groups were washed three times with PBS, fixed with 4% paraformaldehyde for 15 min, permeabilized with 0.5% Triton X-100, and then blocked with 5% goat serum for 30 min. Cells were stained with primary antibodies at 37°C for 1h and were incubated with AlexaFluor488 and AlexaFluor594-conjugated secondary antibodies (1:400). Nuclei were counterstained by 0.2 mg/mL DAPI. Samples were imaged with an Axio Image Z2 fluorescence microscope (Zeiss) and analyzed by TissueQuest and StrataQuest software.

RNA-Sequence (Seq) Analysis

Total RNA was extracted from cells using TRIzol reagent (Invitrogen). Later, all the samples were sent to BGI Corporation (Shenzhen, China) for further RNA-seq detection and analysis using the MGISEQ-2000 sequencer. The Dr. Tom network platform developed by Beijing Genomic Institute (BGI; http://report.bgi.com) was used to perform the protein–protein interaction (PPI) analysis after defining the differentially expressed genes (DEGs), gene ontology (GO) enrichment analysis, and Kyoto Encyclopedia of Genes and Genomes (KEGG) pathway analysis. The 'phyper' function of R software was used for the enrichment analysis, to calculate the P-value and perform FDR correction on the P-value. Q-value ≤ 0.05 was regarded as significant enrichment.

Quantitative Real-Time PCR (qRT-PCR)

Quantitative real-time PCR was performed on selected genes to verify differential gene expression that was observed through RNA-seq analysis. Total RNA was extracted with Trizol reagent (Invitrogen). Complementary DNA was synthesized using ProtoScript® II First-Strand cDNA Synthesis Kit (E6300S, NEB, USA). Afterwards, quantitative PCR was performed with NovoStart® SYBR Green Super Mix Plus (E096-01A, novoprotein, China). Relative mRNA expressions were normalized to peptidylprolyl isomerase A (PPIA) with the $2^{-\Delta\Delta CT}$ method. The used primer sequences were listed in **Supplementary Table 4**. The process was implemented using ABI prism 7500 (Applied Biosystems, USA).

Orthotopic Xenograft Mouse Model *In Vivo*

The mouse orthotopic xenograft tumor model was prepared using 4~6-week-old BALB/c male nude mice (Vital River Laboratory Animal Technology Co., Beijing, China). For the orthotopic xenograft tumor model, Luc-SN12 shNC or Luc-SN12 shFGL1 cells (1×10^6) suspended in 100 μl of sterilized PBS + Matrigel (1:1) were injected orthotopically into the subcapsular space of right kidney of nude mice. Surgical procedures were performed under anesthesia by administering an intraperitoneal injection of pentobarbital sodium (80 mg/kg). The mice were maintained at the animal facility of the Cyagen Laboratory, where they were caged and handled under ethical conditions, according to the rules outlined by the International Animal Welfare Recommendations and in accordance with the local institutional animal welfare guidelines. At the end of experiments, the primary and metastatic tumors were harvested, measured, photographed, and fixed for further histopathological analyses.

Statistical Analyses

Statistical analyses were performed using the GraphPad Prism software version 8.0 (GraphPad software, USA). Normally distributed data were expressed as mean ± standard deviation. Comparisons between two groups were done using unpaired Student's t-test or Mann–Whitney U test. One-way ANOVA test was used to compare three or more groups. Categorical data was analyzed by the chi-squared test or Fisher's exact test. Correlations of gene expression were determined with the Pearson's coefficient test. Kaplan–Meier plots and log-rank tests were used for the overall survival analysis and progression free survival analysis. The univariate and multivariate analyses were executed using the Cox proportional hazards model.

RESULTS

FGL1 Is Significantly Upregulated in ccRCC

Western blotting and IHC were used to examine the expression of FGL1 protein in specimens of ccRCC tumor and adjacent normal tissues. The results showed that FGL1 was significantly higher in cancer tissues than in the adjacent normal tissues (**Figure 1A**). Staining of FGL1 was mainly localized in the extracellular and cytoplasm of ccRCC cells, with varying intensities in different specimens (**Figures 1B–E**). Furthermore, higher FGL1 levels were found to be significantly associated with a strong presence of metastasis (**Figures 1C–E**). In the non-metastatic group, absent/weak immunostaining was observed in 59.7% (108/181) of the tumors, while moderate and strong staining was noted in 40.3% (73/181) of the tumors. By comparison to the non-metastatic group, absent/weak immunostaining was observed in 6.7% (2/30) of the tumors, while moderate and strong staining was noticed in 93.3% (28/30) of the tumors in the metastatic group. This suggested that upregulation of FGL1 may have contributed to the progression of ccRCC by promoting tumor metastasis. In addition, plasma concentration of FGL1 was higher in patients with ccRCC than healthy donors (**Figure 1F**). Patients with high T stage (i.e., T_3 and T_4) had higher plasma FGL1 concentration than those with low T stage (i.e., T_1 and T_2; **Figure 1G**). These results indicated that FGL1 was significantly upregulated in patients with ccRCC.

High FGL1 Expression Is Associated With Poor Prognosis in ccRCC Patients

The correlation between FGL1 expression and the clinicopathologic features of ccRCC patients was shown in **Table 1**. There was significant correlation between FGL1 and age ($P<0.001$), body mass index ($P<0.001$), T stage ($P<0.001$), N stage ($P<0.001$), M stage ($P<0.001$), AJCC stage ($P<0.001$), and Fuhrman grade ($P<0.001$). Immunohistochemistry score of FGL1 was significantly higher in samples from patients with a high T-stage (T3+T4), high Fuhrman grade (G3+G4), N1 stage, M1 stage, and high AJCC stage (III+IV) than in those with a low T-stage (T1+T2), low Fuhrman grade (G3+G4), N0 stage, M0 stage, and low AJCC stage (I+II) (**Figures 2A–E**). The Kaplan–Meier survival analysis indicated that patients with high FGL1 expression had a shorter overall survival and progression-free survival than patients with low FGL1 expression (**Figure 2F, G**). Univariate and multivariate Cox regression analyses indicated that FGL1 expression was an independent prognostic factor for OS (HR = 10.703, P = 0.000) and PFS (HR = 21.954, P = 0.000) in patients with ccRCC (**Table 2**). Therefore, increased FGL1 expression was associated with poor prognosis and might be a novel progression marker for ccRCC.

FGL1 Promote the Migration and Invasion of ccRCC Cells *In Vitro*

In this part, we set out to study the effect of FGL1 on the biological function of ccRCC cells. Firstly, FGL1 was expressed in human normal renal tubular epithelial cell line HK-2, human embryonic kidney derived cell line HEK293T, and seven ccRCC cell lines (ACHN,786-O, Caki-1, Caki-2, A498, SN12, and OSRC2) at varying degrees, among which A498, SN12, and Caki-2 cells exhibited the highest FGL1 expression (**Figure 3A**). Then, we validated the knockdown or overexpression effect of FGL1 on ccRCC cell lines (SN12 and A498) by Western blot when transfected with FGL1 shRNA construct or FGL1 overexpression plasmid (**Figure 3B, C**).

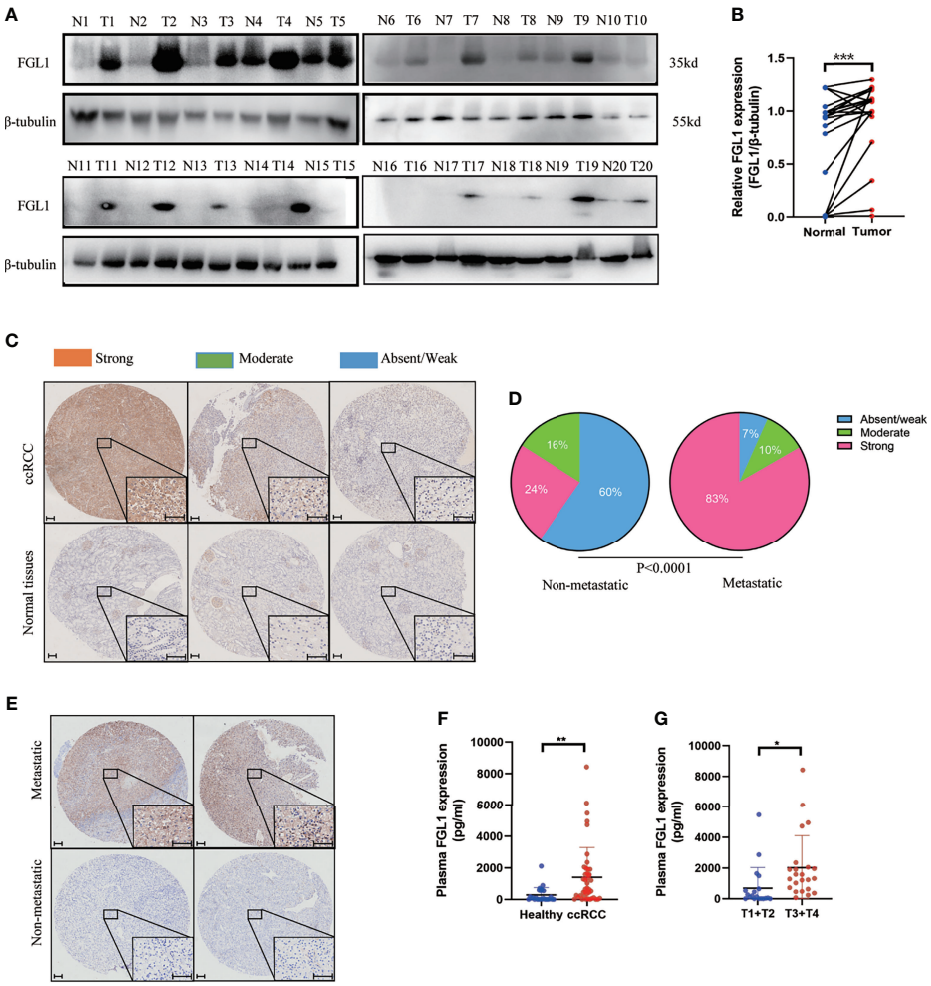

FIGURE 1 | FGL1 is significantly upregulated in ccRCC. **(A, B)** FGL1 protein expression in 20 pairs of ccRCC cancer (T) and adjacent normal tissues (N) by western blot analysis **(A)**. The intensity of bands was quantified using ImageJ software and normalized to β-tubulin **(B)**. The difference between the groups was compared by the student t-test. ***p < 0.001. **(C, D)** Immunohistochemistry (IHC) staining for FGL1 in ccRCC tissues and adjacent normal tissues. FGL1 staining intensity defined into three groups as absent/weak (Blue), moderate (Green), and strong (Red) in clinical ccRCC samples and adjacent normal tissues by IHC **(C)**. Scale bar, 100 μm. Pie chart shows the composition of different staining intensity of FGL1 between metastatic group (n=181) and non-metastatic group (n=30) **(D)**. The difference between the groups was compared by Pearson Chi-square test. **(E)** Distinguished FGL1 protein expression by IHC between representative primary metastatic ccRCC samples (n=2) and nonmetastatic ccRCC samples (n=2). Scale bar, 100 μm. **(F)** Plasma concentrations of FGL1 were measured by ELISA in a cohort of 43 ccRCC patients and 26 healthy donors. The difference between the groups was compared by the student t-test. **p < 0.01, *p < 0.05. **(G)**, Plasma concentrations of FGL1 were measured by ELISA in ccRCC patients of T1+T2 stage (20 cases) vs T3+T4 stage (23 cases). The difference between the groups was compared by the student t-test. *p < 0.05.

The MTS assay was introduced to observe the effect of FGL1 on the proliferation of SN12 and A498 cells. The results showed that neither knocking down nor overexpressing FGL1 had significant effect on the proliferation of A498 and SN12 cells at different time points (**Figure 3D**). To investigate the effect of FGL1 on the migration and invasion ability of ccRCC cells, we performed Transwell assay with or without a Matrigel coating. The results showed that when FGL1 was knocked down, the migration rate of A498 and SN12 cells was significantly slower than shNC cells (**Figures 3E, F**). On the other hand, overexpressing FGL1 resulted in a faster rate of migration of A498 and SN12 cells than in shNC cells (**Figures 3G, H**). In the wound healing assay, knocking down FGL1 caused a slower migration of A498 and SN12 cells into the scratched wound than shNC cells (**Figure 3F**), whereas overexpressing FGL1 lead to a faster migration of A498 and SN12 cells migrated into the scratched than of shNC cells (**Figure 3G**). Therefore, FGL1 did not affect ccRCC cell growth/proliferation, but promoted cell migration and cell invasion *in vitro*.

FGL1 Is Required for EMT Process in ccRCC

Epithelial mesenchymal-transition (EMT) is a key process for tumor migration, invasion, and metastasis. However, the effects of FGL1

TABLE 1 | Relationship between FGL1 expression and clinicopathological features in patients with ccRCC [n (%)].

Variable	No. of patients (%)			χ^2	*P* value
	Patients	FGL1 High	FGL1 Low		
Age (years)					
≤60	149	22 (14.8)	125 (83.9)	30.563	0.000
> 60	62	32 (51.6)	30 (48.4)		
Gender					
Male	156	43 (66.7)	113 (33.3)	1.222	0.269
Female	55	11 (61.8)	44 (38.2)		
Body mass index					
≤23.9	67	34 (50.7)	33 (49.3)	32.619	0.000
> 23.9	144	20 (13.9)	124 (86.1)		
T stage					
T_1+T_2	179	33 (18.4)	146 (81.6)	31.745	0.000
T_3+T_4	32	21 (65.6)	11 (34.4)		
N stage					
N0	198	44 (22.2)	154 (77.8)	16.403	0.000
N1	13	10 (76.9)	3 (23.1)		
M stage					
M0	191	37 (19.4)	154 (80.6)	40.948	0.000
M1	20	17 (85.0)	3 (15.0)		
AJCC Stage					
Stage I+II	162	28 (17.3)	64 (88.9)	60.629	0.006
Stage III+IV	49	36 (73.5)	9 (26.5)		
Fuhrman grade					
Grade 1+2	156	20 (12.8)	136 (87.2)	51.266	0.000
Grade 3+4	55	34 (61.8)	21 (38.2)		

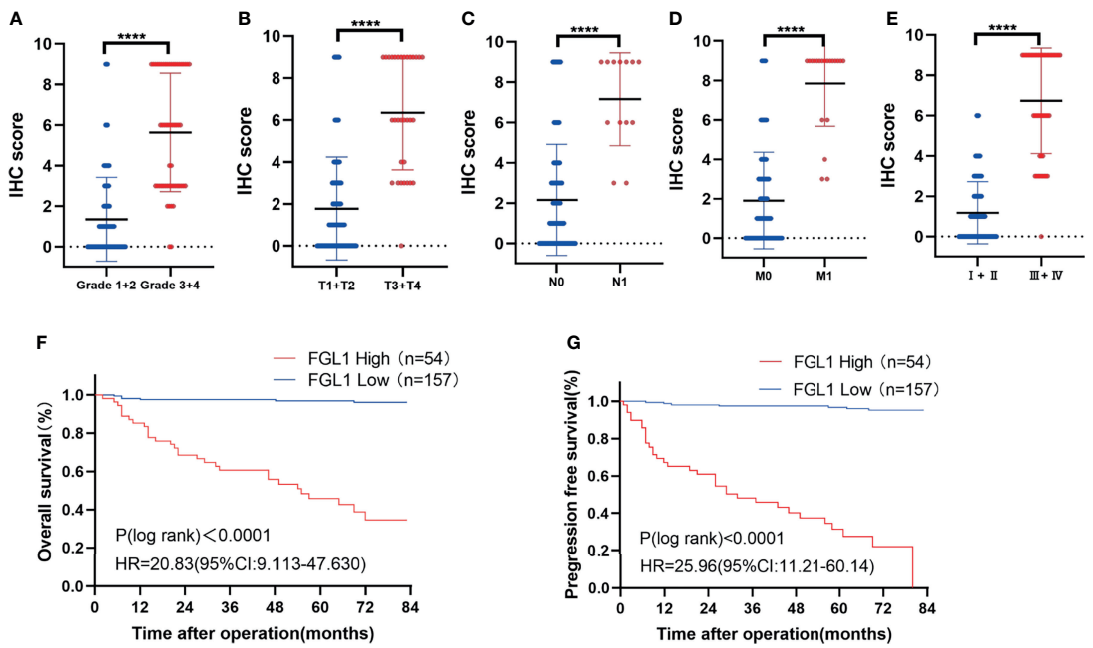

FIGURE 2 | High FGL1 expression is associated with poor prognosis in ccRCC patients. **(A–E)** significantly higher IHC score of FGL1 in patients with high Fuhrman grade (G3 and G4) (n=55) **(A)** advanced T stage (T3 and T4) (n=32) **(B)** positive lymphatic metastasis (N1) (n=13) **(C)** metastasis (M1) (n=20) **(D)** and advanced AJCC stage (III and IV) (n=49) **(E)**. The difference between the groups was compared by the nonparametric test of Mann–Whitney U test. ****p < 0.0001. **(F, G)** Kaplan-Meier curves with log rank test of overall survival **(F)** and progression-free survival **(G)**. High FGL1 expression group (n=54) (red line); low FGL1 expression group (n=157) (blue line).

TABLE 2 | Univariate and multivariable Cox regression models analyzing clinical variables affecting OS and PFS.

Variable	OS				PFS			
	Univariate		Multivariate		Univariate		Multivariate	
	HR (CI95%)	P	HR (CI95%)	P	HR (CI95%)	P	HR (CI95%)	P
Age (years) 1:<60;0:≥60	0.427 (0.226~0.808)	0.009	0.755 (0.389~1.464)	0.405	0.785 (0.424~1.456)	0.443	0.635(0.330~1.224)	0.175
Gender 1:male;0:female	1.279 (0.586~2.791)	0.536	1.601 (0.640~4.006)	0.314	1.283 (0.637~2.587)	0.486	0.669(0.287~1.559)	0.351
BMI 1:<23.9;0:≥23.9	1.732 (0.909~3.299)	0.051	2.088 (0.998~4.371)	0.051	1.731 (0.961~3.118)	0.068	0.412(0.205~0.826)	0.013
T stage 1: ≥T3;0:<T3	4.787 (2.626~8.725)	0.000	0.719 (0.208~2.484)	0.602	4.787 (2.626~8.725)	0.000	1.896(0.581~6.182)	0.289
N stage 1:N1;0: N0	5.960 (2.594~13.695)	0.000	2.343 (0.725~7.577)	0.155	5.474 (2.521~11.888)	0.000	0.663(0.251~1.749)	0.406
M stage 1:M1;0: M0	9.618 (4.833~19.143)	0.000	2.782 (0.727~10.643)	0.135	9.002 (4.467~17.338)	0.000	0.690(0.205~2.323)	0.550
AJCC 1: ≥III;0:<III	8.765 (4.443~17.291)	0.000	0.995 (0.193~5.135)	0.995	10.745 (5.775~20.061)	0.000	0.436(0.103~1.843)	0.259
Fuhrman grade 1: ≤2;0:>2	9.469 (4.685~19.140)	0.000	3.600 (1.646~7.875)	0.001	7.131 (3.900~13.038)	0.000	0.417(0.213~0.817)	0.011
FGL1 1:high;0:low	24.236 (10.013~58.661)	0.000	10.703 (3.876~29.558)	0.000	35.207 (15.273~81.161)	0.000	21.954(8.436~57.134)	0.000

on EMT in ccRCC cells remain unclear. In this study, we observed that after FGL1 knockdown the cells showed a cuboidal cobblestone epithelial shape with tight cell-to-cell adherence, whereas the cells with overexpressed FGL1 had a slender and fibroblast-like shape (**Figure 4A**). These observations suggested that FGL1 participates in the EMT process in ccRCC. As expected, after FGL1 knockdown in A498 and SN12 cells, expression of E-cadherin was upregulated, while it was downregulated in N-cadherin. Moreover, opposite results were observed after overexpression of FGL1 in A498, SN12 cells (**Figure 4B** and **Supplementary Figure S1**). These observations were further validated by immunofluorescence staining (**Figure 4C** and **Supplementary Figure S2**). The features of EMT are regulated by EMT-inducing transcription factors such as Twist and Snail. Our results showed that Twist protein was significantly decreased after FGL1 knockdown in A498 and SN12 cells, and overexpression of FGL1 yielded opposite results. Collectively, these results suggested that FGL1 could promote EMT in ccRCC cells.

To further investigate whether FGL1 could promote EMT in ccRCC, we used IHC to analyze the correlation between FGL1 and EMT markers including E-cadherin, N-cadherin, and Vimentin in ccRCC tissues and paired normal tissues. The results showed that the expression of Vimentin and N-cadherin were significantly higher in ccRCC cancer tissues than in paired normal tissues, whereas the expression of E-cadherin in ccRCC cancer tissues was significantly lower than in paired normal tissues (**Supplementary Figure S3**). Pearson correlation analysis showed that the expression of FGL1 in ccRCC cancer tissues was significantly negatively correlated with E-cadherin expression, whereas significantly positively correlated with N-cadherin expression. No correlation was found between FGL1 and Vimentin expression in ccRCC tissues (**Figures 4D–G**). Altogether, these findings implicate FGL1 with promoting invasion and metastasis by enhancing the EMT process in ccRCC.

Loss of FGL1 Induces Production of Pro-Inflammatory Cytokines/Chemokines in ccRCC Cells

To determine the transcriptional output regulation after knocking down FGL1 in ccRCC cells, we performed RNA-seq detection in A498 shNC, A498 FGL1-sh1, and A498 FGL1-sh2 cells. Firstly, volcano plots showed that a total of total 119 DEGs including 44 upregulated and 75 downregulated expressed genes were detected in shNC vs FGL1-sh1 group (**Figure 5A**), while a total 97 DEGs including 46 upregulated and 51 downregulated expressed genes were detected in shNC vs FGL1-sh2 group (**Supplementary Figure S4**). Then, Venn diagram showed that 56 genes were shared between shNC vs FGL1-sh1 group and shNC vs FGL1-sh2 group (**Supplementary Figure S5**). We assessed key regulatory pathways using gene-set enrichment analysis (GSEA) and discovered that chemokine activity and chemokine receptor are regulatory targets of FGL1 (**Figures 5B, C**). Moreover, KEGG pathway analysis revealed that the major pathways involved in DEGs were 'Cytokine-cytokine receptor interaction pathway', 'renin secretion', and 'vascular smooth muscle contraction' (**Figure 5D**). The PPI network showed that IL-6 was the most prominent hub with nineteen related proteins, and that CXCL8, CXCL2, and CCL5 were secondary hubs. The majority of these hub genes were found to be involved in the cytokine-cytokine receptor interaction pathway (**Supplementary Figure S6**). Expression of the hub genes that were identified on the RNA-seq was confirmed by qPCR. We found higher levels mRNA for IL-6, CXCL2, CXCL8, and CCL5 in FGL1 knockdown cells than in shNC cells, which was consistent with RNA-seq data (**Figure 5E**).

The DEGs were annotated by GO biological function analysis, cellular component analysis, and biological process analysis. The five most enriched GO terms of the DEGs for the biological process were 'inflammatory response', 'positive regulation of urine volume', 'cell-cell signaling', 'negative regulation of T cell activation', and 'intracellular signal transduction' (**Figure 5F**). The four most enriched GO terms of the DEGs for cellular component were 'extracellular space', 'basal part of cell', 'integral component of plasma membrane', and 'extracellular region' (**Supplementary Figure S7**). The most enriched GO terms of the DEGs for molecular function was 'cytokine activity' (**Supplementary Figure S8**).

FGL1 Silencing Suppressed Tumorigenicity and Metastasis in Orthotopic Xenograft Tumor Model

Since FGL1 promotes the migration and invasion of ccRCC cells *in vitro*, we hypothesized that knocking down FGL1 expression

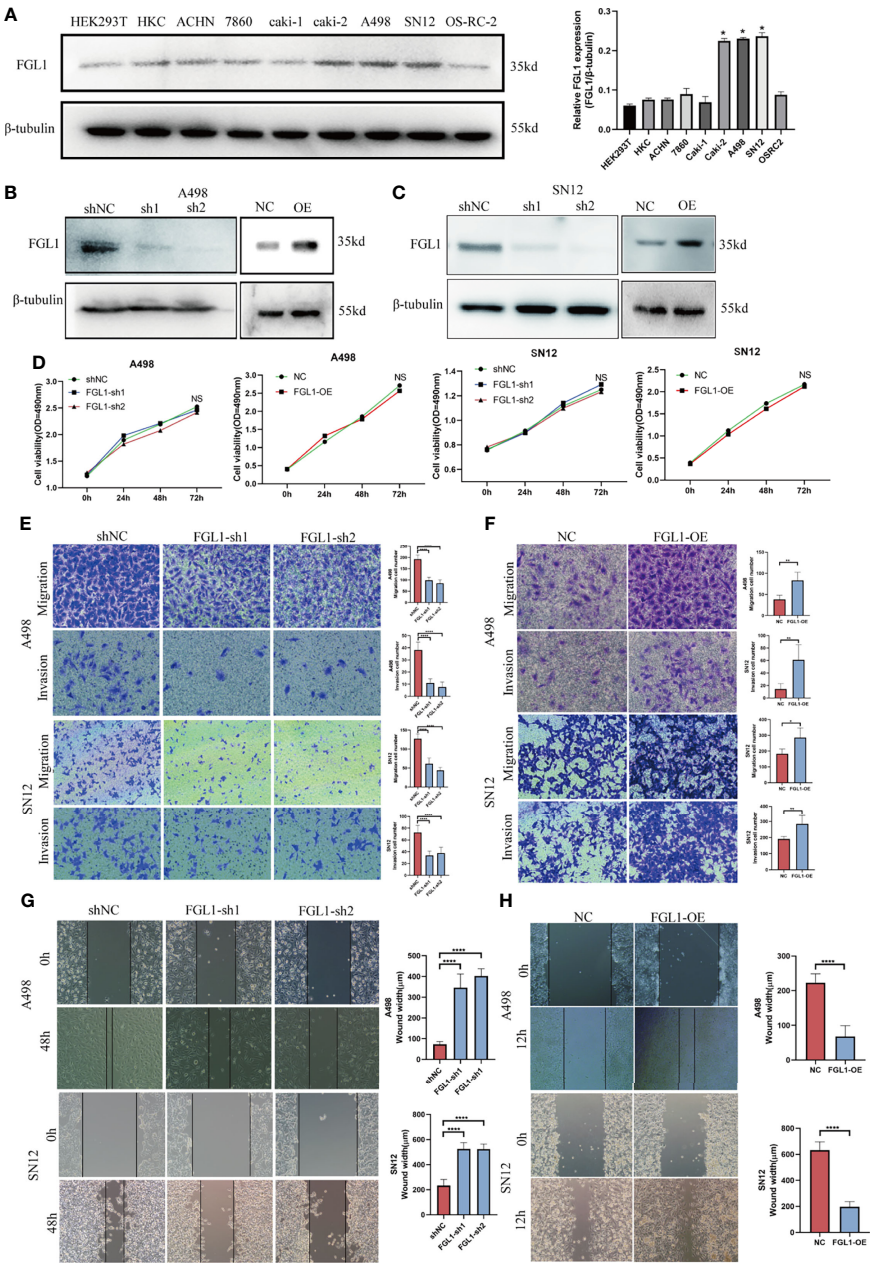

FIGURE 3 | FGL1 promote the migration and invasion of ccRCC cells *in vitro*. **(A)** FGL1 expression was determined by western blot analysis in RCC cell lines (ACHN, 786O, Caki-1, Caki-2, A498, SN12 and OS-RC-2) and normal renal cell lines (HEK293T, HKC) (left). The intensity of bands was quantified using ImageJ software and normalized to β-tubulin (right). *$p < 0.05$ compared to the HKC cell line. **(B, C)** FGL1 knockdown or overexpression effect was confirmed by Western blot analysis in A498 **(B)** and SN12 cells **(C)**. **(D)** MTS assay to detect the effect of FGL1 knockdown or overexpression on cell proliferation of A498 and SN12 cells at 24h, 48h, and 72h. NS denotes no significant difference between groups. **(E, F)** the effect of FGL1 knockdown or overexpression on migration **(E)** and invasion **(F)** ability of A498 and SN12 cells were examined by Transwell assay. Scale bar, 100 μm. Representative images were taken at 16h after cell migration and invasion. The mean migration or invasion cell numbers of the groups were compared using the student t test. *$p < 0.05$, **$p < 0.01$, ****$p < 0.0001$. **(G, H)** the effect of FGL1 knockdown **(G)** or overexpression **(H)** on migration ability of A498 and SN12 cells were examined by wound healing assay. Scale bar, 100 μm. Wound-healing process measured at 24 hours. The mean wound width of the groups was compared using the student t test. ****$p < 0.0001$.

will suppress progression and metastasis *in vivo*. We orthotopically injected shFGL1/Luc or shNC/Luc SN12 cells into subcapsular space of nude mice. Four weeks after injection, the bioluminescent signals in the kidneys were significantly higher in the shNC group than in the shFGL1 group (**Figures 6A, C**). In these two groups, all the mice were sacrificed at the end of the fourth week, and the primary tumors are shown in **Figure 6B**. The shFGL1 group had lighter and

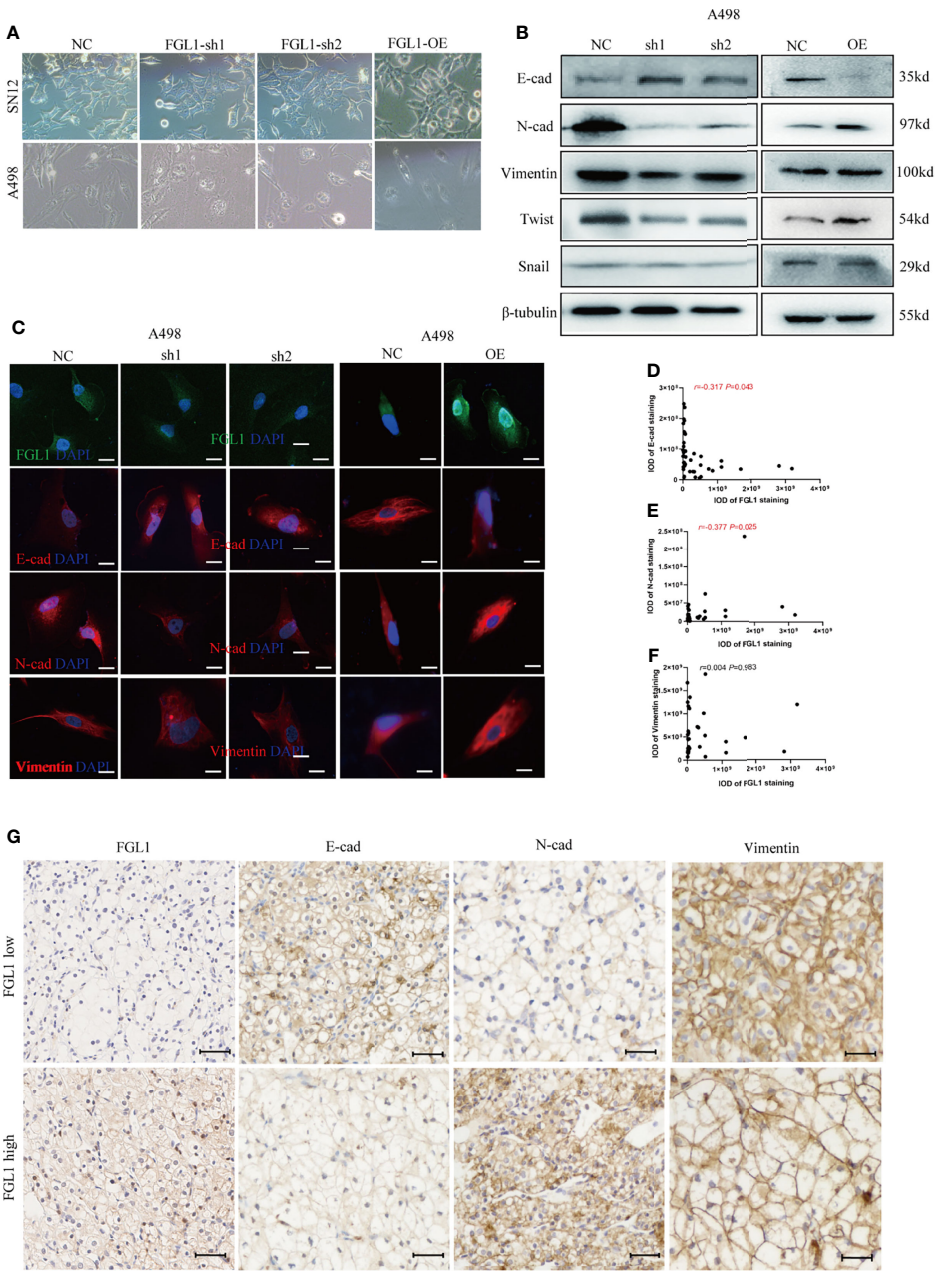

FIGURE 4 | FGL1 is required for EMT process in ccRCC. **(A)** cell morphology of A498 and SN12 cells was observed under bright-field microscopy after FGL1 knockdown or overexpression. **(B)** Western blot analyzed the expression of E-cadherin, N-cadherin, Vimentin, Twist and Snail with FGL1 knockdown or overexpression in A498 cells. **(C)** Immunofluorescence staining of E-cadherin, N-cadherin, Vimentin after FGL1 knockdown or overexpression in A498 cells, with DAPI nuclear staining in blue, FGL1 in green and EMT markers (E-cadherin, N-cadherin, Vimentin) in red. **(D–F)** the correlation between FGL1 and E-cadherin **(D)** N-cadherin **(E)** and vimentin **(F)** expression is represented in a scatter plot. Statistical significance was tested by the Pearson correlation test. In the scatter plot, the symbol r represents the Pearson's correlation coefficient. IOD, integral optical density. **(G)** Representative images of IHC staining for E-cad, N-cad and Vimentin expression in low- and high-FGL1 tumors. Scale bar, 100μm.

smaller tumors than the control group (**Figures 6D, E**). Our data confirmed that knocking down FGL1 inhibits tumor growth *in vivo*. Gross lung specimens were collected and used to elucidate whether knocking down FGL1 affects metastasis *in vivo* (**Supplementary Figure S9**). We found that mice in the shFGL1 group developed fewer lung metastatic foci than those in the shNC group (**Figures 6E, F**). The average tumor size of metastatic nodules in the shFGL1 group was smaller than in the shNC group (**Figure 6G**). Furthermore, we discovered that the shNC group had more CD146 positive microvessels and a higher

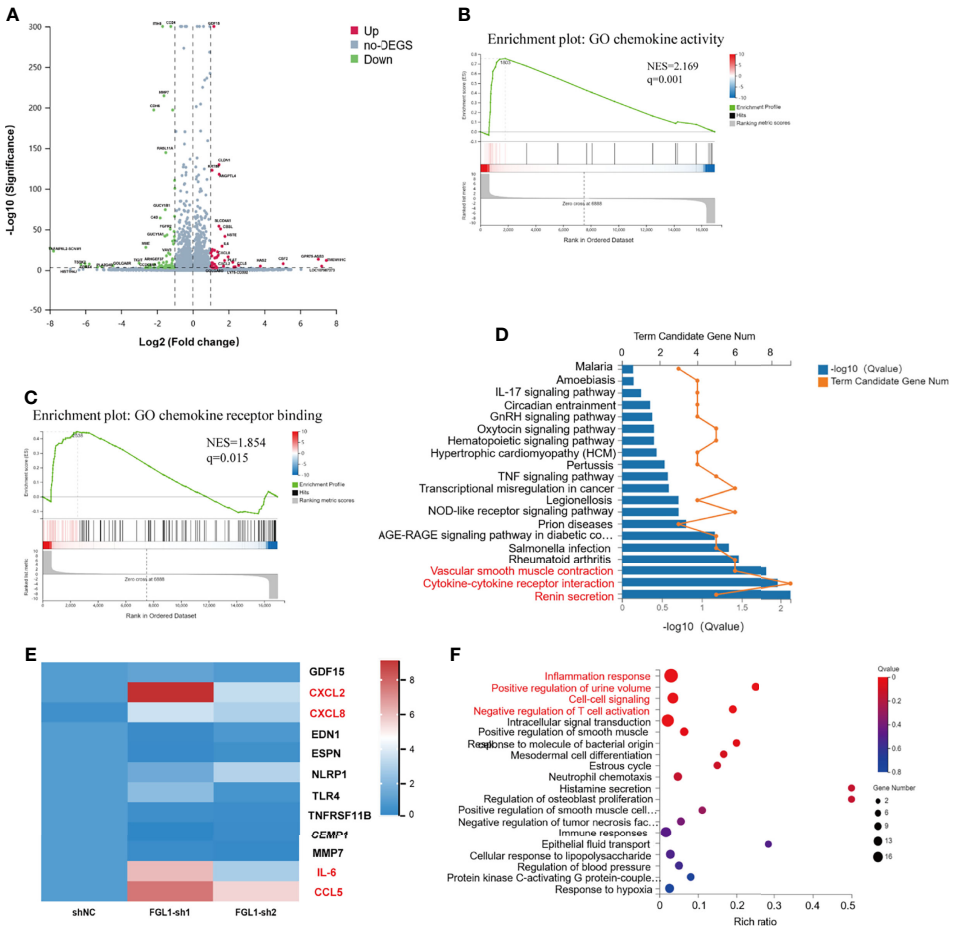

FIGURE 5 | Loss of FGL1 induces production of pro-inflammatory cytokines/chemokines in ccRCC cells. **(A)** Volcano plots were constructed using fold-change values and p-values between shNC and FGL1-sh1 group (log2 FC≥1, FDR< 0.001) by the Dr. Tom network platform. Red represents differentially expressed genes (DEGs) up regulated, blue represents DEG down regulated, and gray represents non-DEG. **(B, C)** GSEA enrichment plot for chemokine activity gene set **(B)** and chemokine receptor binding gene set **(C)** by the Dr. Tom network platform. (Normalized Enrichment Score (NES) > 1, Nominal p-value < 0.05, FDR q-value < 0.25). **(D)** DEGs were analyzed by GO biological process enrichment analysis and showed by histogram chart. The major pathways involved in DEGs were 'Cytokine-cytokine receptor interaction pathway', 'renin secretion', and 'vascular smooth muscle contraction' were showed in red font. **(E)** qRT-PCR validation of the DEGs involved in the cytokine-cytokine receptor interaction pathway. The DEGs, including IL-6, CXCL2, CXCL8, and CCL5, were significantly upregulated in FGL1 knockdown cells and shown in red font. **(F)** Bubble chart for significantly enriched pathway terms using the phyper function in R software to perform the KEGG enrichment analysis. X-axis is the enrichment ratio (Rich Ratio = Term Candidate Gene Num/Term Gene Num), Y-axis is KEGG Pathway.

positivity rate of CD11b+ and Ly-6G+ cells in tumor tissues than in the shFGL1 group (**Figure 6H** and **Supplementary Figure S10**). Therefore, our findings demonstrated that FGL1 knockdown repressed the tumorigenicity and metastasis properties of ccRCC cells *in vivo*.

DISCUSSION

Invasion and metastasis, two of the most significant hallmarks of malignant tumors, are major obstacles to the treatment of malignant tumors, and have effects on the prognosis of patients (25). Although surgical resection can cure certain cancers when diagnosed at early stages, metastatic cancer is largely incurable and results in high mortality rate (26). This is likely because the precise mechanisms of metastatic changes during cancer progression are still largely unknown.

Fibrinogen-like protein 1(FGL1), originally named as human hepassocin (HPS), is a liver-secreted protein that plays a critical role in liver regeneration by activating the MAPK pathway to repair damaged hepatocytes (27, 28). Further experiments indicated that FGL1 regulates metabolism by increasing hepatic lipid accumulation and inducing insulin resistance (29). Recent evidence boosted the research of FGL1 in cancer biology by illustrating a new function of FGL1 in immune suppression where it acts as a major inhibitory ligand of LAG-3 and inhibits antigen-specific T cell activation (14). Recent research suggested that FGL1 is upregulated in gastric cancer tissues, while some

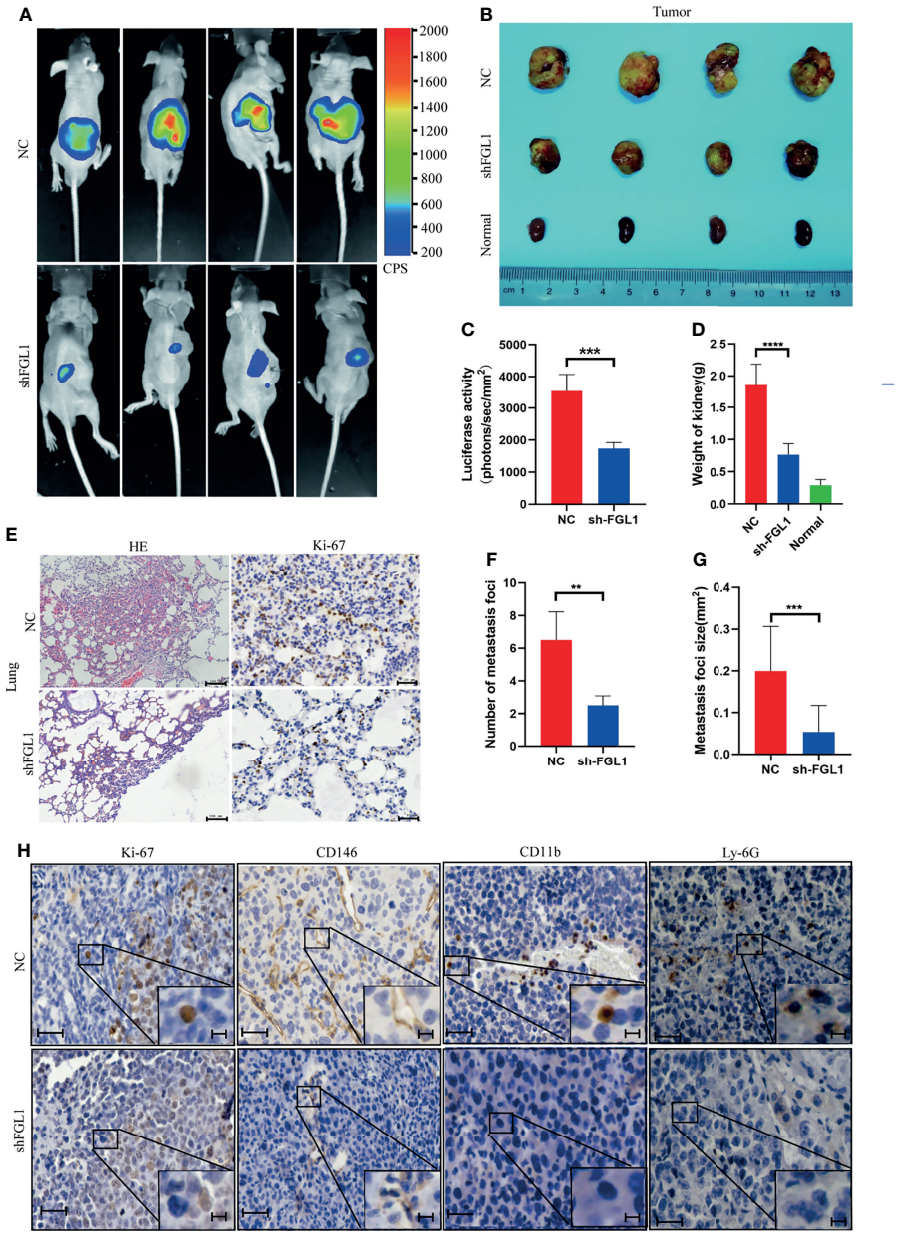

FIGURE 6 | FGL1 silencing suppressed tumorigenicity and metastasis in orthotopic xenograft tumor model. **(A)** Representative bioluminescent images of kidney tumors in shNC (Upper) (n=4) and shFGL1 experimental groups (Lower) (n=4) (four week after cell implantation). CPS, unit of signal intensity in counts per second. **(B)** Gross appearance of kidney tumors in shNC group (n=4), shFGL1 group (n=4) and contralateral normal kidney (n=4). **(C)** Measurement of bioluminescent signals of shNC (n=4) and shFGL1 group (n=4) on day 30. ***P<0.001. **(D)** the histogram shows the weight of tumors in shNC group (n=4) and shFGL1 group (n=4), ***p < 0.001. **(E)** Representative images of hematoxylin-eosin (HE) staining and ki-67 staining of lung metastatic foci in shNC group (n=4) and shFGL1 group (n=4). Scale bar of HE staining, 100 μm. Scale bar of ki-67 staining, 20 μm. **(F, G)** the number **(F)** and size **(G)** of lung metastatic foci was were decreased in shFGL1 group compared to shNC groups. **P<0.01, ***P<0.001. **(H)** Representative images of ki-67 (proliferation marker), CD146 (endothelial cell marker), CD11b (myeloid cell marker) and Ly-6G (neutrophil marker) in tumor tissues from shNC group and shFGL1 group. Scale bar, 20 μm. and scale bar in zoom, 5 μm.

studies revealed that it is downregulated and possibly acts as a tumor suppressor in hepatocellular carcinoma (18, 30). Accordingly, depending on the cell type and origin of the cancer, FGL1 can be upregulated or downregulated acting as an oncogene or tumor suppressor, thus indicating the complexity and diversity of roles played by FGL1 in different cancers. Currently, the expression and function of FGL1 in ccRCC is poorly understood. Herein, we reported for the first time that FGL1 is upregulated in both cancer tissues and plasma of ccRCC patients. High expression of FGL1 in cancer tissues is closely associated with distal metastasis and fatal

outcome in ccRCC patients. Univariate and multivariable Cox proportional hazard regression analyses further showed that, high FGL1 expression in cancer tissues is an independent risk factor for ccRCC patients with poor prognosis, indicating that FGL1 may be an oncogene of ccRCC. Consequently, FGL1 may be used as a new prognostic marker for ccRCC.

Epithelial mesenchymal-transition (EMT) is now widely recognized as an indispensable step in tumor invasion and metastasis (31), and E–cadherin, N–cadherin, and Vimentin are generally accepted as important molecular markers of EMT (32). The loss of E-cadherin, an important feature of EMT, has been linked to invasive and undifferentiated phenotype in malignant tumors (17). Markers such as N-cadherin and vimentin were upregulated during EMT to induce mesenchymal phenotypes and motile behavior (16). Our data showed that overexpression of FGL1 decreased the expression of E-cadherin while increasing the expression of N-cadherin, causing ccRCC cells to evolve into a highly invasive and mesenchymal phenotype. Furthermore, overexpression or knocking down of FGL1 increased or decreased the levels of Twist proteins, respectively. Previous study had indicated that upregulation of Twist proteins resulted in a significant decrease in the expression of E-cadherin and a prominent increase in the expression of N-cadherin, thus promoting the migration and invasion abilities in cancer cells (33). In light of our findings, FGL1 might upregulate Twist to maintain the mesenchymal phenotype and promote the migration and invasion behavior of ccRCC cells. Besides, we also observed a significant association between FGL1 expression and EMT biomarkers in clinical specimens. Therefore, our data elucidated that FGL1 exerts the biological function of promoting tumor cell migration, invasion, and metastasis by facilitating EMT process in ccRCC. However, the detailed mechanism by which FGL1 regulates EMT is unknown, and further research is required.

Numerous studies had reported that FGL1 knockdown either inhibits or promotes tumor cell proliferation. However, our data showed that neither overexpression nor knockdown of FGL1 in ccRCC cell lines had an effect on cell proliferation, but cell migration and invasion were affected. Interestingly, in contrast to the *in vitro* assay, our results showed that FGL1 knockdown inhibited orthotopic tumor growth in xenograft tumor model using T cell-deficient nude mice. We speculated that FGL1 may play an important role in modulating tumor innate immunity. Our results demonstrated that FGL1 knockdown significantly decreased the infiltrated number of myeloid-derived CD11b+ cells and ly6G+ cells in primary tumor tissues. Various types of myeloid cells, such as tumor-associated neutrophils (TANs) and myeloid-derived suppressor cells (MDSC), have been shown to promote tumor progression by inhibiting anti-tumor immunity (34, 35). Neutrophil accumulation in tissue involves different steps including chemotaxis, activation, and transmigration (36, 37). Our study showed that the expression of CD146 was significantly reduced in shFGL1 tumors. Bardin N. et al. (38), reported that CD146, which is found at the junction and apical membrane of human umbilical veins endothelial cells, can contribute to transendothelial migration of monocytes during inflammation. So, knocking down FGL1 can help to repress neutrophil accumulation in tumor by reducing neutrophils transmigration through blood vessels. In addition, our study revealed that some inflammatory cytokines (such as IL-6) and chemokines (such as CXCL2, CXCL8, and CCL5) were elevated after FGL1 knockdown in ccRCC cells. Chemokines, like CXCL2, CXCL8 and CCL5, can mobilize and activate resting NK cells, resulting in tumor cell cytolysis (39). Based on these observations, our study showed that FGL1 achieves its function by influencing the release of cytokines and chemokines from cancer cells, which can dampen anti-tumor immune responses in TME. However, further research in immunocompetent mice is needed to fully understand this effect.

In summary, our report demonstrates that FGL1 is upregulated in ccRCC patients, and that high expression of FGL1 is associated with poor prognosis. Moreover, we validated that FGL1 stimulates the migration, invasion, and metastasis phenotype in ccRCC by promoting the EMT process. Besides mediating T cell suppression, we demonstrated that FGL1 has a novel role in regulating innate immune response. Therefore, targeting FGL1 may help to suppress the progression of ccRCC and improve clinical outcomes. However, many problems remain to be solved. First, the mechanism by which FGL1 regulates the expression of cytokines and chemokines in cancer cells remains largely unknown. Second, future research should focus on how FGL1-regulated cytokines and chemokines modulate immune cell functions. Nevertheless, FGL1 remains a potential therapeutic target in cancer.

DATA AVAILABILITY STATEMENT

The raw data supporting the conclusions of this article will be made available by the authors, without undue reservation.

ETHICS STATEMENT

Patients were asked to sign an informed consent before inclusion in the study and the study was approved by Ethics Committee of Chinese PLA Hospital. The patients/participants provided their written informed consent to participate in this study. Written informed consent was obtained from the individual(s) for the publication of any potentially identifiable images or data included in this article.

AUTHOR CONTRIBUTIONS

The study design, XZ., YH, and ZL. The experiment and performed data analysis, BC and H-YF. The animal experiments: XH, Y-DX, and TW. The clinical data analysis, H-FW and H-YF. The IHC and IF assay: ZL. Manuscript writing, reviewing, and revision: ZL, XM, YH, and XZ. Study supervision: H-ZL, XM, and XZ. All authors contributed to the article and approved the submitted version.

FUNDING

This study was financially supported by the National Natural Science Foundation of China (grant number. 81972389 and 81770790).

SUPPLEMENTARY MATERIAL

The Supplementary Material for this article can be found online at: https://www.frontiersin.org/articles/10.3389/fonc.2021.756843/full#supplementary-material

REFERENCES

1. Siegel RL, Miller KD, Jemal A. Cancer Statistics, 2019. *CA Cancer J Clin* (2019) 69(1):7–34. doi: 10.3322/caac.21551
2. Hsieh JJ, Purdue MP, Signoretti S, Swanton C, Albiges L, Schmidinger M, et al. Renal Cell Carcinoma. *Nat Rev Dis Primers* (2017) 3:17009. doi: 10.1038/nrdp.2017.9
3. Crispen PL, Breau RH, Allmer C, Lohse CM, Cheville JC, Leibovich BC, et al. Lymph Node Dissection at the Time of Radical Nephrectomy for High-Risk Clear Cell Renal Cell Carcinoma: Indications and Recommendations for Surgical Templates. *Eur Urol* (2011) 59(1):18–23. doi: 10.1016/j.eururo.2010.08.042
4. Heng DYC, Wells JC, Rini BI, Beuselinck B, Lee J-L, Knox JJ, et al. Cytoreductive Nephrectomy in Patients With Synchronous Metastases From Renal Cell Carcinoma: Results From the International Metastatic Renal Cell Carcinoma Database Consortium. *Eur Urol* (2014) 66(4):704–10. doi: 10.1016/j.eururo.2014.05.034
5. Cohen HT, McGovern FJ. Renal-Cell Carcinoma. *N Engl J Med* (2005) 353 (23):2477–90. doi: 10.1056/NEJMra043172
6. Motzer RJ, Ravaud A, Patard J-J, Pandha HS, George DJ, Patel A, et al. Adjuvant Sunitinib for High-Risk Renal Cell Carcinoma After Nephrectomy: Subgroup Analyses and Updated Overall Survival Results. *Eur Urol* (2018) 73 (1):62–8. doi: 10.1016/j.eururo.2017.09.008
7. Ravaud A, Motzer RJ, Pandha HS, George DJ, Pantuck AJ, Patel A, et al. Adjuvant Sunitinib in High-Risk Renal-Cell Carcinoma After Nephrectomy. *N Engl J Med* (2016) 375(23):2246–54. doi: 10.1056/NEJMoa1611406
8. Choueiri TK, Halabi S, Sanford BL, Hahn O, Michaelson MD, Walsh MK, et al. Cabozantinib Versus Sunitinib As Initial Targeted Therapy for Patients With Metastatic Renal Cell Carcinoma of Poor or Intermediate Risk: The Alliance A031203 CABOSUN Trial. *J Clin Oncol* (2017) 35(6):591–7. doi: 10.1200/JCO.2016.70.7398
9. Motzer RJ, Barrios CH, Kim TM, Falcon S, Cosgriff T, Harker WG, et al. Phase II Randomized Trial Comparing Sequential First-Line Everolimus and Second-Line Sunitinib Versus First-Line Sunitinib and Second-Line Everolimus in Patients With Metastatic Renal Cell Carcinoma. *J Clin Oncol* (2014) 32(25):2765–72. doi: 10.1200/JCO.2013.54.6911
10. Motzer RJ, Escudier B, McDermott DF, George S, Hammers HJ, Srinivas S, et al. Nivolumab Versus Everolimus in Advanced Renal-Cell Carcinoma. *N Engl J Med* (2015) 373(19):1803–13. doi: 10.1056/NEJMoa1510665
11. Dong H, Strome SE, Salomao DR, Tamura H, Hirano F, Flies DB, et al. Tumor-Associated B7-H1 Promotes T-Cell Apoptosis: A Potential Mechanism of Immune Evasion. *Nat Med* (2002) 8(8):793–800. doi: 10.1038/nm730
12. Motzer RJ, Penkov K, Haanen J, Rini B, Albiges L, Campbell MT, et al. Avelumab Plus Axitinib Versus Sunitinib for Advanced Renal-Cell Carcinoma. *N Engl J Med* (2019) 380(12):1103–15. doi: 10.1056/NEJMoa1816047
13. Rini BI, Plimack ER, Stus V, Gafanov R, Hawkins R, Nosov D, et al. Pembrolizumab Plus Axitinib Versus Sunitinib for Advanced Renal-Cell Carcinoma. *N Engl J Med* (2019) 380(12):1116–27. doi: 10.1056/NEJMoa1816714
14. Wang J, Sanmamed MF, Datar I, Su TT, Ji L, Sun J, et al. Fibrinogen-Like Protein 1 Is a Major Immune Inhibitory Ligand of LAG-3. *Cell* (2019) 176(1-2):334–47. doi: 10.1016/j.cell.2018.11.010
15. Pastushenko I, Blanpain C. EMT Transition States During Tumor Progression and Metastasis. *Trends Cell Biol* (2019) 29(3):212–26. doi: 10.1016/j.tcb.2018.12.001
16. Bhandari A, Zheng C, Sindan N, Sindan N, Quan R, Xia E, et al. COPB2 Is Up-Regulated in Breast Cancer and Plays a Vital Role in the Metastasis *via* N-Cadherin and Vimentin. *J Cell Mol Med* (2019) 23(8):5235–45. doi: 10.1111/jcmm.14398
17. Wong SHM, Fang CM, Chuah L-H, Leong CO, Ngai SC. E-Cadherin: Its Dysregulation in Carcinogenesis and Clinical Implications. *Crit Rev Oncol Hematol* (2018) 121:11–22. doi: 10.1016/j.critrevonc.2017.11.010
18. Zhang Y, Qiao H-X, Zhou Y-T, Hong L, Chen J-H. Fibrinogen–Like–Protein 1 Promotes the Invasion and Metastasis of Gastric Cancer and Is Associated With Poor Prognosis. *Mol Med Rep* (2018) 18(2):1465–72. doi: 10.3892/mmr.2018.9097
19. Bie F, Wang G, Qu X, Wang Y, Huang C, Wang Y, et al. Loss of FGL1 Induces Epithelial–Mesenchymal Transition and Angiogenesis in LKB1 Mutant Lung Adenocarcinoma. *Int J Oncol* (2019) 55(3):697–707. doi: 10.3892/ijo.2019.4838
20. Gao M, Zhan Y-Q, Yu M, Ge C-H, Li C-Y, Zhang J-H, et al. Hepassocin Activates the EGFR/ERK Cascade and Induces Proliferation of L02 Cells Through the Src-Dependent Pathway. *Cell Signal* (2014) 26(10):2161–6. doi: 10.1016/j.cellsig.2014.04.013
21. Sun C, Gao W, Liu J, Cheng H, Hao J. FGL1 Regulates Acquired Resistance to Gefitinib by Inhibiting Apoptosis in Non-Small Cell Lung Cancer. *Respir Res* (2020) 21(1):210. doi: 10.1186/s12931-020-01477-y
22. Huang QB, Ma X, Li HZ, Ai Q, Liu SW, Zhang Y, et al. Endothelial Delta-Like 4 (DLL4) Promotes Renal Cell Carcinoma Hematogenous Metastasis. *Oncotarget* (2014) 5(10):3066–75. doi: 10.18632/oncotarget.1827
23. Zhao T, Ren H, Li J, Chen J, Zhang H, Xin W, et al. LASP1 Is a HIF1α Target Gene Critical for Metastasis of Pancreatic Cancer. *Cancer Res* (2015) 75 (1):111–9. doi: 10.1158/0008-5472.CAN-14-2040
24. Gao Y, Li H, Ma X, Fan Y, Ni D, Zhang Y, et al. KLF6 Suppresses Metastasis of Clear Cell Renal Cell Carcinoma *via* Transcriptional Repression of E2F1. *Cancer Res* (2017) 77(2):330–42. doi: 10.1158/0008-5472.CAN-16-0348
25. Valastyan S, Weinberg RA. Tumor Metastasis: Molecular Insights and Evolving Paradigms. *Cell* (2011) 147(2):275–92. doi: 10.1016/j.cell.2011.09.024
26. Wallis CJD, Klaassen Z, Bhindi B, Ye XY, Chandrasekar T, Farrell AM, et al. First-Line Systemic Therapy for Metastatic Renal Cell Carcinoma: A Systematic Review and Network Meta-Analysis. *Eur Urol* (2018) 74(3):309–21. doi: 10.1016/j.eururo.2018.03.036
27. Hara H, Uchida S, Yoshimura H, Aoki M, Toyoda Y, Sakai Y, et al. Isolation and Characterization of a Novel Liver-Specific Gene, Hepassocin, Upregulated During Liver Regeneration. *Biochim Biophys Acta* (2000) 1492(1):31–44. doi: 10.1016/S0167-4781(00)00056-7
28. Li C-Y, Cao C-Z, Xu W-X, Cao M-M, Yang F, Dong L, et al. Recombinant Human Hepassocin Stimulates Proliferation of Hepatocytes *In Vivo* and Improves Survival in Rats With Fulminant Hepatic Failure. *Gut* (2010) 59 (6):817–26. doi: 10.1136/gut.2008.171124
29. Jung TW, Chung YH, Kim H-C, Abd El-Aty AM, Jeong JH. Hyperlipidemia-Induced Hepassocin in the Liver Contributes to Insulin Resistance in Skeletal Muscle. *Mol Cell Endocrinol* (2018) 470:26–33. doi: 10.1016/j.mce.2017.10.014
30. Yan J, Yu Y, Wang N, Chang Y, Ying H, Liu W, et al. LFIRE-1/HFREP-1, a Liver-Specific Gene, Is Frequently Downregulated and has Growth Suppressor Activity in Hepatocellular Carcinoma. *Oncogene* (2004) 23(10):1939–49. doi: 10.1038/sj.onc.1207306
31. Lourenco AR, Ban Y, Crowley MJ, Lee SB, Ramchandani D, Du W, et al. Differential Contributions of Pre- and Post-EMT Tumor Cells in Breast Cancer Metastasis. *Cancer Res* (2020) 80(2):163–9. doi: 10.1158/0008-5472.CAN-19-1427
32. Zeisberg M, Neilson EG. Biomarkers for Epithelial-Mesenchymal Transitions. *J Clin Invest* (2009) 119(6):1429–37. doi: 10.1172/JCI36183
33. Peng B, Zhu H, Leung PCK. Gonadotropin-Releasing Hormone Regulates Human Trophoblastic Cell Invasion *via* TWIST-Induced N-Cadherin

Expression. *J Clin Endocrinol Metab* (2015) 100(1):E19–29. doi: 10.1210/jc.2014-1897
34. Mollinedo F. Neutrophil Degranulation, Plasticity, and Cancer Metastasis. *Trends Immunol* (2019) 40(3):228–42. doi: 10.1016/j.it.2019.01.006
35. Tcyganov E, Mastio J, Chen E, Gabrilovich DI. Plasticity of Myeloid-Derived Suppressor Cells in Cancer. *Curr Opin Immunol* (2018) 51:76–82. doi: 10.1016/j.coi.2018.03.009
36. Filippi M-D. Neutrophil Transendothelial Migration: Updates and New Perspectives. *Blood* (2019) 133(20):2149–58. doi: 10.1182/blood-2018-12-844605
37. Kolaczkowska E, Kubes P. Neutrophil Recruitment and Function in Health and Inflammation. *Nat Rev Immunol* (2013) 13(3):159–75. doi: 10.1038/nri3399
38. Bardin N, Blot-Chabaud M, Despoix N, Kebir A, Harhouri K, Arsanto J-P, et al. CD146 and Its Soluble Form Regulate Monocyte Transendothelial Migration. *Arterioscler Thromb Vasc Biol* (2009) 29(5):746–53. doi: 10.1161/ATVBAHA.108.183251
39. Robertson MJ. Role of Chemokines in the Biology of Natural Killer Cells. *J Leukoc Biol* (2002) 71(2):173–83. doi: 10.1189/jlb.71.2.173

Conflict of Interest: The authors declare that the research was conducted in the absence of any commercial or financial relationships that could be construed as a potential conflict of interest.

Publisher's Note: All claims expressed in this article are solely those of the authors and do not necessarily represent those of their affiliated organizations, or those of the publisher, the editors and the reviewers. Any product that may be evaluated in this article, or claim that may be made by its manufacturer, is not guaranteed or endorsed by the publisher.

Copyright © 2021 Lv, Cui, Huang, Feng, Wang, Wang, Xuan, Li, Ma, Huang and Zhang. This is an open-access article distributed under the terms of the Creative Commons Attribution License (CC BY). The use, distribution or reproduction in other forums is permitted, provided the original author(s) and the copyright owner(s) are credited and that the original publication in this journal is cited, in accordance with accepted academic practice. No use, distribution or reproduction is permitted which does not comply with these terms.

frontiers in Oncology

ORIGINAL RESEARCH
published: 13 December 2021
doi: 10.3389/fonc.2021.726486

A Novel Prognostic Signature Based on Ferroptosis-Related Genes Predicts the Prognosis of Patients With Advanced Bladder Urothelial Carcinoma

Xiaoqi Li[1†], Junting Huang[1†], Ji Chen[1†], Yating Zhan[1†], Rongrong Zhang[1†], Enze Lu[1], Chunxue Li[1], Yuxiao Zhang[1], Yajing Wang[1], Yeping Li[2], Jianjian Zheng[1] and Wujun Geng[3,4*]*

[1] Key Laboratory of Diagnosis and Treatment of Severe Hepato-Pancreatic Diseases of Zhejiang Province, The First Affiliated Hospital of Wenzhou Medical University, Wenzhou, China, [2] Department of Urology, The First Affiliated Hospital of Wenzhou Medical University, Wenzhou, China, [3] Department of Anesthesiology, The First Affiliated Hospital of Wenzhou Medical University, Wenzhou, China, [4] Wenzhou Key Laboratory of Perioperative Medicine, The First Affiliated Hospital of Wenzhou Medical University, Wenzhou, China

OPEN ACCESS

Edited by:
Francesca Sanguedolce, University of Foggia, Italy

Reviewed by:
Fabrizio Di Maida, Careggi University Hospital, Italy
Yuchen Liu, Shenzhen University, China

***Correspondence:**
Wujun Geng
gengwujun@wzhospital.cn
Jianjian Zheng
120378196@qq.com

[†]These authors have contributed equally to this work

Specialty section:
This article was submitted to Genitourinary Oncology, a section of the journal Frontiers in Oncology

Received: *16 June 2021*
Accepted: *24 November 2021*
Published: *13 December 2021*

Citation:
Li X, Huang J, Chen J, Zhan Y, Zhang R, Lu E, Li C, Zhang Y, Wang Y, Li Y, Zheng J and Geng W (2021) A Novel Prognostic Signature Based on Ferroptosis-Related Genes Predicts the Prognosis of Patients With Advanced Bladder Urothelial Carcinoma. Front. Oncol. 11:726486. doi: 10.3389/fonc.2021.726486

Bladder Urothelial Carcinoma (BLCA) is the major subtype of bladder cancer, and the prognosis prediction of BLCA is difficult. Ferroptosis is a newly discovered iron-dependent cell death pathway. However, the clinical value of ferroptosis-related genes (FRGs) on the prediction of BLCA prognosis is still uncertain. In this study, we aimed to construct a novel prognostic signature to improve the prognosis prediction of advanced BLCA based on FRGs. In the TCGA cohort, we identified 23 differentially expressed genes (DEGs) associated with overall survival (OS) *via* univariate Cox analysis (all $P < 0.05$). 8 optimal DEGs were finally screened to generate the prognostic risk signature through LASSO regression analysis. Patients were divided into two risk groups based on the median risk score. Survival analyses revealed that the OS rate in the high-risk group was significantly lower than that in the low-risk group. Moreover, the risk score was determined as an independent predictor of OS by the multivariate Cox regression analysis (Hazard ratio > 1, 95% CI = 1.724-2.943, $P < 0.05$). Many potential ferroptosis-related pathways were identified in the enrichment analysis in BLCA. With the aid of an external FAHWMU cohort (n = 180), the clinical predication value of the signature was further verified. In conclusion, the prognosis of advanced BLCA could be accurately predicted by this novel FRG-signature.

Keywords: ferroptosis, prognostic signature, bladder urothelial carcinoma, immune status, function analyses

Abbreviations: BC, Bladder cancer; LASSO, Least absolute shrinkage and selection operator; TCGA, The Cancer Genome Atlas; DEGs, Differentially expressed genes; OS, Overall survival; ROC, Receiver operating characteristic; FDR, False discovery rate; GO, Gene Ontology; KEGG, Kyoto Encyclopedia of Genes and Genomes; ssGSEA, Single-sample gene set enrichment analysis; PCA, Principal component analysis; t-SNE, t-distributed stochastic neighbor embedding; AUC, Area under the curve; HR, Hazard ratio; CI, Confidence interval; APC, Antigen presenting cell; AFP, alpha fetoprotein; aDC, Activated dendritic cell; iDC, Immature dendritic cell; pDC, Plasmacytoid dendritic cell; Tfh, T follicular helper cell; TIL, Tumor Infiltrating Lymphocyte; HLA, Human leukocyte antigen; CCR, Cytokine-cytokine receptor.

INTRODUCTION

Bladder cancer (BC), ranking 9th in the incidence of malignant tumors, is a malignant tumor of the bladder mucosa with poor prognosis and high recurrence (1, 2). Usually, BC could be divided into muscle invasive bladder cancer (MIBC) and non-muscle invasive bladder cancer (NMIBC). In comparison with patients with NMIBC, patients with MIBC have a poor prognosis. Bladder Urothelial Carcinoma (BLCA), caused by cigarette smoking and occupational exposure, is the main BC subtype, accounting for 90–95% of cases (3, 4). However, clinical biomarkers that could accurately predict the prognosis of BLCA are still lacking. Most BLCA patients are diagnosed at the late stages, leading to the worse prognosis (4). Therefore, the need of a better predictive signature for the prognosis prediction of BCLA, especially for MIBC, is urgent.

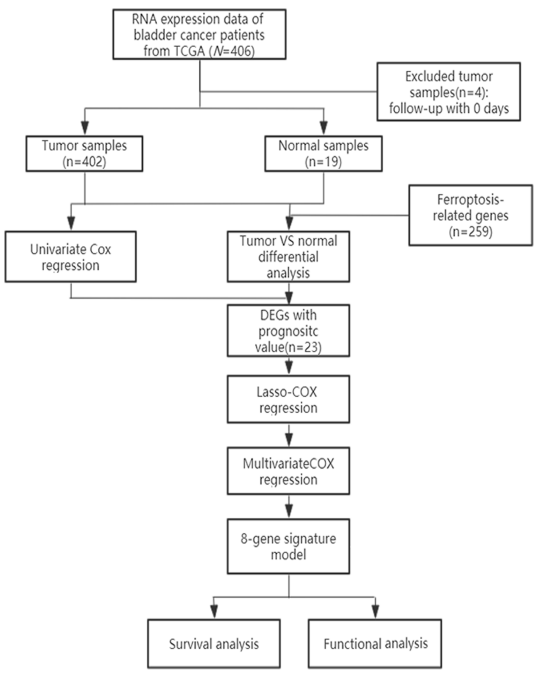

FIGURE 1 | Flowchart of data collection and analysis.

Ferroptosis, results from the accumulation iron-dependent lipid peroxide (LPO), is a new discovered pathway of non-apoptotic cell death (5). Ferroptosis is mainly caused by iron-dependent oxidative damage (6). It has been reported to be involved in the vital biological functions, including a sequence of complex biochemical reactions, gene expression, and signal transduction events (7, 8). Ferroptosis-related genes (FRGs) has been demonstrated to be associated with the prognosis of various human cancers (9–12). However, the clinical value of FRGs in the prognosis of BLCA still remains unknown.

In this study, we constructed a novel prognostic signature to improve the prognosis prediction of BLCA. Due to the reason that most patients with BLCA in TCGA database are with advanced-stage disease, we focused on the clinical value of FRGs in patients with MIBC. With the aid of an extra cohort obtained from the First Affiliated Hospital of Wenzhou Medical University (FAHWMU), the accuracy of this prognostic signature was verified.

MATERIALS AND METHODS

Data Collection

In this study, mRNA expression files [fragment per thousand base pairs per kilobase fragment normalization (FPKM) normalized] and clinical features from 406 BLCA patients were obtained from the TCGA database (https://portal.gdc.cancer.Government/Repository). Using the R package "limma", gene expression profiles were standardized. Data from TCGA are publicly available and use standardized read count values. As this study follows the TCGA data access strategy and release guidelines, it does not require approval by the local ethics committee. The 259 FRGs were selected from the previous studies (13, 14). As an extra cohort data, the FAHWMU cohort (n = 180) was obtained from the First Affiliated Hospital of Wenzhou Medical University (Wenzhou, China).

TABLE 1 | The clinical features of TCGA cohort and the FAHWMU cohort.

	TCGA cohort	FAHWMU cohort
No.of patients	406	180
gender		
female	106 (26.1%)	47 (26.1%)
male	300 (73.9%)	133 (73.9%)
Age		
>65	245 (60.3%)	107 (59.4%)
≤65	161 (39.7%)	73 (40.5%)
status		
alive	227 (55.9%)	93 (51.7%)
dead	179 (44.1%)	87 (48.3%)
stage		
Stage I	2 (0.5%)	21 (11.7%)
Stage II	129 (31.8%)	56 (31.1%)
Stage III	140 (34.5%)	44 (24.4%)
Stage IV	133 (32.8%)	57 (31.7%)
unknown	2 (0.5%)	2 (1.1%)

BLCA samples in the FAHWMU cohort were collected from 2012 to 2020, and OS time was used as the main survival time indicator. The collection of this cohort was reviewed and approved by the human research ethics committee of the First Affiliated Hospital of Wenzhou Medical University. The patients/participants provided their written informed consent to participate in this study.

Generation and Validation of the Signature

In the TCGA cohort, differentially expressed genes (DEGs) between BLCA samples and adjacent nontumorous samples were identified using "limma" with a false discovery rate (FDR) < 0.05. Prognosis related DEGs were screened using univariate Cox analysis of overall survival (OS) ($P < 0.05$), *P*-values were adjusted using Benjamini & Hochberg (BH) correction. The STRING database (version 11.0) generated a protein-to-protein interaction (PPI) network for the interactions among prognostic DEGs (15). The prognostic signature was constructed using the combination of LASSO-penalized Cox regression and multivariate Cox regression (16, 17). The LASSO algorithm was used to select and compress variables. In the regression, the standardized expression matrix of the prognosis related DEGs constituted the independent variable, while the OS and patient status in the TCGA cohort constituted the response variables. Standard ten-fold cross-validation determined the model penalty parameter (λ). The standardized expression level and regression coefficients for each gene were used to calculate patient risk, where the score = sum (each gene's expression × corresponding coefficient). In the TCGA cohort, as determined by the median risk score, all patients were divided into the high-risk and low-risk groups. By using the "prcomp" function from the R package "stats", PCA was performed after the gene expression signature was obtained. t-SNE, produced by the R package "Rtsne", explored group distribution. Time-dependent receiver operating characteristic (ROC) curve analysis was used to assess the performance of gene signatures. The Kaplan-Meier (K-M) survival analysis was performed using the log rank test.

Enrichment Analysis

DEGs (|log2FC|≥1, FDR < 0.05) were identified using the R package "clusterProfiler" based on the risk score. We used the BH method to adjust P values based on Gene Ontology (GO) function enrichment analysis and Kyoto Encyclopedia of Genes and Genomes (KEGG) pathways enrichment analysis. The single-sample gene set enrichment analysis (ssGSEA) was used to calculate the activity of 13 immune-related pathways and the infiltration analysis data of 16 immune cells (18). The gene set of the 13 immune-related pathways and the 16 immune cells is shown in **Table S2**.

Statistical Analysis

Student's t-test was performed to compare gene expression between BLCA and controls. The Mann-Whitney test was used

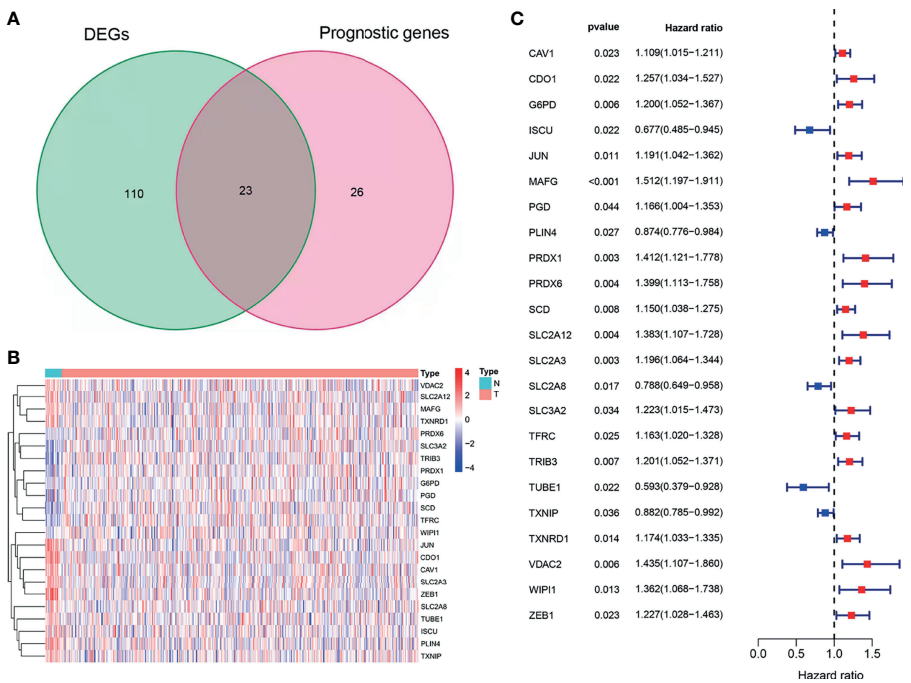

FIGURE 2 | Identification of OS-related DEFRGs in the TCGA cohort. **(A)** Venn plot showing common genes from differential analysis and univariate Cox analysis. **(B)** Heat map of OS-related DEFRGs. **(C)** Forest plots showing OS-related DEFRGs ($P < 0.05$).

to compare ssGSEA scores between high- and low-risk groups. *P* values < 0.05 were considered statistically significant. R software (Version 3.5.3) was used for all statistical analyses.

RESULTS

Identification of 23 OS-Related Differently Expressed Ferroptosis-Related Genes

A schematic representation of data collection and analysis was shown in **Figure 1**. We obtained data for BLCA patients from the TCGA databases. Clinical characteristics were summarized in **Table 1**.

Using BLCA samples from the TCGA cohort, differential expression between BLCA samples and adjacent nontumorous samples was observed in most FRGs (133/259, 51.4%); 23 were related to OS *via* univariate Cox regression (all $P < 0.05$, **Figures 2A–C**). The gene interaction network indicated that PRDX6, TXNRD1, PRDX6, and G6PD were the hub genes (**Figure 3A**). The correlations among genes were shown in **Figure 3B**. It was found that there were significant relationships between 193/318 TFs and DEGs ($P < 0.05$). A TF-based regulatory network was shown in **Figure 3C**.

Generation of the 8 Ferroptosis-Related Prognostic Gene Signature

To prevent over fitting of the model, Lasso-Cox regression was used to screen the identified 21 genes (**Figures 4A, B**). Then, multivariate Cox regression analysis was used to determine the optimal regulatory genes and 8 FRGs were identified to generate the prognostic signature (**Figure 4C**). The risk scores of BLCA patients were calculated using mRNA levels and the estimated regression coefficients. The resulting formula was used:

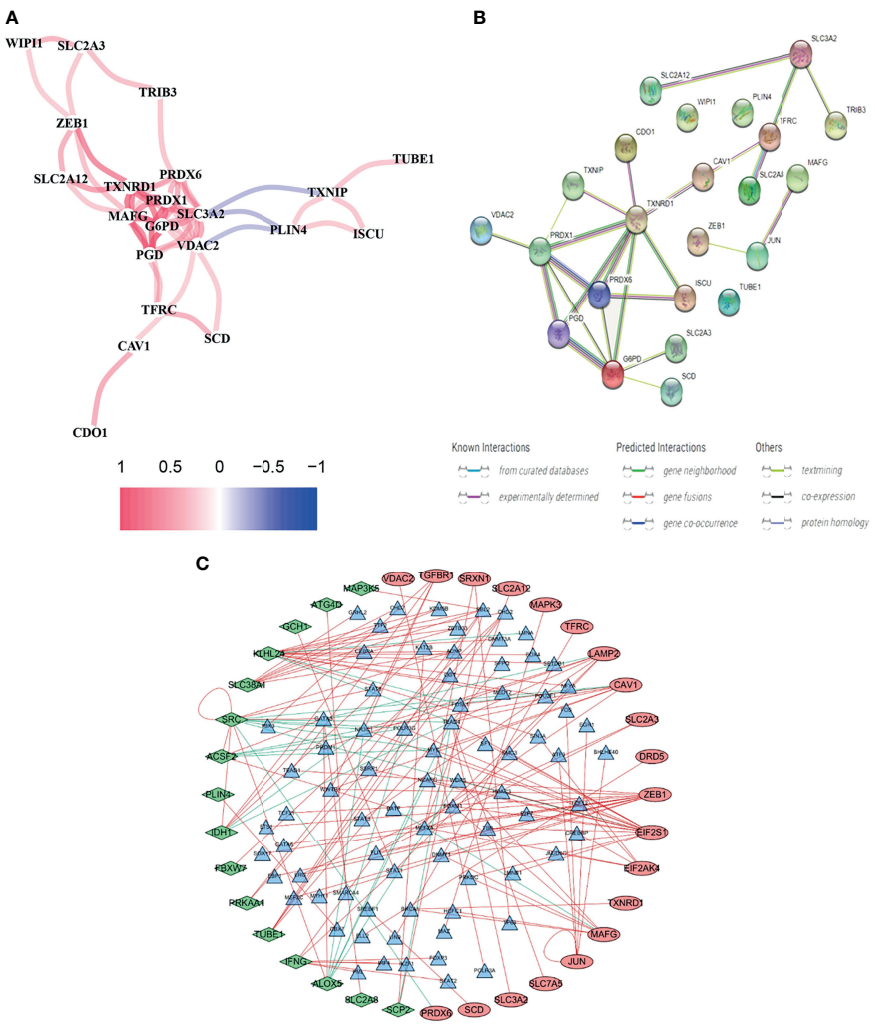

FIGURE 3 | Comprehensive networks of 23 OS-related DEFRGs. **(A)** PPI network **(B)** Correlation network of 23 OS-related DEFRGs. **(C)** Regulatory network of TFs and DEFRGs (green nodes: DEFRGs with low risk; red nodes: DEFRGs with high risk, only nodes with correlation coefficient > 0.4 and $P < 0.05$ were selected).

$$\text{Training cohort risk score} = (0.2758 \times \text{expression of CDO1}) + (0.1851 \times \text{expression of JUN}) + (0.4881 \times \text{expression of MAFG}) + (0.2629 \times \text{expression of PRDX1}) + (0.1766 \times \text{expression of SCD}) + (0.2825 \times \text{expression of SLC2A12}) + (-0.6320 \times \text{expression of TUBE1}) + (-0.1586 \times \text{expression of TXNRD1}).$$

Patients in the TCGA cohort were partitioned into high-risk (n = 203) and low-risk groups (n = 203) according to the median risk score (**Figure 5C**). K-M survival curves indicated that the OS of the low-risk group was higher than that of the high-risk group (**Figure 5A**, $P < 0.05$). Time-dependent ROC curves indicated that area under the curve (AUC) values were 0.704, 0.641, and 0.657 at 1st years, 2nd years and 3rd years (**Figure 5B**). As shown in **Figure 5D**, worse OS was found in high-risk patients, consistent with the results of the K-M curve. PCA and t-SNE analysis indicated two directions in the patient distribution of the two risk groups (**Figures 5E, F**).

Validation of the Prognostic Value of Gene Signature in the FAHWMU Cohort

The FAHWMU cohort was used to verify prognostic signature. Considering that most patients with BLCA in TCGA database are at the advanced-stage, only patients with MIBC in the FAHWMU cohort (n = 110) were used for the next analysis. The risk score was calculated based on the expressions of eight risk genes: CDO1, JUN, MAFG, PRDX6, SCD, SLC2A12, TUBE1 and TXNRD1. According to the calculated median risk score of the FAHWMU cohort, all patients were divided into high-risk (n=55) or low-risk (n=55) groups (**Figures 6C, D**). Similarly, the AUC in 1st years, 2nd years and 3rd years in the FAHWMU cohort was 0.709, 0.832, and 0.877 (**Figure 6B**). K-M survival curve indicated that compared to low-risk patients, the OS of high-risk patients was worse (**Figure 6A**, $P < 0.05$). The results of PCA and t-SNE analysis in the FAHWMU cohort were similar to the results of the TCGA cohort (**Figures 6E, F**). Taken together, our results preliminarily suggest the prognosis prediction of our signature in BLCA.

The Risk Score Was Identified as an Independent Prognostic Predictor

To determine whether the risk score is an independent prognostic marker, univariate and multivariate Cox regression analyses were performed. Univariate Cox regression indicated that the risk score of TCGA cohort was closely related to OS ($P < 0.001$, **Figure 7A**). Multivariate Cox regression analysis further confirmed the risk score as an independent prognostic factor in TCGA cohort ($P < 0.01$, **Figure 7B**).

Function Enrichment Analyses Revealed Potential Molecular Mechanisms

GO enrichment and KEGG pathway analysis were performed to reveal ferroptosis-related potential molecular mechanisms. In the TCGA cohort, various neutrophil-related molecular functions and mitotic nuclear division molecular functions were enriched

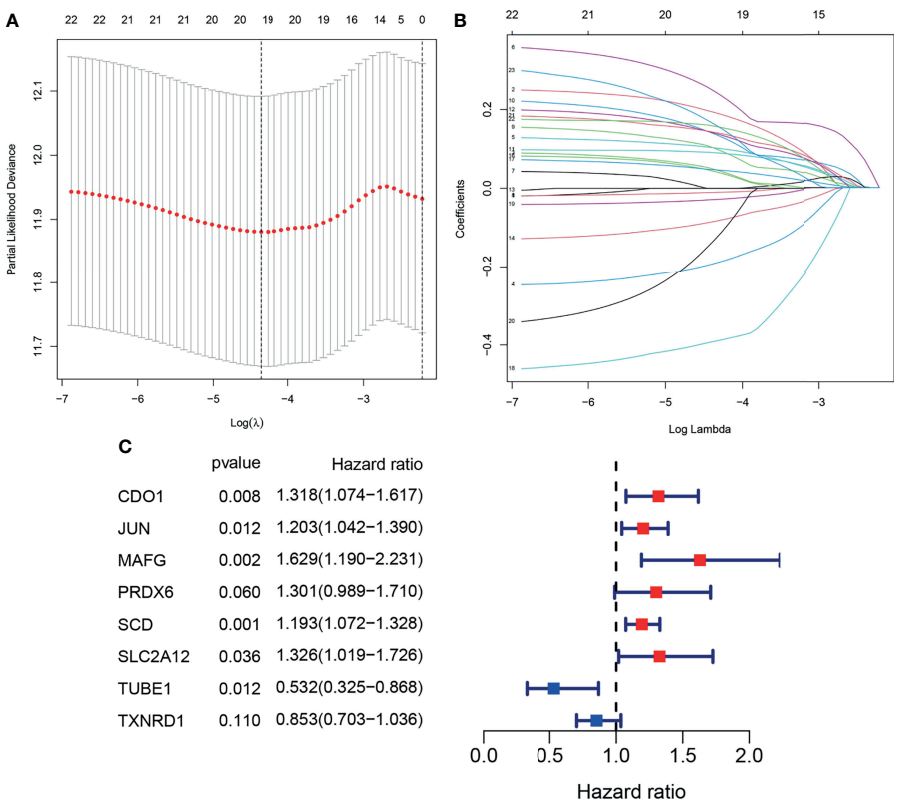

FIGURE 4 | Construction of the prognostic model. **(A, B)**. Lasso-Cox analysis of 23 OS-related DEFRGs. **(C)** Forest plot showing the eight genes in the prognostic risk model.

in the GO analysis ($P < 0.05$, **Figure 8A**). KEGG pathway analysis indicated that DNA replication pathways were enriched in the TCGA cohort ($P < 0.05$, **Figure 8B**).

ssGSEA was performed to analyze the relationships between the risk scores and immune-related cells and pathways in TCGA. In the TCGA cohort, there were significant differences between the low-risk and high-risk groups (all adjusted $P < 0.05$, **Figures 9A, B**), with the differences in aDC, Tfh, Inflammation-promoting and MHC class I.

DISCUSSION

It has been reported that FRGs are involved in the regulation of drug-induced ferroptosis in BLCA (11). Additionally, FRG-related inducers have been found to suppress BC with the help of mTOR inhibitors (19). Recently, ferroptosis participates in the inhibition of cell cycle in BC by obstructing the G0/G1 phase (11). Combined with these, ferroptosis plays a key role in BLCA development. However, the clinical value of FRGs in predicting the OS of BLCA patients was still unknown. In this study, a novel FRG-signature for BLCA was generated. The relationships between FRGs and prognosis of BLCA were explored. Next, the hub FRGs were identified and used to construct this FRG-signature. Our data suggest that this signature could improve the prognosis of advanced BLCA. Notably, the clinical prediction value of our FRG-signature was confirmed in an external FAHWMU cohort.

Herein, 8 FRGs (CDO1, JUN, MAFG, PRDX6, SCD, SLC2A12, TUBE1, TXNRD1) were used to establish the

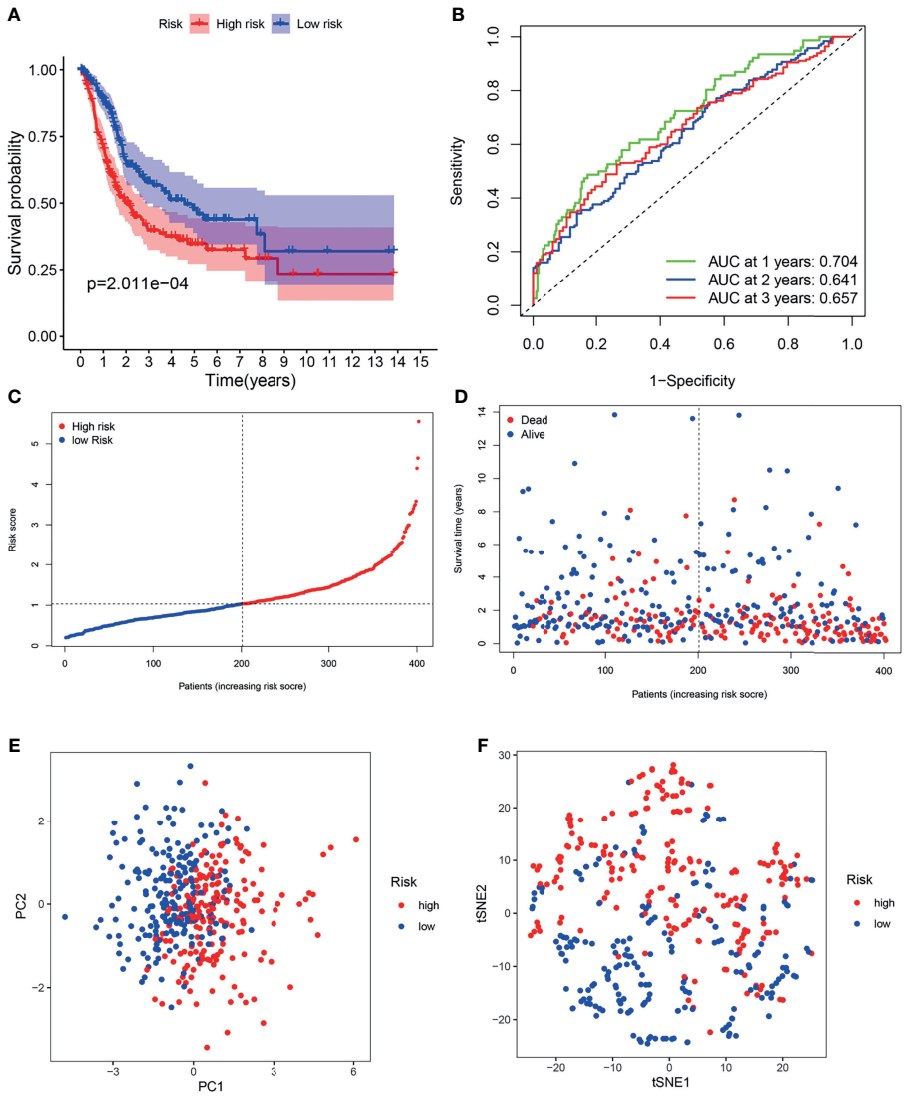

FIGURE 5 | Survival analysis of the TCGA cohort prognostic signature. **(A)** Kaplan-Meier survival curve. **(B)** time-dependent ROC curve. **(C)** The distribution and median value of the risk scores. **(D)** OS-related scatter plot. **(E)** PCA plot. **(F)** t-SNE plot.

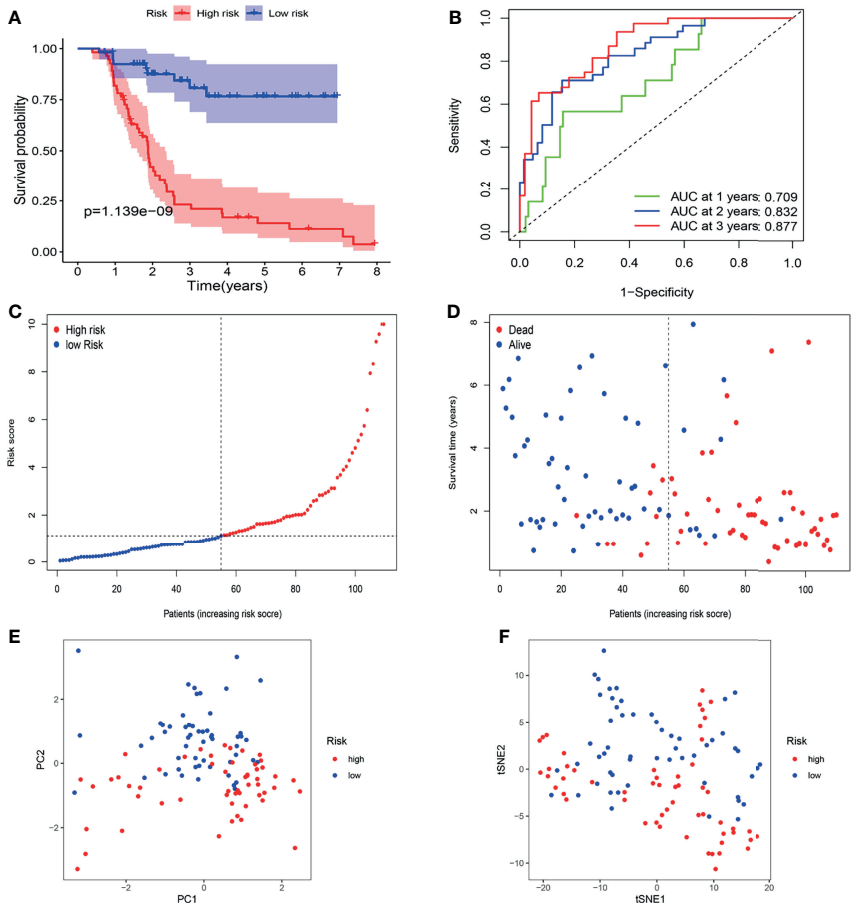

FIGURE 6 | Validation of gene signature in patients with MIBC in the FAHWMU cohort (n = 110). **(A)** Kaplan-Meier survival curve. **(B)** time-dependent ROC curve. **(C)** The distribution and median value of the risk scores. **(D)** OS-related scatter plot. **(E)** PCA plot. **(F)** t-SNE plot.

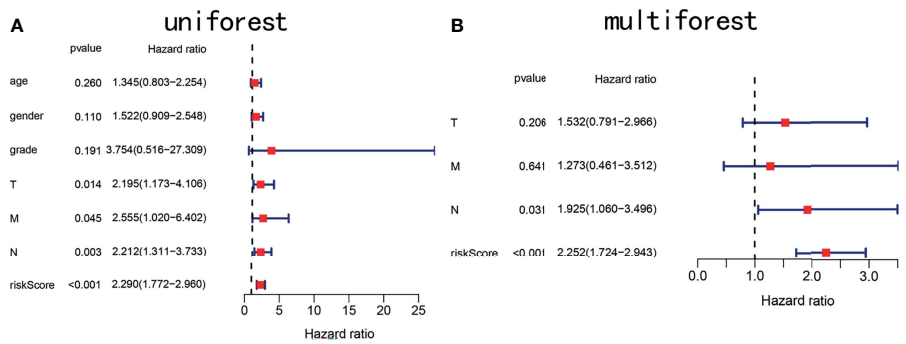

FIGURE 7 | Forest plots showing key clinical factors under the signature. **(A)** Univariate Cox regression analysis of the TCGA cohort. **(B)** Multivariate Cox regression analysis of the TCGA cohort.

prognostic signature. These FRGs could be summarized as four types: iron metabolism (CDO1), lipid metabolism (JUN, TUBE1), (anti)oxidant metabolism (TXNRD1, SCD, SLC2A12) (20) and energy metabolism (MAFG, PRDX6). CDO1, silenced by promoter methylation in BLCA, induces a reduction in the onset of ferroptosis, leading to the inhibition of BLCA invasion (21). JUN has been reported to reduce lipid peroxidation and inhibit ferroptosis, which contributes to the invasion and

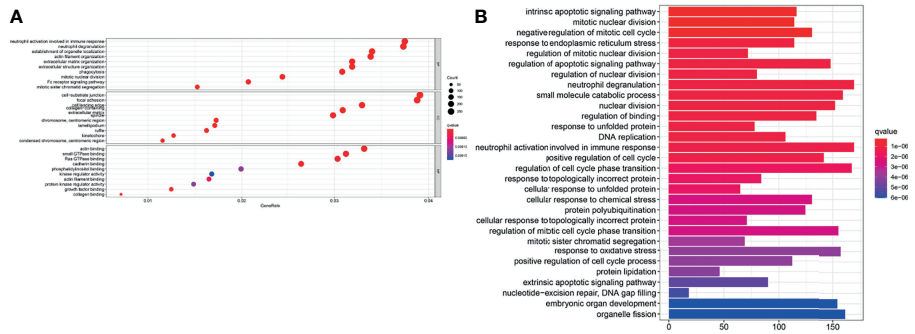

FIGURE 8 | Enrichment analyses of the signature. **(A)** GO enrichment plot of the TCGA cohort. **(B)** KEGG pathway enrichment plot of the TCGA cohort.

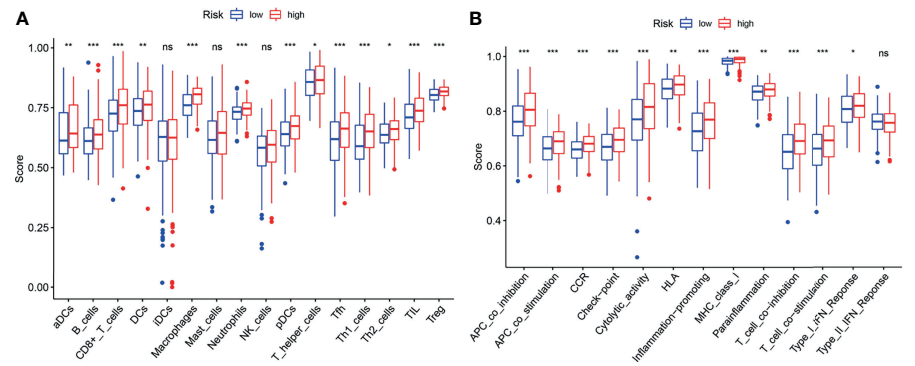

FIGURE 9 | ssGSEA analyses of the signature. **(A, B)** The block diagram showing the scores of 16 immune cells **(A)** and 13 immune-related functions **(B)** of the TCGA cohort. *p < 0.05; **p < 0.01; ***p < 0.001; ns, no significance.

metastasis of BC (22). Pitsava et al. found that TUBE1 suppresses BLCA metastasis by promoting ferroptosis through lipid metabolism (23). High expression of SLC2A12 has been found to be associated with glucose metabolism in ferroptosis, which exacerbates the invasion of BLCA (24). PRDX6 could inhibit the high oxidative damage caused by ferroptosis and thus promote the proliferation of BLCA (25). In addition, SCD promotes the proliferation of BLCA *via* fatty acid metabolic pathway in ferroptosis (26). In sum, these 8 FRGs may participate in the key biological processes such as proliferation, invasion and metastasis of BLCA through ferroptosis pathway.

Increasing studies have shown that there is an association between ferroptosis and tumor immunity (27). In this study, it was found that biological functions associated with immunity such as neutrophil activation in immune response, are enriched in the GO analysis. Moreover, it was found that the proportion of macrophages (28, 29) and Treg cells (29, 30) is increased in the high-risk group. Furthermore, several anti-tumor immunity factors, like NK cells, type I IFN response and type II IFN response were decreased in the high-risk group. Recent studies have demonstrated that high proportion of tumor-related macrophages or Treg cells is associated with poor prognosis of BLCA patients. Accordingly, our results also showed that the high-risk patients with the high proportion of macrophages and Treg cells, were associated with poor prognosis, suggesting the existence of the association of ferroptosis and tumor immunity.

The strengths of this study are that an external FAHWMU cohort was used to further verify the clinical value of our FRG-signature in the prognosis prediction of advanced BLCA. Meanwhile, there are several limitations in this study. First, cell biological experiments should be performed to further validate the functions of 8 FRGs in the future. Second, more sample validation is needed for clinical value of our prognostic signature.

CONCLUSION

In conclusion, we generate a novel prognostic FRG-signature, which contributes to the improvement in the prognosis prediction of advanced BLCA.

DATA AVAILABILITY STATEMENT

Publicly available datasets were analyzed in this study. This data can be found here: https://www.ncbi.nlm.nih.gov/geo/https://portal.gdc.cancer.gov/.

ETHICS STATEMENT

The studies involving human participants were reviewed and approved by Human Research Ethics Committee in The First Affiliated Hospital of Wenzhou Medical University. The patients/participants provided their written informed consent to participate in this study. Written informed consent was obtained from the individual(s) for the publication of any potentially identifiable images or data included in this article. The patients/participants provided their written informed consent to participate in this study.

AUTHOR CONTRIBUTIONS

XL and WG designed the study and analyzed the data. JH, JC, YTZ, and RZ revised the images. EL, CL, YXZ, and YW performed the literature search and collected data for the manuscript. YL and JZ revised the manuscript. All authors contributed to the article and approved the submitted version.

FUNDING

The project was supported by the Zhejiang Provincial Research Center for Cancer Intelligent Diagnosis and Molecular Technology (JBZX-202003).

SUPPLEMENTARY MATERIAL

The Supplementary Material for this article can be found online at: https://www.frontiersin.org/articles/10.3389/fonc.2021.726486/full#supplementary-material

REFERENCES

1. Patel V, Oh W, Galsky M. Treatment of Muscle-Invasive and Advanced Bladder Cancer in 2020. *CA: Cancer J Clin* (2020) 70(5):404–23. doi: 10.3322/caac.21631
2. Gruba N, Stachurski L, Lesner AJC. Biodiversity. Non-Proteasomal Urine Activity in Bladder Cancer. (2021) 18: (3):e2000981. doi: 10.1002/cbdv.202000981
3. Gan J, Skipper P, Gago-Dominguez M, Arakawa K, Ross RK, Yu MC, et al. Alkylaniline-Hemoglobin Adducts and Risk of Non-Smoking-Related Bladder Cancer. *J Natl Cancer Institute* (2004) 96(19):1425–31. doi: 10.1093/jnci/djh274
4. Amara C, Vantaku V, Lotan Y, Putluri N. Recent Advances in the Metabolomic Study of Bladder Cancer. *Expert Rev Proteomics* (2019) 16 (4):315–24. doi: 10.1080/14789450.2019.1583105
5. Yu H, Guo P, Xie X, Wang Y, Chen G. Medicine M. Ferroptosis, a New Form of Cell Death, and Its Relationships With Tumourous Diseases. (2017) 21: (4):648–57. doi: 10.1111/jcmm.13008
6. Ubellacker J, Tasdogan A, Ramesh V, Shen B, Mitchell EC, Martin-Sandoval MS, et al. Lymph Protects Metastasizing Melanoma Cells From Ferroptosis. *Nature* (2020) 585(7823):113–8. doi: 10.1038/s41586-020-2623-z
7. Xu S, He Y, Lin L, Chen P, Chen M, Zhang S. The Emerging Role of Ferroptosis in Intestinal Disease. *Cell Death Dis* (2021) 12(4):289. doi: 10.1038/s41419-021-03559-1
8. Shi Z, Zhang L, Zheng J, Sun H, Shao C. Ferroptosis: Biochemistry and Biology in Cancers. *Front Oncol* (2021) 11:579286. doi: 10.3389/fonc.2021.579286
9. Wang J, Yin X, He W, Xue W, Zhang J, Huang Y. SUV39H1 Deficiency Suppresses Clear Cell Renal Cell Carcinoma Growth by Inducing Ferroptosis. *Acta Pharm Sinica B* (2021) 11(2):406–19. doi: 10.1016/j.apsb.2020.09.015
10. Yang Y, Lin J, Guo S, Xue X, Wang Y, Qiu S, et al. RRM2 Protects Against Ferroptosis and Is a Tumor Biomarker for Liver Cancer. *Cancer Cell Int* (2020) 20(1):587. doi: 10.1186/s12935-020-01689-8
11. Zhao F, Vakhrusheva O, Markowitsch SD, Slade KS, Tsaur I, Cinatl J Jr, et al. Artesunate Impairs Growth in Cisplatin-Resistant Bladder Cancer Cells by Cell Cycle Arrest, Apoptosis and Autophagy Induction. *Cells* (2020) 9(12). doi: 10.3390/cells9122643
12. Jiang X, Stockwell B, Conrad M. Ferroptosis: Mechanisms, Biology and Role in Disease. *Nat Rev Mol Cell Biol* (2021) 22(4):266–82. doi: 10.1038/s41580-020-00324-8
13. Stockwell B, Friedmann Angeli J, Bayir H, Bush AI, Conrad M, Dixon SJ, et al. Ferroptosis: A Regulated Cell Death Nexus Linking Metabolism, Redox Biology, and Disease. *Cell* (2017) 171(2):273–85. doi: 10.1016/j.cell.2017.09.021
14. Hassannia B, Vandenabeele P, Vanden Berghe T. Targeting Ferroptosis to Iron Out Cancer. *Cancer Cell* (2019) 35(6):830–49. doi: 10.1016/j.ccell.2019.04.002
15. Szklarczyk D, Franceschini A, Kuhn M, Simonovic M, Roth A, Minguez P, et al. The STRING Database in 2011: Functional Interaction Networks of Proteins, Globally Integrated and Scored. (2011) 39:D561–8. doi: 10.1093/nar/gkq973
16. Simon N, Friedman J, Hastie T, Tibshirani R. Regularization Paths for Cox's Proportional Hazards Model *via* Coordinate Descent. *J Stat Softw* (2011) 39 (5):1–13. doi: 10.18637/jss.v039.i05
17. Tibshirani R. The Lasso Method for Variable Selection in the Cox Model. *Stat Med* (1997) 16(4):385–95. doi: 10.1002/(sici)1097-0258(19970228)16:4<385::aid-sim380>3.0.co;2-3
18. Rooney M, Shukla S, Wu C, Getz G, Hacohen NJC. Molecular and Genetic Properties of Tumors Associated With Local Immune Cytolytic Activity. (2015) 160:48–61. doi: 10.1016/j.cell.2014.12.033
19. Sun Y, Berleth N, Wu W, Schlutermann D, Deitersen J, Stuhldreier F, et al. Fin56-Induced Ferroptosis Is Supported by Autophagy-Mediated GPX4 Degradation and Functions Synergistically With mTOR Inhibition to Kill Bladder Cancer Cells. *Cell Death Dis* (2021) 12(11):1028. doi: 10.1038/s41419-021-04306-2
20. Wohlhieter C, Richards A, Uddin F, Hulton CH, Quintanal-Villalonga A, Martin A, et al. Concurrent Mutations in STK11 and KEAP1 Promote Ferroptosis Protection and SCD1 Dependence in Lung Cancer. *Cell Rep* (2020) 33(9):108444. doi: 10.1016/j.celrep.2020.108444
21. Brait M, Ling S, Nagpal JK, Chang X, Park HL, Lee J, et al. Cysteine Dioxygenase 1 Is a Tumor Suppressor Gene Silenced by Promoter Methylation in Multiple Human Cancers. *PloS One* (2012) 7(9):e44951. doi: 10.1371/journal.pone.0044951
22. Ren S, Zhang N, Shen L, Lu Y, Chang Y, Lin Z, et al. Lnc00892 Competes With C-Jun to Block NCL Transcription, Reducing the Stability of RhoA/RhoC mRNA and Impairing Bladder Cancer Invasion. *Oncogene* (2021). doi: 10.1038/s41388-021-02033-8
23. Pitsava G, Feldkamp M, Pankratz N, Lane J, Kay DM, Conway KM, et al. Exome Sequencing of Child-Parent Trios With Bladder Exstrophy: Findings in 26 Children. *Am J Med Genet Part A* (2021) 185(10):3028–41. doi: 10.1002/ajmg.a.62439
24. Xiong Y, Lei F. SLC2A12 of SLC2 Gene Family in Bird Provides Functional Compensation for the Loss of SLC2A4 Gene in Other Vertebrates. *Mol Biol Evol* (2021) 38(4):1276–91. doi: 10.1093/molbev/msaa286
25. Gao L, Meng J, Yue C, Wu X, Su Q, Wu H, et al. Integrative Analysis the Characterization of Peroxiredoxins in Pan-Cancer. *Cancer Cell Int* (2021) 21 (1):366. doi: 10.1186/s12935-021-02064-x

26. Sun J, Yue W, You J, Wei X, Huang Y, Ling Z, et al. Identification of a Novel Ferroptosis-Related Gene Prognostic Signature in Bladder Cancer. *Front Oncol* (2021) 11:730716. doi: 10.3389/fonc.2021.730716
27. Li D, Li Y. The Interaction Between Ferroptosis and Lipid Metabolism in Cancer. *Signal Transduction Targeted Ther* (2020) 5(1):108. doi: 10.1038/s41392-020-00216-5
28. Zhang Q, He Y, Luo N, Patel SJ, Han Y, Gao R, et al. Landscape and Dynamics of Single Immune Cells in Hepatocellular Carcinoma. *Cell* (2019) 179(4):829–45.e20. doi: 10.1016/j.cell.2019.10.003
29. Zhou S, Zhou Z, Hu Z, Huang HW, Wang Z, Chen EB, et al. Tumor-Associated Neutrophils Recruit Macrophages and T-Regulatory Cells to Promote Progression of Hepatocellular Carcinoma and Resistance to Sorafenib. *Gastroenterology* (2016) 150(7):1646–58.e17. doi: 10.1053/j.gastro.2016.02.040
30. Fu J, Xu D, Liu Z, Shi M, Zhao P, Fu B, et al. Increased Regulatory T Cells Correlate With CD8 T-Cell Impairment and Poor Survival in Hepatocellular Carcinoma Patients. *Gastroenterology* (2007) 132(7):2328–39. doi: 10.1053/j.gastro.2007.03.102

Conflict of Interest: The authors declare that the research was conducted in the absence of any commercial or financial relationships that could be construed as a potential conflict of interest.

Publisher's Note: All claims expressed in this article are solely those of the authors and do not necessarily represent those of their affiliated organizations, or those of the publisher, the editors and the reviewers. Any product that may be evaluated in this article, or claim that may be made by its manufacturer, is not guaranteed or endorsed by the publisher.

Copyright © 2021 Li, Huang, Chen, Zhan, Zhang, Lu, Li, Zhang, Wang, Li, Zheng and Geng. This is an open-access article distributed under the terms of the Creative Commons Attribution License (CC BY). The use, distribution or reproduction in other forums is permitted, provided the original author(s) and the copyright owner(s) are credited and that the original publication in this journal is cited, in accordance with accepted academic practice. No use, distribution or reproduction is permitted which does not comply with these terms.

frontiers in Oncology

ORIGINAL RESEARCH
published: 21 December 2021
doi: 10.3389/fonc.2021.780906

Potential Clinical Value of Pretreatment De Ritis Ratio as a Prognostic Biomarker for Renal Cell Carcinoma

Jinze Li[1,2†], Dehong Cao[1†], Lei Peng[3], Chunyang Meng[3], Zhongyou Xia[3], Yunxiang Li[3] and Qiang Wei[1*]*

[1] Department of Urology, Institute of Urology, West China Hospital, Sichuan University, Chengdu, China, [2] West China School of Medicine, Sichuan University, Chengdu, China, [3] Department of Urology, Nanchong Central Hospital, The Second Clinical Medical College, North Sichuan Medical College, Nanchong, China

OPEN ACCESS

Edited by:
Marco Borghesi, University of Genoa, Italy

Reviewed by:
Sandeep Gurram, National Institutes of Health (NIH), United States
Kuang-Hung Hsu, Chang Gung University, Taiwan

***Correspondence:**
Yunxiang Li
liyunxinag369@126.com
Qiang Wei
weiqiang339@126.com

[†]These authors have contributed equally to this work

Specialty section:
This article was submitted to Genitourinary Oncology, a section of the journal Frontiers in Oncology

Received: *22 September 2021*
Accepted: *25 November 2021*
Published: *21 December 2021*

Citation:
Li J, Cao D, Peng L, Meng C, Xia Z, Li Y and Wei Q (2021) Potential Clinical Value of Pretreatment De Ritis Ratio as a Prognostic Biomarker for Renal Cell Carcinoma. Front. Oncol. 11:780906. doi: 10.3389/fonc.2021.780906

Background: We performed this study to explore the prognostic value of the pretreatment aspartate transaminase to alanine transaminase (De Ritis) ratio in patients with renal cell carcinoma (RCC).

Methods: PubMed, EMBASE, Web of Science, and Cochrane Library were searched to identify all studies. The hazard ratio (HR) with a 95% confidence interval (CI) for overall survival (OS) and cancer-specific survival (CSS) were extracted to evaluate their correlation.

Results: A total of 6,528 patients from 11 studies were included in the pooled analysis. Patients with a higher pretreatment De Ritis ratio had worse OS (HR = 1.41, $p < 0.001$) and CSS (HR = 1.59, $p < 0.001$). Subgroup analysis according to ethnicity, disease stage, cutoff value, and sample size revealed that the De Ritis ratio had a significant prognostic value for OS and CSS in all subgroups.

Conclusions: The present study suggests that an elevated pretreatment De Ritis ratio is significantly correlated with worse survival in patients with RCC. The pretreatment De Ritis ratio may serve as a potential prognostic biomarker in patients with RCC, but further studies are warranted to support these results.

Keywords: De Ritis ratio, renal cell carcinoma, biomarker, prognosis, survival

INTRODUCTION

Renal cell carcinoma (RCC) is a common malignant tumor in adults, and its incidence has been increasing over the past two decades (1). In 2020, approximately 73,750 new RCC cases and 14,830 deaths were predicted in the United States (2). Despite an increase in early detection of RCC, nearly 20% of patients already have local progression or metastasis disease at initial diagnosis (3). Moreover, postoperative cancer recurrence occurs in 20%–40% of patients with localized RCC (4). Thus, it is of great value to define the prognostic indicators of survival, metastasis, or recurrence in patients with RCC.

Tumor, node, and metastasis (TNM) staging is an essential traditional prognostic factor for RCC, with limited accuracy when used alone (5, 6). Numerous clinical prognostic or predictive factors have been identified based on clinical trials and retrospective univariate or multivariate analysis, including performance status, appearing symptoms, and paraneoplastic syndromes (7–9). Besides, laboratory values were also used for prognosis, such as serum protein, corrected calcium, erythrocyte sedimentation rate, and neutrophil to lymphocyte ratio (10–12).

Aspartate transaminase (AST) and alanine transaminase (ALT) are the most critical transaminase in the body, reflecting hepatocellular damage (13). The ratio of serum AST to ALT, also known as the De Ritis ratio, is usually used to identify the etiology of various hepatitis (14). Recent studies have confirmed that the De Ritis ratio is a biomarker that can predict the prognosis of several tumors, such as breast cancer, gastric adenocarcinoma, and nasopharyngeal cancer (15–17). However, the prognostic value of this ratio in patients with RCC remains unclear. Bezan et al. (18) found that patients with a high De Ritis ratio had inferior overall survival (OS) and metastasis-free survival (MFS), while another study reported no correlation between high DR Ritis rate and OS (19). Therefore, this study aims to explore the prognostic value of the pretreatment De Ritis ratio in patients with RCC and provide higher-level medical evidence for clinical practice.

MATERIALS AND METHODS

Search Strategy

This present study was performed following the Preferred Reporting Items for Systematic Reviews and Meta-Analyses (PRISMA) criteria (20) and was registered in PROSPERO (ID: CRD42021255149). PubMed, EMBASE, Web of Science, and Cochrane Library were searched to identify eligible studies up to April 2021 (update on October 28, 2021) without language restriction. The search items were as follows: renal cell carcinoma (renal cell cancer, renal carcinoma, kidney cancer, kidney neoplasms, clear cell carcinoma, adenocarcinoma, RCC), De Ritis ratio (aspartate transaminase, AST, alanine transaminase, ALT, aspartate transaminase/alanine transaminase ratio, AST/ALT ratio, AST to ALT ratio), and prognosis (recurrence, survival, outcome) as keywords or Mesh term. A list of references to relevant studies was also manually searched. Two authors reviewed the literature independently, and any differences settled through discussion with a third author.

Inclusion and Exclusion Criteria

Qualified studies should meet the following inclusion criteria: (1) cohort studies or observational studies; (2) patients with RCC were histopathologically confirmed; (3) the pretreatment De Ritis ratio was obtained, (4) estimating the relationship between the De Ritis ratio and RCC prognosis; (5) reported available data for analysis, including OS or cancer-specific survival (CSS). Studies excluded were based on the following criteria: (1) studies involving animals; (2) reviews, comments, letters, case reports, and unpublished articles; (3) studies with unavailable data or insufficient data for analyses; (4) duplicated studies based on the same cohort.

Data Extraction and Quality Assessment

Two reviewers independently extracted the required data from eligible studies, which were as follows: the first author's name, year of publication, study region, study design, tumor type, treatment, sample size, patient age, the cutoff value of the De Ritis ratio, analysis method, and follow-up period. Furthermore, all outcome parameters were directly extracted with hazard ratio (HR) and 95% confidence interval (CI). The primary outcome was OS, while the secondary outcome was CSS. When both univariate and multivariate analyses were used in the study, data were extracted from the multivariate analysis. The quality of all included studies was estimated using the Newcastle–Ottawa scale (maximum score 9) (21). In the current study, we considered a study with a score of 7 or higher as a high-quality study (22). All discrepancies were discussed through negotiation or finally decided by a third reviewer.

Statistical Analyses

The statistical analysis of this study was performed using Stata v.15.0 (Stata Corp, College Station, TX, USA). The merged HRs with 95% CIs were adopted to evaluate the correlation between the pretreatment De Ritis ratio and prognosis. Heterogeneity between studies was estimated using Cochran's Q and I^2 tests. $p < 0.10$ or $I^2 > 50\%$ represented a significant heterogeneity. A random-effect model was applied for this meta-analysis. Moreover, we performed a subgroup analysis to investigate the cause of heterogeneity. Sensitivity analysis was also performed by dropping each study individually to assess the stability of the findings. Publication bias was assessed by using Begg's test, as the small number of included studies. Statistical significance was defined as a p value of less than 0.05.

RESULTS

Study Characteristics

Of the 323 initially identified articles through the search strategy, 141 studies remained after removing duplicates (93 publications) and irrelevant studies (89 publications). Subsequently, 114 articles were excluded by viewing titles and abstracts (16 reviews or meta-analysis, 11 meetings or comments, and 87 not related records). Moreover, the full text of 2 articles could not be found. After full-text evaluation, 12 studies were excluded from the remaining 25 potential studies, including 6 without survival outcomes, 3 without adequate survival data, and 5 without De Ritis ratio data. Finally, eleven articles comprising 6,258 patients were included in the present analysis (18, 19, 23–31) (**Figure 1**). **Table 1** records the basic characteristics of all included studies. All studies had a retrospective design, two of which were propensity score-matched analyses. Five studies focused on metastatic RCC (24, 26, 27, 30, 31). Six studies

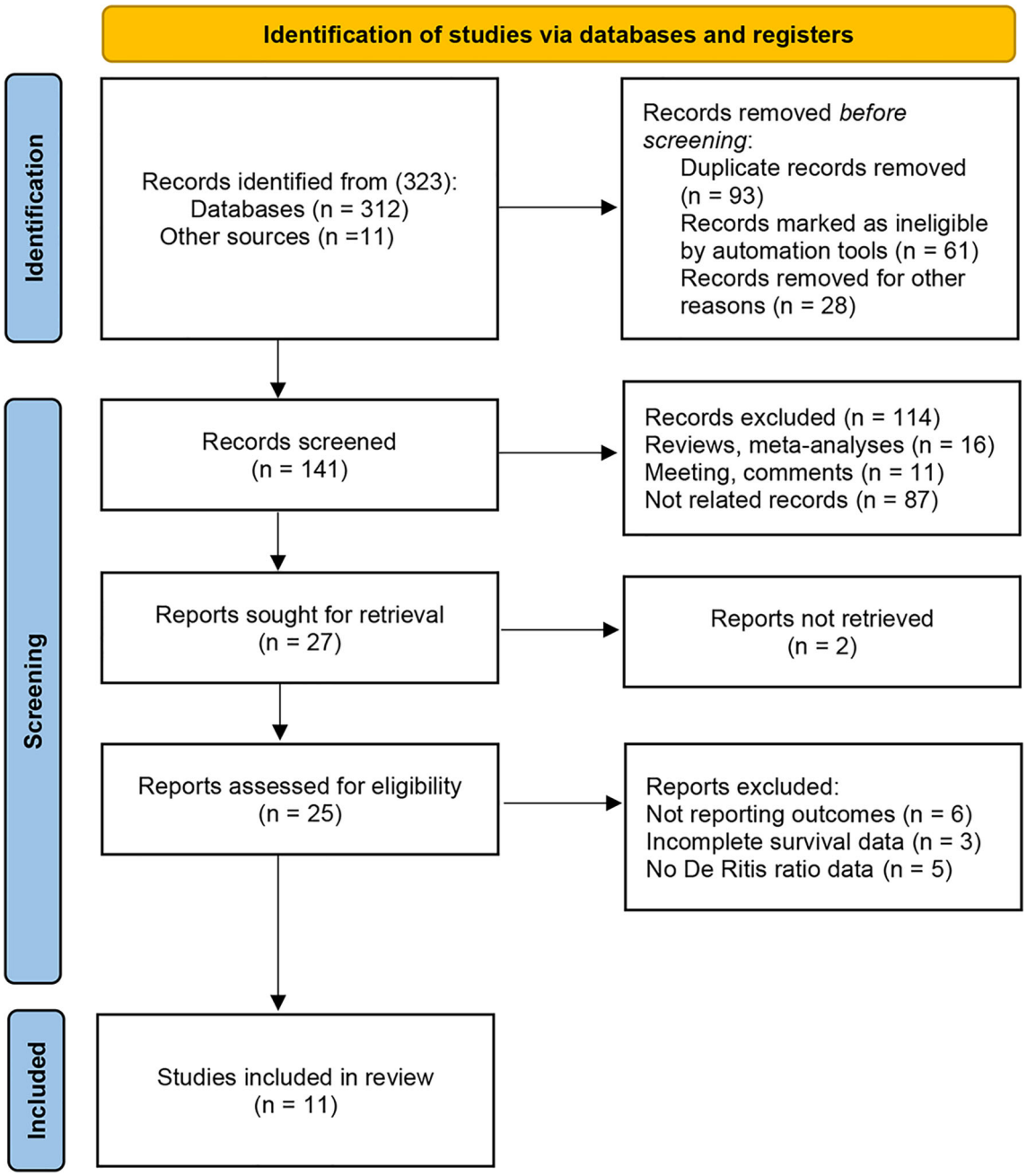

FIGURE 1 | Flow diagram of studies identified, excluded, and included.

focused on non-metastatic RCC (18, 19, 23, 25, 28, 29). These studies were conducted in many countries, including China, Korea, Turkey, Japan, Germany, the United States, and European countries. The median age of patients included in the study ranged from 55 to 65 years. The cutoff values for the De Ritis ratio ranged from 1.0 to 1.5. The median follow-up period for the included studies ranged from 21 to 60 months, and only one study did not report the follow-up period (27). Ten studies recorded the association between De Ritis ratio and OS, and seven studies recorded CSS. All studies were regarded as high-quality based on the NOS score, and the specific quality score of each study is shown in **Supplementary File 1**.

Overall Survival

Nine studies including 6,285 patients recorded about OS (18, 19, 23–27, 29–31). Since moderate heterogeneity was found, the random-effect model was adopted ($I2 = 34.6\%$, $p = 0.131$). The merged results demonstrated that patients with an increased

TABLE 1 | Baseline characteristics of include studies and methodological assessment.

Authors (year)	Region	Study design	Tumor type	Treatment	Number of patients	Age (years)	Cutoff value (AST/ALT)	Analysis method	Outcomes	Follow-up (months)	Quality score
Bezan 2015 (18)	America	Retrospective	Non-metastatic	Surgery	698	Median 65.4 (55.8–73.4)	1.26	Multivariate	OS	Median 60	8
Canat 2017 (19)	Turkey	Retrospective	Non-metastatic	Surgery	298	Median 61 (22–86)	1.5	Univariate	OS, CSS	Mean 37.8 ± 22.3	7
Gu 2017 (23)	China	Retrospective	Non-metastatic	Surgery	185	Mean 56.1 ± 11.8	1.0	Univariate	OS	Median 30.2 (12.1–48.4)	8
Ishihara 2017 (24)	Japan	Propensity score matching	Metastatic	Surgery	118	Median 65	1.24	Multivariate	OS, CSS	Mean 21.0 ± 24.3	9
Lee 2017 (25)	Korea	Propensity score matching	Non-metastatic	Surgery	2965	Median 55 (47–65)	1.5	Multivariate	OS, CSS	Median 37 (24–73)	9
Kang 2018 (26)	Korea	Retrospective	Metastatic	TKI	360	Median 58 (51–67)	1.2	Multivariate	OS, CSS	Median 29 (24.1–33.9)	9
Kim 2018 (27)	Korea	Retrospective	Metastatic	TT	158	Mean 58.6 ± 10.6	1.38	Univariate	OS,	NR	7
Ikeda 2020 (28)	Japan	Retrospective	Non-metastatic	Surgery	243	Median 61 (55–67)	1.42	Multivariate	CSS	Median 60 (25–103)	9
Kang 2020 (29)	Korea	Retrospective	Non-metastatic	Surgery	670	Median 55 (48–61)	1.0	Univariate	OS, CSS	Median 59 (41–81)	8
Laukhtina 2020 (30)	Europe and America	Retrospective	Metastatic	Surgery	613	Median 57 (50–64)	1.2	Multivariate	OS, CSS	Median 31 (16–58)	9
Janisch 2021 (31)	Germany	Retrospective	Metastatic	TKI	220	Median 64 (57–71)	1.08	Multivariate	OS	Median 28 (10–58)	9

TKI, tyrosine kinase inhibitor; TT, targeted therapy; AST, aspartate transaminase; ALT, alanine transaminase; OS, overall survival. CSS, cancer-specific survival; PFS, progression-free survival; MFS, metastasis-free survival; NR, not report.

pretreatment De Ritis ratio had inferior OS (HR = 1.41, 95% CI 1.25 to 1.59, p < 0.001, **Figure 2**).

Cancer-Specific Survival

Seven studies recorded the prognostic role of the pretreatment De Ritis ratio in patients with RCC on CSS, including 5,167 patients (19, 24–26, 28–30). The pooled results revealed that a higher pretreatment De Ritis ratio was related to worse CSS (random-effect model: HR = 1.59, 95% CI 1.28 to 1.97, p < 0.001), and with moderate heterogeneity (I2 = 49.7%, p = 0.063, **Figure 3**).

Subgroup Analyses

Limited to the number of studies included in the meta-analysis, we only conducted subgroup analysis for OS and CSS oncologic outcomes, and stratified by ethnicity, disease stage, treatment method, cutoff value, analysis method, or sample size (**Table 2**). For studies that include the Asian population, the higher pretreatment De Ritis ratio was associated with inferior OS (HR = 1.49, 95% CI 1.25 to 1.77, p < 0.001, I^2 = 20.5%) and CSS (HR = 1.80, 95% CI 1.38 to 2.33, p < 0.001, I^2 = 35.6%). Moreover, in the Caucasian population subgroup, the high De Ritis ratio was also an independent predictor of OS (HR = 1.34, 95% CI 1.11 to 1.62, p = 0.002, I^2 = 53.4%) and CSS (HR = 1.27, 95% CI 1.06 to 1.51, p = 0.009, I^2 = 0%). Subgroup analysis by disease stage demonstrated that the high pretreatment De Ritis ratio was related to worse OS (HR = 1.37, 95% CI 1.21 to 1.54, p < 0.001, I^2 = 0%) and CSS (HR = 1.54, 95% CI 1.14 to 2.08, p < 0.001, I^2 = 60.1%) in patients with metastatic RCC, and similar results were observed in patients with non-metastatic RCC (OS: HR = 1.45, 95% CI 1.13 to 1.86, p = 0.004, I^2 = 58.9%; CSS: HR = 1.66, 95% CI 1.15 to 2.40, p < 0.001, I^2 = 50.7%). In terms of subgroup analysis for the treatment method, the high pretreatment De Ritis ratio in patients with RCC was an independent predictor of OS (surgery: HR = 1.43 95% CI 1.18 to 1.72, p < 0.001, I^2 = 51.3%; non-surgery: HR = 1.41, 95% CI 1.25 to 1.72, p < 0.001, I^2 = 0%). For the subgroup with a cutoff value of > 1.2, the patients with a higher pretreatment De Ritis ratio had poor OS (HR = 1.44, 95% CI 1.18 to 1.76, p < 0.001, I^2 = 51.1%) and CSS (HR = 1.94, 95% CI 1.43 to 2.6, p < 0.001, I^2 = 27.3%). Likewise, in the cutoff value of the ≤1.2 group, the increased De Ritis ratio was correlated with worse OS (HR = 1.39, 95% CI 1.17 to 1.65, p < 0.001, I^2 = 27.0%) and CSS outcomes (HR = 1.45, 95% CI 1.15 to 1.83, p < 0.001, I^2 = 0%). In the multivariate analysis subgroup, the high pretreatment De Ritis ratio was related to poor OS (HR = 1.50, 95% CI 1.29 to 1.58, p < 0.001, I^2 = 21.7%) and CSS (HR = 1.76, 95% CI 1.32 to 2.35, p < 0.001, I^2 = 63.5%). In the univariate analysis subgroup, a higher pretreatment De Ritis ratio had worse OS (HR = 1.28, 95% CI 1.04 to 1.58, p = 0.020, I^2 = 40.8%) but not in CSS (HR = 1.25, 95% CI 0.90 to 1.75, p = 0.184, I^2 = 0.0%). Additionally, stratified by sample size, the higher pretreatment De Ritis ratio had steep inferior OS (HR = 1.45, 95% CI 1.23 to 1.71, p < 0.001, I^2 = 34.1%) and CSS (HR = 1.42, 95% CI 1.28 to 1.73, p = 0.001, I^2 = 29.8%) in the sample size >300 subgroup, which was consistent with the results of the sample size ≤300 subgroup

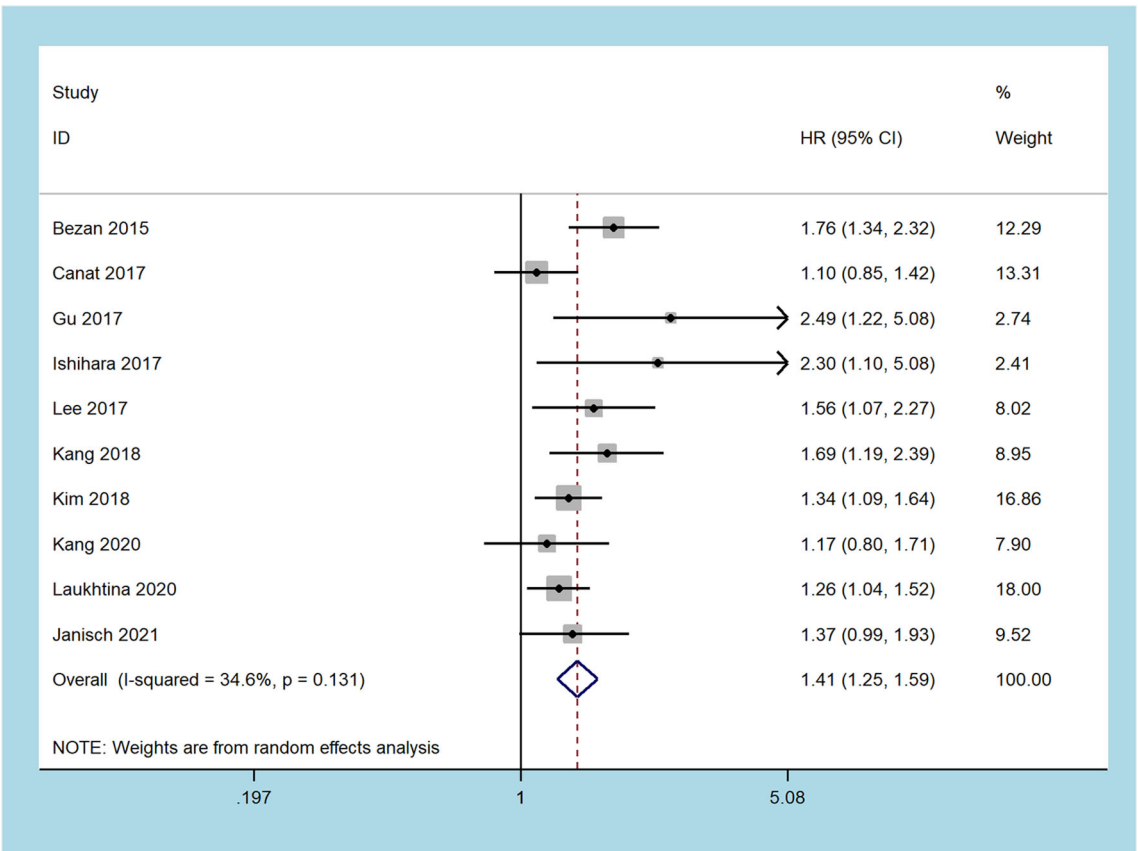

FIGURE 2 | Forest plots of the association between the De Ritis ratio and overall survival.

(OS: HR = 1.38, 95% CI 1.12 to 1.71, p = 0.003, I^2 = 43.3%; CSS: HR = 1.97, 95% CI 1.25 to 3.10, p = 0.004, I^2 = 51.4%).

Sensitivity Analysis and Meta-Regression Analysis

Restricted to the number of articles included in the study, we performed a sensitivity analysis for OS and CSS outcomes. After performing the leave-one-out test or excluding small studies (<200 patients), no significant change in the pooled HR was observed, which undoubtedly proved the reliability of our results (**Supplementary File 2**). We also performed a meta-regression analysis to explore the suspected reasons for the heterogeneity of OS and CSS outcomes. The results showed that ethnicity (p = 0.409), disease stage (p = 0.935), treatment method (p = 0.897), cutoff value (p = 0.877), analysis method (p = 0.220), and sample size (p = 0.692) did not significantly affect the heterogeneity of OS. In addition, ethnicity (p = 0.086), disease stage (p = 0.809), cutoff value (p = 0.067), analysis method (p = 0.278), and sample size (p = 0.250) had no influence on CSS heterogeneity (**Table 2**).

Publication Bias

Begg's test was applied to estimate the publication bias. A visual inspection of Begg's funnel plots revealed asymmetry (**Figure 4**). This raises the possibility of publication bias, although the Begg's test was not statistically significant (OS: p = 0.152, CSS: p = 0.072). Because of this, we used the trim and fill method to further detect publication bias, and two filled funnel plots demonstrated that even if the uncollected literature was included, it did not affect the results of the combined effect, which indicates that our results are relatively robust (**Figure 4**).

DISCUSSION

RCC is one of the most common solid lesions in the kidney, accounting for about 80%–90% of all renal malignancies (1). The prognosis of RCC is affected by various factors, including patient age, clinical manifestations, laboratory values, and tumor pathologic variables such as pathological stage, nuclear grade, and histological subtype (32, 33). Tumor stage and grade are considered as common prognostic markers for RCC, but the application of these factors in clinical practice remains problematic (34). How to more accurately identify those patients with poor prognosis before treatment and carry out the risk stratification of tumors are of great significance for choosing treatment options and the guidance of postoperative

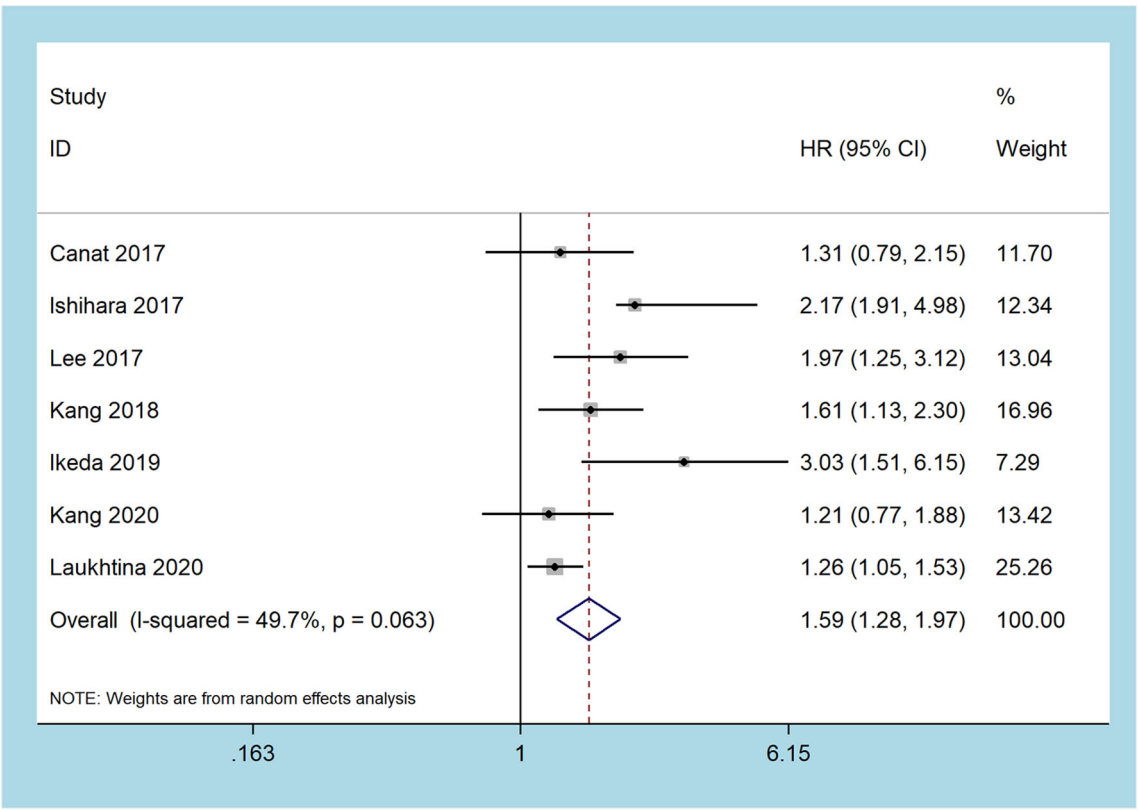

FIGURE 3 | Forest plots of the association between the De Ritis ratio and cancer-specific survival.

TABLE 2 | Subgroup analyses of OS and CSS.

Outcome	Variable	No. of studies	Model	HR (95% CI)	p	Heterogeneity		Pm
						I^2 (%)	p	
OS	All	10	Random	1.41 (1.25, 1.59)	< 0.001	34.6	0.131	
Ethnicity	Asian	6	Random Random	1.49 (1.25, 1.77)	< 0.001	20.5	0.279	0.409
	Caucasian	4		1.34 (1.11, 1.62)	0.002	53.4	0.092	
Disease stage	Metastatic	5	Random Random	1.37 (1.21, 1.54)	< 0.001	0.0	0.414	0.935
	Non-metastatic	5		1.45 (1.13, 1.86)	0.004	58.9	0.045	
Treatment method	Surgery	7	Random	1.43 (1.18, 1.72)	< 0.001	51.3	0.055	0.897
	Non-surgery	3	Random	1.41 (1.25, 1.65)	< 0.001	0.0	0.521	
Cutoff value	>1.2	5	Random Random	1.44 (1.18, 1.76)	<0.001	51.1	0.085	0.877
	≤1.2	5		1.39 (1.17, 1.65)	<0.001	27.0	0.242	
Analysis method	Multivariate	6	Random Random	1.50 (1.29, 1.73)	<0.001	21.7	0.271	0.220
	Univariate	4		1.28 (1.04, 1.58)	0.020	40.8	0.167	
Sample size	>300	5	Random Random	1.45 (1.23, 1.71)	<0.001	34.1	0.194	0.629
	≤300	5		1.38 (1.12, 1.71)	0.003	43.3	0.132	
CSS	All	7	Random	1.59 (1.28, 1.97)	<0.001	49.7	0.063	
Ethnicity	Asian	5	Random Random	1.80 (1.38, 2.33)	<0.001	35.6	0.184	0.086
	Caucasian	2		1.27 (1.06, 1.51)	0.009	0.0	0.887	
Disease stage	Metastatic	3	Random	1.54 (1.14, 2.08)	<0.001	60.1	0.082	0.809
	Non-metastatic	4	Random	1.66 (1.15, 2.40)	<0.001	50.7	0.107	
Cutoff value	>1.2	4	Random	1.94 (1.43, 2.64)	<0.001	27.3	0.248	0.067
	≤1.2	3	Random	1.45 (1.15, 1.83)	0.001	0.0	0.063	
Analysis method	Multivariate	5	Random	1.76 (1.32, 2.35)	<0.001	63.5	0.027	0.278
	Univariate	2	Random	1.25 (0.90, 1.75)	0.184	0.0	0.816	
Sample size	>300	4	Random Random	1.42 (1.28, 1.73)	0.001	29.8	0.233	0.250
	≤300	3		1.97 (1.25, 3.10)	0.004	51.4	0.128	

OS, overall survival; CSS, cancer-specific survival; HR, hazard ratio; CI, confidence interval.

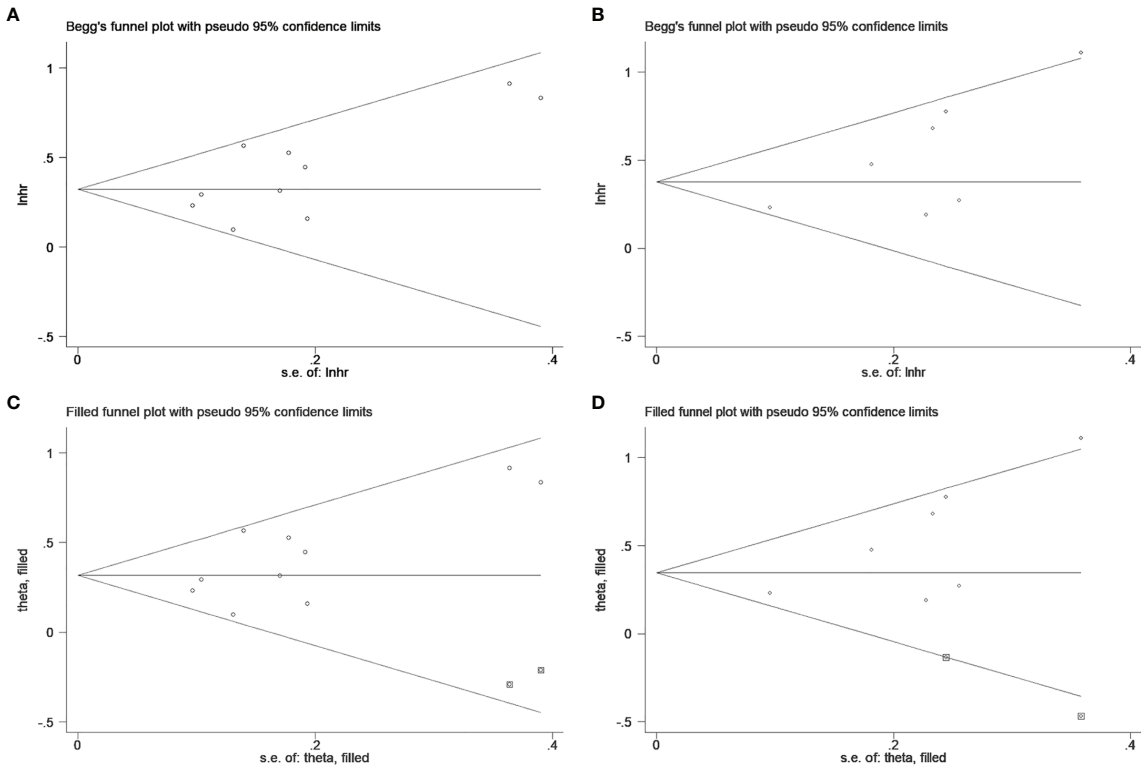

FIGURE 4 | Begg's test for **(A)** overall survival and **(B)** cancer-specific survival; Trim and fill method for **(C)** overall survival and **(D)** cancer-specific survival.

follow-up. Therefore, finding potential prognostic markers for RCC prognosis has become a hot spot in clinical research.

Initially, the serum De Ritis ratio was adopted to evaluate the prognosis of various liver diseases, including viral hepatitis, alcoholic hepatitis, and fatty liver (14). Because laboratory tests are routinely performed before treating cancer patients, the De Ritis ratio can be a simple, convenient, and inexpensive measurement method. Previous studies have reported that the De Ritis ratio was significantly associated with the prognosis of several tumors, including RCC (15–18). However, the actual prognostic value of this ratio in patients with RCC remains controversial. Su et al. (35) conducted a meta-analysis to explore the prognostic value of the De Ritis ratio in urological cancers, and 6 articles focused on RCC were included. They claimed that the patients with a higher De Ritis ratio had inferior OS (4 studies involved). A problem of the study by Su is their interpretation of OS since the data provided by the original research in their studies all indicated that an elevated De Ritis ratio had poor survival. Furthermore, a recent study reported that the De Ritis ratio was not associated with RCC prognosis (31). Thus, it is necessary to reevaluate the role of the De Ritis ratio in the prognosis of RCC based on the existing literature to better guide clinical practice.

Compared with the study by Su, the advantage of the current meta-analysis is that we included five more recent articles and eventually included 6,528 RCC patients for the analysis. The study revealed that patients with a higher pretreatment De Ritis ratio had worse survival outcomes regarding OS and CSS. Subgroup analyses of OS and CSS by ethnicity, disease stage, treatment method, cutoff value, analysis method, or sample size obtained similar results. Previous studies have suggested that histological subtypes are also prognostic factors for RCC (33). However, it was not possible to perform a subgroup analysis to assess the impact of different histological subtypes of the De Ritis ratio on prognosis due to lack of data. Remarkably, Lee et al. (25) found that a higher De Ritis ratio was associated with OS and CSS in localized clear-cell RCC patients, but not in non-clear-cell RCC. Janisch et al. (31) also revealed that an elevated De Ritis ratio was an unfavorable factor for OS in patients with clear-cell histology. Since these favorable results were obtained based on limited studies and insufficient sample sizes, therefore, a prospective large-scale cohort is needed to validate the conclusion.

It should be noted that sensitivity analyses indicated that our results were robust, but moderate heterogeneity among the included studies was found in both survival outcomes, a finding that may be due to different baseline characteristics of individual studies. Therefore, the meta-regression analysis was performed using ethnicity, disease stage, treatment method, cutoff value, analysis method, and sample size to explore the potential sources of heterogeneity. However, none of these factors can explain the heterogeneity of OS. Similar results

were obtained for CSS. We also performed a subgroup analysis to investigate the cause of heterogeneity. The results showed that the heterogeneity of most subgroup analyses was slightly reduced, but it was still statistically significant in several subgroups. Thus, the random-effect model was used to calculate the effect size to minimize the impact of heterogeneity on the combined results. In addition, although we have conducted an extensive literature search, we still found a potential publication bias in the study reporting survival outcomes. We used the trim and fill method for further analysis and found that the inclusion of uncollected studies did not influence the results of the pooled effect, which suggests that publication bias may not have a significant effect on the overall findings. Therefore, the results of this study are relatively robust and reliable.

ALT and AST are often used to reflect hepatocellular damage or death. ALT is mainly present in the liver, while AST is widely distributed in various tissues such as the heart, liver, brain, muscle, and kidney tissues (14). Hence, ALT suggests liver disease specifically, while AST may be associated with several diseases that affect other organs. Pathological processes that have been proved to cause tissue damage, high proliferative states, and faster tumor cell turnover tend to enhance the serum AST level rather than ALT level, making the De Ritis (AST/ALT) ratio an attractive potential clinical biomarker (36).

Although the De Ritis ratio is a promising marker, the specific mechanism of this higher ratio and the inferior prognosis of cancer patients remain unclear. Indeed, cancer cells have a higher rate of glycolysis compared with normal cells, even in the presence of oxygen, and abnormal glycolytic metabolism produces sufficient ATP to promote cancer cell proliferation; this phenomenon is known as the "Warburg effect" (37, 38). Increased glycolysis in tumor cells is thought to be related to changes in nicotinamide adenine dinucleotide (NAD)-related enzymes and glucose transporters within mitochondria, according to Dorward et al. (39). A higher lactate dehydrogenase and cytosolic (NADH)/NAD+ ratio plays an essential role in maintaining enhanced glycolysis (40). It must be highlighted that AST is a pivotal component of the malate–aspartate shuttle in the glycolysis pathway that relocates NADH into mitochondria (14). Moreover, the previous study had confirmed that von Hippel-Lindau (VHL) significantly associated with renal clear-cell type RCC was presented in the cytoplasm of mitochondria (41). The loss of VHL and an increase in hypoxia-inducible factor expression influence several metabolic pathways, including glycolysis and oxidative phosphorylation (42). Accordingly, AST may be related to the glycolysis mechanism of clear-cell type RCC with VHL loss (25). However, further investigation is needed to explore the exact mechanism.

Considering that serum ALT and AST are commonly used indicators of clinical hematology, they are simple and easy to measure, and the cost is low. Therefore, the pretreatment De Ritis ratio can be used as an effective prognostic marker in patients with RCC and applied in clinical diagnosis and treatment. Our meta-analysis affirms that patients with an increased pretreatment De Ritis ratio had worse survival outcomes. It could be a potential selection criterion for the hierarchical management of risk factors for RCC (18). Given that a prognostic factor must be verified in well-designed, large-scale with an independent cohort before it can be applied universally, the findings should be interpreted cautiously.

Although the study provides more substantial evidence for the prognostic value of the pretreatment De Ritis ratio in patients with RCC, there are certain limitations. Firstly, the sample size of some of the included studies is relatively small, which may lead to a biased conclusion. Secondly, all included studies were retrospective, which may have an inherent structural bias, and the duration of follow-up was relatively short. Thirdly, similar to the study by Su (35), since this study only includes published literature, it may have potential publication bias. Fourth, patients could not be stratified according to histology due to lack of data. However, we conducted subgroup analysis based on sample size, study population, and disease status to explore potential sources of heterogeneity, which made our results more robust. Fifth, although the included studies attempted to exclude all patients with liver disease, there were still undetected liver pathological conditions that could affect the serum AST or ALT levels and distort the De Ritis ratio.

CONCLUSION

Available evidence suggests that patients with an increased pretreatment De Ritis ratio have worse OS and CSS, indicating that this ratio may serve as a potential prognostic biomarker in RCC patients. However, prospective, well-designed, and large-scale studies are warranted to validate our findings.

DATA AVAILABILITY STATEMENT

The original contributions presented in the study are included in the article/**Supplementary Material**. Further inquiries can be directed to the corresponding authors.

ETHICS STATEMENT

Ethical review and approval were not required for the study on human participants in accordance with the local legislation and institutional requirements. Written informed consent for participation was not required for this study in accordance with the national legislation and the institutional requirements.

AUTHOR CONTRIBUTIONS

YL and QW: conception and design. JL, DC, CM, and LP: acquisition of data and critical revision of the manuscript for important intellectual content. JL, DC, and ZX: analysis and interpretation of data. JL and DC: drafting of the manuscript.

QW: supervision. All authors contributed to the article and approved the submitted version.

FUNDING

This work was funded by the National Natural Science Foundation of China (Grant Number 82000721), Post-Doctor Research Project, West China Hospital, Sichuan University (Grant Number 2019HXBH089), Health Commission of Sichuan province (Grant Number 20PJ036), and the Sichuan Province Science and Technology Planning Project (Grant Numbers 2020YJ0054, 2020YFS0320).

ACKNOWLEDGMENTS

This manuscript has been released as a pre-print at Research Square. The authors thank Ms. Mengqi Chen for providing continuous encouragement to Dr. Jinze Li to pursue his career in medicine.

SUPPLEMENTARY MATERIAL

The Supplementary Material for this article can be found online at: https://www.frontiersin.org/articles/10.3389/fonc.2021.780906/full#supplementary-material

REFERENCES

1. Ljungberg B, Albiges L, Abu-Ghanem Y, Bensalah K, Dabestani S, Fernandez-Pello S, et al. European Association of Urology Guidelines on Renal Cell Carcinoma: The 2019 Update. *Eur Urol* (2019) 75:799–810. doi: 10.1016/j.eururo.2019.02.011
2. Siegel RL, Miller KD, Jemal A. Cancer Statistics, 2020. *CA Cancer J Clin* (2020) 70:7–30. doi: 10.3322/caac.21590
3. Brufau BP, Cerqueda CS, Villalba LB, Izquierdo RS, Gonzalez BM, Molina CN. Metastatic Renal Cell Carcinoma: Radiologic Findings and Assessment of Response to Targeted Antiangiogenic Therapy by Using Multidetector CT. *Radiographics* (2013) 33:1691–716. doi: 10.1148/rg.336125110
4. Chow WH, Devesa SS. Contemporary Epidemiology of Renal Cell Cancer. *Cancer J* (2008) 14:288–301. doi: 10.1097/PPO.0b013e3181867628
5. Sun M, Shariat SF, Cheng C, Ficarra V, Murai M, Oudard S, et al. Prognostic Factors and Predictive Models in Renal Cell Carcinoma: A Contemporary Review. *Eur Urol* (2011) 60:644–61. doi: 10.1016/j.eururo.2011.06.041
6. Moch H, Gasser T, Amin MB, Torhorst J, Sauter G, Mihatsch MJ. Prognostic Utility of the Recently Recommended Histologic Classification and Revised TNM Staging System of Renal Cell Carcinoma: A Swiss Experience With 588 Tumors. *Cancer* (2000) 89:604–14. doi: 10.1002/1097-0142(20000801)89:3<604::AID-CNCR16>3.0.CO;2-Q
7. Klatte T, Rossi SH, Stewart GD. Prognostic Factors and Prognostic Models for Renal Cell Carcinoma: A Literature Review. *World J Urol* (2018) 36:1943–52. doi: 10.1007/s00345-018-2309-4
8. Karakiewicz PI, Briganti A, Chun FK, Trinh QD, Perrotte P, Ficarra V, et al. Multi-Institutional Validation of a New Renal Cancer-Specific Survival Nomogram. *J Clin Oncol* (2007) 25:1316–22. doi: 10.1200/JCO.2006.06.1218
9. Motzer RJ, Bukowski RM, Figlin RA, Hutson TE, Michaelson MD, Kim ST, et al. Prognostic Nomogram for Sunitinib in Patients With Metastatic Renal Cell Carcinoma. *Cancer* (2008) 113:1552–8. doi: 10.1002/cncr.23776
10. Ohno Y. Role of Systemic Inflammatory Response Markers in Urological Malignancy. *Int J Urol* (2019) 26:31–47. doi: 10.1111/iju.13801
11. Sekar RR, Patil D, Baum Y, Pearl J, Bausum A, Bilen MA, et al. A Novel Preoperative Inflammatory Marker Prognostic Score in Patients With Localized and Metastatic Renal Cell Carcinoma. *Asian J Urol* (2017) 4:230–8. doi: 10.1016/j.ajur.2017.04.002
12. Motzer RJ, Mazumdar M, Bacik J, Berg W, Amsterdam A, Ferrara J. Survival and Prognostic Stratification of 670 Patients With Advanced Renal Cell Carcinoma. *J Clin Oncol* (1999) 17:2530–40. doi: 10.1200/JCO.1999.17.8.2530
13. Ozer J, Ratner M, Shaw M, Bailey W, Schomaker S. The Current State of Serum Biomarkers of Hepatotoxicity. *Toxicology* (2008) 245:194–205. doi: 10.1016/j.tox.2007.11.021
14. Botros M, Sikaris KA. The De Ritis Ratio: The Test of Time. *Clin Biochem Rev* (2013) 34:117–30.
15. Thornburg JM, Nelson KK, Clem BF, Lane AN, Arumugam S, Simmons A, et al. Targeting Aspartate Aminotransferase in Breast Cancer. *Breast Cancer Res* (2008) 10:R84. doi: 10.1186/bcr2154
16. Chen SL, Li JP, Li LF, Zeng T, He X. Elevated Preoperative Serum Alanine Aminotransferase/Aspartate Aminotransferase (ALT/AST) Ratio Is Associated With Better Prognosis in Patients Undergoing Curative Treatment for Gastric Adenocarcinoma. *Int J Mol Sci* (2016) 17:911. doi: 10.3390/ijms17060911
17. Wu J, Li S, Wang Y, Hu L. Pretreatment Aspartate Aminotransferase-To-Alanine Aminotransferase (De Ritis) Ratio Predicts the Prognosis of Nonmetastatic Nasopharyngeal Carcinoma. *Onco Targets Ther* (2019) 12:10077–87. doi: 10.2147/OTT.S232563
18. Bezan A, Mrsic E, Krieger D, Stojakovic T, Pummer K, Zigeuner R, et al. The Preoperative AST/ALT (De Ritis) Ratio Represents a Poor Prognostic Factor in a Cohort of Patients With Nonmetastatic Renal Cell Carcinoma. *J Urol* (2015) 194:30–5. doi: 10.1016/j.juro.2015.01.083
19. Canat L, Ataly HA, Agalarov S, Alkan İ, Alturende F. The Effect of AST/ALT (De Ritis) Ratio on Survival and Its Relation to Tumor Histopathological Variables in Patients With Localized Renal Cell Carcinoma. *Int Braz J urol* (2018) 44:288–95. doi: 10.1590/s1677-5538.ibju.2017.0173
20. Page MJ, McKenzie JE, Bossuyt PM, Boutron I, Hoffmann TC, Mulrow CD, et al. The PRISMA 2020 Statement: An Updated Guideline for Reporting Systematic Reviews. *Bmj* (2021) 372:n71. doi: 10.1136/bmj.n71
21. Stang A. Critical Evaluation of the Newcastle-Ottawa Scale for the Assessment of the Quality of Nonrandomized Studies in Meta-Analyses. *Eur J Epidemiol* (2010) 25:603–5. doi: 10.1007/s10654-010-9491-z
22. Yuhara H, Steinmaus C, Cohen SE, Corley DA, Tei Y, Buffler PA. Is Diabetes Mellitus an Independent Risk Factor for Colon Cancer and Rectal Cancer? *Am J Gastroenterol* (2011) 106:1911–1921; quiz 1922. doi: 10.1038/ajg.2011.301
23. Gu L, Wang Z, Chen L, Ma X, Li H, Nie W, et al. A Proposal of Post-Operative Nomogram for Overall Survival in Patients With Renal Cell Carcinoma and Venous Tumor Thrombus. *J Surg Oncol* (2017) 115:905–12. doi: 10.1002/jso.24575
24. Ishihara H, Kondo T, Yoshida K, Omae K, Takagi T, Iizuka J, et al. Evaluation of Preoperative Aspartate Transaminase/Alanine Transaminase Ratio as an Independent Predictive Biomarker in Patients With Metastatic Renal Cell Carcinoma Undergoing Cytoreductive Nephrectomy: A Propensity Score Matching Study. *Clin Genitourin Cancer* (2017) 15:598–604. doi: 10.1016/j.clgc.2017.04.011
25. Lee H, Lee SE, Byun SS, Kim HH, Kwak C, Hong SK. De Ritis Ratio (Aspartate Transaminase/Alanine Transaminase Ratio) as a Significant Prognostic Factor After Surgical Treatment in Patients With Clear-Cell Localized Renal Cell Carcinoma: A Propensity Score-Matched Study. *BJU Int* (2017) 119:261–7. doi: 10.1111/bju.13545
26. Kang M, Yu J, Sung HH, Jeon HG, Jeong BC, Park SH, et al. Prognostic Impact of the Pretreatment Aspartate Transaminase/Alanine Transaminase Ratio in Patients Treated With First-Line Systemic Tyrosine Kinase Inhibitor Therapy for Metastatic Renal Cell Carcinoma. *Int J Urol* (2018) 25:596–603. doi: 10.1111/iju.13574
27. Kim SH, Park EY, Joo J, Chung J. The De Ritis and Neutrophil-To-Lymphocyte Ratios May Aid in the Risk Assessment of Patients With Metastatic Renal Cell Carcinoma. *J Oncol* (2018) 2018:1953571. doi: 10.1155/2018/1953571
28. Ikeda T, Ishihara H, Takagi T, Fukuda H, Yoshida K, Iizuka J, et al. The De Ritis (Aspartate Transaminase/Alanine Transaminase) Ratio as a

Prognosticator in Patients With End-Stage Renal Disease-Associated Renal Cell Carcinoma. *Clin Genitourin Cancer* (2020) 18:236–40. doi: 10.1016/j.clgc.2019.12.012
29. Kang M, Shin SJ, Sung HH, Jeon HG, Jeong BC, Jeon SS, et al. Clinical Significance of Pre-To-Postoperative Dynamics of Aspartate Transaminase/Alanine Transaminase Ratio in Predicting the Prognosis of Renal Cell Carcinoma After Surgical Treatment. *Dis Markers* (2020) 2020:8887605. doi: 10.1155/2020/8887605
30. Laukhtina E, Pradere B, D DA, Rosiello G, Luzzago S, Pecoraro A, et al. Association of Preoperative Serum De Ritis Ratio With Oncological Outcomes in Patients Treated With Cytoreductive Nephrectomy for Metastatic Renal Cell Carcinoma. *Urol Oncol* (2020) 38:936.e937–936.e914. doi: 10.1016/j.urolonc.2020.08.013
31. Janisch F, Klotzbücher T, Marks P, Kienapfel C, Meyer CP, Yu H, et al. Predictive Value of De Ritis Ratio in Metastatic Renal Cell Carcinoma Treated With Tyrosine-Kinase Inhibitors. *World J Urol* (2021) 39:2977–85. doi: 10.1007/s00345-021-03628-2
32. Lane BR, Kattan MW. Prognostic Models and Algorithms in Renal Cell Carcinoma. *Urol Clin North Am* (2008) 35:613–625; vii. doi: 10.1016/j.ucl.2008.07.003
33. Gudbjartsson T, Hardarson S, Petursdottir V, Thoroddsen A, Magnusson J, Einarsson GV. Histological Subtyping and Nuclear Grading of Renal Cell Carcinoma and Their Implications for Survival: A Retrospective Nation-Wide Study of 629 Patients. *Eur Urol* (2005) 48:593–600. doi: 10.1016/j.eururo.2005.04.016
34. Delahunt B. Advances and Controversies in Grading and Staging of Renal Cell Carcinoma. *Mod Pathol* (2009) 22(Suppl 2):S24–36. doi: 10.1038/modpathol.2008.183
35. Su S, Liu L, Li C, Zhang J, Li S. Prognostic Role of Pretreatment De Ritis Ratio (Aspartate Transaminase/Alanine Transaminase Ratio) in Urological Cancers: A Systematic Review and Meta-Analysis. *Front Oncol* (2020) 10:1650. doi: 10.3389/fonc.2020.01650
36. Conde VR, Oliveira PF, Nunes AR, Rocha CS, Ramalhosa E, Pereira JA, et al. The Progression From a Lower to a Higher Invasive Stage of Bladder Cancer Is Associated With Severe Alterations in Glucose and Pyruvate Metabolism. *Exp Cell Res* (2015) 335:91–8. doi: 10.1016/j.yexcr.2015.04.007
37. Koppenol WH, Bounds PL, Dang CV. Otto Warburg's Contributions to Current Concepts of Cancer Metabolism. *Nat Rev Cancer* (2011) 11:325–37. doi: 10.1038/nrc3038
38. Lunt SY, Vander Heiden MG. Aerobic Glycolysis: Meeting the Metabolic Requirements of Cell Proliferation. *Annu Rev Cell Dev Biol* (2011) 27:441–64. doi: 10.1146/annurev-cellbio-092910-154237
39. Dorward A, Sweet S, Moorehead R, Singh G. Mitochondrial Contributions to Cancer Cell Physiology: Redox Balance, Cell Cycle, and Drug Resistance. *J Bioenerg Biomembr* (1997) 29:385–92. doi: 10.1023/A:1022454932269
40. Fantin VR, St-Pierre J, Leder P. Attenuation of LDH-A Expression Uncovers a Link Between Glycolysis, Mitochondrial Physiology, and Tumor Maintenance. *Cancer Cell* (2006) 9:425–34. doi: 10.1016/j.ccr.2006.04.023
41. Shiao YH, Resau JH, Nagashima K, Anderson LM, Ramakrishna G. The Von Hippel-Lindau Tumor Suppressor Targets to Mitochondria. *Cancer Res* (2000) 60:2816–9.
42. Sudarshan S, Karam JA, Brugarolas J, Thompson RH, Uzzo R, Rini B, et al. Metabolism of Kidney Cancer: From the Lab to Clinical Practice. *Eur Urol* (2013) 63:244–51. doi: 10.1016/j.eururo.2012.09.054

Conflict of Interest: The authors declare that the research was conducted in the absence of any commercial or financial relationships that could be construed as a potential conflict of interest.

Publisher's Note: All claims expressed in this article are solely those of the authors and do not necessarily represent those of their affiliated organizations, or those of the publisher, the editors and the reviewers. Any product that may be evaluated in this article, or claim that may be made by its manufacturer, is not guaranteed or endorsed by the publisher.

Copyright © 2021 Li, Cao, Peng, Meng, Xia, Li and Wei. This is an open-access article distributed under the terms of the Creative Commons Attribution License (CC BY). The use, distribution or reproduction in other forums is permitted, provided the original author(s) and the copyright owner(s) are credited and that the original publication in this journal is cited, in accordance with accepted academic practice. No use, distribution or reproduction is permitted which does not comply with these terms.

frontiers in Oncology

ORIGINAL RESEARCH
published: 21 December 2021
doi: 10.3389/fonc.2021.771545

Prognostic Significance of NLR About NETosis and Lymphocytes Perturbations in Localized Renal Cell Carcinoma With Tumor Thrombus

Bingqing Shang[1†], Liping Guo[2†], Rongfang Shen[3], Chuanzhen Cao[1], Ruiyang Xie[1], Weixing Jiang[4], Li Wen[1], Xingang Bi[1], Hongzhe Shi[1], Shan Zheng[5], Changling Li[1], Jianhui Ma[1], Kaitai Zhang[3], Lin Feng[3*] and Jianzhong Shou[1*]*

[1] Department of Urology, National Cancer Center/National Clinical Research Center for Cancer/Cancer Hospital, Chinese Academy of Medical Sciences and Peking Union Medical College, Beijing, China, [2] Peking University People's Hospital, Peking University Institute of Hematology, National Clinical Research Center for Hematologic Disease, Beijing Key Laboratory of Hematopoietic Stem Cell Transplantation, Beijing, China, [3] State Key Laboratory of Molecular Oncology, Department of Etiology and Carcinogenesis, National Cancer Center/National Clinical Research Center for Cancer/Cancer Hospital, Chinese Academy of Medical Sciences and Peking Union Medical College, Beijing, China, [4] Department of Urology, Beijing Friendship Hospital, Capital Medical University, Beijing, China, [5] Department of Pathology, National Cancer Center/National Clinical Research Center for Cancer/Cancer Hospital, Chinese Academy of Medical Sciences and Peking Union Medical College, Beijing, China

Background: Non-metastatic renal cell carcinoma (RCC) with tumor thrombus showed a greater tendency for developing metastases after surgery. Early identification of patients with high risk of poor prognosis is especially important to explore adjuvant treatment of improving outcomes. Neutrophil-to-lymphocyte ratio (NLR) was a systemic inflammation marker and outcome predictor in RCC, reflecting the chaos in systemic immune status in cancer as myeloid cell expansion and lymphatic cell suppression. Neutrophil extracellular traps (NET) formation (NETosis) is the process of neutrophils generating an extracellular DNA net-like structure. NETosis in tumor was demonstrated to conduce to the subsequent metastases of tumor. However, the role of NLR for systemic immune status and tumor local immune infiltration, especially for neutrophil-associated NETs, in non-metastatic RCC with thrombus remains unclear.

Patients and Methods: In our clinical cohort, we enrolled the clinical, pathologic, and preoperative laboratory parameters of 214 RCC patients with tumor thrombus who were treated surgically. The clinical endpoint was defined as cancer-specific survival (CSS). In our basic research cohort, RNA-seq, TCR-seq, and scRNA-seq data were analyzed. Patients who reached the endpoint as recurrence-free survival (RFS) were defined as the "High-risk" group. Otherwise, they were separated into the "Low-risk" group.

Results: In the clinical cohort, NLR≥4 was an independent risk factor for 203 localized RCC with tumor thrombus. In the basic research cohort, tumor thrombi were separated into NETosis-thrombi belonging to the "High-risk" group and non-NETosis-thrombi to the "Low-risk" group. NETs induced by tumor-derived G-CSF in tumor thrombus has a mechanistic role in unfavorable prognosis. Besides, NETs-score from single sample

OPEN ACCESS

Edited by:
Marijo Bilusic, University of Miami Health System, United States

Reviewed by:
Maolake Aerken, University at Buffalo, United States
Liangyou Gu, People's Liberation Army General Hospital, China

***Correspondence:**
Kaitai Zhang
zhangkt@cicams.ac.cn
Lin Feng
fenglin@cicams.ac.cn
Jianzhong Shou
shoujzh2021@163.com

[†]*These authors have contributed equally to this work*

Specialty section:
This article was submitted to Genitourinary Oncology, a section of the journal Frontiers in Oncology

Received: *06 September 2021*
Accepted: *25 November 2021*
Published: *21 December 2021*

Citation:
Shang B, Guo L, Shen R, Cao C, Xie R, Jiang W, Wen L, Bi X, Shi H, Zheng S, Li C, Ma J, Zhang K, Feng L and Shou J (2021) Prognostic Significance of NLR About NETosis and Lymphocytes Perturbations in Localized Renal Cell Carcinoma With Tumor Thrombus. Front. Oncol. 11:771545. doi: 10.3389/fonc.2021.771545

GSEA (ssGSEA) algorithm was an independent prognostic factor validated in the TCGA data. Apart from the neutrophils-associated NETosis, systemic immune perturbations of lymphocytes occurred in the "High-risk" group, represented with decreased TCR diversity and increasingly high proportion of CD4-positive effector memory T (Tem) cells, which indirectly represented the state of lymphopenia.

Conclusions: Our findings firstly demonstrated that neutrophils-associated NETosis and systemic lymphocytes perturbations were considered as tumor progression in patients of localized RCC with tumor thrombus, which reflected NLR≥4 as an independent risk factor for patients.

Keywords: NETosis, renal cell carcinoma, tumor thrombus, prognosis, NLR

INTRODUCTION

According to statistics, the incidence rate and mortality of renal cell carcinoma (RCC) increase year by year, with an estimated 403,262 new cases and 175,098 deaths worldwide in 2018 (1). Among them, about 4–36% patients are characterized with vein tumor thrombus (2, 3). Almost half of patients with non-metastatic RCC with tumor thrombus developed metastases after surgery, and the median recurrence-free survival (RFS) was 37.3 months (4). Sidana et al. previously reported that the 5-year cancer-specific survival (CSS) of non-metastatic RCC with tumor thrombus was 58% (5). To date, most large series of patients with RCC with thrombus have focused on clinical and oncological risk factors such as BMI, age, thrombus level, tumor size, nuclear grade, and perinephric fat invasion, which were independent prognostic factors (6–8). In recent years, the immunological research of kidney cancer has been popular. Many studies have focused on the prognosis of some immunization indicators. Neutrophil-to-lymphocyte ratio (NLR) was considered as a systemic inflammatory marker and prognostic predictor of RCC (9, 10), which reflected the unstable systemic immune status of tumor, such as myeloid expansion and lymphatic suppression (11). Peyton CC et al. demonstrated the prognostic value of NLR for the metastatic RCC with thrombus (12). Whereas, the prognostic value and biological underpinnings of NLR for systemic immune status and the immune cell infiltration in tumor, especially for neutrophils, were undefined in non-metastatic RCC with thrombus.

Neutrophils exert an important role in the immune defense in the face of stimuli (13). The recent research in neutrophil biology has shed light on the ability of neutrophils to free their decondensed chromatin and generate large extracellular DNA net-like structures called neutrophil extracellular traps (NETs) (14). NET formation (NETosis) is considered as a tactic to catch and kill bacteria initially, and thus protects the host against microbial invasion (15). Now, it is well identified that the releasing of NETs has more complicated consequences. Of note, NETosis in tumor was identified to capture the circulating tumor cells (CTCs), allowing their migration and invasion (16), contributing to the subsequent metastases in the distant tissues and organs (17). In our prior research, our results indicated that NETs released by peripheral neutrophils could act as a protective shelter for helping the metastasis of CTCs in RCC (18). What is more, excessive NETs in cancer, which afforded a physical scaffold for thrombus formation by binding red blood cells (RBCs), platelets, even with tumor cells, could contribute to vessel thrombus (19–22). Treatment with targeted inhibitors abrogating NET formation has been shown to reduce thrombotic events in neoplasms (22, 23). Meanwhile, it lacks the NETosis-related research for RCC with tumor thrombus. What is more, NETosis inhibitions are promising as targeted therapy for RCC. Thus, we investigated the role of NETosis in tumor thrombus of RCC. In this study, we explored the immune-oncology landscape of localized RCC with thrombus and identified the role of NLR in NETosis as a prognostic risk factor and immune repertoire in tumor progression.

PATIENTS AND METHODS

Study Cohort and Public Datasets

Our study was approved by the Ethics Committee of National Cancer Center/Cancer Hospital, Chinese Academy of Medical Sciences (NCC/CHCAMS) (ID Num: NCC2016YJC-08). It was separated into two parts: the clinical cohort and basic research cohort. We enrolled RCC patients with tumor thrombus who were treated surgically from NCC/CHCAMS from January 2000 to December 2019. Patient consent was not required. Patients were followed every 3–6 months for the first 5 years after surgery and then yearly thereafter. All follow-ups were concluded on May 30, 2021. None of these patients received preoperative chemotherapy, radiotherapy, or targeted therapy.

In the clinical cohort, we investigated the prognosis factor for RCC patients with thrombus. The clinical, pathologic, and preoperative laboratory parameters were abstracted from the clinical database. Clinical variables included gender, body mass index (BMI), age at surgery, and paraneoplastic syndrome. Pathologic information included maximum tumor size, tumor laterality, tumor necrosis, Fuhrman grade, sarcomatoid differentiation, perirenal fat invasion, and lymph node metastasis at surgery. Preoperative laboratory parameters included absolute neutrophil, lymphocyte, platelet counts, Hb, LDH, ALT, AST, IgA, IgG, and IgM. NLR was calculated by dividing the absolute neutrophil count by the absolute lymphocyte count. Cutoff values were selected based on our institutional-specific laboratory guidelines, median values, or through related literature review.

The clinical-pathological-blood characteristics of the enrolled patients are shown in **Supplementary Material, Table S1**. The clinical endpoint in our clinical cohort was defined as CSS.

To further investigate the underlying mechanisms of the prognosis factor, we collected 10 treatment-naive patients of non-metastatic RCC with tumor thrombus from the basic research cohort. Multiple tumor and tumor thrombus regions and peripheral blood mononuclear cell (PBMC) samples were selected for RNA sequencing (RNA-seq). The detailed information of the enrolled patients is shown in **Supplementary Material, Table S2**. All of the specimens were verified by histopathology. To early recognize the patients of poor prognosis, we chose recurrence-free survival (RFS) for the outcome endpoint as the time from diagnosis to documented recurrence or metastasis in our basic research cohort. Patients were divided into two groups according to the 3-year RFS. Patients who reached the endpoint were defined as the "High-risk" group. Otherwise, they were separated into the "Low-risk" group.

Public expression data for a further 39 tumor samples from stage III RCC patients with tumor thrombus in TCGA were obtained from UCSC (University of California, Santa Cruz) Xena (https://xenabrowser.net/datapages/). Gene expression data from TCGA datasets were to construct a prognostic gene set for RCC with tumor thrombus.

Statistical Analysis and Survival Analysis

Statistical analysis was performed using R (version 3.6.0, http://www.r-project.org). Univariable and multivariable Cox proportional hazards regression model were used to estimate hazard ratios (HRs) *via* the R package "survival." In addition, the HR, 95% CI, and statistical significance of each key prognostic factor were estimated and demonstrated using a forest plot *via* the R package "survminer." The main packages used included survival, survminer, and dplyr.

Next-Generation Sequencing and Data Processing

QC-qualified RNA samples of the preoperation peripheral leukocytes, tumor, and tumor thrombus tissues from the basic research cohort were analyzed using RNA-seq. Strand-specific mRNA libraries were prepared using a NEBNext® Ultra™ RNA Library Prep Kit (Illumina; cat. no. E7530L). Subsequently, the eligible libraries were sequenced on an HiSeq XTen platform of 150 bp paired-end reads (Illumina; cat. no. FC-501-2521), yielding approximately 20 million (M) reads per sample. Adapter sequences and low-quality reads were cleaned up using Cutadapt and Sickle (http://github.com/najoshi/sickle/) software. Clean reads were quantified against an Ensembl catalog (GRCh37) using Salmon software at the transcript level (24) and aggregated with the R package "tximport" at the gene level; transcripts per million reads (TPM) values were estimated by Salmon gene expression quantification software, and genes with detectable TPM counts over 80% of the samples were maintained. The proportion of immune cells in PBMC was validated by single-cell RNA sequencing (scRNA) information. After the RNA was extracted in PBMC samples, the SMART-based UMI-corrected TCRB libraries were constructed for sequencing, which was detailed in our previous work (25). Data were dealt with the MIGEC, MiXCR, and CellRanger software and the R packages "Seurat", "immunarch", and "scRepertoire".

NETs-Related Gene Sets

The gene sets of NETs were derived from two parts. One was a summary gene set of NETs-associated genes, mainly consisting of the ligands and receptors that promote the NETosis, downstream associated signals, and the molecules that illustrated to adhere to the structure of NETs. The other genes came from the neutrophil-associated genes from the weighted correlation network analysis (WGCNA) in the basic research cohort. In total, we converged the 44 overlapping genes in the NETs-associated gene set for signature constructing.

Enrichment Score of Marker Gene Sets Calculated With Single-Sample Gene Set Enrichment Analysis

We acquired the marker gene sets for immune cells (26) and classic oncologic pathways (27) from other articles. We carried out ssGSEA to calculate the enrichment score of each term using the R package GSVA" (28). With the above methods, the counts for every immune cell type and the expression for each classic oncologic pathways in each specimen were referred to as the immune-cell score and pathway-activated score. The counts of NETs calculated hereafter stood for as the NETs-score. The signature of NETs in localized RCC with thrombus was constructed from the 44 NETs-associated genes according to the Cox proportional hazard regression model in TCGA cohort, in which each characteristic gene obtained P value <0.05. Every patient could obtain a NETs-score with the signature of NETs.

Constructing Weighted Gene Co-Expression Network

In this study, WGCNA was restricted to the top 8,000 varying genes according to their standard deviation. Therefore, WGCNA was constructed to find phenotype-related module and hub genes *via* the "WGCNA" package and R tutorials (29). Finally, highly similar modules and their relationship to phenotype traits (tissue types and prognosis risk) were identified.

Additional Bioinformatic

By analyzing RNA-seq of tumor and tumor thrombus with an unsupervised clustering algorithm, we separated diverse status on the basis of the infiltration of immune cells and expression of oncological pathway at a much higher resolution. To distinguish the differentially expressed genes (DEGs) in RCC of progression risk group, expression profiles in the "High-risk" tissue were compared with those in "Low-risk" through the "limma" package in R software. Genes with an adjusted P-value < 0.05 and the cutoff value of $|\log_2$ fold changes$|> 2$ ($\log_2$FC) were defined as DEGs. GSEA was applied to enrich hallmark gene sets downloaded from the Molecular Signatures Database v6.0 (MSigDB) with "GSVA" package in R software. Input genes were listed in descending order according to the $\log_2$FC values. Genes with false discovery rate (FDR) p-value less than 0.05 and nominal p-value less than 0.05 were considered significantly enriched. To investigate Gene Ontology (GO) of a comprehensive set of functionally annotated

genes, the R package "clusterProfiler" was used (30), with a cutoff criterion of adjusted $p < 0.05$.

Immunohistochemistry Assay

IHC was performed on archival formalin-fixed paraffin-embedded tumor and tumor thrombus tissue. Tumor thrombus tissues were stained with the following antibodies to identify specific proteins: anti- citrullinated histone H3 (anti-H3Cit) (citrulline R2 + R8 + R17) antibody (Abcam, ab5103; dilution 1:200) and anti-myeloperoxidase (anti-MPO) antibody (Abcam, ab25989; dilution 1:200). NET formation was visually determined as the percentage of neutrophils identified positive for a DAPI and H3Cit signal (31). IHC images were evaluated with image J software.

RESULTS

NLR ≥ 4 as an Independent Prognosis Factor for RCC With Tumor Thrombus

A total of 214 patients of non-metastatic RCC with tumor thrombus were treated surgically in the period 2000–2019 from NCC/CHCAMS. Clinical-pathological-blood characteristics of these selected patients in our clinical cohort are summarized in **Supplementary Material, Table S1**. Of these patients, 203 had available follow-up data and blood count data to calculate preoperative NLR; therefore, this research focused on these patients. The median [interquartile range (IQR)] follow-up was 46.0 months. Median survival time was 127 months (95% CI: 104.2~150.0). The 5-year CSS was 66.3%.

Univariable Cox proportional hazards regression identified the following risk factors: perinephric fat invasion, paraneoplastic syndrome, blood transfusion, BMI, tumor laterality, tumor size, Fuhrman grade 3/4, tumor necrosis, sarcomatoid differentiation, preoperative platelet count, NLR, hemoglobin level, IgG, and IgA (**Table 1**). A multivariable Cox hazards regression model identified the following independent prognostic factors: NLR ≥ 4 (HR 2.46; 95% CI 1.18–5.1; P = 0.016), Fuhrman grade 3/4 (HR 4.07; 95% CI 1.80–9.2; P < 0.001), and Tumor laterality (left) (HR 2.05; 95% CI 1.08–3.9; P = 0.028) (**Table 1**).

Tumor in "High-Risk" Group Was Highly Immune-Cell Infiltrated and Proliferative

To further investigate the mechanism of NLR as prognosis factor, we analyzed the local immune infiltration and oncologic features of tumor and tumor thrombus samples from our basic research cohort. Unsupervised clustering on the basic research cohort showed that the tissue samples were predominantly separated into two clusters: low immune cell infiltration (Low-CI) and high immune cell infiltration (High-CI). Patients in the High-CI cluster were featured with rich leukocyte infiltration, such as CD4+ T cells, CD8+ T cells, as well as myeloid cells of macrophages and Neutrophils (**Figure 1A**). The immune characteristic of tumor was consistent with its paired tumor thrombus. In addition, two clusters of unsupervised clustering were consistent with the progression risk group (see the definition in *Methods*). That is to say, patients in the "High-risk" group characterized as High-CI cluster had the most immune cells highly immersed including T cells, B cells, and Treg cells, compared to the "Low-risk" group

TABLE 1 | Univariate and multivariable Cox proportional hazard regression analysis of CSS in our clinical cohort.

	Univariate		Multivariate	
	hazard ratio (95% CI)	**P-value**	**hazard ratio (95% CI)**	**P-value**
Age (years)	1 (0.98–1)	0.92		
Gender (Male)	0.89 (0.49–1.6)	0.7		
BMI ≥ 24.7 Kg/m2	0.44 (0.26–0.74)	0.0019	0.74 (0.39–1.4)	0.354
Tumor size ≥7 cm	3.6 (2–6.6)	<0.001	1.94 (0.98–3.8)	0.059
Tumor laterality (Left)	2.1 (1.2–3.7)	0.0076	2.05 (1.08–3.9)	0.028*
Paraneoplastic syndrome	3 (1.6–5.7)	<0.001	1.71 (0.77–3.8)	0.185
Blood transfusion	3.2 (1.9–5.3)	<0.001	0.98 (0.52–1.9)	0.957
Fuhrman grade 3/4	6.6 (3.4–13)	<0.001	4.07 (1.80–9.2)	<0.001***
Tumor necrosis	2.2 (1.3–3.7)	0.0029	0.81 (0.41–1.6)	0.552
Sarcomatoid differentiation	3.9 (2.3–6.6)	<0.001	1.84 (0.93–3.7)	0.082
Perineal fat invasion	3 (1.8–5)	<0.001	1.83 (0.99–3.4)	0.055
LN metastasis	1.6 (0.63–4)	0.33		
Hb	0.98 (0.98–0.99)	<0.001	1 (0.99–1.0)	0.966
LDH	1 (1–1)	0.051		
ALT	1 (0.98–1)	0.95		
AST	1 (0.98–1)	0.66		
Neutrophil	1.1 (0.95–1.3)	0.18		
Platelet	1 (1–1)	<0.001	1 (1–1)	0.911
NLR≥4	4 (2.2–7.2)	<0.001	2.46 (1.18–5.1)	0.016*
IgG	1.1 (1–1.2)	0.0021	1.01 (0.92–1.1)	0.894
IgA	1.3 (1.1–1.5)	0.0022	1.24 (0.97–1.6)	0.084
IgM	0.97 (0.78–1.2)	0.81		

ALT, alanine aminotransferase; AST, aspartate aminotransferase; BMI, body mass index; Hb, hemoglobin; LDH, lactate dehydrogenase; LN, lymph nodes; NLR, neutrophil-to-lymphocyte ratio.
**p < 0.05, ***p < 0.001.*

(**Figure 1B**). Besides, the total NK cells were with low infiltration in the "High-risk" group (**Figure 1B**).

To further investigate the oncologic pathway-level analyses, we explored simplified signatures of representative genes associated with angiogenesis, cell cycle, antigen presenting machinery, the complement cascade, EMT feature, and metabolism-related pathways, including Fatty Acid Synthesis (FAS)/pentose phosphate and Fatty Acid Oxidation/AMP-activated protein kinase (FAO/AMPK) signaling (**Figure 1A**). Patient tumors in "High-risk" group were primarily characterized as highly proliferative, with enrichment of "cell cycle" pathway related genes (**Figure 1B**). "Low-risk" group also showed increased FAO/AMPK gene signature expression (**Figure 1B**).

NETosis in the RCC Tumor Thrombus Contributes to the Unfavorable Prognosis

To further understand the relationship between neutrophil and prognosis, the infiltration of neutrophil in tumor and tumor

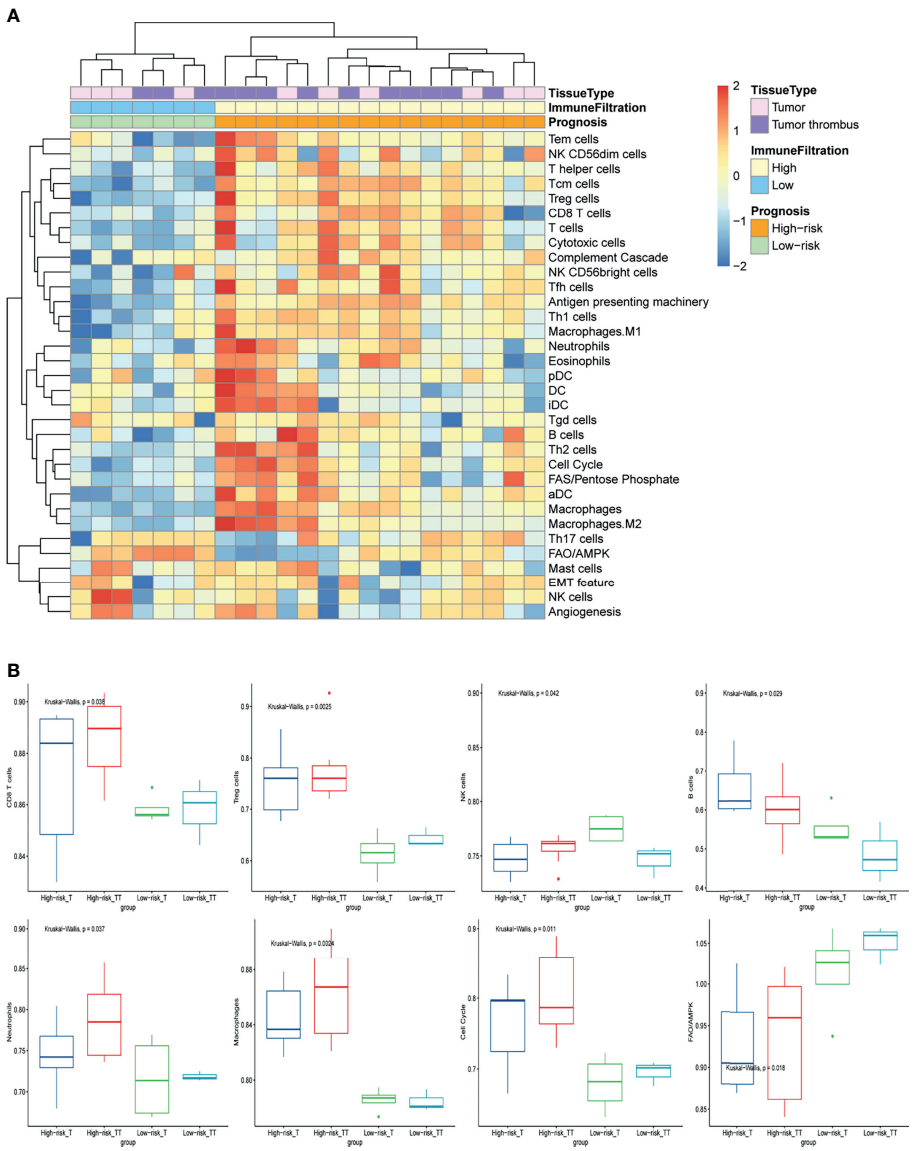

FIGURE 1 | The immune-oncology landscape of localized RCC with tumor thrombus. **(A)** Heatmap of the ssGSEA score, as estimated using gene sets for immune cells and classic oncologic pathways. The top bar indicates the groups stratified by the tissue of tumor or tumor thrombus, the second bar indicates the immune cell infiltration group, and the third bar on the x-axis represents the prognosis of the patients. **(B)** The average expression of cell cycle and FAO/AMPK signaling and changes in the constituent ratios of infiltrated cell subpopulations including CD8 T cells, Treg cells, NK cells, B cells, neutrophils, and macrophages in the four subgroups for "High-risk" or "Low-risk" group of tumor or tumor thrombus. Data were analyzed using the Kruskal-Wallis test. High-risk_T, tumor tissue in the "High-risk" group; High-risk_TT, tumor thrombus tissue in the "High-risk" group; Low-risk _T, tumor tissue in the "Low-risk" group; Low-risk_TT, tumor thrombus tissue in the "Low-risk" group.

thrombus tissues were analyzed. Patients in the "High-risk" group showed an increase in neutrophil infiltration, especially for tumor thrombus (**Figure 1B**). Tumor-derived granulocyte colony stimulating factor (G-CSF) as a NET-inducing factor, and NETs-associated marker genes including Histone family, peptidyl arginine deiminase 4 (PADI4), and matrix metalloproteinase 9 (MMP9), were significantly overexpressed in the tumor thrombus (**Figure 2A**), rather than tumor, of patients with unfavorable prognosis in the "High-risk" group. GSEA revealed that the leukocytes in the peripheral blood of patients with unfavorable prognosis groups were similar to G-CSF-treated PBMCs (**Figure 2B**).

Next, we confirmed that NETosis was morphologically detectable in the tumor thrombus through testing positive for a DAPI, H3Cit, and MPO signal with IHC. NETosis was identified in the "High-risk" group instead of "Low-risk" group (**Figure 2C**). The quantification of IHC staining results indicated that H3Cit and MPO were significantly expressed in the "High-risk" group (**Figure 2D**). These overall modulations suggest that tumor thrombi were divided into NETosis-thrombi in the "High-risk" group and non-NETosis-thrombi in the "Low-risk" group. And NETs induced by tumor cell-derived G-CSF in tumor thrombus have a mechanistic effect of the poor prognosis with RCC.

NETs-Score Was an Independent Prognostic Factor Validated in the TCGA Data

In WGCNA analysis, the gene co-expression networks were constructed from the basic research cohort. With each module assigned a color, a total of 16 modules were identified and their association with four clinical phenotypes was analyzed, including tissue type (tumor and tumor thrombus) and progression risk (High-risk and Low-risk). The results of the module-trait relationships are presented in **Figure 3A**, revealing that the black module was found to have the highest association with tumor thrombus tissues with high risk (black module: r = 0.61, p = 0.002). To investigate the underlying function of the genes in black

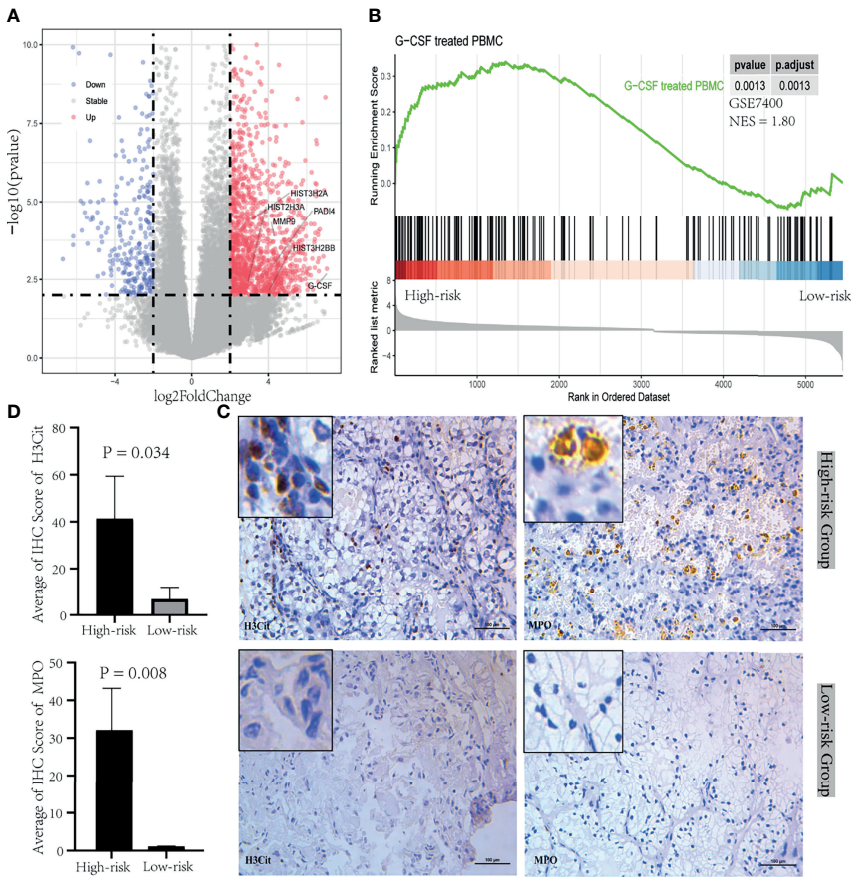

FIGURE 2 | NETosis induced by tumor-derived G-CSF in tumor thrombus of RCC. **(A)** Volcano plot of the upregulated (red) and downregulated (blue) genes between the group between "High-risk" and "Low-risk" of tumor thrombus. G-CSF and NETs-associated marker genes including Histone family, PADI4, and MMP9, were significantly overexpressed in the "High-risk" group. **(B)** GSEA plot of the enriched hallmark gene sets derived from GSE7400 was performed with DEGs between "High-risk" and "Low-risk" group of PBMC. **(C)** IHC was performed in tumor thrombus specimens. H3Cit and MPO were stained during NETosis. **(D)** The bar plot of the IHC score quantification for H3Cit and MPO between the "High-risk" group and "Low-risk" group. Data were expressed as mean ± SD.

module for the "High-risk_TT" group, we performed GO analysis. In GO analysis, GO terms such as neutrophil activation, neutrophil-mediated immunity, and neutrophil degranulation were enriched in the black module (**Figure 3B**).

As shown in **Figure 3C**, 486 genes were found in the black module, and 41 genes in neutrophil-characteristic GO-terms in this module. The other was a summary gene set of NETs-associated genes in prior research (see in *Methods*). As a consequence, the 44 overlapping genes were converged in the NETs-associated gene set for signature constructing (**Figure 3C**). Based on the data of TCGA cohort, a total of 44 genes related to NETs was adapted to Univariable Cox analysis. As a result, a set of five genes—ATAD3B, ADAM8, F3, PSMD13, and SLC11A1—was initially obtained, with a cutoff criterion of adjusted p< 0.05. Subsequently, we got a NETs-score with ssGSEA analysis of these five genes.

Based on the data of TCGA RNA-seq of non-metastatic RCC with thrombus, NETs-score was adapted to the Cox regression analysis, and each variable was given a regression coefficient β (see **Table 2**). The factors of age and NETs-score were candidate risk factors in univariable Cox regression analysis ($p < 0.05$). Due to Fuhrman grade as an important prognosis factor in RCC, we added it in multivariable Cox analysis with age and NETs-score. As a result, NETs-score ($p = 0.021$, HR 6.5) and age ($p = 0.001$, HR 1.1) were independent prognostic factors identified (**Table 2**

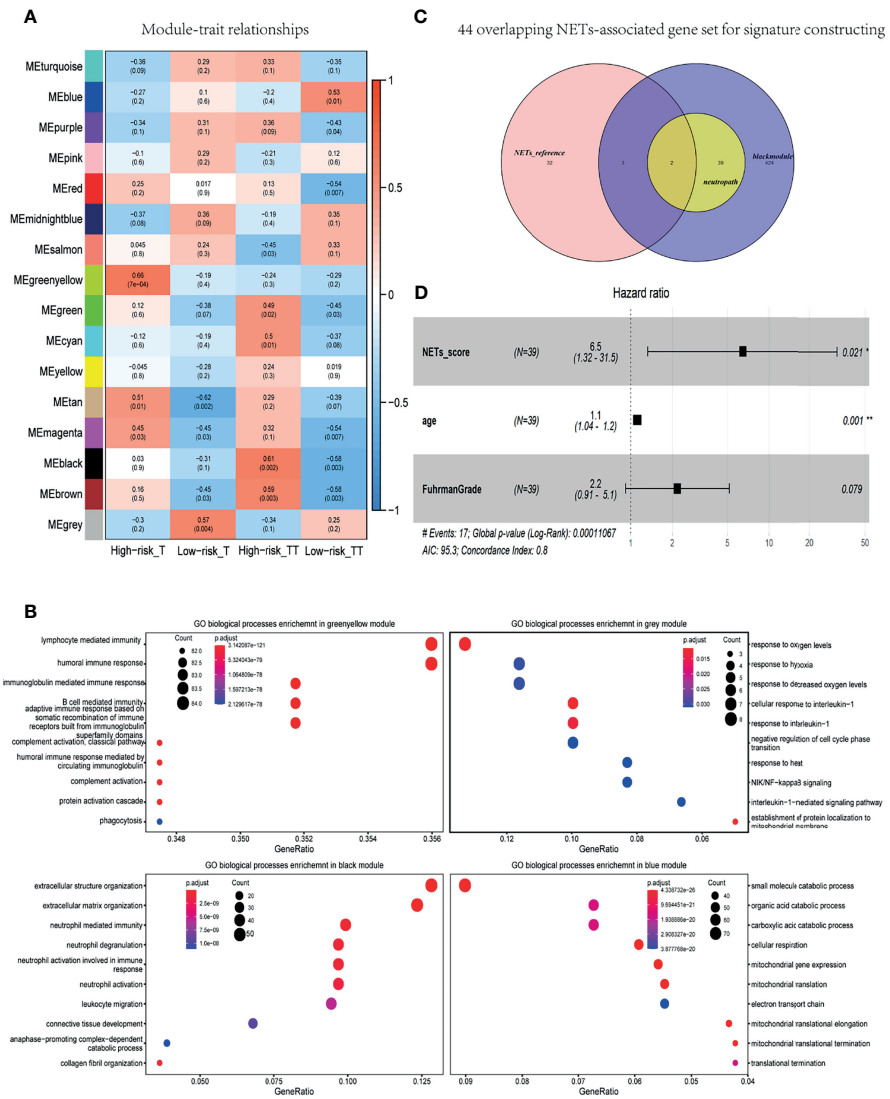

FIGURE 3 | NETs-score was an independent prognostic factor for localized RCC with tumor thrombus. **(A)** Heat map of module-trait associations; rows represent the module eigengene, and columns represent clinical traits. **(B)** Dot plot of the biological process enrichment results in the black module. The dot size and color represent the gene count and enrichment level, respectively. **(C)** Venn diagram of the 44 overlapping genes were converged in the NETs-associated gene set for signature constructing. black module: 486 genes were found in the black module; neutropath: 41 genes in neutrophil-characteristic GO-terms in this black module; NETs-reference: a summary gene set of NETs-associated genes in prior research. **(D)** Forest plot of pooled HRs and 95% CI for OS in the TCGA validated data.

TABLE 2 | Univariate and multivariable Cox proportional hazard regression analysis in the TCGA cohort.

	Univariate		Multivariate	
	hazard ratio (95% CI)	P-value	hazard ratio (95% CI)	P-value
NETs-score	8.1 (1.8–37)	0.0064	6.5 (1.32–31.5)	0.021*
Age	1.1 (1–1.2)	0.002	1.1 (1.04–1.2)	0.001**
Gender (Male)	0.74 (0.29–1.9)	0.54		
Fuhrman grade	2.2 (0.97–5)	0.058	2.2 (0.91–5.1)	0.079
Tumor laterality (Left)	1.5 (0.57–3.8)	0.43		

*Annotation details for two tables: The second classification variables have been labeled with cutoff values or grouped indicators. Variables that are not labeled with cutoff values were analyzed as continuous variables. *p < 0.05, **p < 0.01.*

and **Figure 3D**), indicating the NETs-score was a hazard factor for significantly curtailed survival.

Systemic Immune Perturbations of Lymphocytes Induced in the "High-Risk" Group

According to the TCR repertoire analysis of PBMC *via* bulk TCR sequencing for the patients in our basic research cohort, the index chao1, a symbol of diversity and richness, was decreased in the "High-risk" group (**Figure 4A**). Each clonotype in the top 25% of two representative patients in the High-risk/Low-risk group was graphically represented (**Figure 4B**), which illustrated that the high-abundance overwhelming clonotypes increased in the "High-risk" group.

Hence, we further investigated the preoperative PBMC transcriptome levels and immune repertoire *via* scRNA sequencing between two patients in "High-risk" and "Low-risk" groups (**Figure 5A**). Removing the low-quality cells, we acquired single-cell RNA sequencing (scRNA-seq) profiles from 13,532 cells. After normalization of gene expression and principal component analysis (PCA), we used uniform manifold approximation and projection (UMAP) clustering to separate the cells into 16 clusters (**Figure 5B**). These clusters could be assigned to seven known cell lineages through marker genes (**Figure 5C**): Monocytes (2,373 cells, 17.5%, marked with CD14 and FCGR3A), NK cells (1,280 cells, 9.5%, marked with NKG7, GZMH, and GZMA), Dendritic cells (63 cells, 0.47%, marked with FCER1A); macrophages (40 cells, 0.3%, marked with CD68); platelets (110 cells, 0.81%, marked with PPBP); B cells (1,722 cells, 12.72%, marked with MS4A1, CD19, and MZB1); and T cells (7,944 cells, 58.7%, marked with CD4, CD8A). The proportion of each cell lineage varying, obviously, the counts of lymphocytes including naive B cells and CD4 positive central memory T cells (Tcm) decreased while CD4 and CD8 positive effector memory T (Tem) and Treg cells increased in the patient of "High-risk" group (**Figure 5D**). Integrated with the corresponding single-cell immune repertoire data, we confirmed that the increasingly high proportion of clonal expansion (defined as over one T cells shared the same α-β TCR pair) of the CD4 positive Tem cells occurred in the "High-risk" group (**Figure 5E**). Systemic perturbations of lymphocytes existed in the "High-risk" group of non-metastatic RCC with thrombus, featured with TCR diversity decrease and immune function inhibition, which also explains that NLR≥4 was associated with poor prognosis in the clinical cohort.

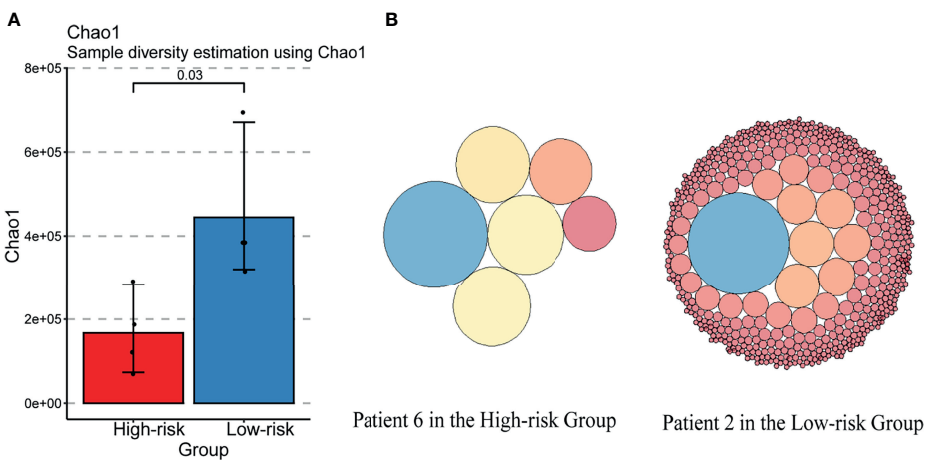

FIGURE 4 | TCR diversity was decreased in the "High-risk" group. **(A)** Changes in the TCRB diversity Chao1 in "High-risk" and "Low-risk" groups. **(B)** Changes of TOP25% clonotypes in the two representative patients of "High-risk" and "Low-risk" groups. Each circle indicates a clonotype. The size of the circle represents the amount of the clonotype.

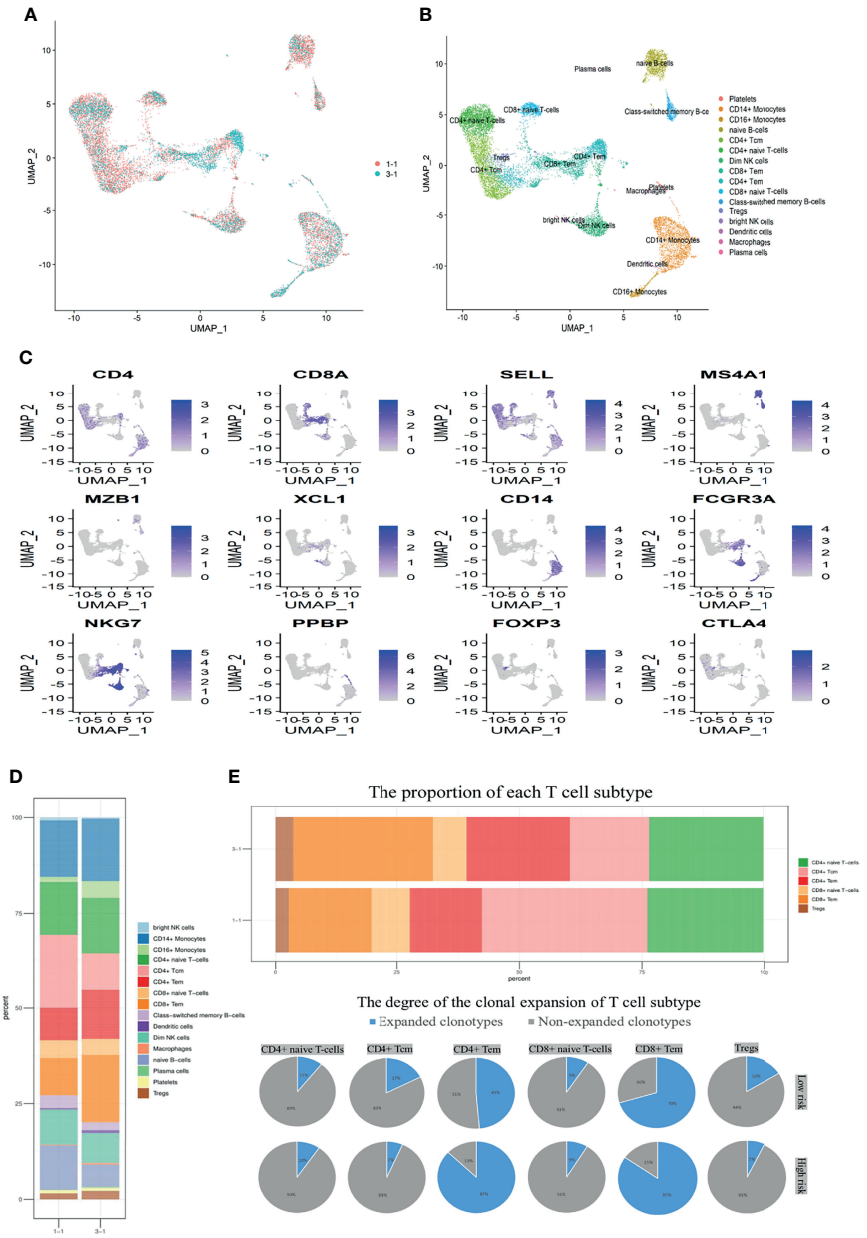

FIGURE 5 | Perturbations of lymphocytes were induced in the "High-risk" group determined by scRNA. **(A)** Perioperative PBMC for "High-risk" (3-1) and "Low-risk" (1-1) samples from two treatment-naive localized RCC patients with tumor thrombus are shown. Each dot represents a cell. **(B)** Sixteen clusters were identified by principal component analysis and visualized with UMAP. **(C)** UMAP plots show the expression levels of canonical marker genes for 16 cell types. **(D)** The stack bar plot shows the proportions of all cell subtypes of PBMC. **(E)** The stack bar plot represents the proportions of all T-cell subtypes of PBMC. The pie chart shows the distribution of TCRB clonotypes in different T-cell subtypes. Expanded clonotype was defined as which is detected more than once.

DISCUSSION

In spite of the hallmark improvements in perioperative care and surgical treatment, locally advanced RCC with tumor thrombus symbolized a relatively adverse prognosis.

The prior research demonstrated that the 5-year CSS of RCC of tumor thrombus without metastasis remains only 58% (5). In this study, the median follow-up was 46.0 months. Median survival time was 127 months. And the 5-year CSS was 66.3% for non-metastasis RCC with tumor thrombus. Apart from clinical and tumor features, our study firstly investigated the blood characteristics as prognosis predictors in the non-metastasis RCC with tumor thrombus. In the clinical cohort, this study has illustrated three clinical-pathologic-blood variables, namely tumor laterality (left), Fuhrman Grade (G3/4), and NLR (≥4), which were independently predictive of unfavorable prognosis using our retrospective research of 203

patients with non-metastatic RCC with thrombus. Consistent with the finding of Xiao R et al., Fuhrman Grade was an unfavorable prognostic factor in localized RCC patients with tumor thrombus (7). Strauss A et al. illustrated that left-sided RCC of the SEER dataset in surgically treated patients tended to present at more advanced stage and has in general adverse CSS (32). Compared to a right side of thrombus of RCC, Thiel DD et al. demonstrated that a left-side thrombus may be associated with poor prognosis that was more aggressive (33). What is more, surgery for the left RCC with tumor thrombus was more complicated than the right. NLR, an established signature of inflammation, has been considered as a prognosis risk factor in the metastatic RCC with thrombus (12).

Considering that approximately 40% of patients with non-metastatic RCC with tumor thrombus developed metastases after surgery, with 37.3 months of the median RFS (4), early recognition of patients at high risk for tumor recurrence is particularly important in exploring adjuvant treatments to achieve better prognosis, such as targeted therapy and immunotherapy therapy of clinical trials (34, 35). In the basic research cohort, patients who reached the endpoint were defined as the "High-risk" group. Otherwise, they were separated into the "Low-risk" group.

Firstly, we compared the local immune and oncologic characteristic of tumor and its paired tumor thrombus according to the RNA-seq data. Compared with the "Low-risk" group, the tumor and tumor thrombus tissue of patients in the "High-risk" group were featured with rich leukocyte infiltrates, such as CD4+ T cells, CD8+ T cells, as well as myeloid cells of macrophages and Neutrophils. This is consistent with previous reports that a high level of local immune cells infiltration in tumor tissue, including T cells and neutrophils, was associated with poor prognosis in RCC (36–38). However, few studies focused on immune cell infiltration of tumor thrombus of RCC, possibly because of the difficulty in obtaining the tumor thrombosis tissue. In our basic research cohort, tumor thrombus shared similar but not identical characteristics with its paired tumor. Interestingly, patients in the "High-risk" group showed an increase in the infiltration level of neutrophils, especially in tumor thrombus tissues.

In response to stimuli, activated neutrophils could release net-like structures as NETs that are composed of DNA-histone scaffold and cytoplasmic and granular proteins. NETs, found in both mouse and human tumors (39, 40), facilitated tumor invasion and metastasis and encouraged tumor progression. NETs could be promoted by tumor-cell-derived factors, primarily G-CSF that can accumulate in the blood of tumor-bearing mice and cancer patients (20, 21, 41). Intriguingly, NETs not only booster tumor progression but also serve as risk factors for cancer-associated thrombosis seen in the cancer of tumor-free mice (21). Furthermore, NETs-associated microthrombi for ischemic stroke and high circulating levels of G-CSF were easily found in patients with cancer (20). In this study, we firstly reported that instead of in the tumor tissue, tumor cells in tumor thrombus released G-CSF. Tumor-thrombus-derived G-CSF was identified to promote neutrophils to form NETs in tumor thrombus. As a result, tumor thrombi could be separated into two types: NETosis- thrombi and non-NETosis-thrombi. NETosis-related thrombus was the unfavorable prognostic factor. Therefore, better NETs-associated biomarkers for progression and prognosis of RCC with tumor thrombus are demanded. In this study, a total of five significant genes for NETs-score were identified for localized RCC with thrombus in the TCGA. NETs-score was an independent factor ($p = 0.021$, HR 6.5). Non-metastatic RCC with tumor thrombus was treated only with the operation with the excision of venous vena caval thrombus, and no distinct surgical method was superior to it (42). If the prognosis could be predicted in advance according to NETs-score, these patients could receive early intervention of NETosis inhibition to improve survival outcome. However, except for inflammation diseases and pancreatic cancer (23, 43–45), it lacks the NETosis-inhibition-related research for RCC. In the next step, our study intends to conduct research on animal or clinical trials related to the molecular pathway or inhibitors of NETosis.

Tumor cells blocked the effective response of antitumor immunity, including the upregulation of suppressive molecules on the T cells, which were associated with overall survival (46, 47). Morizawa Y et al. identified that the elevated NLR in blood was correlated with the increase of Foxp3+ Treg cells in muscle-invasive bladder cancer (48).

Secondly, apart from the central role of neutrophils in NETosis, this study explored the systemic immune status in non-metastatic RCC with thrombus. We confirmed that the systemic perturbations of lymphocytes were induced in the "High-risk" group. The proportion of Treg cells was increased. Meanwhile, the TCR repertoire diversity was decreased, and the increasingly expanded clonotypes of CD4 positive Tem occurred in the "High-risk" group. In the prior studies, the overwhelming expansion of CD4 positive Tem was found in the state of lymphopenia (49, 50). As the peripheral blood is a limited pool to restore T cells, the expansion clonotype of one T cell subtype may result in suppression of the others (51, 52). As a result, there is not enough room for the enriched naïve T cells. These findings identified that, although the immune system generated much more expanded tumor-associated T cells with the identical TCR clonotype, these expanded immune cells not only failed to kill tumor cells but also impacted the homeostasis of TCR repertoire. The systemic perturbations of T cells in quantity and function may promote the unfavorable prognosis in the "High-risk" group of RCC with thrombus. There are several limitations worth noting, such as the retrospective design in clinical cohort and the limited sample size of basic research cohort in this study. In addition, the prognostic prediction of NETs-score was prone to model based on RNA-seq profile and algorithms. Furthermore, this signature was only validated in localized RCC with thrombus in the TCGA cohort. Therefore, further validation in prospective observational studies with larger sample size is expected.

CONCLUSION

In summary, NLR, a hematological biomarker, was an independent prognostic risk factor for non-metastatic RCC with tumor thrombus. What is more, this study was the first to

further investigate the molecular mechanism of NLR as a prognosis risk factor. Increased neutrophil infiltration and more NETs stimulated by tumor cell-derived G-CSF in the tumor thrombus occurred in the "High-risk" group. Moreover, the lymphocytes in the "High-risk" group showed a systemic disorder, including TCR diversity decreasing and CD4 Tem amplification occurring, which was found in the state of lymphopenia in prior studies.

DATA AVAILABILITY STATEMENT

The datasets presented in this study can be found in online repositories. The names of the repository/repositories and accession number(s) can be found below: http://bigd.big.ac.cn/gsa-human, HRA000049 and HRA000042. Further inquiries can be directed to the corresponding author.

AUTHOR CONTRIBUTIONS

BS was responsible for data analysis and writing of the draft of the manuscript. LG conducted the experiments. RS, CC, RX, WJ, and LW researched data. XB, HS, and SZ evaluated images and contributed to discussion. CL and JM were responsible for data revision. KZ, LF, and JS reviewed/edited the manuscript. All authors contributed to the article and approved the submitted version.

FUNDING

This work was supported by the National Natural Science Foundation of China (ID Number: 82072837). This study was also funded by Beijing Municipal Natural Science Foundation (ID Number: 7212083) and CAMS Initiative for Innovative Medicine (CAMS-I2M) [2016-I2M-1-007].

SUPPLEMENTARY MATERIAL

The Supplementary Material for this article can be found online at: https://www.frontiersin.org/articles/10.3389/fonc.2021.771545/full#supplementary-material

REFERENCES

1. Bray F, Ferlay J, Soerjomataram I, Siegel RL, Torre LA, Jemal A. Global Cancer Statistics 2018: GLOBOCAN Estimates of Incidence and Mortality Worldwide for 36 Cancers in 185 Countries. *CA Cancer J Clin* (2018) 68 (6):394–424. doi: 10.3322/caac.21492
2. Blute ML, Leibovich BC, Lohse CM, Cheville JC, Zincke H. The Mayo Clinic Experience With Surgical Management, Complications and Outcome for Patients With Renal Cell Carcinoma and Venous Tumour Thrombus. *BJU Int* (2004) 94(1):33–41. doi: 10.1111/j.1464-410X.2004.04897.x
3. Pouliot F, Shuch B, Larochelle JC, Pantuck A, Belldegrun AS. Contemporary Management of Renal Tumors With Venous Tumor Thrombus. *J Urol* (2010) 184(3):833–41; quiz 1235. doi: 10.1016/j.juro.2010.04.071
4. Baboudjian M, Gondran-Tellier B, Khene Z, Bigot P, Mejean A, Lang H, et al. Predictive Factors of Recurrence After Surgery in Patients With Non-Metastatic Renal Cell Carcinoma With Venous Tumor Thrombus (UroCCR-56 Study). *World J Urol* (2021). doi: 10.1007/s00345-021-03640-6
5. Sidana A, Goyal J, Aggarwal P, Verma P, Rodriguez R. Determinants of Outcomes After Resection of Renal Cell Carcinoma With Venous Involvement. *Int Urol Nephrol* (2012) 44(6):1671–9. doi: 10.1007/s11255-012-0314-x
6. Wang BS, Ma RZ, Liu YQ, Liu Z, Tao LY, Lu M, et al. Body Mass Index as an Independent Risk Factor for Inferior Vena Cava Resection During Thrombectomy for Venous Tumor Thrombus of Renal Cell Carcinoma. *World J Surg Oncol* (2019) 17(1):17. doi: 10.1186/s12957-019-1560-5
7. Xiao R, Xu C, He W, Liu L, Zhang H, Liu C, et al. Preoperative Anaemia and Thrombocytosis Predict Adverse Prognosis in Non-Metastatic Renal Cell Carcinoma With Tumour Thrombus. *BMC Urol* (2021) 21(1):31. doi: 10.1186/s12894-021-00796-6
8. Cho MC, Kim JK, Moon KC, Kim HH, Kwak C. Prognostic Factor for Korean Patients With Renal Cell Carcinoma and Venous Tumor Thrombus Extension: Application of the New 2009 TNM Staging System. *Int Braz J Urol* (2013) 39(3):353–63. doi: 10.1590/S1677-5538.IBJU.2013.03.08
9. Agizamhan S, Qu F, Liu N, Sun J, Xu W, Zhang L, et al. Preoperative Neutrophil-to-Lymphocyte Ratio Predicts the Surgical Outcome of Xp11.2 Translocation/TFE3 Renal Cell Carcinoma Patients. *BMC Urol* (2018) 18 (1):60. doi: 10.1186/s12894-018-0374-z
10. Rebuzzi SE, Signori A, Banna GL, Maruzzo M, De Giorgi U, Pedrazzoli P, et al. Inflammatory Indices and Clinical Factors in Metastatic Renal Cell Carcinoma Patients Treated With Nivolumab: The Development of a Novel Prognostic Score (Meet-URO 15 Study). *Ther Adv Med Oncol* (2021) 13:17588359211019642. doi: 10.1177/17588359211019642
11. Hiam-Galvez KJ, Allen BM, Spitzer MH. Systemic Immunity in Cancer. *Nat Rev Cancer* (2021) 21(6):345–59. doi: 10.1038/s41568-021-00347-z
12. Peyton CC, Abel EJ, Chipollini J, Boulware DC, Azizi M, Karam JA, et al. The Value of Neutrophil to Lymphocyte Ratio in Patients Undergoing Cytoreductive Nephrectomy With Thrombectomy. *Eur Urol Focus* (2020) 6 (1):104–11. doi: 10.1016/j.euf.2018.08.023
13. Castanheira FVS, Kubes P. Neutrophils and NETs in Modulating Acute and Chronic Inflammation. *Blood* (2019) 133(20):2178–85. doi: 10.1182/blood-2018-11-844530
14. Brinkmann V, Reichard U, Goosmann C, Fauler B, Uhlemann Y, Weiss DS, et al. Neutrophil Extracellular Traps Kill Bacteria. *Science* (2004) 303 (5663):1532–5. doi: 10.1126/science.1092385
15. Wang J. Neutrophils in Tissue Injury and Repair. *Cell Tissue Res* (2018) 371 (3):531–9. doi: 10.1007/s00441-017-2785-7
16. Cools-Lartigue J, Spicer J, McDonald B, Gowing S, Chow S, Giannias B, et al. Neutrophil Extracellular Traps Sequester Circulating Tumor Cells and Promote Metastasis. *J Clin Invest* (2013) 123(8):3445–58. doi: 10.1172/JCI67484
17. Lee W, Ko SY, Mohamed MS, Kenny HA, Lengyel E, Naora H. Neutrophils Facilitate Ovarian Cancer Premetastatic Niche Formation in the Omentum. *J Exp Med* (2019) 216(1):176–94. doi: 10.1084/jem.20181170
18. Wen L, Guo L, Zhang W, Li Y, Jiang W, Di X, et al. Cooperation Between the Inflammation and Coagulation Systems Promotes the Survival of Circulating Tumor Cells in Renal Cell Carcinoma Patients. *Front Oncol* (2019) 9:504(504). doi: 10.3389/fonc.2019.00504
19. Pfeiler S, Stark K, Massberg S, Engelmann B. Propagation of Thrombosis by Neutrophils and Extracellular Nucleosome Networks. *Haematologica* (2017) 102(2):206–13. doi: 10.3324/haematol.2016.142471
20. Thalin C, Demers M, Blomgren B, Wong SL, von Arbin M, von Heijne A, et al. NETosis Promotes Cancer-Associated Arterial Microthrombosis Presenting as Ischemic Stroke With Troponin Elevation. *Thromb Res* (2016) 139:56–64. doi: 10.1016/j.thromres.2016.01.009
21. Demers M, Krause DS, Schatzberg D, Martinod K, Voorhees JR, Fuchs TA, et al. Cancers Predispose Neutrophils to Release Extracellular DNA Traps That Contribute to Cancer-Associated Thrombosis. *Proc Natl Acad Sci USA* (2012) 109(32):13076–81. doi: 10.1073/pnas.1200419109

22. Wolach O, Sellar RS, Martinod K, Cherpokova D, McConkey M, Chappell RJ, et al. Increased Neutrophil Extracellular Trap Formation Promotes Thrombosis in Myeloproliferative Neoplasms. *Sci Transl Med* (2018) 10 (436). doi: 10.1126/scitranslmed.aan8292
23. Boone BA, Murthy P, Miller-Ocuin J, Doerfler WR, Ellis JT, Liang X, et al. Chloroquine Reduces Hypercoagulability in Pancreatic Cancer Through Inhibition of Neutrophil Extracellular Traps. *BMC Cancer* (2018) 18(1):678. doi: 10.1186/s12885-018-4584-2
24. Patro R, Duggal G, Love MI, Irizarry RA, Kingsford C. Salmon Provides Fast and Bias-Aware Quantification of Transcript Expression. *Nat Methods* (2017) 14(4):417–9. doi: 10.1038/nmeth.4197
25. Guo L, Bi X, Li Y, Wen L, Zhang W, Jiang W, et al. Characteristics, Dynamic Changes, and Prognostic Significance of TCR Repertoire Profiling in Patients With Renal Cell Carcinoma. *J Pathol* (2020) 251(1):26–37. doi: 10.1002/path.5396
26. Senbabaoglu Y, Gejman RS, Winer AG, Liu M, Van Allen EM, de Velasco G, et al. Tumor Immune Microenvironment Characterization in Clear Cell Renal Cell Carcinoma Identifies Prognostic and Immunotherapeutically Relevant Messenger RNA Signatures. *Genome Biol* (2016) 17(1):231. doi: 10.1186/s13059-016-1092-z
27. Motzer RJ, Banchereau R, Hamidi H, Powles T, McDermott D, Atkins MB, et al. Molecular Subsets in Renal Cancer Determine Outcome to Checkpoint and Angiogenesis Blockade. *Cancer Cell* (2020) 38(6):803–17 e4. doi: 10.1016/j.ccell.2020.10.011
28. Subramanian A, Tamayo P, Mootha VK, Mukherjee S, Ebert BL, Gillette MA, et al. Gene Set Enrichment Analysis: A Knowledge-Based Approach for Interpreting Genome-Wide Expression Profiles. *Proc Natl Acad Sci USA* (2005) 102(43):15545–50. doi: 10.1073/pnas.0506580102
29. Langfelder P, Horvath S. WGCNA: An R Package for Weighted Correlation Network Analysis. *BMC Bioinf* (2008) 9:559. doi: 10.1186/1471-2105-9-559
30. Yu G, Wang LG, Han Y, He QY. Clusterprofiler: An R Package for Comparing Biological Themes Among Gene Clusters. *OMICS* (2012) 16(5):284–7. doi: 10.1089/omi.2011.0118
31. Arpinati L, Shaul ME, Kaisar-Iluz N, Mali S, Mahroum S, Fridlender ZG. NETosis in Cancer: A Critical Analysis of the Impact of Cancer on Neutrophil Extracellular Trap (NET) Release in Lung Cancer Patients vs. Mice. *Cancer Immunol Immunother* (2020) 69(2):199–213. doi: 10.1007/s00262-019-02474-x
32. Strauss A, Uhlig J, Lotz J, Trojan L, Uhlig A. Tumor Laterality in Renal Cancer as a Predictor of Survival in Large Patient Cohorts: A STROBE Compliant Study. *Med (Baltimore)* (2019) 98(17):e15346. doi: 10.1097/MD.0000000000015346
33. Thiel DD, Lohse CM, Arnold ML, Cheville JC, Leibovich BC, Parker AS. Does Left Side Renal Cell Carcinoma (RCC) With Renal Vein/Vena Cava Thrombus Predict Worse Prognosis Than Equivalent Right Side RCC Tumor Thrombus? *Int Urol Nephrol* (2012) 44(4):1005–12. doi: 10.1007/s11255-012-0168-2
34. Ravaud A, Motzer RJ, Pandha HS, George DJ, Pantuck AJ, Patel A, et al. Adjuvant Sunitinib in High-Risk Renal-Cell Carcinoma After Nephrectomy. *N Engl J Med* (2016) 375(23):2246–54. doi: 10.1056/NEJMoa1611406
35. Choueiri TK, Tomczak P, Park SH, Venugopal B, Ferguson T, Chang YH, et al. Adjuvant Pembrolizumab After Nephrectomy in Renal-Cell Carcinoma. *N Engl J Med* (2021) 385(8):683–94. doi: 10.1056/NEJMoa2106391
36. Vuong L, Kotecha RR, Voss MH, Hakimi AA. Tumor Microenvironment Dynamics in Clear-Cell Renal Cell Carcinoma. *Cancer Discovery* (2019) 9 (10):1349–57. doi: 10.1158/2159-8290.CD-19-0499
37. Wang J, Liu L, Bai Q, Ou C, Xiong Y, Qu Y, et al. Tumor-Infiltrating Neutrophils Predict Therapeutic Benefit of Tyrosine Kinase Inhibitors in Metastatic Renal Cell Carcinoma. *Oncoimmunology* (2019) 8(1):e1515611. doi: 10.1080/2162402X.2018.1515611
38. Fridman WH, Zitvogel L, Sautes-Fridman C, Kroemer G. The Immune Contexture in Cancer Prognosis and Treatment. *Nat Rev Clin Oncol* (2017) 14(12):717–34. doi: 10.1038/nrclinonc.2017.101
39. Albrengues J, Shields MA, Ng D, Park CG, Ambrico A, Poindexter ME, et al. Neutrophil Extracellular Traps Produced During Inflammation Awaken Dormant Cancer Cells in Mice. *Science* (2018) 361(6409). doi: 10.1126/science.aao4227
40. Yang L, Liu Q, Zhang X, Liu X, Zhou B, Chen J, et al. DNA of Neutrophil Extracellular Traps Promotes Cancer Metastasis *via* CCDC25. *Nature* (2020) 583(7814):133–8. doi: 10.1038/s41586-020-2394-6
41. Iriondo O, Yu M. Unexpected Friendship: Neutrophils Help Tumor Cells En Route to Metastasis. *Dev Cell* (2019) 49(3):308–10. doi: 10.1016/j.devcel.2019.04.021
42. Lardas M, Stewart F, Scrimgeour D, Hofmann F, Marconi L, Dabestani S, et al. Systematic Review of Surgical Management of Nonmetastatic Renal Cell Carcinoma With Vena Caval Thrombus. *Eur Urol* (2016) 70(2):265–80. doi: 10.1016/j.eururo.2015.11.034
43. Yost CC, Schwertz H, Cody MJ, Wallace JA, Campbell RA, Vieira-de-Abreu A, et al. Neonatal NET-Inhibitory Factor and Related Peptides Inhibit Neutrophil Extracellular Trap Formation. *J Clin Invest* (2016) 126 (10):3783–98. doi: 10.1172/JCI83873
44. Okeke EB, Louttit C, Fry C, Najafabadi AH, Han K, Nemzek J, et al. Inhibition of Neutrophil Elastase Prevents Neutrophil Extracellular Trap Formation and Rescues Mice From Endotoxic Shock. *Biomaterials* (2020) 238:119836. doi: 10.1016/j.biomaterials.2020.119836
45. Kajioka H, Kagawa S, Ito A, Yoshimoto M, Sakamoto S, Kikuchi S, et al. Targeting Neutrophil Extracellular Traps With Thrombomodulin Prevents Pancreatic Cancer Metastasis. *Cancer Lett* (2021) 497:1–13. doi: 10.1016/j.canlet.2020.10.015
46. Diaz-Montero CM, Rini BI, Finke JH. The Immunology of Renal Cell Carcinoma. *Nat Rev Nephrol* (2020) 16(12):721–35. doi: 10.1038/s41581-020-0316-3
47. Riemann D, Cwikowski M, Turzer S, Giese T, Grallert M, Schutte W, et al. Blood Immune Cell Biomarkers in Lung Cancer. *Clin Exp Immunol* (2019) 195(2):179–89. doi: 10.1111/cei.13219
48. Morizawa Y, Miyake M, Shimada K, Hori S, Tatsumi Y, Nakai Y, et al. Correlation of Immune Cells and Cytokines in the Tumor Microenvironment With Elevated Neutrophil-To-Lymphocyte Ratio in Blood: An Analysis of Muscle-Invasive Bladder Cancer. *Cancer Invest* (2018) 36(7):395–405. doi: 10.1080/07357907.2018.1506800
49. Zhou Y, Leng X, Mo C, Zou Q, Liu Y, Wang Y. The P53 Effector Perp Mediates the Persistence of CD4(+) Effector Memory T-Cell Undergoing Lymphopenia-Induced Proliferation. *Immunol Lett* (2020) 224:14–20. doi: 10.1016/j.imlet.2020.05.001
50. Ellestad KK, Anderson CC. Two Strikes and You're Out? The Pathogenic Interplay of Coinhibitor Deficiency and Lymphopenia-Induced Proliferation. *J Immunol* (2017) 198(7):2534–41. doi: 10.4049/jimmunol.1601884
51. Lythe G, Callard RE, Hoare RL, Molina-Paris C. How Many TCR Clonotypes Does a Body Maintain? *J Theor Biol* (2016) 389:214–24. doi: 10.1016/j.jtbi.2015.10.016
52. Grossman Z, Min B, Meier-Schellersheim M, Paul WE. Concomitant Regulation of T-Cell Activation and Homeostasis. *Nat Rev Immunol* (2004) 4(5):387–95. doi: 10.1038/nri1355

Conflict of Interest: The authors declare that the research was conducted in the absence of any commercial or financial relationships that could be construed as a potential conflict of interest.

Publisher's Note: All claims expressed in this article are solely those of the authors and do not necessarily represent those of their affiliated organizations, or those of the publisher, the editors and the reviewers. Any product that may be evaluated in this article, or claim that may be made by its manufacturer, is not guaranteed or endorsed by the publisher.

Copyright © 2021 Shang, Guo, Shen, Cao, Xie, Jiang, Wen, Bi, Shi, Zheng, Li, Ma, Zhang, Feng and Shou. This is an open-access article distributed under the terms of the Creative Commons Attribution License (CC BY). The use, distribution or reproduction in other forums is permitted, provided the original author(s) and the copyright owner(s) are credited and that the original publication in this journal is cited, in accordance with accepted academic practice. No use, distribution or reproduction is permitted which does not comply with these terms.

frontiers in Oncology

ORIGINAL RESEARCH
published: 22 December 2021
doi: 10.3389/fonc.2021.795837

Evaluation of Serum miR-17-92 Cluster as Noninvasive Biomarkers for Bladder Cancer Diagnosis

Jingyao Wang[1†], *Xiqi Peng*[1,2†], *Rongkang Li*[1,3†], *Kaihao Liu*[1,3], *Chunduo Zhang*[1], *Xuan Chen*[1,2], *Guocheng Huang*[1,2], *Liwen Zhao*[1,3], *Zebo Chen*[4*] and *Yongqing Lai*[1,3*]

[1] Department of Urology, Guangdong and Shenzhen Key Laboratory of Male Reproductive Medicine and Genetics, Peking University Shenzhen Hospital, Shenzhen, China, [2] Shantou University Medical College, Shantou, China, [3] Anhui Medical University, Hefei, China, [4] Department of Urology, Peking University Shenzhen Hospital, Shenzhen, China

OPEN ACCESS

Edited by:
Elena Ranieri,
University of Foggia, Italy

Reviewed by:
Felice Crocetto,
Federico II University Hospital, Italy
Giuseppe Simone,
Regina Elena National Cancer Institute (IRCCS), Italy

***Correspondence:**
Yongqing Lai
yqlord@163.com
Zebo Chen
szchenzebo@sina.com

[†]These authors have contributed equally to this work and share first authorship

Specialty section:
This article was submitted to Genitourinary Oncology, a section of the journal Frontiers in Oncology

Received: 15 October 2021
Accepted: 29 November 2021
Published: 22 December 2021

Citation:
Wang J, Peng X, Li R, Liu K, Zhang C, Chen X, Huang G, Zhao L, Chen Z and Lai Y (2021) Evaluation of Serum miR-17-92 Cluster as Noninvasive Biomarkers for Bladder Cancer Diagnosis. Front. Oncol. 11:795837. doi: 10.3389/fonc.2021.795837

Previous studies have shown that the miR-17-92 cluster is involved in the occurrence and development of bladder cancer. However, the role of serum miR-17-92 cluster in the diagnosis of bladder cancer has not been studied. In the present study, we evaluated the expression of miR-17-92 cluster members in bladder cancer tissues by analyzing 428 cases from TCGA database. Next, we collected the sera of 74 bladder cancer patients and 90 controls, and used qRT-PCR to detect the relative expression of the cluster. The results showed that the expression of the cluster members in the sera of patients were significantly higher than that of the controls, and they were positively correlated with the clinical stage and pathological grade of the patients. We evaluated their ability to diagnose bladder cancer using ROC, of which miR-92a-3p (AUC = 0.902), miR-17-5p (AUC = 0.845) and miR-20a-5p (AUC = 0.806) were the most prominent. Finally, we established a diagnostic model by logistic regression (AUC = 0.969). We further validated the results of the study using another dataset from the GEO database. Moreover, we evaluated the prognostic value of the cluster. The results revealed that miR-20a-5p was correlated with recurrence of bladder cancer. In summary, the present study validated the overexpression of serum miR-17-92 cluster in bladder cancer. The model composed of the three cluster members were confirmed to be a promising noninvasive biomarker for bladder cancer diagnosis.

Keywords: bladder cancer, circulating biomarker, non-invasive detection, diagnosis, logistic regression model

INTRODUCTION

Bladder cancer (BC) is the sixth most common cancer worldwide, with the eighth highest mortality rate (1). Unfortunately, little improvement in the diagnosis and treatment of BC has been made over the past three decades, unlike many other tumors (2). The main reason was that the existing diagnostic methods for BC cannot meet the needs of clinical work. A good BC diagnosis method can not only help the early diagnosis and treatment of BC, but can also monitor the recurrence after surgery. At present, cystoscopy is the gold standard for detecting BC, but its detection method is invasive (3). It is usually accompanied by risks of bleeding, UTI, and difficulty urinating, so it is not

suitable for early cancer screening. Also, long-term frequent cystoscopy after surgery will bring a great mental burden to patients (4). Therefore, it is necessary to find new feasible diagnostic methods for BC.

In recent years, the research on BC diagnostic biomarkers has aroused great interest, but most of them has not yet been clinically available (5, 6). Biomarkers with high specificity and sensitivity from body fluids may be effective tools for non-invasive BC detection.

microRNAs (miRNAs) are small non-coding and endogenous RNAs which can bind to the 3′-UTR of target mRNAs, regulate gene expression and thus lead to mRNA degradation or translation inhibition (7, 8). Mounting evidence has shown that circulating miRNAs are promising biomarkers for tumor detection for the reason that miRNAs can be stably detected in circulating blood (9–11).

Many miRNAs are located in polycistronic miRNA "clusters", where multiple miRNAs are produced from a single primary transcript. The miR-17-92 cluster, also named as oncomiR-1, is a frequently amplified locus in cancer (12). The cluster encodes six mature miRNAs: miR-17-5p, miR-18a-5p, miR-19a-3p, miR-20a-5p, miR-19b-3p and miR-92a-3p. Many studies have reported that members of the miR-17-92 cluster are upregulated in BC cells and play a carcinogenic role (13–17). Therefore, we want to know whether this cluster can be used as new circulating markers to diagnose BC.

In the present study, we tested the relative expression levels of miR-17-92 cluster members in BC tissues and patient sera. We evaluated the diagnostic ability of serum miR-17-92 cluster. We also constructed a three-miRNA model, which has a high sensitivity and specificity for BC diagnosis. These results were also confirmed in the external verification set. Furtherly, we explored the relationship between the cluster and BC recurrence.

MATERIALS AND METHODS

Study Design

We firstly tested the differential expression of the miR-17-92 cluster (miR-17-5p, miR-18a-5p, miR-19a-3p, miR-20a-5p, miR-19b-3p and miR-92a-3p) in BC and adjacent normal bladder tissues using data from The Cancer Genome Atlas (TCGA) database. We then analyzed the differential expression of circulating miR-17-92 cluster in the sera from 74 BC patients and 90 healthy controls (HCs) using the quantitative reverse transcription-polymerase chain reaction (qRT-PCR) method. Also, we discovered the expression trends of miR-17-92 cluster members of BC patients with different pathological grades and stages. We evaluated the diagnostic ability of miR-17-92 cluster by ROC analysis. A logistic regression model was established to enhance the sensitivity and specificity of diagnosis. A GEO dataset (including 492 samples) was used as an external validation set to furtherly confirmed the diagnostic value of serum miR-17-92 cluster in BC. We also test the expression of the cluster in BC cell lines and a normal transitional epithelial cell line (SV-HUC-1). The culture medium was used to illustrate the origin of circulating miRNAs. Moreover, Cox regression analysis and Kaplan-Meier analysis were used to evaluate their relationship with BC recurrence. The design of this study was shown in **Figure 1**.

Enrollment of Participants

The present study enrolled a total of 74 BC patients from Peking University Shenzhen Hospital between June 2017 and July 2019. All serum samples were collected before accepting any treatment. The histological grade was classified according to the standards of World Health Organization. The tumor stage was confirmed based the TNM staging system. We enrolled a total of 90 HCs who came to the hospital for physical examination and had no history to tumors and other diseases. The age and gender of HCs and BC patients were matched. The demographic and clinical characteristics of the participants was listed in **Table 1**. No significant differences were found in age or gender distribution among BC and HCs group ($p > 0.05$). All participants in this study had signed informed consent forms before their blood samples being collected, and agreed to be included in this study. This study had been approved by the Ethics Committee of Peking University Shenzhen Hospital. The study was processed following the Declaration of Helsinki. The specimen collection process was implemented according to regulations of the committee.

Data Acquisition

We obtained the miRNA-sequencing data of the Bladder Urothelial Carcinoma (BLCA) from TCGA database, which contained 19 normal bladder epithelial tissues, 409 bladder urothelial carcinoma tissues. The corresponding clinical information of the patients were also obtained. A serum miRNA expression profile matrix GSE113486, which consist of serum samples from multiple tumors and normal controls, were downloaded from the GEO database. It was performed on GPL21263 Toray Industries platform. The expression data and clinical information of 392 BC patients and 100 non-cancer controls inside it were utilized in our study. All miRNA expression data were standardized and log2 transformation for further analysis.

Serum Sample Collection

We collected 10ml peripheral blood of each participant before their accepting any treatment. The peripheral blood was centrifuged at 1000 g for 10 minutes and 15,000 g for 5 minutes at 4°C within 2 hours. 2 μl of 10 nmol/L synthetic C. Elegans miRNA-39 (RiboBio, Guangzhou, China) was spiked into each serum sample before the experiments to control the variability during the extraction and purification process.

Cell Culture

The normal transitional epithelial cell (SV-HUC-1) and BC cell lines including RT4, J82, UM-UC-3, 5637 and T24, were obtained from Shanghai Institute of Biochemistry and Cell Biology (Shanghai, China). The cells were maintained in Dulbecco's modified Eagle's medium (DMEM; Gibco; Thermo Fisher Scientific. Inc., Waltham, MA, USA) or RPMI-1640 (Gibco; Thermo Fisher Scientific, Inc., Waltham, MA, USA)

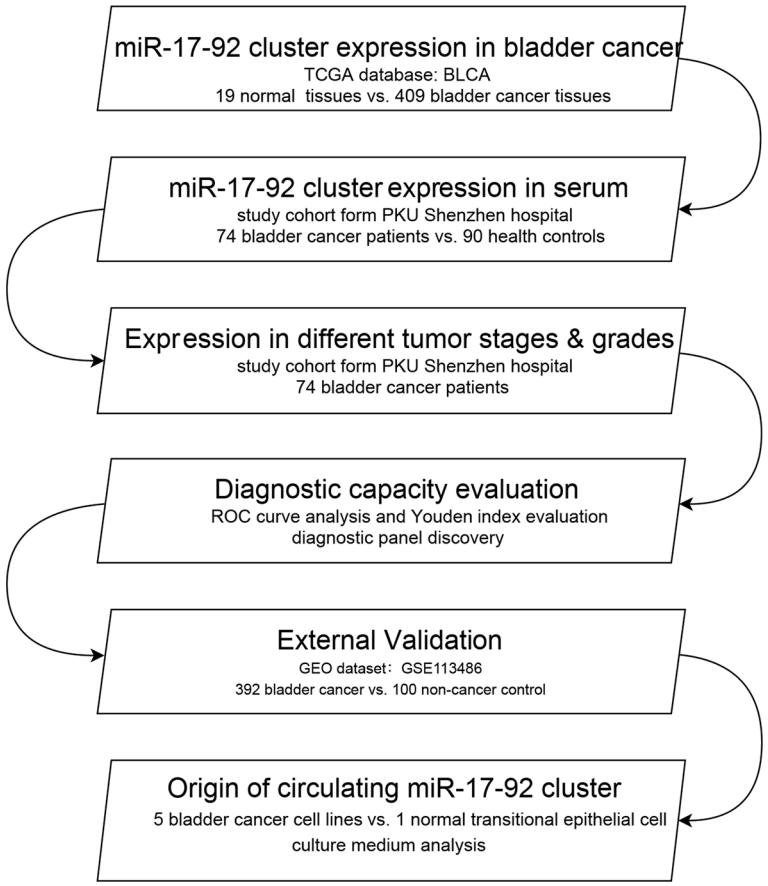

FIGURE 1 | The flowchart of the study design. BLCA, bladder urothelial carcinoma; ROC, receiver operating characteristic.

supplemented with fetal bovine serum (FBS; 10% Gibco; Thermo Fisher Scientific, Inc.), antibiotics (1% 100 μl/ml penicillin and 100 mg/ml streptomycin sulfates) and glutamine (1%) in 37°C with 5% CO2. We collected the culture media from culture plates after the cells were cultivated for 24h, 48h, and 72h.

RNA Extraction and Quantitative Reverse Transcription-Polymerase Chain Reaction

Total RNA was extracted from sera, cell lines and culture media using the TRIzol LS isolation kit (Thermo Fisher Scientific, Waltham, MA, USA) in accordance with the manufacturer's

TABLE 1 | Demographic and clinical characteristics of 164 participants enrolled in the study.

	BC patients	HCs
Total number	74	90
Age (Mean ± SD)	63.8 ± 13.5	56.6 ± 13.1
Gender (%)		
Male	54 (73.0)	42 (46.7)
Female	20 (27.0)	48 (53.3)
Tumor stage (%)		
TaN0M0	26 (35.1)	
T1N0M0	30 (40.5)	
T2N0M0	13 (17.6)	
≥pT3	5 (6.8)	
Pathological grade (%)		
Low grade	35 (47.3)	
High grade	39 (52.7)	

BC, bladder cancer; HCs, healthy controls.

instructions. Later, total RNA was resuspended with 30 μl RNase-free water and stored at −80°C for further experiments. Using the NanoDrop 2000 spectrophotometer (NanoDrop, Wilmington, DE, USA), we evaluated the concentration and purity of the extracted RNA.

The amplification of miRNAs was conducted using the specific reverse transcription primers from Bulge-Loop miRNA qRT-PCR Primer Set (RiboBio, Guangzhou, China). The real-time polymerase chain reaction was performed using SYBR Green qPCR kit (SYBR Pre-mix Ex Taq II, TaKaRa) in 384-well plates on LightCycler 480 Real-Time PCR System (Roche Diagnostics, Mannheim, Germany) at 95°C for 30 s, followed by 35 cycles in 95°C for 10 s, 60°C for 20 s and then 70°C for 10 s. The specificity of the PCR product was confirmed by melting curve analysis at last. The relative expression levels of target miRNAs were calculated by the $2-\triangle\triangle Cq$ method (18) and normalized to the spiked-in control cel-miR-39. All reactions had repeated three times or more.

Statistical Analysis

The differential expression of each miRNA between BC and HCs groups were analyzed using Students' T-test or Mann–Whitney U test. Multiple comparisons among different phases were analyzed using the Kruskal-Wallis rank test. Binary logistic regression analysis was performed to build the miRNA signature. And we evaluated the calibration by the Hosmer-Lemeshow goodness-of-fit test. Thee diagnostic ability of the miRNAs were evaluated by Receiver operating characteristic (ROC) curves and the area under the ROC curve (AUC). The optimal cut-off was determined by the Youden index (calculated as J = Sensitivity + Specificity − 1). Cox regression analysis and Kaplan-Meier analysis were used for prognostic analysis. We evaluated the calibration using the Hosmer-Lemeshow goodness-of-fit test. We used Receiver operating characteristic (ROC) curves and the area under the ROC curve (AUC) to evaluate the diagnostic ability of miRNAs. The Youden index was used to determine the optimal cut-off (Youden index= Sensitivity + Specificity − 1). Cox regression analysis and Kaplan-Meier analysis were used for prognostic analysis. All statistical analyses in this study were performed using SPSS software (Version 20, Chicago, USA), GraphPad Prism (Version 8, LaJolla, CA), and Medcalc (Version 19, Ostend, Belgium). Differences were considered to be significant when p-value was less than 0.05.

RESULTS

Expression of miR-17-92 Cluster Members Was Remarkably Elevated in BC

We downloaded miRNA-isoform sequencing data of BLCA from the TCGA database, including 409 bladder cancer tissues and 19 normal bladder epithelium tissues. The differential expression ratio (logFC) and expression level (logTPM) of miR-17-92 cluster in BC tissues and para-carcinoma tissues are shown in **Table 2**. The higher the fold change (FC) value indicates the greater the difference in expression of the miRNA between the two groups, and it can better distinguish the two groups of samples. The higher the TPM value indicates the higher the expression level of the miRNA, which means it can be found in a smaller amount of sample. As shown in **Figure 2**, all 6 members of the miR-17-92 cluster are highly upregulated in BC tissues. The TPM value of miR-92a-3p is the highest among all. Such results support previous studies that the miR-17-92 cluster may play a carcinogenic role in BC.

We detected the miR-17-92 cluster relative expression levels of the preoperative sera of 74 BC patients and the sera of 90 HCs. The results were consistent with tissue. As shown in **Figure 3** and **Table 2**, all members in miR-17-92 cluster were enriched in sera of BC patients. Among them, the expression differences of miR-18a-5p and miR-19a-3p in the two groups of sera were relatively small ($0.05>P> 0.01$), while the other miR-17-92 cluster members were significantly enriched in the sera of BC patients ($P<0.01$).

Expression of miR-17-92 Cluster Members in Sera of Patients With Different Stages and Grades

We divided the 74 BC patients from our cohort into four groups based on different clinical stages, and into two groups based on different pathological grades. There were 5 patients with ≥pT3, 13 T2N0M0 patients, 30 T1N0M0 patients, and 26 TaN0M0 patients. There were 39 high-grade and 35 low-grade BC patients. The expression levels of miR-17-5p, miR-18a-5p, miR-20a-5p and miR-92a-3p in patients' sera were significantly positively correlated with patients' clinical grade (**Figure 4A**). But for miR-19a-3p and miR-19b-3p, this trend is not obvious. The expression levels of miR-17-5p, miR-20a-5p and miR-92a-3p in the sera of high-grade BC patients are much higher than those in low-grade patients (**Figure 4B**). The expression of serum miR-18a-5p, miR-19a-3p and miR-19b-3p was not related to BC pathological grade.

TABLE 2 | The expression profiles of miR-17-92 cluster members in BC tissues and patient sera.

miRNAs	Tissue (TCGA-BLCA)			Serum (PKU-shenzhen hospital)			Serum (GSE113486)		
	logFC	FDR	logTPM	logFC	p-value	AveCT	logFC	FDR	AveExpr
miR-17-5p	2.07	<0.01	9.37	1.81	<0.01	17.34	2.30	<0.01	2.02
miR-18a-5p	2.55	<0.01	4.97	1.34	0.03	20.10	2.64	<0.01	1.41
miR-19a-3p	1.93	<0.01	5.38	1.33	0.02	21.09	3.14	<0.01	0.56
miR-20a-5p	1.92	<0.01	8.89	1.93	<0.01	19.57	2.56	<0.01	1.45
miR-19b-3p	1.28	<0.01	7.57	1.71	<0.01	17.89	2.60	<0.01	2.26
miR-92a-3p	0.98	<0.01	13.72	1.89	<0.01	16.11	2.18	<0.01	6.32

FC, fold change; FDR, false discovery rate; TPM, Transcripts Per Kilobase of exonmodel per Million mapped reads; AveCT, average CT value; AveExpr, average expression.

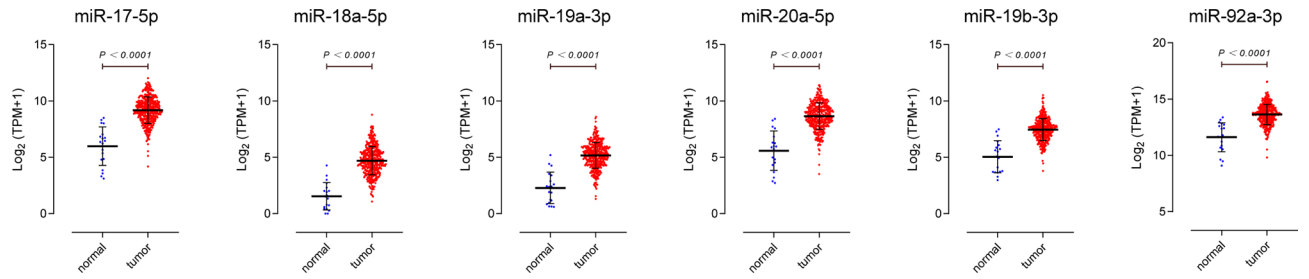

FIGURE 2 | Expression profiles of miR-17-92 cluster members in bladder cancer tissues. Data were downloaded from The Cancer Genome Atlas database, including 19 para-carcinoma tissues (normal), 409 bladder urothelial carcinoma tissues(tumor).

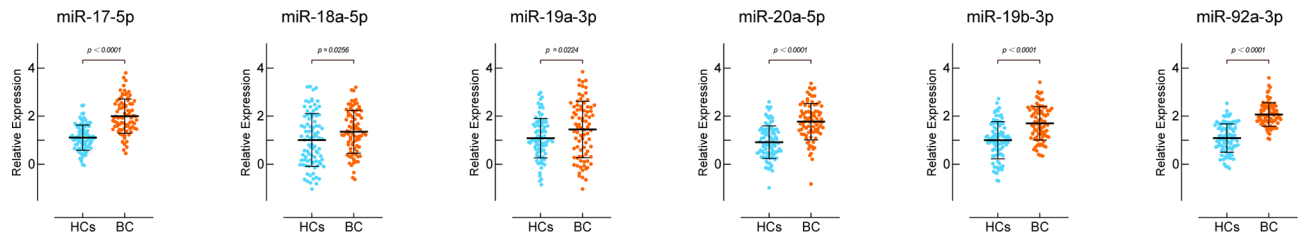

FIGURE 3 | Expression of miR-17-92 cluster members in the sera of bladder cancer patients. HCs group includes sera of 90 healthy controls and BC group includes sera of 74 patients.

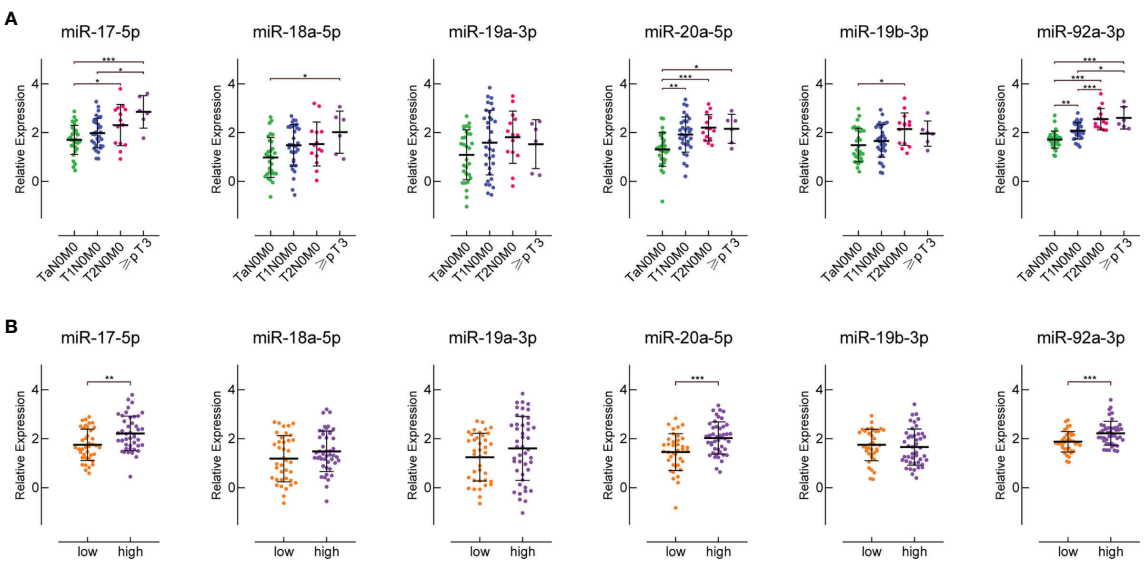

FIGURE 4 | The expression of miR-17-92 cluster members in the sera of patients with different clinical stages and pathological grades. **(A)** shows their expression in the sera of patients with different clinical stages. There are 26 TaN0M0 patients, 30 T1N0M0 patients, 13 T2N0M0 patients, and 5 patients with ≥pT3. **(B)** shows their expression in the sera of patients with different pathological grades. There are 35 low-grade and 39 high-grade BC patients. *P < 0.05, **P < 0.01, ***P < 0.001.

Evaluation of the Diagnostic Ability of miR-17-92 Cluster Members in BC

To assess the diagnostic value of the serum miR-17-92 cluster members in discriminating BC patients from healthy controls, ROC curve analyses were conducted. As shown in **Figure 5A** and **Table 3**, of the six miR-17-92 cluster members investigated, serum miR-92a-3p exhibited the highest accuracy in diagnosing BC, with an AUC of 0.902 (p = 0.022). Serum miR-17-5p (AUC = 0.845), miR-20a-5p (AUC = 0.806) and miR-19b-3p (AUC = 0.741) have moderate diagnostic ability. In contrast, serum miR-18a-5p (AUC = 0.597) and miR-19a-3p (AUC = 0.596) BC diagnosis ability is very low.

Construction of BC Diagnostic Model

Usually, one single biomarker is unable to achieve great sensitivity and specificity simultaneously. To achieve better diagnostic ability, it is practicable to combine several miRNAs into one diagnostic model. Therefore, we selected three miRNAs (miR-17-5p, miR-20a-5p and miR-92a-3p) with AUC over 0.8 to construct a diagnostic model using the stepwise logistic regression method. We found that the AUC for the three-miRNA model was 0.969 (95% CI: 0.931 - 0.989; sensitivity = 90.36%, specificity = 94.44%; **Figure 5B**). The Hosmer-Lemeshow P value of the model was 0.885, suggesting adequate calibration. The model was calculated with the formula:

$$\text{Logit}(P) = 2.43 \times \text{Exp}_{\text{miR-17-5p}} + 1.64 \times \text{Exp}_{\text{miR-20a-5p}} + 3.51 \times \text{Exp}_{\text{miR-92a-3p}} - 11.60$$

External Validation of miR-17-92 Cluster Expression in Sera of BC Patients

To further prove our results, GSE113486 was used as the external validation set for this study. GSE113486 contained 392 BC serum samples and 100 control serum samples. **Figure 6** shows the signal intensity of miR-17-92 cluster members in each group of samples. Affected by the sensitivity of gene microarray detection and the low titer of miRNA expression in serum, many cases of the miR-17-92 cluster members were undetected, both in the tumor and the control group. However, this situation had no much effect on the results. The results in **Table 2** show that the logFC values of miR-17-92 cluster members were all above 2, meaning they were significantly up-regulated in the sera of BC patients from the external validation set. But their absolute expression levels in serum are different. For example, the average expression level of miR-19a-3p is only 0.56, indicating that it is low both in the sera of patients and in the sera of controls. In contrast, the average expression level of miR-92a-3p is 6.32, indicating that it has a high basal content in serum and is more suitable as a biomarker.

Origin of Serum miR-17-92 Cluster

To verify the hypothesis that serum miR-17-92 cluster was released into circulation by BC tumor cells, we detected the miR-17-92 cluster relative expression levels in a normal transitional epithelial cell line SV-HUC-1 and 5 BC cell lines. The results showed that miR-17-5p, miR-18a-5p, miR-20a-5p, miR-19b-3p, miR-92a-3p were significantly upregulated in three or more BC cell lines, especially in 5637, T24 and UM-UC-3 (**Supplementary Figure S1A**). miR-19a-3p was only upregulated in UM-UC-3 cell line. Later, we detect miR-17-92 cluster expression in the culture media at different time points after cultivation. We observed that expression level of the miR-17-92 cluster from culture media of 5637, UM-UC-3 and T24 cell lines increased with time while no obvious change was found in normal transitional epithelial cell line SV-HUC-1 culture media (**Supplementary Figure S1B**). These results indicated that BC-related miR-17-92 cluster could enter into the cell culture media.

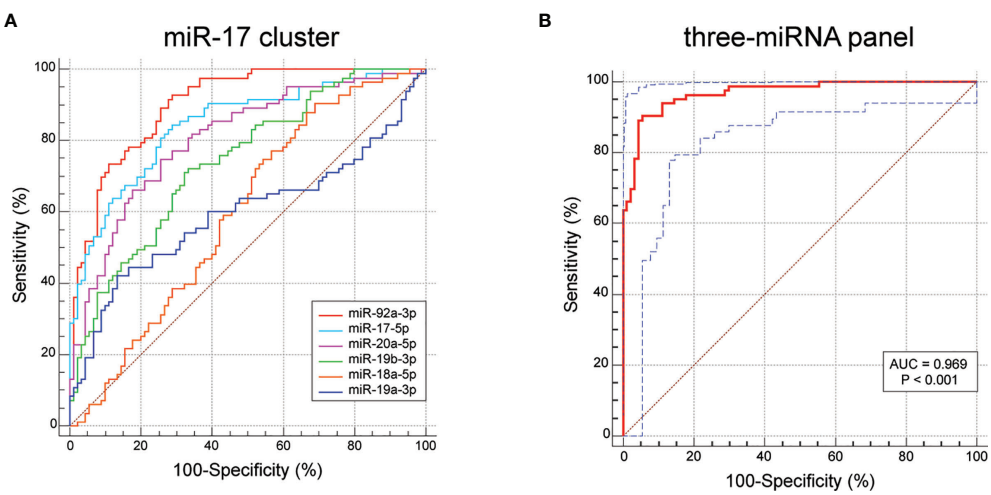

FIGURE 5 | ROC results for the miR-17-92 cluster members and the three-miRNA diagnostic model (miR-130a-3p, miR-130b-3p and miR-301a-3p). **(A)** The AUC value of miR-17-5p is 0.845, miR-18a-5p is 0.597, miR-19a-3p is 0.596, miR-20a-5p is 0.806, miR-19b-3p is 0.741, miR-92a-3p is 0.902. **(B)** The AUC value of the three-miRNA model is 0.969 (95% CI: 0.931 - 0.989; sensitivity = 90.36%, specificity = 94.44%).

TABLE 3 | Outcomes of ROC and Youden index for miR-17-92 cluster members.

	AUC	Standard Error	95% CI	Sensitivity (%)	Specificity (%)
miR-17-5p	0.845	0.030	0.782 - 0.895	84.34	71.11
miR-18a-5p	0.597	0.043	0.520 - 0.671	90.36	31.11
miR-19a-3p	0.596	0.045	0.519 - 0.670	42.17	86.67
miR-20a-5p	0.806	0.033	0.739 - 0.862	74.70	74.44
miR-19b-3p	0.741	0.037	0.669 - 0.804	72.29	66.67
miR-92a-3p	0.902	0.022	0.847 - 0.942	92.77	71.11
three-miRNA panel	0.969	0.011	0.931 - 0.989	90.36	94.44

AUC, area under curve; CI, confidence interval.

Prognostic Value of Serum miR-17-92 Cluster in Predicting Recurrence of BC Patients

To explore the prognostic value of serum miR-17-92 cluster, we followed up the BC patients after surgery to observe if their tumors recur. Among them, 8 BC patients had undergone radical cystectomy and therefore were excluded. Other patients, including 26 with TaN0M0, 30 with T1N0M0, and 10 with T2N0M0, were treated with transurethral resection of bladder tumor surgery (TURBT). After surgery, these patients were treated by bladder perfusion chemotherapy with gemcitabine. Patients were given pirarubicin at 30 mg per week for first 8 weeks after surgery, followed by pirarubicin at 30 mg per month for 10 months. In the patients we followed, all recurrences occurred in the bladder. The results of univariate Cox regression analysis showed that pathological grade, miR-18a-5p, miR-20a-5p, miR-19b-3p, and miR-92a-3p were correlated with the recurrence of BC (**Table S1**). In multivariate Cox regression analysis, miR-20a-5p and miR-92a-3p were the more significant factors (**Table S1**). The results of Kaplan-Meier analysis revealed that high serum miR-20a-5p expression was correlated with high recurrence risk in BC patients ($p = 0.004$) (**Figure S2**). The rest of miR-17-92 cluster members showed no significant correlation with recurrence in Kaplan-Meier analysis.

DISCUSSION

Liquid biopsy is a very promising method that has been extensively researched over the last decade. Liquid biopsy is anticipated to be used as the foundation for precise medical patient selection, including therapy selection and real-time monitoring of treatment impact. Furthermore, liquid biomarkers in urine and blood, such as DNA methylation and mutations, protein-based assays, gene signatures, and non-coding RNAs, might pave the way for molecular diagnosis and tailored therapy of bladder cancer (19). After therapy, biomarkers in urine may be useful in estimating residual illness or recurrence of bladder cancer; hence, liquid biopsy in urine may be a valuable source of personalized medicine prognostic biomarkers (19).

Emerging research indicates that microRNAs have tremendous promise for use in the diagnosis, prognosis, and therapy of urinary malignancies, and that microRNAs have considerable potential as biological fluid indicators of urinary system tumors, such as serum and urine (20). For example, Sebastian L Hofbauer et al. identified a 6-microRNA signature in urine for diagnosis of bladder cancer (21) and Wataru Usuba et al. identified a 7-miRNA panel in serum for specific and early detection in bladder cancer (22). In terms of prognosis research, the study found that let-7c cluster evaluation may enhance prognosis by recognizing patients' risk of progression and addressing early radical therapy in high grade non-muscle-invasive bladder cancer (23).

Early detection of BC is also critical to a better prognosis and quality of life. Because it is non-invasive, serum-based miRNA screening is an unique and widely available diagnostic method. In this study, we selected the serum miR-17-92 cluster members (miR-17-5p, miR-18a-5p, miR-19a-3p, miR-20a-5p, miR-19b-3p and miR-92a-3p) as candidate biomarkers for BC diagnosis.

The miR-17-92 cluster is located in the open reading frame 25 of chromosome 13 (C13orf25) and is a highly conserved polycistronic miRNA cluster. The miRNA-17-92 cluster is highly expressed in various tumor cells, such as lung cancer, breast cancer, pancreatic cancer, prostate cancer and BC (24, 25). Therefore, it is also called "oncomiR1". Recently, basic researches on miR-17-92 cluster members in BC have also received attention. For example, modification of the SNHG16/miR-17-5p/TIMP3 signal may help delay the progression of BC (15). Circ-ITCH upregulates the expression of miR-17-5p target genes p21 and PTEN by stimulating miR-17-5p, thereby inhibiting the malignant biological behavior of BC (14). miR-19a-3p promotes BC invasion and EMT by targeting RhoB (26). Similarly, miR-20a-5p can also promote BC cell growth and invasion by targeting PTEN (16).

Nonetheless, the connection between serum miR-17-92 cluster and BC has not been studied. Also, there are no studies on the clinical application of miR-17-92 cluster members in the diagnosis and treatment of BC. The present study aimed to explore the potential of miR-17-92 cluster to be diagnostic biomarkers for BC and the results were satisfactory. We confirmed the overexpression of miR-17-92 cluster in BC tissues using TCGA-BLCA data, which was consistent with previous studies. We then evaluated the differential expression of miR-17-92 cluster in serum. It was found that serum miR-92a-3p (AUC = 0.902) has extremely high BC diagnostic ability. Serum miR-17-5p (AUC = 0.845), miR-20a-5p (AUC = 0.806) and miR-19b-3p (AUC = 0.741) have moderate diagnostic ability. Then, we constructed a three-miRNA diagnostic model through logistic regression to improve specificity and sensitivity.

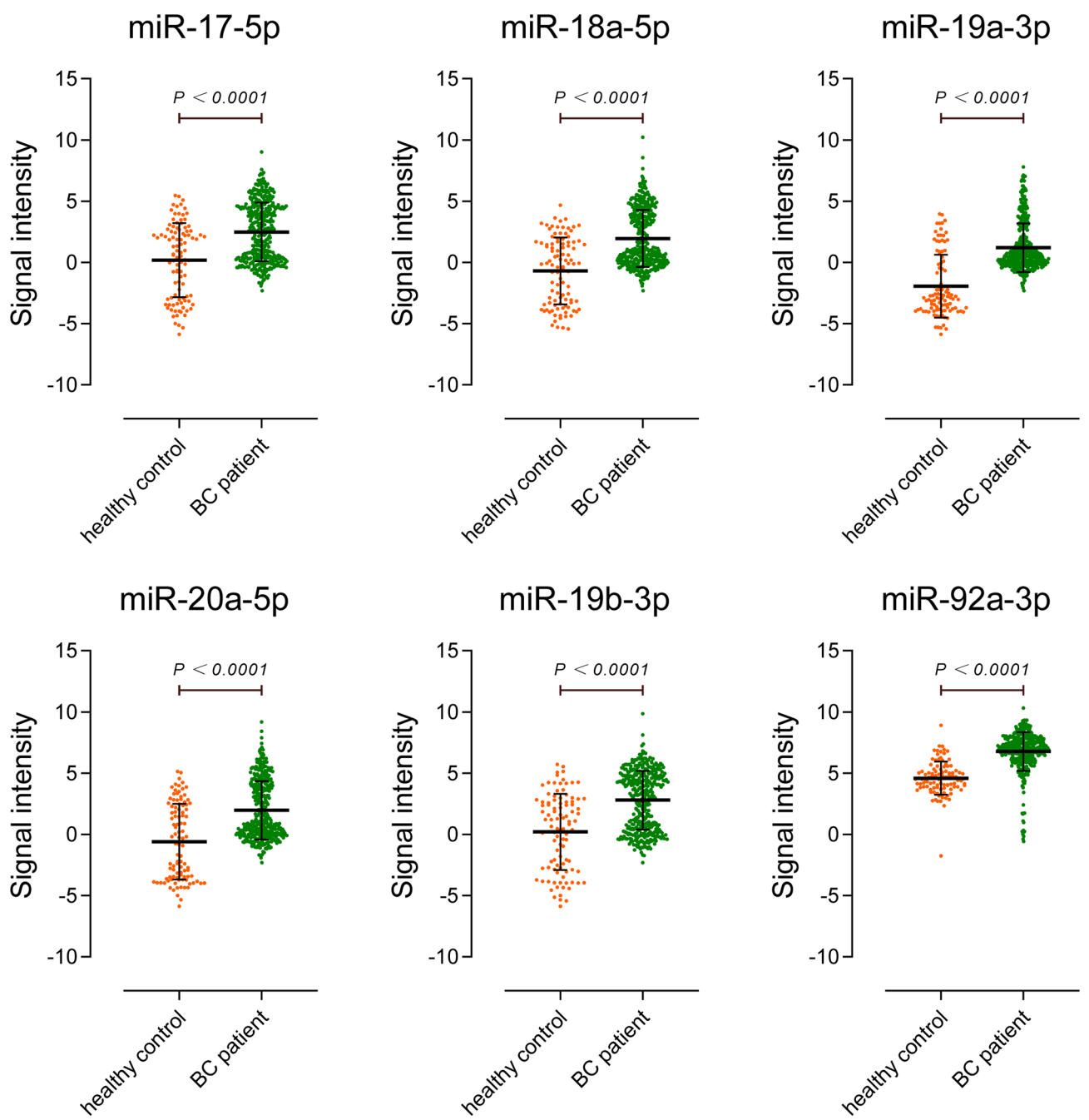

FIGURE 6 | External validation of miR-17-92 cluster expression in sera of bladder cancer patients. The validation set included 392 BC patients and 100 non-cancer controls.

The AUC of the model is as high as 0.969 (95% CI: 0.931 - 0.989; sensitivity = 90.36%, specificity = 94.44%), showing an excellent diagnostic ability for BC. The following external data validation (492 cases) also confirmed the reliability of our results. We also proved the overexpression of miR-17-92 cluster in BC cell lines. And we observed that miR-17-92 in the culture media of BC cell lines was gradually increased with incubation times, supporting our hypothesis that elevated serum miR-17-92 cluster was released into circulation by BC tumor cells. Among members of miR-17-92 cluster, serum miR-20a-5p expression level was associated with the recurrence of BC patients and have the potential to serve as a prognostic indicator.

In spite of the meaningful findings we obtained, certain limitations should be mentioned. All sera used in this study were taken from patients before surgery and postoperative sera were deficient. Moreover, the sample size of this study was

relatively small, and multicenter study in the future is needed. The follow-up period after surgery was not long enough to obtain a more accurate conclusion. We will continue to recruit new cases and follow up, to furtherly confirm the clinical value of miR-17-92 cluster in our future work. Also, microRNAs in urine have great prospects in the diagnosis of urinary tumors (20). We will further evaluate the miRNA model in urine of patients with bladder cancer to test the role of the tool as a non-invasive biomarker for urine. Many miRNAs are involved in the inhibition of chemoresistance, while others are involved in the induction of chemoresistance (27). For example, miR-17-5p is overexpressed in pancreatic cancer and miR-17-5p inhibitor heightens the sensitivity of gemcitabine chemotherapy by up regulating the expression of Bim (28). It's worth evaluating the expression levels of the miR-17-92 cluster correlate with the pharmacological response to drugs conventionally used in bladder treatment.

In conclusion, we confirmed that miR-17-92 cluster expression was significantly upregulated in BC tissue, cell lines, and serum compared to normal controls. Serum miR-17-92 cluster members could serve as potential diagnostic biomarkers for BC. Among them, the three-miRNA model constructed by miR-92a-3p, miR-17-5p and miR-20a-5p exhibited excellent diagnostic ability (AUC = 0.969), showing its potential to be a new noninvasive biomarker for the diagnosis of BC.

DATA AVAILABILITY STATEMENT

The datasets presented in this study can be found in online repositories. The names of the repository/repositories and accession number(s) can be found in the article/**Supplementary Material**.

ETHICS STATEMENT

This study had been approved by the Ethics Committee of Peking University Shenzhen Hospital. The patients/participants provided their written informed consent to participate in this study.

AUTHOR CONTRIBUTIONS

JW, XP, YL, and ZC conceived and designed this study. JW, XP, KL, and CZ performed the experiments. XC, GH, and LZ collected the serum samples and the clinical information. JW, XP, and RL performed statistical analysis and wrote the original manuscript. YL and ZC reviewed and edited the manuscript. All authors contributed to the article and approved the submitted version.

FUNDING

This study was supported by Shenzhen High-level Hospital Construction Fund, Basic Research Project of Peking University Shenzhen Hospital (JCYJ2017001, JCYJ2017004, JCYJ2017005, JCYJ2017006, JCYJ2017007, JCYJ2017012), Clinical Research Project of Peking University Shenzhen Hospital (LCYJ2017001), Science and Technology Development Fund Project of Shenzhen (no. JCYJ20180507183102747) and Clinical Research Project of Shenzhen Health Commission (no. SZLY2018023).

SUPPLEMENTARY MATERIAL

The Supplementary Material for this article can be found online at: https://www.frontiersin.org/articles/10.3389/fonc.2021.795837/full#supplementary-material

REFERENCES

1. Siegel RL, Miller KD, Jemal A. Cancer Statistics, 2020. *CA: Cancer J Clin* (2020) 70(1):7–30. doi: 10.3322/caac.21590
2. Berdik C. Unlocking Bladder Cancer. *Nature* (2017) 551(7679):S34–s5. doi: 10.1038/551S34a
3. Burke DM, Shackley DC, O'Reilly PH. The Community-Based Morbidity of Flexible Cystoscopy. *BJU Int* (2002) 89(4):347–9. doi: 10.1046/j.1464-4096.2001.01899.x
4. Raharja PAR, Hamid A, Mochtar CA, Umbas R. Recent Advances in Optical Imaging Technologies for the Detection of Bladder Cancer. *Photodiagnosis Photodynamic Ther* (2018) 24:192–7. doi: 10.1016/j.pdpdt.2018.10.009
5. Uttley L, Whiteman BL, Woods HB, Harnan S, Philips ST, Cree IA. Building the Evidence Base of Blood-Based Biomarkers for Early Detection of Cancer: A Rapid Systematic Mapping Review. *EBioMedicine* (2016) 10:164–73. doi: 10.1016/j.ebiom.2016.07.004
6. Feber A, Dhami P, Dong L, de Winter P, Tan WS, Martinez-Fernandez M, et al. UroMark-A Urinary Biomarker Assay for the Detection of Bladder Cancer. *Clin Epigenet* (2017) 9:8. doi: 10.1186/s13148-016-0303-5
7. Bartel DP. MicroRNAs: Genomics, Biogenesis, Mechanism, and Function. *Cell* (2004) 116(2):281–97. doi: 10.1016/s0092-8674(04)00045-5
8. Calin GA, Croce CM. MicroRNA Signatures in Human Cancers. *Nat Rev Cancer* (2006) 6(11):857–66. doi: 10.1038/nrc1997
9. Todeschini P, Salviato E, Paracchini L, Ferracin M, Petrillo M, Zanotti L, et al. Circulating miRNA Landscape Identifies miR-1246 as Promising Diagnostic Biomarker in High-Grade Serous Ovarian Carcinoma: A Validation Across Two Independent Cohorts. *Cancer Lett* (2017) 388:320–7. doi: 10.1016/j.canlet.2016.12.017
10. Lin XJ, Chong Y, Guo ZW, Xie C, Yang XJ, Zhang Q, et al. A Serum microRNA Classifier for Early Detection of Hepatocellular Carcinoma: A Multicentre, Retrospective, Longitudinal Biomarker Identification Study With a Nested Case-Control Study. *Lancet Oncol* (2015) 16(7):804–15. doi: 10.1016/S1470-2045(15)00048-0
11. Zhou J, Yu L, Gao X, Hu J, Wang J, Dai Z, et al. Plasma microRNA Panel to Diagnose Hepatitis B Virus-Related Hepatocellular Carcinoma. *J Clin Oncol Off J Am Soc Clin Oncol* (2011) 29(36):4781–8. doi: 10.1200/JCO.2011.38.2697
12. Concepcion CP, Bonetti C, Ventura A. The microRNA-17-92 Family of microRNA Clusters in Development and Disease. *Cancer J* (2012) 18 (3):262–7. doi: 10.1097/PPO.0b013e318258b60a
13. Tao J, Wu D, Li P, Xu B, Lu Q, Zhang W. microRNA-18a, a Member of the Oncogenic miR-17-92 Cluster, Targets Dicer and Suppresses Cell Proliferation in Bladder Cancer T24 Cells. *Mol Med Rep* (2012) 5(1):167–72. doi: 10.3892/mmr.2011.591
14. Yang C, Yuan W, Yang X, Li P, Wang J, Han J, et al. Circular RNA Circ-ITCH Inhibits Bladder Cancer Progression by Sponging miR-17/miR-224 and Regulating P21, PTEN Expression. *Mol Cancer* (2018) 17(1):19. doi: 10.1186/s12943-018-0771-7
15. Peng H, Li H. The Encouraging Role of Long Noncoding RNA Small Nuclear RNA Host Gene 16 in Epithelial-Mesenchymal Transition of Bladder Cancer *via* Directly Acting on miR-17-5p/Metalloproteinases 3 Axis. *Mol Carcinogenesis* (2019) 58(8):1465–80. doi: 10.1002/mc.23028
16. Zhong XL, Wang L, Yan X, Yang XK, Xiu H, Zhao M, et al. MiR-20a Acted as a ceRNA of lncRNA PTENPL and Promoted Bladder Cancer Cell Proliferation and Migration by Regulating PDCD4. *Eur Rev Med Pharmacol Sci* (2020) 24(6):2955–64. doi: 10.26355/eurrev_202003_20660

17. Feng Y, Liu J, Kang Y, He Y, Liang B, Yang P, et al. miR-19a Acts as an Oncogenic microRNA and Is Up-Regulated in Bladder Cancer. *J Exp Clin Cancer Res CR* (2014) 33:67. doi: 10.1186/PREACCEPT-9242556491295527
18. Livak KJ, Schmittgen TD. Analysis of Relative Gene Expression Data Using Real-Time Quantitative PCR and the 2(-Delta Delta C(T)) Method. *Methods (San Diego Calif)* (2001) 25(4):402–8. doi: 10.1006/meth.2001.1262
19. Ferro M, La Civita E, Liotti A, Cennamo M, Tortora F, Buonerba C, et al. Liquid Biopsy Biomarkers in Urine: A Route Towards Molecular Diagnosis and Personalized Medicine of Bladder Cancer. *J Pers Med* (2021) 11(3):237. doi: 10.3390/jpm11030237
20. Fendler A, Stephan C, Yousef GM, Kristiansen G, Jung K. The Translational Potential of microRNAs as Biofluid Markers of Urological Tumours. *Nat Rev Urol* (2016) 13(12):734–52. doi: 10.1038/nrurol.2016.193
21. Hofbauer SL, de Martino M, Lucca I, Haitel A, Susani M, Shariat SF, et al. A Urinary microRNA (miR) Signature for Diagnosis of Bladder Cancer. *Urol Oncol* (2018) 36(12):531.e1–e8. doi: 10.1016/j.urolonc.2018.09.006
22. Usuba W, Urabe F, Yamamoto Y, Matsuzaki J, Sasaki H, Ichikawa M, et al. Circulating miRNA Panels for Specific and Early Detection in Bladder Cancer. *Cancer Sci* (2019) 110(1):408–19. doi: 10.1111/cas.13856
23. Spagnuolo M, Costantini M, Ferriero M, Varmi M, Sperduti I, Regazzo G, et al. Urinary Expression of Let-7c Cluster as Non-Invasive Tool to Assess the Risk of Disease Progression in Patients With High Grade Non-Muscle Invasive Bladder Cancer: A Pilot Study. *J Exp Clin Cancer Res* (2020) 39(1):68. doi: 10.1186/s13046-020-01550-w
24. Fang LL, Wang XH, Sun BF, Zhang XD, Zhu XH, Yu ZJ, et al. Expression, Regulation and Mechanism of Action of the miR-17-92 Cluster in Tumor Cells (Review). *Int J Mol Med* (2017) 40(6):1624–30. doi: 10.3892/ijmm.2017.3164
25. Mogilyansky E, Rigoutsos I. The miR-17/92 Cluster: A Comprehensive Update on Its Genomics, Genetics, Functions and Increasingly Important and Numerous Roles in Health and Disease. *Cell Death Diff* (2013) 20(12):1603–14. doi: 10.1038/cdd.2013.125
26. Li Z, Li Y, Wang Y. miR-19a Promotes Invasion and Epithelial to Mesenchymal Transition of Bladder Cancer Cells by Targeting RhoB. *J BUON Off J Balkan Union Oncol* (2019) 24(2):797–804.
27. Ashrafizadeh M, Zarrabi A, Orouei S, Kiavash H, Hakimi A, Amirhossein Z, et al. MicroRNA-Mediated Autophagy Regulation in Cancer Therapy: The Role in Chemoresistance/Chemosensitivity. *Eur J Pharmacol* (2021) 892:173660. doi: 10.1016/j.ejphar.2020.173660
28. Yan HJ, Liu WS, Sun WH, Wu J, Ji M, Wang Q, et al. miR-17-5p Inhibitor Enhances Chemosensitivity to Gemcitabine *via* Upregulating Bim Expression in Pancreatic Cancer Cells. *Dig Dis Sci* (2012) 57(12):3160–7. doi: 10.1007/s10620-012-2400-4

Conflict of Interest: The authors declare that the research was conducted in the absence of any commercial or financial relationships that could be construed as a potential conflict of interest.

Publisher's Note: All claims expressed in this article are solely those of the authors and do not necessarily represent those of their affiliated organizations, or those of the publisher, the editors and the reviewers. Any product that may be evaluated in this article, or claim that may be made by its manufacturer, is not guaranteed or endorsed by the publisher.

Copyright © 2021 Wang, Peng, Li, Liu, Zhang, Chen, Huang, Zhao, Chen and Lai. This is an open-access article distributed under the terms of the Creative Commons Attribution License (CC BY). The use, distribution or reproduction in other forums is permitted, provided the original author(s) and the copyright owner(s) are credited and that the original publication in this journal is cited, in accordance with accepted academic practice. No use, distribution or reproduction is permitted which does not comply with these terms.

frontiers in Oncology

CASE REPORT
published: 22 December 2021
doi: 10.3389/fonc.2021.736969

Case Report: Molecular Characterization of Aggressive Malignant Retroperitoneal Solitary Fibrous Tumor: A Case Study

Haruna Nonaka[1], Shuya Kandori[1], Satoshi Nitta[1], Masanobu Shiga[1], Yoshiyuki Nagumo[1], Tomokazu Kimura[1], Takashi Kawahara[1], Hiromitsu Negoro[1], Akio Hoshi[1], Takahiro Kojima[2], Koji Kawai[3], Bryan J. Mathis[4], Takuro Tamura[5], Taka-Aki Sato[5], Mariko Yamato[6], Masayuki Noguchi[6] and Hiroyuki Nishiyama[1]*

[1] Department of Urology, Faculty of Medicine, University of Tsukuba, Tsukuba, Japan, [2] Department of Urology, Aichi Cancer Center Hospital, Nagoya, Japan, [3] Department of Urology, School of Medicine, International University of Health and Welfare, Narita, Japan, [4] International Medical Center, University of Tsukuba Affiliated Hospital, Tsukuba, Japan, [5] Research and Development Centre for Precision Medicine, University of Tsukuba, Tsukuba, Japan, [6] Department of Pathology, Faculty of Medicine, University of Tsukuba, Tsukuba, Japan

OPEN ACCESS

Edited by:
Marijo Bilusic, University of Miami Health System, United States

Reviewed by:
An Zhao, University of Chinese Academy of Sciences, China
Zuheir Alshehabi, Tishreen University, Syria

***Correspondence:**
Shuya Kandori
shuya79@md.tsukuba.ac.jp

Specialty section:
This article was submitted to Genitourinary Oncology, a section of the journal Frontiers in Oncology

Received: *06 July 2021*
Accepted: *22 November 2021*
Published: *22 December 2021*

Citation:
Nonaka H, Kandori S, Nitta S, Shiga M, Nagumo Y, Kimura T, Kawahara T, Negoro H, Hoshi A, Kojima T, Kawai K, Mathis BJ, Tamura T, Sato T-A, Yamato M, Noguchi M and Nishiyama H (2021) Case Report: Molecular Characterization of Aggressive Malignant Retroperitoneal Solitary Fibrous Tumor: A Case Study. Front. Oncol. 11:736969. doi: 10.3389/fonc.2021.736969

Solitary fibrous tumors (SFT) are mesenchymal neoplasms with a favorable prognosis usually originating from the visceral pleura. Rarely, they may occur at various extrapleural sites and show malignant behavior coupled with dedifferentiation. NAB2-STAT6 fusion gene and STAT6 nuclear expression are biomarkers for diagnosis of SFT in addition to CD34, Bcl-2, and CD99. Furthermore, several reports have shown specific NAB2-STAT6 fusion variants and loss of STAT6 protein expression are associated with malignancy. We report a rare case of retroperitoneal SFT which rapidly progressed to death within 35 days after admission. Autopsy found a primary tumor containing both benign and malignant histologies, with multiple metastatic sites similar to the malignant, dedifferentiated tumor. STAT6 was detected in the primary differentiated tumor but not in the primary dedifferentiated tumor or lung/liver metastases. However, the NAB2-STAT6 fusion gene (NAB2ex6/STAT6ex16 variant) was detected in the primary tumor and lung/liver metastases. Intriguingly, fusion gene expression at the transcriptional level was downregulated in the dedifferentiated tumors compared to the differentiated tumor. We further performed target DNA sequencing and found gene mutations in TP53, FLT3, and AR in the dedifferentiated tumors, with TP53 mutations especially found among them. We demonstrate that downregulation of NAB2-STAT6 fusion gene at the transcriptional level is associated with malignant SFT for the first time. Moreover, the present study supports the idea that TP53 mutations promote malignancy in SFTs.

Keywords: malignant solitary fibrous tumor, *NAB2-STAT6* fusion gene, STAT6 nuclear expression, target DNA sequencing, *TP53* mutation

INTRODUCTION

Solitary fibrous tumors (SFT) are mesenchymal neoplasms usually originating from the visceral pleura but can occur at various extrapleural sites (1). They are usually slow-growing with favorable prognoses but approximately 10-20% develop malignancy (2, 3). SFTs are diagnosed by histologic features and CD34 immunostaining while positive findings for Bcl-2 and CD99 are supportive for diagnosis (1). However, recent advances in next generation sequencing have established a fusion gene of juxtaposed NGFI-A binding protein 2 (NAB2) and signal transducer and activator of transcription 6 (STAT6) as the genetic hallmark of SFT (4, 5). Subsequently, immunohistochemical detection of STAT6 nuclear expression is reported as a highly sensitive and specific biomarker for SFT diagnosis (6, 7). Here, we present a rare case of retroperitoneal SFT where the primary tumor contained a clear delineation between benign (CD34- and STAT6-positive) and malignant (CD34- and STAT6-negative) histologies. After diagnosis, the patient quickly died from rapid exacerbation of metastases. Here, we analyze the molecular characteristics of this unique case and discuss mechanisms for the observed malignant phenotype.

MATERIAL AND METHODS

Immunohistochemistry

The tissue specimens were cut into 4μm-thick sections from formalin-fixed, paraffin-embedded (FFPE) blocks before deparaffinization and antigen retrieval using PT Link (Dako, Agilent Technologies). Target retrieval solution 'high' was used for staining of CD34 and STAT6 while 'low' was used for Ki67. Immunostaining was performed using a Dako Autostainer Link 48 (Agilent Technologies) with the primary antibody (anti-Ki67 antibody [Cat#:IR626, Dako], anti-CD34 antibody [Cat#:IR632, Dako] or anti-STAT6 antibody [1:400 dilution, Cat#: SC-621, SantaCruz]) and REAL Envision HRP rabbit/mouse (Agilent Technologies) as a secondary antibody. Immunoreactivity was detected with DAB (Dako REAL EnVision Detection system, Agilent Technologies) and counterstaining was performed with hematoxylin.

RT-PCR and Sanger Sequencing

Total RNA was extracted from frozen samples by RNeasy Mini Kit (Qiagen). The RNA was then reverse-transcribed into cDNA using a High Capacity cDNA Reverse Transcription Kit (Thermo Fisher Scientific). PCR was performed by Quick Taq® HS DyeMix (TOYOBO) according to the manufacturer's instructions. The primer sets for the detection of NAB2-STAT6 fusion genes were previously designed by Tai et al. (8). Hypoxanthine phosphoribosyltransferase 1 (HPRT) was used as an internal control. Primer sequences are listed in **Supplementary Table 1**. PCR products were loaded onto 2% agarose gels with ethidium bromide and visualized under UV illumination. Confirmed PCR products were directly sequenced using an Applied Biosystems 3730xl Genetic Analyzer (Thermo Fisher Scientific).

Next-Generation Sequencing

DNA was extracted from frozen samples by QIAamp DNA Mini Kit (Qiagen) or from FFPE samples by AllPrep DNA/RNA FFPE kit (Qiagen). A QIAseq Human Comprehensive Cancer Panel (DHS-3501Z-12, Qiagen) was used for library construction according to the manufacturer's instructions. The libraries were assessed using a Bioanalyzer High Sensitivity DNA Kit (5067-4626, Agilent Technologies) and applied to a MiSeq sequencer (Illumina) to obtain 2x151-base reads. FASTQ files were imported to CLC Genomics Workbench (ver.12.0, Qiagen) and compared with normal kidney to remove the germline mutations. Somatic mutations were selected by allele frequency >=5% and coverage >=100x.

CASE PRESENTATION

Clinical Summary

A 53-year-old man with an unremarkable past medical history presented to our department with lower abdominal pain. Enhanced chest and abdominal computed tomography (CT) showed a 10x10x10 cm pelvic tumor and, although central necrosis was revealed, the anterior-to-left periphery of the tumor was markedly enhanced. The tumor margin was clear in most parts but had partly invaded into the right pelvic wall. Marked hypermetabolism in the invasive area of the tumor was seen on 18F-fluorodeoxyglucose-positron emission tomography (FDG PET) (**Figures 2A, B**) and both CT and FDG PET revealed multiple lung and bone metastases. We clinically diagnosed retroperitoneal sarcoma or malignant mesenchymal tumors based on the image findings. Therefore, we next carried out percutaneous needle biopsy of the primary masses to determine a pathological diagnosis, finding specimens composed of spindle-shaped malignant cells positive for STAT6 that led to a pathological diagnosis of solitary fibrous tumor (SFT). Cytotoxic chemotherapy was planned but the patient's condition rapidly deteriorated, with respiratory failure, disseminated intravascular coagulation, and finally death from multiple organ failure occurring 35 days after admission. A chronological summary of the case report is shown in **Figure 1**.

Autopsy Findings

Figure 2C shows the gross findings from the tumor autopsy, namely a well-circumscribed and smooth area on the left side and a poorly margined and lobulated area on the right side corresponding to radiological imaging findings (**Figures 2A, B**). Pathological findings also differed between the left (**Figures 3A–E**) and right sides (**Figures 3F–J**) of the tumor. On the left side, spindle-shaped tumor cells with mild atypia and collagen fiber proliferation were observed. The mitotic activity was 0.3/10 HPF and tumor necrosis was not observed. The Ki-67-positive rate was low, around 1% (**Figure 3B**), but cells were diffusely stained with CD34 (**Figure 3C**) and tumor cell nuclei were positively stained with STAT6 (**Figure 3D**). The left side findings fit the definition of SFT in the WHO Classification (9). On the right side, round or short spindle-shaped tumor cells with

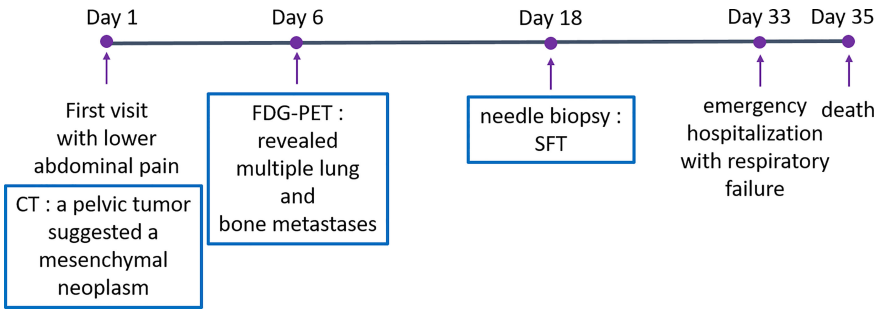

FIGURE 1 | Case report timeline.

high N/C ratios proliferated in a honeycomb pattern. In contrast to the left side, the mitotic activity was 80-100/10 HPF and tumor necrosis was detected. Moreover, the around 80% of these tumor cells were stained with Ki-67 (**Figure 3G**) but completely negative for CD34 and STAT6 (**Figures 3H, I**). Tumor cells from both sides were positive for CD99 (**Figures 3E, J**), focally positive for BCL-2, and negative for p53 (data not shown). From these observations, the left side lesion was considered to be the differentiated SFT while the right side lesion was composed of a dedifferentiated tumor. We next conducted a complete histological examination of the multiple metastatic sites revealed at autopsy, including more than 30 lung metastases, 2 liver metastases, 3 bone metastases and 1 adrenal metastasis, and pathological findings for all sites were similar to the right-side dedifferentiated tumor. We thus diagnosed the dedifferentiated tumors as malignant SFT, which were transformed from the differentiated SFT on the left side of the primary site.

Molecular Findings

Detecting the NAB2/STAT6 fusion gene is the gold standard for SFT diagnosis but, in the present case, STAT6 protein expression within dedifferentiated tumors was not observed. To clarify NAB2/STAT6 fusion gene status, we performed RT-PCT analysis of the primary differentiated tumor, primary dedifferentiated tumor, and lung/liver metastases. The NAB2 exon 6/STAT6 exon 16 (NAB2ex6/STAT6ex16) variant was identified in the primary differentiated tumor (**Figure 4A**), with Sanger sequencing revealing a stretch (111bp) of NAB2 intronic sequence between the NAB2 exon 6 and STAT6 exon 16 (**Figure 4B**). The NAB2ex6/STAT6ex16 variant was also detected in the primary dedifferentiated tumor and lung/liver metastases (**Figure 4C**), albeit at lower levels compared to the primary differentiated tumor.

We next performed target DNA sequencing using a comprehensive cancer panel for the primary differentiated tumor, primary dedifferentiated tumor, and lung/liver metastases. All non-synonymous variants are listed in **Supplementary Tables 2-5**. The number of gene mutations was 164 in the primary differentiated tumor, 105 in the primary dedifferentiated tumor, 69 in the lung metastasis and 139 in the liver metastasis (**Figures 5A, B**). At the primary site, 75 genes were shared between the differentiated and dedifferentiated tumors. In the dedifferentiated tumors, 33 genes were shared between the primary and metastatic sites. Oncoprinting of gene mutations among four lesions is shown in **Supplementary Table 6**. Mutations with variant allele frequency <10% were excluded from further analysis to clarify the significance of the mutations and a summary is shown in **Figure 5C**. The gene mutations in TP53, FLT3, and AR were found in dedifferentiated tumors while the TP53 mutation (c.97del; p.Ser33fs) was especially found in all dedifferentiated tumors.

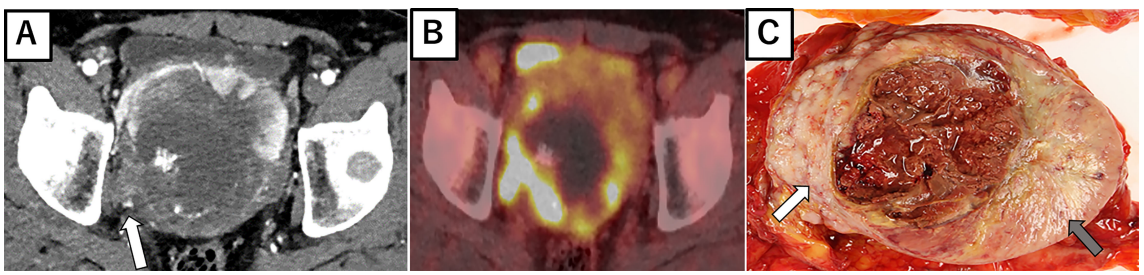

FIGURE 2 | Radiological imaging and macroscopic findings of primary site. **(A)** Enhanced abdominal CT showing central necrosis and the marked enhancement of anterior to left periphery of the tumor. At the right periphery, the tumor is seen invading the pelvic wall (white arrow). **(B)** 18F-fluorodeoxyglucose-positron emission tomography showing the marked hypermetabolism in the right invasive area of the tumor. **(C)** Autopsy specimen, with a well-circumscribed and smooth area (left side: gray arrow) and poorly margined and lobulated area (right side: white arrow).

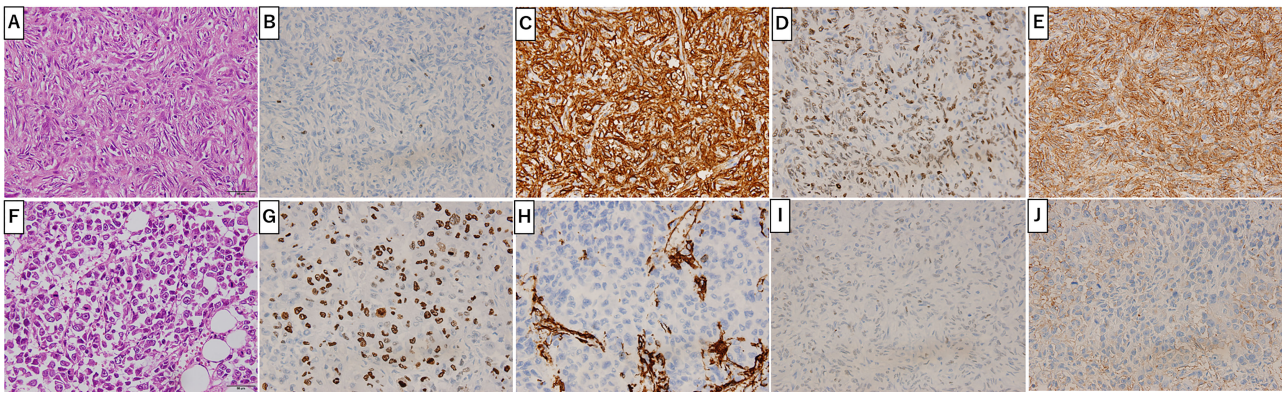

FIGURE 3 | Primary Site Pathology. Pathologic findings were distinct between the left **(A-E)** and right **(F-J)** sides of the tumor. On the left side (gray arrow in **Figure 2C**), spindle-shaped tumor cells with mild atypia and collagen fiber proliferation are seen **(A)**. Ki-67 positive cells were around 1% **(B)**. Tumor cells positively stained with CD34 **(C)**, STAT6 **(D)** and CD99 **(E)**. On the right side (white arrow in **Figure 2C**), round or short spindle-shaped tumor cells with high N/C ratios proliferating in a honeycomb pattern are seen **(F)**. Around 80% of tumor cells were positive for Ki-67 **(G)** and CD99 **(J)** but not CD34 **(H)** or STAT6 **(I)**. Scale bar: 50μm.

DISCUSSION AND CONCLUSIONS

Here, we present a rare case of retroperitoneal SFT with clear delineation between benign and malignant histologies within a single primary tumor. The malignant side met the criteria for a pathological judgement of malignancy, namely high cellularity and mitotic activity (more than four mitotic figures per 10 high-power fields), pleomorphism, hemorrhage, and necrosis (10). Pathological findings of all metastatic sites obtained at autopsy were similar to the malignant, dedifferentiated lesion. Demicco et al. reported a risk stratification model for SFT incorporating patient age, tumor size, mitotic activity and necrosis to predict metastatic risk (11). According to this model, no metastases were seen in low risk cases, while intermediate risk patients had a 10%

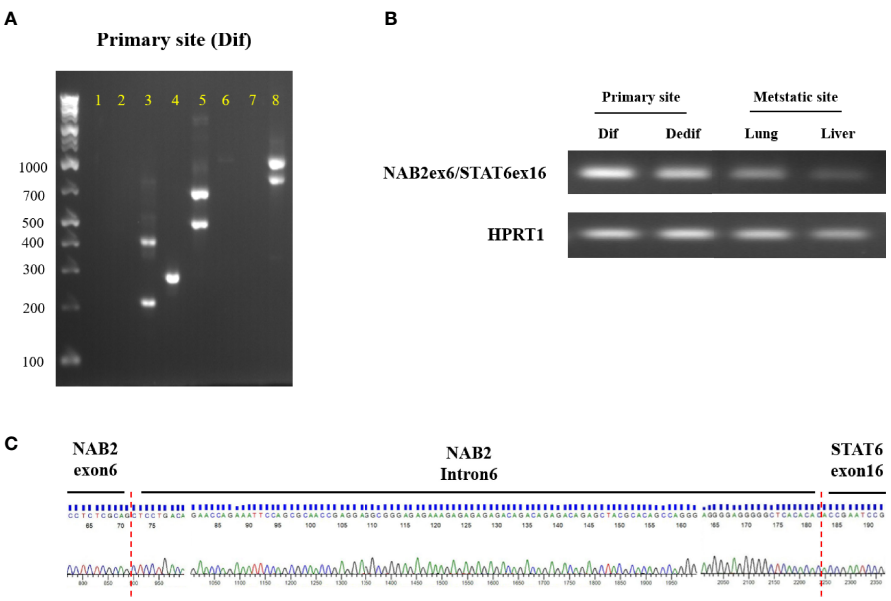

FIGURE 4 | NAB2-STAT6 fusion gene status in primary and metastatic sites. **(A)** Agarose gel separation of a NAB2-STAT6 fusion-specific RT-PCR product (NAB2ex6/STAT6ex16, Lane 4) from the primary differentiated tumor. **(B)** Detection of NAB2ex6/STAT6ex16 fusion gene from the primary site (differentiated and dedifferentiated tumors) and metastatic sites. **(C)** Sanger sequencing chromatogram of a NAB2/STAT6 fusion-specific RT-PCR product. Dif: differentiated tumor. Dedif: dedifferentiated tumor.

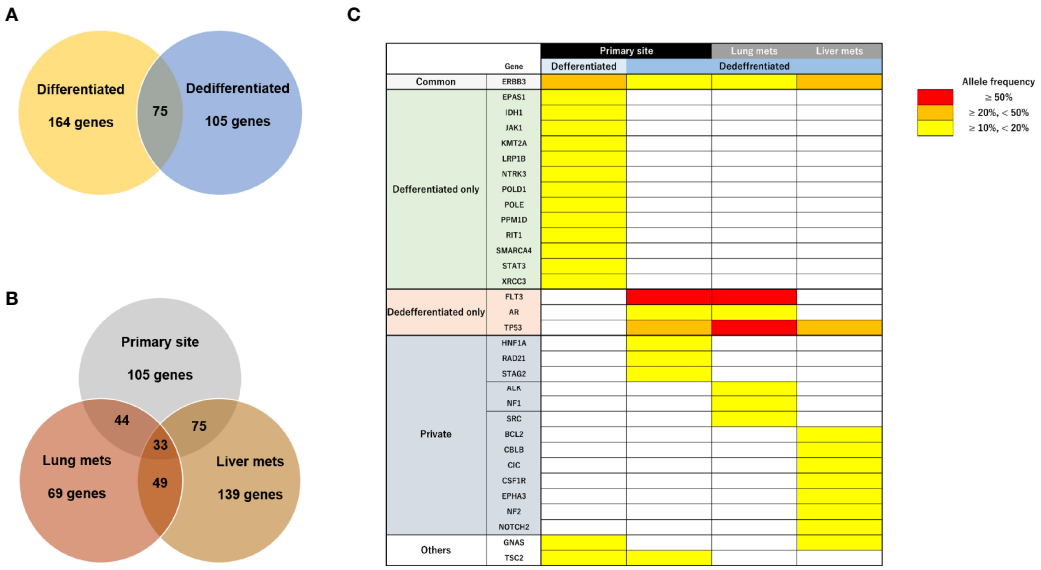

FIGURE 5 | Characteristics of genomic alterations in primary and metastatic sites. **(A)** Number of all gene mutations between primary differentiated and dedifferentiated tumors. **(B)** Number of all gene mutations between primary and metastatic sites in dedifferentiated tumors. **(C)** Mutational heatmap for the primary differentiated tumor, primary dedifferentiated tumor, and lung/liver metastases. Mutations with variant allele frequency <10% were excluded.

risk of metastasis at 10 years and high-risk SFT had a 73% risk of metastasis at 5 years. The present case was categorized as intermediate risk; nevertheless, the disease rapidly progressed and patient condition quickly deteriorated. This suggests that clinicopathological classification has limits to its prognostic power and molecular characterization may be more precise in this regard.

In the present case, we planned a conventional chemotherapy regimen but the rapid death precluded any treatment, highlighting the fact that systemic therapeutic options for unresectable or metastatic SFT disease are particularly limited. Anthracycline-based regimens have been advocated as a first-line chemotherapy, with several retrospective studies showing that the median progression-free survival (PFS) was 3-5 months in such patients with advanced SFT (12). On the other hand, some anti-angiogenic agents, such as sunitinib or pazopanib, have demonstrated efficacy for patients with advanced SFT and the median PFS was 4.7-9.7 months in those studies (12). Although a number of therapeutic agents have been tested in patients with advanced SFT, the efficacy of systemic therapies is limited. Therefore, an approach based on molecular mechanisms, particularly those driving tumorigenesis or progression of SFT, might pave the way to new therapeutic strategies.

With regard to these molecular strategies, NAB2-STAT6 fusion, recognized as a hallmark of SFT, was first identified by Robinson et al. and Chmielecki et al. from whole-exome sequencing studies (4, 5). These fusion genes drive STAT6 nuclear expression and immunohistochemical detection has been generally recognized as a definitive biomarker for diagnosis of SFT. A meta-analysis revealed that more than 40 NAB2-STAT6 fusion variant types were present in up to 83% (452/546) of SFTs, with NAB2ex6-STAT6ex16/17/18 and NAB2ex4-STAT6ex2/3 being the most frequent variants (13). In the present case, the NAB2ex6–STAT6ex16 variant was identified in primary and metastatic sites by RT-PCR and Sanger sequencing (**Figure 4**). Barthelmess et al. reported that NAB2ex6–STAT6ex16/17 was significantly associated with malignant phenotype and high recurrence in SFTs (14). Similarly, Akaike et al. showed that SFTs with NAB2ex6–STAT6ex16/18 harbored aggressive histological features (15). However, several studies have reported that NAB2-STAT6 fusion variants were not associated with malignant SFTs (16–19) and, therefore, the association between NAB2-STAT6 fusion variants and malignant potential remains controversial (14–19). These findings suggest that some other molecular mechanism promoted the malignant transformation seen in the present case.

Several studies reported that 7% to 10% of SFTs are negative for CD34 (6, 16) while, in contrast, STAT6 is highly positive in SFTs. Tai et al. reported that 87 of 88 (99%) tumors diagnosed as SFT (75 nonmalignant and 13 malignant) were positive for STAT6 (8) but STAT6 was positive in 7 of 8 CD34-negative SFTs. Other studies also reported that positive rates of STAT6 in SFTs were from 98% to 100% (6, 7). On the other hand, Dagrada et al. showed that STAT6 protein expression in dedifferentiated recurrent/metastatic tumors was lost whereas expression in primary usual/malignant tumors was positive in 4 SFT cases (16). RT-PCT analysis found the NAB2-STAT6 fusion gene in 3 of 4 cases in that report (16). Zhang et al. also reported a case with mediastinal malignant SFT carrying a NAB2-STAT6 fusion gene but negative STAT6 immunohistochemical staining (20). In the present case, the primary differentiated tumor was positive for CD34 and STAT6 but the primary dedifferentiated tumor

and lung/liver metastases were completely negative (**Figures 3C, D, H, I**). Moreover, NAB2ex6-STAT6ex16 fusion gene expression was downregulated in the dedifferentiated tumors compared to the differentiated tumor (**Figure 4B**). These findings suggest that NAB2-STAT6 chimeric protein downregulation promotes malignant transformation and might involve some transcriptional mechanism.

Previous reports have shown that other molecular factors, such as mutations in TP53, TERT promoter, and APAF1, were associated with malignant transformation or dedifferentiation (15–17, 21–24). Park et al. demonstrated that TP53 immunohistochemical positive in SFTs was significantly associated with malignant cases and TP53 mutations were detected in 41% of malignant SFTs (17). Similarly, TP53 mutations were detected only in dedifferentiated tumors in the present case. The identified mutation (c.97del in TP53) was previously found in patients with head and neck or esophageal squamous cell carcinoma (25, 26). Although this mutation has been linked to malignant transformation or dedifferentiation of SFT (15–17, 22–24), the mechanisms remain to be fully elucidated. On the other hand, FLT3 mutations (c.20A>G; p.Asp7Gly) were detected in the primary dedifferentiated tumor and lung metastases of the present case with high allele frequencies (77.6% and 93.1%), contributing to respiratory failure due to rapid progression of multiple lung metastases. As FLT3 mutations frequently occur in acute myeloid leukemia (AML) (27) and are associated with transformation to AML in myelodysplastic syndrome (MDS) patients (28, 29), these findings led us to speculate that an FLT3 mutation also promoted the malignant transformation of the dedifferentiated tumors in the present case.

In conclusion, we experienced a rare case of retroperitoneal SFT with rapid and lethal progression. Interestingly, two morphologic tumor types (differentiated and dedifferentiated) coexisted at the primary site but metastatic sites contained dedifferentiated tumors that commonly featured loss of STAT6 protein and TP53 mutations. Here, we demonstrate that downregulation of the NAB2-STAT6 fusion gene at the transcriptional level is associated with malignant SFT for the first time. These findings suggest that specific molecular alterations are associated with malignant behaviors, indicating that vigilance is required against SFT cases with loss of STAT6 protein expression and TP53 mutations.

DATA AVAILABILITY STATEMENT

The datasets of this study have been deposited with links to BioProject accession number PRJDB11977 in the DDBJ BioProject database.

ETHICS STATEMENT

This study was reviewed and approved by the Ethics Committee of the University of Tsukuba (Approval Number: H28-104). The written informed consent was obtained from the bereaved families of the patient at the time of autopsy.

AUTHOR CONTRIBUTIONS

HNo: data collection and manuscript writing. SK: conception and manuscript writing. revising. SN, MS, TKi, TKa, and AH: data collection. YN, MY, and TT: data analysis and interpretation. HNe, TKo, KK, and BM: manuscript revising. T-AS, MN, and HNi: supervision. All authors have read and agreed to the published version of the manuscript. All authors contributed to the article and approved the submitted version.

FUNDING

This work was supported by a grant from COI-NEXT (JPMJPF2017).

ACKNOWLEDGMENTS

We are thankful for the skillful technical assistance of Mrs. Noriko Kunita and Mrs. Naoko Ueki (University of Tsukuba).

SUPPLEMENTARY MATERIAL

The Supplementary Material for this article can be found online at: https://www.frontiersin.org/articles/10.3389/fonc.2021.736969/full#supplementary-material

REFERENCES

1. Davanzo B, Emerson RE, Lisy M, Koniaris LG, Kays JK. Solitary Fibrous Tumor. *Transl Gastroenterol Hepatol* (2018) 3:94. doi: 10.21037/tgh.2018.11.02
2. Lahon B, Mercier O, Fadel E, Ghigna MR, Petkova B, Dartevelle P, et al. Solitary Fibrous Tumor of the Pleura: Outcomes of 157 Complete Resections in a Single Center. *Ann Thorac Surg* (2012) 94(2):394–400. doi: 10.1016/j.athoracsur.2012.04.028
3. Gholami S, Cassidy MR, Kirane A, Kuk D, Zanchelli B, Brennan M, et al. Size and Location Are the Most Important Risk Factors for Malignant Behavior in Resected Solitary Fibrous Tumors. *Ann Surg Oncol* (2017) 24(13):3865–71. doi: 10.1245/s10434-017-6092-z
4. Robinson DR, Wu YM, Chinnaiyan AM, Kalyana-S S, Cao X, Lonigro RJ. Identification of Recurrent NAB2-STAT6 Gene Fusions in Solitary Fibrous Tumor by Integrative Sequencing. *Nat Genet* (2013) 45(2):180–5. doi: 10.1038/ng.2509
5. Chmielecki J, Crago AM, Rosenberg M, O'Connor R, Walker SR, Meyerson M, et al. Whole-Exome Sequencing Identifies a Recurrent NAB2-STAT6 Fusion in Solitary Fibrous Tumors. *Nat Genet* (2013) 45(2):131–2. doi: 10.1038/ng.2522
6. Doyle LA, Vivero M, Fletcher CD, Mertens F, Hornick JL. Nuclear Expression of STAT6 Distinguishes Solitary Fibrous Tumor From Histologic Mimics. *Mod Pathol* (2014) 27(3):390–5. doi: 10.1038/modpathol.2013.164
7. Cheah AL, Billings SD, Goldblum JR, Carver P, Tanas MZ, Rubin BP. STAT6 Rabbit Monoclonal Antibody Is a Robust Diagnostic Tool for the Distinction

of Solitary Fibrous Tumour From Its Mimics. *Pathology* (2014) 46(5):389–95. doi: 10.1097/PAT.0000000000000122
8. Tai HC, Chuang IC, Chen TC, Li CF, Huang SC, Huang HY, et al. NAB2-STAT6 Fusion Types Account for Clinicopathological Variations in Solitary Fibrous Tumors. *Mod Pathol* (2015) 28(10):1324–35. doi: 10.1038/modpathol.2015.90
9. WHO Classification of Tumours Editorial Board. *Soft Tissue & Bone Tumours WHO Classification of Tumours. 5th ed* Vol. 3. Lyon (France):World Health Organization (2020) p. 104–8.
10. England DM, Hochholzer L, McCarthy MJ. Localized Benign and Malignant Fibrous Tumors of the Pleura. A Clinicopathologic Review of 223 Cases. *Am J Surg Pathol* (1989) 13(8):640–58. doi: 10.1097/00000478-198908000-00003
11. Demicco EG, Wagner MJ, Maki RG, Gupta V, Iofin I, Wang WL, et al. Risk Assessment in Solitary Fibrous Tumors: Validation and Refinement of a Risk Stratification Model. *Modern Pathol* (2017) 30:1433–42. doi: 10.1038/modpathol.2017.54
12. Martin-Broto J, et al. A Comprehensive Review on Solitary Fibrous Tumor: New Insights for New Horizons. *Cancers (Basel)* (2021) 13(12):2913. doi: 10.3390/cancers12122913
13. Nakada S, Minato H, Nojima T. Clinicopathological Differences Between Variants of the NAB2-STAT6 Fusion Gene in Solitary Fibrous Tumors of the Meninges and Extra-Central Nervous System. *Brain Tumor Pathol* (2016) 33 (3):169–74. doi: 10.1007/s10014-016-0264-6
14. Barthelmess S, Geddert H, Boltze C, Moskalev EA, Bieg M, Haller F, et al. Solitary Fibrous Tumors/Hemangiopericytomas With Different Variants of the NAB2-STAT6 Gene Fusion are Characterized by Specific Histomorphology and Distinct Clinicopathological Features. *Am J Pathol* (2014) 184(4):1209–18. doi: 10.1016/j.ajpath.2013.12.016
15. Akaike K, Kurisaki-Arakawa A, Hara K, Suehara Y, Takagi T, Saito T, et al. Distinct Clinicopathological Features of NAB2-STAT6 Fusion Gene Variants in Solitary Fibrous Tumor With Emphasis on the Acquisition of Highly Malignant Potential. *Hum Pathol* (2015) 46(3):347–56. doi: 10.1016/j.humpath.2014.11.018
16. Dagrada GP, Spagnuolo RD, Mauro V, Tamborini E, Cesana L, Pilotti S, et al. Solitary Fibrous Tumors: Loss of Chimeric Protein Expression and Genomic Instability Mark Dedifferentiation. *Modern Pathol* (2015) 28(8):1074–83. doi: 10.1038/modpathol.2015.70
17. Park HK, Yu DB, Sung M, Oh E, Kim M, Choi YL, et al. Molecular Changes in Solitary Fibrous Tumor Progression. *J Mol Med* (2019) 97(10):1413–25. doi: 10.1007/s00109-019-01815-8
18. Chuang IC, Liao KC, Huang HY, Kao YC, Li CF, Lin PC, et al. NAB2-STAT6 Gene Fusion and STAT6 Immunoexpression in Extrathoracic Solitary Fibrous Tumors: The Association Between Fusion Variants and Locations. *Pathol Int* (2016) 66(5):288–96. doi: 10.1111/pin.12408
19. Yuzawa S, Nishihara H, Wang L, Tsuda M, Kimura T, Tanaka S, et al. Analysis of NAB2-STAT6 Gene Fusion in 17 Cases of Meningeal Solitary Fibrous Tumor/Hemangiopericytoma: Review of the Literature. *Am J Surg Pathol* (2016) 40(8):1031–40. doi: 10.1097/PAS.0000000000000625
20. Zhang P, Xiong K, Lv P, Zhang H, Wang Y, Song W, et al. Malignant Solitary Fibrous Tumor Occurring in the Mediastinal Pleura Showing NAB2ex4-STAT6ex2 Fusion and Negative STAT6 Immunohistochemistry: A Case Report. *Thorac Cancer* (2020) 11(5):1344–9. doi: 10.1111/1759-7714.13395
21. Yokoi T, Tsuzuki T, Yatabe Y, Suzuki M, Kurumaya H, Kakudo K, et al. Solitary Fibrous Tumor: Significance of P53 and CD34 Immunoreactivity in its Malignant Transformation. *Histopathology* (1998) 32(5):423–32. doi: 10.1046/j.1365-2559.1998.00412.x
22. Bahrami A, Lee S, Schaefer IM, Boland JM, Patton KT, Fletcher CD, et al. TERT Promoter Mutations and Prognosis in Solitary Fibrous Tumor. *Mod Pathol* (2016) 29(12):1511–22. doi: 10.1038/modpathol.2016.126
23. Machado I, Morales GN, Cruz J, Lavernia J, Giner F, Llombart-Bosch A, et al. Solitary Fibrous Tumor: A Case Series Identifying Pathological Adverse Factors-Implications for Risk Stratification and Classification. *Virchows Arch* (2020) 476(4):597–607. doi: 10.1007/s00428-019-02660-3
24. Subramaniam MM, Lim XY, Venkateswaran K, Shuen CS, Soong R, Petersson F, et al. Dedifferentiated Solitary Fibrous Tumor of the Nasal Cavity: The First Case Reported With Molecular Characterization of a TP53 Mutation. *Histopathology* (2011) 59(6):1269–74. doi: 10.1111/j.1365-2559.2011.03997.x
25. Cabelguenne A, Blons H, Waziers I, Carnot F, Houllier AM, Laurent-Puig P, et al. P53 Alterations Predict Tumor Response to Neoadjuvant Chemotherapy in Head and Neck Squamous Cell Carcinoma: A Prospective Series. *J Clin Oncol* (2000) 18(7):1465–73. doi: 10.1200/JCO.2000.18.7.1465
26. Lin DC, Hao JJ, Nagata Y, Xu L, Shang L, Koeffler HP, et al. Genomic and Molecular Characterization of Esophageal Squamous Cell Carcinoma. *Nat Gene* (2014) 46(5):467–73. doi: 10.1038/ng.2935
27. Daver N, Schlenk RF, Russell NH, Levis MJ. Targeting FLT3 Mutations in AML: Review of Current Knowledge and Evidence. *Leukemia* (2019) 33 (2):299–312. doi: 10.1038/s41375-018-0357-9
28. Takahashi K, Jabbour E, Wang X, Luthra R, Bueso-Ramos C, Garcia-Manero G, et al. Dynamic Acquisition of FLT3 or RAS Alterations Drive a Subset of Patients With Lower Risk MDS to Secondary AML. *Leukemia* (2013) 27 (10):2081–83. doi: 10.1038/leu.2013.165
29. Makishima H, Yoshizato T, Yoshida K, Sekeres MA, Radivoyevitch T, Maciejewski JP, et al. Dynamics of Clonal Evolutions in Myelodysplastic Syndromes. *Nat Genet* (2017) 49(2):204–12. doi: 10.1038/ng.3742

Conflict of Interest: The authors declare that the research was conducted in the absence of any commercial or financial relationships that could be construed as a potential conflict of interest.

Publisher's Note: All claims expressed in this article are solely those of the authors and do not necessarily represent those of their affiliated organizations, or those of the publisher, the editors and the reviewers. Any product that may be evaluated in this article, or claim that may be made by its manufacturer, is not guaranteed or endorsed by the publisher.

Copyright © 2021 Nonaka, Kandori, Nitta, Shiga, Nagumo, Kimura, Kawahara, Negoro, Hoshi, Kojima, Kawai, Mathis, Tamura, Sato, Yamato, Noguchi and Nishiyama. This is an open-access article distributed under the terms of the Creative Commons Attribution License (CC BY). The use, distribution or reproduction in other forums is permitted, provided the original author(s) and the copyright owner(s) are credited and that the original publication in this journal is cited, in accordance with accepted academic practice. No use, distribution or reproduction is permitted which does not comply with these terms.

frontiers in Oncology

ORIGINAL RESEARCH
published: 05 January 2022
doi: 10.3389/fonc.2021.774279

Pyroptosis Regulators and Tumor Microenvironment Infiltration Characterization in Clear Cell Renal Cell Carcinoma

Xi Zhang[1†], *Xiyi Wei*[1†], *Yichun Wang*[1†], *Shuai Wang*[1], *Chengjian Ji*[1], *Liangyu Yao*[1] *and Ninghong Song*[1,2*]

[1] *The State Key Lab of Reproductive Medicine, Department of Urology, The First Affiliated Hospital of Nanjing Medical University, Nanjing, China,* [2] *Department of Urology, The Affiliated Kezhou People's Hospital of Nanjing Medical University, Kezhou, China*

OPEN ACCESS

Edited by:
Marijo Bilusic,
University of Miami Health System, United States

Reviewed by:
Luciana Buonerba,
Azienda Sanitaria Locale Salerno, Italy
Gopalakrishnan Natarajan,
University of Nebraska Medical Center, United States

****Correspondence:***
Ninghong Song
songninghong_urol@163.com

[†]These authors have contributed equally to this work

Specialty section:
This article was submitted to Genitourinary Oncology, a section of the journal Frontiers in Oncology

Received: *11 September 2021*
Accepted: *25 November 2021*
Published: *05 January 2022*

Citation:
Zhang X, Wei X, Wang Y, Wang S, Ji C, Yao L and Song N (2022) Pyroptosis Regulators and Tumor Microenvironment Infiltration Characterization in Clear Cell Renal Cell Carcinoma. Front. Oncol. 11:774279. doi: 10.3389/fonc.2021.774279

Background: It is well known that chronic inflammation can promote the occurrence and progression of cancer. As a type of proinflammatory death, pyroptosis can recast a suitable microenvironment to promote tumor growth. However, the potential role of pyroptosis in clear cell renal cell carcinoma (ccRCC) remains unclear.

Methods: The transcriptome expression profile and mutation profile data of ccRCC with clinical characteristics included in this study were obtained from The Cancer Genome Atlas (TCGA) and Gene Expression Omnibus (GEO) databases. Consensus clustering was used for clustering. Gene set enrichment analysis (GSEA) analysis were applied to evaluate the biological mechanisms. Single sample gene set enrichment analysis (ssGSEA) was applied for evaluating the proportion of various immune infiltrating cells. The ESTIMATE algorithm was involved to compute the immune microenvironment scores.

Results: Among the 17 pyroptosis regulators, a total of 15 pyroptosis regulators were differential expressed between tumor and normal tissues, in which 12 of them emerged strong correlations with prognoses. According to the pyroptosis components, the ccRCC patients were divided into four pyroptosis subtypes with different clinical, molecular, and pathway characteristics. Compared with other clusters, cluster B showed the pyroptosis heat phenotype, while cluster D represented the pyroptosis cold phenotype with poor overall survival. In addition, we performed principal component analysis (PCA) on the differential genes between clusters to construct the pyroptosis index. Furthermore, the pyroptosis index was significantly correlated with survival in different tumor mutation statuses and different grades and stages. Besides, the expression of pyroptosis-related regulators was related to the infiltration of immune cells and the expression of immune checkpoints, among which *AIM2* was considered as the most significant immune-related pyroptosis regulator. Ultimately, we found that *AIM2* was related to the immune activation pathway and was significantly overexpressed in tumor tissues.

Conclusion: This study revealed that pyroptosis regulators and pyroptosis index played an important role in the development and prognoses of ccRCC. Moreover, *AIM2* can be used as a predictor of the response of immunotherapy. Assessing the pyroptosis patterns may help evaluate the tumor status and guide immunotherapy strategies.

Keywords: pyroptosis, pyroptosis index, clear cell renal cell carcinoma, *AIM2*, immune microenvironment

INTRODUCTION

As a frequent malignant tumor of the urinary system, renal cell carcinoma (RCC) originated from the renal tubular epithelial system, which accounted for 80% to 90% of the malignant renal tumors (1, 2). RCC accounted for about 2% of all cancer diagnoses and cancer deaths in the world, and about 295,000 new cases of RCC were diagnosed worldwide every year, with about 134,000 deaths recorded (3). Histologically, clear cell renal cell carcinoma (ccRCC) is the prominent subtype of RCC, accounting for approximately 75% of RCC cases (4). Currently, early resection is considered the basic treatment for ccRCC patients, but nearly 30% of local ccRCC patients had recurrence and metastasis after tumor resection (5). Besides, its curative effects remained inadequate for these terminal ccRCC patients (6). Although great progress had been made in screening, diagnosis, surgery, and various treatments, the clinical results of advanced ccRCC were still unsatisfactory (6). Therefore, in order to provide better treatment for ccRCC patients, it was necessary to comprehensively understand the biological mechanism of ccRCC development.

Recently, the role of pyroptosis in cancer growth, invasion, and metastasis has been given more and more attention, and pyroptosis has gradually become a good opportunity to improve the efficacy of cancer immunotherapy (7, 8). Besides, pyroptosis is a newly discovered programmed death mode of inflammatory cells (9). It mainly mediated the activation of a variety of caspases including caspase-1 through inflammasomes, bringing about the ceaseless extension of cells until the break of the cell membrane, which led to the release of cell substance and after that enacted a solid inflammatory response (9, 10).

The aims of the research were to investigate the mechanism of pyroptosis-related regulators (PRRs) in ccRCC and to explore the effect of PRRs in the prognoses of ccRCC patients. We divided ccRCC samples into four pyroptosis clusters and constructed the pyroptosis index (PI) based on the diverse genes between different clusters to predict the survival rate and progress of ccRCC. In addition, we analyzed the correlation of PRRs with the infiltration of immune cells and the expression of immune checkpoints, which may help guide ccRCC immunotherapy strategies.

METHODS

Clear Cell Renal Cell Carcinoma Dataset Source and Preprocessing

In this study, a total of two eligible ccRCC cohorts [GSE29609 and The Cancer Genome Atlas-Kidney renal clear cell carcinoma (TCGA-KIRC)] were collected for further analysis. Public gene expression data and complete clinical annotations of ccRCC in the GEO and TCGA databases were obtained for analysis, among which cases without survival information and survival status were excluded. Besides, we downloaded somatic mutation data from the TCGA database. R (version 4.1.1) and R Bioconductor package were utilized for analysis. The Wilcoxon test was used to identify differentially expressed PRRs. At the same time, $|\text{LogFC}| > 2$ and $P < 0.05$ were used as the criteria for screening differentially expressed PRRs. Real-time quantitative PCR (RT-qPCR) was utilized to assess the *AIM2* expression in ccRCC (**Table S1**).

Establishment of Pyroptosis Clusters

Based on the expression of 17 PRRs, we applied unsupervised cluster analysis to identify disparate PRR modification patterns and classified patients for further analysis. The number of clusters and their steadiness was decided by the consensus clustering calculation. We utilized the ConsensusClusterPlus package to perform the procedures and repeated it 1,000 times to ensure the stability of the classification (11). The overall survival (OS) for each pyroptosis cluster was calculated by employing the Kaplan Meier (KM) curve. Meanwhile, the log-rank test was utilized to evaluate the distinction in survival between the high-expression group and low-expression group with a criteria level of $P < 0.05$.

Identification of the Immune Characteristics of Clusters

In order to further explore the role of PRRs in biological pathway, we utilized the "GSVA" R package to perform gene set variation analysis (GSVA). In non-parametric and unsupervised strategies, GSVA was as a rule utilized to assess changes in pathways and biological process movement in expression dataset tests. We downloaded the gene set of "c2.cp.kegg.v7.4.symbols" from the MSigDB database for running GSVA. A balanced *P*-value of less than 0.05 was considered statistically critical. The ssGSEA score was used to quantify the enrichment level of 23 immune signatures in each KIRC sample. Charoentong's research had stored various human immune cell subtypes, including activated CD8 T cells, activated dendritic cells, and regulatory T cells. Therefore, we obtained the genome of each TME-infiltrating immune cell type from this study. The relative abundance of each TME-infiltrated cell in each sample was represented by the enrichment score calculated by ssGSEA. In addition, we further analyzed the difference of each cluster and used the VennDiagram package to draw the Venn diagram of the genes that overlap between each cluster. To

further confirm the potential functions of the intersection genes, the data were analyzed through function enrichment. Gene Ontology (GO) is a widely used tool for annotating functional genes, especially molecular functions (MFs), biological pathways (BPs), and cellular components (CCs). The Kyoto Encyclopedia of Genes and Genomes (KEGG) enrichment analysis is practical and can be used to analyze gene function and related advanced genome function information. To comprehend the carcinogenic impacts of target genes, the clusterProfiler package was utilized to analyze the GO functions of the overlapping genes and enhance the KEGG pathway. Besides, we also used GSEA to determine the potential molecular mechanism of *AIM2* in KIRC.

Establishment of the Pyroptosis Index

To measure the PRRs alteration of cancer, we built a set of the scoring framework to assess the PRR adjustment of patients with ccRCC—the pyroptosis index (PI). The strategies established by PI mainly included the following points: the different expression PRRs recognized from different clusters were firstly normalized among all ACRG (Asian Cancer Research Group) tests and the overlapping genes were extricated. At that point, we performed the prognostic analysis for each gene within the signature utilizing the univariate Cox regression model. The genes with a critical prognosis were extricated for advanced investigation. Both central components 1 and 2 were chosen to act as signature scores. This strategy had the advantage of centering the score on the set with the largest block of well-connected (or anticorrelated) qualities within the set; while down-weighting contributions from genes that do not track with other set members. We at that point characterize the index employing a strategy comparable to GGI (12, 13):

$$\text{Index} = \sum(\text{PC1}_i + \text{PC2}_i)$$

Where i represents the expression of PRRs.

Correlation Between Pyroptosis Index and Other Related Biological Processes

According to the correlation between PI and patient survival rate, the survival R package was utilized to decide the cutoff point of each dataset subgroup. The work of the surv-cutpoint was to more than once test all potential cutoff points to discover the biggest rank measurement so that patients were separated into high and low PI groups based on the biggest chosen log-rank measurement to diminish the calculated batch effect. We used the ggalluvial R package to draw an alluvial map to show the changes between cluster, PI, and survival status. We performed correlation analysis on the PI to further reveal the connection between the PI and immune cells. The maftools function was used to present a waterfall chart of the mutation landscape of patients with high and low PI clusters. The KM method was used to analyze the survival correlation between the high and low PI groups and clinical grouping information. Finally, we downloaded the scoring data of 537 cases of KIRC immunotherapy from The Cancer Immunome Database (TCIA) and analyzed the correlation between high- and low-risk groups and immunotherapy. All statistical *P*-values were two-sided, with $P < 0.05$ as statistically critical. All data preparation was completed by R 4.1.1 software.

RESULTS

Genetic Variation Prognoses of Pyroptosis Regulators in Clear Cell Renal Cell Carcinoma

After merging the GEO and TCGA databases, we finally identified 17 PRRs. Among the 336 samples, only 7 samples had PRR mutations, and the mutation rate was 2.08%. It was found that only *GBP1*, *CASP8*, *TLR4*, *GBP2*, and *LBP* had mutations, and none of the other genes showed any mutations in the KIRC samples (**Figure 1A**). **Figure 1B** showed the copy number variation (CNV) changes of the PRRs on the chromosome. In addition, through the analysis of the frequency of CNV changes, it was found that CNV changes were common in 17 genes and most of them were concentrated in the loss of copy number, while the loss of MYD88 was the most obvious. In addition, only the copy number of *AIM2* was amplified (**Figure 1C**). To determine whether the abovementioned genetic variation affected the expression of PRRs in ccRCC patients, we further analyzed the expression levels of PRRs in normal and tumor samples. It was discovered that the genes other than *TNF* and *LBP* were significantly separate between normal and tumor samples (**Figure 1D**). However, compared with normal tissues, the expression of PRRs deleted in CNV was significantly higher in tumor tissues (**Figures 1C, D**). The above results showed that although the expression of PRRs was highly heterogeneous in normal and tumor samples, the alteration of CNV may not be the main factor causing the perturbation of PRRs. To clarify the impacts of these 17 PRRs on the prognoses of ccRCC, we carried out the survival analysis. The results showed that a total of 12 PRRs have significant differences, of which 7 PRRs were negatively correlated with prognoses and the rest were positively correlated. In addition, 5 genes were not different between tumor and normal tissues (**Figure 2**).

Identification of the Immune Characteristics and Prognoses of Each Pyroptosis Cluster

We used the ConsensusClusterPlus package to classify patients depending on the expression levels of 17 PRRs and finally distinguished 4 diverse clusters (**Figure 3A**). Next, survival analysis was conducted based on the four clusters. The results showed that there was critical statistical diversity between the clusters, and cluster A had the most significant survival advantage (**Figure 3B**). In addition, the correlation heat map indicated the expression of PRRs and various clinical information including survival status, grade, TMN, and age among clusters A–D. The outcomes showed that the expression of PRRs was generally higher in B and C (**Figure 3C**). Besides, to explore the immune atlas of pyroptosis clusters, we first investigated the layout of 23 immune cells in each cluster. The results showed that innate

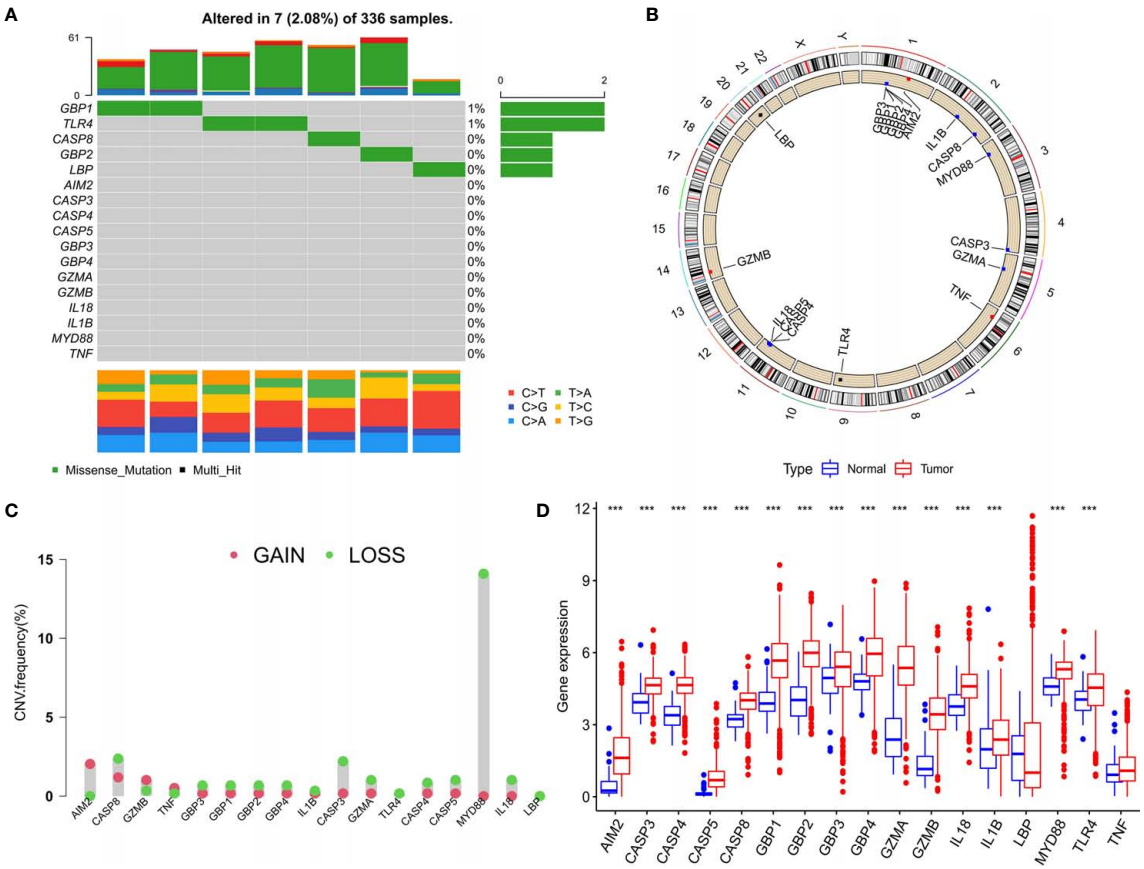

FIGURE 1 | Expression and genetic variation of pyroptosis regulators in clear cell renal cell carcinoma. **(A)** The mutation frequency of 17 pyroptosis regulatory factors for 336 ccRCC patients in the TCGA-KIRC cohort. **(B)** The location of CNV alteration of pyroptosis regulators on 23 chromosomes. **(C)** The CNV variation frequency of pyroptosis regulators. red circle: amplified frequency; green circle: missing frequency. **(D)** The expression difference of 17 pyroptosis regulatory factors between normal tissue and ccRCC tissue. The asterisk represents the statistical p value (*P < 0.05; **P < 0.01; ***P < 0.001).

immune cell infiltration was significantly enriched in cluster B including activated CD8 T cell, immature B cell, natural killer cell, MDSC, mast cell, T follicular helper cell, and type 1 T helper cell (**Figure 3D**). In addition, patients in cluster B showed better survival advantage (**Figure 3B**). However, although the degree of innate immune cell infiltration was low in cluster A, it had an obvious survival advantage (**Figures 3B, D**).

Identification of GSVA and Functional Enrichment Analysis Between Pyroptosis Clusters

To investigate the biological behaviors of these PRRs, we performed GSVA. Cluster A showed obvious immunosuppression, where adipocytokine_SIGNALING_PATHWAY, INOSITOL_PHOSPHATE_Metabolism, and notch_SIGNALING_Pathway were significantly enriched (**Figures 4A, B**). Cluster B showed enrichment pathways related to complete immune activation, including CHEMOKINE_SIGNALING_PATHWAY, T_CELL_RECEPTOR_SIGNALING_PATHWAY, and toll_LIKE_RECEPTOR_SIGNALING_ PATHWAY (**Figure 4A**). Besides, the P53 SIGNALING PATHWAY, JAK–STAT SIGNALING PATHWAY, and CHEMOKINE SIGNALING PATHWAY were significantly enriched in cluster C (**Figure 4F**). Similarly, cluster D showed obvious immunosuppression (**Figure 4E**). To our surprise, we found that cluster C was significantly enriched in innate immune cell infiltration, including natural killer cells, macrophages, CD4-positive T cells, and MDSC cells. However, patients with this PRR modification pattern showed the worst survival advantage. We speculated that this may be related to the abnormal activation of the JAK–STAT signaling pathway and p53 signaling pathway. Then, we screened the differential genes between the two clusters according to the adjusted P <0.001 standards. Then, the differential genes in these 6 groups (A–B, A–C, A–D, B–C, B–D, C–D) were crossed, and finally, 70 crossed genes were obtained (**Figure 5A**). The selected 70 intersection genes were further analyzed by GO annotation and KEGG enrichment. The results of BP showed that the 70 intersection genes were mainly concentrated in T-cell activation, regulation of T-cell activation, lymphocyte differentiation, T-cell differentiation, leukocyte cell–cell adhesion, and regulation of leukocyte cell–cell adhesion. Regarding MFs, the target genes were usually enriched in cytokine binding, cytokine receptor

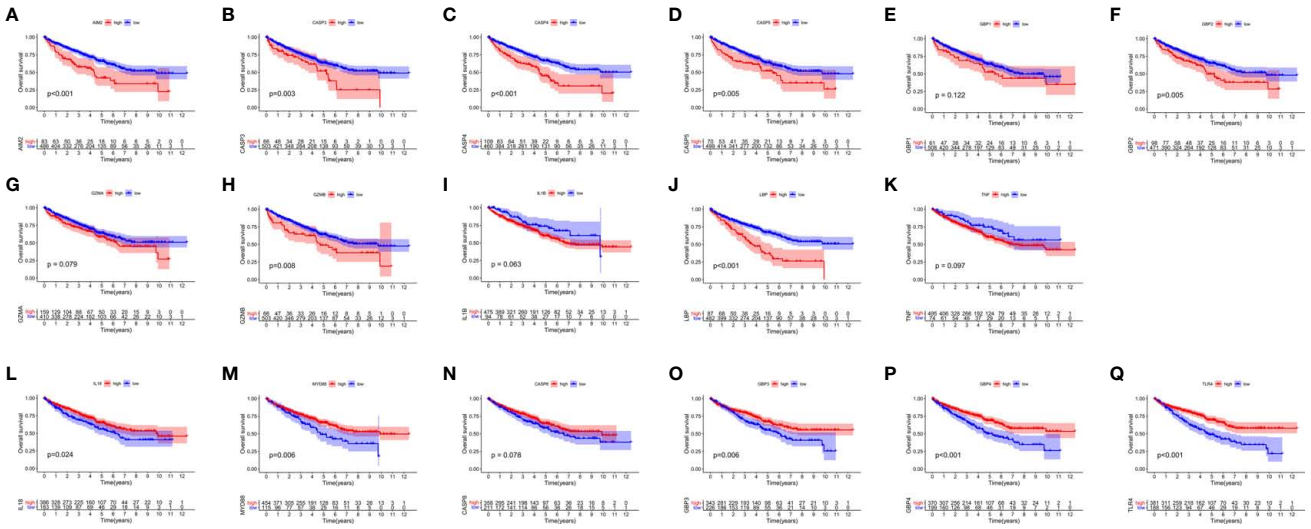

FIGURE 2 | The OS Kaplan-Meier curve of 17 pyroptosis regulators in the TCGA-KIRC. **(A–K)** 11 pyroptosis regulators were negatively correlated with survival. **(L–Q)** 6 pyroptosis regulators were positively correlated with survival.

activity, and immune receptor activity. Regarding CCs, target genes were mainly concentrated on the external side of the plasma membrane, plasma membrane signaling receptor complex, and immunological synapse (**Figure 5B**). KEGG annotation results demonstrated enrichment in hematopoietic cell lineage, cytokine–cytokine receptor interaction, chemokine signaling pathway, and human immunodeficiency virus 1 infection (**Figure 5C**).

Identification of the Tumor Mutation Burden and Clinical Characteristics of the Pyroptosis Index

Because of the heterogeneity and complexity of PRR modification, we constructed the PI to evaluate the PRR modification pattern of individual patients. The alluvial map was used to visualize the attribute changes of a single patient (**Figure 6A**). To more usefully outline the characteristics of the PI, we, moreover, analyzed the relationship between immune cells and PI. The outcomes appeared that the index was closely associated with immature B cell, natural killer cell, regulatory T cell, and T follicular helper cell (**Figure 6B**). The results of the Kruskal–Wallis test revealed that compared with other clusters, cluster B showed a significantly increased index (**Figure 6C**). Moreover, the results showed that the index was positively related to the patient prognoses (**Figure 6D**). There was no doubt that the L-TMB had a better survival advantage (**Figure 6E**). Survival analysis combining mutation and index proved the accuracy of the above results (**Figure 6F**). In order to explore whether the index applied to patients of various clinical groups, we used the KM curve to analyze whether there were prognosis contrasts between high and low PI groups among diverse clinical groups. The results showed that there were critical statistical differences between high index and low index in age ≤65, G1–2, M0, N0, and T3–4 groups. Compared with the low-index group, the high-index group had a significant survival advantage (**Figure 7**). Then, the maftools package was employed to investigate the discrepancy of somatic mutations between the low-index group and the high-index group in the TCGA-KIRC cohort. **Figures S1A, B** reveal that the high-index group presented broader tumor mutation burden than the low-index group. In addition, we investigated the relationship between the PI and survival status. The consequence of the histogram and block diagram indicated that the high-index group had better survival advantages (**Figures S1C, D**). Besides, we tested whether PI can be used as an independent prognostic biomarker for ccRCC. Therefore, we constructed a nomogram to speculate the prognoses of KIRC (**Figure S2A**). Meanwhile, multivariate Cox regression analysis confirmed that PI was a credible and independent prognostic biomarker for assessing the prognoses of ccRCC patients (HR = 0.945; 0.901–0.991) (**Figures S2B, C**). In particular, we inspected the capacity of PI to predict the curative effect of immunotherapy in ccRCC patients. Besides, anti-PD-1 therapy was more suitable for high-index patients (**Figure S2D**), while anti-CTLA-4 therapy response was not different between the high- and low-index groups (**Figure S2E**).

Identification of the Immune Characteristics of Pyroptosis Regulators

In order to systematically study the potential influence of PRRs on the immune microenvironment of ccRCC, we utilized correlation analysis for PRRs and infiltrating immunocytes and immune checkpoints. The expression level of immune checkpoints was positively related to PRRs (**Figure 8A**). Considering the known role of checkpoints in the immunosuppressive microenvironment, PRRs may have important biological functions in ccRCC immunotherapy. Besides, correlation analysis found that PRRs were negatively associated with various immune cells (**Figure 8B**).

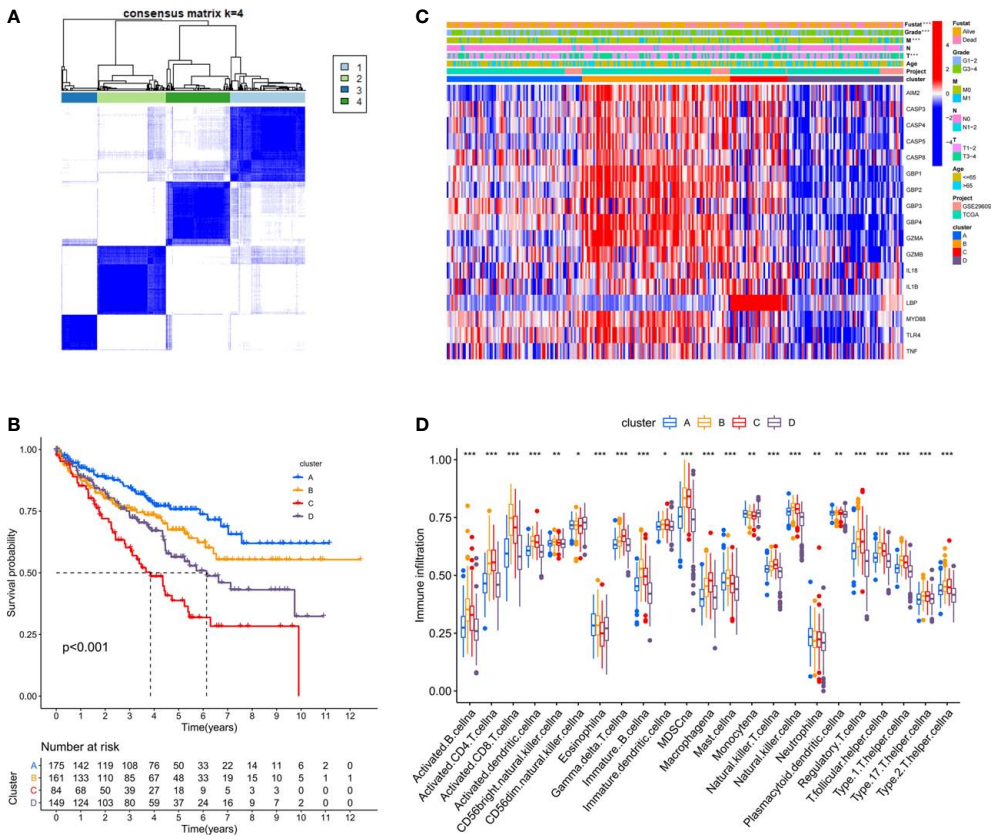

FIGURE 3 | Identification of potential pyroptosis clusters in ccRCC patients. **(A)** Sample distribution of different clusters. **(B)** The OS Kaplan-Meier curve of different clusters in ccRCC patients. **(C)** The heatmap showing gene expression and clinical correlation among different clusters of ccRCC. **(D)** Differential expression of immune cells among the KIRC pyroptosis clusters. The asterisk represents the statistical p value (*P < 0.05; **P < 0.01; ***P < 0.001).

Collectively, PRRs were positively correlated with $CD8^+$ T cell, follicular helper T cell, and gamma delta T cell and negatively correlated with mast cell, monocyte, and myeloid dendritic cell. In view of the remarkable mutation characteristic, prognostic, and immunoregulatory effects of *AIM2*, GSEA was used to examine *AIM2*-related signaling pathways. GSEA results showed that *AIM2* was involved in multiple malignant pathways, including JAK–STAT SIGNALING PATHWAY, B-CELL RECEPTOR SIGNALING PATHWAY, NATURAL KILLER CELL-MEDIATED CYTOTOXICITY, and T-CELL RECEPTOR SIGNALING PATHWAY (**Figures 8C–G**).

Validation of *AIM2* in Tissues and Cell Lines

RT-qPCR was carried out in 15 pairs of ccRCC tissues and normal renal tissues and 4 cell lines, consisting of 3 tumor cell lines and 1 normal renal cell line. Compared with normal renal cell lines, the expression of *AIM2* in tumor cell lines was significantly higher, and the expression was the highest in 786-O cell lines (**Figure 9A**). Besides, in tumor tissues, the expression level of *AIM2* was significantly higher than that in normal renal tissues (**Figure 9B**). The above experimental results were consistent with the results predicted by bioinformatics methods. In addition, the Human Protein Atlas (HPA) database explicitly uncovered that in ccRCC tissues, the expression levels of *AIM2* were significantly higher than those in normal renal tissue (**Figures 9C, D**).

DISCUSSION

In recent years, the morbidity and mortality of RCC have gradually increased, which has become the most fatal adult renal malignancy (14). With the development of scientific research, the traditional histopathological features (tumor size, stage, and grade) may not meet the needs of diagnosis and prognoses (15, 16). Pyroptosis, the lytic programmed cell death, was a pivotal fibrotic mechanism in the development of renal pathology, which has been broadly investigated in inflammatory disease models (17, 18). Recently, more and more shreds of evidence have shown that in the absence of any bacterial or viral infection, pyroptosis can be chemically induced in cancer cells (19, 20). Therefore, we investigated the expression of PRRs in ccRCC and established PI to further predict the role of PRRs in prognoses. In addition, we analyzed the biological function of *AIM2*, which may be an effective immune target.

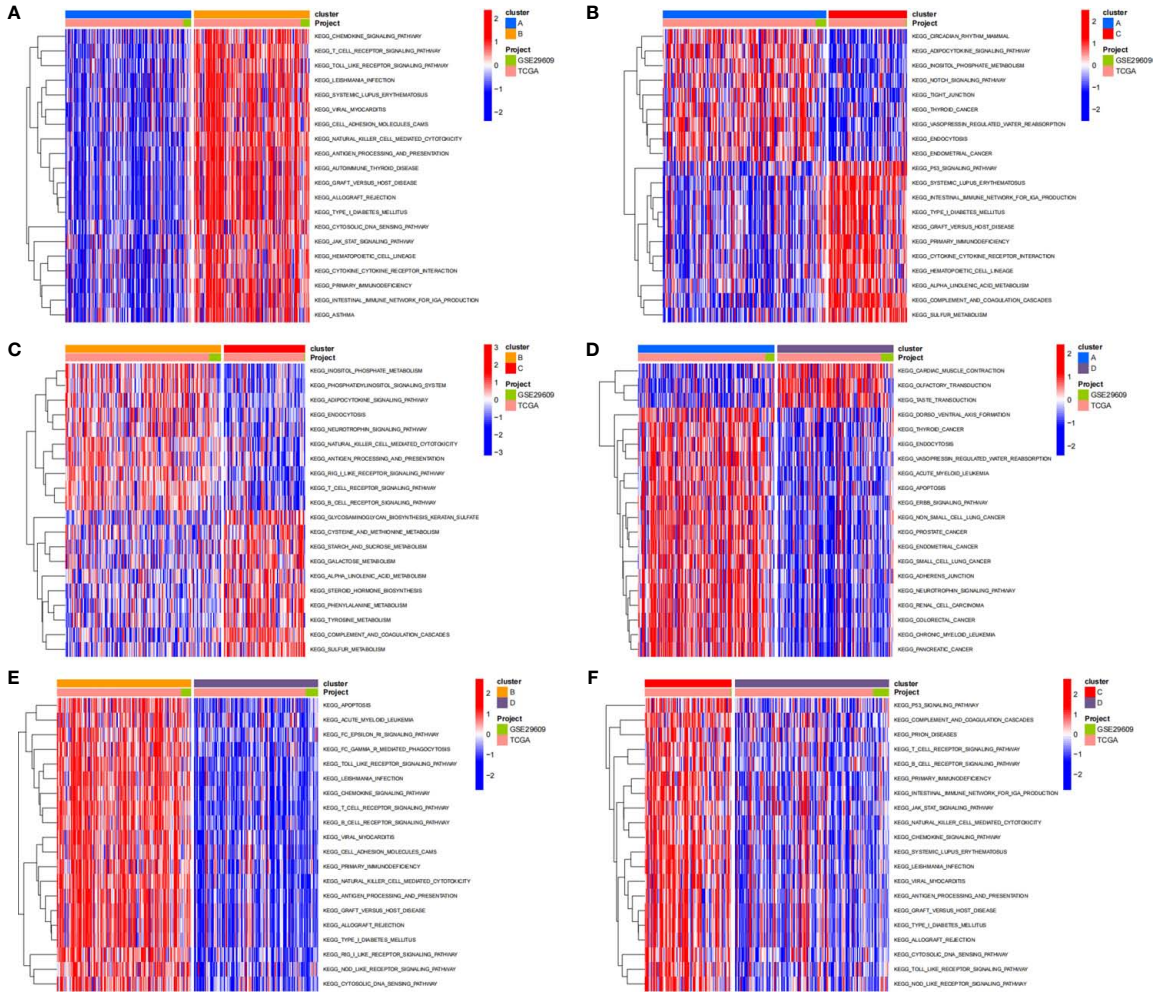

FIGURE 4 | The results of GSVA enrichment analysis. The heatmap showing the results of GSVA enrichment analysis among different pyroptosis clusters. Red represented activated pathways; blue represented inhibited pathways. (**A**: cluster A vs cluster B; **B**: cluster A vs cluster C; **C**: cluster B vs cluster C; **D**: cluster A vs cluster D; **E**: cluster B vs cluster D; **F**: cluster C vs cluster D).

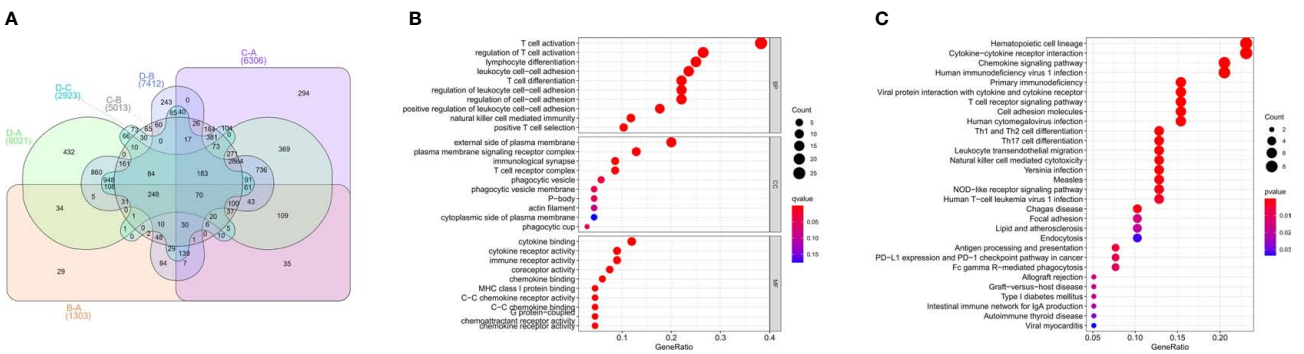

FIGURE 5 | GO, KEGG analysis of intersective differential genes between clusters. **(A)** Venn diagram of 70 intersection genes. **(B)** Bubble of GO enrichment analysis results for 70 intersection genes. **(C)** Bubble of KEGG enrichment analysis results for 70 intersection genes.

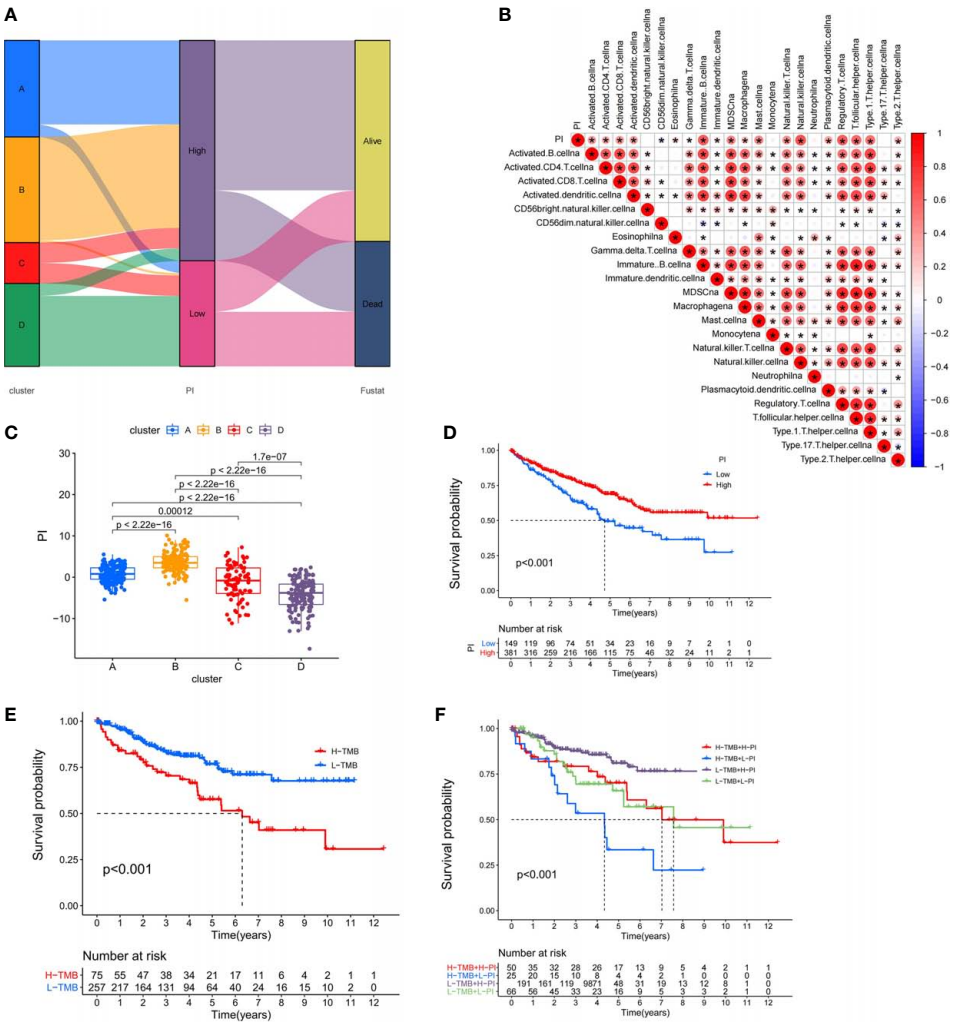

FIGURE 6 | Immunological and tumor somatic mutation characteristics of pyroptosis index. **(A)** Alluvial diagram showing the changes of clusters, index, and fustat. **(B)** Correlations between the PI and immune cells. **(C)** Differential expression of PI among the KIRC pyroptosis clusters. **(D)** The OS Kaplan-Meier curve of High and Low PI. **(E)** The OS Kaplan-Meier curve of high and low TMB groups. **(F)** The OS Kaplan-Meier curve of the combination of PI and TMB.

Through the results, we found that the PRRs played important roles in the development and invasion of ccRCC. The expression of the majority of PRRs in tumor tissues was significantly increased compared with that in normal tissues. Most of the PRRs were critically associated with the prognoses of ccRCC and appeared to be cancer-promoting genes, which led to poor prognoses. With more and more research carried out, scholars found that PRRs performed disparate roles in various cancers (21). For instance, the upregulation of PRR expression in non-small cell lung cancer and breast cancer (BC) was related to poor prognoses (21, 22). On the contrary, many studies have also shown the antitumor activity of the PRRs. The low expression of PRRs in gastric cancer (GC), hepatocellular carcinoma (HCC), and colorectal cancer (CRC) was associated with poor prognoses (23–26).

Here, the KIRC cohort was divided into four clusters *via* the 17 PRRs. Among them, B and C were closely related to PRRs, while cluster A and cluster D were the opposite. In addition, there was more immune cell infiltration in cluster B and cluster C and less in cluster A and cluster D. We speculated that the PRRs had used two signaling pathways (the classical pathway that depended on caspase-1 and the non-classical pathway that depended on caspase-4, 5, and 11) to cleave the precursors of IL-1β and IL-18 to form active IL-1β and IL-18. The active IL-1β and IL-18 were released to the outside of the cell, which recruited immune cells to gather and amplified the inflammatory response (27). Although cluster C was rich in immune cells, it failed to match the corresponding survival advantage. It was possibly because cancer cells may functionally shape their microenvironment by secreting various cytokines, chemokines,

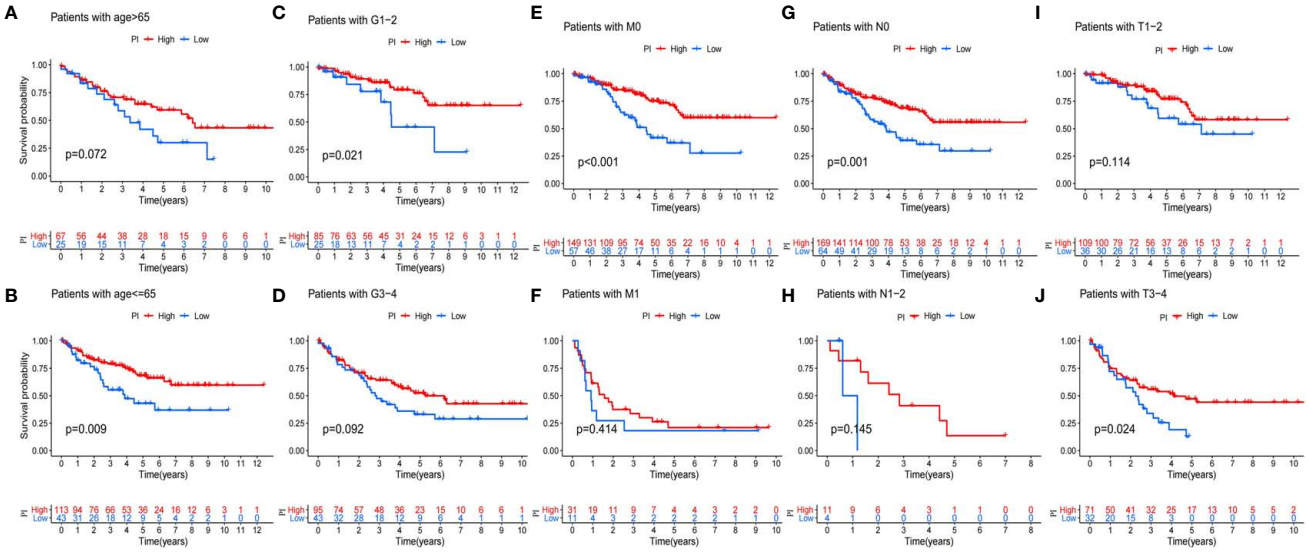

FIGURE 7 | Validation of the prognosis of PI under the stratifications of different clinical parameters. **(A, B)** age > 65 and age <=65; **(C, D)** histological grade 1-2 and 3-4; **(E, F)** M stage 0 and 1 **(G, H)** N stage 0 and 1; **(I, J)** T stage 1-2 and 3-4.

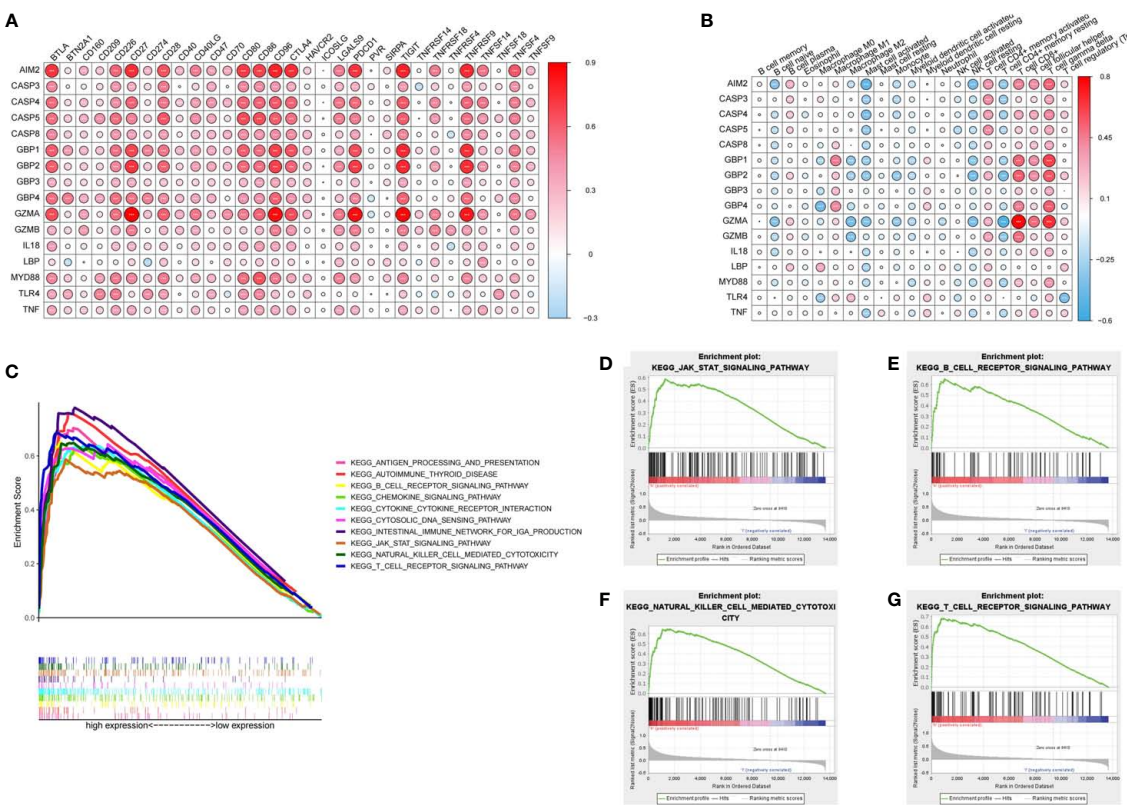

FIGURE 8 | Immune characteristics and enrichment pathway characteristics of pyroptosis related regulators **(A)** Association between pyroptosis regulators and immune cells. **(B)** Association between pyroptosis regulators and immune checkpoints. **(C–G)** The results of GSEA analysis of AIM2.

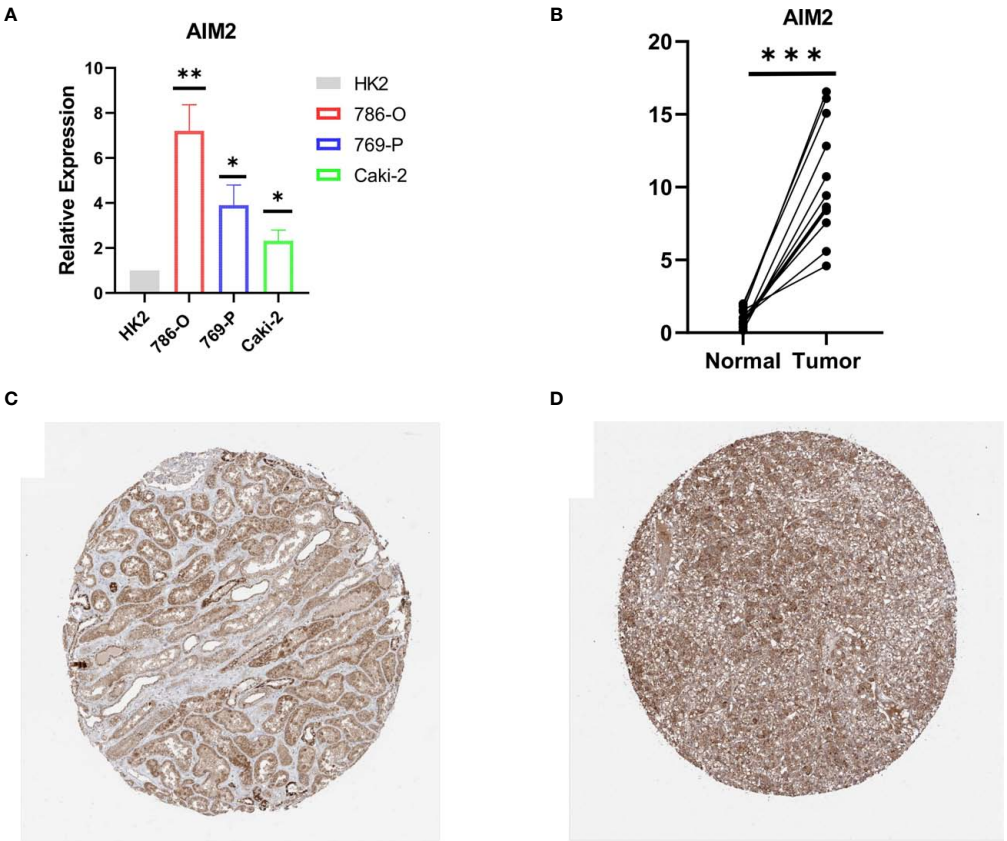

FIGURE 9 | Validation of AIM2 in ccRCC tissues and cell lines. **(A)** Bar plot for the relative expression of AIM2 in ccRCC cell lines and normal HK2 cell line. **(B)** Bar plot for the relative expression of AIM2 between ccRCC tissues and normal tissues. **(C)** Immunohistochemical analysis of AIM2 in normal kidney tissues. **(D)** Immunohistochemical analysis of TRIM2 in ccRCC tissues.

and other factors, which led to the reprogramming of the surrounding immune cells. Eventually, a microenvironment that promoted tumor growth and metastasis was formed, which showed the phenomenon of immune evasion (28, 29). The JAK–STAT pathway regulated and controlled tumor cell proliferation, differentiation, and metastasis and played a significant part in regulating the tumor microenvironment (30). The abnormal activation of the JAK–STAT pathway in cluster C promoted the production of some tumor-derived factors such as IL-6, TGF-β, VEGF, and other factors. In addition, it also promoted the recruitment and activation of dendritic cells (DCs), myeloid-derived suppressor cells (MDSCs), tumor-associated macrophages (TAMs), and other cells in the microenvironment. Meanwhile, it released a great quantity of the immunosuppressive factors, recruited the abundance of the immunosuppressive cells, and finally formed a vicious circle of immunosuppressive tumor microenvironment (30). In addition, the JAK/STAT3 pathway may enhance TGF-β-induced epithelial–mesenchymal transition (EMT) to promote tumor metastasis (31).

Considering the individual heterogeneity of genetic modification of pyroptosis, there was an urgent need to quantify the pattern of genetic modification of pyroptosis in individual tumors. To this end, we established the PI to evaluate the PRR modification pattern for individual KIRC patients. We demonstrated that the index can be used to evaluate the prognosis characteristics of patients. Similarly, the PI can be used as an independent prognostic biomarker to predict patient survival. Other than that, we were able to, moreover, foresee the adequacy of the clinical reaction of patients to PD-L1 immunotherapy through the PI. Previously, Khadirnaikar et al. developed and verified an immune lncRNA prognostic score for KIRC patients, which may be used as an independent indicator for judging the prognoses of KIRC patients (32). Diversely, we used PRRs to establish the pyroptosis index for KIRC patients. Besides, Sun et al. constructed a prognostic risk model related to pyroptosis, which can divide KIRC patients into low- and high-risk subgroups with different prognoses and immune cell infiltration. They also systematically analyzed the prognostic value of PRRs in KIRC, their role in TME, their response to ICIs, and drug sensitivity, providing new insights into the role of pyroptosis in KIRC patients in TME and even helping to develop new treatment strategies (33). Compared with us, we firstly systematically and comprehensively analyzed the prognostic

characteristics and immune correlation of all PRRs. Secondly, we determined that *AIM2* was the most significant immune-related PRRs in ccRCC, and through *in vitro* experiments, we were able to verify our conclusions.

AIM2 was confirmed to be closely related to immune activation through GSEA and was positively correlated with immune checkpoints. *AIM2* contained a PYD domain matching the NLRP and a hematopoietic IFN-inducible nucleoprotein with a 200 amino acid repeat (HIN200) domain that recognized exogenous dsDNA. In addition to these two pattern recognition receptors, there were two other proteins, ASC and caspase-1, which were related to the formation of the inflammatory complex. Besides, *AIM2* played a significant part in the development and invasion of tumors and played pro- or anticancerous roles in different tumors. For instance, low expression of *AIM2* in HCC was related to lower OS (34). The reason may be that *AIM2* deficiency enhanced the expression of fibronectin-1 and EMT, thus promoting the metastasis of HCC (34). In addition, *AIM2* may inhibit the growth of HCC by inhibiting the mTOR/S6K1 pathway (35). The high expression of *AIM2* was associated with a higher survival rate in EBV-induced nasopharyngeal carcinoma (NPC). The effect of *AIM2* may be related to IL-1β and immune stimulation of neutrophils to accumulate into tumors to mediate antitumor activity (36). Furthermore, *AIM2* played an protumor role in colorectal tumors because overexpression of *AIM2* in colorectal cancer cells induced the expression of invasion-associated genes such as *VIM* and *MCAM* (37). *AIM2* was overexpressed in non-small cell lung cancer and facilitated cell proliferation (38, 39). In addition, our research showed that *AIM2* was highly expressed in ccRCC and promoted tumor development through immune activation pathways.

CONCLUSION

In a word, our research indicated that PRRs served as critical parts in the development and prognoses of ccRCC. In addition, we established the PI, which can be used to evaluate the clinical, prognostic, and immune patterns. Besides, *AIM2* may regulate the expression of the immune checkpoints, which was a potential immunotherapy target.

DATA AVAILABILITY STATEMENT

The datasets presented in this study can be found in online repositories. The names of the repository/repositories and accession number(s) can be found in the article/**Supplementary Material**.

ETHICS STATEMENT

The studies involving human participants were reviewed and approved by the Ethical Committee of The First Affiliated Hospital of Nanjing Medical University. The patients/participants provided their written informed consent to participate in this study.

AUTHOR CONTRIBUTIONS

NS designed this work. XZ and XW wrote the manuscript. YW performed the bioinformatics analysis. CJ, LY, and SW performed the data review. All authors contributed to the article and approved the submitted version.

FUNDING

This work was supported by the National Natural Science Foundation of China (grant number 82071638).

SUPPLEMENTARY MATERIAL

The Supplementary Material for this article can be found online at: https://www.frontiersin.org/articles/10.3389/fonc.2021.774279/full#supplementary-material

Supplementary Figure 1 | Characteristics of tumor somatic mutation and survival in high and low index groups. **(A, B)** The waterfall plot of tumor somatic mutation established by high and low PI groups. **(C)** Proportion distribution of fustat in the PI groups. **(D)** Differential expression of PI in fustat of KIRC patients.

Supplementary Figure 2 | The role of pyroptosis index in immunotherapy and prognoses evaluation **(A)** The nomogram to predict ccRCC patients. **(B, C)** Univariate and Multivariate Cox regression analysis for PI in KIRC shown by the forest plot. **(D–G)** Differential expression of anti-CTLA4 and anti-PD1 combination immunotherapy among the KIRC PI.

REFERENCES

1. Ljungberg B, Bensalah K, Canfield S, Dabestani S, Hofmann F, Hora M, et al. EAU Guidelines on Renal Cell Carcinoma: 2014 Update. *Eur Urol* (2015) 67 (5):913–24. doi: 10.1016/j.eururo.2015.01.005
2. Gansler T, Ganz PA, Grant M, Greene FL, Johnstone P, Mahoney M, et al. Sixty Years of CA: A Cancer Journal for Clinicians. *CA Cancer J Clin* (2010) 60(6):345–50. doi: 10.3322/caac.20088
3. Barata PC, Rini BI. Treatment of Renal Cell Carcinoma: Current Status and Future Directions. *CA Cancer J Clin* (2017) 67(6):507–24. doi: 10.3322/caac.21411
4. Weng S, DiNatale RG, Silagy A, Mano R, Attalla K, Kashani M, et al. The Clinicopathologic and Molecular Landscape of Clear Cell Papillary Renal Cell Carcinoma: Implications in Diagnosis and Management. *Eur Urol* (2021) 79 (4):468–77. doi: 10.1016/j.eururo.2020.09.027
5. Gulati S, Vaishampayan U. Current State of Systemic Therapies for Advanced Renal Cell Carcinoma. *Curr Oncol Rep* (2020) 22(3):26. doi: 10.1007/s11912-020-0892-1
6. Garcia JA, Rini BI. Recent Progress in the Management of Advanced Renal Cell Carcinoma. *CA Cancer J Clin* (2007) 57(2):112–25. doi: 10.3322/canjclin.57.2.112
7. Tan Y, Chen Q, Li X, Zeng Z, Xiong W, Li G, et al. Pyroptosis: A New Paradigm of Cell Death for Fighting Against Cancer. *J Exp Clin Cancer Res* (2021) 40(1):153. doi: 10.1186/s13046-021-01959-x
8. Tan Y, Chen Q, Li X, Zeng Z, Xiong W, Li G, et al. Correction to: Pyroptosis: A New Paradigm of Cell Death for Fighting Against Cancer. *J Exp Clin Cancer Res* (2021) 40(1):219. doi: 10.1186/s13046-021-02101-7
9. Yu P, Zhang X, Liu N, Tang L, Peng C, Chen X. Pyroptosis: Mechanisms and Diseases. *Signal Transduct Target Ther* (2021) 6(1):128. doi: 10.1038/s41392-021-00507-5

10. Bedoui S, Herold MJ, Strasser A. Emerging Connectivity of Programmed Cell Death Pathways and Its Physiological Implications. *Nat Rev Mol Cell Biol* (2020) 21(11):678–95. doi: 10.1038/s41580-020-0270-8
11. Wilkerson MD, Hayes DN. ConsensusClusterPlus: A Class Discovery Tool With Confidence Assessments and Item Tracking. *Bioinformatics* (2010) 26 (12):1572–3. doi: 10.1093/bioinformatics/btq170
12. Zeng D, Li M, Zhou R, Zhang J, Sun H, Shi M, et al. Tumor Microenvironment Characterization in Gastric Cancer Identifies Prognostic and Immunotherapeutically Relevant Gene Signatures. *Cancer Immunol Res* (2019) 7(5):737–50. doi: 10.1158/2326-6066.CIR-18-0436
13. Sotiriou C, Wirapati P, Loi S, Harris A, Fox S, Smeds J, et al. Gene Expression Profiling in Breast Cancer: Understanding the Molecular Basis of Histologic Grade to Improve Prognosis. *J Natl Cancer Inst* (2006) 98(4):262–72. doi: 10.1093/jnci/djj052
14. Scelo G, Larose TL. Epidemiology and Risk Factors for Kidney Cancer. *J Clin Oncol* (2018) 36(36):Jco2018791905. doi: 10.1200/JCO.2018.79.1905
15. Penticuff JC, Kyprianou N. Therapeutic Challenges in Renal Cell Carcinoma. *Am J Clin Exp Urol* (2015) 3(2):77–90.
16. Tenold M, Ravi P, Kumar M, Bowman A, Hammers H, Choueiri TK, et al. Current Approaches to the Treatment of Advanced or Metastatic Renal Cell Carcinoma. *Am Soc Clin Oncol Educ Book* (2020) 40:1–10. doi: 10.1200/EDBK_279881
17. Bergsbaken T, Fink SL, Cookson BT. Pyroptosis: Host Cell Death and Inflammation. *Nat Rev Microbiol* (2009) 7(2):99–109. doi: 10.1038/nrmicro2070
18. Cookson BT, Brennan MA. Pro-Inflammatory Programmed Cell Death. *Trends Microbiol* (2001) 9(3):113–4. doi: 10.1016/S0966-842X(00)01936-3
19. Wang Y, Gao W, Shi X, Ding J, Liu W, He H, et al. Chemotherapy Drugs Induce Pyroptosis Through Caspase-3 Cleavage of a Gasdermin. *Nature* (2017) 547(7661):99–103. doi: 10.1038/nature22393
20. Wellenstein MD, de Visser KE. Cancer-Cell-Intrinsic Mechanisms Shaping the Tumor Immune Landscape. *Immunity* (2018) 48(3):399–416. doi: 10.1016/j.immuni.2018.03.004
21. Xia X, Wang X, Cheng Z, Qin W, Lei L, Jiang J, et al. The Role of Pyroptosis in Cancer: Pro-Cancer or Pro-"Host"? *Cell Death Dis* (2019) 10(9):650. doi: 10.1038/s41419-019-1883-8
22. Gao J, Qiu X, Xi G, Liu H, Zhang F, Lv T, et al. Downregulation of GSDMD Attenuates Tumor Proliferation *via* the Intrinsic Mitochondrial Apoptotic Pathway and Inhibition of EGFR/Akt Signaling and Predicts a Good Prognosis in Non–Small Cell Lung Cancer. *Oncol Rep* (2018) 40(4):1971–84. doi: 10.3892/or.2018.6634
23. Wei Q, Zhu R, Zhu J, Zhao R, Li M. E2-Induced Activation of the NLRP3 Inflammasome Triggers Pyroptosis and Inhibits Autophagy in HCC Cells. *Oncol Res* (2019) 27(7):827–34. doi: 10.3727/096504018X15462920753012
24. Dihlmann S, Tao S, Echterdiek F, Herpel E, Jansen L, Chang-Claude J, et al. Lack of Absent in Melanoma 2 (*AIM2*) Expression in Tumor Cells Is Closely Associated With Poor Survival in Colorectal Cancer Patients. *Int J Cancer* (2014) 135(10):2387–96. doi: 10.1002/ijc.28891
25. Chen C, Wang B, Sun J, Na H, Chen Z, Zhu Z, et al. DAC can Restore Expression of NALP1 to Suppress Tumor Growth in Colon Cancer. *Cell Death Dis* (2015) 6(1):e1602. doi: 10.1038/cddis.2014.532
26. Wang WJ, Chen D, Jiang MZ, Xu B, Li XW, Chu Y, et al. Downregulation of Gasdermin D Promotes Gastric Cancer Proliferation by Regulating Cell Cycle-Related Proteins. *J Dig Dis* (2018) 19(2):74–83. doi: 10.1111/1751-2980.12576
27. Martinon F, Burns K, Tschopp J. The Inflammasome: A Molecular Platform Triggering Activation of Inflammatory Caspases and Processing of proIL-Beta. *Mol Cell* (2002) 10(2):417–26. doi: 10.1016/S1097-2765(02)00599-3
28. Bahcecioglu G, Basara G, Ellis BW, Ren X, Zorlutuna P. Breast Cancer Models: Engineering the Tumor Microenvironment. *Acta Biomater* (2020) 106:1–21. doi: 10.1016/j.actbio.2020.02.006
29. Hinshaw DC, Shevde LA. The Tumor Microenvironment Innately Modulates Cancer Progression. *Cancer Res* (2019) 79(18):4557–66. doi: 10.1158/0008-5472.CAN-18-3962
30. Yu H, Pardoll D, Jove R. STATs in Cancer Inflammation and Immunity: A Leading Role for STAT3. *Nat Rev Cancer* (2009) 9(11):798–809. doi: 10.1038/nrc2734
31. Liu RY, Zeng Y, Lei Z, Wang L, Yang H, Liu Z, et al. JAK/STAT3 Signaling Is Required for TGF-β-Induced Epithelial-Mesenchymal Transition in Lung Cancer Cells. *Int J Oncol* (2014) 44(5):1643–51. doi: 10.3892/ijo.2014.2310
32. Khadirnaikar S, Kumar P, Pandi SN, Malik R, Dhanasekaran SM, Shukla SK. Immune Associated LncRNAs Identify Novel Prognostic Subtypes of Renal Clear Cell Carcinoma. *Mol Carcinog* (2019) 58(4):544–53. doi: 10.1002/mc.22949
33. Sun Z, Jing C, Guo X, Zhang M, Kong F, Wang Z, et al. Comprehensive Analysis of the Immune Infiltrates of Pyroptosis in Kidney Renal Clear Cell Carcinoma. *Front Oncol* (2021) 11:716854. doi: 10.3389/fonc.2021.716854
34. Chen SL, Liu LL, Lu SX, Luo RZ, Wang CH, Wang H, et al. HBx-Mediated Decrease of *AIM2* Contributes to Hepatocellular Carcinoma Metastasis. *Mol Oncol* (2017) 11(9):1225–40. doi: 10.1002/1878-0261.12090
35. Ma X, Guo P, Qiu Y, Mu K, Zhu L, Zhao W, et al. Loss of *AIM2* Expression Promotes Hepatocarcinoma Progression Through Activation of mTOR-S6K1 Pathway. *Oncotarget* (2016) 7(24):36185–97. doi: 10.18632/oncotarget.9154
36. Chen LC, Wang LJ, Tsang NM, Ojcius DM, Chen CC, Ouyang CN, et al. Tumour Inflammasome-Derived IL-1β Recruits Neutrophils and Improves Local Recurrence-Free Survival in EBV-Induced Nasopharyngeal Carcinoma. *EMBO Mol Med* (2012) 4(12):1276–93. doi: 10.1002/emmm.201201569
37. Patsos G, Germann A, Gebert J, Dihlmann S. Restoration of Absent in Melanoma 2 (*AIM2*) Induces G2/M Cell Cycle Arrest and Promotes Invasion of Colorectal Cancer Cells. *Int J Cancer* (2010) 126(8):1838–49. doi: 10.1002/ijc.24905
38. Kong H, Wang Y, Zeng X, Wang Z, Wang H, Xie W. Differential Expression of Inflammasomes in Lung Cancer Cell Lines and Tissues. *Tumour Biol* (2015) 36(10):7501–13. doi: 10.1007/s13277-015-3473-4
39. Sorrentino R, Terlizzi M, Terlizzi VG, Popolo A, Pecoraro M, Perillo G, et al. Human Lung Cancer-Derived Immunosuppressive Plasmacytoid Dendritic Cells Release IL-1α in an *AIM2* Inflammasome-Dependent Manner. *Am J Pathol* (2015) 185(11):3115–24. doi: 10.1016/j.ajpath.2015.07.009

Conflict of Interest: The authors declare that the research was conducted in the absence of any commercial or financial relationships that could be construed as a potential conflict of interest.

Publisher's Note: All claims expressed in this article are solely those of the authors and do not necessarily represent those of their affiliated organizations, or those of the publisher, the editors and the reviewers. Any product that may be evaluated in this article, or claim that may be made by its manufacturer, is not guaranteed or endorsed by the publisher.

Copyright © 2022 Zhang, Wei, Wang, Wang, Ji, Yao and Song. This is an open-access article distributed under the terms of the Creative Commons Attribution License (CC BY). The use, distribution or reproduction in other forums is permitted, provided the original author(s) and the copyright owner(s) are credited and that the original publication in this journal is cited, in accordance with accepted academic practice. No use, distribution or reproduction is permitted which does not comply with these terms.

Advantages of publishing in Frontiers

OPEN ACCESS
Articles are free to read for greatest visibility and readership

FAST PUBLICATION
Around 90 days from submission to decision

HIGH QUALITY PEER-REVIEW
Rigorous, collaborative, and constructive peer-review

TRANSPARENT PEER-REVIEW
Editors and reviewers acknowledged by name on published articles

Frontiers
Avenue du Tribunal-Fédéral 34
1005 Lausanne | Switzerland

Visit us: www.frontiersin.org
Contact us: frontiersin.org/about/contact

REPRODUCIBILITY OF RESEARCH
Support open data and methods to enhance research reproducibility

DIGITAL PUBLISHING
Articles designed for optimal readership across devices

FOLLOW US
@frontiersin

IMPACT METRICS
Advanced article metrics track visibility across digital media

EXTENSIVE PROMOTION
Marketing and promotion of impactful research

LOOP RESEARCH NETWORK
Our network increases your article's readership